Synthesis and Applications of P-Chiral Molecules in the Design of P-Chiral Brønsted Acids and Ligands for Asymmetric Catalytic Reactions

Ifenna I. Mbaezue

Department of Chemistry, McGill University

Montreal, QC, Canada

January 2024

A thesis submitted to McGill University in partial fulfillment of the requirements of the degree of Doctor of Philosophy

To my parents, Nkwute and Uche, and my siblings, Chioma, Ugonna and Munachi.

Abstract

Novel approaches towards the synthesis and applications of *P*-chiral molecules were investigated and applied in the design of *P*-chiral Brønsted acid organocatalysts. These catalysts were evaluated in the asymmetric transfer hydrogenation of quinolines to tetrahydroquinolines. Among these substrates, the organocatalytic asymmetric transfer hydrogenation of deactivated quinolines was investigated for the first time. Additionally, these novel approaches were applied in the first enantiospecific phosphonylation of imidazoles via a solvent-switchable, site-selective, 1,4-palladium migration/C-H activation cascade. As a proof of concept of the utility of these compounds, the stereoretentive reduction of one phosphonyl imidazole product was achieved, leading to the first reported *P*-chiral phosphinyl imidazole ligand. This *P*-chiral ligand was found to induce high enantioselectivity in the Pd-catalyzed Suzuki-Miyaura cross-coupling reaction of two sterically demanding aromatic systems to give an atropisomer in high enantiomeric purity.

Résumé

De nouvelles approches vers la synthèse et les applications de molécules P-chirales ont été étudiées et appliquées dans la conception d'organocatalyseurs d'acide de Brønsted P-chiraux. Ces catalyseurs ont été évalués dans l'hydrogénation par transfert asymétrique des quinolines en tétrahydroquinolines. Parmi ces substrats, l'hydrogénation par transfert asymétrique organocatalytique de quinolines désactivées a été étudiée pour la première fois. De plus, ces nouvelles approches ont été appliquées à la première phosphonylation énantiospécifique des imidazoles via une cascade régiosélective de migration 1,4 du palladium et d'activation C-H, commutable par solvant. Comme preuve de concept de l'utilité de ces composés, la réduction, avec rétention de chiralité, d'un produit phosphonyle imidazole a été obtenue, conduisant au premier ligand phosphinylimidazole P-chiral signalé. Il a été constaté que ce ligand P-chiral induisait une énantiosélectivité élevée dans la réaction de couplage croisé Suzuki-Miyaura, catalysée par le Palladium, de deux systèmes aromatiques exigeants stériquement pour donner un atropisomère de haute pureté énantiomère.

Preface

Parts of the material included in the following thesis are adapted from published papers and are under copyright.

The material in Chapter 2 is adapted from:

Yuan, M.; Mbaezue, I. I.; Zhou, Z.; Topic, F.; Tsantrizos, Y. S. *P*-Chiral, *N*-Phosphoryl Sulfonamide Brønsted Acids with an Intramolecular Hydrogen Bond Interaction that Modulates Organocatalysis. *Org. Biomol. Chem*. **2019**, *17*, 8690 – 8694. © Royal Society of Chemistry (2019).

The material in Chapter 3 is adapted from:

Mbaezue, I. I.; Topic, F.; Tsantrizos, Y. S. Re-evaluation of *P*-Chiral, *N*-Phosphoryl Sulfonamide Brønsted Acids in the Asymmetric Synthesis of 1,2,3,4-Tetrahydroquinoline-2-carboxylate Esters via Biomimetic Transfer Hydrogenation. *Synlett* **2023**, *34*, 1709-1714. © Georg Thieme Verlag KG (2023).

The material in Chapter 4 is adapted from a manuscript in preparation.

Acknowledgements

I am sincerely grateful to my Ph.D. supervisor, Prof. Youla S. Tsantrizos, for her mentorship and unwavering support throughout this journey. I am also grateful for the remarkable research opportunities she has provided, which have allowed me to acquire valuable skills and knowledge.

I would also like to acknowledge the efforts of my colleagues, past and present, who have contributed to the research projects described herein. I especially thank Dr. Shi-Guang Li, Dr. Mingle Yuan and Dr. Angula Reddy for their contributions and collaborative endeavours. I am also grateful to the entire Tsantrizos group for their support and friendship.

I would like to thank the members of my review committee, Prof. Masad Damha, Prof. Tomislav Friščić and Prof. Bruce Arndtsen for their feedback, evaluation and suggestions regarding my research progress. I am also grateful to the all the faculty and staff of the Department of Chemistry at McGill University. especially Dr. Robin Stein, Dr. Tara Sprules and Dr. Kirill Levin (NMR), Dr. Alex Wahba and Nadim Saadé (mass spectrometry) and Dr. Hatem Titi and Dr. Filip Topic (X-ray analysis). I would also like to thank all the administrative and IT staff, especially Chantal Marotte, Chelsea Briand-Pitts, Linda Del Paggio, Nikoo Taghavi and Robert Workman, for making this journey possible.

Finally, I would like to thank my family for their all their support and encouragement and for instilling in me, the values of perseverance and dedication. I am most fortunate to have them.

Table of Contents

List of Figures

List of Schemes

List of Tables

Frequently used Symbols and Abbreviations

BALT	binaphthyl-allyl-tetrasulfone
BPA	BINOL-derived phosphoric acid
BTPA	BINOL-derived thiophosphoric acid
[H_8]-BPA	partially reduced BINOL-derived phosphoric acid
cat.	catalyst
Cp	cyclopentadienyl
Cy	cyclohexyl
de	diastereomeric excess
DFT	density functional theory
dr	diastereomeric ratio
DSI	disulfonimide
EDG	electron donating group
ee	enantiomeric excess
er	enantiomeric ratio
EWG	electron withdrawing group
GC	gas chromatography
HEH	Hantzsch ester
IDP	imidodiphosphate
IDPi	imidodiphosphoamidate
JINGLEs	Binaphthyl-2,2′-bis(sulfuryl)imides
L	Ligand
MBH	Morita-Baylis-Hillman

Men	menthol
M.S.	molecular sieves
ND	not determined
NMP	N-methyl-2-pyrrolidone
NPA	N-triflylphosphoramide
NR	no reaction
NSPA	N-triflylselenophosphoramide
NTPA	N-triflylthiophosphoramide
PC	propylene carbonate
Ph	phenyl
PTSA	P-toluenesulfonic acid
rt	room temperature
SPO	secondary phosphine oxide
Tf	triflyl
THF	tetrahydrofuran
TPO	tertiary phosphine oxide
TRIP	3,3’-bis(2,4,6-triisopropylphenyl)-1,1’-binaphthyl-2,2’-diyl hydrogenphosphate

Chapter 1: Introduction

1.1 Synthesis of *P*-Chiral Secondary Phosphine Oxides (SPOs)

Organophosphorus compounds constitute an important class of catalysts and ligands in asymmetric reactions. The high degree of tunability displayed by phosphorus allows for the synthesis of compounds bearing a wide range of attributes. While their electronic properties can be modulated by the installation of various aryl and alkyl groups, steric congestion is often improved by *t*-butyl and adamantly substituents. Moreover, such steric congestion often enhances the ability of *P*-chiral compounds to promote asymmetric transformations.

Among the numerous organophosphorus compounds reported, the unique nature of secondary phosphine oxides (SPOs) allows for their versatility in organic synthesis and in some cases, their use as ligands in metal-catalyzed reactions. The tautomerization of trivalent phosphinous acid **1.1** to pentavalent SPO **1.2** is favoured under ambient conditions (Scheme 1.1). However, upon coordination as a neutral ligand to metals, the equilibrium favours phosphinous acid-metal complex **1.3**. Under basic conditions, the corresponding anionic *P*-bound complex **1.4** and *O*-bound complex **1.5** are formed.[1]

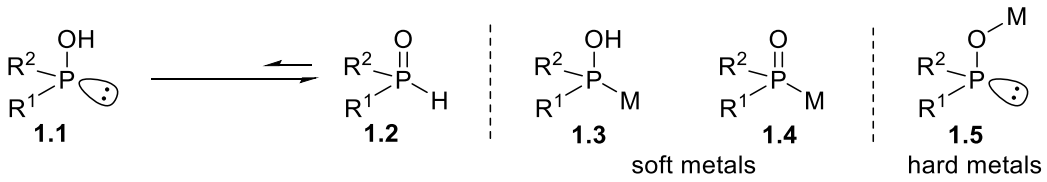

Scheme 1.1. Models of SPO Coordination.

This coordination property has enabled their utility as ligands in various reactions such as asymmetric imine hydrogenation[2] and alkylidenecyclopropanation reactions.[3] In addition, SPOs also serve as precursors to more complex compounds such as tertiary phosphine oxides (TPOs), phosphine ligands and Brønsted acid catalysts. In the design of the *P*-chiral Brønsted acids (Chapters 2 and 3) and

phosphonyl/phosphinyl imidazoles (Chapter 4) reported in this thesis, the synthesis and derivatization of various chiral SPOs was employed. As such, an overview of the various synthetic routes to their acquisition is important. In general, these protocols are grouped into two: the use of chiral auxiliaries and chiral resolution.

1.1.1 The use of Chiral Auxiliaries in the Synthesis of *P*-Chiral SPOs

1.1.1.1 Menthol as a Chiral Auxiliary

Diastereomeric complexes of a racemic SPO and a chiral auxiliary may be formed via substitution reactions. By exploiting differences in physical properties, separation methods such as fractional crystallisation may be successful in isolating these diastereomers. Subsequent cleavage of the requisite bond(s) yields the enantioenriched SPO and the recovery of the auxiliary. The application of this process dates back to 1968, when Emmick and co-workers reported the first attempt to synthesize enantioenriched SPOs with L-(-)-menthol as the chiral auxiliary.[4] The reaction of phenyl phosphonous dichloride **1.6** with L-(-)-menthol yielded H-phosphinate **1.7** (Scheme 1.2a). However, this diastereomeric mixture was inseparable and the subsequent substitution of compound **1.7** with benzylmagnesium chloride afforded SPO **1.8** as a racemate (Scheme 1.2a). Alternatively, the reaction of phenylphosphonic dichloride **1.9** with L-(-)-menthol yielded **1.10**. Subsequently, substitution with benzylmagnesium chloride afforded a diastereomeric mixture of phosphinate **1.11** which was isolated by crystallization. While Emmick and co-workers claimed that enantioenriched SPO **1.8** was obtained by the reduction of **1.11** with $LiAlH_4$, (Scheme 1.2b), subsequent efforts by Mislow to reproduce this protocol led to racemic SPO **1.8**.[5] Mislow also reported that diastereomeric SPOs **1.12** undergo *P*-epimerization to SPO **1.13** in the presence of $LiAlH_4$, via two possible intermediates (Scheme 1.2c).[5] Thus, this method of reduction was deemed detrimental to stereoretention. Subsequently, Mislow and coworkers showed that H-phosphinate **1.7** could in fact be isolated in 95:5 dr by crystallisation from hexane.[6] However, their

efforts were directed towards the synthesis of chiral TPOs instead. It was not until 2007 that Giordano and Buono reported the first application of (R_P)-**1.7** towards the synthesis of chiral SPOs (Scheme 1.3a).[7]

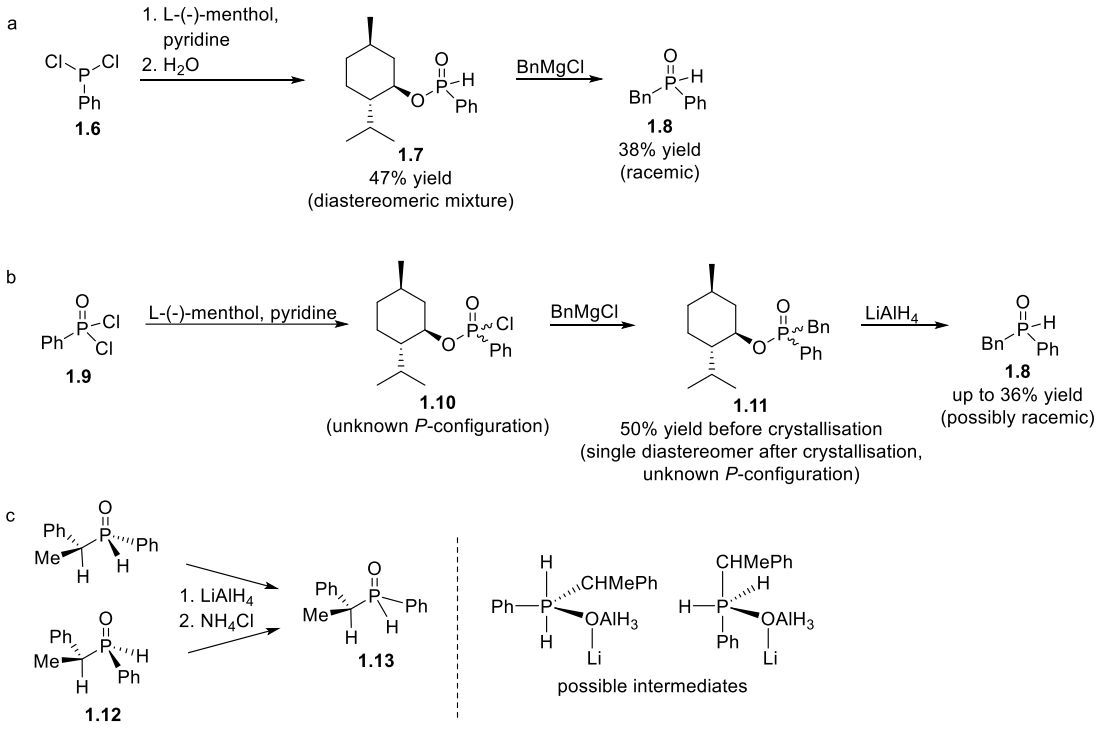

Scheme 1.2. Seminal Synthesis and Stability Studies of SPOs.

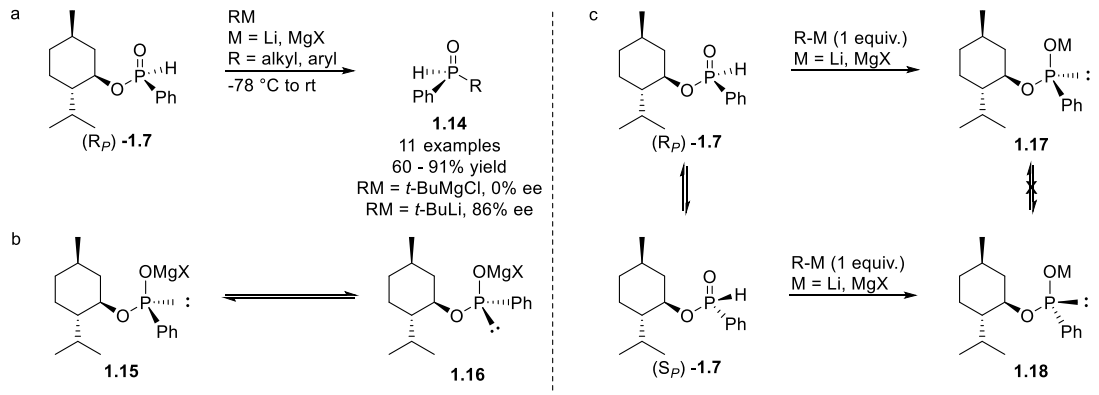

Scheme 1.3. Synthesis of *P*-Chiral SPOs using L-(-)-Menthol as a Chiral Auxiliary.

While their methodology tolerated an array of alkyl and aryl nucleophiles in the substitution of (R_P)-**1.7**, organolithium reagents outperformed the corresponding organomagnesium reagents in stereoretention. For instance, while *t*-BuMgCl afforded the *t*-butyl substituted SPO **1.14** as a racemic product, *t*-BuLi yielded this compound in 86% ee.[7] The authors attributed this phenomenon to a reversible *P*-epimerisation of **1.15** to **1.16**, obtained after the first equivalent of Grignard reagent abstracts the phosphinate proton of (R_P)-**1.7** (Scheme 1.3b).[7] The nucleophilic attack of compound **1.15** by a second equivalent of a bulky Grignard reagent like *t*-BuMgCl, was deemed to proceed slower than *P*-epimerisation to **1.16**, whereas the more reactive *t*-BuLi afforded stereoretention. However, Han latter reported a thorough mechanistic investigation that highlighted the unlikely *P*-epimerisation of **1.15** to **1.16**, or that of **1.17** to **1.18** (Scheme 1.3c).[8] It was demonstrated that after the reaction of (R_P)-**1.7** with 1 equivalent of *t*-BuMgCl at -80 °C to give **1.15**, quenching of the reaction led to the recovery of (R_P)-**1.7** in >99% de. Han also showed that metal alkoxides such as (-)MenOLi generated from the substitution of (R_P)-**1.7** by organometallic reagents were implicated in the *P*-epimerisation of (R_P)-**1.7** to (S_P)-**1.7** (Scheme 1.3c). In addition, other impurities such as menthol and water were reported to be detrimental to stereoretention.[8]

1.1.1.2 Amines and Amino Alcohols/Phenols as Chiral Auxiliaries

In addition to chiral alcohols such as L-(-)-menthol, chiral amines and amino-alcohols also serve as important auxiliaries towards the acquisition of *P*-chiral SPOs. In 2003, Kolodiazhnyi reported the first diastereoselective reaction of phosphorus(III) chlorides **1.19a-c** with chiral *N*-(1-methylbenzyl)amines, to furnish enriched aminophosphines **1.20a-c** (Scheme 1.4).[9] Their reaction with BH_3.THF, gave adducts which could be crystallised to yield compounds **1.21a-c** as single diastereomers. The deborylation of **1.21a** with diethylamine and subsequent hydrolysis afforded SPO (S_P)-**1.22**.

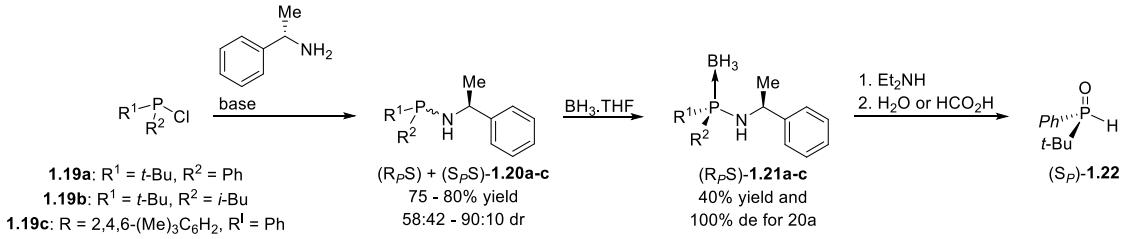

Scheme 1.4. Synthesis of *P*-Chiral SPOs using N-(1-methylbenzyl)amine as a Chiral Auxiliary.

Shortly after, Buono and co-workers reported a one-pot, two-step synthesis of both enantiomers of **1.22** from oxazaphospholidine **1.23** (Scheme 1.5).[10] The reaction of amino alcohol (S)-(+)-prolinol with $PhP(NMe_2)_2$ gave **1.23** and the cleavage of the formed P-O bond with *t*-BuLi furnished **1.24**. Upon work-up with acids having pK_a values $\leq$ 1, (R_P)-**1.22** was obtained in up to 88% yield and 91% ee. Moreover, acids with pK_a values of approximately 3 – 5, gave (S_P)-**1.22** in up to 77% yield and 85% ee. Buono also reported the transformation of unprotected ephedrine-based oxazaphospholidine **1.25** to (R_P)-**1.22**. After *t*-BuLi mediated ring-opening and PTSA/H_2O acidolysis, (R_P)-**1.22** was obtained in similar selectivity (85% ee) when compared to the prolinol-based phosphine route (Scheme 1.5b). However, (R_P)-**1.22** was obtained in lower yield at 40%.

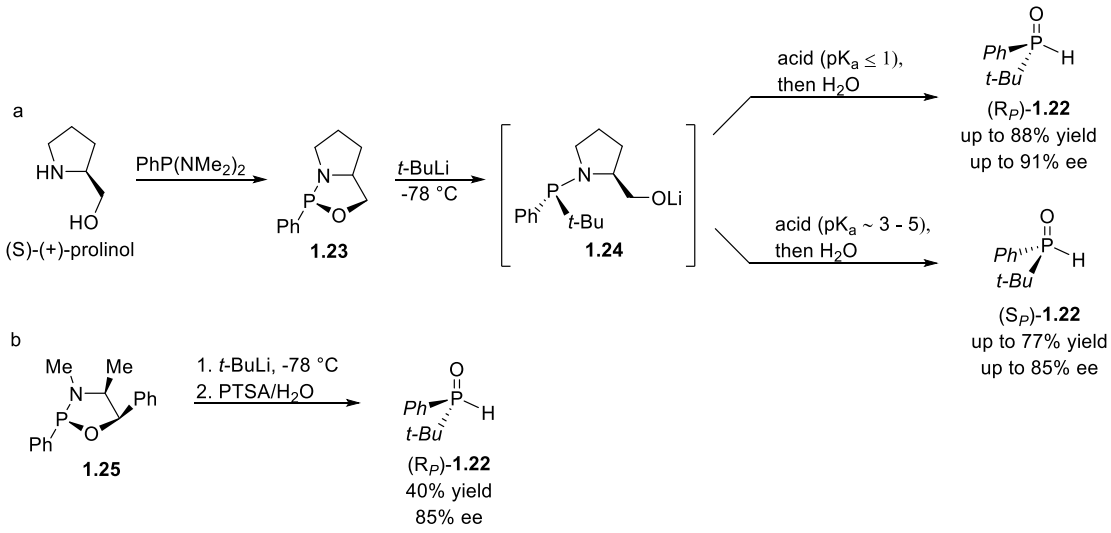

Scheme 1.5. Seminal Synthesis of *P*-Chiral SPOs using Prolinol and Ephedrine.

In 2017, Han and coworkers reported the synthesis of SPO (S_P)-**1.22** using (1R,2S)-norephedrine **1.26** as a chiral auxiliary (Scheme 1.6a).[11] The treatment of **1.26** with $PhPCl_2$ under basic conditions afforded intermediate **1.27**. Subjecting **1.27** to hydrolysis led to selective P-N bond cleavage, yielding **1.28**. Subsequently, the P-O bond cleavage of **1.28** was achieved with *t*-BuLi, to give (S_P)-**1.22** in 65% yield and 99.2:0.8 er. A similar approach was amenable to (*1S,2R*) aminoindanol **1.29**, furnishing phosphinates **1.30** in good to excellent dr (Scheme 16b). The reaction of these compounds with *t*-BuLi gave SPOs (S_P)-**1.31** in up to 92% yield and 99.5:0.5 er. In both instances, aryl-substituted phosphine dichlorides were employed. However, it was also demonstrated that the sequential reaction of phosphine trichloride and the requisite aryl-Grignard reagent with either **1.26** or **1.29**, yielded phosphinates **1.32** or **1.30** respectively (Schemes 16c-d). This protocol allowed for the modular installation of various aryl groups, while avoiding the separate synthesis of aryl-substituted phosphine dichlorides. Finally, the reactions of **1.32** or **1.30** with *t*-BuLi, furnished SPOs (S_P)-**1.31** in up to 91% yield and 99.9:0.1 er.

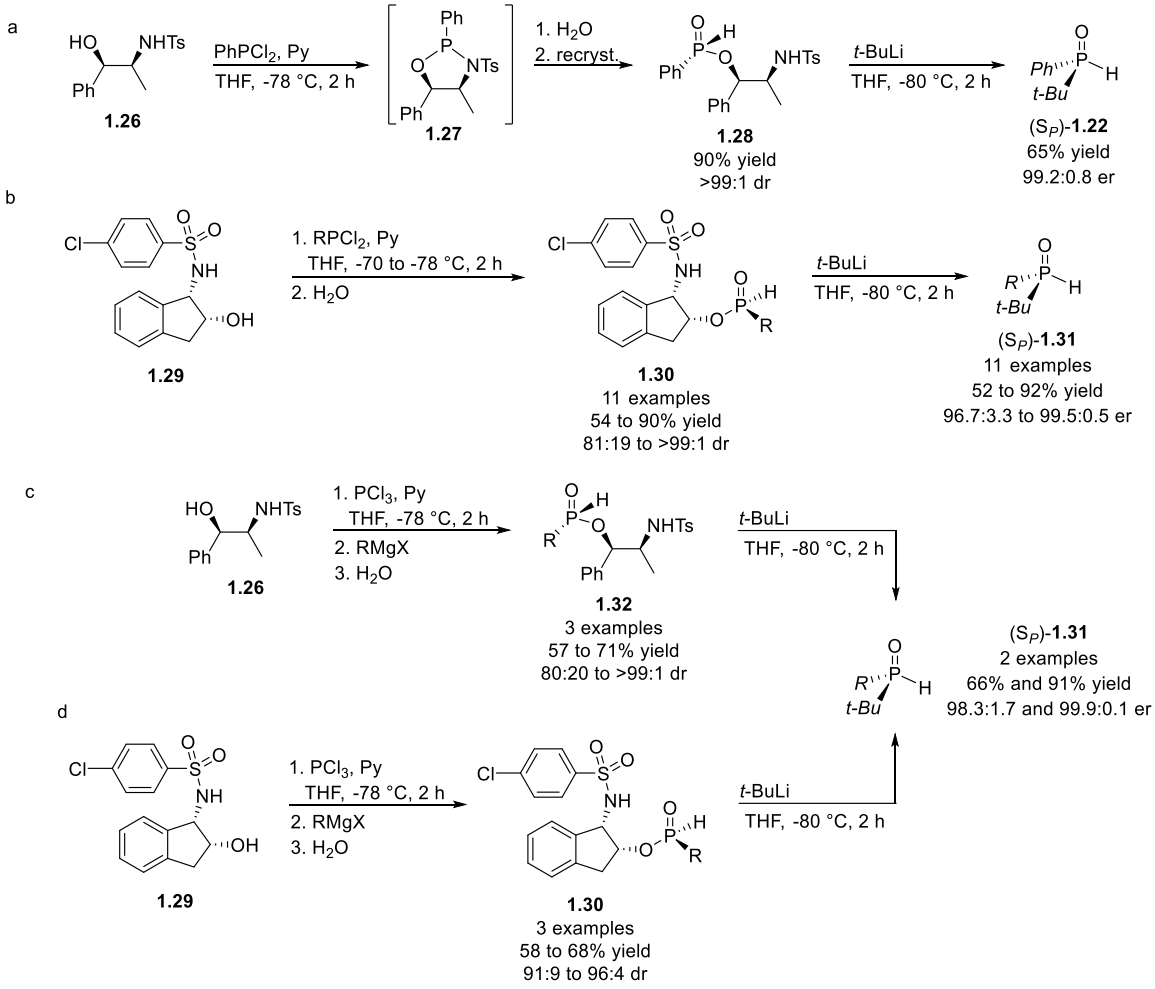

Scheme 1.6. Synthesis of *P*-Chiral SPOs using Norephedrine and Aminoindanol as Chiral Auxiliaries.

In the synthesis of SPOs from chiral auxiliaries, *t*-BuLi is conventionally used to install the *t*-butyl group while simultaneously cleaving the requisite P-OR bonds (Schemes 1.3, 1.5, 1.6). However, due to the extreme pyrophoric nature of this organolithium reagent, methodologies that circumvent its use are advantageous. In 2019, our group reported a novel route to the acquisition of SPOs, via the pre-installation of the *t*-butyl group using *t*-$BuPCl_2$.[12] Auxiliary **1.33** was reacted with *t*-$BuPCl_2$ to give **1.34** and subsequently, the more labile P-N bond was hydrolysed to give H-phosphinate **1.35** in good yield and excellent dr (Scheme 1.7). The choice of auxiliary **1.33** was strategic: the aryloxy backbone incorporated into H-phosphinate **1.35** is a good leaving group. Consequently, the P-O bond of **1.35** is susceptible to

cleavage by nucleophiles weaker than *t*-BuLi. Thus, various Grignard reagents were successfully utilized in P-O bond cleavage, to afford SPOs (R_P)-**1.31** in 40 – 96% yield and up to 99% ee (Scheme 1.7).

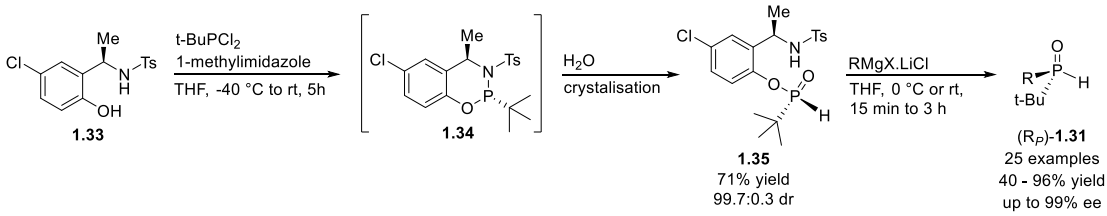

Scheme 1.7. Synthesis of *P*-Chiral SPOs using an Aminophenol as a Chiral Auxiliary.

1.1.2 Synthesis of *P*-Chiral SPOs by Resolution

1.1.1.3 Resolution of SPOs using Chiral Bi-naphthol and Carboxylic Acids

The synthesis of enantioenriched SPOs from chiral auxiliaries is often expensive and lacking in atom economy. Thus, despite the yield limitations of methodologies such as kinetic resolution, this approach may be fairly efficient when SPO racemates are readily accessible. Moreover, if the separation of the resulting diastereomeric complexes is facile, accessibility to the desired compounds may be further improved. In 1999, Mikołajczyk reported the first kinetic resolution of racemic SPO **1.22** using optically active reagents.[13] Preliminary investigations commenced by stirring (rac)-**1.22** (2 equiv.) with (R)-(+)-1,1'-Bi(2-naphthol) (1 equiv.), in water (Scheme 1.8a). Consequently, a crystalline diastereomeric complex of (S_P)-**1.22** and (R)-(+)-1,1'-Bi(2-naphthol) was isolated by filtration. Via chromatography, (S_P)-**1.22** was isolated in 58% ee. The extraction of the mother liquor yielded (R_P)-**1.22** in 60% ee and by repeating the resolution, it was obtained in 77% ee. Next, the resolving properties of (S)-(+)-mandelic acid were investigated. By stirring equimolar quantities of (rac)-**1.22** and (S)-(+)-mandelic acid in ether, a crystalline diastereomeric complex of (S_P)-**1.22** and (S)-(+)-mandelic acid was obtained (Scheme 1.8b). Moreover, the mother liquor contained a diastereomeric complex of (R_P)-**1.22** and (S)-(+)-mandelic

acid. The decomposition of the crystalline complex in aqueous potassium carbonate furnished (S_P)-**1.22** in 28% yield and 99% ee. Similarly, the isolation and decomposition of the complex in the mother liquor gave (R_P)-**1.22** in 52% yield and 39% ee.

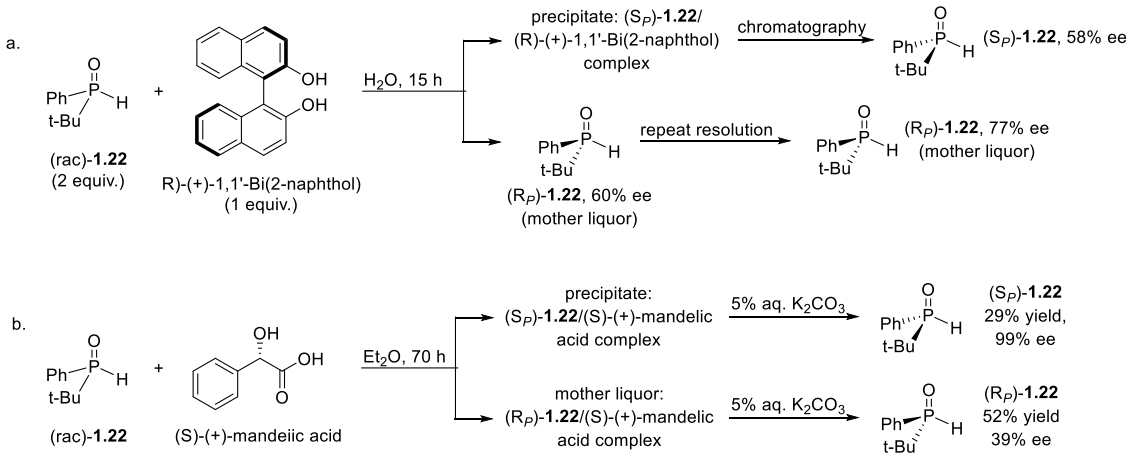

Scheme 1.8. Kinetic Resolution using (R)-(+)-1,1[1]-Bi(2-naphthol) and (S)-(+)-Mandelic Acid.

Mikołajczyk also highlighted the potential of dibenzoyl-L-tartaric acid to resolve SPO (rac)-**1.22**. However, it was not until 2009 that Minaard reported the application of this acid for this purpose.[14] Under optimised conditions, (rac)-**1.22** was dissolved in a 4:1 benzene:acetone solution at reflux, and following the addition of an equimolar quantity of dibenzoyl-L-tartaric acid, a crystalline diastereomeric complex of (R_P)-**1.22** and dibenzoyl-L-tartaric acid was obtained at ambient temperature. The decomposition of this complex in aqueous sodium hydroxide gave (R_P)-**1.22** in 31% yield and >99% ee. Similarly, the isolation and decomposition of the complex in the mother liquor gave (S_P)-**1.22** in 31% yield and 97% ee (Scheme 1.9a).

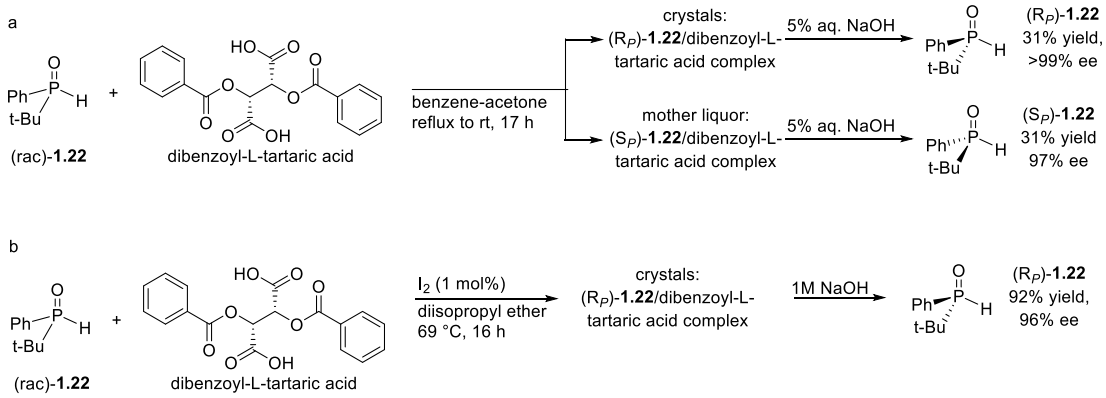

Scheme 1.9. SPO Resolution using Dibenzoyl-L-Tartaric Acid.

In 2014, Minaard reported an extension of this methodology via a radical-mediated, crystallisation-induced dynamic resolution of (rac)-**1.22** (Scheme 1.9b).[15] By heating a mixture of (rac)-**1.22**, dibenzoyl-L-tartaric acid and catalytic iodine in diisopropyl ether, a crystalline diastereomeric complex of (R_P)-**1.22** and dibenzoyl-L-tartaric acid was obtained. The decomposition of this complex under basic conditions afforded (R_P)-**1.22** in 92% yield and 96% ee. After a thorough mechanistic investigation, it was concluded that iodine promoted the radical-mediated *P*-epimerisation equilibrium of (R_P)-**1.22** to (S_P)-**1.22**. This allowed for the *in-situ* deracemization of the SPO via the preferential binding of one enantiomer to the dibenzoyl-L-tartaric acid, hence, leading to the formation of the favoured chiral SPO-tartaric acid complex.

1.1.1.4 Resolution of SPOs by Asymmetric Coupling

Kinetic resolution via the asymmetric coupling of a racemic compound and another substrate presents the opportunity to recover some of the compound enantioenriched, as well as obtain a new *P*-chiral product. An efficient application of this concept in the resolution of SPOs, was first reported by Zhang in 2020.[16] The Le-Phos catalysed asymmetric allylation of (rac)-**1.36** with Morita-Baylis-Hillman (MBH)

carbonates **1.37** gave SPOs (R_P)-**1.36** in up to 99% ee. In addition, TPOs **1.38** were obtained in up to 95% ee (Scheme 1.10).

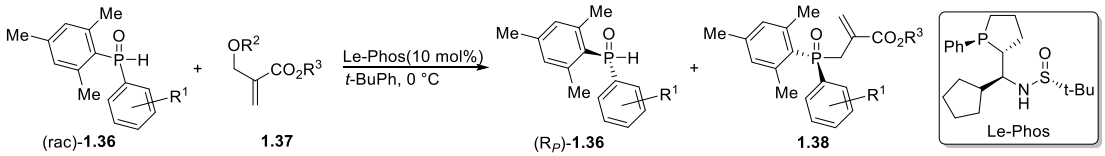

Scheme 1.10. Resolution via Asymmetric Allylation.

1.2 Brønsted Acids as Efficient Organocatalysts for Asymmetric Reactions

In recent years, organocatalytic methodologies for asymmetric synthesis have gained attention as a powerful tool in green and metal-free chemistry. Brønsted acids, a subset of organocatalysts, have become ubiquitous in asymmetric reactions, with the BINOL-derived phosphoric acids being the most common types. The entry of these catalysts into modern chemistry is attributed to Akiyama[17] and Terada[18] who in 2004, independently reported highly asymmetric Mannich-type reactions catalysed by these phosphoric acids (Scheme 1.11). Since then, the field of Brønsted acid catalysis has undergone tremendous growth towards the development of strategies for asymmetric bond construction.[19] As such, electrophiles of varying strengths have been successfully activated under mild reaction conditions. For instance, while imines are relatively easy to activate using BINOL-based phosphoric acids (Scheme 1.11), the activation of challenging electrophiles such as olefins was only recently reported by List, using highly acidic IDPi Brønsted acids.[20]

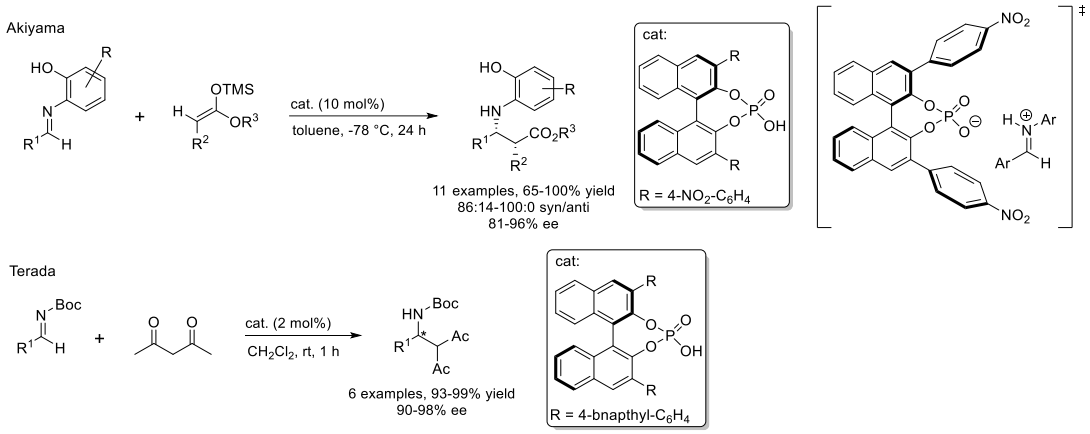

Scheme 1.11. Asymmetric Mannich-type Reactions Catalysed by Phosphoric Brønsted Acids.

Based on their pK_a, chiral Brønsted acids can be grouped into weaker and stronger categories (Figure 1.1).[21] Weaker Brønsted acids such as chiral thioureas, squaramides and TADDOL derivatives have higher pK_a and catalyse asymmetric reactions via hydrogen bonding. However, stronger Brønsted acids have lower pK_a values. In addition, stronger catalysts display hydrogen bonding and/or ion pairing modes of activation, depending on the nature of the electrophile and solvent.[19, 22] Thus, stronger Brønsted acids (subsequently referred to as Brønsted acids) display versatile properties that can be tuned to promote otherwise difficult asymmetric transformations, without employing harsh reaction conditions.

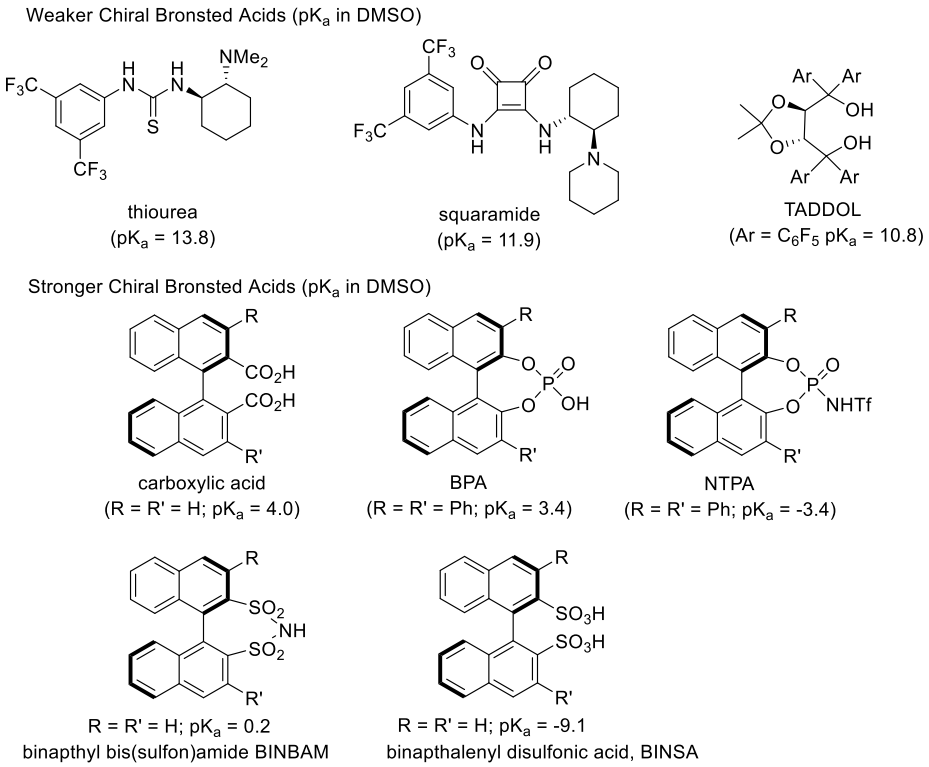

Figure 1.1. Classification of Chiral Brønsted Acids based on pK_a (values in DMSO).

1.2.1 The Rational Design of Brønsted Acids Towards Increased Reactivity and Selectivity

Enantioselectivity is often dependent on the nature and size of the R and R' substituents on the BINOL scaffold of Brønsted acids (Figure 1.1). Moreover, the various modes by which an electrophile can be activated by Brønsted acid catalysts, in addition to the catalyst-controlled delivery of a nucleophile, can also play a crucial role in enantioselectivity. However, reaction rate is primarily determined by the acidity of the catalyst.[23] Although it is important to distinguish between the factors controlling enantioselectivity and reaction rate, the holistic approach presented herein will attempt to show how these factors are complementary in asymmetric catalysis.

1.2.2 The Role of Acidity in Reactivity

While O'Donoghue and Berkessel have reported the pK_a values of a range of Brønsted acids in DMSO,[24] Rueping and Leito established an acidity scale for commonly used Brønsted acids in MeCN.[23] BINOL-derived phosphoric acids (BPAs) were reported to have pK_a values between 12 and 14, the N-triflylphosphoramides (NPAs) between 6 and 7, and Binaphthyl-2,2′-bis(sulfuryl)imides (JINGLEs) at around 5 (Figure 1.2). In addition, Rueping and Leito showed that the pK_a of these acids were positively correlated with their activities. Thus, more acidic catalysts promote higher reaction rates and vice versa. List also reported the pk_a of imidodiphosphate (IDP), disulfonimide (DSI), binaphthyl-allyl-tetrasulfone (BALT) and imidodiphosphoamidate (IDPi) catalysts in MeCN (Figure 1.2).[25] Of these Brønsted acids, the IDPis are the most acidic. In order to clearly present this pK_a-dependent trend in reactivity, the Brønsted acids reviewed in this chapter have been grouped according to similarities in their structures (Figure 1.3).

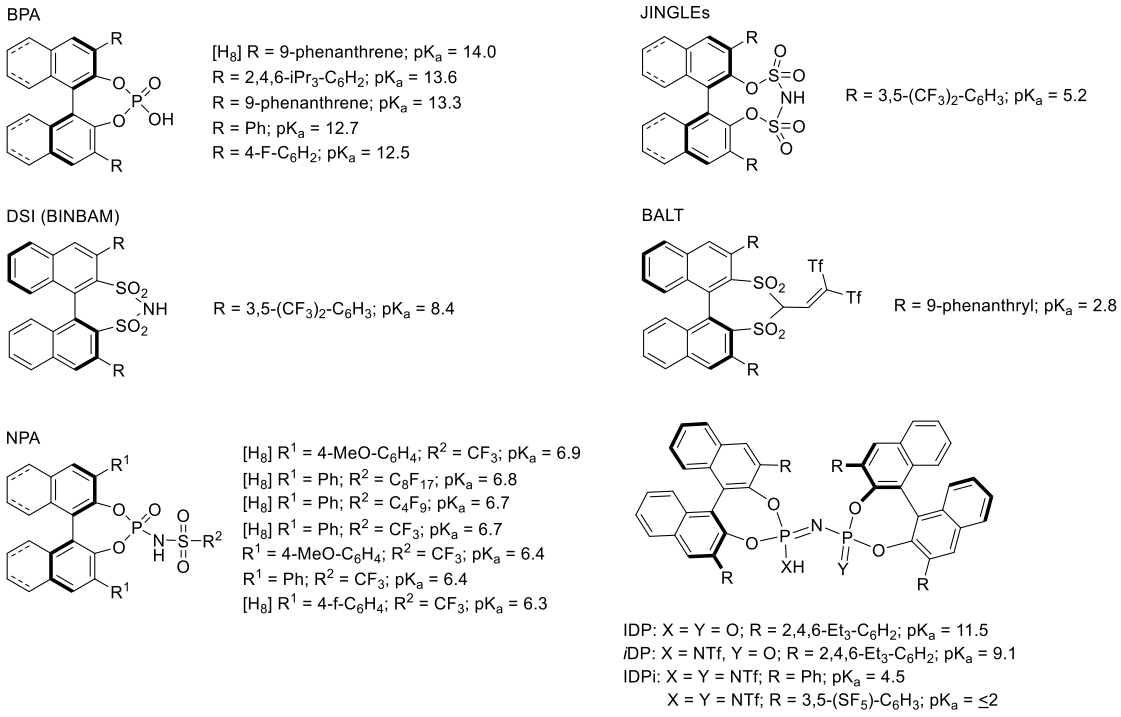

Figure 1.2. pK_a Values of Chiral Brønsted Acids in MeCN.

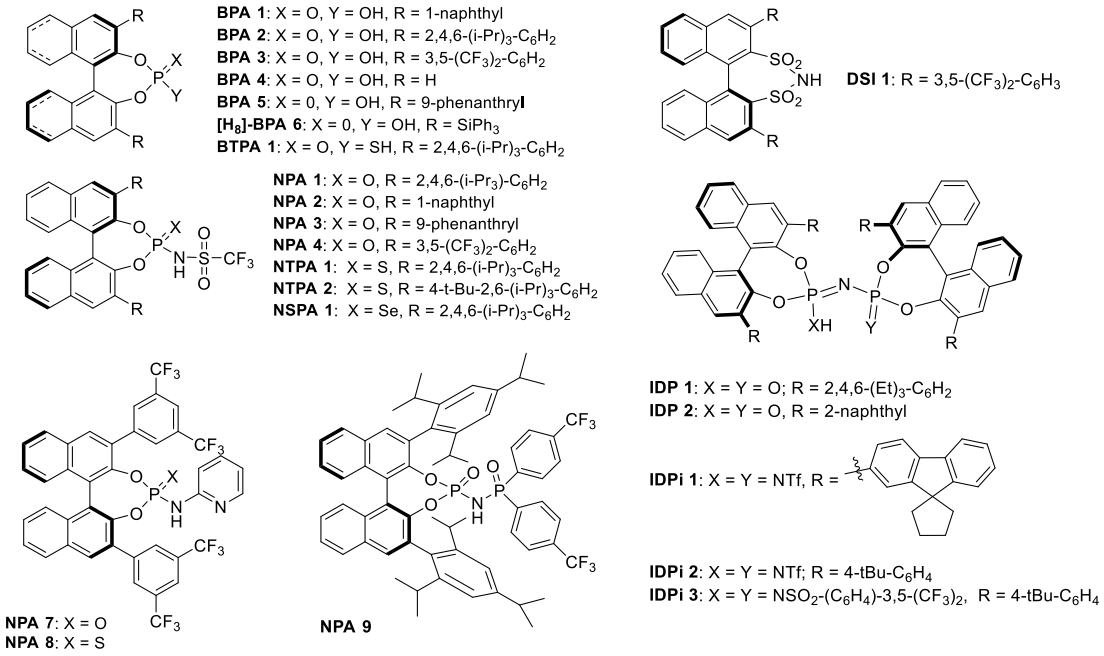

Figure 1.3. Structures of BINOL-derived Brønsted Acids Reviewed.

1.2.3 The Progression of Catalyst Design from Phosphoric Acids to Phosphoramides

BPAs, partially reduced BINOL-derived phosphoric acids ([H_8]-BPAs) and NPAs (Figure 1.3) are by far the most common types of BINOL-based Brønsted acids encountered in asymmetric reactions. The ability to synthesize these acids from cheap and commercially available BINOL, as well as elaborate their scaffold through standard cross-coupling reactions, has led to the design of catalysts of varying steric and electronic properties. For the majority of these compounds, the typical synthetic route[19] begins with the protection of BINOL (R or S) to obtain **1.39** (Scheme 1.12). Subsequently, *ortho*-lithiation with *n*-BuLi, followed by borylation or halogenation gives **1.40** or **1.41** respectively. Under Pd(0) cross-coupling conditions, the desired substituents at the 3,3'-positions are installed and subsequent deprotection gives **1.42**. Phosphorylation using $POCl_3$ affords intermediate **1.43**, from which amidation gives the NPA. However, an acidic work-up of **1.43** yields the BPA and a subsequent

reduction under H_2-Pd/C conditions affords the partially reduced [H_8]-BPA (Scheme 1.12).[19, 26]

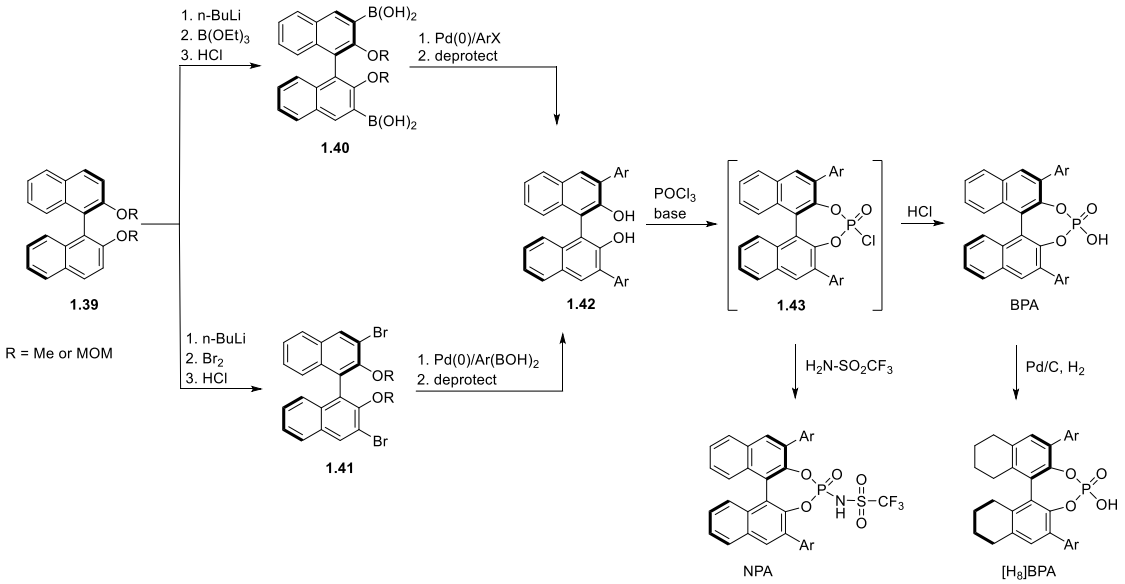

Scheme 1.12. A General Synthetic Route to BPA, [H_8]-BPA and NPA.

Brønsted acids may activate substrates either through mono-activation, dual-activation or bifunctional activation transition states (Figure 1.4).[19] When the substrate contains an acidic proton in proximity to the reaction center, dual activation mode **A** occurs. However, when the substrate contains a Lewis basic group in proximity to the reaction centre, dual activation mode **B** occurs. The bifunctional activation model is possibly the most common transition state encountered in BINOL-based asymmetric reactions. [19, 27] This model, as well as the dual activation models, highlight the Brønsted and Lewis basic nature of these catalysts in the activation and delivery of nucleophiles. In conjunction with the steric bulk provided by the 3,3'-substituents, these transition states may also control enantioselectivity.

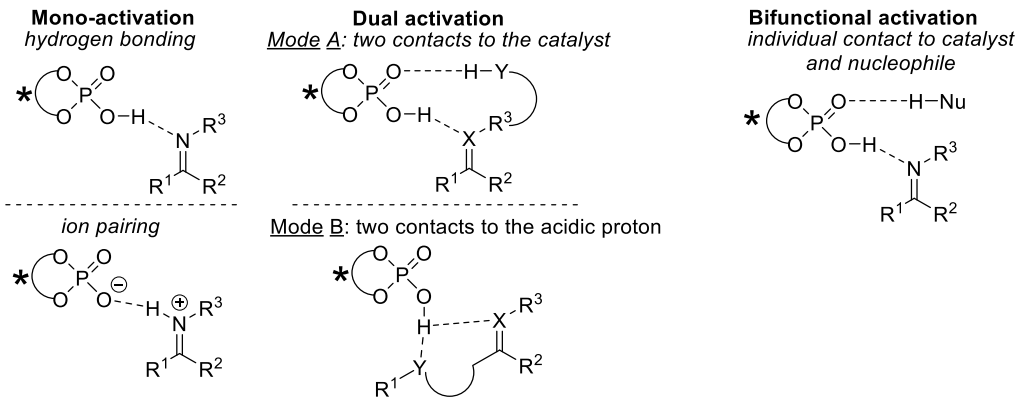

Figure 1.4. Various Modes of Electrophile Activation by BINOL-based Brønsted Acids.

BPAs and [H_8]-BPAs have shown remarkable success in numerous asymmetric reactions such as Mannich-type,[17,18,28] intra-molecular Michael additions,[29] transacetalization,[30] hydrophosphonylation,[31] the transfer hydrogenation of imines[32] and N-heterocycles,[33] Friedel-Crafts,[34] Strecker[35] and Biginelli[36] reactions. However, the majority of these transformations involve the activation of reactive electrophiles such as imines and aziridines.[19] For weaker electrophiles such as aldehydes, ketones and olefins, the relatively high pk_a values of BPAs and [H_8]-BPAs often render these activations unsuccessful. In the effort to increase the acidity of these Brønsted Acids, Yamamoto introduced the electron withdrawing triflyl moiety as a replacement of the -OH group.[26] This modification allowed for the asymmetric activation of α,β-unsaturated ketones **1.44** by (S)-**NPA 1**. The subsequent reaction of the activated electrophiles with dienes **1.45** afforded Diels-Alder adducts **1.46** in moderate to excellent yields and excellent enantioselectivity (Scheme 1.13).

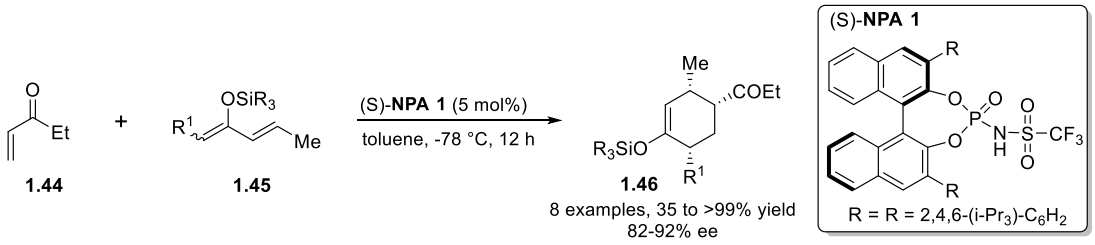

Scheme 1.13. Brønsted Acid Catalysed Asymmetric Diels-Alder Reaction.

In addition, when applied to other reactions that can be catalysed by BPAs, NPAs show significant improvements in yields and enantioselectivities. This may be due to the ability of NPAs to accommodate milder reaction conditions than BPAs, while retaining their high reactivity. For example, in 2007, Rueping reported the first asymmetric organocatalyzed Nazarov cyclization of pentenones to divinyl ketones using NPAs.[37] In the optimisation of the cyclisation of **1.47** to **1.48 a/b**, (R**)-BPA 1** was able to catalyse the reaction in up to 81% ee, although a higher temperature (60 °C) was required. However, with (R)-**NPA 2** and (R)-**NPA 3**, full conversion of the starting material to the desired product was observed at 0 °C, in 10 minutes. Furthermore, enantioselectivity (up to 96% ee) and diastereoselectivity (*cis/trans* ratio up to 7:1) were markedly improved using NPAs (Scheme 1.14).

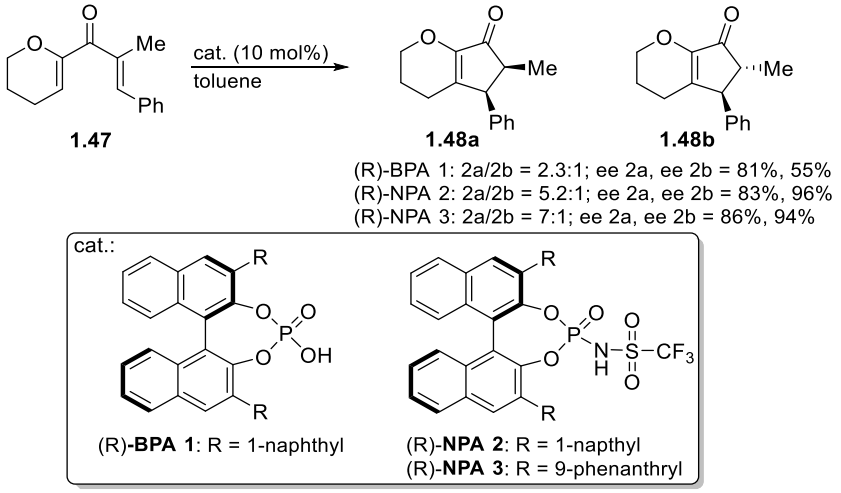

Scheme 1.14. Optimisation of a Brønsted Acid Catalysed Nazarov Cyclization.

To further increase the reactivities of NPAs, Yamamoto envisioned that more acidic analogues could be obtained by replacing the P=0 moiety with P=S or P=Se.[38] It was reasoned that the ability of the respective N-triflylthiophosphoramides (NTPAs) and N-triflylselenophosphoramides (NSPAs) to form more stable conjugate bases than NPAs, would lower their pk_a. These analogues proved superior to NPAs, in the asymmetric protonation of silyl enol ethers (Scheme 1.15).[38]

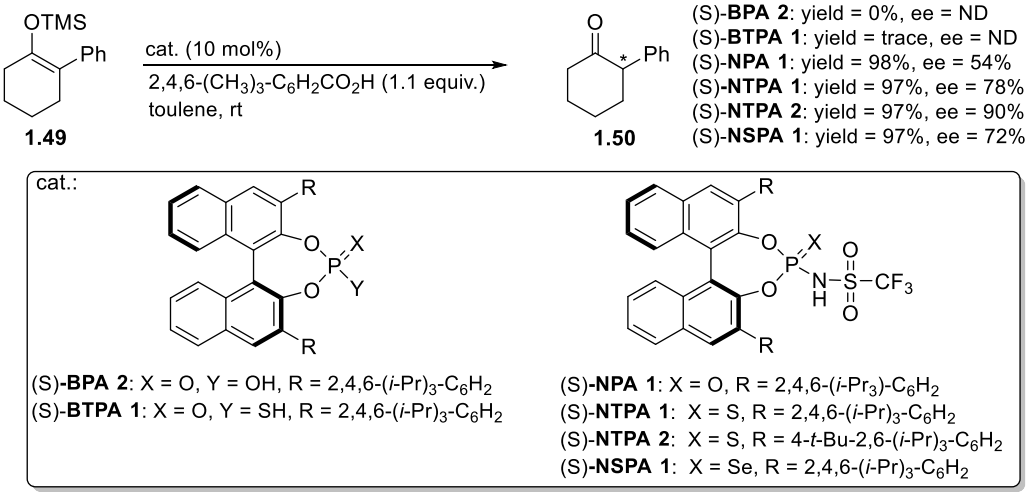

Scheme 1.15. Optimisation of a Brønsted Acid Catalyzed Asymmetric Protonation.

While investigating a suitable Brønsted acid for this reaction, Yamamoto showed that (S)-**BPA 2** failed to catalyse the transformation of **1.49** to **1.50,** while the sulfur analogue, (S)-**BTPA 1**, only gave **1.50** in trace amounts after 96 h (Scheme 1.15). However, with (S)-**NPA 1**, **1.50** was obtained in 98% yield and 54% ee after only 4.5 h. Furthermore, the thio- and seleno- analogues, (S)-**NTPA 1** and (S)-**NSPA 1** afforded **1.50** in similar yields but higher ee, in a shorter time of 3.5 h. Further optimisation using the bulkier (S)-**NTPA 2** improved selectivity, and a substrate scope with ee as high as 90% was reported.[38]

As a result of their higher acidity, NPAs and NTPAs have since been successfully applied to other challenging asymmetric transformations including the 1,3-dipolar cycloaddition of nitrones with ethyl vinyl ethers[39] and the Mukaiyama aldol reaction of aldehydes with silyl enol ethers.[40] However, in some cases, there is a correlation between the higher reaction rates obtained with NPAs and the erosion of enantioselectivity. An examples of this phenomenon was reported by List in the asymmetric desymmetrisation of *meso* cyclic anhydrides.[41] While (S)-**BPA 3** could catalyse the conversion of **1.51** to **1.52** in 80% yield and 22% ee in 24 h, the more

acidic (S)-**NPA 4** gave a similar yield in the same time, but the product was racemic (Scheme 1.16). By replacing the Tf group of (S)-**NPA 4** with a pyridyl group, List introduced a Brønsted basic site that better activated and delivered MeOH with improved yields and enantioselectivity (Scheme 1.16). While this Brønsted acid/base, (S)-**NPA 7**, gave **1.52** in quantitative yield and 80% ee in just 5 h, the thio-analogue, (S)-**NPA 8**, gave similar results in only 3 h. Thus, the mode of substrate activation was crucial in improving yields and controlling enantioselectivity. The importance of an additional basic site was also exemplified in the asymmetric *N*,*O*-acetalization of aldehydes;[42] List showed that in the reaction of **1.53** and **1.54**, the more acidic (S)-**NPA 1** gave **1.55** with lower selectivity, compared to that obtained with (S)-**BPA 2** (Scheme 1.17). However, the use of N-phosphonyl phosphoramide (S)-**NPA 9**, gave **1.55** in the highest enantiomeric excess. List proposed a transition state where the second phosphonyl group of the catalyst activates the hydroxyl nucleophile and enables its delivery to the *re*-enantioface of the iminium intermediate (Scheme 1.17).

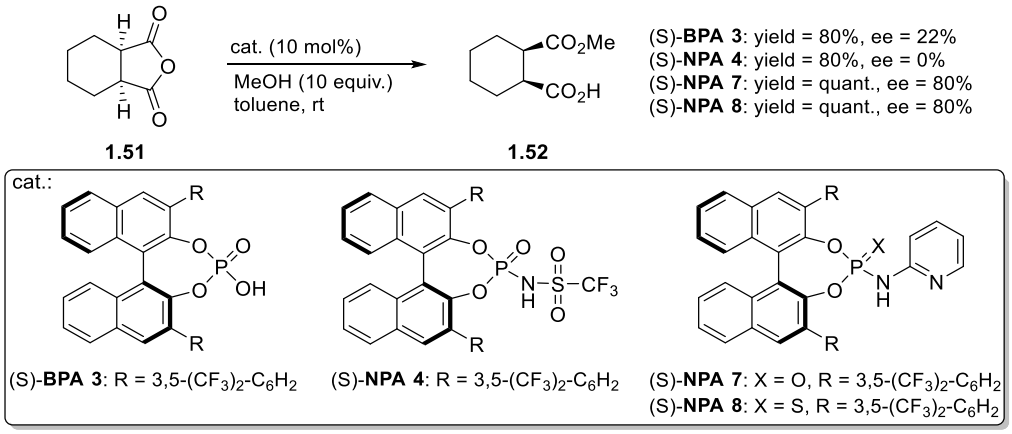

Scheme 1.16. Asymmetric Desymmetrisation of Meso Anhydrides.

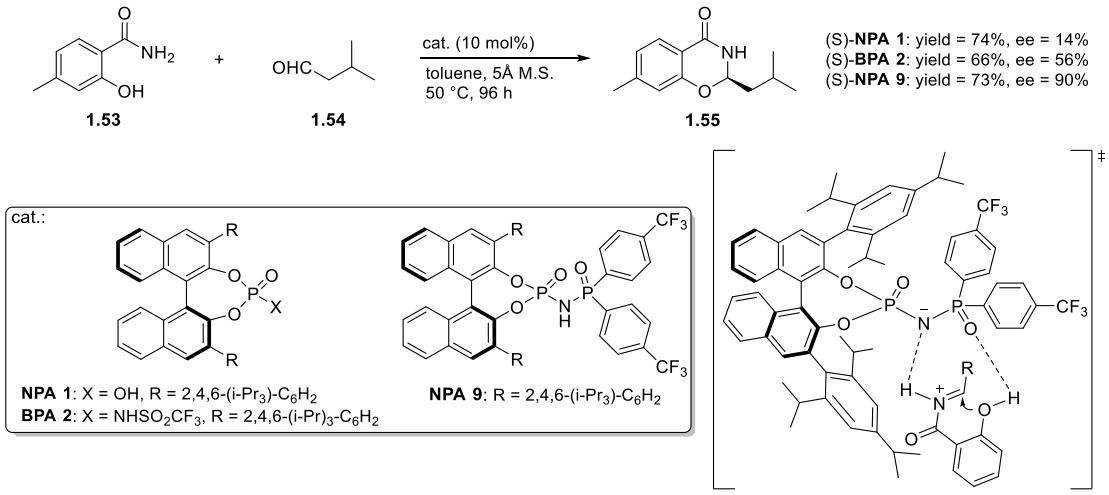

Scheme 1.17. Asymmetric *N,O*-Acetalization of Aldehydes.

1.2.4 The Design and Applications of imidophosphates and Imidodiphosphoramidates

While BPAs and NPAs have been extensively applied in asymmetric catalysis, a limitation to their usage is the absence of a confined cavity. This requirement is crucial in controlling the enantiofacial bias of intermediates that lack well-defined interactions with the catalyst.[43] In addition, it is difficult to overcome this challenge with the installation of bulkier 3,3'-substituents on the BINOL scaffold of BPAs/NPAs, since they radiate away from the active site.[43] To overcome this limitation, List envisioned a model catalyst that would provide a cavity, much like the deep binding pocket of an enzyme. By assembling two identical BINOL subunits through a -P=N-P- linkage, and locking the *O,O*-syn conformation with bulky 3,3'-substituents, imidodiphosphates (IDPs) with well defined confinement were obtained (Scheme 1.18a//b). This rigidification also prevented unwanted Brønsted basicity at the -N- site, leaving only one Brønsted basic site at P=O (Scheme 1.18c).[43] Subsequently, List explored the asymmetric spirocyclization of hydroxyenol ethers **1.56** to **1.57** using these IDPs and showed that they were superior to BPAs/NPAs in achieving excellent selectivities (Scheme 1.18d). Since then, List and co-workers have successfully applied IDP

asymmetric catalysis to other reactions including the acetalization of aldehydes,[44], Prins cyclization[45] and *oxa*-Pictet-Spingler reactions.[46]

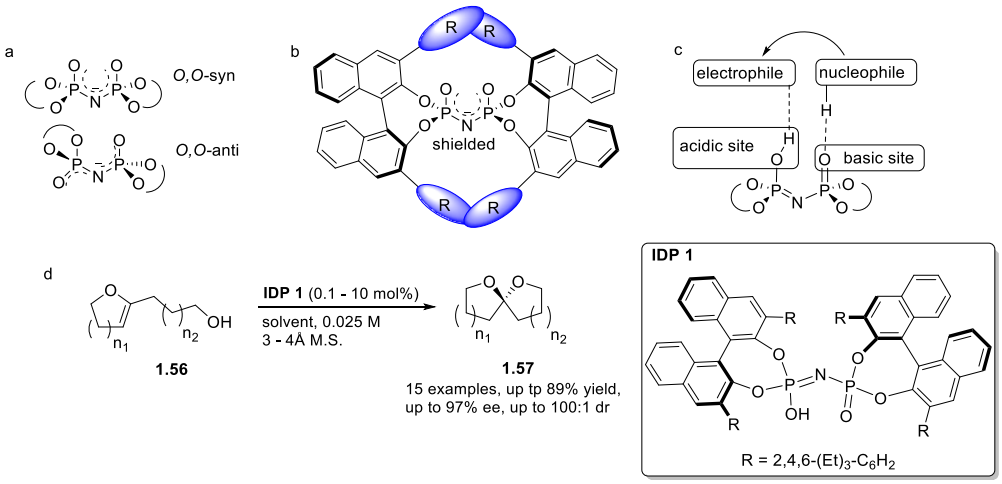

Scheme 1.18. The Rational Design of Imidophosphates.

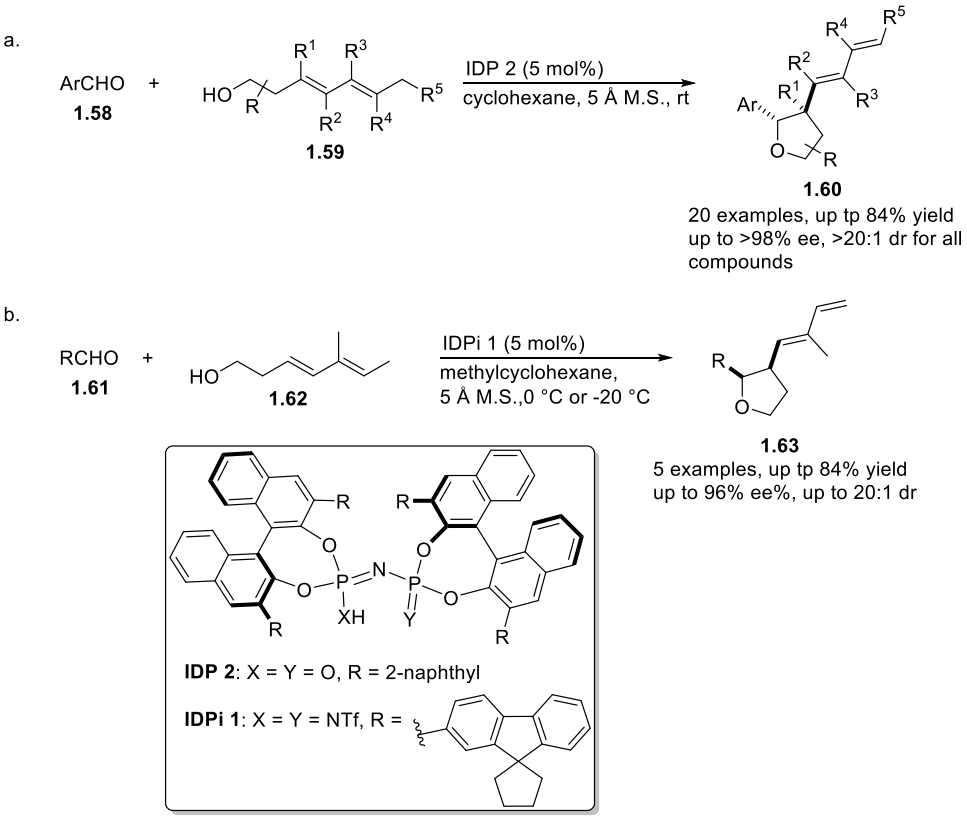

Scheme 1.19. The Application of IDP and IDPi in Asymmetric Cyclisation Reactions.

A limitation of IDPs is their high pK_a (**IDP 1** = 11.5 in MeCN). As a result, they exhibit only moderate reactivity compared to other Brønsted acids of lower pk_a For instance, while investigating the asymmetric vinylogous Prims cyclization of aromatic aldehydes **1.58** with dienyl homoallylic alcohols **1.59**, List and co-workers were able to obtain the corresponding THF products **1.60** in high yields and selectivities, with **IDP 2** (Scheme 1.19a).[47] However, when less reactive aliphatic aldehydes were investigated, the IDP-catalysed transformation failed, even at elevated temperatures. To remedy this, the more acidic imidodiphosphoramidate, **IDPi 1**, was introduced, facilitating the cyclisation of aliphatic aldehydes **1.61** and linear/branched alcohols **1.62** to yield THF products **1.63** (Scheme 1.19b). Depending on the aliphatic aldehyde, the IDPi-catalysed reaction could be carried out at either 0 °C or -20 °C, in comparison to the IDP-catalysed reaction of aromatic aldehydes, which were performed at room temperature. This synergistic effect of confinement and acidity displayed by IDPi catalysts, is further exemplified in the intramolecular hydroalkoxylation of simple olefins **1.64** (Scheme 1.20).[20]

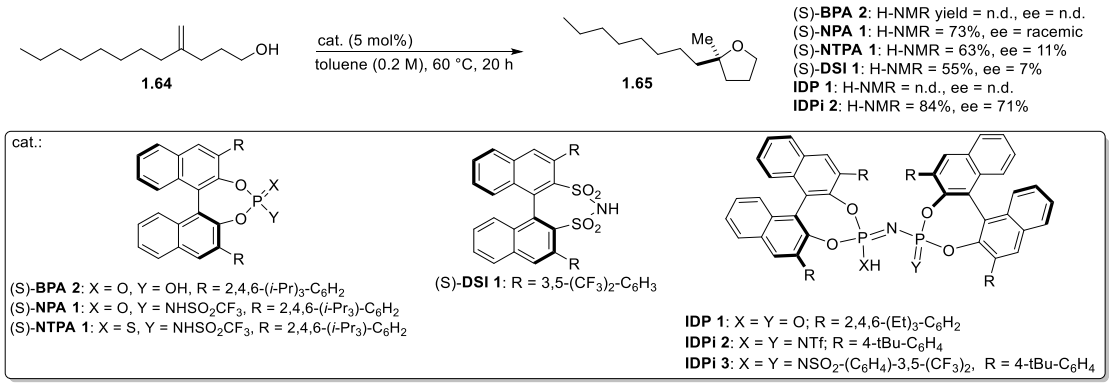

Scheme 1.20. A Comparison of Catalysts in the Hydroalkoxylation of Olefins.

In the optimisation of this reaction, a plethora of catalysts ranging from the BINOL-derived phosphoric acids and their *N*-triflyl analogues, to the disulfonimides and imidodiphosphoramidates were explored. While (S)-**BPA 2** and **IDP 1** showed no reactivity, the more acidic analogues, (S)-**NPA 1**, (S)-**NTPA 1** and (S)-**DS1 1** gave THF product **1.65** in modest to good yields and racemic to poor ee However, under the

same reaction conditions, the confined and more acidic **IDPi 2** delivered **1.65** in 84% yield and 71% ee. Further optimisation with **IDPi 3** afforded **1.65** in 91% isolated yield and 95% ee.

1.2.5 Design, Synthesis and Applications of *P*-Chiral Phosphinamide Brønsted Acids

As exemplified by NPAs, DSI, IDPs and IDPis (Figure 1.3), the amine functionality of Brønsted acids can be tuned to improve catalyst reactivity. However, since these catalysts are based on the BINOL scaffold, structural diversity is primarily dependent upon the nature of the substituents at the 3,3' positions. In the effort to develop a new class of diverse Brønsted acids, Han and co-workers envisioned a *P*-chiral phosphinamide model amenable to structural tunability (Scheme 1.21a).[48] At the core of its architecture, this class of acids is devoid of C_2-symmetry common to the BINOL-based catalysts. Moreover, the R^1 and R^2 substituents on phosphorus may be tuned to modulate selectivity and the acidity of N-H. The synthesis of these catalysts was achieved via either of two routes (Schemes 1.21b,c).

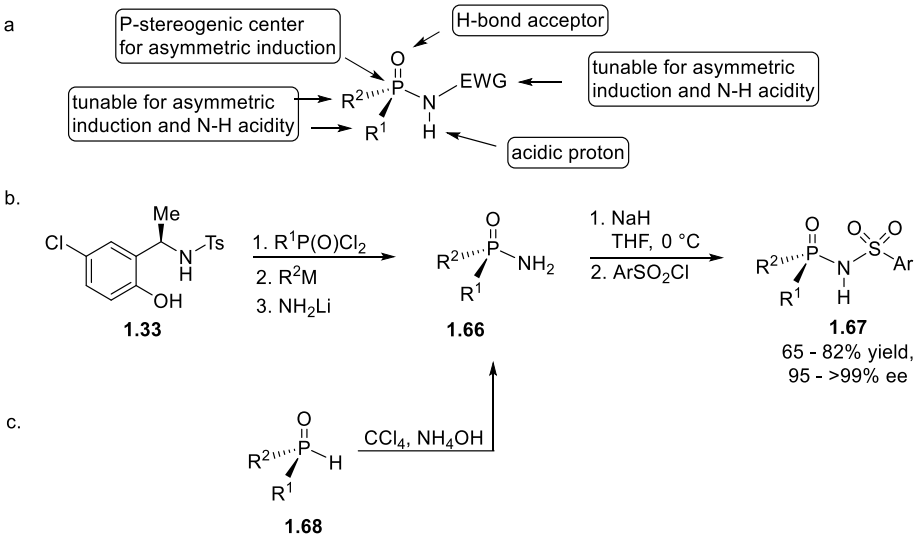

Scheme 1.21. Design and Synthesis of Phosphinamide Brønsted Acids.

Via the first route, chiral auxiliary **1.33** was cyclised using the requisite phosphonyl dichloride. Afterwards, P-N and P-O bond cleavage were achieved with

R^2M and NH_2Li respectively, to give phosphinamide **1.66**. Subsequently, the requisite sulfonyl moieties were installed via substitution on aryl sulfonyl chlorides, yielding Brønsted acids **1.67** (Schemes 1.21b). Alternatively, subjecting SPO **1.68** to Atherton-Todd conditions yielded **1.66** (Scheme 1.21c) from which Brønsted Acids **1.67** were synthesised. Subsequently, Han and co-workers examined the properties of catalysts **1.67a-d** as well as BINOL-based (R)-**BPA 4** in the asymmetric transfer hydrogenation of quinolines **1.69a-b** (Table 1.1). With quinoline **1.69a** as the substrate, catalysts (R)-**BPA 4** and (S)-**1.67a-b** performed comparably, yielding product **1.70a** in 6-11% ee. However, with the *t*-butyl substituted catalyst (R)-**1.67c**, enantioselectivity was improved to 30%. Moreover, the more congested (S)-**1.67d** gave an improvement to 36% ee. In the transfer hydrogenation of **1.69b**, catalysts (R)-**1.67c** and (S)-**1.67d** outperformed (R)-**BPA 4**, yielding tetrahydroquinoline **1.70b** in up to 45% ee (Table 1.1). In the transfer hydrogenation of benzoxazine **1.71**, phosphinamide-based catalysts (R)-**1.67c** and (S)-**1.67d** also outperformed (R)-**BPA 4**. However, in comparison to (S)-**1.67d**, the *t*-butyl substituted (R)-**1.67c** afforded dihydrobenzoxazine **1.72** in a higher ee of 68% (Scheme 1.22).

Table 1.1. A Comparison of Phosphinamide and BINOL-based Brønsted Acids Catalysts in the Asymmetric Transfer Hydrogenation of Quinolines.

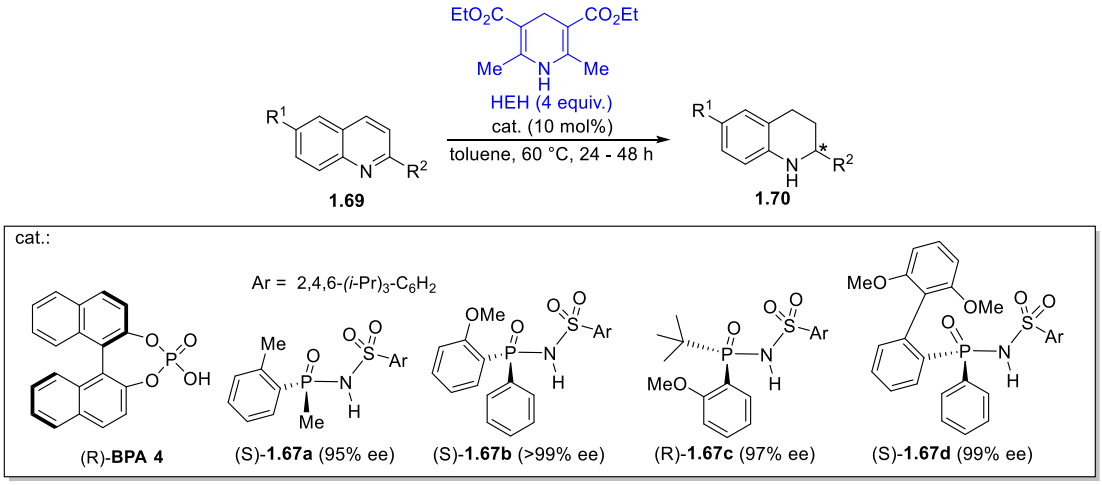

Substrate	R^1, R^2	Cat.	Time (h)	Product	%ee
1.69a	Br, Me	(*R*)-**BPA 4**	24	(S)-**1.70a**	11
		(*S*)-**1.67a**	48	(R)-**1.70a**	6
		(*S*)-**1.67b**	24	(S)-**1.70a**	11
		(*R*)-**1.67c**	24	(S)-**1.70a**	30
		(*S*)-**1.67d**	36	(S)-**1.70a**	36
1.69b	H, Ph	(*R*)-**BPA 4**	48	(R)-**1.70b**	12
		(*R*)-**1.67c**			45
		(*S*)-**1.67d**			35

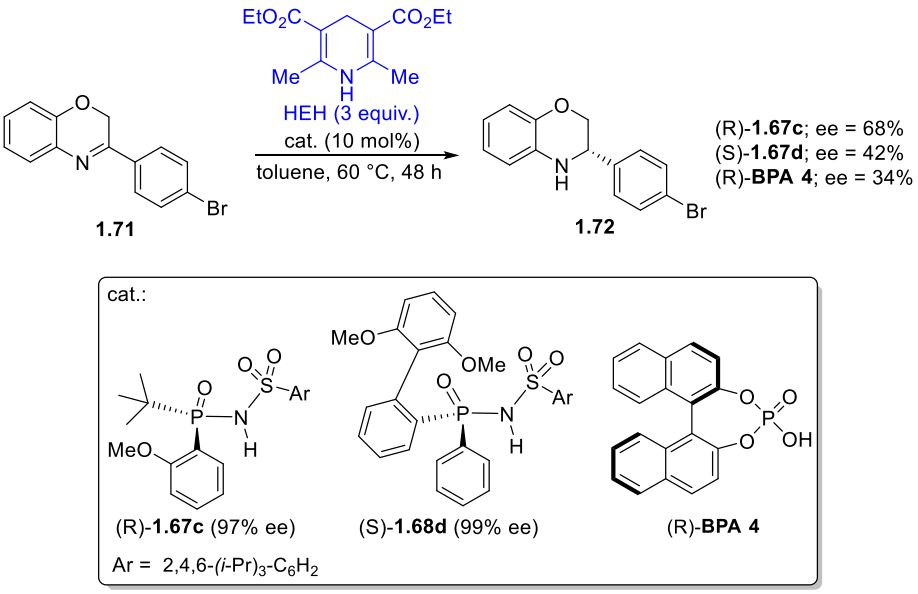

Scheme 1.22. Phosphinamide Brønsted Acid Catalysed Asymmetric Transfer Hydrogenation of Benzoxazine.

1.3 C2-Substituted Phosphinyl imidazole Ligands in Catalysis

1.3.1 Synthesis and Characteristics of C2-Substituted Phosphinyl Imidazole Ligands

Of the various classes of phosphorus-based ligands, C2-substituted phosphinyl imidazoles (subsequently referred to as phosphinyl imidazoles; Figure 1.5) have emerged as promising ligands for various transformations. Generally, the synthesis of these ligands begins with the C2-metalation of the requisite imidazole **1.73**. Quenching the resultant anion with the desired chloro-substituted phosphine gives the phosphinyl imidazole ligand, **L** (Scheme 1.23).

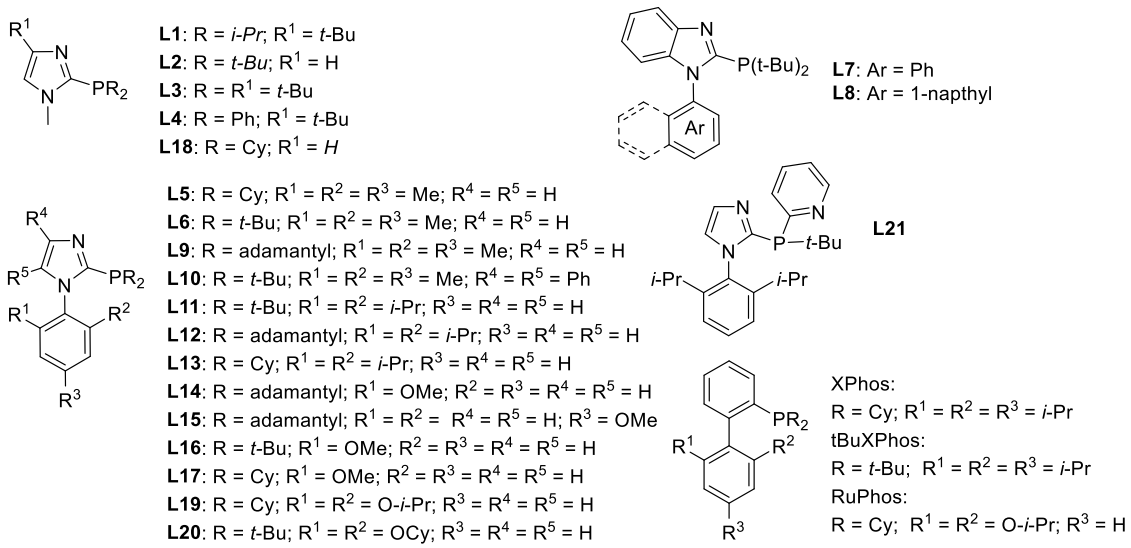

Figure 1.5. Structures of Phosphinyl Imidazoles and Buchwald Ligands Reviewed.

Scheme 1.23. General Synthetic Protocol for Phosphinyl Imidazole Ligands.

In addition to their ability to act as monodentate ligands, phosphinyl imidazoles may also display bidentate η^2 *P*,*N*-chelation of metals. In 2006, Grotjahn reported a thorough investigation on the denticity of these ligands, by evaluating the coordination properties of **L1-3** to Pd.[49] To synthesize the requisite Pd(0) species, **L1-3** were reacted with CpPd(allyl), furnishing Pd-(**L1-3**)$_2$ (Scheme 1.24). When the less phosphorus-encumbered Pd-(**L1**)$_2$ was reacted with iodobenzene, oxidative addition gave **1.74**. This two-coordinate, 16-electron species was obtained, despite the availability of the imidazole N-3 atom(s) to engage in η^2 P,N-chelation with Pd. However, when the more phosphorus-encumbered Pd-(**L2-3**)$_2$ were reacted with bromo- and iodobenzene, η^2 P,N-chelation occurred, affording monomeric species **1.75a-c** (Scheme 1.24a).

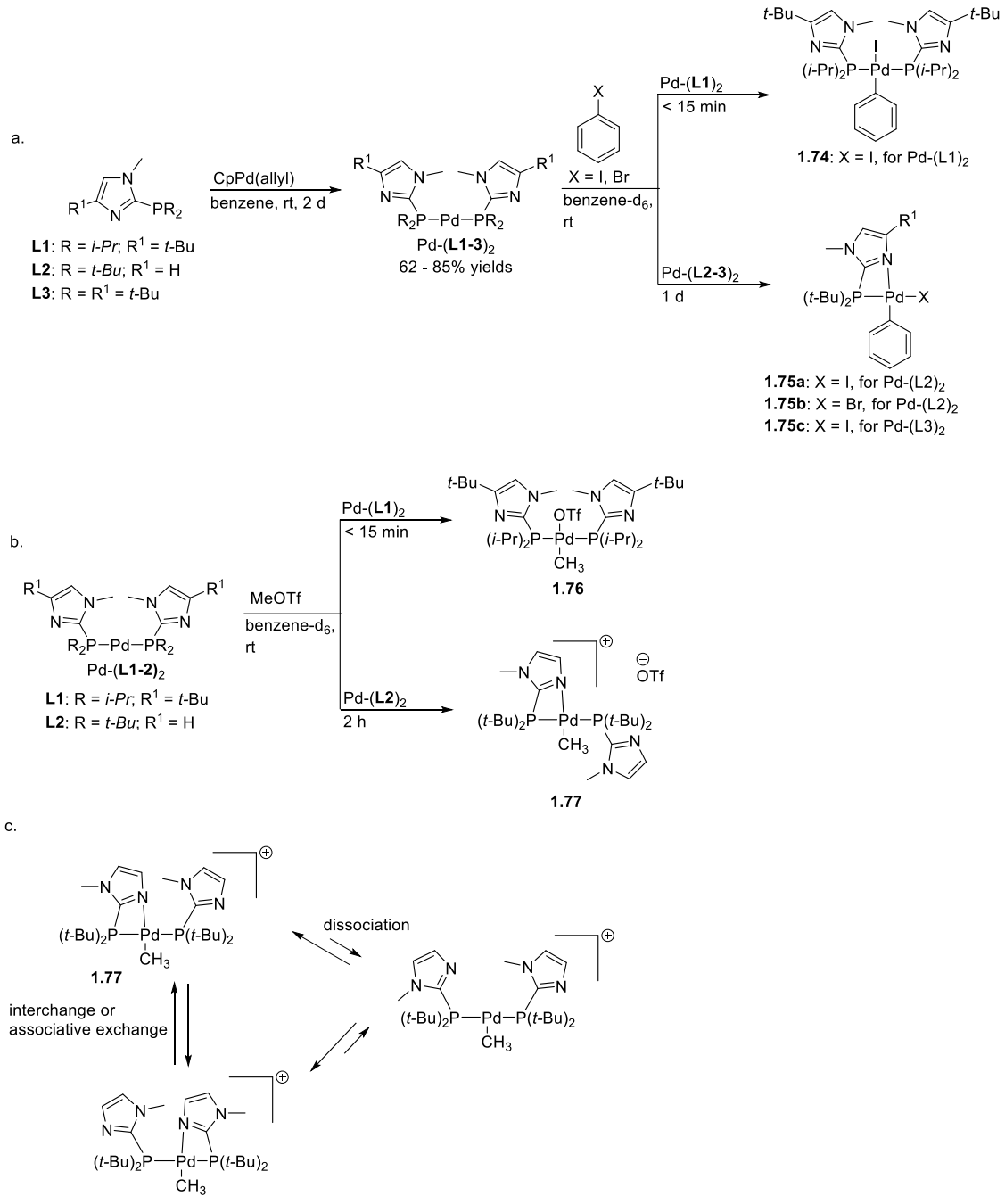

Scheme 1.24. Denticity of Phosphinyl Imidazole Ligands.

Similarly, the oxidative addition of Pd-(**L1**)$_2$ to MeOTf yielded the monodentate, two-coordinate species **1.76** (Scheme 1.24b). However, in the analogous oxidative addition of Pd-(**L2**)$_2$ to give **1.77**, a bidentate η^2 *P*,*N*-chelation to Pd was observed for one imidazole ligand. Moreover, the second imidazole ligand displayed only monodentate *P*-chelation. After variable temperature NMR analysis, fluxionality

of **1.77** was proposed to exist in solution (Scheme 1.24c). In addition to changes in denticity, varying the steric encumbrance on phosphorus affected the rate of oxidative addition. For instance, while *i*-Pr substituted Pd-(**L1**)$_2$ reacted with iodobenzene in under 15 minutes, *t*-Bu substituted Pd-(**L2-3**)$_2$ reacted with the aryl iodide in 1 day.

1.3.2 Applications of C2-Substituted Phosphinyl Imidazole Ligands

Inspired by metalloenzymes, Grotjahn envisioned that the cooperative effect of a metal and phosphinyl imidazole ligands could provide a binding pocket for polar molecules. The synthesis of this proposed complex was accomplished by the reaction of **L4** (Figure 1.5), H_2O and CpRu(MeCN)$_3$OTf, furnishing CpRu-**L4** in 98% yield (Scheme 1.25a).[50] As expected, the metal ion and the strategically placed imidazole groups of **L4** were able to participate in hydrogen-bonding with water. This interaction was deemed to be crucial in stabilizing the catalyst and promoting its reactivity. In 2001, Grotjahn reported a highly selective anti-Markovnikov hydration of terminal alkynes **1.78** to aldehydes **1.79**, using CpRu-**L4** (Scheme 1.25b). Furthermore, typically labile functionalities such as acid-sensitive alcohol-protecting groups were tolerated. In addition to this success of CpRu-**L4**, other Ru-phosphinyl imidazoyl complexes have been utilized in reactions such as olefin isomerisation.[51,52]

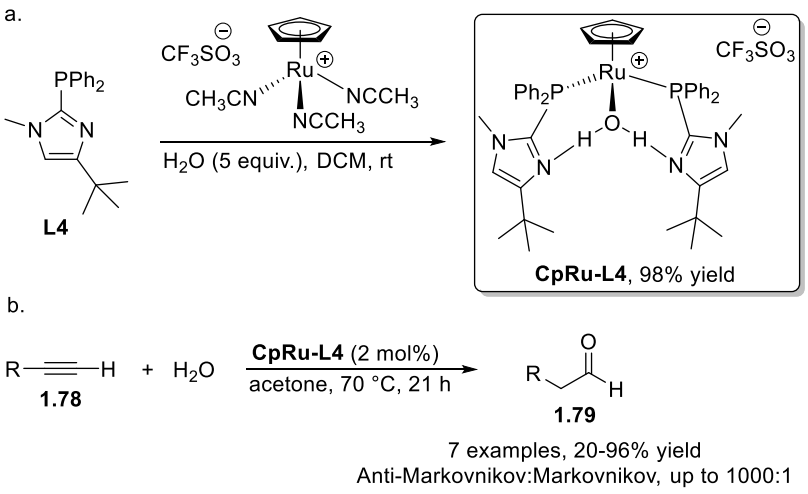

Scheme 1.25. Anti-Markovnikov Hydration of Terminal Alkynes.

Shortly after the introduction of **L1-4**, Beller reported the applications of **L5-8** in the Pd-catalysed coupling of aryl chlorides via Buchwald-Hartwig amination and Suzuki cross coupling reactions.[53] In order to investigate the properties of **L5-8** in the amination reactions, chlorobenzene **1.80** and aniline **1.81** were evaluated as test substrates. While **L5** afforded product **1.82** in 87% yield, **L7** gave the product in 92% yield. However, **L6** and **L8** furnished **1.82** in the best yield of 99%. The relatively lower yield achieved with **L5** was attributed to the decreased steric encumbrance of the cyclohexyl moieties (Scheme 1.26). In the case of the Suzuki cross-coupling reaction, aryl chloride **1.83** and boronic acid **1.84** were evaluated as test substrates. Under optimised conditions, **L6** and **L8** gave biphenyl **1.85** in yield ranges of 50-83% and 59-95% respectively. However, only **L7** gave a reproducible yield of 86% (Scheme 1.27).

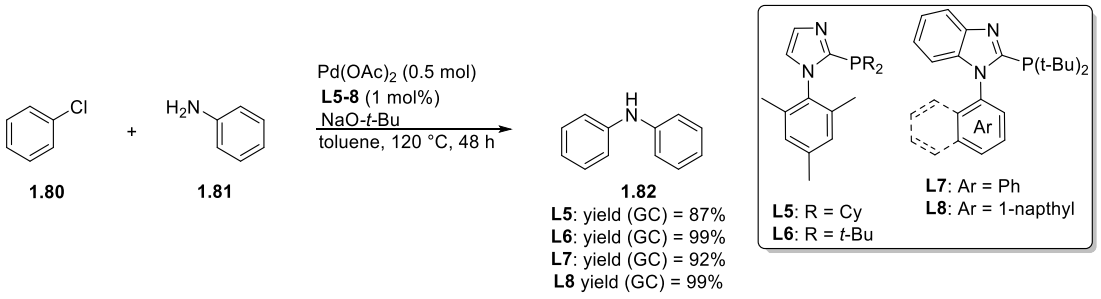

1.80 **1.81** **1.82**

L5: yield (GC) = 87%
L6: yield (GC) = 99%
L7: yield (GC) = 92%
L8 yield (GC) = 99%

Scheme 1.26. Aryl Chloride Buchwald-Hartwig Amination with Phosphinyl Imidazole Ligands.

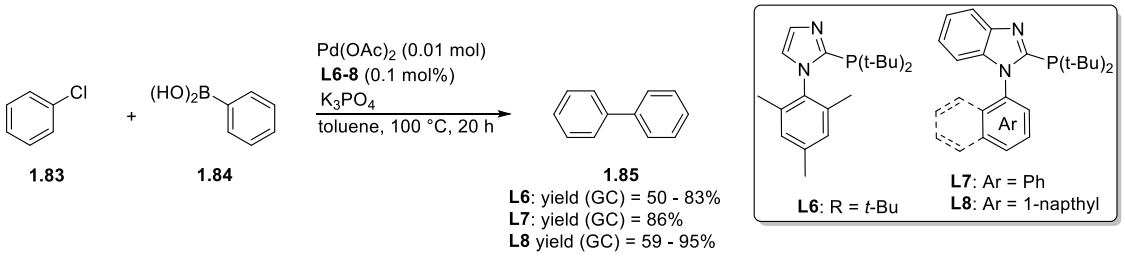

1.83 **1.84** **1.85**

L6: yield (GC) = 50 - 83%
L7: yield (GC) = 86%
L8 yield (GC) = 59 - 95%

Scheme 1.27. Aryl Chloride Suzuki Cross-Coupling with Phosphinyl Imidazole Ligands.

In 2009, Beller reported a methodology for the Sonogashira cross-coupling of aryl chlorides that did not require the addition of copper salts.[54] During the evaluation of ligands for the reaction, phosphinyl imidazoles generally outperformed other ligands including the structurally related Buchwald ligand, XPhos (Scheme 1.28). For instance, when the coupling of thiophene chloride **1.86** and octyne **1.87** was examined, XPhos gave alkyne **1.88** in only 6% yield. However, phosphinyl imidazole ligands **L5-6** and **L9-12** furnished **1.88** in yields ranging from 1-68%. Within this class of phosphinyl imidazoles, a general trend was observed: the more sterically hindered ligands gave **1.88** in higher yields potentially due to accelerated reductive elimination. However, an exception to this trend arose in the comparison of **L11** to **L12**. While **L11** gave **1.88** in the best yield of 68%, the more hindered **L12** afforded **1.88** in only 25% yield.

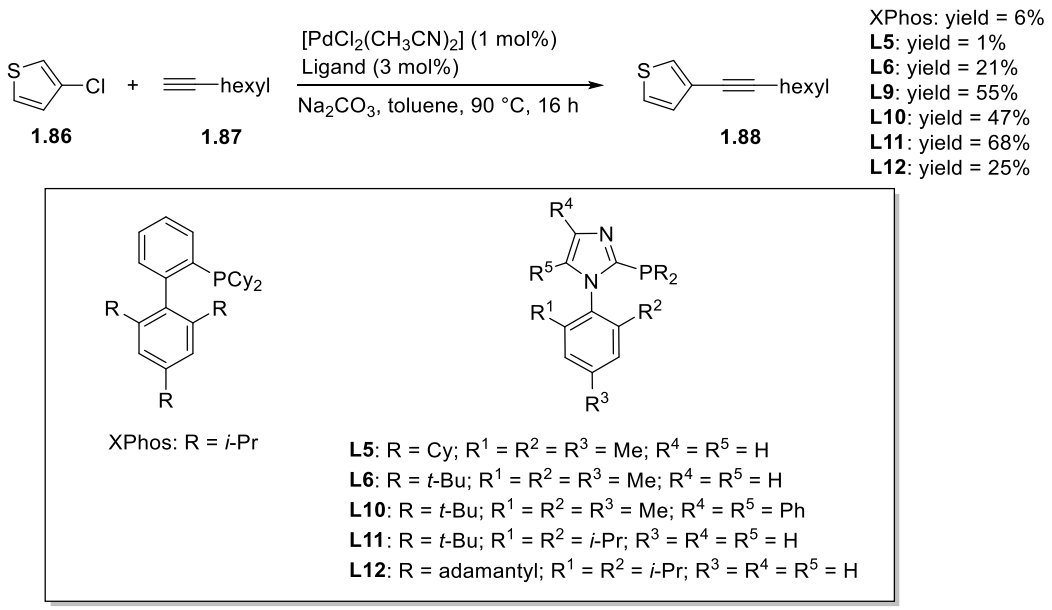

Scheme 1.28. Aryl Chloride Sonogashira Cross-Coupling with Phosphinyl Imidazole Ligands.

In the same year, Beller also reported the hydroxylation of aryl halides using phosphinyl imidazole ligands.[55] A representative scope of various chloro- and bromoarenes **1.89** were tolerant of the reaction conditions, affording phenols **1.90** in

yields of up to 99% (Scheme 1.29a). Furthermore, a high chemoselectivity of >95%, for the bromide moiety was observed with 1-bromo-2-chlorobenzene. In the optimisation phase, the hydroxylation of **1.89a** to **1.90a** was studied using various ligands. Similar to the aforementioned reactions, product yields were correlated with the steric encumbrance of the phosphinyl imidazole ligands. Thus, while **L13** failed to give phenol **1.90a**, the more hindered **L11** and **L12** furnished the phenol in 49% and 77% yields respectively. Moreover, the failure of ligands **L14-15** was attributed to the lack of substituents at both ortho positions of their phenyl rings. In comparison to **L11-12**, Buchwald ligands XPhos and tBuXPhos performed poorly, giving the phenol in 1% and 8% yields respectively (Scheme 1.29b).

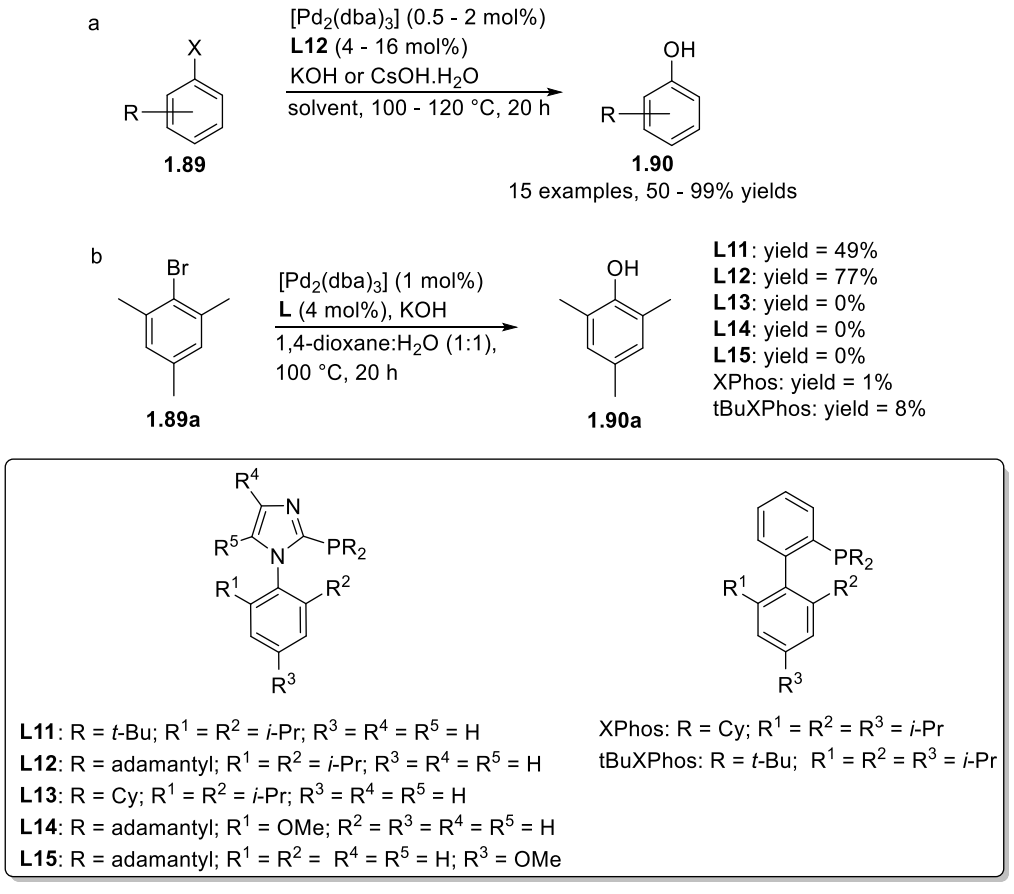

Scheme 1.29. Hydroxylation of Aryl Halides with Phosphinyl Imidazole Ligands.

The success of sterically hindered phosphinyl imidazoles is further exemplified in reactions such as the carbonylative Heck coupling of aryl halides and olefins (Scheme 1.30).[56] However, quite remarkably, this trend is not universal. In 2013, Beller and co-workers highlighted one such aberration in their report of a Ru-catalysed hydroformylation of olefins (Scheme 1.31).[57] Whereas the hindered *P*-Ad substituted **L14** and *P*-*t*-Bu substituted **L16** gave no conversion, the less hindered *P*-Cy substituted **L17** and **L18** yielded products (aldehyde and isomers) in 79% yield. Furthermore, less hindered phosphinyl imidazoles have proven advantageous over more hindered analogues, in similar reactions including the regioselective domino hydroformylation/reduction of olefins.[58]

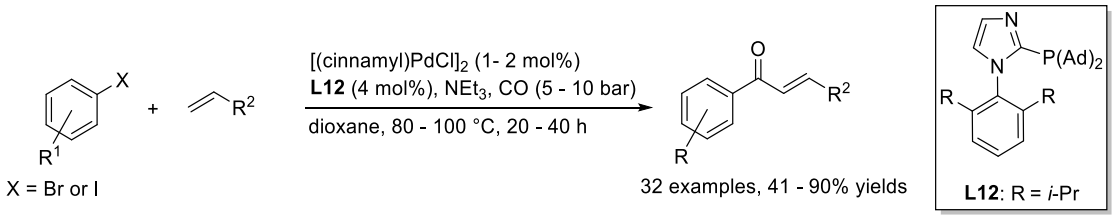

Scheme 1.30. Carbonylative Heck Cross-Coupling with Phosphinyl Imidazole Ligands.

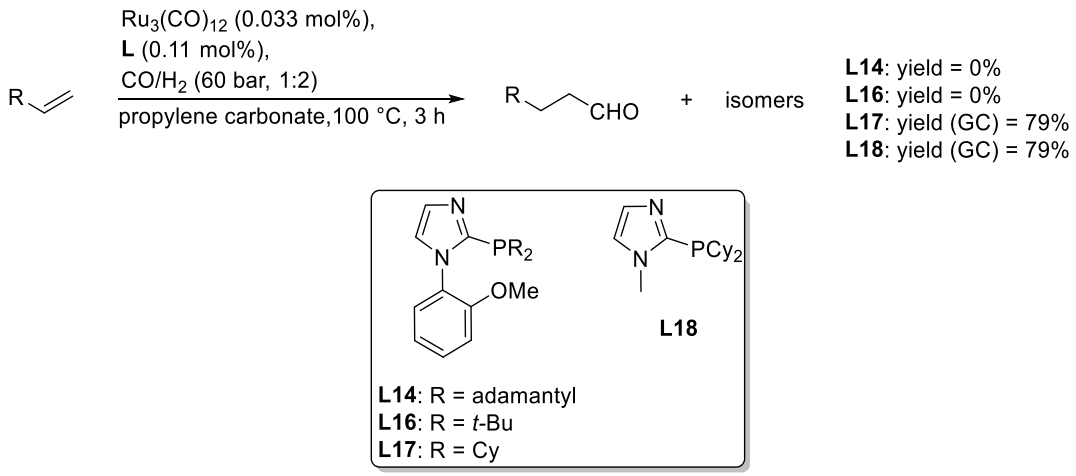

Scheme 1.31. Hydroformylation of Olefins with Phosphinyl Imidazole Ligands.

It is of noteworthy mention that for some reactions, phosphinyl imidazoles do not out-perform analogous Buchwald-type ligands. For instance, in the Barbier-Negishi cross-coupling of triflate **1.91** with bromide **1.92**, Baudoin reported that product **1.93** was obtained in <5% yield with **L19**. In comparison, the analogous Buchwald-type ligand, RuPhos, gave **1.93** in 88% yield.[59] However, while the more sterically encumbered **L20** gave **1.93** in a lower yield of 83% yield, it was selected as the preferred ligand because it induced better selectivity for **1.93** (Scheme 1.32).

In addition to phosphinyl imidazoles bearing the same *P*-substituents, *P*-unsymmetrical analogues have also proven to be important ligands for metal-mediated catalysis. In 2019, Beller reported the first Pd-catalysed reductive methylation of nitroarenes with **L21** as the ligand (Scheme 1.33a).[60] In a proposed mechanism, it was suggested that the pyridyl nitrogen of **L21** engages in hydrogen-bonding with methanol (Scheme 1.33b). This interaction facilitates the Pd-catalysed decomposition of methanol to hydrogen and formaldehyde via a β-H elimination/reductive elimination cascade. The subsequent reaction of aniline with the aldehyde to generate the imine, followed by hydrogenation, furnishes the methylaniline.

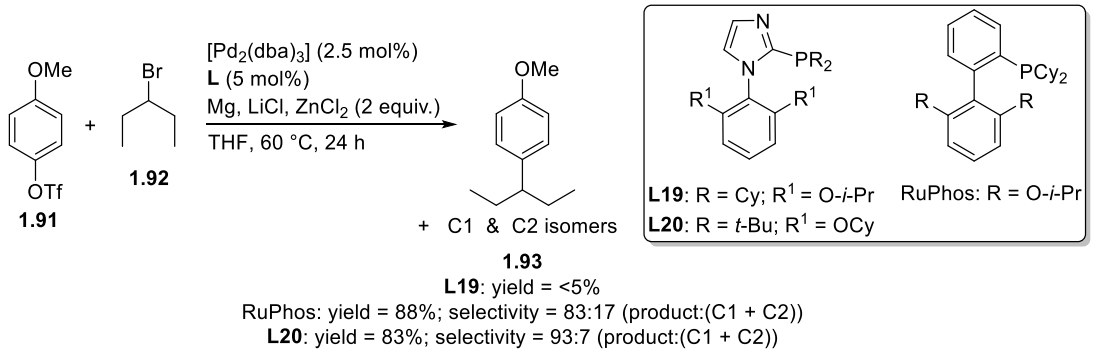

Scheme 1.32. Barbier-Negishi Cross-Coupling with Phosphinyl Imidazole Ligands.

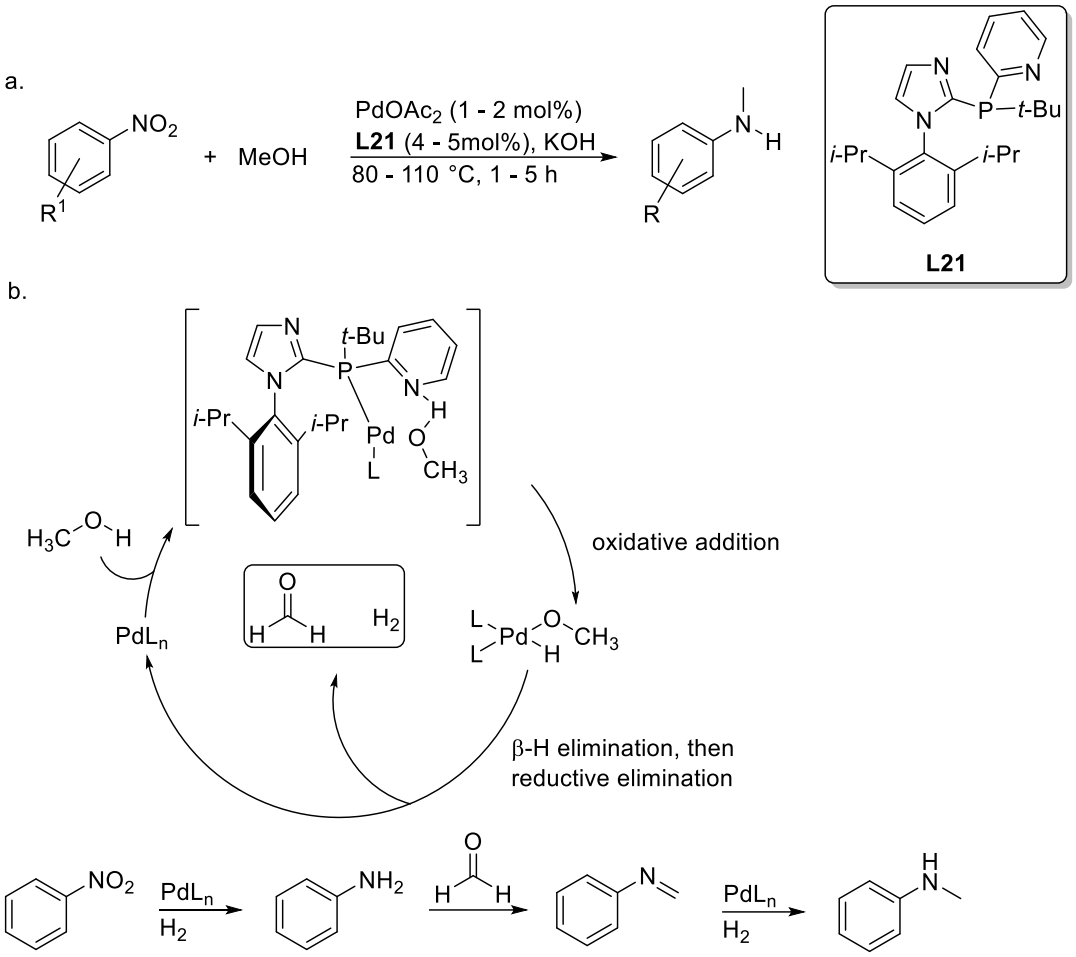

Scheme 1.33. Methylation of Nitroarenes.

1.4 Synthesis of Chiral Tetrahydroquinolines via Asymmetric HydrogenationTransfer Hydrogenation

Chiral tetrahydroquinolines are privileged motifs found in numerous biologically active compounds such as NK2 receptor agonist, TAK-480[61] and DNA-gyrase inhibitor, Zoliflodacin[62] (Figure 1.6). Synthetically, the asymmetric hydrogenation/transfer hydrogenation of quinolines provide a direct and atom-economical route to the acquisition of tetrahydroquinolines. In Chapters 2 and 3 of this thesis, the applications of *P*-chiral Brønsted acids in the asymmetric transfer hydrogenation of quinolines was studied. Thus, an overview of key metal-mediated and organocatalytic endeavours is presented herein.

Since Zhou's 2003 report on the asymmetric Ir-catalysed[63] hydrogenation of quinolines (Scheme 1.34a), numerous methodologies employing different metals such as Ru[64,65] (Scheme 1.34b,c) and Rh[66] (Scheme 1.34d) have been reported. While these reactions are usually high-yielding and provide the desired tetrahydroquinolines in high enantioselectivity, metal-free protocols circumvent the possibility of metal contaminants in final products. In 2006, Rueping reported the first asymmetric, metal-free, Brønsted acid-catalysed transfer hydrogenation of quinolines, with a Hantzsch ester (HEH) as a biomimetic hydride source (Scheme 1.34e).[33]

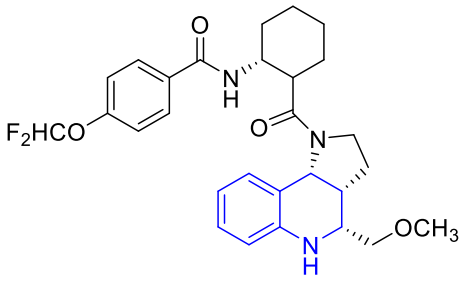

TAK-480
NK2 receptor agonist

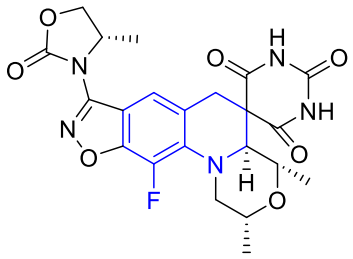

Zoliflodacin (AZD0914, ETX0914)
DNA-gyrase inhibitor

Figure 1.6. Examples of Biologically Active Tetrahydroquinolines.

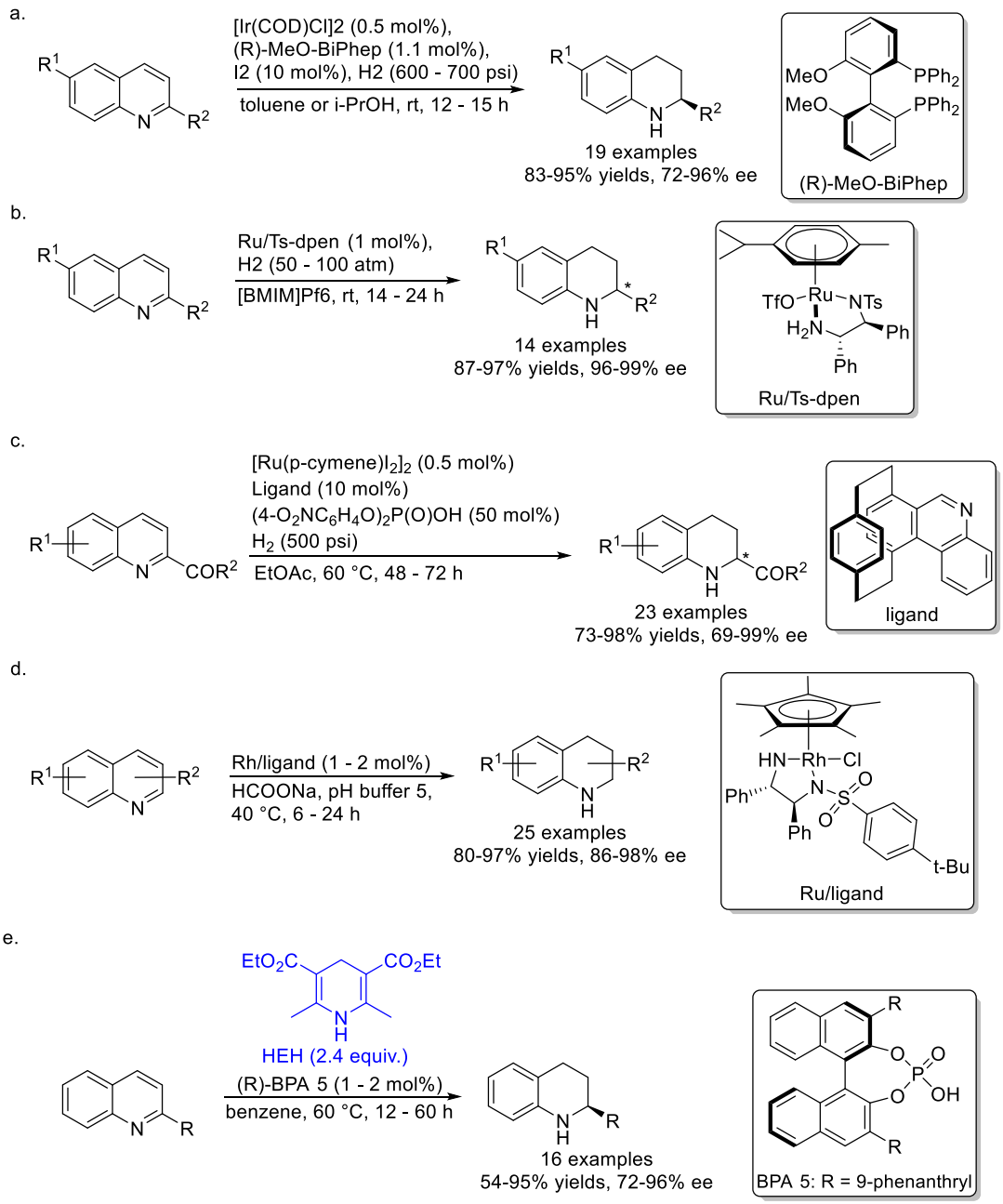

Scheme 1.34. Seminal Examples of Asymmetric Hydrogenation/Transfer Hydrogenation of Quinolines.

This methodology tolerated a range of C2-substituted quinolines, including those bearing alkyl, aromatic and heteroaromatic substituents, to furnish the desired tetrahydroquinolines in high yields and enantioselectivities. It was proposed that the first step of the mechanism is the protonation of the quinoline by the Brønsted acid to form iminium ion **A** (Scheme 1.35). Subsequently, 1,4-hydride transfer from the

Hantzsch ester generates enamine **B** and the pyridinium salt which regenerates the catalyst. The protonation of **B** to form iminium **C**, followed by an asymmetric 1,2-hydride transfer to the less hindered face gives the tetrahydroquinoline **D**.

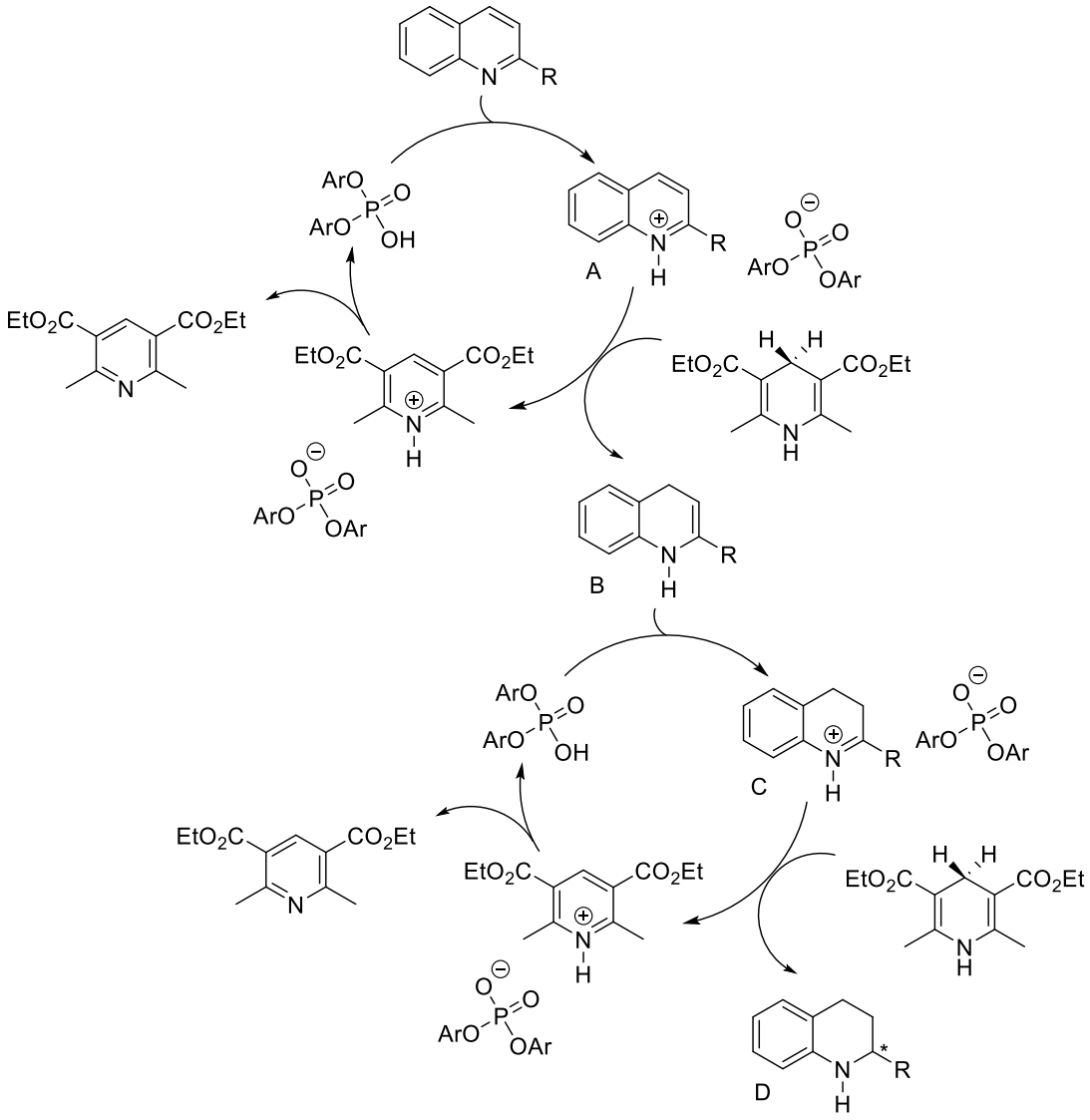

Scheme 1.35. Mechanism of Brønsted Acid-Catalyzed Transfer Hydrogenation of C2-Substituted Quinolines.

In an extension of this methodology, Rueping reported the asymmetric transfer hydrogenation of C3-substituted quinolines shortly after (Scheme 1.36).[67] In contrast to the transfer hydrogenation of C2-substituted quinolines, the origin of enantioselectivity via this methodology relied on the enantioselective protonation of the

enamine (Scheme 1.36a). In the reaction optimisation phase, interestingly, 3,3'-susbtituted 9-phenanthryl catalyst (R)-**BPA 5** gave only racemic product even though this catalyst was very successful in the transfer hydrogenation of C2-substituted quinolines (Scheme 1.34e vs. Scheme 1.36b). However, under optimised conditions, partially reduced (R)-**[H_8]-BPA 6** furnished the C3-substituted tetrahydroquinolines in 30-84% yield and 77-86% ee (Scheme 1.36c).

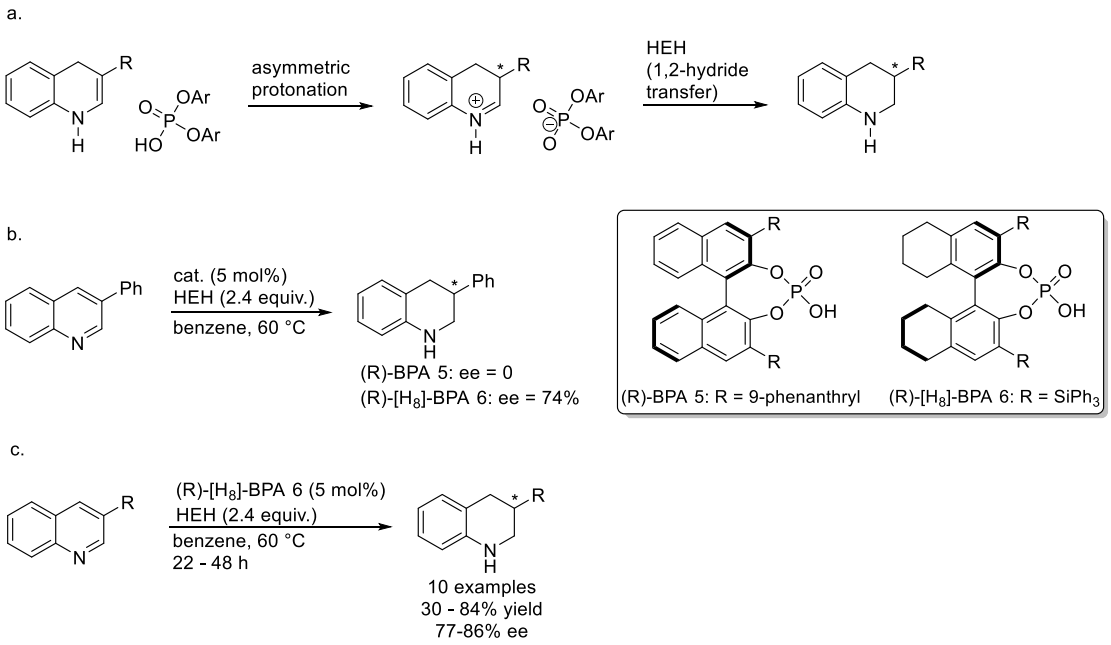

Scheme 1.36. Asymmetric Brønsted Acid-Catalyzed Transfer Hydrogenation of C3-Substituted Quinolines.

Rueping further demonstrated the utility of this organocatalytic protocol by investigating the transfer hydrogenation of C4-substituted quinolines.[68] Under optimised conditions with (R)-**[H_8]-BPA 6** as the catalyst, the corresponding tetrahydroquinolines were obtained in 67-98% yield and 72-92% ee (Scheme 1.37a). Mechanistically, the enantioselectivity of this reaction is determined during the 1,4-hydride attack of the quinoline (Scheme 1.37b).

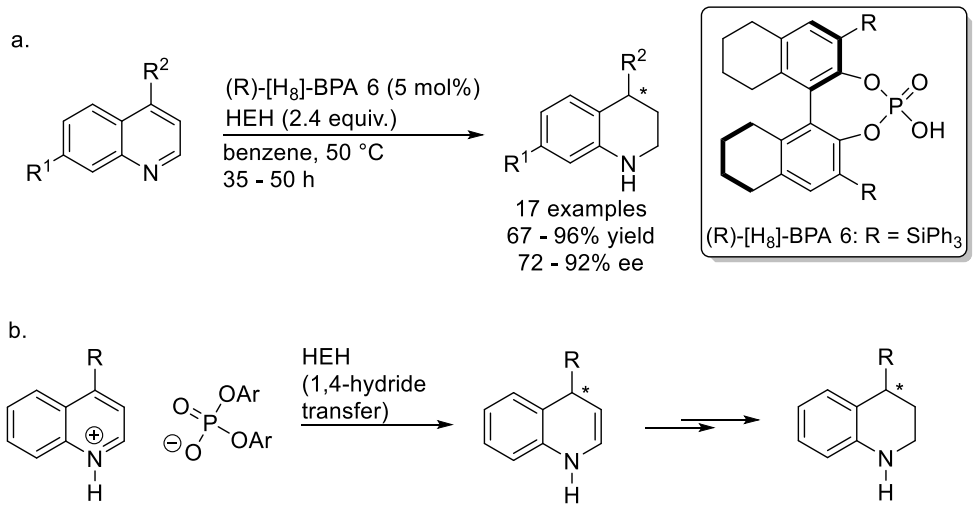

Scheme 1.37. Asymmetric Brønsted Acid-Catalyzed Transfer Hydrogenation of C4-Substituted Quinolines.

1.5 Research Goals: The Design and Applications of *P*-Chiral Brønsted Acids and Ligands

The first objective of this Ph.D. thesis was to design a class of novel *P*-chiral *N*-phosphoryl sulfonamide Brønsted acid catalysts and investigate their application in the metal-free asymmetric transfer hydrogenation of quinolines. We hypothesised that a key intramolecular hydrogen-bonding interaction could stabilize the catalyst-substrate transition state and improve reaction rates and enantioselectivity. Chapter 2 reports the design and application of this class of catalysts, as well as evidence for the role of hydrogen-bonding in promoting reaction rate and enantioselectivity. Subsequently, in Chapter 3, the applications of these catalysts to the asymmetric transfer hydrogenation of 2-carboxymethyl quinolines to yield rigidified bioisosteres of amino acids, is reported. In addition, catalyst stability is thermally probed and their rearrangement at elevated temperatures is observed. In addition to our endeavours to develop novel *P*-chiral Brønsted acid organocatalysts, we sought to explore the design and applications of novel *P*-chiral ligands for metal-mediated catalysis. In Chapter 4, the synthesis and application of a novel *P*-chiral phosphinyl imidazole ligand in an asymmetric Suzuki-Miyaura is reported. The synthesis of this ligand was enabled by a solvent-switchable,

site-selective remote C-H activation, which allowed for the acquisition of its phosphonyl imidazole precursor.

1.6 References

1. van Leeuwen, P. W. N. M.; Cano, I.; Freixa, Z. Secondary Phosphine Oxides: Bifunctional Ligands in Catalysis. *Chemcatchem* **2020,** *12*, 3982-3994.
2. Jiang, X. B.; Minnaard, A. J.; Hessen, B.; Feringa, B. L.; Duchateau, A. L.; Andrien, J. G.; Boogers, J. A.; de Vries, J. G. Application of Monodentate Secondary Phosphine Oxides, a New Class of Chiral Ligands, in Ir(i)-Catalyzed Asymmetric Imine Hydrogenation. *Org. Lett.* **2003**, *5*, 1503-1506.
3. Bigeault, J.; Giordano, L.; de Riggi, I.; Gimbert, Y.; Buono, G., Platinum(II)-Coordinated Phosphinous Acid-Catalyzed Alkylidenecyclopropanation of Bicyclic Alkenes with Terminal Alkynes. *Org. Lett.* **2007**, *9*, 3567-3570.
4. Emmick, T. L.; Letsinge.R. L. Unsymmetrical Secondary Phosphine Oxides . Synthetic Isotopic Exchange and Stereochemical Studies. *J. Am. Chem. Soc.* **1968**, *90*, 3459-3465.
5. Farnham, W. B.; Lewis, R. A.; Murray, R. K.; Mislow, K. Lithium Aluminum Hydride Induced Stereomutation of Secondary Phosphine Oxides. *J. Am. Chem. Soc.* **1970**, *92*, 5808-5809.
6. Farnham, W. B.; Murray, R. K.; Mislow, K. Stereospecific Alkylation of Menthyl Phenylphosphinate. *J. Am. Chem. Soc.* **1970**, *92*, 5809-5810.
7. Leyris, A.; Bigeault, J.; Nuel, D.; Giordano, L.; Buono, G. Enantioselective Synthesis of Secondary Phosphine Oxides from (R-P)-(-)-Menthylhydrogenophenylphosphinate. *Tetrahedron Lett.* **2007**, *48*, 5247-5250.
8. Xu, Q.; Zhao, C. Q.; Han, L. B. Stereospecific Nucleophilic Substitution of Optically Pure H-Phosphinates: a General Way for the Preparation of Chiral *P*-Stereogenic Phosphine Oxides. *J. Am. Chem. Soc.* **2008**, *130*, 12648-12655.

9. Kolodiazhnyi, O. I.; Gryshkun, E. V.; Andrushko, N. V.; Freytag, M.; Jones, P. G.; Schmutzler, R. Asymmetric Synthesis of Chiral N-(1-Methylbenzyl)aminophosphines. *Tetrahedron: Asymmetry* **2003**, *14*, 181-183.

10. Leyris, A.; Nuel, D.; Giordano, L.; Achard, M.; Buono, G. Enantioselective Synthesis of Both Enantiomers of tert-Butylphenylphosphine Oxide from (S)-Prolinol. *Tetrahedron Lett.* **2005**, *46*, 8677-8680.

11. Han, Z. S.; Wu, H.; Xu, Y.; Zhang, Y.; Qu, B.; Li, Z.; Caldwell, D. R.; Fandrick, K. R.; Zhang, L.; Roschangar, F.; Song, J. J.; Senanayake, C. H. General and Stereoselective Method for the Synthesis of Sterically Congested and Structurally Diverse P-Stereogenic Secondary Phosphine Oxides. *Org. Lett.* **2017**, *19*, 1796-1799.

12. Li, S. G.; Yuan, M. L.; Topic, F.; Han, Z. X. S.; Senanayake, C. H.; Tsantrizos, Y. S. Asymmetric Library Synthesis of P-Chiral t-Butyl-Substituted Secondary and Tertiary Phosphine Oxides. *J. Org. Chem.* **2019**, *84*, 7291-7302.

13. Drabowicz, J.; Lyzwa, P.; Omelanczuk, J.; Pietrusiewicz, K. M.; Mikolajczyk, M. New Procedures for the Resolution of Chiral tert-Butylphenylphosphine Oxide and Some of its Reactions. *Tetrahedron: Asymmetry* **1999**, *10*, 2757-2763.

14. Holt, J.; Maj, A. M.; Schudde, E. P.; Pietrusiewicz, K. M.; Sieron, L.; Wieczorek, W.; Jerphagnon, T.; Arends, I. W. C. E.; Hanefeld, U.; Minnaard, A. J. On the Resolution of Secondary Phosphine Oxides via Diastereomeric Complex Formation: The Case of tert-Butylphenylphosphine Oxide. *Synthesis* **2009**, 2061-2065.

15. Kortmann, F. A.; Chang, M. C.; Otten, E.; Couzijn, E. P. A.; Lutz, M.; Minnaard, A. J. Consecutive Dynamic Resolutions of Phosphine Oxides. *Chem. Sci.* **2014**, *5*, 1322-1327.

16. Qiu, H.; Dai, Q.; He, J.; Li, W.; Zhang, J. Access to *P*-chiral sec- and tert-Phosphine Oxides Enabled by Le-Phos-Catalyzed Asymmetric Kinetic Resolution. *Chem. Sci.* **2020**, *11*, 9983-9988.

17. Akiyama, T.; Itoh, J.; Yokota, K.; Fuchibe, K. Enantioselective Mannich-Type Reaction Catalyzed By a Chiral Bronsted Acid. *Angew. Chem. Int. Ed.* **2004**, *43*, 1566-1568.

18. Uraguchi, D.; Terada, M. Chiral Bronsted Acid-Catalyzed Direct Mannich Reactions via Electrophilic Activation. *J. Am. Chem. Soc.* **2004**, *126*, 5356-5357.

19. Parmar, D.; Sugiono, E.; Raja, S.; Rueping, M. Complete Field Guide to Asymmetric BINOL-Phosphate Derived Bronsted Acid and Metal Catalysis: History and Classification by Mode of Activation; Bronsted Acidity, Hydrogen bonding, Ion Pairing, and Metal Phosphates. *Chem. Rev.* **2014**, *114*, 9047-9153.

20. Tsuji, N.; Kennemur, J. L.; Buyck, T.; Lee, S.; Prevost, S.; Kaib, P. S. J.; Bykov, D.; Fares, C.; List, B. Activation of Olefins via Asymmetric Bronsted Acid Catalysis. *Science* **2018**, *359*, 1501-1505.

21. Akiyama, T.; Mori, K., Stronger Bronsted Acids: Recent Progress. *Chem. Rev.* **2015**, *115*, 9277-9306.

22. Fleischmann, M.; Drettwan, D.; Sugiono, E.; Rueping, M.; Gschwind, R. M. Bronsted Acid Catalysis: Hydrogen Bonding versus Ion Pairing in Imine Activation. *Angew. Chem. Int. Ed.* **2011**, *50*, 6364-6369.

23. Kaupmees, K.; Tolstoluzhsky, N.; Raja, S.; Rueping, M.; Leito, I. On the Acidity and Reactivity of Highly Effective Chiral Bronsted Acid Catalysts: Establishment of an Acidity Scale. *Angew. Chem. Int. Ed.* **2013**, *52*, 11569-11572.

24. Christ, P.; Lindsay, A. G.; Vormittag, S. S.; Neudorfl, J. M.; Berkessel, A.; O'Donoghue, A. C. pKa Values of Chiral Bronsted Acid Catalysts: Phosphoric Acids/Amides, Sulfonyl/sulfuryl Imides, and Perfluorinated TADDOLs (TEFDDOLs). *Chem. Eur. J.* **2011**, *17*, 8524-8528.

25. Schreyer, L.; Properzi, R.; List, B. IDPi Catalysis. *Angew. Chem. Int. Ed.* **2019**, *58*, 12761-12777.

26. Nakashima, D.; Yamamoto, H. Design of Chiral N-Triflyl Phosphoramide as a Strong Chiral Bronsted Acid and its Application to Asymmetric Diels-Alder Reaction. *J. Am. Chem. Soc.* **2006**, *128*, 9626-9627.

27. Simon, L.; Goodman, J. M. A Model for the Enantioselectivity of Imine Reactions Catalyzed by BINOL-Phosphoric Acid Catalysts. *J. Org. Chem.* **2011**, *76*, 1775-1788.

28. Guo, Q. X.; Liu, H.; Guo, C.; Luo, S. W.; Gu, Y.; Gong, L. Z. Chiral Bronsted Acid-Catalyzed Direct Asymmetric Mannich Reaction. *J. Am. Chem. Soc.* **2007**, *129*, 3790-3791.

29. Zhang, L. D.; Zhong, L. R.; Xi, J.; Yang, X. L.; Yao, Z. J. Enantioselective Total Synthesis of Lycoposerramine-Z Using Chiral Phosphoric Acid Catalyzed Intramolecular Michael Addition. *J. Org. Chem.* **2016**, *81*, 1899-1904.

30. Coric, I.; Vellalath, S.; List, B. Catalytic Asymmetric Transacetalization. *J. Am. Chem. Soc.* **2010,** *132*, 8536-8537.

31. Akiyama, T.; Morita, H.; Itoh, J.; Fuchibe, K. Chiral Bronsted Acid Catalyzed Enantioselective Hydrophosphonylation of Imines: Asymmetric Synthesis of Alpha-Amino Phosphonates. *Org. Lett.* **2005**, *7*, 2583-2585.

32. Hoffmann, S.; Seayad, A. M.; List, B. A Powerful Bronsted Acid Catalyst for the Organocatalytic Asymmetric Transfer Hydrogenation of Imines. *Angew. Chem. Int. Ed.* **2005**, *44*, 7424-7427.

33. Rueping, M.; Antonchick, A. P.; Theissmann, T. A Highly Enantioselective Bronsted Acid Catalyzed Cascade Reaction: Organocatalytic Transfer Hydrogenation of Quinolines and their Application in the Synthesis of Alkaloids. *Angew. Chem. Int. Ed.* **2006**, 45, 3683-3686.

34. Kang, Q.; Zhao, Z. A.; You, S. L. Highly Enantioselective Friedel-Crafts Reaction of Indoles with Imines by a Chiral Phosphoric Acid. *J. Am. Chem. Soc.* **2007**, *129*, 1484-1485.

35. Rueping, M.; Sugiono, E.; Azap, C. A Highly Enantioselective Bronsted Acid Catalyst for the Strecker Reaction. *Angew. Chem. Int. Ed.* **2006**, *45*, 2617-2619.

36. Chen, X. H.; Xu, X. Y.; Liu, H.; Cun, L. F.; Gong, L. Z. Highly Enantioselective Organocatalytic Biginelli Reaction. *J. Am. Chem. Soc.* **2006**, *128*, 14802-14803.

37. Rueping, M.; Ieawsuwan, W.; Antonchick, A. P.; Nachtsheim, B. J. Chiral Bronsted Acids in the Catalytic Asymmetric Nazarov Cyclization--the First

Enantioselective Organocatalytic Electrocyclic Reaction. *Angew. Chem. Int. Ed.* **2007**, *46*, 2097-2100.

38. Cheon, C. H.; Yamamoto, H. A Bronsted Acid Catalyst for the Enantioselective Protonation Reaction. *J. Am. Chem. Soc.* **2008**, *130*, 9246-9247.

39. Jiao, P.; Nakashima, D.; Yamamoto, H. Enantioselective 1,3-Dipolar Cycloaddition of Nitrones with Ethyl Vinyl Ether: the Difference between Bronsted and Lewis Acid Catalysis. *Angew. Chem. Int. Ed.* **2008**, *47*, 2411-2413.

40. Cheon, C. H.; Yamamoto, H. *N*-Triflylthiophosphoramide Catalyzed Enantioselective Mukaiyama Aldol Reaction of Aldehydes with Silyl Enol Ethers of Ketones. *Org. Lett.* **2010**, *12*, 2476-2479.

41. Wakchaure, V. N.; List, B. A New Structural Motif for Bifunctional Bronsted Acid/Base Organocatalysis. *Angew. Chem. Int. Ed.* **2010**, *49*, 4136-4139.

42. Vellalath, S.; Coric, I.; List, B. *N*-Phosphinyl Phosphoramide--a Chiral Bronsted Acid Motif for the Direct Asymmetric *N*,*O*-Acetalization of Aldehydes. *Angew. Chem. Int. Ed.* **2010**, *49*, 9749-9752.

43. Coric, I.; List, B. Asymmetric Spiroacetalization Catalysed by Confined Bronsted Acids. *Nature* **2012**, *483*, 315-319.

44. Kim, J. H.; Coric, I.; Vellalath, S.; List, B. The Catalytic Asymmetric Acetalization. *Angew. Chem. Int. Ed.* **2013**, *52*, 4474-4477.

45. Tsui, G. C.; Liu, L.; List, B. The Organocatalytic Asymmetric Prins Cyclization. *Angew. Chem. Int. Ed.* **2015**, *54*, 7703-7706.

46. Das, S.; Liu, L.; Zheng, Y.; Alachraf, M. W.; Thiel, W.; De, C. K.; List, B. Nitrated Confined Imidodiphosphates Enable a Catalytic Asymmetric Oxa-Pictet-Spengler Reaction. *J. Am. Chem. Soc.* **2016**, *138*, 9429-9432.

47. Xie, Y.; Cheng, G. J.; Lee, S.; Kaib, P. S.; Thiel, W.; List, B, Catalytic Asymmetric Vinylogous Prins Cyclization: A Highly Diastereo- and Enantioselective Entry to Tetrahydrofurans. *J. Am. Chem. Soc.* **2016**, *138*, 14538-14541.

48. Han, Z. X. S.; Wu, H.; Qu, B.; Wang, Y. W.; Wu, L.; Zhang, L.; Xu, Y. B.; Wu, L. L.; Zhang, Y. D.; Lee, H.; Roschangar, F.; Song, J. J.; Senanayake, C. H.

New Class of *P*-stereogenic Chiral Bronsted Acid Catalysts Derived from Chiral Phosphinamides. *Tetrahedron Lett.* **2019**, *60*, 1834-1837.

49. Grotjahn, D. B.; Gong, Y.; Zakharov, L.; Golen, J. A.; Rheingold, A. L. Changes in Coordination of Sterically Demanding Hybrid Imidazolylphosphine Ligands on Pd(0) and Pd(II). *J. Am. Chem. Soc.* **2006**, *128*, 438-453.

50. Grotjahn, D. B.; Incarvito, C. D.; Rheingold, A. L. Combined Effects of Metal and Ligand Capable of Accepting a Proton or Hydrogen Bond Catalyze Anti-Markovnikov Hydration of Terminal Alkynes. *Angew. Chem. Int. Ed.* **2001**, *40*, 3884-3887.

51. Grotjahn, D. B.; Larsen, C. R.; Gustafson, J. L.; Nair, R.; Sharma, A. Extensive Isomerization of Alkenes using a Bifunctional Catalyst: an Alkene Zipper. *J. Am. Chem. Soc.* **2007**, *129*, 9592-9593.

52. Larsen, C. R.; Grotjahn, D. B. Stereoselective Alkene Isomerization over One Position. *J. Am. Chem. Soc.* **2012**, *134*, 10357-10360.

53. Harkal, S.; Rataboul, F.; Zapf, A.; Fuhrmann, C.; Riermeier, T.; Monsees, A.; Beller, M. Dialkylphosphinoimidazoles as New Ligands for Palladium-Catalyzed Coupling Reactions of Aryl Chlorides. *Adv. Synth. Catal/* **2004,** *346*, 1742-1748.

54. Torborg, C.; Huang, J.; Schulz, T.; Schaffner, B.; Zapf, A.; Spannenberg, A.; Borner, A.; Beller, M. Improved Palladium-Catalyzed Sonogashira Coupling Reactions of Aryl Chlorides. *Chem. Eur. J.* **2009**, *15*, 1329-1336.

55. Schulz, T.; Torborg, C.; Schaffner, B.; Huang, J.; Zapf, A.; Kadyrov, R.; Borner, A.; Beller, M. Practical Imidazole-Based Phosphine Ligands for Selective Palladium-Catalyzed Hydroxylation of Aryl Halides. *Angew. Chem. Int. Ed.***2009**, *48*, 918-921.

56. Wu, X. F.; Neumann, H.; Spannenberg, A.; Schulz, T.; Jiao, H.; Beller, M. Development of a General Palladium-Catalyzed Carbonylative Heck Reaction of Aryl Halides. *J. Am. Chem. Soc.* **2010**, *132*, 14596-14602.

57. Fleischer, I.; Wu, L.; Profir, I.; Jackstell, R.; Franke, R.; Beller, M. Towards the Development of a Selective Ruthenium-Catalyzed Hydroformylation of Olefins. *Chem. Eur. J.* **2013,** *19*, 10589-10594.

58. Fleischer, I.; Dyballa, K. M.; Jennerjahn, R.; Jackstell, R.; Franke, R.; Spannenberg, A.; Beller, M. From Olefins to Alcohols: Efficient and Regioselective Ruthenium-Catalyzed Domino Hydroformylation/Reduction Sequence. *Angew. Chem. Int. Ed.* **2013**, *52*, 2949-2953.

59. Zhang, K. F.; Christoffel, F.; Baudoin, O. Barbier-Negishi Coupling of Secondary Alkyl Bromides with Aryl and Alkenyl Triflates and Nonaflates. *Angew. Chem. Int. Ed.* **2018**, *57*, 1982-1986.

60. Wang, L.; Neumann, H.; Beller, M. Palladium-Catalyzed Methylation of Nitroarenes with Methanol. *Angew. Chem. Int. Ed.* **2019**, *58*, 5417-5421.

61. Tanaka, T.; Tanaka, A.; Nakamura, A.; Matsushita, K.; Imanishi, A.; Matsumoto-Okano, S.; Inatomi, N.; Miura, K.; Toyoda, M.; Mizojiri, G.; Tsukimi, Y. Effects of TAK-480, a Novel Tachykinin NK(2)-Receptor Antagonist, on Visceral Hypersensitivity in Rabbits and Ricinoleic Acid-Induced Defecation in Guinea Pigs. *J. Pharmacol. Sci.* **2012**, *120*, 15-25.

62. Jacobsson, S.; Golparian, D.; Oxelbark, J.; Franceschi, F.; Brown, D.; Louie, A.; Drusano, G.; Unemo, M. Pharmacodynamic Evaluation of Zoliflodacin Treatment of Neisseria gonorrhoeae Strains With Amino Acid Substitutions in the Zoliflodacin Target GyrB Using a Dynamic Hollow Fiber Infection Model. *Front. Pharmacol.* **2022**, *13*, 874176.

63. Wang, W. B.; Lu, S. M.; Yang, P. Y.; Han, X. W.; Zhou, Y. G. Highly Enantioselective Iridium-Catalyzed Hydrogenation of Heteroaromatic Compounds, Quinolines. *J. Am. Chem. Soc.* **2003,** *125*, 10536-10537.

64. Zhou, H.; Li, Z.; Wang, Z.; Wang, T.; Xu, L.; He, Y.; Fan, Q. H.; Pan, J.; Gu, L.; Chan, A. S. Hydrogenation of Quinolines using a Recyclable Phosphine-Free Chiral Cationic Ruthenium Catalyst: Enhancement of Catalyst Stability and Selectivity in an Ionic Liquid. *Angew. Chem. Int. Ed.* **2008**, *47*, 8464-8467.

65. Zhao, Z. B.; Wang, J.; Zhu, Z. H.; Chen, M. W.; Zhou, Y. G. Enantioselective Synthesis of 2-Functionalized Tetrahydroquinolines through Biomimetic Reduction. *Org. Lett.* **2021**, *23*, 9112-9117.

66. Wang, C.; Li, C.; Wu, X.; Pettman, A.; Xiao, J. pH-Regulated Asymmetric Transfer Hydrogenation of Quinolines in Water. *Angew. Chem. Int. Ed.* **2009**, *48*, 6524-6528.

67. Rueping, M.; Theissmann, T.; Raja, S.; Bats, J. W. Asymmetric Counterion Pair Catalysis: An Enantioselective Bronsted Acid-Catalyzed Protonation. *Adv. Synth. Catal.* **2008**, *350*, 1001-1006.

68. Rueping, M.; Theissmann, T.; Stoeckel, M.; Antonchick, A. P. Direct Enantioselective Access to 4-Substituted Tetrahydroquinolines by Catalytic Asymmetric Transfer Hydrogenation of Quinolines. *Org. Biomol. Chem.* **2011**, *9*, 6844-6850.

<u>Chapter 2:</u> P-Chiral, N-Phosphoryl Sulfonamide Brønsted Acids with an Intramolecular Hydrogen Bond Interaction that Modulates Organocatalysis

2.1 Preface

Asymmetric Brønsted acid organocatalysis presents an attractive route for the synthesis of chiral molecules: the metal-free nature of such methodologies may allow for milder reaction protocols, while circumventing the use of potentially toxic transition-metals. While BINOL-based phosphoric acid organocatalysts are prevalent in the literature, *P*-chiral analogues are rare, highlighting the underexplored potential for electronic and steric modifications on phosphorus, in the design of organocatalysts. Thus, the synergistic combination of phosphorus-based tunability, and the robust nature of organocatalysis could furnish *P*-chiral Brønsted acids bearing interesting and desirable catalytic properties. Herein, the design and applications of a novel class of *P*-chiral, *N*-phosphoryl sulfonamide Brønsted acid organocatalysts is reported.

The work presented in this chapter has been published as shown: Yuan, M.; Mbaezue, I. I.; Zhou, Z.; Topic, F.; Tsantrizos, Y. S. P-Chiral, N-Phosphoryl Sulfonamide Brønsted Acids with an Intramolecular Hydrogen Bond Interaction that Modulates Organocatalysis. *Org. Biomol. Chem*. **2019**, *17*, 8690 – 8694.

Dr. Zhi Zhou synthesised the first generation of *P*-chiral, *N*-phosphoryl sulfonamide Brønsted acids catalysts and evaluated their properties in the asymmetric transfer hydrogenation of quinolines. Dr. Minglei Yuan synthesised the second generation of catalysts and optimised the reaction conditions for the transfer hydrogenation. Ifenna I. Mbaezue re-synthesised catalysts, synthesised the substrates and performed the experiment required to investigate the substrate scope. Dr. Filip Topic analysed the X-ray crystallographic data. Youla S. Tsantrizos, Minglei Yuan and Ifenna I. Mbaezue co-wrote the manuscript.

2.2 Abstract

Brønsted acids exemplified by OttoPhosa I (**2.5c**) were designed and evaluated in the asymmetric transfer hydrogenation of quinolines. Their catalytic properties are modulated by an intramolecular hydrogen bond that rigidifies their catalytic cavity, accelerates the reaction rate and improves enantioselectivity.

2.3 Introduction

Phosphorus-based Brønsted acids have emerged as a highly promising class of organocatalysts. Many molecular designs have contributed to this field, including the most valuable BINOL-based Brønsted acids **2.1** and **2.2** (Fig. 2.1).[1] Brønsted acids **2.1** were first reported by Akiyama[2] and Terada,[3] and have been shown to efficiently catalyse a plethora of asymmetric reactions, including Mannich-type[2a,3,4] and Diels–Alder reactions,[5] the enantioselective hydrophosphonylation of imines,[6] reductive aminations,[7] imine transfer hydrogenations,[8] Friedel–Crafts alkylations,[9] intramolecular Michael additions,[10] the N,O-acetalization of aldehydes[11] and the transfer hydrogenation of various heterocyclic compounds.[12] These Brønsted acids were also reported to catalyse metal-free asymmetric 6π-electrocyclization reactions, leading to enantiomerically enriched 1,4-dihydropyridazines.[13] Recently, List reported the design of BINOL-based dimeric and sterically highly confined imidodiphosphorimidate analogs (IDPi; **2.2**, Fig. 2.1).[14] IDPi analogs were shown to catalyse the protonation of olefins, which then react with intramolecular hydroxyl groups to form chiral 5- and 6-membered ring ethers.[14a] Additionally, they can catalyse enantioselective C–C bond formation in Mukaiyama aldol-type reactions with a remarkably low concentration of the catalyst.[14b]

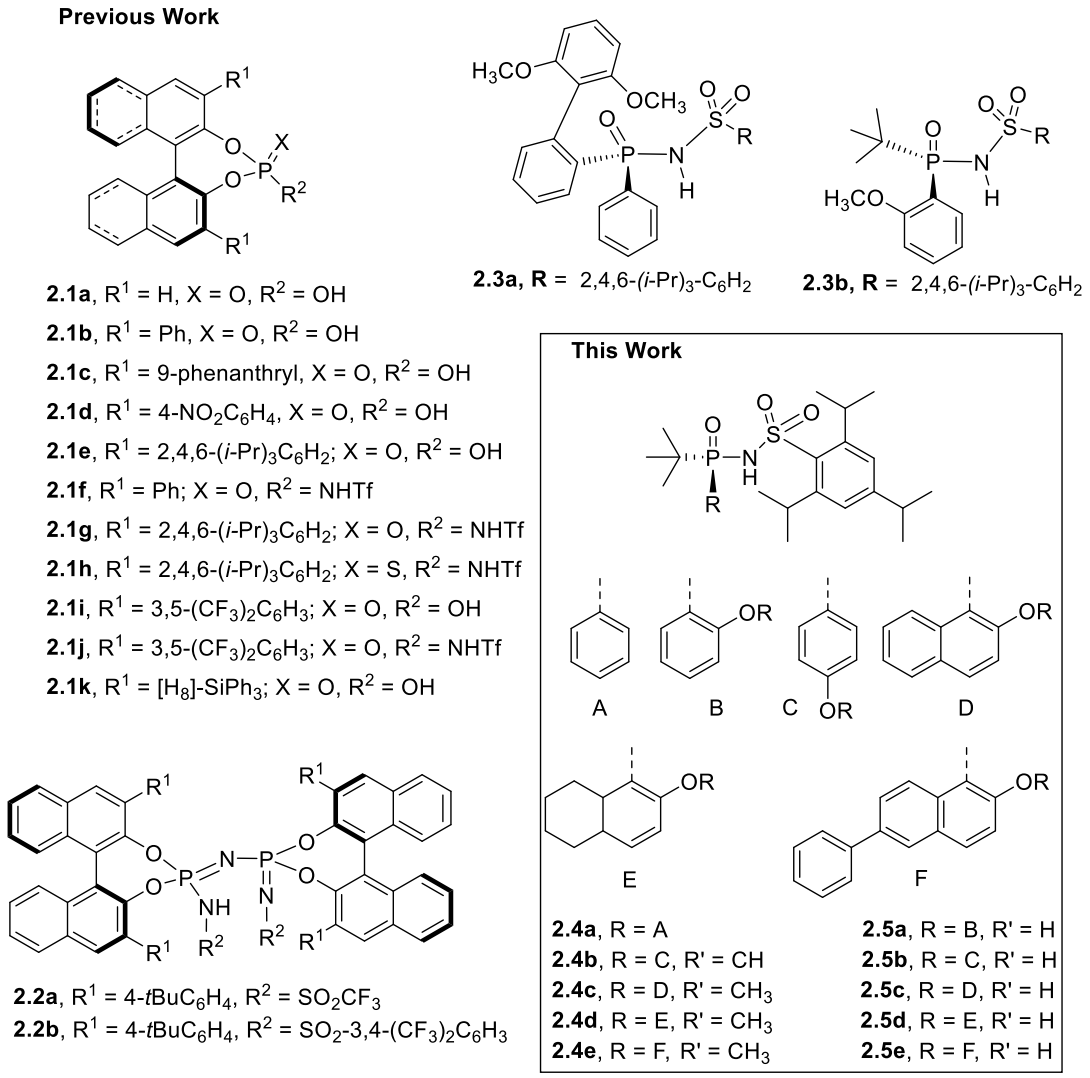

Figure 2.1. Phosphorus-Based Brønsted Acid Organocatalysts.

N-Phosphoryl sulfonamide derivatives of **2.1** (e.g. **2.1f**) were first introduced by Yamamoto and shown to possess greater ability to activate substrates with low reactivity, such as aldehydes, ketones and silyl enol ethers.[5,15] This observation is consistent with the higher acidity of the *N*-triflyl Brønsted acid;[16] the pK_a values of many analogs of **2.1** have been determined in acetonitrile[17] and DMSO.[18] However, the higher reaction rates observed with the *N*-triflyl Brønsted acid, as compared to the corresponding phosphoric acids, were often also associated with lower enantioselectivity.[4b,c] For example, List reported that direct asymmetric *N,O*-acetalization of aldehydes with Brønsted acids **2.1e** and **2.1g** resulted in products with 61% ee and 14% ee, respectively.[19a] Similarly, asymmetric methanolysis of cis-1,2-

cyclohexanedicarboxylic anhydride with a phosphinic acid and its corresponding phosphoramide led to 22% ee and 0% ee, respectively.[19b] Recently, Han reported the synthesis of *P*-stereogenic analogs **2.3** (e.g. **2.3a,b**) and observed that these compounds catalyzed the transfer hydrogenation of 2-phenylquinolines in only 30–36% enantiomeric excess.[20]

Based on the collective knowledge in this field, we decided to explore the impact of an intramolecular non-covalent interaction that could potentially participate in stabilizing the reaction intermediates in the transfer hydrogenation of heterocyclic compounds. We aimed to combine the higher catalytic activity of phosphoramides with the steric effect of *t*-butyl-substituted *P*-chiral phosphines into a new class of Brønsted acids, typified by analog **2.5c** (Fig. 2.1). In the design of these compounds, we presumed that a hydrogen bond between a heteroatom attached to the backbone of the catalyst and the acidic NH could (a) further increase the acidity of the catalyst, (b) rigidify the catalytic cavity, (c) stabilize the transition state of the reaction, and (d) potentially recruit the Hantzsch ester, thus leading to faster conversion at RT and good enantioselectivity. Herein we report the properties of a prototype, analog **2.5c** (OttoPhosa I), having a strategically placed phenolic moiety, as a key structural element (Fig. 2.1).

2.4 Results and Discussion

Recently, we reported a library synthesis of structurally diverse *t*-butyl-substituted *P*-chiral secondary phosphine oxides (SPOs) in high enantiomeric purity, starting from precursor **2.6** (Scheme 2.1).[21] Preparation of analogs **2.7a**, **2.7c** and **2.7d** was reported and the same methodology was used for the syntheses of **2.7e** and **2.7f** in good yields and high enantiomeric purity.[21] In order to probe the impact of the intramolecular hydrogen bond characterizing Brønsted acids **2.5** in a head-to-head comparison with analogs missing only that feature, we also synthesized the previously disclosed SPO **2.7b** (the precursor to Brønsted acid **2.3b**) using the method previously

reported.[22] Intermediates **2.7** were treated with aqueous ammonia in the presence of Et_3N and CCl_4 to obtain the phosphinamides **2.8** via an Atherton–Todd-type reaction.[23] These intermediates were treated with 2,4,6-triisopropylbenzenesulfonyl chloride under basic conditions to give the *P*-chiral, *N*-phosphoryl sulfonamides **2.3b** and **2.4**. Finally, analogs **2.3b** and **2.4b–e** were treated with BBr_3 to cleave the methyl ether and obtain the phenolic Brønsted acids **2.5a–e** (Fig. 2.1). Due to the polarity of these compounds (**2.4** and **2.5**), chiral HPLC analysis proved to be very challenging. Consequently, the reported enantiomeric purities of analogs **2.4** were based on the enantiomeric purity of the corresponding phosphinamides **2.8**. However, in cases where both compounds **2.8** and the corresponding analogs **2.4** could be analyzed by chiral HPLC, a negligible difference in enantiomeric excess was observed (e.g. for **2.8a** and **2.4a**, 96.6% ee and 96.0% ee, respectively).

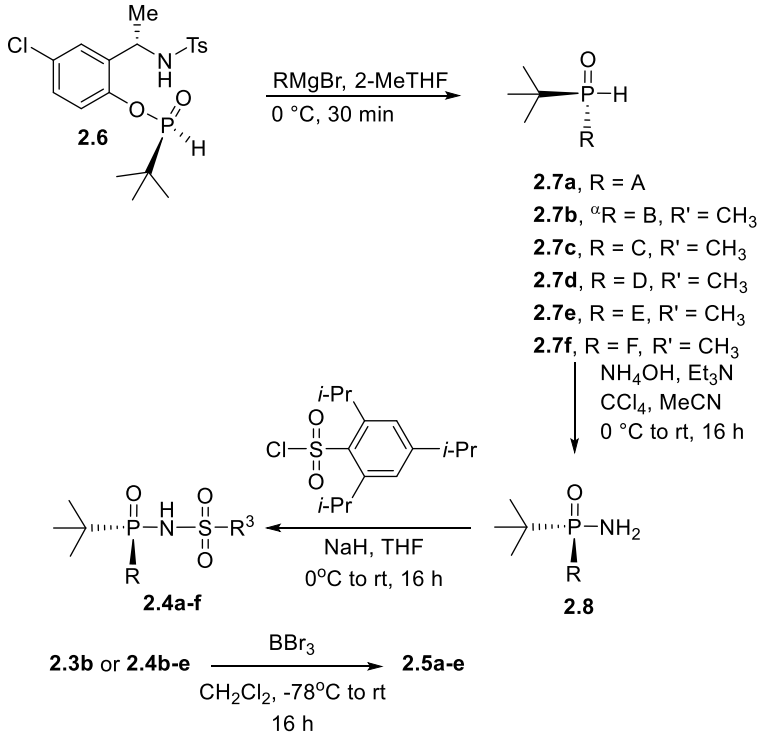

Scheme 2.1. Synthesis of Brønsted Acids ([α]prepared as previously reported[22]).

As a proof of concept, we decided to study the ability of our compounds to catalyze the asymmetric transfer hydrogenation of quinolines, which is an extensively investigated reaction with many BINOL-based Brønsted acids **2.1**. Rueping first

reported using Brønsted acids **2.1** (Fig. 2.1)[24] as a greener approach for the preparation of chiral 1,2,3,4-tetrahydroquinolines (as compared to the classical metal-mediated hydrogenation under high pressure of H_2). The hydride source for these reactions is derived from the Hantzsch ester **2.9** (Table 2.1), a bioisostere of NADH/NADPH.[25] Chiral tetrahydroquinolines are valuable scaffolds for the synthesis of many biologically active compounds, including natural products[26,27] and human therapeutics (Fig. 2.2).[28] The transfer hydrogenation of the 6-bromo-2-methylquinoline **(2.10a**) to the 1,2,3,4-tetrahydroquinoline **2.11a** was first investigated using the previously reported Brønsted acid **2.3b** (Table 2.1; entry 3).

Table 2.1. Asymmetric Transfer Hydrogenation of Quinolines.

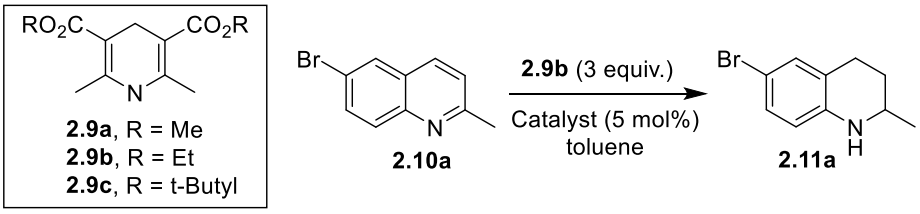

Entry	Catalyst	Temp./°C	Time/h	Yield/%	2.11a %ee[a]
1	none	60	48	50	-
2	none	22	48	-	-
3	**2.3b**	22	48	75	40
4	**2.4a**	22	48	72	40
5	**2.5a**	22	2	99	58
6	**2.5b**	22	24	99	40
7	**2.5c**	22	2	99	80(93[b])
8[c]	**2.5c**	22	0.5	99	80
9[d]	**2.5c**	22	5	99	89
10	**2.5d**	22	2	99	60
11	**2.5e**	22	2	99	84

[a]%ee of the crude product. [b]%ee of the isolated crystalline product. [c]Reaction was run in $CHCl_{33}$. [d]Reaction was run in cyclohexane.

In parallel, the same reaction was carried out in the absence of a catalyst at 60 °C, 40 °C and 22 °C, to exclude the possibility of any competing reaction. Surprisingly, a significant amount of **2.11a** was formed at high temperatures even in the absence of a catalyst (entry 1), which was suppressed at RT (entry 2). To the best of our knowledge, this observation has not been previously reported. Although the 2-methoxy group in Brønsted acid **2.3b** could potentially hydrogen-bond with the NH, the rate of the reaction and enantioselectivity were identical to those of the simple phenyl analog **2.4a** (entry 3 vs. 4). In contrast, the corresponding phenolic Brønsted acid **2.5a** led to quantitative conversion in 2 h and higher enantioselectivity (entry 3 vs. 5). A much slower reaction rate was observed with the 4-phenol derivative **2.5b** and the enantioselectivity was also reduced to that observed with **2.3b** and **2.4a** (entry 6 vs. 3 and 4, respectively). These results strongly support our hypothesis of a beneficial intramolecular cooperative interaction.

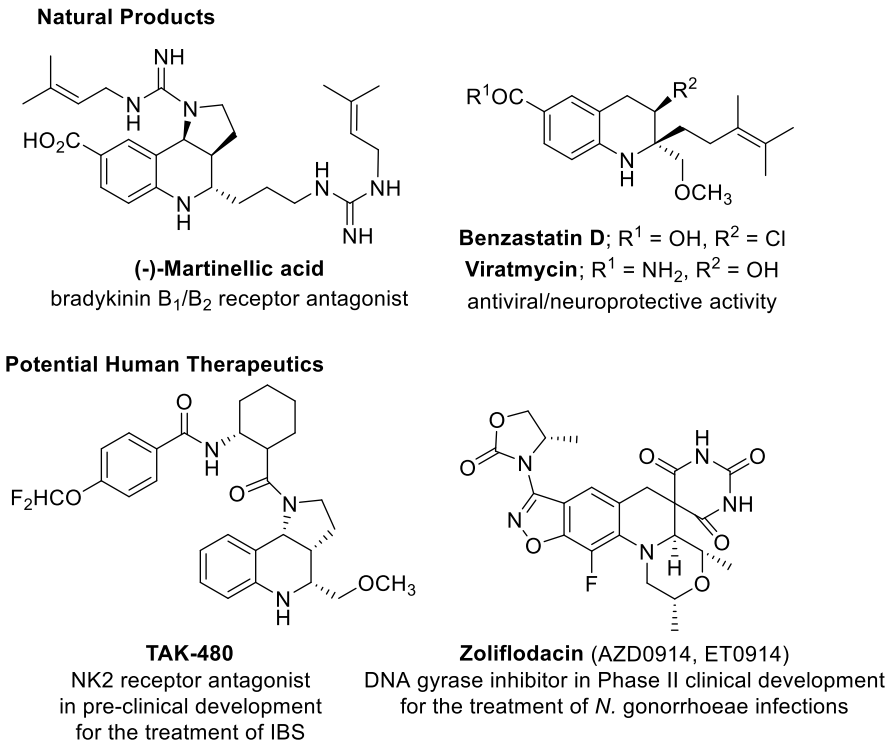

Figure 2.2. Examples of Bioactive Tetrahydroquinolines.

Extension of the π-system to the naphthalen-2-ol derivative **2.5c** led to further improvement in enantioselectivity, giving a crude product in a 1:9 R:S ratio and a quantitative yield after 2 h at RT; enantiomeric purity was increased to a 3.5:96.5 R:S ratio upon crystallization of the product (entry 7). Furthermore, the same reaction could be completed in only 30 min if run in $CHCl_3$ without any loss in enantioselectivity (entry 8). The best enantioselectivity was observed when the reaction was run in cyclohexane (89% ee); however, the reaction time was a little longer (entry 9). Interestingly, the corresponding 5,6,7,8-tetrahydronaphthalen-2-ol derivative **2.5d** gave very similar results to the simple phenol **2.5a** (entry 5 vs. 10), suggesting that π-stacking interactions between the catalyst and the substrate play a significant role in this reaction. Extension of the π-system to the 6-phenylnaphthalen-2-ol analog **2.5e** provided some further improvement in enantioselectivity (entry 7 vs. 11); this aspect of our catalyst design merits further investigation in future studies. The absolute stereochemistries of the (S)-6-bromo-2-methyl1,2,3,4-tetrahydroquinoline (**2.11a**) and the Brønsted acids R$_p$-**2.5a** and R$_p$-**2.5c** were confirmed by their single-crystal X-ray structures (Fig. 3a–c, respectively). The structures of R$_p$-**2.5a** and R$_p$-**2.5c** also clearly showed the presence of a hydrogen bond between the phenolic oxygen and the acidic NH and provided a molecular view of a small substrate-binding cavity (e.g. Fig. 2.3d; 2.5c).

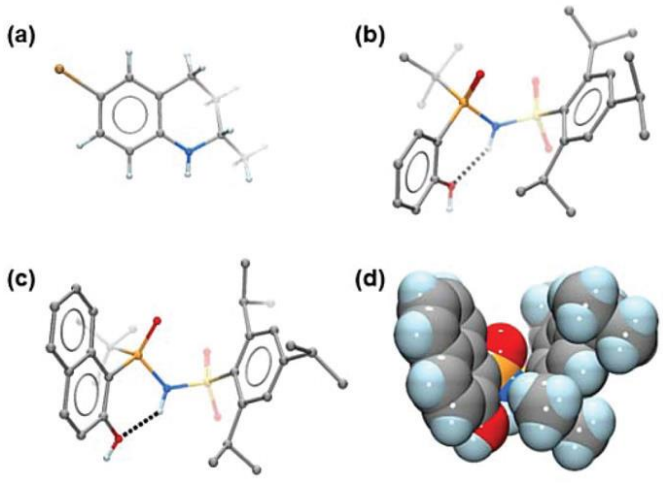

Figure 2.3. (a) (S)-**2.11a**; (b) R$_P$-**2.5a**; (c) R$_P$-**2.5c**; (d) space-filling model based on the X-ray of R$_P$-**2.5c**.

Optimization of the reaction conditions for the solvent and the Hantzsch ester effects in the presence of catalyst **2.5c** were also studied (Tables 2.3 and 2.4). The effects of the Hantzsch esters (**2.9a–c**) investigated so far did not result in any major differences. The substrate scope was subsequently explored and the results were compared to those reported for BINOL-based Brønsted acids **2.1b** and **2.1c** (Table 2.2); the objective of this study was to simply gain further insight into the catalytic properties of catalyst **2.5** in comparison to BINOL-based Brønsted acids **2.1** that have similar size (or slightly larger) substrate binding cavities. Although catalyst optimization is often required for each different type of reaction, certain structural trends are well known about organocatalysts **2.1**.[1] For example, large substituents at the 3,3′-positions of the BINOL-based Brønsted acids **2.1** typically provide better enantioselectivity, due to higher steric bulk and larger substrate-binding catalytic cavities (e.g. Table 2.2, entry 8 vs. 9).[24]

Table 2.2. Substrate Scope and Catalyst Effect.

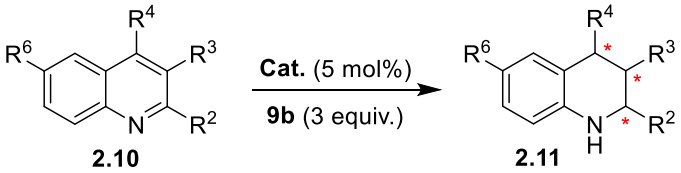

Entry	Catalyst	R^2	$R^3/R^4/R^6$	Time/h	Yield/%	2.11 %ee[a]
1	**2.5c**	Me	H/H/H	16	73	88
2	**2.5c**	Me	H/H/Br	5	99	88(93[b])
3	**2.5c**	Me	H/H/NO_2	3	83	86(96[b])
4	**2.5c**	Me	H/H/OMe	168	<5	-
5	**2.5c**	Et	H/H/H	9	72	75
6	**2.5c**	*i*-Pr	H/H/H	22	77	66
7	**2.5c**	Ph	H/H/H	12	95	59
8[c]	**2.1b**	Ph	H/H/H	-	nd	5
9[c]	**2.1c**	Ph	H/H/H	12	92	97
10	**2.5c**	H	H/Me/H	96	70	30
11[c]	**2.1b**	H	H/Me/H	35-60	nd	35
12	**2.5c**	H	Me/H/H	16	71	14
13	**2.5c**	H	Ph/H/H	86	51[d]	4
14[c]	**2.1c**	H	Ph/H/H	22-48	nd	Racemic
15[e]	**2.5c**	CO_2Me	H/H/H	4	71	30

Most reactions catalyzed by **2.5c** were run at RT. [a]%ee of the product. [b]%ee after crystallization. [c]Data obtained at 60 °C.[24,30] [d]Yield based on the recovered starting material. [e]Data obtained at 50 °C.

Screening of various substituents at the C-2 position of the quinoline substrate revealed that substituents with larger steric bulk led to lower enantioselectivity (Table 2.2; entry 1 vs. 5 and 6). Substitution with an electron-withdrawing group at C-6 accelerated the reaction rate (entries 2 and 3), whereas an electron-donating group dramatically reduced the rate of the reaction (entry 4). These observations are consistent with the general mechanism for this type of reaction.[1,24] Hydrogenation of the 2-phenylquinoline resulted in lower enantioselectivity than expected (59% ee; entry 7),

suggesting a possible competing π-stacking interaction between the catalyst and the C-2 phenyl group, instead of the quinoline core. It is noteworthy that in spite of its small cavity size, compound **2.5c** catalyzed the transfer hydrogenation of the 2-phenylquinoline with significantly higher enantioselectivity than catalyst **2.1b** (entry 7 vs. 8),[24] whereas hydrogenation of the 4-methylquinoline catalyzed by **2.5c** results in a similar enantioselectivity to that reported with catalyst **2.1b**[29] (entry 10 vs. 11). We also examined the hydrogenation of the 3-methyl and 3-phenyl substituted quinolines but observed low enantioselectivity and slower reaction rates (entries 12 and 13, respectively). Our observations are consistent with those reported by Rueping for the 3-substituted vs. the 2-substituted quinoline. For example, whereas hydrogenation of the 2-phenylquinoline with catalyst **2.1c** leads to 97% ee of the tetrahydroquinoline **2.11** (entry 9),[24] the 3-phenylquinoline was reported to give a racemic mixture of the corresponding product (entry 14). However, sterically more congested catalysts, such as **2.1k**, were shown to lead to the formation of the 3-phenyl-1,2,3,4-tetrahydroquinoline in 74% ee, under the same reaction conditions.[30] Finally, we examined the transfer hydrogenation of methylquinoline-2-carboxylate (entry 15). A strongly electron-withdrawing substituent at C-2 is expected to decrease the electron density on the quinoline nitrogen and significantly decrease the rate of this reaction.[31] In fact, the transfer hydrogenation of methylquinoline-2-carboxylate catalyzed by a Brønsted acid has not been previously reported. We were pleased to see quantitative conversion in 4 hours, albeit in modest enantioselectivity (the isolated yield of the pure product was only 71% due to partial co-elution of the Hantzsch esters with the product during chromatography). It is reasonable to assume that the high acidity of Brønsted acid **2.5c** is able to compensate for the electronic effects of the C-2 carboxylate moiety.

Although we have not yet fully explored the mechanistic differences between catalyst **2.5c** and the BINOL-based Brønsted acids **2.1**, our current data are generally consistent with the established mechanism for this reaction.[1,24,29] The rate acceleration and enantioselectivity differences observed between catalysts **2.3b** and **2.5a** (Table 1; entry 3 vs. 5) are consistent with our original hypothesis, which presumed that

protonation of the quinoline by the catalyst could lead to an intramolecular cooperative ion pair (Fig. 2.4; **II**), stabilizing the conjugate base of the catalyst.

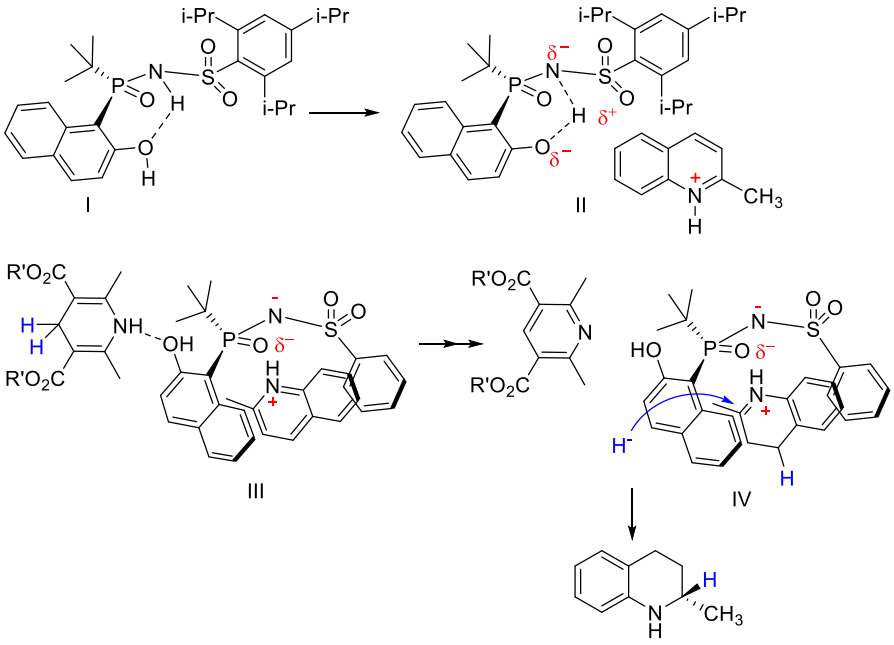

Figure 2.4. Proposed Catalytic Mechanism of Brønsted Acid **2.5c**.

Whether the shared proton in the ionized form **II** is derived from the OH or the NH of the original catalyst (**I**) is inconsequential to the proposed intermediate **II**. Additionally, once the protonated quinoline is bound to the catalyst, it is likely that the OH moiety recruits the Hantzsch ester, leading to a more stable trimolecular complex (**III**) and guiding the delivery of the hydride species from the side of the naphthol ring (**IV**). Binding of the 2-methylquinoline to **2.5c** through favorable π-stacking interactions and placement of the quinoline nitrogen near the acidic NH of the catalyst necessitates that the 2-methyl group becomes buried in the catalytic pocket and near the *t*-butyl substituent on the phosphorus. Therefore, entrance of the hydride from the side of the naphthol would simultaneously push the 2-methyl group away from the steric bulk of the *t*-butyl group.

2.5 Conclusion

In summary, we aimed to demonstrate that the incorporation of an intramolecular H-bond between a phenolic substituent on a *P*-stereogenic center of a Brønsted acid and the NH of its *N*-phosphoryl sulfonamide can stabilize the conformation of the catalytic cavity, accelerate the reaction rate and increase enantioselectivity for the transfer hydrogenation of quinolines. OttoPhosa I (**2.5c**) represents a prototype of this new class of Brønsted acid organocatalysts. Its catalytic properties compare favorably with those of BINOL-based Brønsted acids **2.1** having a similarly small substrate-binding pocket. The synthesis of analogues **2.5** and fine-tuning of their catalytic properties for different chemical transformations can be easily achieved in a modular library mode[21] and is currently in progress.

2.6 Experimental Section

Genera Procedure: All reactions were carried out under anhydrous conditions and under an atmosphere of dry argon unless otherwise indicated. Compounds were purified by normal phase flash column chromatography on silica gel (SDS, 60 Å C. C. 40-63 mm) as the stationary phase. Thin Layer Chromatography (TLC) was performed on alumina plates pre-coated with silica gel (Merck silica gel, 60 F254), which were visualized by UV when applicable (λmax = 254 nm and/or 366 nm) and/or by staining with vanillin or anisadehyde in acidic ethanol and/or $KMnO_4$ in basic water followed by heating. Key compounds were fully characterized by ^{1}H, $^{13}C\{^{1}H\}$ and $^{31}P\{^{1}H\}$ NMR and HRMS. Chemical shifts (δ) are reported in ppm relative to the internal deuterated solvent or external H_3PO_4 (δ 0.00 ^{31}P), unless indicated otherwise. High-resolution MS spectra were recorded using electrospray ionization (ESI+/-) and Fourier transform ion cyclotron resonance mass analyzer (FTMS).

The reactions were monitored either by TLC or analytical HPLC/MS to confirm completion and homogeneity of the products. Analytical HPLC was performed using a

reversed phase C18 5 µm column on a Waters Atlantis T3 instrument and the solvent system indicated below:

Solvent A: H_2O, 0.1% formic acid

Solvent B: CH_3CN, 0.1% formic acid

Mobile phase: linear gradient from 95%A and 5%B to 5%A and 95%B in 13 min, then 2 min at 100% B

Flow rate: 1 mL/min

Compounds 6-bromo-2-methylquinoline (**2.10a**), 2-methylquinoline (**2.10b**), 2-phenylquinoline (**2.10c**) and 4-methylquinoline (**2.10d**) were purchased from Sigma Aldrich. The 2-ethylquinoline (**2.10e**),[32] 2-isopropylquinoline (**2.10f**),[33] 6-nitro-2-methylquinoline (**2.10g**)[34] and 6-methoxy-2-methylquinoline (**2.10h**)[34] were synthesized according to the literature procedures indicated.

The enantiomeric purity of chiral compounds was determined by chiral HPLC using an Agilent 1100 or Agilent 1260 series instrument and the column and solvent system indicated for each compound. The absolute stereochemistry of all compounds was assigned based on several factors, including the single crystal X-ray of the previously reported key precursor compound **2.6**,[21] the single crystal X-ray structures of intermediate phosphinic amide **2.8d** (refer to Appendix I, Table I-1), the single crystal X-ray structures of catalysts **2.5a** and **2.5c**, the single crystal X-ray structure of compound (*S*)-2-bromo-6-methyl-3,4-dihydro-*2H*-1λ^2-quinoline (**2.11a**), and by analogy with previously reported compounds in the literature.

The names of all compounds were generated using ChemBioDraw Ultra 12.0.

<u>General synthesis of secondary phosphine oxides (SPOs) **2.7**:</u>

We recently reported the synthesis of SPO intermediates **2.6**, **2.7a,** 2.**7c** and **2.7d**.[21] The synthesis of analogs **2.7e** and **2.7f** was achieved using the same protocol.[21] The

synthesis of SPO analogs **2.7b** was achieved using the previously reported methodology.[22]

(S)-tert-Butyl(2-methoxy-5,6,7,8-tetrahydronaphthalen-1-yl)phosphine oxide (2.7e)

Precursor compound 5-bromo-6-methoxy-1,2,3,4-tetrahydronaphthalene (used to prepare the Grignard reagent) was synthesized according to the method reported by Smith and co-workers.[35]

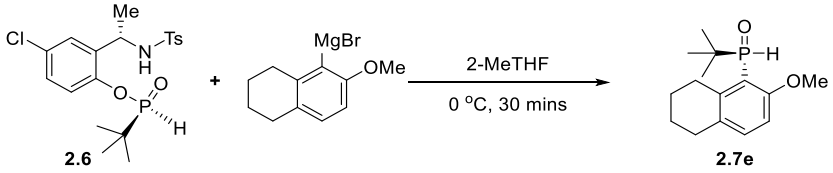

A three-neck flask under argon was charged with SPO **2.6** (1 mmol) in 2-MeTHF (3 mL) and cooled to 0°C. 2-Methoxy-5,6,7,8-tetrahydronaphthalen-1-yl magnesium bromide (1 M in 2-MeTHF, 4 mmol, 4 mL) was added slowly while keeping the internal temperature <5 °C. The reaction mixture was stirred for 40 min to completion. Saturated and degassed aqueous NH_4Cl solution (5 mL) was added slowly to quench the reaction. The organic layer was collected and the aqueous residue was extracted with DCM (25 mL x3). The combined organic extracts were dried over anhydrous Na_2SO_4 and concentrated. The residue was purified by flash column chromatography on silica gel (deactivated with 10% water) using a solvent gradient of hexane/EtOAc (from 50:50 to 0:100, v/v) to obtain the desired product (141 mg) in 53% yield. ^{1}H NMR (400 MHz, $CDCl_3$): δ 8.28 (s, 0.5 H), 7.17 (d, *J* = 8.5 Hz, 1H), 7.06 (s, 0.5 H), 6.71 (dd, *J* = 8.5, 5.1 Hz, 1H), 3.77 (s, 3H), 3.54 – 3.39 (m, 1H), 2.93 (dt, *J* = 17.0, 5.6 Hz, 1H), 2.72 (t, *J* = 6.2 Hz, 2H), 1.83 – 1.66 (m, 4H), 1.20 (d, *J* = 16.6 Hz, 9H). ^{31}P NMR (162 MHz, $CDCl_3$): δ 36.57.

More detailed characterization and estimation of the enantiomeric purity was performed at the subsequent step, when **2.7e** was converted to the corresponding *P*-chiral (*tert*-butyl)-P-arylphosphinic amide **2.8e**.

(S)-tert-Butyl(2-methoxy-6-phenylnaphthalen-1-yl)phosphine oxide (2.7f)

The precursor 1-bromo-2-methoxy-6-phenylnaphthalene (used to prepare the Grignard reagent) was synthesized according to the method reported by Smith and co-workers.[35]

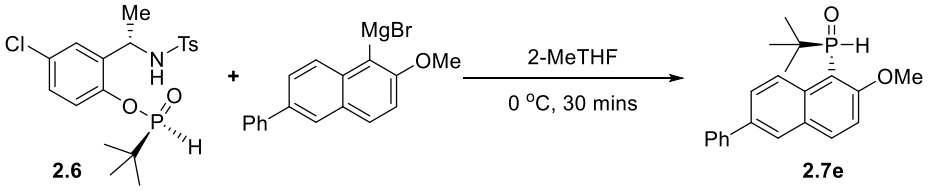

A three-neck flask under argon was charged with SPO **2.6** (1 mmol) dissolved in 2-MeTHF (3 mL) and cooled to 0 °C. A solution of 2-methoxy-6-phenylnaphthalen-1-yl magnesium bromide (1 M in 2-MeTHF, 4 mmol, 4 ml; prepared as previously reported[6]) was added slowly, while keeping the internal temperature <5 °C. The reaction mixture was stirred for 40 min to complete the reaction. Saturated and degassed aqueous NH_4Cl solution (5 mL) was added slowly to quench the reaction. The organic layer was collected and the aqueous residue was extracted with DCM (25 mL x3). The combined organic extracts were dried over anhydrous Na_2SO_4 and concentrated. The residue was purified by silica gel chromatography (on deactivated silica with 10% water) eluted with a solvent gradient of hexane/EtOAc gradient (50:50 to 0:100, v/v) to obtained the desired product (189 mg) in 56% yield. ^{1}H NMR (400 MHz, $CDCl_3$): δ 9.04 (d, *J* = 9.0 Hz, 1H), 8.54 (s, 0.5 H), 8.07 (d, *J* = 9.1 Hz, 1H), 7.98 (s, 1H), 7.81 (dd, *J* = 9.0, 2.1 Hz, 1H), 7.70 (d, *J* = 7.1 Hz, 2H), 7.48 (t, *J* = 7.7 Hz, 2H), 7.37 (t, *J* = 7.4 Hz, 1H), 7.31 (s, 0.5 H), 7.30 – 7.26 (m, 1H), 3.98 (s, 3H), 1.26 (d, *J* = 16.8 Hz, 9H). ^{31}P NMR (162 MHz, $CDCl_3$): δ 36.19.

More detailed characterization and estimation of the enantiomeric purity was performed at the subsequent step, when **2.7f** was converted to the corresponding *P*-chiral (*tert*-butyl)-P-arylphosphinic amide **2.8f**.

General procedure for the conversion of SPOs **2.7** to the *P*-Chiral (*t*-butyl)-*P*-arylphosphinic amides **2.8**:

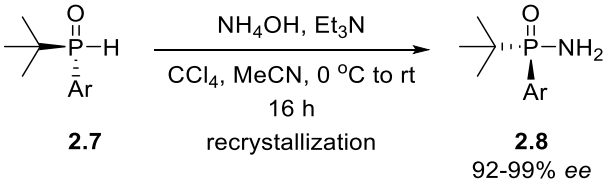

2.7 **2.8**
92-99% *ee*

Chiral SPO **2.7** (1.0 mmol) was dissolved in 6 mL of degassed acetonitrile and cooled to 0 °C. CCl_4 (1.0 mL), Et_3N (2.0 mmol) and saturated aqueous solution of NH_4OH (28% in water, 0.5 mL) were sequentially added dropwise while stirring. The solution was stirred at 0 °C for 30 min and then warmed to RT and allowed to stir for 16 h. Water (5 mL) was added to the reaction mixture and then extracted with EtOAc, the organic layers were combined, dried over anhydrous Na_2SO_4 and concentrated to give the crude product. The pure product was obtained after first passing the crude through a short silica gel column and then doing a crystallization in DCM/Et_2O (1:5, v/v) at -20 °C to obtain the phosphoramide products as highly enriched single enantiomers (92-99% ee).

(R)-P-(tert-butyl)-P-phenylphosphinic amide **(2.8a)**; characterization data consistent with previously reported.[36]

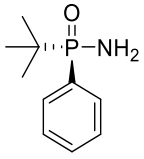

Isolated as a white solid in 82% yield (162 mg) and 96.7% ee. ^{1}H NMR (500 MHz, $CDCl_3$): δ 7.90–7.84 (m, 2H), 7.57–7.52 (m, 1H), 7.49–7.43 (m, 2H), 2.72 (brs, 2H), 1.16 (d, *J* = 15.3 Hz, 9H). ^{31}P NMR (202 MHz, $CDCl_3$): δ 41.34. Chiral HPLC method:

Chiralcel OD, hexane/IPA = 80/20, 1.0 mL/min, λ = 220 nm; (R)-enantiomer t_R (major) = 5.88 min, (*S*)-enantiomer t_R (minor) = 7.60 min.

(R)-P-(tert-butyl)-P-(2-methoxyphenyl)phosphinic amide **(2.8b)**

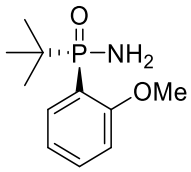

Isolated as a white solid in 73% yield (166 mg) and 95% ee. ^{1}H NMR (500 MHz, $CDCl_3$): δ 7.90 (ddd, *J* = 11.9, 7.5, 1.8 Hz, 1H), 7.49 – 7.40 (m, 1H), 7.10 – 7.02 (m, 1H), 6.93 – 6.87 (m, 1H), 3.83 (s, 3H), 3.17 (s, 2H), 1.08 (d, *J* = 15.9 Hz, 9H). ^{13}C NMR (126 MHz, $CDCl_3$): δ 159.2 (d, *J* = 3.9 Hz), 135.5 (dd, *J* = 5.5, 3.0 Hz), 133.3, 121.0 (dd, *J* = 10.6, 2.5 Hz), 119.4 (d, *J* = 101.4 Hz), 110.6 (d, *J* = 7.0 Hz), 55.2, 34.3 (d, *J* = 93.7 Hz), 24.2. ^{31}P NMR (203 MHz, $CDCl_3$): δ 46.01. HRMS: calculated for $C_{11}H_{18}NnaO_2P^+$ $[M+H]^+$: 250.0967, found: 250.0967. Chiral HPLC method: Chiralcel OD, hexane/IPA = 80/20, 1.0 mL/min, λ = 220 nm; (*S*)-enantiomer t_R (minor) = 7.38 min, (R)-enantiomer t_R (major) = 10.23 min.

(R)-*P*-(*tert*-butyl)-*P*-(4-methoxyphenyl)phosphinic amide (2.8c)

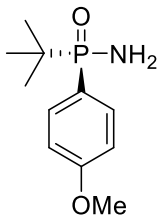

Isolated as a white solid in 48% yield (109 mg) and >99% ee. ^{1}H NMR (500 MHz, $CDCl_3$) δ 7.77 – 7.70 (m, 2H), 6.92 (dd, *J* = 8.9, 2.4 Hz, 2H), 3.83 (s, 3H), 2.84 (s, 2H), 1.11 (d, *J* = 15.2 Hz, 9H). ^{13}C NMR (126 MHz, $CDCl_3$): δ 162.4 (d, *J* = 2.9 Hz), 135.0 (d, *J* = 9.6 Hz), 121.4 (d, *J* = 123.0 Hz), 113.6 (d, *J* = 12.5 Hz), 55.2, 32.3 (d, *J* = 93.5

Hz), 24.8. ^{31}P NMR (203 MHz, $CDCl_3$): δ 41.44. HRMS: calculated for $C_{11}H_{18}NNaO_2P^+$ $[M+H]^+$: 250.0967, found: 250.0968. Chiral HPLC method: Chiralcel OD, hexane/IPA = 80/20, 1.0 mL/min, λ = 220 nm; (*R*)-enantiomer t_R (major) = 7.08 min, (*S*)-enantiomer t_R (minor) = 12.49 min.

(*R*)-*P*-(*tert*-butyl)-*P*-(2-methoxynaphthalen-1-yl)phosphinic amide (2.8d)

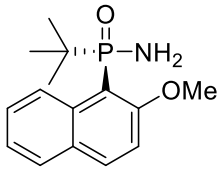

Isolated as a white solid in 42% yield (116 mg) and >99% ee. ^{1}H NMR (400 MHz, $CDCl_3$): δ 9.59 (d, *J* = 8.5 Hz, 1H), 7.99 (d, *J* = 9.1 Hz, 1H), 7.76 (dt, *J* = 8.2, 1.7 Hz, 1H), 7.54 (ddd, *J* = 8.6, 6.7, 1.5 Hz, 1H), 7.38 (ddd, *J* = 8.0, 6.8, 1.2 Hz, 1H), 7.31 – 7.23 (m, 1H), 3.99 (s, 3H), 3.22 (s, 2H), 1.16 (d, *J* = 16.0 Hz, 9H). ^{13}C NMR (101 MHz, $CDCl_3$): δ 158.7 (d, *J* = 3.2 Hz), 136.7 (d, *J* = 6.7 Hz), 134.7, 129.4 (d, *J* = 9.1 Hz), 128.0, 127.6 (d, *J* = 2.2 Hz), 127.5, 124.2, 112.8, 111.9, 111.8, 56.0, 35.9 (d, *J* = 93.2 Hz), 24.4. ^{31}P NMR (162 MHz, $CDCl_3$): δ 50.06. HRMS: calculated for $C_{15}H_{20}NNaO_2P^+$ $[M+H]^+$: 300.1124, found: 300.1115. Chiral HPLC method: Chiralcel OD, hexane/IPA = 80/20, 1.0 mL/min, λ = 220 nm; (*S*)-enantiomer t_R = 8.46 min, (*R*)-enantiomer t_R (single peak) = 28.96 min.

(*R*)-*P*-(tert-butyl)-*P*-(2-methoxy-5,6,7,8-tetrahydronaphthalen-1-yl)phosphinic amide (2.8e)

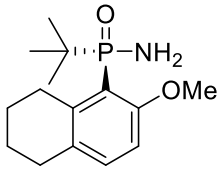

Isolated as a white solid in 45% yield (126 mg) and >99% ee. ^{1}H NMR (500 MHz, $CDCl_3$): δ 7.15 (d, *J* = 8.5 Hz, 1H), 6.72 (dd, *J* = 8.5, 4.8 Hz, 1H), 3.79 (s, 3H), 3.65 – 3.56 (m, 1H), 3.20 (dt, *J* = 17.7, 5.7 Hz, 1H), 3.12 (s, 2H), 2.72 (t, *J* = 6.6 Hz, 2H), 1.86 – 1.77 (m, 1H), 1.75 – 1.66 (m, 2H), 1.65 – 1.55 (m, 1H), 1.13 (d, *J* = 15.8 Hz, 9H). ^{13}C NMR (126 MHz, $CDCl_3$): δ 158.09 (d, *J* = 4.6 Hz), 145.82 (d, *J* = 7.0 Hz), 133.25 (d, *J* = 2.1 Hz), 131.73 (d, *J* = 10.3 Hz), 117.61 (d, *J* = 95.2 Hz), 108.24 (d, *J* = 7.4 Hz), 55.16, 35.83 (d, *J* = 91.8 Hz), 29.87, 28.51 (d, *J* = 2.2 Hz), 24.41 (d, *J* = 0.9 Hz), 22.39 (d, *J* = 84.5 Hz). ^{31}P NMR (203 MHz, $CDCl_3$): δ 50.18. HRMS: calculated for $C_{15}H_{24}NNaO_2P^+$ $[M+H]^+$: 304.1437, found: 304.1142. Chiral HPLC method: Chiralcel OD, hexane/IPA = 80/20, 1.0 mL/min, λ = 220 nm; (*S*)-enantiomer t_R = 4.96 min, (*R*)-enantiomer t_R (single peak) = 6.20 min.

(*R*)-*P*-(*tert*-butyl)-*P*-(2-methoxy-6-phenylnaphthalen-1-yl)phosphinic amide (2.8f)

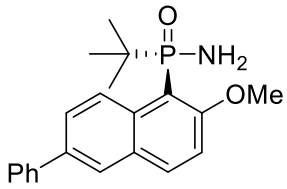

Isolated as a white solid in 60% yield (212 mg) and >99% ee. ^{1}H NMR (500 MHz, $CDCl_3$): δ 9.64 (d, *J* = 9.1 Hz, 1H), 8.00 (d, *J* = 9.0 Hz, 1H), 7.94 (s, 1H), 7.80 (dd, *J* = 9.1, 2.1 Hz, 1H), 7.70 (d, *J* = 7.0 Hz, 2H), 7.47 (t, *J* = 7.7 Hz, 2H), 7.36 (t, *J* = 7.4 Hz, 1H), 7.24 (dd, *J* = 9.0, 4.3 Hz, 1H), 3.95 (s, 3H), 3.31 (brs, 2H), 1.17 (d, *J* = 16.1 Hz, 9H). ^{13}C NMR (126 MHz, $CDCl_3$): δ 158.7 (d, *J* = 3.2 Hz), 140.6, 136.5, 135.9 (d, *J* = 6.7 Hz), 134.9 (d, *J* = 2.1 Hz), 129.7 (d, *J* = 9.0 Hz), 128.9, 128.2 (d, *J* = 2.1 Hz), 127.3,

127.2, 127.0, 125.63, 112.4 (d, J = 93.6 Hz), 112.3 (d, J = 7.7 Hz), 56.0, 35.9 (d, J = 93.2 Hz), 24.4. ^{31}P NMR (203 MHz, $CDCl_3$): δ 50.11. HRMS: calculated for $C_{21}H_{25}NO_2P^+$ $[M+H]^+$: 354.1617, found: 354.1618. Chiral HPLC method: Chiralcel OD, hexane/IPA = 80/20, 1.0 mL/min, λ = 220 nm; (*S*)-enantiomer t_R = 10.91 min, (*R*)-enanatiomer (single peak) t_R = 15.34 min.

General procedure for the conversion of arylphosphinic amides **2.8** to Brønsted acids **2.3b** and **2.4**:

A slurry of NaH (3 equiv of 60% NaH in oil) in anhydrous THF (3.0 mL) at 0 °C was added to a solution of phosphinamide **2.8** (0.5 mmol, 1 equiv) and the mixture was stirred for 30 min. The arylsulfonyl chloride (1.5 equiv) was added slowly, and the mixture was warmed to RT and monitored by TLC. After complete conversion (~12-15 h), NH_4Cl (0.1 g) was added portion-wise, the mixture was diluted with THF and filtered. The filtrate was concentrated and the crude residue was purified by flash column chromatography on silica gel to give the desired product. The product was dissolved in DCM (15 mL) and thoroughly washed with 4 M HCl (2x) to remove any salt impurities and completely protonate the catalyst. The organic layer was separated and concentrated under reduced pressure. The residue was taken up in toluene (5 mL), evaporated to dryness again and dried under high vacuum for 24 h to give the catalyst.

Note: Upon completion of the coupling reaction between intermediate **2.8** and the sulfonyl chloride, some analogs **2.4** were used directly in the subsequent demethylation step (without isolation/purification) to get the final catalysts **2.5**.

(**R)-N-(tert-butyl(2-methoxyphenyl)phosphoryl)-2,4,6-triisopropylbenzenesulfonamide (2.3b)**: This compound was recently reported by Han and coworkers.[20]

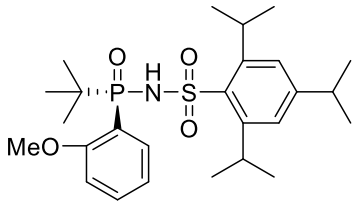

Isolated as a yellow solid in 97% yield (240 mg). ^{1}H NMR (500 MHz, CD_3OD): δ 7.74 (ddd, *J* = 7.0, 1.5 Hz, 1H), 7.37 (t, *J* = 7.3 Hz, 1H), 7.11 (s, 2H), 6.91 (dd, *J* = 7.8, 5.3 Hz, 1H), 6.77 (t, *J* = 7.0 Hz, 1H), 4.49 - 4.40 (m, 2H), 3.54 (s, 3H), 2.88 (hept, *J* = 6.9 Hz, 1H), 1.27 – 1.21 (m, 12H), 1.14 – 1.04 (m, 15H). ^{31}P NMR (202 MHz, CD_3OD): δ 33.97. HRMS: calculated for $C_{26}H_{40}NO_4PSNa$ [M+Na]: 516.2308, found: 516.2305.

(R)-N-(tert-butyl(phenyl)phosphoryl)-2,4,6-triisopropylbenzenesulfonamide (2.4a)

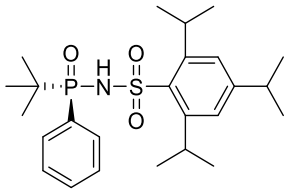

Isolated as a yellow solid in 96% yield (223 mg). ^{1}H NMR (500 MHz, CD_3OD): δ 7.66-7.62 (m, 2H), 7.35 (td, *J* = 7.5, 1.5 Hz, 1H), 7.22 (td, *J* = 8.0, 3.0 Hz, 2H), 7.04 (s, 2H), 4.51-4.45 (m, 2H), 2.88-2.82 (m, 1H), 1.23 (d, *J* = 7.0 Hz, 6H), 1.21 (d, *J* = 6.5 Hz, 6H), 1.06 (d, *J* = 7.0 Hz, 6H), 1.01 (d, *J* = 15.5 Hz, 9H); ^{13}C NMR (125 MHz, CD_3OD): δ 150.8, 149.2, 142.7, 134.8 (d, *J* = 112.0 Hz), 134.5 (d, *J* = 8.1 Hz), 131.3 (d, *J* = 1.8 Hz), 128.1 (d, *J* = 10.9 Hz), 123.6, 35.3, 33.9 (d, *J* = 103.8 Hz), 30.2, 25.6, 25.2, 25.1, 24.33, 24.30; ^{31}P NMR (202 MHz, CD_3OD): δ 31.74; HRMS: calculated for $C_{25}H_{38}NO_3PSNa$ $[M+Na]^+$: 486.2202, found: 486.2194.

(R)-N-(tert-butyl(4-methoxyphenyl)phosphoryl)-2,4,6-triisopropylbenzenesulfonamide (2.4b)

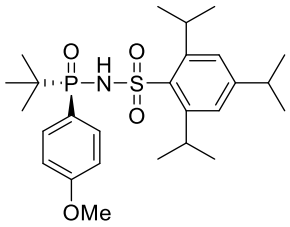

Upon completion of the coupling reaction with the sulfonyl chloride, compound **2.4b** was used directly in the subsequent demethylation step to get the final catalyst **2.5b**.

(R)-N-(tert-butyl(2-methoxynaphthalen-1-yl)phosphoryl)-2,4,6-triisopropylbenzenesulfonamide (2.4c)

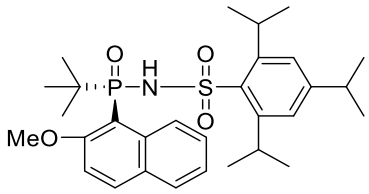

Compound was isolated as a white solid in 98% yield (173 mg). ^{1}H NMR (500 MHz, $CDCl_3$): δ 9.43 (d, *J* = 8.9 Hz, 1H), 8.02 (d, *J* = 9.1 Hz, 1H), 7.75 (d, *J* = 8.0 Hz, 1H), 7.56 – 7.43 (m, 2H), 7.37 (t, *J* = 8.0 Hz, 1H), 7.32 – 7.27 (m, 1H), 7.05 (s, 2H), 4.16 (hept, *J* = 6.5 Hz, 2H), 4.10 (s, 3H), 2.81 (hept, *J* = 7.0 Hz, 1H), 1.31 – 1.11 (m, 21H), 1.10 (d, *J* = 6.8 Hz, 6H). ^{13}C NMR (126 MHz, $CDCl_3$): δ 158.42, 152.56, 150.27, 136.80 (d, *J* = 7.6 Hz), 135.92 (d, *J* = 2.3 Hz), 135.43, 129.60 (d, *J* = 10.0 Hz), 128.28, 127.99, 127.57 (d, *J* = 2.3 Hz), 124.64, 123.75, 111.89 (d, *J* = 8.2 Hz), 110.79, 110.03, 56.53, 37.40 (d, *J* = 89.4 Hz), 34.18, 29.91, 24.91 (d, *J* = 3.4 Hz), 24.60, 23.63 (d, *J* = 5.8 Hz). ^{31}P NMR (203 MHz, $CDCl_3$): δ 43.1. HRMS: calculated for $C_{30}H_{41}O_4NPS$: 542.2499, found: 542.2491.

(R)-N-(tert-butyl(2-methoxy-5,6,7,8-tetrahydronaphthalen-1-yl)phosphoryl)-2,4,6-triisopropylbenzenesulfonamide (2.4d)

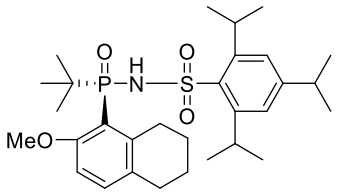

^{1}H NMR (500 MHz, $CDCl_3$): δ 7.47 (s, 1H), 7.17 (d, *J* = 8.5 Hz, 1H), 7.08 (s, 2H), 6.74 (dd, *J* = 8.5, 5.2 Hz, 1H), 4.18 (hept, *J* = 6.7 Hz, 2H), 3.89 (s, 3H), 3.40 (dt, *J* = 18.0, 6.2 Hz, 1H), 3.03 (dt, *J* = 17.9, 5.5 Hz, 1H), 2.85 (hept, *J* = 6.9 Hz, 1H), 2.74 – 2.64 (m, 2H), 1.73 – 1.56 (m, 4H), 1.26 (d, *J* = 6.7 Hz, 6H), 1.24 – 1.15 (m, 15H), 1.13 (d, *J* = 6.7 Hz, 6H). ^{31}P NMR (203 MHz, $CDCl_3$): δ 44.0.

Upon completion of the coupling reaction with the sulfonyl chloride, the crude compound **2.4d** was used directly in the subsequent demethylation step to get the final catalyst **2.5d**.

(R)-N-(tert-butyl(2-methoxy-6-phenylnaphthalen-1-yl)phosphoryl)-2,4,6-triisopropylbenzenesulfonamide (2.4e)

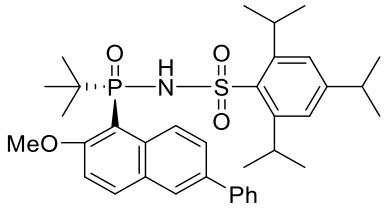

^{1}H NMR (500 MHz, $CDCl_3$) δ 9.51 (d, *J* = 9.2 Hz, 1H), 8.08 (d, *J* = 9.1 Hz, 1H), 7.95 (t, *J* = 2.1 Hz, 1H), 7.75 (dd, *J* = 9.2, 2.1 Hz, 1H), 7.68 (dd, *J* = 8.3, 1.3 Hz, 2H), 7.52 (d, *J* = 6.4 Hz, 1H), 7.47 (t, *J* = 7.7 Hz, 2H), 7.39 – 7.34 (m, 1H), 7.31 (dd, *J* = 9.1, 4.7 Hz, 1H), 7.06 (s, 2H), 4.18 (hept, *J* = 6.7 Hz, 2H), 4.11 (s, 3H), 2.81 (hept, *J* = 6.8 Hz, 1H), 1.26 – 1.20 (m, 15H), 1.18 (dd, *J* = 6.9, 2.4 Hz, 6H), 1.12 (d, *J* = 6.7 Hz, 6H). ^{31}P NMR (203 MHz, $CDCl_3$): δ 43.2.

Upon completing of the coupling reaction with the sulfonyl chloride, compound **2.4e** the crude product was used directly in the subsequent demethylation step to get the final catalyst **2.5e**.

General procedure for the synthesis of Brønsted acids **2.5**:

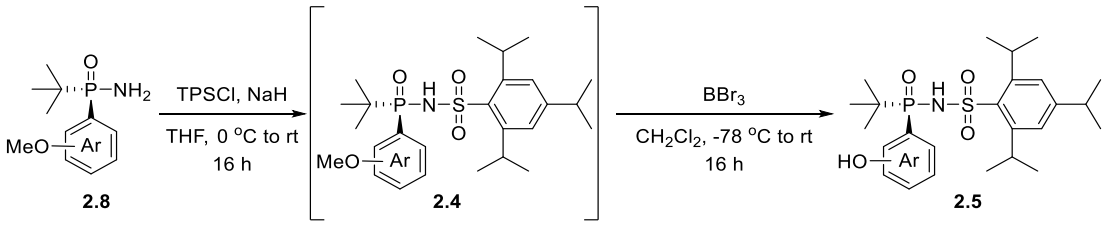

Note: Upon completion of the coupling reaction between intermediate **2.8** and the sulfonyl chloride, some analogs **2.4** were used directly in the subsequent demethylation step to get the final catalysts **2.5**.

Demethylation step: A solution of intermediates **2.3b** or **2.4** in dry DCM (5 mL) was cooled to -78 °C, then BBr_3 (1.2 equiv in hexane) was added slowly over a 5 min period. After the addition was finished, the reaction mixture was allowed to warm-up to RT and stirred overnight. The reaction was quenched with water and diluted with DCM. The organic fraction was washed with 1 N HCl, dried over anhydrous $MgSO_4$, concentrated and purified by flash column chromatography on silica gel. The isolated product was re-dissolved in DCM (15 mL) and thoroughly washed with 4 M HCl (15 mL x 2) to remove any metal impurities and completely protonate the catalyst. The organic layer was separated and concentrated under reduced pressure. The residue was taken up in toluene (5 mL), evaporated to dryness again and allowed to dry under high vacuum for a minimum of 24 h to give (*R*)-phenolic catalyst.

(R)-N-(tert-butyl(2-hydroxyphenyl)phosphoryl)-2,4,6-triisopropylbenzenesulfonamide (2.5a)

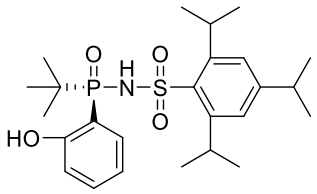

Compound was isolated as a yellow solid in 92% yield (221 mg). ^{1}H NMR (400 MHz, $CDCl_3$): δ 10.60 (s, 1H), 7.42 (ddt, *J* = 8.4, 7.1, 1.4 Hz, 1H), 7.31-7.23 (m, 1H), 7.14 (s, 2H), 6.97 – 6.89 (m, 1H), 6.84 – 6.75 (m, 1H), 6.41 (d, *J* = 8.7 Hz, 1H), 3.91 (hept, *J* = 6.6 Hz, 2H), 2.90 (hept, *J* = 6.9 Hz, 1H), 1.30 – 1.14 (m, 27H). ^{13}C NMR (126 MHz, $CDCl_3$): δ 163.6 (d, *J* = 5.0 Hz), 153.7, 150.3, 135.1 (d, *J* = 2.1 Hz), 134.2 (s), 133.0 (d, *J* = 8.4 Hz), 123.9, 118.8 (d, *J* = 12.5 Hz), 118.0 (d, *J* = 9.3 Hz), 107.5 (d, *J* = 117.5 Hz), 34.6 (d, *J* = 86.2 Hz), 34.2, 30.1, 24.7 (d, *J* = 47.0 Hz), 23.8, 23.5 (d, *J* = 4.2 Hz). ^{31}P NMR (162 MHz, $CDCl_3$): δ 45.42. HRMS: calculated for $C_{25}H_{39}NO_4PS^+$ $[M+H]^+$: 480.2332, found: 480.2336.

***(R)-N-(tert-butyl(4-hydroxyphenyl)phosphoryl)-2,4,6-triisopropylbenzenesulfonamide*: (2.5b)**

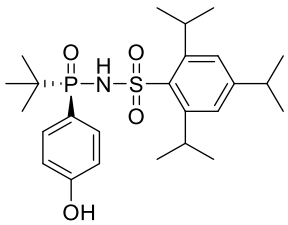

Isolated as a yellow solid, in 80% yield (193 mg). ^{1}H NMR (500 MHz, MeOD): δ 7.51–7.44 (m, 2H), 7.17 (s, 2H), 6.77 (dd, *J* = 8.5, 2.5 Hz, 2H), 4.27–4.14 (m, 2H), 2.96–2.87 (m, 1H), 1.31–1.20 (m, 12H), 1.18–1.03 (m, 15H). ^{13}C NMR (126 MHz, MeOD): δ 161.4, 152.4, 149.6, 136.6, 134.8 (d, *J* = 11.0 Hz), 123.1, 116.5 (d, *J* = 125.4 Hz), 114.7 (d, *J* = 13.8 Hz), 34.0, 33.1 (d, *J* = 93.4 Hz), 28.9, 23.8 (d, *J* = 38.7 Hz), 23.0, 22.7 (d,

J = 6.2 Hz). ^{31}P NMR (203 MHz, MeOD): δ 41.15. HRMS: calculated for $C_{25}H_{39}NO_4PS^+$ $[M+H]^+$: 480.2332, found: 480.2335.

(R)-N-(tert-butyl(2-hydroxynaphthalen-1-yl)phosphoryl)-2,4,6-triisopropylbenzenesulfonamide **(2.5c)**

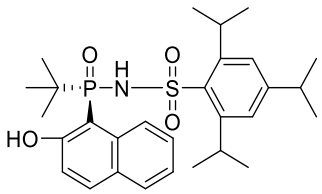

Isolated as a yellow solid in 95% yield (252 mg). ^{1}H NMR (400 MHz, $CDCl_3$): δ 12.55 (s, 1H), 8.15 (m, 1H), 7.88 (d, *J* = 8.9 Hz, 1H), 7.70 (m, 1H), 7.25 – 7.20 (m, 2H), 7.15 – 7.06 (m, 3H), 6.56 (s, 1H), 3.88 (hept, *J* = 6.7 Hz, 2H), 2.88 (hept, *J* = 6.9 Hz, 1H), 1.36 – 1.14 (m, 21H), 1.11 (d, *J* = 6.7 Hz, 6H). ^{13}C NMR (126 MHz, $CDCl_3$): δ 166.5 (d, *J* = 4.8 Hz), 153.4, 150.1, 136.5 (d, *J* = 2.3 Hz), 134.6, 133.6 (d, *J* = 8.6 Hz), 128.4 (d, *J* = 10.2 Hz), 128.0 (d, *J* = 197.2 Hz), 125.5 (d, *J* = 4.2 Hz), 123.9, 123.2, 120.4 (d, *J* = 11.1 Hz), 36.8 (d, *J* = 85.8 Hz), 34.2, 30.2, 24.8, 24.7 (d, *J* = 39.8 Hz), 23.5 (d, *J* = 4.6 Hz). ^{31}P NMR (162 MHz, $CDCl_3$): δ 47.72. HRMS: calculated for $C_{29}H_{41}NO_4PS^+$ $[M+H]^+$: 530.2488, found: 530.2496.

(R)-N-(tert-butyl(2-hydroxy-5,6,7,8-tetrahydronaphthalen-1-yl)phosphoryl)-2,4,6-triisopropylbenzenesulfonamide **(2.5d)**:

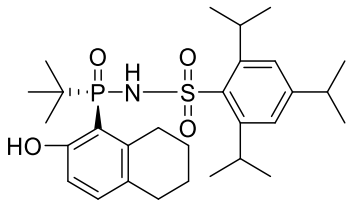

Isolated as a yellow solid in 93% yield (248 mg). ^{1}H NMR (400 MHz, $CDCl_3$): δ 11.50 (s, 1H), 7.17 (s, 2H), 7.14 (d, *J* = 8.4 Hz, 1H), 6.75 (dd, *J* = 8.4, 5.2 Hz, 1H), 6.19 (d, *J* = 10.9 Hz, 1H), 3.97 (hept, *J* = 6.5 Hz, 2H), 3.13 (ddd, *J* = 15.9, 10.1, 5.4 Hz, 1H), 2.95

– 2.78 (m, 2H), 2.75 – 2.67 (m, 2H), 1.98 – 1.68 (m, 4H), 1.31 (d, *J* = 6.6 Hz, 6H), 1.27 – 1.22 (m, 12H), 1.18 (d, *J* = 16.6 Hz, 9H). ^{13}C NMR (126 MHz, $CDCl_3$): δ 162.9 (d, *J* = 5.6 Hz), 153.3, 150.2, 140.3 (d, *J* = 9.1 Hz), 136.0, 135.0, 128.9 (d, *J* = 10.4 Hz), 124.0, 116.4 (d, *J* = 11.0 Hz), 106.3 (d, *J* = 109.8 Hz), 36.2 (d, *J* = 83.9 Hz), 34.1, 30.3, 29.5, 24.8 (d, *J* = 84.6 Hz), 24.8 (d, *J* = 14.8 Hz), 24.3, 23.6, 22.4, 22.1. ^{31}P NMR (162 MHz, $CDCl_3$): δ 49.00. HRMS: calculated for $C_{29}H_{45}NO_4PS^+$ $[M+H]^+$: 534.2801, found: 534.2808.

(R)-N-(tert-butyl(2-hydroxy-6-phenylnaphthalen-1-yl)phosphoryl)-2,4,6-triisopropylbenzenesulfonamide **(2.5e)**

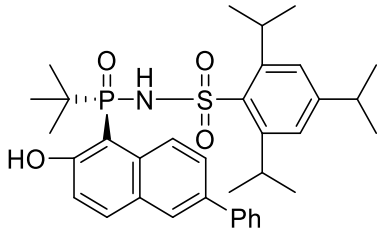

Isolated as a yellow solid in 88% yield (267 mg). ^{1}H NMR (500 MHz, $CDCl_3$) δ 12.49 (s, 1H), 8.30 (d, J = 8.9 Hz, 1H), 7.85 (d, J = 8.9 Hz, 1H), 7.64 (s, 1H), 7.44 – 7.30 (m, 6H), 7.17 (s, 2H), 7.13 (dd, J = 8.9, 4.7 Hz, 1H), 3.98 (hept, J = 6.7 Hz, 2H), 2.89 (hept, J = 6.9 Hz, 1H), 1.35 (d, J = 6.7 Hz, 6H), 1.28 – 1.12 (m, 21H). ^{13}C NMR (126 MHz, $CDCl_3$): δ 166.2 (d, *J* = 4.3 Hz), 153.6, 150.6, 140.0, 136.8, 135.3, 134.7, 132.9 (d, *J* = 8.7 Hz), 128.6 (d, *J* = 10.1 Hz), 128.3, 126.9, 126.6 (d, *J* = 126.9 Hz), 126.3 (d, *J* = 4.1 Hz), 124.0, 120.3 (d, *J* = 10.8 Hz), 98.3 (d, *J* = 111.8 Hz), 36.9 (d, *J* = 85.1 Hz), 34.2, 30.3, 25.2, 24.6, 23.5 (d, *J* = 6.9 Hz). ^{31}P NMR (203 MHz, $CDCl_3$): δ 48.88. HRMS: calculated for $C_{35}H_{45}NO_4PS^+$ $[M+H]^+$: 606.2801, found: 606.2803.

General procedure for the transfer hydrogenation of quinolines **2.10** to the tetrahydroquinolines **2.11**:

General procedure for the synthesis of the racemic tetrahydroquinolines:

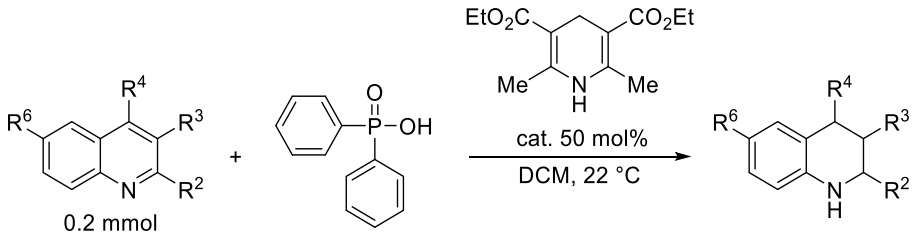

An oven dried 2 dram vial equipped with a stir bar was cooled to ambient temperature in a desiccator and subsequently charged with the requisite quinoline (0.200 mmol). DCM (1 mL), Hantzsch ester (152 mg, 0.600 mmol) and diphenylphosphinic acid (21.8 mg, 0.500 mmol). The vial was capped under air, sealed with parafilm and the mixture was stirred at RT for 2-24 h. Progress of the reaction was monitored by TLC (20% EtOAc and 80% hexanes). The crude product was purified by flash chromatography on silica gel (using EtOAc/hexanes) to afford the desired tetrahydroquinoline.

*General procedure for the asymmetric transfer hydrogenation of quinolines **2.10** to the tetrahydroquinolines **2.11***:

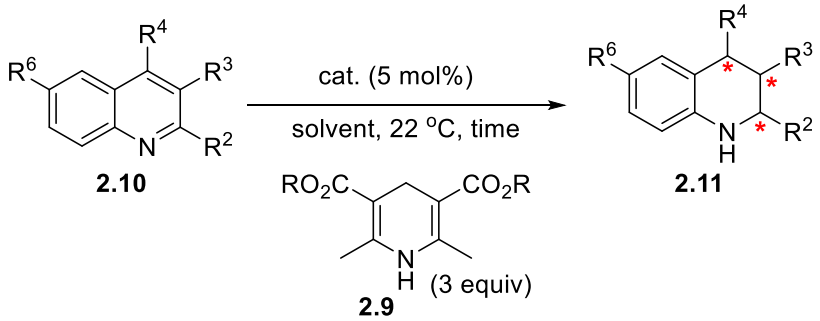

An oven-dried flask was fitted with magnetic stirring bar and charged with the quinoline (reactions were typically carried out at a 0.1-0.2 mmol scale), catalyst (5 mol%), Hantzsch ester (3.0 equiv) and solvent (0.5-1.0 mL). The resulting mixture was stirred at RT (~22 °C), unless otherwise indicated and monitored by TLC. When all starting

material was consumed, the solvent was removed under reduced pressure and the residue was purified by flash column chromatography on silica gel using the solvent system indicated to isolate the corresponding product.

(S)-6-bromo-2-methyl-1,2,3,4-tetrahydroquinoline (2.11a)

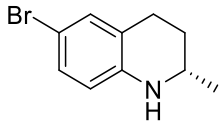

Reaction time: 5 h using catalyst **2.5c**. Known compound[37], purified using a 0-2% EtOAc/hexanes eluent gradient; isolated as white solid in 98% yield (44.2 mg) and 88% ee. The compound was crystallized from DCM/hexanes to afford the tetrahydroquinoline **2.11e** in 93% ee. ^{1}H NMR (500 MHz, $CDCl_3$): δ 7.09 – 7.05 (d, *J* = 2.4 Hz, 1H), 7.03 (dd, *J* = 8.4, 2.4 Hz, 1H), 6.34 (d, *J* = 8.4 Hz, 1H), 3.76 (s, 1H), 3.38 (dqd, *J* = 9.3, 6.3, 2.9 Hz, 1H), 2.80 (ddd, *J* = 17.0, 11.5, 5.7 Hz, 1H), 2.75 – 2.64 (dt, 1H), 1.98 – 1.87 (m, 1H), 1.55 (m, 1H), 1.20 (d, *J* = 6.3 Hz, 3H). ^{13}C NMR (101 MHz, CDCl3): δ 143.9, 131.8, 129.5, 123.3, 115.5, 108.4, 47.2, 29.8, 26.5, 22.6. Chiral HPLC method: chiralcel OD-H, hexane/IPA = 98/2, 1.0 mL/min, λ = 254 nm; (*R*)-enantiomer t_R (minor) = 8.6 min, (*S*)-enantiomer t_R (major) = 11.2 min.

For the purpose of comparison the product was also analyzed using the same chiral HPLC column and solvent system as previously reported:[37] [9] Chiralcel OJ-H, hexane/IPA = 95/5, 0.8 mL/min, λ = 254 nm; (*S*)-enantiomer t_R (major) = 19.04 min, (*R*)-enatiomer t_R (minor) = 23.19 min.

(S)-2-methyl-1,2,3,4-tetrahydroquinoline (2.11b)

NMR and chiral HPLC data consistent with those previously reported.[38]

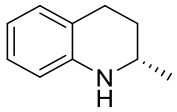

Compound was purified using a 0-1% EtOAc/hexanes as the eluent; isolated as a pale-yellow oil in 73% yield (21.6 mg) and 88% ee. ^{1}H NMR (500 MHz, $CDCl_3$): δ 7.02 – 6.90 (m, 2H), 6.60 (td, *J* = 7.3, 1.2 Hz, 1H), 6.47 (dd, *J* = 8.4, 1.2 Hz, 1H), 3.70 (broad s, 1H), 3.40 (dqd, *J* = 10.0, 6.3, 2.8 Hz, 1H), 2.90 – 2.78 (m, 1H), 2.73 (ddd, *J* = 16.3, 5.2, 3.4 Hz, 1H), 1.93 (dddd, *J* = 12.8, 5.6, 3.4, 2.8 Hz, 1H), 1.63 – 1.55 (m, 1H), 1.21 (d, *J* = 6.3 Hz, 3H). ^{13}C NMR (126 MHz, $CDCl_3$): δ 144.9, 129.4, 126.8, 121.3, 117.1, 114.1, 47.3, 30.3, 26.7, 22.8. Chiral HPLC method: Chiralcel OD, hexane/IPA = 98/2, 1.0 mL/min, λ = 254 nm; (*R*)-enantiomer t_R (minor) = 6.78 min, (*S*)-enantiomer (majot) t_R = 7.79 min.

(R)-2-phenyl-1,2,3,4-tetrahydroquinoline (2.11c)

NMR and chiral HPLC data consistent with those previously reported.[38]

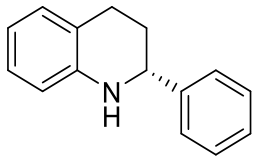

Compound was purified using a 0-3% EtOAc/hexanes eluent and isolated as a white solid 95% yield (39.9 mg) and 59.3% ee. ^{1}H NMR (500 MHz, $CDCl_3$): δ 7.45 – 7.33 (m, 4H), 7.32 – 7.27 (m, 1H), 7.07 – 6.97 (m, 2H), 6.66 (td, *J* = 7.3, 1.2 Hz, 1H), 6.55 (d, *J* = 7.5 Hz, 1H), 4.45 (dd, *J* = 9.4, 3.3 Hz, 1H), 4.05 (s, 1H), 2.93 (ddd, *J* = 16.2, 10.7, 5.5 Hz, 1H), 2.75 (dt, *J* = 16.3, 4.8 Hz, 1H), 2.13 (dddd, *J* = 13.1, 5.4, 4.5, 3.3 Hz, 1H), 2.00 (dddd, *J* = 13.0, 10.7, 9.3, 5.1 Hz, 1H). ^{13}C NMR (126 MHz, CDCl3): δ 144.9, 144.9, 129.4, 128.7, 127.6, 127.0, 126.7, 121.0, 117.3, 114.1, 56.4, 31.1, 26.5. Chiral HPLC method: Chiralcel OD, hexane/IPA = 98/2, 1.0 mL/min, λ = 254 nm; (*S*)-enantiomer t_R (minor) = 15.13 min, (*R*)-enantiomer t_R (major) = 21.39 min (major).

(R)-4-methyl-1,2,3,4-tetrahydroquinoline (2.11d)

NMR and chiral HPLC data consistent with those previously reported[29]

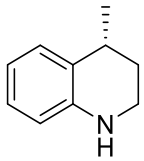

Compound purified using a 0-20% Et_2O in pentane and isolated a pale-yellow oil in 70% yield and 30% ee. ^{1}H NMR (500 MHz, $CDCl_3$): δ 7.06 (d, J = 7.6 Hz, 1H), 6.96 (tdd, *J* = 7.3, 1.7, 0.8 Hz, 1H), 6.63 (td, *J* = 7.4, 1.2 Hz, 1H), 6.48 (dd, *J* = 7.9, 1.2 Hz, 1H), 3.91 (s, 1H), 3.39 – 3.23 (m, 2H), 2.92 (h, *J* = 6.6 Hz, 1H), 2.04 – 1.94 (m, 1H), 1.68 (dddd, *J* = 13.0, 6.9, 6.1, 3.5 Hz, 1H), 1.29 (d, *J* = 7.0 Hz, 3H). ^{13}C NMR (126 MHz, CDCl3): δ 144.3, 128.6, 126.9, 126.8, 117.1, 114.3, 39.2, 30.4, 30.0, 22.8. Chiral HPLC method: Chiralcel OD, hexane/IPA = 98/2, 0.6 mL/min, λ = 254 nm; (*S*)-enantiomer t_R (minor) = 16.41 min, (*R*)-enantiomer t_R (major) = 17.67 min.

(S)-2-ethyl-1,2,3,4-tetrahydroquinoline (2.11e)

NMR and chiral HPLC data consistent with those previously reported.[38]

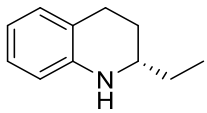

Compound was purified using a 0-2% EtOAc in hexanes and isolated as a pale-yellow oil in 72% yield (23.1 mg) and 75% ee. ^{1}H NMR (500 MHz, $CDCl_3$): δ 6.96 (ddt, *J* = 8.2, 7.4, 0.8 Hz, 2H), 6.60 (td, *J* = 7.4, 1.2 Hz, 1H), 6.48 (dt, *J* = 7.4, 1.3 Hz, 1H), 3.77 (s, 1H), 3.17 (dtd, *J* = 9.4, 6.4, 2.9 Hz, 1H), 2.88 – 2.77 (m, 1H), 2.73 (ddd, *J* = 16.3, 5.4, 4.0 Hz, 1H), 1.98 (dddd, *J* = 12.7, 5.6, 4.0, 2.9 Hz, 1H), 1.65 – 1.56 (m, 1H), 1.56 – 1.49 (m, 2H), 1.00 (t, *J* = 7.5 Hz, 3H). ^{13}C NMR (126 MHz, $CDCl_3$): δ 144.9, 129.4, 126.8, 121.5, 117.0, 114.1, 53.2, 29.6, 27.7, 26.6, 10.2. Chiral HPLC method: Chiralcel OD, hexane/IPA = 98/2, 1.0 mL/min, λ = 254 nm; (*R*)-enantiomer t_R (minor) = 6.56 min, (*S*)-enantiomer t_R (major) = 7.91 min.

(R)-2-isopropyl-1,2,3,4-tetrahydroquinoline (2.11f)

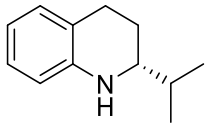

NMR and chiral HPLC data consistent with those previously reported,[38] purified using a 0-2% EtOAc/hexanes eluent; isolated as a pale-yellow oil in 77% yield (27.0 mg) and 66% ee.^{1}H NMR (500 MHz, $CDCl_3$): δ 7.00 – 6.91 (m, 2H), 6.59 (td, *J* = 7.3, 1.2 Hz, 1H), 6.52 – 6.45 (m, 1H), 3.76 (s, 1H), 3.04 (ddd, *J* = 10.0, 5.9, 2.9 Hz, 1H), 2.81 (ddd, *J* = 16.5, 11.3, 5.5 Hz, 1H), 2.77 – 2.70 (m, 1H), 1.92 (dddd, *J* = 12.5, 5.5, 3.9, 2.9 Hz, 1H), 1.77 – 1.60 (m, 2H), 1.00 (d, *J* = 6.8 Hz, 3H), 0.98 (d, *J* = 6.8 Hz, 3H). ^{13}C NMR (126 MHz, $CDCl_3$): δ 145.2, 129.3, 126.8, 121.6, 116.9, 114.1, 57.4, 32.7, 26.8, 24.7, 18.7, 18.4. Chiral HPLC method: Chiralcel OD, hexane/IPA = 98/2, 1.0 mL/min, λ = 254 nm; (*S*)-enantiomer t_R (minor) = 5.90 min, (*R*)-enantiomer t_R (major) = 8.53 min.

(S)-2-methyl-6-nitro-1,2,3,4-tetrahydroquinoline (2.11g)

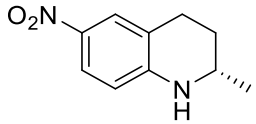

NMR and chiral HPLC data consistent with those previously reported.[39] Compound was purified by flash column chromatography on silica gel (silica gel was deactivated with a 1% Et_3N in hexanes solution) using a 0-15% EtOAc/hexanes eluent gradient; isolated an orange solid in 83% yield (31.8 mg) and 86% ee. The compound was recrystallized from DCM/hexanes to afford the tetrahydroquinoline in 96% ee. ^{1}H NMR (500 MHz, $CDCl_3$): δ 7.95 – 7.86 (m, 2H), 6.42 – 6.32 (m, 1H), 4.53 (s, 1H), 3.55 (dqd, *J* = 9.7, 6.4, 3.4 Hz, 1H), 2.90 – 2.74 (m, 2H), 2.00 (dtd, *J* = 12.9, 4.8, 3.4 Hz, 1H), 1.58 (dtd, *J* = 13.0, 9.8, 6.2 Hz, 1H), 1.28 (d, *J* = 6.4 Hz, 3H). ^{13}C NMR (126 MHz, $CDCl_3$): δ 150.4, 137.5, 125.9, 124.4, 119.8, 112.2, 47.6, 29.0, 26.3, 22.4. Chiral HPLC method: Chiralcel OD, hexane/IPA = 95/5, 1 mL/min, λ = 254 nm; (*R*)-enantiomer t_R (minor) =

19.35 min, (*S*)-enantiomer t_R (major) = 20.67 min (major).

(R)-3-methyl-1,2,3,4-tetrahydroquinoline (2.11h)

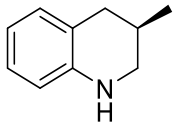

NMR and chiral HPLC data consistent with those previously reported.[40] Compound was purified by flash column chromatography on silica gel using a 0-10% pentane/Et_2O eluent; isolated as a pale-yellow oil in 71% yield (20.9 mg) and 14% ee. ^{1}H NMR (400 MHz, $CDCl_3$): δ 7.01-6.91 (m, 2H), 6.61 (td, *J* = 7.4, 1.2 Hz, 1H), 6.49 (dd, *J* = 7.9, 1.2 Hz, 1H), 3.89 (s, 1H), 3.27 (ddd, *J* = 11.0, 3.7, 2.0 Hz, 1H), 2.90 (dd, *J* = 11.0, 9.6 Hz, 1H), 2.78 (ddd, *J* = 16.0, 5.0, 2.0 Hz, 1H), 2.43 (dd, *J* = 16.0, 10.2 Hz, 1H), 2.14 – 1.99 (m, 1H), 1.05 (d, *J* = 6.6 Hz, 3H). ^{13}C NMR (126 MHz, $CDCl_3$) δ 144.4, 129.7, 126.8, 121.3, 117.1, 114.0, 49.0, 35.6, 27.3, 19.2. Chiral HPLC method: Chiralcel OJ-H, hexane/IPA = 90/10, 0.5 mL/min, λ = 210 nm; (*R*)-enantiomer t_R = 30.77 min (major), (S)- enantiomer t_R = 37.77 min (minor).

(R)-3-phenyl-1,2,3,4-tetrahydroquinoline **(2.11i)**

The precursor 3-phenylquinoline was synthesized according to literature procedure.[41]

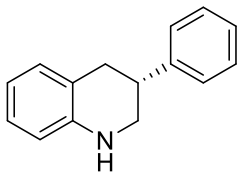

NMR and chiral HPLC data consistent with those previously reported.[30] Compound was purified by flash column chromatography on silica gel using 0-6% EtOAc/hexanes as the eluent; isolated as a pale-yellow solid in 51% yield (10.5 mg; yield based on recovered starting material) and 4% ee. ^{1}H NMR (400 MHz, $CDCl_3$) δ 7.39 – 7.30 (m, 2H), 7.30 – 7.22 (m, 3H), 7.02 (d, *J* = 7.4 Hz, 2H), 6.66 (td, *J* = 7.4, 1.2 Hz, 1H), 6.57

(dd, *J* = 8.4, 1.3 Hz, 1H), 4.15 (s, 1H), 3.47 (ddd, *J* = 11.2, 3.7, 1.9 Hz, 1H), 3.35 (t, *J* = 10.7 Hz, 1H), 3.16 (tdd, *J* = 10.2, 5.8, 3.7 Hz, 1H), 3.09 – 2.93 (m, 2H). ^{13}C NMR (101 MHz, $CDCl_3$) δ 144.1, 144.0, 129.7, 128.8, 127.4, 127.1, 126.8, 121.6, 117.3, 114.3, 48.5, 38.8, 34.8. Chiral HPLC method: Chiralcel OD, hexane/IPA = 98/2, 1 mL/min, λ = 254 nm; (R)-enantiomer t_R = 18.81 min (major), (S)- 10.5 mg t_R = 24.04 min (minor).

Methyl (R)-1,2,3,4-tetrahydroquinoline-2-carboxylate **(2.11j**)

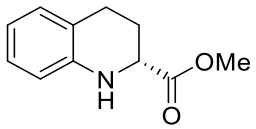

Reaction time: 4 h at 50 °C using catalyst **5c**. NMR and chiral HPLC data consistent with those previously reported.[42] purified using a 0-8% Et_2O/hexanes eluent; isolated as a colourless oil in 71% yield (27.2 mg) and 30% ee. ^{1}H NMR (400 MHz, $CDCl_3$) δ 7.05 – 6.96 (m, 1H), 6.96 (d, *J* = 7.5 Hz, 1H), 6.65 (td, *J* = 7.3, 1.2 Hz, 1H), 6.59 (dd, *J* = 8.0, 1.2 Hz, 1H), 4.40 (s, 1H), 4.05 (dd, *J* = 8.8, 3.8 Hz, 1H), 3.78 (s, 3H), 2.90 – 2.71 (m, 2H), 2.29 (dtd, *J* = 13.0, 5.6, 3.8 Hz, 1H), 2.01 (dtd, *J* = 13.0, 9.1, 5.3 Hz, 1H). ^{13}C NMR (101 MHz, $CDCl_3$) δ 173.8, 143.1, 129.3, 127.2, 120.7, 117.8, 114.7, 54.1, 52.5, 26.0, 24.8. Chiral HPLC method: Chiralpak AD, hexane/IPA = 80/20, 1 mL/min, λ = 254 nm; (R)-t_R = 7.62 min (major), (S)-t_R = 9.04 min (minor).

Table 2.3. Solvent Screening and Optimization of Reaction Conditions.

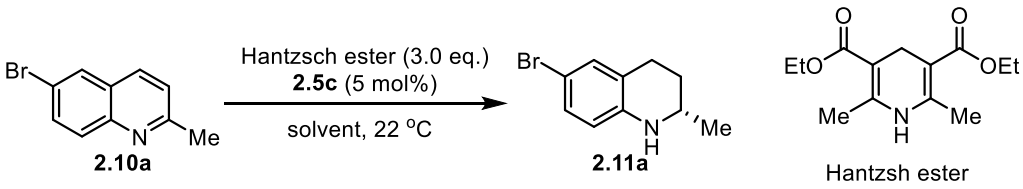

Entry	Solvent	Time (h)	Yield (%)	*ee* (%)
1	toluene	2	99	80
2	CH_2Cl_2	1.5	99	75
3	$CHCl_3$	0.5	99	80
4	CCl_4	1.5	99	86
5	DCE	1.5	99	78
6	cyclohexane	5	99	89
7	*n*-hexane	5	99	86
8	Et_2O	3	99	85
9	*t*-BuOMe	3	99	85
10	EtOAc	2	99	84

Table 2.4. Optimization of Hantzsch Ester.

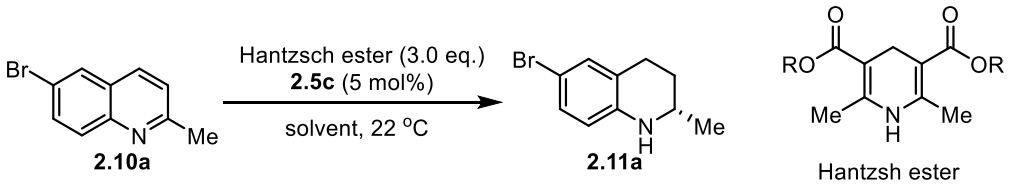

Entry	R	Time (h)	Yield (%)	*ee* (%)
1	Me	5	99	88
2	Et	5	99	89
3	*t*-Bu	3	99	85

2.7 Associated Content

NMR spectra and chiral HPLC data are provided in Appendix I.

2.8 Author Information

Corresponding Author

*Phone 514-398-3638. Fax 514-398-3797. Email: youla.tsantrizos@mcgill.ca

2.9 Acknowledgements

We are grateful to the Natural Sciences and Engineering Research Council of Canada (NSERC) for financial support (RGPIN-2015-05529). We wish to thank Boehringer-Ingelheim Pharmaceuticals Inc., USA, for their generous gift of the chiral auxiliary (R)-*N*-(1-(5-chloro-2-hydroxyphenyl)ethyl)-4-methylbenzenesulfonamide and Prof. Tomislav Friščić for access to his X-ray facility.

2.10 References

1. For an extensive review see: Parmar, D.; Sugiono, E.; Raja, S.; Rueping, M. Complete Field Guide to Asymmetric BINOL-Phosphate Derived Brønsted Acid and Metal Catalysis: History and Classification by Mode of Activation; Brønsted Acidity, Hydrogen Bonding, Ion Pairing, and Metal Phosphates. *Chem. Rev*. **2014**, *114*, 9047-9153; Additions and Corrections: Chem. Rev. **2017**, *117*, 10608-10620.

2. (a) Akiyama, T.; Itoh, J.; Yokota, K.; Fuchibe, K. Enantioselective Mannich-Type Reaction Catalyzed by a Chiral Brønsted Acid. *Angew. Chem. Int. Ed.* **2004**, *43*, 1566-1568. (b) Akiyama, T. Stronger Brønsted Acids. *Chem. Rev*. **2007**, *107*, 5744–5758.

3. Uraguchi, D.; Terada, M. Chiral Brønsted Acid-Catalyzed Direct Mannich Reactions via Electrophilic Activation. *J. Am. Chem. Soc.* **2004**, *126*, 5356-5357.

4. (a) Rueping, M.; Sugiono E.; Schoepke, F. R. Development of the First Brønsted Acid Assisted Enantioselective Brønsted Acid Catalyzed Direct Mannich Reaction. *Synlett* **2007**, *1441*-1445 (b) Guo, Q-X.; Liu, H.; Guo, C.; Luo, S-W.; Gu, Y.; Gong, L-Z. Chiral Brønsted Acid-Catalyzed Direct Asymmetric Mannich Reaction. *J. Am. Chem. Soc.* **2007**, *129*, 3790-3791 (c) Gridnev, I. D.; Kouchi, M.; Sorimachi, K.; Terada, M. On the Mechanism of Stereoselection in Direct Mannich Reaction Catalyzed by BINOL-derived Phosphoric Acids. *Tetrahedron Lett* **2007**, *48*, 497-500.

5. Nakashima, D.; Yamamoto, H. Design of Chiral *N*-Triflyl Phosphoramide as a Strong Chiral Brønsted Acid and Its Application to Asymmetric Diels−Alder Reaction. *J. Am. Chem. Soc*. **2006**, *128*, 9626-9627.

6. Akiyama, T.; Morita, H.; Itoh, J.; Fuchibe, K. Chiral Brønsted Acid Catalyzed Enantioselective Hydrophosphonylation of Imines: Asymmetric Synthesis of α-Amino Phosphonates. *Org. Lett.* **2005**, *7*, 2583-2585.

7. Storer, R. I.; Carrera, D. E.; Ni, Y.; MacMillan, D. W. C. Enantioselective Organocatalytic Reductive Amination. *J. Am. Chem. Soc.* **2006**, *128*, 84-86.

8. (a) Hoffmann, S.; Seayad, A. M.; List, B. A Powerful Brønsted Acid Catalyst for the Organocatalytic Asymmetric Transfer Hydrogenation of Imines. *Angew. Chem., Int. Ed*. **2005**, *44*, 7424-7427. (b) Rueping, M.; Sugiono, E.; Azap, C.; Theissmann, T.; Bolte, M. Enantioselective Brønsted Acid Catalyzed Transfer Hydrogenation: Organocatalytic Reduction of Imines. *Org. Lett.* **2005**, ***7***, 3781-3783. (c) Nguyen, T. B.; Bousserrouel, H.; Wang, Q.; Guéritte, F. Chiral Phosphoric Acid-Catalyzed Enantioselective Transfer Hydrogenation of ortho-Hydroxyaryl Alkyl N−H Ketimines. *Org. Lett.* **2010**, *12*, 4705-4707. (d) Greindl, J.; Hioe, J.; Sorgenfrei, N.; Morana, F.; Gschwind, R. M. Brønsted Acid Catalysis—Structural Preferences and Mobility in Imine/Phosphoric Acid Complexes. *J. Am. Chem. Soc.* **2016**, *138*, 15965-15971.

9. (a) Itoh, J.; Fuchibe, K.; Akiyama, T. Chiral Phosphoric Acid Catalyzed Enantioselective Friedel–Crafts Alkylation of Indoles with Nitroalkenes: Cooperative Effect of 3 Å Molecular Sieves. *Angew. Chem. Int. Ed.* **2008**, *47*, 4016-4018. (b) Zeng, M.; Kang, Q.; He, Q-L.; You, S-L. Highly Enantioselective Friedel–Crafts Reaction of 4,7-Dihydroindoles with β,γ-Unsaturated α-Keto Esters by Chiral Brønsted Acids. *Adv. Synth. Catal.* **2008**, *350*, 2169-2173. (c) Zhang, J-W.; Cai, Q.; Shi, X-X.; Zhang, W.; You, S-L. Enantioselective Synthesis of Tetrahydropyrano[3,4-b]indoles Catalyzed by Chiral N-Triflyl Phosphoramide via Intramolecular Friedel-Crafts Alkylation Reaction. *Synlett*, **2011**, 1239-1242.

10. Zhang, L-D.; Zhong, L-R.; Xi, J.; Yang, X-L.; Yao, Z-J. Enantioselective Total Synthesis of Lycoposerramine-Z Using Chiral Phosphoric Acid Catalyzed Intramolecular Michael Addition. *J. Org. Chem.* **2016**, *81*, 1899-1904.

11. Vellalath, S.; Čorić, I.; List, B. N-Phosphinyl Phosphoramide—A Chiral Brønsted Acid Motif for the Direct Asymmetric N,O-Acetalization of Aldehydes. *Angew. Chem. Int. Ed.* **2010**, *49*, 9749-9752.

12. For recent reviews, see: (a) Rueping, M.; Dufour, J.; Schoepke, F. R. Advances in Catalytic Metal-Free Reductions: from Bio-Inspired Concepts to Applications in the Organocatalytic Synthesis of Pharmaceuticals and Natural Products. *Green Chem.* **2011**, *13*, 1084-1105. (b) Phillips, A. M. F.; Pombeiro, A. J. L. Recent Advances in Organocatalytic Enantioselective Transfer Hydrogenation. *Org. Biomol. Chem.* **2017**, *15*, 2307-2340.

13. Das, A.; Volla, C. M. R.; Atodiresei, I.; Bettray, W.; Rueping, M. Asymmetric Ion Pair Catalysis of 6π Electrocyclizations: Brønsted Acid Catalyzed Enantioselective Synthesis of Optically Active 1,4-Dihydropyridazines. *Angew. Chem. Int. Ed.* **2013**, ***52***, 8008-8011.

14. (a) Tsuji, N.; Kennemur, J. L.; Buyck, T.; Lee, S.; Prévost, S.; Kaib, P. S. J.; Bykov, D.; Farès, C.; List, B. Activation of Olefins via Asymmetric Brønsted Acid Catalysis. *Science*, **2018**, *359*, 1501-1505. (b) Bae, H. Y.; Höfler, D.; Kaib, P. S. J.; Kasaplar, P.; De, C. K.; Döhring, A.; Lee, S.; Kaupmees, K.; Leito, I.; List, B.

Approaching Sub-ppm-level Asymmetric Organocatalysis of a Highly Challenging and Scalable Carbon–Carbon Bond Forming Reaction. *Nat. Chem.*, **2018**, *10*, 888-894.

15. (a) Cheon, C. H.; Yamamoto, H. A Brønsted Acid Catalyst for the Enantioselective Protonation Reaction. *J. Am. Chem. Soc.* **2008**, *130*, 9246-9247. (b) Cheon, C. H.; Yamamoto, H. A. N-Triflylthiophosphoramide Catalyzed Enantioselective Mukaiyama Aldol Reaction of Aldehydes with Silyl Enol Ethers of Ketones. *Org. Lett.* **2010**, *12*, 2476-2479.

16. Rueping, M.; Azap, C.; Sugiono, E.; Theissmann, T. Brønsted Acid Catalysis: Organocatalytic Hydrogenation of Imines. *Synlett* **2005**, 2367-2369.

17. Kaupmees, K.; Tolstoluzhsky, N.; Raja, S,; Rueping, M.; Leito, I. On the Acidity and Reactivity of Highly Effective Chiral Brønsted Acid Catalysts: Establishment of an Acidity Scale. *Angew. Chem. Int. Ed.* **2013**, *52*, 11569-11572.

18. (a) Christ, P.; Lindsay, A. G.; Vormittag, S. S.; Neudörfl, J. M.; Berkessel, A.; O'Donoghue, A. C. pK_a Values of Chiral Brønsted Acid Catalysts: Phosphoric Acids/Amides, Sulfonyl/Sulfuryl Imides, and Perfluorinated TADDOLs (TEFDDOLs). *Chem. Eur. J.* **2011**, *17*, 8524-8528. (b) Yang, C.; Xue, X-S.; Jin, J-L.; Li, X.; Cheng J-P. Theoretical Study on the Acidities of Chiral Phosphoric Acids in Dimethyl Sulfoxide: Hints for Organocatalysis. *J. Org. Chem.*, **2013**, *78*, 7076-7085.

19. (a) Vellalath, S.; Čorić, I.; List, B. *N*-Phosphinyl Phosphoramide—A Chiral Brønsted Acid Motif for the Direct Asymmetric *N*,*O*-Acetalization of Aldehydes. *Angew. Chem. Int. Ed.* **2010**, *49*, 9749-9752. (b) Wakchaure, V. N.; List, B. A New Structural Motif for Bifunctional Brønsted Acid/Base Organocatalysis. *Angew. Chem. Int. Ed.* **2010**, *49*, 4136-4139.

20. Han, Z. S.; Wu, H.; Qu, B.; Wang, Y.; Wu, L.; Zhang, L.; Xu, Y.; Wu, L.; Zhang, Y.; Lee, H.; Roschangar, F.; Song, J. J.; Senanayake, C. H. New Class of *P*-Stereogenic Chiral Brønsted Acid Catalysts Derived from Chiral Phosphinamides. *Tetrahedron Lett.* **2019**, *60*, 1834-1837.

21. Li, S-G.; Yuan, M.; Topic, F.; Han, Z. S.; Senanayake, C. H. Tsantrizos, Y. S. Asymmetric Library Synthesis of P-Chiral t-Butyl-Substituted Secondary and Tertiary Phosphine Oxides. *J. Org. Chem.* **2019**, *84*, 7291-7302.

22. Han, Z. S.; Wu, H.; Xu, Y.; Zhang, Y.; Qu, B.; Li, Z.; Caldwell, D. R.; Fandrick, K. R.; Zhang, L.; Roschangar, F.; Song, J. J.; Senanayake, C. H. General and Stereoselective Method for the Synthesis of Sterically Congested and Structurally Diverse P-Stereogenic Secondary Phosphine Oxides. *Org. Lett.*, **2017**, *19*, 1796-1799.

23. (a) Atherton, F. R.; Openshaw, H. T.; Todd, A. R. Studies on Phosphorylation. Part II. The Reaction of Dialkyl Phosphites with Polyhalogen Compounds in Presence of Bases. A New Method for the Phosphorylation of Amines. *J. Chem. Soc.* **1945**, 660-663. (b) Le Corre, S. S.; Berchel, M.; Couthon-Gourvès, H.; Haelters, J-P.; Jaffrès, P-A. Atherton-Todd Reaction: Mechanism, Scope and Applications. *Beilstein J. Org. Chem.* **2014**, *10*, 1166-1196.

24. Rueping, M.; Antonchick, A. P.; Theissmann, T. A Highly Enantioselective Brønsted Acid Catalyzed Cascade Reaction: Organocatalytic Transfer Hydrogenation of Quinolines and their Application in the Synthesis of Alkaloids. *Angew. Chem. Int. Ed.* **2006**, *45*, 3683-3686.

25. (a) Mauzerall, D.; Westheimer, F. H. 1-Benzyldihydronicotinamide—A Model for Reduced DPN. *J. Am. Chem. Soc.* **1955**, *77*, 2261-2264. (b) Abeles, R.; Westheimer, F. H. The Reduction of Ketoacids with a Derivative of 1,4-Dihydropyridine. *J. Am. Chem. Soc.* **1958**, *80*, 5459-5460. (c) Richter, D.; Mayr, H. Hydride-Donor Abilities of 1,4-Dihydropyridines: A Comparison with π Nucleophiles and Borohydride Anions. *Angew. Chem. Int. Ed.* **2009**, *48*, 1958-1961.

26. (a) Snider, B. B.; Ahn, Y.; O'Hare, S. M. Total Synthesis of (±)-Martinellic Acid. *Org. Lett.* **2001**, *3*, 4217-4220. (b) Davies, S. G.; Fletcher, A. M. Lee, J. A.; Lorkin, T. J. A.; Roberts, P. M.; Thomson, J. E. Asymmetric Synthesis of (−)-Martinellic Acid. *Org. Lett.* **2013**, *15*, 2050-2053.

27. Tsutsumi, H.; Katsuyama, Y.; Izumikawa, M.; Takagi, M.; Fujie, M.; Satoh, N.; Shinya, K.; Ohnishi, Y. Unprecedented Cyclization Catalyzed by a Cytochrome P450 in Benzastatin Biosynthesis. *J. Am. Chem. Soc.* **2018**, *140*, 6631-6639.

28. (a) Basarab, G. S.; Doig, P.; Galullo, V.; Kern, G..; Kimzey, A.; Kutschke, A.; Newman, J. P.; Morningstar, M.; Mueller, J.; Otterson, L.; Vishwanathan, K.; Zhou, F.; Gowravaram, M. Discovery of Novel DNA Gyrase Inhibiting Spiropyrimidinetriones: Benzisoxazole Fusion with N-Linked Oxazolidinone Substituents Leading to a Clinical Candidate (ETX0914). *J. Med. Chem.*, **2015**, *58*, 6264-6282. (b) Taylor, S. N.; Marrazzo, J.; Batteiger, B. E.; Hook III, E. W.; Seña, A. C.; Long, J.; Wierzbicki, M. R.; Kwak, H.; Johnson, S. M.; Lawrence, K.; Mueller, J. Single-Dose Zoliflodacin (ETX0914) for Treatment of Urogenital Gonorrhea. *N. Engl. J. Med.* **2018**, *379*, 1835-1845.

29. Rueping, M.; Theissmann, T.; Stoeckel, M.; Antonchick, A. P. Direct Enantioselective Access to 4-Substituted Tetrahydroquinolines by Catalytic Asymmetric Transfer Hydrogenation of Quinolines. *Org. Biomol. Chem.* **2011**, *9*, 6844-6850.

30. Rueping, M.; Theissmann, T.; Raja, S.; Bats, J. W. Asymmetric Counterion Pair Catalysis: An Enantioselective Brønsted Acid-Catalyzed Protonation. *Adv. Synth. Catal.* **2008**, *350*, 1001-1006.

31. Park, D. Y.; Lee, S. Y.; Jeon, J.; Cheon, C-H. Enantioselective Synthesis of Tetrahydroquinolines from 2-Aminochalcones via a Consecutive One-Pot Reaction Catalyzed by Chiral Phosphoric Acid. *J. Org. Chem.* **2018**, *83*, 12486-12495.

32. Qian, B.; Guo, S.; Shao, J.; Zhu, Q.; Yang, L.; Xia, C.; Huang, H. Palladium-Catalyzed Benzylic Addition of 2-Methyl Azaarenes to N-Sulfonyl Aldimines via C−H Bond Activation. *J. Am. Chem. Soc*. **2010**, *132*, 3650–3651.

33. Wen, J.; Tan, R.; Liu, S.; Zhao, Q.; Zhang, X. Strong Brønsted Acid Promoted Asymmetric Hydrogenation of Isoquinolines and Quinolines Catalyzed by a Rh–Thiourea Chiral Phosphine Complex via Anion Binding. *Chem. Sci*., **2016**, *7*, 3047–3051.

34. (a) Matsugi, M.; Tabusa, F.; Minamikawa, J. Doebner-Miller Synthesis in a Two-phase System: Practical Preparation of Quinolines. *Tetrahedron Lett*. **2000**, *41*, 8523–8525. (b) Tahtaoui, C.; Guillier, F.; Klotz, P.; Galzi, J-L.; Hibert, M.; Ilien, B. On the Use of Nonfluorescent Dye Labeled Ligands in FRET-Based Receptor Binding Studies. *J. Med. Chem*. **2005**, *48*, 7847-7859.

35. Jolliffe, J.D.; Armstrong, R.J.; Smith, M.D. Catalytic Enantioselective Synthesis of Atropisomeric Biaryl by a Cation-Directed O-Alkylation. *Nature Chem*. **2017**, *9*, 558-562.

36. Han, Z. S.; Zhang, L,; Xu, Y.; Sieber, J. D.; Marsini, M. A.; Li, Z.; Reeves, J. T.; Fandrick, K. R.; Patel, N. D.; Desrosiers, J.; Qu, B.; Chen, A.; Rudzinski, D. M.; Samankumara, L. P.; Ma, S.; Grinberg, N.; Roschangar, F.; Yee, N. K.; Wang, G.; Song,J. J.; Senanayake, C. H. Efficient Asymmetric Synthesis of Structurally Diverse *P*-Stereogenic Phosphinamides for Catalyst Design. *Angew. Chem. Int. Ed*. **2015**, *54*, 5474-5477.

37. Yang, T.; Yin, Q.; Gu, G.; Zhang, X. A One-Pot Process for the Enantioselective Synthesis of Tetrahydroquinolines and Tetrahydroisoquinolines via Asymmetric Reductive Amination (ARA). *Chem. Commun*. **2018**, *54*, 7247-7250.

38. Wang, C.; Li, C.; Wu, X.; Pettman A.; Xiao, J. pH-Regulated Asymmetric Transfer Hydrogenation of Quinolines in Water. *Angew. Chem. Int. Ed*. **2009**, *48*, 6524–6528.

39. Gou, F-R.; Zhang, X.; Liang, Y-M. Iridium-Catalyzed Asymmetric Hydrogenation of Quinoline Derivatives with C3*-TunePhos. *Adv. Synth. Catal.* **2010**, *352*, 2441-2444.

40. Zhao, X.; Xiao, J.; Tang. W. Enantioselective Reduction of 3-Substituted Quinolines with a Cyclopentadiene-Based Chiral Brønsted Acid. *Synthesis*, **2017**, *49*, 3157–3164.

41. Batsyts, S.; Vedmid, R.; Namyslo, J. C.; Nieger, M.; Schmidt, A. 3-Aryl Substituted 1-Methylquinolinium Salts as Carbene Precursors. Eur. J. Org. Chem., 2019, 1301–1310.

42. Takamura, M.; Funabashi, K.; Kanai, M.; Shibasaki, M. Asymmetric Reissert-type Reaction Promoted by Bifunctional Catalyst. *J. Am. Chem. Soc*. **2000**, *122*, 6327-6328.

43. Bruker. APEX3. Bruker AXS Inc., Madison, Wisconsin, USA, 2012.

44. Krause, L.; Herbst-Irmer, R.; Sheldrick, G.M.; Stalke, D. Comparison of Silver and Molybdenum Microfocus X-ray Sources for Single-Crystal Structure Determination. *J. Appl. Crystallogr*. **2015**, 48, 3-10.

45. Sheldrick, G. M. SHELXT – Integrated Space-Group and Crystal-Structure Determination. *Acta Crystallogr*. *A Found. Adv.* **2015**, *71*, 3-8.

46. Sheldrick, G. M. Crystal Structure Refinement with SHELXL. *Acta Crystallogr. C Struct. Chem*. **2015**, *71*, 3-8.

47. Dolomanov, O. V.; Bourhis, L. J.; Gildea, R. J.; Howard, J. A. K.; Puschmann, H. OLEX2: a Complete Structure Solution, Refinement and Analysis Program. *J. Appl. Crystallogr*. **2009**, *42*, 339-341.

48. Farrugia, L. J. WinGX and ORTEP for Windows: an update. *J. Appl. Crystallogr*. **2012**, *45*, 849-854.

<u>Chapter 3:</u> Re-evaluation of *P*-Chiral, *N*-Phosphoryl Sulfonamide Brønsted Acids in the Asymmetric Synthesis of 1,2,3,4-Tetrahydroquinoline-2-carboxylate Esters via Biomimetic Transfer Hydrogenation

3.1 Preface

The organocatalytic, asymmetric transfer hydrogenation of pro-chiral molecules is a powerful strategy for the synthesis of chiral compounds, owing to the atom economical, and green nature of this protocol. Conventional BINOL-based phosphoric acids, such as TRIP, are often effective in catalysing the transfer hydrogenation of reactive quinoline precursors to the corresponding tetrahydroquinolines. However, in the case of deactivated quinolines, these phosphoric acids are less effective. Herein, the catalytic properties of a novel class of *P*-chiral N-phosphoryl sulfonamide Brønsted acids are further evaluated in the asymmetric transfer hydrogenation of deactivated, C2-carboxylate ester-substituted quinolines. The scope of this research also includes an investigation of the thermal stability of this class of *P*-chiral Brønsted acids, highlighting a rearrangement that occurs at elevated temperature.

The work presented in this chapter has been published as shown: Mbaezue, I. I.; Topic, F.; Tsantrizos, Y. S. Re-evaluation of P-Chiral, N-Phosphoryl Sulfonamide Brønsted Acids in the Asymmetric Synthesis of 1,2,3,4-Tetrahydroquinoline-2-carboxylate Esters via Biomimetic Transfer Hydrogenation. *Synlett* **2023**, *34*, 1709-1714.

Ifenna I. Mbaezue synthesised all compounds and conducted all experiments reported in this manuscript. Dr. Filip Topic analysed X-ray crystallography data of key substrates and catalysts. Youla Tsantrizos and Ifenna I. Mbaezue co-wrote the manuscript.

3.2 Abstract

Enantioenriched heterocyclic and rigidified bioisosteres of amino acids are valuable building blocks in drug discovery, particularly in the design of peptidomimetic drugs. The rigidified bioisostere of phenylalanine, 1,2,3,4-tetrahydroquinoline-2-carboxylic acid, is found in several biologically active compounds. However, only a small number of successful methodologies have been reported for its asymmetric synthesis. To develop an environmentally benign and metal-free organocatalytic process for the preparation of this compound, a number of novel *P*-chiral, *N*-phosphoryl sulfonamide Brønsted acids were synthesized and evaluated in a biomimetic transfer hydrogenation reaction of quinoline-2-carboxylates to give the (R)-1,2,3,4-tetrahydroquinoline-2- carboxylates.

3.3 Introduction

Chiral molecules that can serve as bioisosteres of amino acids constitute valuable building blocks for medicinal chemistry, particularly in the synthesis of biologically active peptidomimetics. These bioisosteres often play a significant role in optimizing the biopharmaceutical properties of human therapeutics, improving their cell-based potency, metabolic stability, solubility in biological fluids and oral bioavailability.[1] Examples of such enormously valuable building blocks are those characterizing the structures of the clinically validated drugs shown in Figure 3.1. Amino acid bioisosteres also serve as precursors in the synthesis of other chiral molecules that are equally valuable in medicinal chemistry and organic synthesis/catalysis (Figure 3.2). Examples include intermediates **3.6** and **3.7**, which have been used in the preparation the chiral *N*-heterocyclic carbene ligand (NHC) of the Ru-based catalyst **3.9**,[2] and the multikilogram production of the Bcl-2/Bcl-xL dual antagonist **3.10**, [3] respectively (Figure 3.2). For both of these examples, the rigidified phenylalanine bioisostere **3.8** was used as the starting material, which was initially

accessed from the hydrogenation of inexpensive and commercially available quinoline-2-carboxylic acid.[2,3]

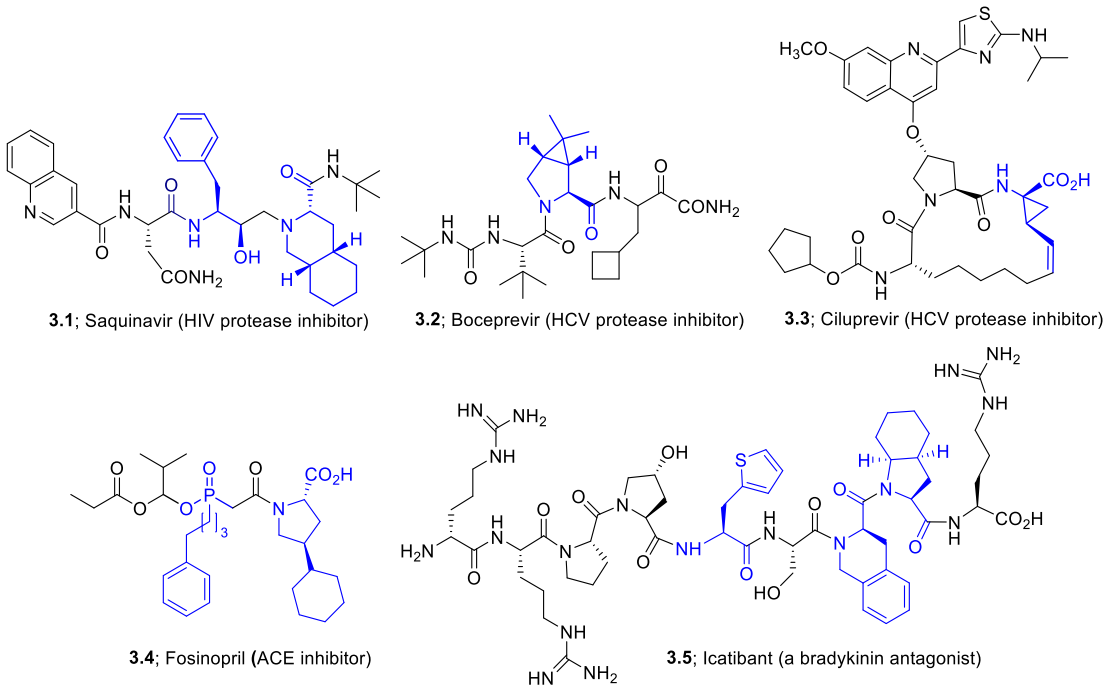

Figure 3.1. Examples of Amino Acid Bioisosteres (highlighted in blue) in Human Therapeutics.

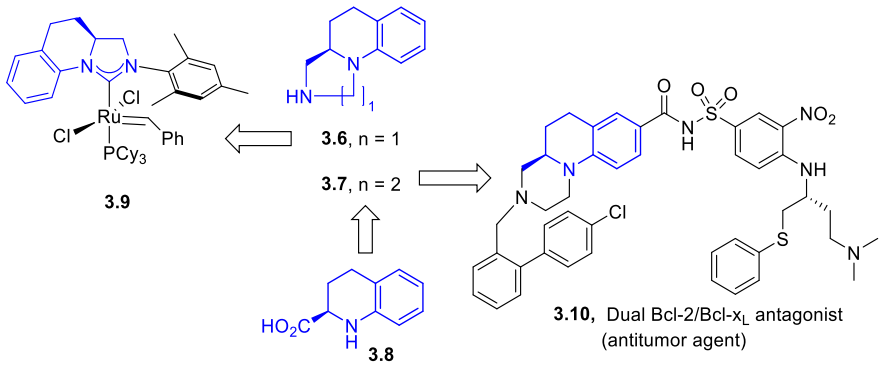

Figure 3.2. An Example of a Chiral Ligand (**3.9**) and a Human Therapeutic (**3.10**), Synthesized from Chiral Tetrahydroquinoline-2-Carboxylic Acid (**3.8**).

Tetrahydroquinoline scaffolds are a common structural motif of biologically active natural products and human therapeutics.[4] A number of efficient methodologies

have already been reported on the asymmetric synthesis of such compounds that include metal-catalyzed asymmetric hydrogenation,[5] as well as biomimetic transfer hydrogenation catalyzed by Brønsted acids,[6] of their precursor quinolines. However, a very limited number of reports describe the asymmetric hydrogenation of quinolines having a C-2 electron-withdrawing substituent, such as a ketone, carboxylic acid, amide or ester moiety (Scheme 3.1).

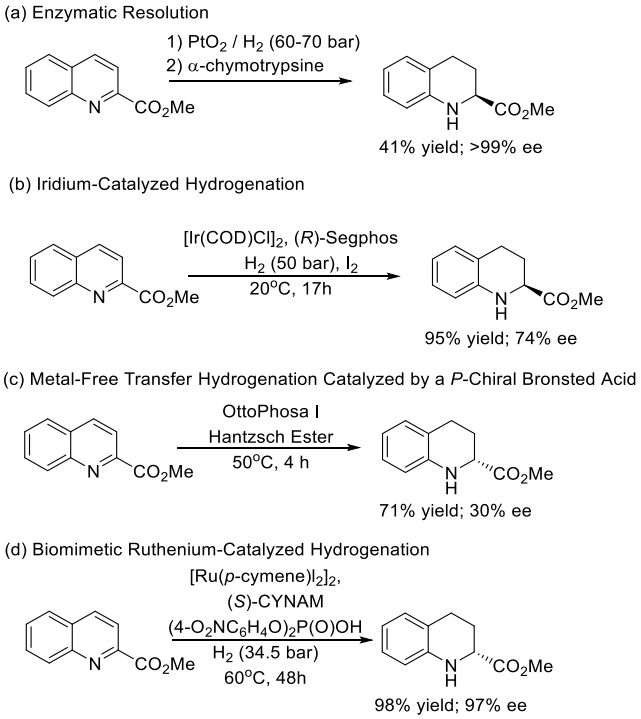

Scheme 3.1. Asymmetric hydrogenation of quinoline-2-carboxylate.

In the course of our medicinal chemistry investigations, enantioenriched tetrahydroquinoline-2-carboxylic acid (Figure 3.2; **3.8**) was required for the preparation of peptidomimetic inhibitors targeting the zinc metalloprotease STE24 (ZMPSTE24).[7] Earlier reports on the synthesis of **3.8** (as its methyl ester) directly from the quinoline-2-carboxylate methyl ester include classical hydrogenation followed by enzymatic separation of the enantiomers (Scheme **3.1a**),[8] iridium-catalyzed asymmetric hydrogenation of quinoline2-carboxylate ester (Scheme **3.1b**),[9] and biomimetic, metal-free transfer hydrogenation catalyzed by a *P*-chiral, *N*-phosphoryl sulfonamide Brønsted acid (Scheme **3.1c**).[10] Most recently, a very efficient Ru-catalyzed

asymmetric reduction that utilizes a regenerable bioisostere of NADH/NADPH [(S)-CYNAM][11] and a Brønsted acid (Scheme **3.1d**) was also reported.[12] Phosphorus-based Brønsted acids are highly valuable organocatalysts,[6] with the BINOL-based derivatives catalyzing numerous transformations. These organocatalysts were first reported by Akiyama[13] and Terada,[14] and have been reported to catalyze a plethora of asymmetric reactions, including Mannich-type[13a,14,15] and Diels–Alder reactions,[16] the enantioselective hydrophosphonylation of imines,[17] reductive aminations,[18] imine transfer hydrogenations,[19] Friedel–Crafts alkylations,[20] intramolecular Michael additions,[21] the *N*,*O*-acetalization of aldehydes[22] and the transfer hydrogenation of various heterocyclic compounds.[6,23] These Brønsted acids were also reported to catalyze metal-free asymmetric 6π-electrocyclization reactions, leading to enantiomerically enriched 1,4-dihydropyridazines.[24] BINOL-based dimeric and sterically highly confined imidodiphosphorimidate analogs were designed by List,[25] and shown to catalyze the formation of highly enantioenriched five- and six-membered ring ethers from the intramolecular nucleophilic attachment of an alcohol onto a double bond.[25a] Additionally, these molecules can also catalyze enantioselective C–C bond formation in Mukaiyama aldol-type reactions at remarkably low concentration of the catalyst.[25b]

3.4 Results and Discussion

P-Chiral, *N*-phosphoryl sulfonamide Brønsted acids, such as **3.12**, were originally reported by Han, Senanayake and co-workers,[26] and were used in the transfer hydrogenation of quinolines to tetrahydroquinolines with modest enantioselectivity (e.g., Table 3.1, entry 1).

Table 3.1. Asymmetric Transfer Hydrogenation of Quinolines.[a]

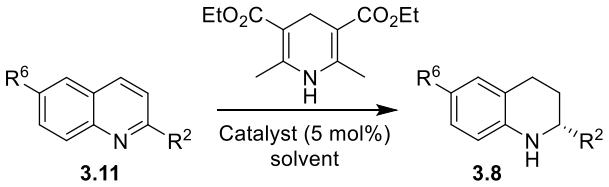

3.11 3.8

Entry	Cat.	R^2/R^6	Temp. (°C)	Time (h)	Solvent	Yield (%)[a]	ee (%)[b]
1	**3.12**	Me/Br	48	48	Toluene	75	40
2	**3.13**	Me/Br	22	2	Toluene	99	58
3	**3.14b**	Me/Br	22	2	Toluene	71	80(93)[c]
4	**3.14b**	CO_2Me/H	50	4	Cyclohexane	71	30
5	**3.14a**	CO_2Me/H	35	12	Toluene	71	23
6	**3.14b**	CO_2Me/H	35	12	Toluene	70	13
7	**3.14c**	CO_2Me/H	35	12	Toluene	72	26
8	**3.14d**	CO_2Me/H	35	12	Toluene	73	0
9	**3.14e**	CO_2Me/H	35	12	Toluene	73	45
10	**3.14e**	CO_2Me/H	50	4	Toluene	75	44
11	none	CO_2Me/H	50	48	Toluene	0	-
12	**3.16**	CO_2Me/H	50	4	Toluene	0	-
13	**3.14e**	CO_2Me/H	50	4	Cyclohexane	73	49
14	none	CO_2Me/H	50	4	Cyclohexane	0	-
15	**3.14e**	CO_2Me/F	50	4	Cyclohexane	83	48
16	**3.14e**	CO_2Me/Br	50	4	Cyclohexane	76	46(66)[d]

[a]The absolute stereochemistry was assigned based on comparison of the chiral HPLC data previously reported. [b]Isolated yield. In some cases, the isolated yield is lower than expected, based on the 100% conversion observed, due to co-elution of the Hantzsch pyridine by-product with products having C2 = CO_2Me, making the purification more challenging. [c]% ee of crystalline product after crystallization. [d]% ee of the mother liquor after crystallization.

We speculated that the introduction of an intramolecular hydrogen bond/ion pair (Figure 3.3; e.g., **3.13**),[10] could modulate the catalytic activity of these organocatalysts,

stabilizing the conformation of the catalytic cavity, and potentially acting as a 'hydride shuttle', which could lead to significant acceleration of the reaction rate and increase in enantioselectivity.[10]

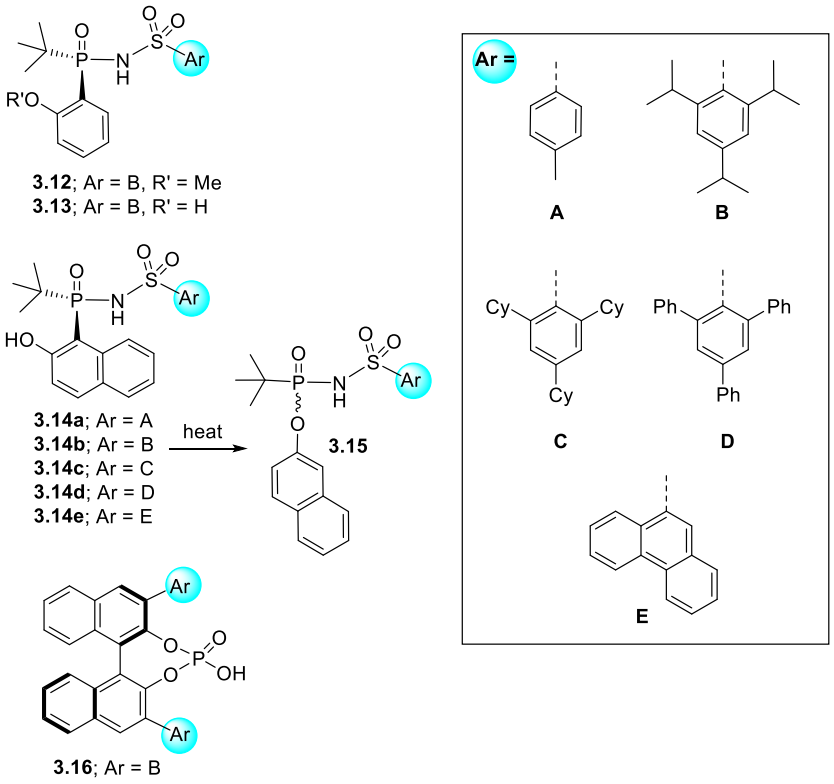

Figure 3.3. Brønsted Acid Catalysts Explored in the Transfer Hydrogenation of Quinoline-2-Carboxylate Methyl Ester.

During our initial evaluation of organocatalyst **3.13**, we observed a dramatic acceleration of the reaction rate and substantial improvement in enantioselectivity, when compared to **3.12** (Table 3.1, entry 1 vs. 2).[10] After some screening of the aromatic substituent attached to the phosphorus atom,[10] the optimized analog OttoPhosa I (**3.14b**) was identified and found to further increase enantioselectivity to 80% ee (entry 3). We were also pleased to find that analog **3.14b** could catalyze the asymmetric transfer hydrogenation of the methyl quinoline-2-carboxylate **3.11** (R^2=CO_2Me, R^6=H) to the corresponding methyl (R)-1,2,3,4-tetrahydroquinoline2-carboxylate (**3.8**), albeit

with much lower enantioselectivity and only at higher temperature (entry 4). The basicity of the quinoline nitrogen plays a major role in the rate of this reaction and, consequently, it is not surprising that electron-withdrawing substituents at the C-2 carbon decelerate the reaction rate. In fact, our previous report is the first example of a Brønsted acid catalyzed transfer hydrogenation of quinoline-2-carboxylate (**3.11**; R^6=H).[10] However, after further evaluation of Brønsted acid **3.14b**, we observed significant decomposition of this molecule at high temperature. The decomposition of **3.14b** was followed by ^{31}P NMR (in $CDCl_3$) and it was found to begin within 5 hours at 40 °C and lead almost quantitatively to the racemic phosphonamidate **3.15** within 24 hours (Figure 3.3). The structure of this rearranged product (**3.15**) was confirmed by its single-crystal X-ray structure (Figure 3.4).

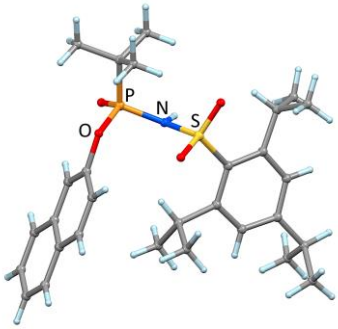

Figure 3.4. Single-Crystal X-ray Structure of Racemic Phosphonamidate **3.15**.

In the last decade alone, numerous [1,2]-phospha-Brook rearrangements have been employed in synthetic methodologies. Examples include the preparation of optically active phosphoric esters,[27] Brønsted base catalyzed [2,3]- Witting rearrangements of 2-allyloxy-2-phosphonoacetates,[28] intramolecular cyclization of alkynyl α-ketoanilide,[29] asymmetric organocatalytic reductive coupling of benzylidene pyruvates and aldehydes,[30] the synthesis of 3-aryloxindoles,[31] preparation of 2,3-allenylamides,[32] Brønsted base catalyzed three-component coupling reactions of α-ketoesters, imines and diethyl phosphite,[33] intramolecular addition of benzyl anion to alkyne,[34] the generation of homoenolate equivalent compounds,[35] preparation of

tetrasubstituted furans,[36] transformation of α,β-epoxyketones to allylic alcohols,[37] and the fluorinative ring expansion of 2- benzoylpyrrolidines.[38] Most recently, the use of this rearrangement has also been reported in the preparation of (difluoromethyl)cycloalkenes,[39] the Passerini–Smiles reaction of α-ketophosphonates,[40] and the asymmetric synthesis of enantioenriched axial chiral allenes.[41] All of the above mentioned reactions proceed under basic conditions, and examples of a Lewis acid catalyzed reaction are extremely rare.[42] To our knowledge, the Brønsted acid catalyzed [1,4]-phospha-Brook rearrangements observed in this study, for the conversion of organocatalyst **3.14b** into the phosphonamidate **3.15**, has not been previously reported. At high temperatures, it is likely that the electron-deficient phosphorus atom of **3.14b** can drive the nucleophilic attachment of the phenol to induce the rearrangement. It is also plausible that during the transfer hydrogenation of **3.11** to give **3.8** (Table 3.1) the accumulating 1,2,3,4-tetrahydroquinoline product (Figure 3.5; Path A; i.e., during the 2nd step of the catalytic cycle) is sufficiently basic to hydrogen-bond or deprotonate the weakly acidic phenol and accelerate an [1,4]-phospha-Brook rearrangement (Figure 3.5; Path B). The latter mechanism may explain why even at slightly higher temperatures (from 35 to 50 °C, corresponding to the temperatures at which **3.14b** is fairly stable and unstable, respectively, over a period of 4 hours) there is no significant deterioration of the enantioselectivity. Another possibility is that intramolecular rearrangement, involving a configurationally labile trigonal bipyramidal intermediate on the phosphorus atom, may be involved in the formation of **3.15**; such intermediates have been proposed in the racemization of *P*-chiral SPOs in the presence of $LiAlH_4$. [43]

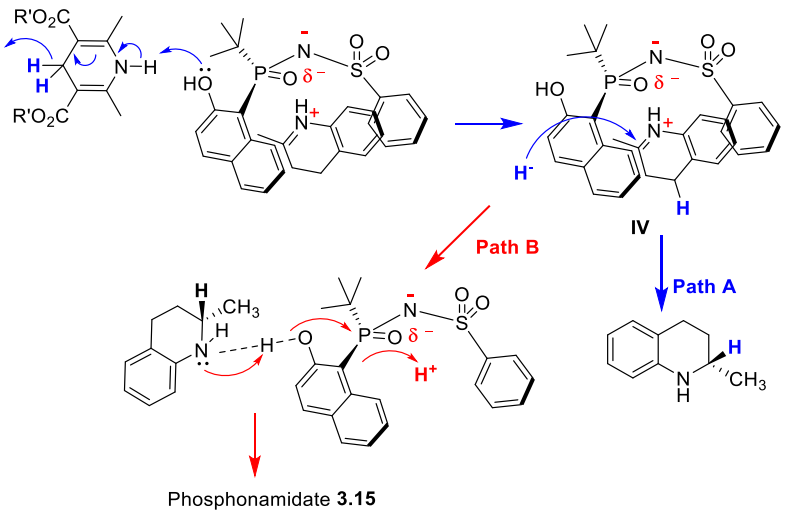

Figure 3.5. Plausible Mechanism for the [1,4]-phospha-Brook Rearrangement of Organocatalyst **3.14b** to the Phosphonamidate **3.15**.

In the hope of identifying a better organocatalyst within this structural class of Brønsted acids, which could catalyze the asymmetric hydrogenation of quinolines having a C-2 electron-withdrawing group at low temperatures and in higher enantioselectivity, we turned our attention to the role of the sulfonamide moiety. Several new derivatives were synthesized (Figure 3.3; analogs **3.14a**, **3.14c,d,e**) in order to evaluate the relative contributions to thermal stability and ability to induce enantioselectivity in the transfer hydrogenation specifically of quinoline-2-carboxylate methyl esters (**3.11**). Initially, we carried out these reactions at 35 °C, which was found to be the highest temperature at which catalyst **3.14b** was chemically stable over a period of 48 hours. Interestingly, when the catalytic properties of Brønsted acid **3.14b** were compared with those of **3.14a** and **3.14c**, having a less sterically congested and a more sterically congested catalytic cavity, respectively, the reaction rates and yields were found to be virtually identical, and only a slightly higher enantiomeric excess of the product was observed with **3.14a** and **3.14c**, as compared to **3.14b** (Table 3.1; entries 5–7). Although these differences are very small, they suggested that steric hindrance may not play a very significant role in inducing enantioselectivity in this transformation. However, a more extended aromatic system on the sulfonamide

moieties, such as analog **3.14d** and **3.14e**, lead to significantly different outcomes. Whereas Brønsted acid **3.14e** catalyzed the transfer hydrogenation of **3.11** to **3.8** with higher enantiomeric excess (entry 9), **3.14d** led to a completely racemic product (entry 8). These results seem to suggest that π-stacking interaction plays an important role in directing the binding of quinoline **3.11** within the catalytic cavity, allowing for the formation of a salt-bridge with the nitrogen or the oxygen anion, or even a bifurcated interaction with both. However, π-stacking interactions distal to the *N*–/*O*– may be detrimental in controlling the orientation of substrate binding. In spite of some decomposition of catalyst **3.14e** at higher temperatures (presumably due to the equivalent rearrangement product as **3.15**, these decomposition products did not appear to have any significant catalytic function), since increasing the temperature of the reaction to 50 °C led to 100% conversion (75% isolated yield) over a 4 h period with equivalent enantioselectivity (44–45% ee, entry 9 vs. 10). This result also suggests that catalyst loading lower than 5% may be sufficient to catalyze this reaction, albeit with a longer reaction time. We also confirmed that, in the absence of an organocatalysts, the transfer hydrogenation of **3.11** to **3.8** did not proceed at all, even at 50 °C temperature and over the same period (entry 10 vs. 11 and 14). To further validate the unique catalytic properties of compound **3.14e**, the same reaction was also run using the commercially available Brønsted acid **3.16** [(R)-3,3′-bis(2,4,6-triisopropylphenyl)-1,1′-binaphthyl-2,2′-diylhydrogenphosphate; (R)-TRIP] at both 35 °C and 50 °C, and for an extended reaction period (4–48 h); however, we did not observe any conversion (entry 12). Finally, based on our previous solvent screening studies,[10] this transfer hydrogenation reaction was also run using cyclohexane as the solvent (entry 13); however, only a very slight increase in enantiomeric excess was observed (entry 13). The yield and enantiomeric excess observed at the 1 mmol scale were essentially identical to those observed at the 0.2 mmol scale (entry 13).[44] To further probe the outcome observed in the transfer hydrogenation of methyl quinoline-2-carboxylate substrate **3.11** (with R^2 = CO_2Me, R^6 = H), the 6-fluoro- and 6-bromoquinoline-2-carboxylate methyl esters were also exposed to the same reaction conditions and found

to give very similar outcomes (entry 13 vs. 15 and 16). Although, crystallization could be used to improve the enantiomeric purity of **3.8** when R^2 = Me and R^6 = Br (entry 3) from 80 to 93%, crystallization of **3.8** when R^2 = CO_2Me and R^6 = H, F or Br proved to be more challenging. For example, crystallization of the reaction mixture containing the methyl 6-bromo-1,2,3,4-tetrahydroquinoline-2-carboxylate (**3.11**, entry 16; 46% ee) led to enantiomeric enrichment of the mother liquor (rather than the crystalline material) from 46 to 66% ee (entry 16).

3.5 Conclusion

In summary, in this study we have identified a serious limitation in using *P*-chiral, *N*-phosphoryl sulfonamide Brønsted acids at high temperatures, due to their facile rearrangement into a racemic phosphonamidate product. Nonetheless, this class of organocatalysts leads to much faster reaction rates at nearly ambient temperature, as compared to many BINOL-based Brønsted acids, and has the ability to induce the metal- and hydrogen-gas-free transfer hydrogenation of quinolines bearing a C-2 electron-withdrawing substituent, such as an ester moiety. Although establishing a large substrate scope was beyond the purpose of this study, and the enantiomeric ratio achieved was only ca. 75:25 (R/S), it is conceivable that, upon crystallization, a significant improvement in the enantiomeric purity of product(s) would be possible.

3.6 Experimental Section

General Procedure: All reactions were carried out under anhydrous conditions and under an atmosphere of dry argon, except transfer hydrogenation reactions, which were carried out under air in sealed vessels. Compounds were purified by normal phase flash column chromatography on silica gel (SDS, 60 Å C. C. 40-63 mm) as the stationary phase. Thin Layer Chromatography (TLC) was performed on alumina plates pre-coated with silica gel (Merck silica gel, 60 F254), which were visualized by UV when applicable (λmax = 254 nm and/or 366 nm) and/or by staining with vanillin or

anisadehyde in acidic ethanol and/or $KMnO_4$ in basic water followed by heating. Key compounds were fully characterized by ^{1}H, $^{13}C\{^{1}H\}$ and $^{31}P\{^{1}H\}$ NMR and HRMS. Chemical shifts (δ) are reported in ppm relative to the internal deuterated solvent or external H_3PO_4 (δ 0.00 ^{31}P), unless indicated otherwise. High-resolution MS spectra were recorded using electrospray ionization (ESI+/-) and Fourier transform ion cyclotron resonance mass analyzer (FTMS).

The reactions were monitored either by TLC or analytical HPLC/MS to confirm completion and homogeneity of the products. Analytical HPLC was performed using a reversed phase C18 5 μm column on a Waters Atlantis T3 instrument and the solvent system indicated below:

Solvent A: H_2O, 0.1% formic acid

Solvent B: CH_3CN, 0.1% formic acid

Mobile phase: linear gradient from 95%A and 5%B to 5%A and 95%B in 13 min, then 2 min at 100% B

Flow rate: 1 mL/min

The enantiomeric purity of chiral compounds was determined by chiral HPLC using an Agilent 1100 or Agilent 1260 series instrument and the column and solvent system indicated for each compound. The absolute stereochemistry of all compounds was assigned based on several factors, including the single crystal X-ray of the previously reported key precursor compounds.

Chloroform ($CHCl_3$) used in screening, was passed through SiO_2 to remove residual EtOH (preservative) and used immediately after. Methoxy-2-quinoline carboxylate was purchased from Sigma Aldrich. All other substituted quinolines were synthesized according to literature procedure from the precursor methyl quinolines, via sequential tribromination,[45] carboxylation[46] and esterification.[47]

Procedure for the Synthesis of Catalysts **3.14a-e**:

(*R*)-*P*-(*tert*-butyl)-*P*-(2-methoxynaphthalen-1-yl)phosphinic amide and catalyst **3.14b** were synthesised according to previously reported literature protocol.[48,10]

(*R*)-*N*-(*tert*-butyl(2-methoxynaphthalen-1-yl)phosphoryl)-4-methylbenzenesulfonamide

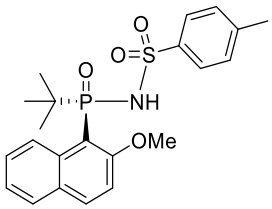

An oven-dried 25 mL flask equipped with an oven-dried stir bar was cooled to ambient temperature in a desiccator. Subsequently, phosphinic amide (90.5 mg, 0.326 mmol) was added to the flask and put through one cycle of evacuation and Ar-backfilling. Dry THF (3 mL) was added to the flask under Ar, to dissolve the phosphinic amide. While stirring, the solution was cooled to an external temperature of 3 °C in an ice bath and t-BuOK (110 mg, 0.979 mmol) was added in one portion. The mixture was stirred for 30 minutes at this temperature and then 4-toluenesulfonyl chloride (249 mg, 1.31 mmol) was added in one portion, under Ar. The mixture was stirred vigorously while sitting in the bath, where it slowly warmed up to RT and was stirred for 14 h. Subsequently, the reaction was quenched with NH_4Cl (8 mL) and diluted with EtOAc (10 mL). The mixture was transferred to a separatory funnel. The flask was washed with EtOAc (4 mL x 2) and the resulting solution was transferred to the separatory funnel. Brine (10 mL) was added and the organic layer was separated. The aqueous layer was further extracted with EtOAc (10 mL) and the combined organic layers was dried over Na_2SO_4, filtered and concentrated. The crude was purified on SiO_2 via flash column chromatography (0-3% DCM/MeOH) to afford the desired product as a light brown oil. Re-dissolving the oil in $CDCl_3$ and evaporating gave a light-yellow solid in 78% yield (110 mg, 0.255 mmol). ^{1}H NMR (400 MHz, $CDCl_3$): δ 9.36 (d, J = 8.9 Hz, 1H), 8.00

(d, *J* = 9.1 Hz, 1H), 7.89 (d, *J* = 8.1 Hz, 2H), 7.73 (d, *J* = 8.1 Hz, 1H), 7.50 (ddd, *J* = 8.7, 6.8, 1.7 Hz, 1H), 7.38 (ddd, *J* = 8.0, 6.8, 1.1 Hz, 1H), 7.22 (dd, *J* = 9.2, 4.9 Hz, 1H), 7.07 (d, *J* = 8.0 Hz, 2H), 4.06 (s, 3H), 2.25 (s, 3H), 1.13 (d, *J* = 17.4 Hz, 9H). ^{13}C NMR (126 MHz, $CDCl_3$): δ 158.4, 143.4, 138.9, 136.7 (d, *J* = 7.8 Hz), 135.9 (d, *J* = 1.9 Hz), 129.6, 129.2, 128.3, 128.2, 127.7, 127.4 (d, *J* = 2.3 Hz), 124.7, 111.9 (d, *J* = 8.2 Hz), 109.8 (d, *J* = 97.1 Hz), 56.7, 37.3 (d, *J* = 89.7 Hz), 24.3, 21.6. ^{31}P NMR (162 MHz, $CDCl_3$): δ 42.96. HRMS (ESI+, *m/z*): calcd for $C_{22}H_{27}NO_4PS$ [M+H]: 432.1393, found: 432.1407.

(*R*)-*N*-(*tert*-butyl(2-hydroxynaphthalen-1-yl)phosphoryl)-4-methylbenzenesulfonamide (3.14a)

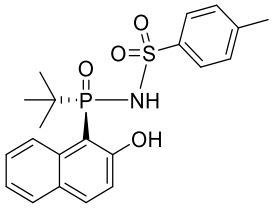

An oven dried 25 mL round bottom flask was charged with an oven dried stir-bar and cooled to ambient temperature in a desiccator. The starting material (83.3 mg, 0.193 mmol) was added and the flask was put through a cycle of evacuation and Ar-backfilling. Dry DCM (2 mL) was added under Ar and the flask was cooled to -70 °C. 1M BBr_3 in DCM (0.23 mL, 0.23 mmol) was added dropwise over 2 minutes while stirring. The flask was allowed to slowly warm up to rt in the bath, over 5 h and stirring was continued for another 2 h at RT. After a TLC showed complete consumption of starting material (5% MeOH/95% DCM), the flask was cooled to 0 °C in an ice bath and the reaction was quenched with deionised water (5 mL). The reaction was diluted with DCM (5 mL) and transferred to a 60 mL separatory funnel. The flask was rinsed with DCM (1 mL x2) and transferred to the separatory funnel and the organic layer was separated. The aqueous was further extracted with DCM (5 mL) and the combined organic layers was washed with 1N HCl (2 mL). The organic layer was dried over Na_2SO_4, filtered and concentrated under reduced pressure (at 35 °C). The crude product

was purified via flash column chromatography on Et_3N-deactivated SiO_2 (0-2% MeOH/DCM) to yield a brown oil. The oil was redissolved in DCM (5 mL) and washed thoroughly with 2N HCl (1 mL) to reveal a cloudy yellow organic layer which was collected. The aqueous layer was extracted with DCM (1 mL) and the combined organic layers was washed once more with 2N HCl (1 mL). The aqueous layer was extracted with DCM (2 mL) and the combined organic layers was concentrated under reduced pressure. The resulting white solid was suspended in toluene (5 mL), evaporated to dryness (at 30 °C) and concentrated under high vacuum for 24 h, to afford the desired compound as a light yellow solid in78% yield (63.0 mg. 0.151 mmol). ^{1}H NMR (400 MHz, $CDCl_3$): δ 12.51 (s, 1H), 8.13 (d, J = 8.6 Hz, 1H), 7.84 (dd, J = 15.4, 8.7 Hz, 3H), 7.71 (m, 1H), 7.38 (ddd, J = 8.6, 6.9, 1.6 Hz, 1H), 7.33 – 7.25 (m, 1H), 7.14 (d, J = 8.0 Hz, 2H), 7.09 (dd, J = 9.0, 4.7 Hz, 1H), 2.35 (s, 3H), 1.21 (d, J = 17.0 Hz, 9H). ^{13}C NMR (126 MHz, $CDCl_3$): δ 166.5, 144.7, 137.5, 136.5, 133.5, 129.5, 129.3, 128.7, 128.6, 127.7, 127.4, 125.0 (d, J = 4.0 Hz), 123.4, 120.8 (d, J = 11.0 Hz), 36.9 (d, J = 85.5 Hz), 24.8, 21.7. ^{31}P NMR (162 MHz, $CDCl_3$): δ 48.49. HRMS (ESI-, *m/z*): calcd for $C_{21}H_{23}NO_4PS$ [M-H]: 416.1091, found: 416.1107.

(R)-N-(*tert*-butyl(2-methoxynaphthalen-1-yl)phosphoryl)-2,4,6-tricyclohexylbenzenesulfonamide

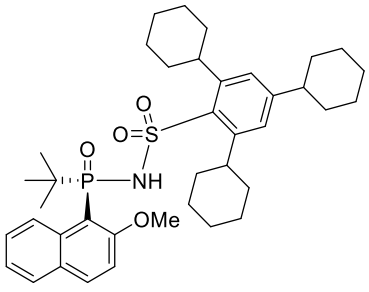

An oven-dried 25 mL flask equipped with an oven-dried stir bar was cooled to ambient temperature in a desiccator. Subsequently, phosphinic amide (73.7 mg, 0.266 mmol) was added to the flask and put through one cycle of evacuation and Ar-backfilling. Dry THF (3 mL) was added to the flask under Ar, to dissolve the phosphinic amide. While

stirring, the solution was cooled to an external temperature of 3 °C in an ice bath. t-BuOK (89.5 mg, 0.797 mmol) was added in one portion. The mixture was stirred for 30 minutes at this temperature and then the sulfonyl chloride (337 mg, 0.797 mmol) was added in one portion, under Ar. The mixture was stirred vigorously while sitting in the bath, where it slowly warmed up to RT and then stirred for 20 h. Subsequently, the reaction was quenched with NH_4Cl (8 mL) and diluted with EtOAc (10 mL). The mixture was transferred to a separatory funnel. The flask was washed with EtOAc (4 mL x 2) and the resulting solution was transferred to the separatory funnel. Brine (10 mL) was added and the organic layer was extracted. The aqueous layer was further extracted with EtOAc (10 mL) and the combined organic layers was dried over Na_2SO_4, filtered and concentrated. The crude was purified on SiO_2 by flash column chromatography (0-2% DCM/MeOH) to afford the desired product as a light brown oil. Re-dissolving this oil in $CDCl_3$ and evaporating gave a white solid in 81% yield ()143 mg, 0.216 mmol). ^{1}H NMR (400 MHz, $CDCl_3$): δ 9.36 (d, J = 8.8 Hz, 1H), 8.03 (d, J = 9.1 Hz, 1H), 7.75 (d, J = 8.1 Hz, 1H), 7.45 (ddd, J = 8.7, 6.7, 1.6 Hz, 1H), 7.36 (ddd, J = 8.0, 6.8, 1.2 Hz, 1H), 7.31 (dd, J = 9.1, 4.8 Hz, 1H), 7.01 (s, 2H), 4.12 (s, 3H), 3.80 – 3.61 (m, 2H), 2.67 – 2.22 (m, 1H), 1.91 (d, J = 11.6 Hz, 2H), 1.80 (d, J = 8.1 Hz, 4H), 1.75 – 1.65 (m, 5H), 1.65 – 1.46 (m, 7H), 1.42 – 1.09 (m, 21H). ^{13}C NMR (126 MHz, $CDCl_3$): δ 158.7, 151.6, 149.3, 135.7, 128.2, 128.0, 127.6, 124.9, 124.7, 124.5, 56.7, 44.6, 40.8, 37.5, 36.8, 35.1, 34.9, 34.1, 34.0, 27.3, 27.1, 26.9, 26.5, 26.2, 24.7. ^{31}P NMR (162 MHz, $CDCl_3$): δ 42.06. HRMS (ESI+, m/z): calcd for $C_{39}H_{55}NO_4PS$ [M+H]: 664.3584, found: 664.3588.

(*R*)-*N*-(*tert*-butyl(2-hydroxynaphthalen-1-yl)phosphoryl)-2,4,6-tricyclohexylbenzenesulfonamide (3.14c)

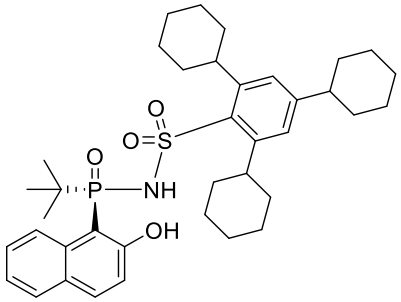

An oven dried 25 mL round bottom flask was charged with an oven dried stir-bar and cooled to ambient temperature in a desiccator. The starting material (121 mg, 0.182 mmol) was added and the flask was put through a cycle of evacuation and Ar backfilling. Dry DCM (2 mL) was added under Ar and the flask was cooled to -70 °C. 1M BBr_3 in DCM (0.22 mL, 0.22 mmol) was added dropwise over 2 minutes, while stirring. The flask was allowed to slowly warm up to rt in the bath, over 6 h and stirring was continued for another 2 h at RT. After a TLC showed complete consumption of starting material (5% MeOH/95% DCM), the flask was cooled to 0 °C in an ice bath and the reaction was quenched with of deionised water (5 mL). The reaction was diluted with DCM (5 mL) and transferred to a 60 mL separatory funnel. The flask was rinsed with DCM (1 mL x 2), transferred to the separatory funnel and the organic layer was separated. The aqueous layer was further extracted with DCM (5 mL x 2) and the combined organic layer was washed with 1N HCl (2 mL) and the resulting organic layer was collected. The acidic-aqueous layer was further extracted with DCM (5 mL). The combined organic layer was dried over Na_2SO_4, filtered and concentrated under reduced pressure (at 30 °C). The crude product was purified via flash column chromatography on Et_3N-deactivated SiO_2 (0-2% MeOH/DCM) to yield a brown oil. This was redissolved in 5 mL DCM and washed thoroughly with 2N HCl (1 mL) to reveal a cloudy yellow organic layer which was collected. The aqueous layer was extracted with DCM (1 mL) and the combined organic layer was washed once more with 2N HCl (1 mL). The aqueous layer was extracted with DCM (2 mL) and the

combined organic layer was concentrated under reduced pressure. The resulting white foam was suspended in toluene (5 mL), evaporated to dryness (at 30 °C) and concentrated under high vacuum for 24 h, to afford the pure compound as a light-yellow solid in 87% yield (103.4 mg. 0.159 mmol). ^{1}H NMR (400 MHz, $CDCl_3$): δ 12.60 (s, 1H), 8.09 (d, *J* = 7.9 Hz, 1H), 7.88 (d, *J* = 9.1 Hz, 1H), 7.69 (d, *J* = 7.7 Hz, 1H), 7.24 – 7.17 (m, 2H), 7.12 (dd, *J* = 9.0, 4.7 Hz, 1H), 7.03 (s, 2H), 6.37 (s, 1H), 3.47 – 3.24 (m, 2H), 2.50 – 2.40 (m, 1H), 1.96 – 1.82 (m, 6H), 1.81 – 1.74 (m, 3H), 1.69 (d, *J* = 10.6 Hz, 4H), 1.56 (d, *J* = 12.2 Hz, 4H), 1.46 – 1.32 (m, 6H), 1.32 – 1.03 (m, 16H). ^{13}C NMR (126 MHz, $CDCl_3$): δ 155.8, 152.4, 151.8, 148.4, 136.5 (d, J = 2.3 Hz), 135.0, 129.2, 129.1, 128.4, 126.8, 125.2, 123.3, 120.8 (d, *J* = 10.9 Hz), 44.7, 41.5, 36.5, 35.1, 34.1, 34.1, 27.3, 27.1, 26.9, 26.3, 26.2, 25.2. ^{31}P NMR (162 MHz, $CDCl_3$): δ 47.50. HRMS (ESI-, m/z): calcd for $C_{38}H_{51}NO_4PS$ [M-H]: 664.3282, found: 664.3307.

(*R*)-*N*-(*tert*-butyl(2-methoxynaphthalen-1-yl)phosphoryl)-5'-phenyl-[1,1':3',1''-terphenyl]-2'-sulfonamide

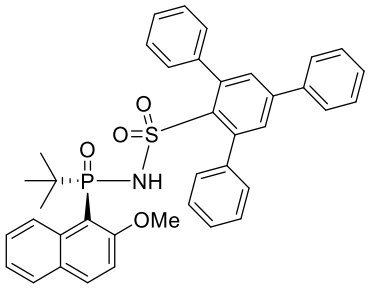

An oven-dried 50 mL flask equipped with an oven-dried stir bar was cooled to ambient temperature in a desiccator. Subsequently, phosphinic amide (75.2 mg, 0.271 mmol) was added to the flask and put through one cycle of evacuation and Ar-backfilling. Dry THF (4 mL) was added to the flask under Ar, to dissolve the phosphinic amide. While stirring, the solution was cooled to an external temperature of 3°C in an ice bath. t-BuOK (91.3 mg, 0.813 mmol) was added in one portion. The mixture was stirred for 30 minutes at this temperature and then sulfonyl chloride (220 mg, 0.542 mmol) was added in one portion, under Ar. The mixture was stirred vigorously while sitting in the

bath, where it slowly warmed up to RT and stirred for 18 h. Subsequently, the reaction was cooled to 3 °C in an ice bath, quenched with NH_4Cl (8 mL) and diluted with EtOAc (10 mL). The mixture was transferred to a separatory funnel. The flask was washed with EtOAc (4 mL x 2) and the resulting solution was transferred to the separatory funnel. Brine (10 mL) was added and the organic layer was extracted. The aqueous layer was extracted with EtOAc (15 mL x 3) and the combined organic layer was dried over Na_2SO_4, filtered and concentrated. The crude was purified on SiO_2 via flash column chromatography (0-2% DCM/MeOH) to afford the desired product as a light-yellow solid in 77% yield (135.6 mg, 0.210 mmol). ^{1}H NMR (400 MHz, $CDCl_3$): δ 9.43 (d, J = 8.8 Hz, 1H), 8.04 (d, J = 9.2 Hz, 1H), 7.81 (d, J = 8.1 Hz, 1H), 7.65 – 7.46 (m, 4H), 7.45 – 7.28 (m, 9H), 7.21 (tt, J = 7.5, 1.3 Hz, 2H), 7.16 – 7.01 (m, 3H), 6.82 (d, J = 6.9 Hz, 2H), 3.68 (s, 3H), 1.00 (d, J = 17.8 Hz, 9H). ^{13}C NMR (126 MHz, $CDCl_3$): δ 157.7, 143.0, 141.8, 139.0, 138.5, 136.8 (d, J = 7.4 Hz), 135.3, 130.9, 129.7, 129.5, 129.4, 128.9, 128.3, 127.5, 127.4, 127.1, 126.8, 124.6, 111.6, 111.6, 109.9, 109.2, 55.5, 37.8 (d, J = 89.3 Hz), 25.4. ^{31}P NMR (162 MHz, $CDCl_3$): δ 44.28. HRMS (ESI+, m/z): calcd for $C_{39}H_{37}NO_4PS$ [M+H]: 646.2175, found: 646.2195.

(*R*)-*N*-(*tert*-butyl(2-hydroxynaphthalen-1-yl)phosphoryl)-5'-phenyl-[1,1':3',1''-terphenyl]-2'-sulfonamide (3.14d)

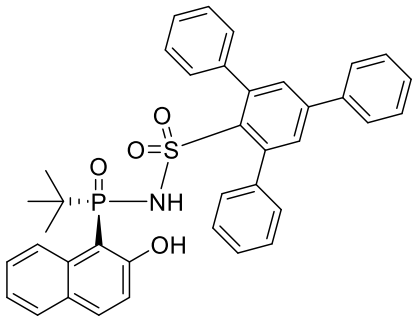

An oven dried 25 mL round bottom flask was charged with an oven dried stir-bar and cooled to ambient temperature in a desiccator. The starting material (100 mg, 0.155 mmol) was added and the flask was put through 2 cycles of evacuation and Ar backfilling. Dry DCM (3 mL) was added under Ar. The flask was cooled to -78 °C and

1M BBr_3 in DCM (0.20 mL, 0.202 mmol) was added dropwise over 5 minutes, while stirring. The flask was allowed to slowly warm up to RT over 5 h and stirred for an additional 24 h at RT. After a TLC showed almost complete consumption of starting material (5% MeOH/95% DCM), the flask was cooled to 0 °C in an ice bath and the reaction was quenched with deionised water (5 mL). The reaction was diluted with DCM (5 mL) and transferred to a 60 mL separatory funnel. The flask was rinsed with DCM (1 mL x 2) and transferred to the separatory funnel and the organic layer was separated. The aqueous layer was further extracted with DCM (5 mL x 2) and the combined organic layer was washed with 1N HCl (2 mL) and the resulting organic layer was collected. The acidic-aqueous layer was further extracted with DCM (5 mL). The combined organic layer was dried over Na_2SO_4, filtered and concentrated under reduced pressure (at 30 °C). The crude product was purified via flash column chromatography on SiO_2 (0-6% MeOH/DCM) to yield a purple-blue solid. This was redissolved in DCM (8 mL) and MeCN (1 mL) and washed thoroughly with 2N HCl (2 mL) to reveal a cloudy yellow organic layer which was collected. The aqueous layer was extracted with DCM (1 mL) and the combined organic layers was washed once more with 2N HCl (2 mL). The aqueous layer was extracted with DCM (2 mL) and the combined organic layer was concentrated under reduced pressure. The resulting yellow solid was suspended in toluene (5 mL), and concentrated (at 30 °C) and then under high vacuum at rt for 24 h, to afford the pure compound as a yellow solid in 88% yield (86.2 mg. 0.137 mmol). ^{1}H NMR (400 MHz, $CDCl_3$): δ 12.40 (s, 1H), 7.87 (d, J = 9.0 Hz, 1H), 7.72 (d, J = 8.1 Hz, 1H), 7.67 – 7.59 (m, 2H), 7.56 – 7.36 (m, 8H), 7.25 – 7.11 (m, 8H), 7.11 – 7.02 (m, 2H), 1.05 (d, J = 17.6 Hz, 9H). ^{13}C NMR (126 MHz, $CDCl_3$): δ 157.7, 143.0, 141.8, 139.0, 138.5, 136.8 (d, J = 7.4 Hz), 135.3, 130.9, 129.7, 129.5, 129.4, 128.9, 128.3, 127.5, 127.4, 127.1, 126.8, 124.6, 111.6, 111.6, 109.9, 109.2, 55.5, 37.8 (d, J = 89.3 Hz), 25.4. ^{31}P NMR (162 MHz, $CDCl_3$): δ 50.57. HRMS (ESI-, m/z): calcd for $C_{38}H_{33}NO_4PS$ [M-H]: 630.1873, found: 630.1894.

(*R*)-*N*-(*tert*-butyl(2-methoxynaphthalen-1-yl)phosphoryl)phenanthrene-9-sulfonamide

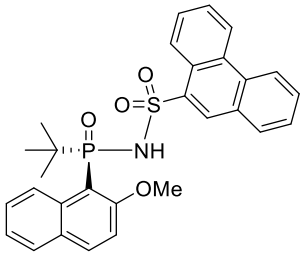

An oven-dried 25 mL flask equipped with an oven-dried stir bar, was cooled to ambient temperature in a desiccator. Subsequently, phosphinic amide (67.4 mg, 0.243 mmol) was added to the flask and put through one cycle of evacuation and Ar-backfilling. Dry THF (3 mL) was added to the flask under Ar, to dissolve the phsphinic amide. While stirring, the solution was cooled to an external temperature of 3 °C in an ice bath. Subsequently, t-BuOK (81.8 mg, 0.729 mmol) was added in one portion. The mixture was stirred for 30 minutes at this temperature and then aryl sulfonyl chloride (202 mg, 0.729 mmol) was added in one portion, under Ar. The mixture was stirred vigorously while sitting in the bath, where it slowly warmed up to RT and stirred for 42 h. Subsequently, the reaction was cooled to 0 °C in an ice bath, quenched with NH_4Cl (8 mL), diluted with EtOAc (10 mL) after which the mixture was transferred to a separatory funnel. The flask was washed with EtOAc (4 mL x2) and the resulting solution was transferred to the separatory funnel. Deionised water (10 mL) was added to dissolve the salts and the organic layer was separated. The aqueous layer was further extracted with EtOAc (15 mL x3) and the combined organic layer was dried over Na_2SO_4, filtered and concentrated. The crude was purified on SiO_2 (flash column chromatography; 0-3% DCM/MeOH) to afford the desired product as a light brown solid in 95% yield (104 mg, 0.202 mmol). ^{1}H NMR (500 MHz, $CDCl_3$): δ 9.08 (d, J = 8.8 Hz, 1H), 8.80 – 8.70 (m, 2H), 8.54 – 8.47 (m, 1H), 8.40 (d, *J* = 8.2 Hz, 1H), 7.84 (d, *J* = 8.0 Hz, 1H), 7.74 (d, *J* = 9.1 Hz, 1H), 7.63 (ddd, *J* = 8.3, 7.0, 1.4 Hz, 1H), 7.61 – 7.46 (m, 5H), 7.22 (ddd, *J* = 8.8, 6.9, 1.6 Hz, 1H), 7.17 (ddd, *J* = 8.0, 6.7, 1.2 Hz, 1H), 6.89 (dd, *J* = 9.2, 4.9 Hz, 1H), 3.98 (s, 3H), 1.10 (d, *J* = 17.4 Hz, 9H). ^{13}C NMR (126 MHz, $CDCl_3$): δ 136.1, 136.1, 135.7, 134.6, 134.0, 132.2, 131.1, 129.5, 129.4, 129.2,

128.0, 127.8, 127.3, 127.0, 126.9, 126.0, 125.1, 124.5, 123.3, 122.3, 111.1, 108.8, 60.5, 56.3, 37.7, 37.0, 24.3, 14.4. ^{31}P NMR (203 MHz, $CDCl_3$): δ 43.5. HRMS (ESI+, m/z): calcd for $C_{29}H_{28}NNaO_4PS$ [M+Na]+: 540.1369, found: 540.1388.

(*R*)-*N*-(*tert*-butyl(2-hydroxynaphthalen-1-yl)phosphoryl)phenanthrene-9-sulfonamide (3.14e)

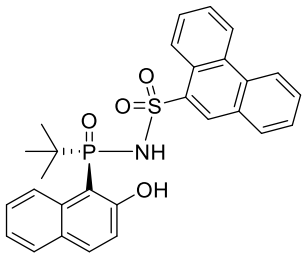

A flame-dried 10 mL round bottom flask and stir-bar were cooled to ambient temperature under a stream of Ar. Subsequently, starting material (75.2 mg, 0.145 mmol) was added and the flask was fitted with a rubber septum. The flask was put through a cycle of evacuation and backfilling with Ar and dry DCM (3 mL) was added under Ar. The flask was cooled to -78 °C and 1M BBr_3 in DCM (0.20 mL, 0.203 mmol) was added dropwise, while stirring. The flask was allowed to slowly warm up to RT in the bath, while stirring for 12 h. The flask was cooled to 0 °C in an ice bath and the reaction was quenched with deionised water (5 mL). The reaction was diluted with DCM (5 mL) and transferred to a 60 mL separatory funnel. The flask was rinsed with DCM (1 mL x2) and transferred to the separatory funnel and the organic layer was collected. The aqueous was further extracted with DCM (5 mL x2) and the combined organic layer was washed with a 1M HCl solution (2 mL) after which the resulting organic layer was collected. The acidic-aqueous layer was further extracted with DCM (5 mL). The combined organic layer was dried over Na_2SO_4, filtered and concentrated under reduced pressure (at 30 °C). The crude product was purified via flash column chromatography on SiO_2 (0-7% MeOH/DCM) to yield a whitish-blue solid. This was redissolved in DCM (5 mL) and MeCN (1 mL) and washed thoroughly with 2N HCl (2 mL) to reveal a cloudy yellow organic layer which was collected. The aqueous layer

was extracted with DCM (1 mL) and the combined organic layers were washed once more with 2N HCl (2 mL). The aqueous layer was extracted with DCM (2 mL) and the combined organic layer was concentrated under reduced pressure. The resulting white foam was suspended in toluene (5 mL x2), evaporated to dryness (at 30 °C) and concentrated under high vacuum for 24 h, to afford the pure compound as a light-yellow solid (42.1 mg. 0.0836 mmol, 58% yield). ^{1}H NMR (500 MHz, $CDCl_3$): δ 12.49 (s, 1H), 8.76 (d, J = 7.3 Hz, 1H), 8.66 (d, *J* = 8.2 Hz, 1H), 8.57 (d, *J* = 8.6 Hz, 1H), 8.45 (s, 1H), 7.81 (d, *J* = 8.5 Hz, 1H), 7.76 (ddd, *J* = 7.4, 4.0, 2.3 Hz, 2H), 7.69 (ddd, *J* = 8.3, 7.1, 1.5 Hz, 2H), 7.65 (ddd, J = 8.2, 6.9, 1.4 Hz, 1H), 7.59 (t, *J* = 7.5 Hz, 1H), 7.44 (d, *J* = 7.8 Hz, 1H), 7.00 – 6.93 (m, 2H), 6.89 (t, *J* = 7.7 Hz, 1H), 1.16 (d, *J* = 17.1 Hz, 9H). ^{13}C NMR (201 MHz, $CDCl_3$): δ 166.7 (d, *J* = 4.5 Hz), 136.4 (d, *J* = 2.6 Hz), 134.2, 133.5, 133.1 (d, *J* = 8.9 Hz), 132.6, 131.3, 131.1, 130.2, 129.2, 129.0, 128.9, 128.4, 128.3 (d, *J* = 10.1 Hz), 128.0, 127.6 (d, *J* = 9.6 Hz), 126.9, 125.7, 124.7 (d, *J* = 4.4 Hz), 124.6, 123.7, 122.8 (d, *J* = 75.0 Hz), 120.7 (d, *J* = 10.9 Hz), 97.8 (d, *J* = 112.4 Hz), 37.2 (d, *J* = 85.0 Hz), 25.0. ^{31}P NMR (203 MHz, $CDCl_3$): δ 49.4. HRMS (ESI+, m/z): calcd for $C_{28}H_{27}NO_4PS$ [M]+: 504.1393, found: 504.1410.

Thermal Stability Studies of Catalysts 3.14b and 3.14e

Investigation of the decomposition of catalyst **3.14b** by ^{31}P NMR at high temperature

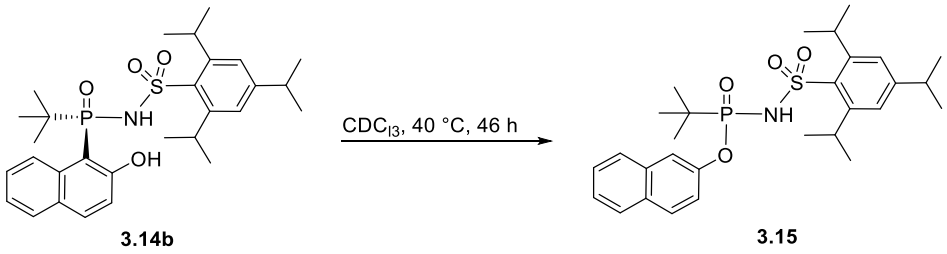

In ^{31}P NMR in $CDCl_3$: An aliquot of **3.14b** was heated in dry $CDCl_3$ at 40 °C, over 46 h; 97% conversion to **3.15** was observed (estimated by ^{31}P NMR; Figure 3.6).

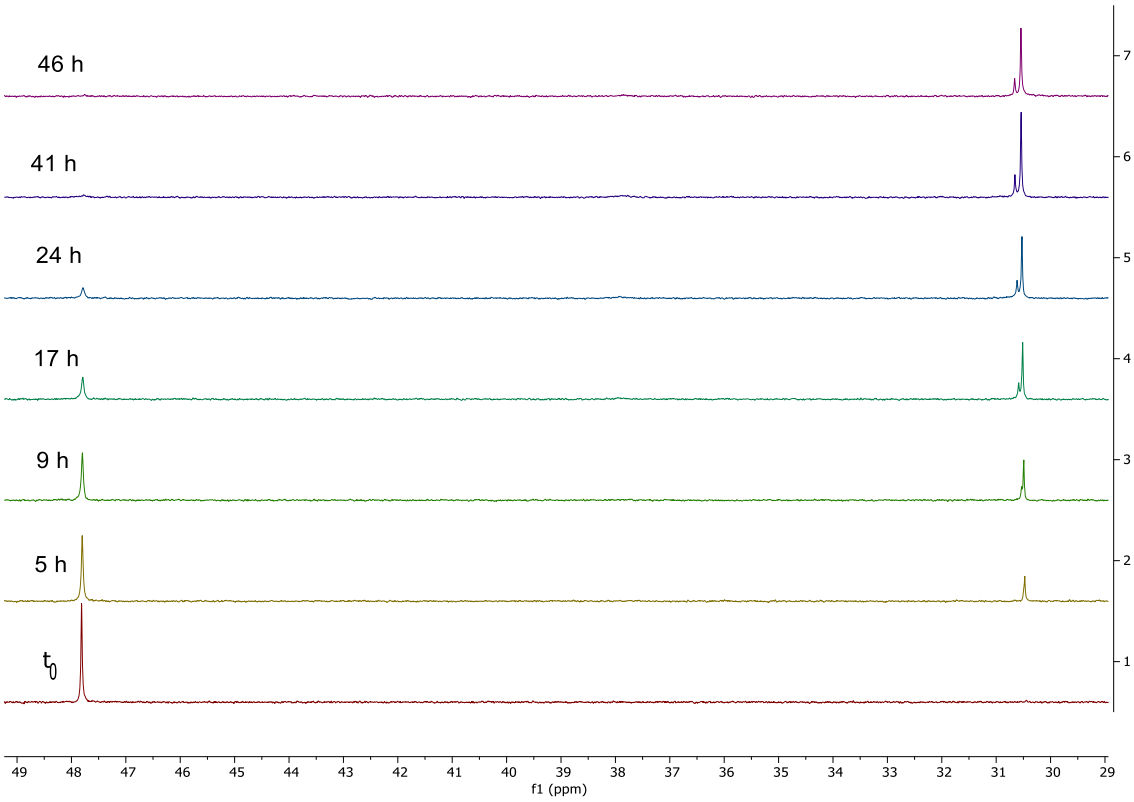

Figure 3.6. ^{31}P NMR ($CDCl_3$) showing Phospha-Brook Rearrangement of Catalyst **3.14b** over 46 h.

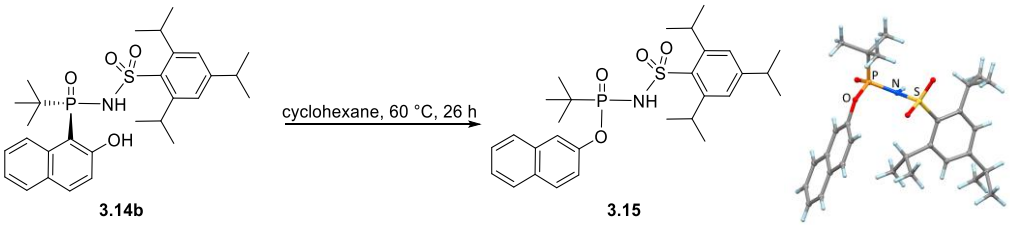

In cyclohexane: **3.14b** (18.5 mg, 0.0349 mmol) was suspended in dry cyclohexane (2 mL) and the mixture was stirred at 60 °C for 26 h, after which full conversion to **3.15** was observed. After concentrating the reaction mixture, the crude was purified on SiO_2 (0-5% MeOH/DCM) and crystallised from DCM/hexanes. ^{1}H and ^{31}P NMR analysis showed the possibility of rotomers at RT. However, at 50 °C, ^{1}H and ^{31}P NMRs showed peak coalescence.

Naphthalen-2-yl P-(tert-butyl)-*N*-((2,4,6-triisopropylphenyl)sulfonyl)phosphonamidite (3.15b)

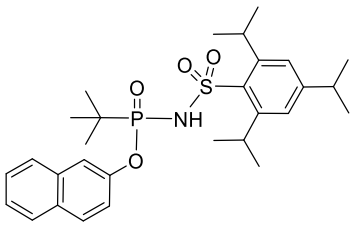

^{1}H NMR (500 MHz, $CDCl_3$): δ 7.78 – 7.68 (m, 1H), 7.67 – 7.53 (m, 1H), 7.42 – 7.30 (m, 3H), 7.20 – 7.14 (m, 1H), 7.14 – 7.09 (m, 1H), 7.07 (s, 2H), 6.23 (s, 1H), 4.09 – 3.97 (m, 2H), 2.94 – 2.79 (m, 1H), 1.41 (overlapping d, J = 18.5 Hz, 9H), 1.29 – 1.14 (m, 12H), 0.93 (overlapping d, J = 6.8 Hz, 6H). 1H NMR at 50 °C (400 MHz, $CDCl_3$) δ 7.77 – 7.66 (m, 1H), 7.62 (d, J = 8.9 Hz, 1H), 7.46 – 7.33 (m, 4H), 7.13 (dd, J = 8.9, 2.4 Hz, 1H), 7.08 (s, 2H), 6.01 (s, 1H), 4.07 (hept, J = 7.5 Hz, 2H), 2.85 (hept, J = 6.5 Hz, 1H), 1.42 (d, J = 18.5 Hz, 9H), 1.33 – 1.15 (m, 12H), 0.99 (d, J = 6.7 Hz, 6H). ^{13}C NMR (126 MHz, $CDCl_3$): δ 153.43, 150.41, 150.37, 148.40 (d, J = 11.0 Hz), 134.40, 133.89, 130.73, 129.75, 129.19, 128.37, 127.61, 126.63, 125.43, 124.10, 119.73 (d, J = 6.0 Hz), 116.06 (d, J = 5.0 Hz), 34.82, 34.24, 33.80, 30.08, 24.99, 24.66 (d, J = 3.3 Hz), 24.55, 23.68, 23.63, 21.61. ^{31}P NMR (203 MHz, $CDCl_3$): δ 30.54, 30.43. ^{31}P NMR at

50 °C (162 MHz, $CDCl_3$): δ 30.34. HRMS (ESI-, m/z): calcd for $C_{29}H_{39}NO_4PS$ [M-H]+: 528.2332, found: 528.2340.

Investigation of the decomposition of catalyst **3.14e** by ^{31}P NMR at high temperature

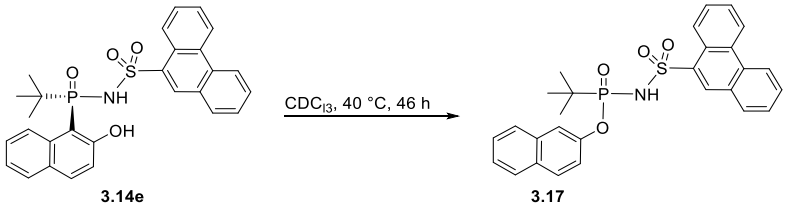

In $CDCl_3$: An aliquot of **3.14e** was heated in dry $CDCl_3$ at 40 °C, over 46 h; 95% conversion to **3.17** was observe (estimated by ^{31}P NMR; Figure 3.7).

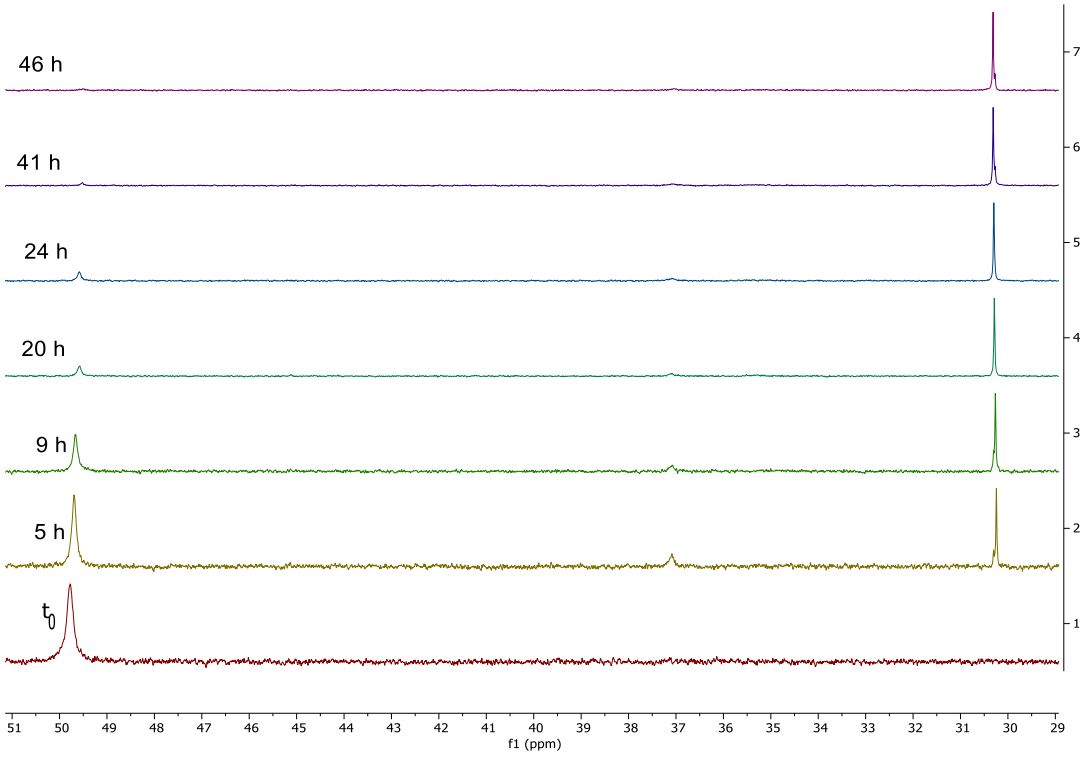

Figure 3.7. ^{31}P NMR ($CDCl_3$) showing Phospha-Brook Rearrangement of Catalyst **3.14e** over 46 h.

Scope of the Asymmetric Transfer Hydrogenation of Quinolines

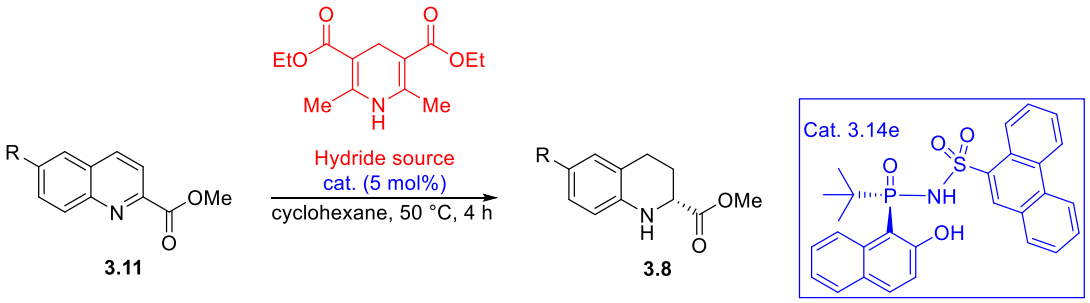

An oven dried pressure vial was cooled to ambient temperature in a desiccator and charged with the requisite quinoline-2-carboxylate (0.200 mmol), Hantzsch ester (0.500 mmol) and **3.14e** (0.0100 mmol). Subsequently, dry cyclohexane (1 mL) was added. The vial was crimp-capped and the mixture was stirred vigorously, at 50 °C for 4 h. The resulting solution was diluted with DCM (1 mL) and SiO_2 was added. The mixture was concentrated *in vacuo* and the crude was first purified by flash chromatography (0-10% EtOAc/hexanes), with the co-elution of some Hantzsch pyridine by-product. Subsequent flash chromatography on Et_3N-deactivated SiO_2 (0-10% EtOAc/hexanes) on this mixture, was sufficient to purify the product.

This reaction was repeated at 1.0 mmol scale with the same outcome in terms of yield and %ee of the product.

Methyl (*R*)-1,2,3,4-tetrahydroquinoline-2-carboxylate (3.8a)

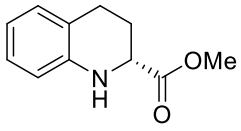

Known compound.[10] Isolated as a light-yellow oil in 73% yield (28.0 mg, 0.146 mmol) and 49% ee. ^{1}H NMR (400 MHz, $CDCl_3$); δ 7.00 (t, J = 7.6 Hz, 1H), 6.96 (d, J = 7.4 Hz, 1H), 6.65 (td, J = 7.3, 1.2 Hz, 1H), 6.59 (d, J = 8.0 Hz, 1H), 4.36 (s, 1H), 4.05 (dd, J = 8.8, 3.8 Hz, 1H), 3.78 (s, 3H), 2.84 (ddd, J = 15.1, 9.3, 5.4 Hz, 1H), 2.75 (dt, J =

16.3, 5.5 Hz, 1H), 2.29 (dtd, J = 13.0, 5.6, 3.8 Hz, 1H), 2.01 (dtd, *J* = 12.9, 9.1, 5.2 Hz, 1H). ^{13}C NMR (101 MHz, $CDCl_3$): δ 173.8, 143.1, 129.3, 127.2, 120.7, 117.8, 114.7, 54.1, 52.5, 26.0, 24.8. Chiral HPLC method: Chiralpak AD, hexane/IPA = 80/20, 1 mL/min, λ = 254 nm; (*R*)-t_R = 6.52 min (major), (*S*)-t_R = 7.82 min (minor).

Methyl (*R*)-6-fluoro-1,2,3,4-tetrahydroquinoline-2-carboxylate (3.8b)

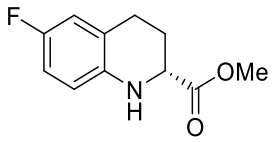

Known compound.[12] Isolated as a colourless oil (which solidifies at low temperature) in 83% yield (34.8 mg, 0.166 mmol) and 48% ee. ^{1}H NMR (500 MHz, $CDCl_3$): δ 6.72 (td, *J* = 8.5, 2.9 Hz, 1H), 6.68 (dd, *J* = 9.1, 2.9 Hz, 1H), 6.52 (dd, *J* = 8.7, 4.8 Hz, 1H), 4.25 (s, 1H), 4.01 (dd, *J* = 8.6, 3.7 Hz, 1H), 3.78 (s, 3H), 2.81 (ddd, *J* = 14.8, 8.9, 5.6 Hz, 1H), 2.73 (dt, *J* = 16.6, 5.7 Hz, 1H), 2.26 (dtd, *J* = 12.9, 5.8, 3.8 Hz, 2H), 2.05 – 1.94 (m, 1H). ^{13}C NMR (126 MHz, $CDCl_3$): δ 173.8, 155.9 (d, *J* = 235.4 Hz), 139.2 (d, *J* = 2.1 Hz), 122.0 (d, *J* = 6.9 Hz), 115.5, 115.4 (d, *J* = 29.5 Hz), 113.8 (d, *J* = 22.5 Hz), 54.1, 52.5, 26.0, 24.6. ^{19}F NMR (471 MHz, $CDCl_3$) δ -127.5. Chiral HPLC method: Chiralcel OJ-H, hexane/IPA = 70/30, 1 mL/min, 30 °C, λ = 254 nm; (*S*)-t_R = 9.97 min (minor), (*R*)-t_R = 12.80 min (major).

Methyl (*R*)-6-bromo-1,2,3,4-tetrahydroquinoline-2-carboxylate (3.8c)

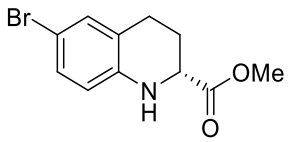

Known compound.[12] Isolated as a white solid in 76% yield (41.1 mg, 0.152 mmol) and 46% ee. Re-crystallisation: The purified compound was dissolved in a minimal quantity of hot hexanes. After cooling to rt and then at -20 °C for 12 h, the enantioenriched

mother liquor was collected using a Pasteur pipet. After drying, the process was repeated and the mother liquor was collected, dried and passed through a short SiO_2 column (0-10% EtOAc/hexanes) to obtain the enantioenriched tetrahydroquinoline in 66% ee. ^{1}H NMR (500 MHz, $CDCl_3$): δ 7.12 – 7.03 (m, 2H), 6.46 (d, J = 8.7 Hz, 1H), 4.37 (s, 1H), 4.02 (dd, J = 8.6, 3.8 Hz, 1H), 3.78 (s, 3H), 2.79 (ddd, J = 16.5, 9.1, 5.4 Hz, 1H), 2.72 (dt, J = 16.5, 5.6 Hz, 1H), 2.26 (dddd, J = 13.1, 6.3, 5.4, 3.9 Hz, 1H), 1.98 (dtd, J = 13.2, 8.9, 5.2 Hz, 1H). ^{13}C NMR (126 MHz, $CDCl_3$): δ 173.5, 142.1, 131.7, 129.9, 122.7, 116.1, 109.3, 53.8, 52.6, 25.7, 24.4. Chiral HPLC method: Chiralcel OJ-H, hexane/IPA = 70/30, 1 mL/min, 30 °C, λ = 254 nm; (*S*)-t_R = 11.20 min (minor), (*R*)-t_R = 12.65 min (major).

3.7 Associated Content

NMR spectra and chiral HPLC data are provided in Appendix II.

3.8 Author Information

Corresponding Author

*Phone 514-398-3638. Fax 514-398-3797. Email: youla.tsantrizos@mcgill.ca

3.9 Acknowledgements

We are grateful for financial support from the Natural Sciences and Engineering Research Council of Canada (NSERC) and the Fonds de recherche du Québec (FRQNT).

3.10 References

1. Reviews: (a) Meanwell, N. A. Synopsis of Some Recent Tactical Application of Bioisosteres in Drug Design. *J. Med. Chem*. **2011**, *54*, 2529-2591. (b) Meanwell, N.

A. Fluorine and Fluorinated Motifs in the Design and Application of Bioisosteres for Drug Design. *J. Med. Chem*. **2018**, *61*, 5822-5880. (c) Subbaiah, M. A. M.; Meanwell, N. A. Bioisosteres of the Phenyl Ring: Recent Strategic Applications in Lead Optimization and Drug Design. *J. Med. Chem*. **2021**, *64*, 14046-14128.

2. Kannenberg, A.; Rost, D.; Eibauer, S.; Tiede, S.; Blechert, S. A Novel Ligand for the Enantioselective Ruthenium-Catalyzed Olefin Metathesis. *Angew. Chem. Int. Ed*. **2011**, *50*, 3299-3302.

3. Hardouin, C.; Baillard, S.; Barière, F.; Copin, C.; Craquelin, A.; Janvier, S.; Lemaitre, S.; Le Roux, S.; Russo, O.; Samson, S. Multikilogram Synthesis of a Potent Dual Bcl-2/Bcl-xL Antagonist. 1. Manufacture of the Acid Moiety and Development of Some Key Reactions. *Org. Process Res. Dev.* **2020**, *24*, 652-669.

4. For a recent review see: (a) Sridharan, V.; Suryavanshi, P. A.; Menéndez, J. C. Advances in the Chemistry of Tetrahydroquinolines. *Chem. Rev*. **2011**, *111*, 7157-7259. For select examples, see: (b) Snider, B. B.; Ahn, Y.; O'Hare, S. M. Total Synthesis of (±)-Martinellic Acid. *Org. Lett*. **2001**, *3*, 4217-4220. (c) Rueping, M.; Antonchick, A. P.; Theissmann, T. A Highly Enantioselective Brønsted Acid Catalyzed Cascade Reaction: Organocatalytic Transfer Hydrogenation of Quinolines and their Application in the Synthesis of Alkaloids. *Angew. Chem. Int. Ed.* **2006**, *45*, 3683-3686. (d) Davies, S. G.; Fletcher, A. M.; Lee, J. A.; Lorkin, T. J. A.; Roberts, P. M.; Thomson, J. E. Asymmetric Synthesis of (−)-Martinellic Acid. *Org. Lett*. **2013**, *15*, 2050-2053. (e) Basarab, G. S.; Doig, P.; Galullo, V.; Kern, G.; Kimzey, A.; Kutschke, A.; Newman, J. P.; Morningstar, M.; Mueller, J.; Otterson, L.; Vishwanathan, K.; Zhou, F.; Gowravaram, M. Discovery of Novel DNA Gyrase Inhibiting Spiropyrimidinetriones: Benzisoxazole Fusion with N-Linked Oxazolidinone Substituents Leading to a Clinical Candidate (ETX0914). *J. Med. Chem*. **2015**, *58*, 6264-6282. (f) Alm, R. A.; Lahiri, S. D.; Kutschke, A.; Otterson, L. G.; McLaughlin, R. E.; Whiteaker, J. D.; Lewis, L. A.; Su, X.; Huband, M. D.; Gardner, H.; Mueller, J. P. Characterization of the Novel DNA Gyrase Inhibitor AZD0914: Low Resistance Potential and Lack of Cross-Resistance in Neisseria Gonorrhoeae. *Antimicrob. Agents Chemother.* **2015**, *59*, 1478-1486. (g)

Tsutsumi, H.; Katsuyama, Y.; Izumikawa, M.; Takagi, M.; Fujie, M.; Satoh, N.; Shin-ya, K.; Ohnishi, Y. Unprecedented Cyclization Catalyzed by a Cytochrome P450 in Benzastatin Biosynthesis. *J. Am. Chem. Soc*. **2018**, *140*, 6631-6639. (h) Taylor, S. N.; Marrazzo, J.; Batteiger, B. E.; Hook, E. W. III.; Seña, A. C.; Long, J.; Wierzbicki, M. R.; Kwak, H.; Johnson, S. M.; Lawrence, K.; Mueller, J. Single-Dose Zoliflodacin (ETX0914) for Treatment of Urogenital Gonorrhea. *N. Engl. J. Med*. **2018**, *379*, 1835-1845.

5. Reviews: (a) Wang, D. S.; Chen, Q.-A.; Lu, S.-M.; Zhou, Y.-G. Asymmetric Hydrogenation of Heteroarenes and Arenes. *Chem. Rev*. **2012**, *112*, 2557-2590. (b) He, Y.-M.; Song, F.-T.; Fan, Q.-H. Advances in Transition Metal-Catalyzed Asymmetric Hydrogenation of Heteroaromatic Compounds. *Top. Curr. Chem*. **2013**, *343*, 145-190. (c) Kim, A. N.; Stoltz, B. M. Recent Advances in Homogeneous Catalysts for the Asymmetric Hydrogenation of Heteroarenes. *ACS Catal*. **2020**, *10*, 13834-13851.

6. Reviews: (a) Akiyama, T. Stronger Brønsted Acids. *Chem. Rev*. **2007**, *107*, 5744-5758. (b) Rueping, M.; Dufour, J.; Schoepke, F. R. Advances in Catalytic Metal-Free Reductions: from Bio-Inspired Concepts to Applications in the Organocatalytic Synthesis of Pharmaceuticals and Natural Products. *Green Chem*. **2011**, *13*, 1084-1105.

7. Matralis, A. M.; Xanthopoulos, D.; Huot, G.; Lopes-Paciencia, S.; Cole, C.; de Vries, H.; Ferbeyre, G.; Tsantrizos, Y. S. Molecular Tools that Block Maturation of the Nuclear Lamin A and Decelerate Cancer Cell Migration. *Bioorg. Med. Chem*. **2018**, *26*, 5547-5554.

8. Alatorre-Santamaría, S.; Gotor-Fernández, V.; Gotor, V. Stereoselective Synthesis of Optically Active Ayclic α- and β-Amino Esters through Lipase-Catalyzed Transesterification or Interesterification Processes. *Tetrahedron: Asymmetry* **2010**, *21*, 2307-2313.

9. Maj, A. M.; Suisse, I.; Hardouin, C.; Agbossou-Niedercorn, F. Synthesis of New Chiral 2-Functionalized-1,2,3,4-Tetrahydroquinoline Derivatives via Asymmetric Hydrogenation of Substituted Quinolines. *Tetrahedron* **2013**, *69*, 9322-9328.

10. Yuan, M.; Mbaezue, I. I.; Zhou, Z.; Topic, F.; Tsantrizos, Y. S. *P*-Chiral, *N*-Phosphoryl Sulfonamide Brønsted Acids with an Intramolecular Hydrogen Bond Interaction that Modulates Organocatalysis .*Org. Biomol. Chem.* **2019**, *17*, 8690-8694.

11. Zhu, Z.-H.; Ding, Y.-X.; Wu, B.; Zhou, Y.-G. Design and Synthesis of Chiral and Regenerable [2.2]Paracyclophane-Based NAD(P)H Models and Application in Biomimetic Reduction of Flavonoids. *Chem. Sci*. **2020**, *11*, 10220-10224.

12. Zhao, Z.-B.; Wang, J.; Zhu, Z.-H.; Chen, M.-W.; Zhou, Y.-G. Enantioselective Synthesis of 2-Functionalized Tetrahydroquinolines through Biomimetic Reduction. *Org. Lett*. **2021**, *23*, 9112-9117.

13. (a) Akiyama, T.; Itoh, J.; Yokota, K.; Fuchibe, K. Enantioselective Mannich-Type Reaction Catalyzed by a Chiral Brønsted Acid. *Angew. Chem. Int. Ed.* **2004**, *43*, 1566-1568. (b) Akiyama, T. Stronger Brønsted Acids. *Chem. Rev*. **2007**, *107*, 5744–5758.

14. Uraguchi, D.; Terada, M. Chiral Brønsted Acid-Catalyzed Direct Mannich Reactions via Electrophilic Activation. *J. Am. Chem. Soc.* **2004**, *126*, 5356-5357.

15. (a) Rueping, M.; Sugiono, E.; Schoepke, F. R. Development of the First Brønsted Acid Assisted Enantioselective Brønsted Acid Catalyzed Direct Mannich Reaction. *Synlett* **2007**, 1441-1445. (b) Guo, Q.-X.; Liu, H.; Guo, C.; Luo, S.-W.; Gu, Y.; Gong, L.-Z. Chiral Brønsted Acid-Catalyzed Direct Asymmetric Mannich Reaction. *J. Am. Chem. Soc.* **2007**, *129*, 3790-3791. (c) Gridnev, I. D.; Kouchi, M.; Sorimachi, K.; Terada, M. On the Mechanism of Stereoselection in Direct Mannich Reaction Catalyzed by BINOL-derived Phosphoric Acids. *Tetrahedron Lett* **2007**, *48*, 497-500.

16. Nakashima, D.; Yamamoto, H. Design of Chiral *N*-Triflyl Phosphoramide as a Strong Chiral Brønsted Acid and Its Application to Asymmetric Diels−Alder Reaction. *J. Am. Chem. Soc*. **2006**, *128*, 9626-9627.

17. Akiyama, T.; Morita, H.; Itoh, J.; Fuchibe, K. Chiral Brønsted Acid Catalyzed Enantioselective Hydrophosphonylation of Imines: Asymmetric Synthesis of α-Amino Phosphonates. *Org. Lett.* **2005**, *7*, 2583-2585.

18. Storer, R. I.; Carrera, D. E.; Ni, Y.; MacMillan, D. W. C. Enantioselective Organocatalytic Reductive Amination. *J. Am. Chem. Soc.* **2006**, *128*, 84-86.

19. (a) Hoffmann, S.; Seayad, A. M.; List, B. A Powerful Brønsted Acid Catalyst for the Organocatalytic Asymmetric Transfer Hydrogenation of Imines. *Angew. Chem., Int. Ed.* **2005**, *44*, 7424-7427. (b) Rueping, M.; Sugiono, E.; Azap, C.; Theissmann, T.; Bolte, M. Enantioselective Brønsted Acid Catalyzed Transfer Hydrogenation: Organocatalytic Reduction of Imines. *Org. Lett.* **2005**, ***7***, 3781-3783. (c) Nguyen, T. B.; Bousserrouel, H.; Wang, Q.; Guéritte, F. Chiral Phosphoric Acid-Catalyzed Enantioselective Transfer Hydrogenation of ortho-Hydroxyaryl Alkyl N−H Ketimines. *Org. Lett.* **2010**, *12*, 4705-4707. (d) Greindl, J.; Hioe, J.; Sorgenfrei, N.; Morana, F.; Gschwind, R. M. Brønsted Acid Catalysis—Structural Preferences and Mobility in Imine/Phosphoric Acid Complexes. *J. Am. Chem. Soc.* **2016**, *138*, 15965-15971.

20. (a) Itoh, J.; Fuchibe, K.; Akiyama, T. Chiral Phosphoric Acid Catalyzed Enantioselective Friedel–Crafts Alkylation of Indoles with Nitroalkenes: Cooperative Effect of 3 Å Molecular Sieves. *Angew. Chem. Int. Ed.* **2008**, *47*, 4016-4018. (b) Zeng, M.; Kang, Q.; He, Q-L.; You, S-L. Highly Enantioselective Friedel–Crafts Reaction of 4,7-Dihydroindoles with β,γ-Unsaturated α-Keto Esters by Chiral Brønsted Acids. *Adv. Synth. Catal.* **2008**, *350*, 2169-2173. (c) Zhang, J-W.; Cai, Q.; Shi, X-X.; Zhang, W.; You, S-L. Enantioselective Synthesis of Tetrahydropyrano[3,4-b]indoles Catalyzed by Chiral N-Triflyl Phosphoramide via Intramolecular Friedel-Crafts Alkylation Reaction. *Synlett*, **2011**, 1239-1242.

21. Zhang, L-D.; Zhong, L-R.; Xi, J.; Yang, X-L.; Yao, Z-J. Enantioselective Total Synthesis of Lycoposerramine-Z Using Chiral Phosphoric Acid Catalyzed Intramolecular Michael Addition. *J. Org. Chem.* **2016**, *81*, 1899-1904.

22. Vellalath, S.; Čorić, I.; List, B. N-Phosphinyl Phosphoramide—A Chiral Brønsted Acid Motif for the Direct Asymmetric N,O-Acetalization of Aldehydes. *Angew. Chem. Int. Ed.* **2010**, *49*, 9749-9752.

23. For recent reviews, see: Phillips, A. M. F.; Pombeiro, A. J. L. Recent Advances in Organocatalytic Enantioselective Transfer Hydrogenation. *Org. Biomol. Chem.* **2017**, *15*, 2307-2340.

24. Das, A.; Volla, C. M. R.; Atodiresei, I.; Bettray, W.; Rueping, M. Asymmetric Ion Pair Catalysis of 6π Electrocyclizations: Brønsted Acid Catalyzed Enantioselective Synthesis of Optically Active 1,4-Dihydropyridazines. *Angew. Chem. Int. Ed.* **2013**, ***52***, 8008-8011.

25. (a) Tsuji, N.; Kennemur, J. L.; Buyck, T.; Lee, S.; Prévost, S.; Kaib, P. S. J.; Bykov, D.; Farès, C.; List, B. Activation of olefins via asymmetric Brønsted acid catalysis. *Science*, **2018**, *359*, 1501-1505. (b) Bae, H. Y.; Höfler, D.; Kaib, P. S. J.; Kasaplar, P.; De, C. K.; Döhring, A.; Lee, S.; Kaupmees, K.; Leito, I.; List, B. Approaching sub-ppm-level asymmetric organocatalysis of a highly challenging and scalable carbon–carbon bond forming reaction. *Nat. Chem.*, **2018**, *10*, 888-894.

26. Han, Z. S.; Wu, H.; Qu, B.; Wang, Y.; Wu, L.; Zhang, L.; Xu, Y.; Wu, L.; Zhang, Y.; Lee, H.; Roschangar, F.; Song, J. J.; Senanayake, C. H. New class of P-stereogenic chiral Brønsted acid catalysts derived from chiral phosphinamides. *Tetrahedron Lett.* **2019**, *60*, 1834-1837.

27. Hayashi, M.; Nakamura, S. Catalytic Enantioselective Protonation of α-Oxygenated Ester Enolates Prepared through Phospha-Brook Rearrangement. *Angew. Chem. Int. Ed*. **2011**, *50*, 2249-2252.

28. Kondoh, A.; Terada, M. Brønsted Base Catalyzed [2,3]-Wittig/Phospha-Brook Tandem Rearrangement Sequence. *Org. Lett*. **2013**, *15*, 4568-4571.

29. Kondoh, A.; Aoki, T.; Terada, M. Intramolecular Cyclization of Alkynyl α-Ketoanilide Utilizing [1,2]-Phospha-Brook Rearrangement Catalyzed by Phosphazene Base. *Org. Lett*. **2014**, *16*, 3528-3531.

30. Horwitz, M. A.; Zavesky, B. P.; Martinez-Alvarado, J. I.; Johnson, J. S. Asymmetric Organocatalytic Reductive Coupling Reactions between Benzylidene Pyruvates and Aldehydes. *Org. Lett*. **2016**, *18*, 36-39.

31. Kondoh, A.; Takel, A.; Terada, M. Novel Methodology for the Efficient Synthesis of 3-Aryloxindoles: [1,2]-Phospha-Brook Rearrangement–Palladium-Catalyzed Cross-Coupling Sequence. *Synlett* **2016**, *27*, 1848-1853.

32. Kondoh, A.; Ishiukawa, S.; Aoki, T.; Terada, M. Synthesis of 2,3-Allenylamides Utilizing [1,2]-Phospha-Brook Rearrangement and their Application to Gold-Catalyzed Cycloisomerization Providing 2-Aminofuran Derivatives. *Chem. Commun.* **2016**, *52*, 12513-12516.

33. Kondoh, A.; Terada, M. Brønsted Base-Catalyzed Three-Component Coupling Reaction of α-Ketoesters, Imines, and Diethyl Phosphite Utilizing [1,2]-Phospha-Brook Rearrangement. *Org. Biomol. Chem.* **2016**, *14*, 4704-4711.

34. Kondoh, A.; Ozawa, R.; Aoki, T.; Terada, M. Intramolecular Addition of Benzyl Anion to Alkyne Utilizing [1,2]-Phospha-Brook Rearrangement under Brønsted Base Catalysis. *Org. Biomol. Chem*. **2017**, *15*, 7277-7281.

35. Kondoh, A.; Aoki, T.; Terada, M. Generation and Application of Homoenolate Equivalents Utilizing [1,2]-Phospha-Brook Rearrangement under Brønsted Base Catalysis. *Chem. Eur. J*. **2017**, *23*, 2769-2773.

36. Kondoh, A.; Aita, K.; Ishikawa, S.; Terada, M. Synthesis of Tetrasubstituted Furans through One-Pot Formal [3 + 2] Cycloaddition Utilizing [1,2]-Phospha-Brook Rearrangement. *Org. Lett*. **2020**, *22*, 2105-2110.

37. Kondoh, A.; Tasato, N.; Aoki, A.; Terada, M. Brønsted Base-Catalyzed Transformation of α,β-Epoxyketones Utilizing [1,2]-Phospha-Brook Rearrangement for the Synthesis of Allylic Alcohols Having a Tetrasubstituted Alkene Moiety. *Org. Lett*. **2020**, *22*, 5170-5175.

38. Kondoh, A.; Ojima, R.; Terada, M. Formal Fluorinative Ring Opening of 2-Benzoylpyrrolidines Utilizing [1,2]-Phospha-Brook Rearrangement for Synthesis of 2-Aryl-3-fluoropiperidines. *Org. Lett*. **2021**, *23*, 7894-7899.

39. Yamamoto, Y.; Tshida, Y.; Takamizu, Y.; Yasui, T. Synthesis of (Difluoromethyl)cycloalkenes from 2-Cycloalkenones by Utilizing Phospha-Brook Rearrangement. *Adv. Synth. Catal*. **2019**, *361*, 3739-3743.

40. Cheibas, C.; Fincias, N.; Casaretto, N.; Garrec, J.; Et Kaïm, L. Passerini–Smiles Reaction of α-Ketophosphonates: Platform for Phospha-Brook/Smiles Embedded Cascades. *Angew. Chem. Int. Ed*. **2022**, *61*, e202116249.

41. Lin, Q.; Zheng, S.; Chen, L.; Wu, J.; Li, J.; Liu, P.; Dong, S.; Liu, X.; Peng, Q.; Feng, X. Catalytic Regio- and Enantioselective Protonation for the Synthesis of Chiral Allenes: Synergistic Effect of the Counterion and Water. *Angew. Chem. Int. Ed*. **2022**, *61*, e202203650.

42. Yang, J.; Qian, D.-W.; Yang, S.-D. Lewis Acid-Catalyzed Pudovik Reaction–Phospha-Brook Rearrangement Sequence to Access Phosphoric Esters. *Beilstein J. Org. Chem*. **2022**, *18*, 1188-1194.

43. For a recent review, see: Glueck, D. S. Asymmetric Synthesis of *P*-Stereogenic Secondary Phosphine -Oxides (SPOs). *Synthesis* **2022**, *54*, 271-280.

44. An oven-dried pressure vessel was cooled to ambient temperature in a desiccator and charged with methyl quinoline-2-carboxylate (188 mg, 1.00 mmol), Hantzsch ester (634 mg, 2.50 mmol) and **2.14e** (25.2 mg, 0.0501 mmol). Subsequently, anhydrous cyclohexane (5.0 mL) was added. The vial was capped, and the mixture was stirred vigorously at 50 °C for 4 h. The resulting solution was diluted with DCM (2.5 mL) and SiO_2 was added. The mixture was concentrated in vacuo and the crude material was first purified on Et_3N-deactvated SiO_2 by flash chromatography (0–3% EtOAc/hexanes), with the co-elution of some Hantzsch pyridine by-product. Purification by flash column chromatography on SiO_2 (0–5% EtOAc/hexanes) afforded the desired product **2.8** (R^2 = CO_2Me, R^6=H), as a yellow oil in 69% yield (130 mg, 0.681 mmol) and 46% ee. Chiral HPLC method: Chiralpak AD, hexane/IPA = 80:20, 1 mL/min, λ = 254 nm; t_R = 6.49 [(R)-, major], 7.78 [(S)-, minor] min. ^{1}H NMR (400 MHz, $CDCl_3$): δ = 7.00 (t, *J* = 7.6 Hz, 1 H), 6.96 (d, *J* = 7.4 Hz, 1 H), 6.65 (td, *J* = 7.3, 1.2 Hz, 1 H), 6.59 (d, *J* = 8.0 Hz, 1 H), 4.36 (s, 1 H), 4.05 (dd, *J* = 8.8, 3.8 Hz, 1 H), 3.78 (s, 3 H), 2.84 (ddd, *J* = 15.1, 9.3, 5.4 Hz, 1 H), 2.75 (dt, *J* = 16.3, 5.5 Hz, 1 H), 2.29 (dtd, *J* = 13.0, 5.6, 3.8 Hz, 1 H), 2.01 (dtd, *J* = 12.9, 9.1, 5.2 Hz, 1 H). ^{13}C NMR

(101 MHz, $CDCl_3$): δ = 173.8, 143.1, 129.3, 127.2, 120.7, 117.8, 114.7, 54.1, 52.5, 26.0, 24.8.

45. Campbell, K. N.; Helbing, C. H.; Kerwin, J. F. Studies in the Quinoline Series. V. The Preparation of Some α-Dialkylaminomethyl-2-quinolinemethanols *J. Am. Chem. Soc*. **1946**, *68*, 1840 – 1843.

46. Junbo, Z.; Shuhao, Z.; Xiaoxin, Q. Compounds for Modulating Fxr. WO2020249064A1, 2020/12/17.

47. Weitgenant, J. A.; Mortison, J, D.; Helquist, P. Samarium-Promoted Coupling of Pyridine-Based Heteroaryl Analogues of Benzylic Acetates with Carbonyl Compounds. *Org. Lett.* **2005**, *7*, 3609 – 3612.

48. Li, S-G.; Yuan, M.; Topic, F.; Han, Z. S.; Senanayake, C. H. Tsantrizos, Y. S. Asymmetric Library Synthesis of P-Chiral t-Butyl-Substituted Secondary and Tertiary Phosphine Oxides. *J. Org. Chem.* **2019**, *84*, 7291-7302.

49. Zhao, Z-B.; Wang, J.; Zhu, Z-H.; Chen, M-W.; Zhou, Y-G. *Org. Lett*. **2022**, *23*, 9112 – 9117.

<u>Chapter 4:</u> Solvent-Switchable Remote C-H Activation via 1,4-Palladium Migration Enables Site-Selective C-P Bond Formation: A New Tool for the synthesis of P-Chiral Phosphinyl Imidazole Ligands

4.1 Preface

The ability to directly functionalise C-H bonds via transition-metal catalysis, is a challenging, yet powerful tool towards the rapid synthesis of molecules. Due to their inertness and ubiquity, C-H bonds may be selectively activated using strategies such as the pre-installation of a directing group. However, in the interest of step-economy, the direct usage of the desired starting materials without pre-functionalization, is advantageous. Herein, we report the first traceless, enantiospecific, solvent-switchable strategy for the construction of C-P bonds, via a C-H activation/1,4-Pd migration cascade.

The work presented in this chapter has been adapted from a manuscript in preparation: Mbaezue, I. I.; Li, S-G.; Reddy, A. C. S.; Titi, H. M.; Tsantrizos, Y. S.

Dr. Shi-Guang Li discovered the solvent-switchable site-selectivity via 1,4-plladium migration, contributed to the optimization of the reaction conditions and the optimization of the asymmetric Suzuki-Miyaura cross-coupling to give **4.9**. Dr. Angula C. S. Reddy contributed to the optimization of the reaction conditions, synthesized one SPO and two imidazoles and contributed to the reaction design for the stereoretentive reduction of **4.5g**. Dr. Hatem M. Titi collected X-ray crystallography data used in identifying the absolute configuration and substitution patterns of the compounds. Ifenna I. Mbaezue contributed to the reaction optimization, synthesized the remaining starting materials and performed the substrate scope, synthesized ligand **4.6** and applied it in the Suzuki-Miyaura cross-coupling reaction to give **4.9,** and performed the mechanistic studies. Youla S. Tsantrizos, Ifenna I. Mbaezue and Shi-Guang Li co-wrote the manuscript.

4.2 Abstract

Solvent-switchable site-selective phosphorylation of imidazoles at the C2 or C5 position of the imidazole ring was achieved via 1,4-palladium migration. *P*-chiral *tert*-butyl(aryl)phosphine oxides were cross-coupled to 1-(2-bromophenyl)-1*H*-imidazoles with high enantiospecificity, leading to a novel class of chiral imidazole-based phosphine oxides. As proof of concept, reduction of an analog yielded the corresponding *P*-chiral 2-phosphinyl imidazole ligand, which was shown to induce high enantioselectivity in the formation of atropisomers, synthesized via a Pd-catalyzed Suzuki-Miyaura cross-coupling reaction.

4.3 Introduction

Numerous metal-mediated catalytic transformations involve exchangeable phosphorus- and/or nitrogen-based ligands. In 2001, Grotjahn introduced the 2-phosphinyl imidazole ligands and demonstrated that they can form Ru-complexes capable of accepting a proton or a hydrogen bond, and catalyze the anti-Markovnikov hydration of terminal alkynes.[1] In addition to their monodentate properties,[2] these hemilabile ligands can engage in bidentate η^2 *P*,*N*-chelation of metals, through the formation of four-membered metallacycles.[3] Soon after, Beller reported the applications of 2-phosphinyl imidazole ligand (Figure 4.1a; **L4.1a-h**) in complexes with metals for several reactions, including Buchwald-Hartwig amination and Suzuki-Miyaura cross-coupling (Pd-**L4.1a**,**b**),[4a] Sonogashira cross-coupling (Pd-**L4.1c**),[4b] hydroxylation of aryl halides (Pd-**L4.1c,d**),[4c] carbonylative Heck cross-coupling (Pd-**L4.1d**),[4d] and hydroformylation of olefins (Os-**L4.1f**, Ru-**L4.1e-h**, Ru-**L4.2**).[4e-g] More recently, Baudoin reported the Pd-catalyzed Barbier-Negishi coupling of secondary alkyl bromides with aryl and alkenyl triflates, as well as nonaflates with limited isomerization of the alkylpalladium complex (Pd-**L4.1i**,**j**).[5] In addition to their applications as ligands for cross-coupling, 2-phosphinyl imidazoles have displayed excellent amenability to other reactions such as Ru-catalyzed alkene isomerizations.[6]

Beller also reported the remarkable utility of *P*-pyridyl substituted 2-phosphinyl imidazole ligand **L4.3**, which catalyzes the methylation of nitroarenes to methylanilines (Figure 4.1b).[7] Interestingly, significant differences in catalytic properties have been observed between metal complexes of 2-phosphinyl imidazoles and those of the structurally related Buchwald-type ligands (Fig 4.1a; **L4.4**, **L4.5**). For example, whereas the Pd-catalyzed hydroxylation of aryl halides in the presence of **L4.1c** proceeds with acceptable yield, the same reaction provides only trace amounts of product with *t*-BuXPhos (Figure 4.1b**, L4.4**).[4c] In contrast, the Pd-RuPhos complex (Pd-**L4.5**) catalyzes the Barbier-Negishi coupling of secondary alkyl bromides far more efficiently than the Pd-**L4.1k** complex (Figure 4.1c),[5] highlighting the importance of structural diversity in ligand design.

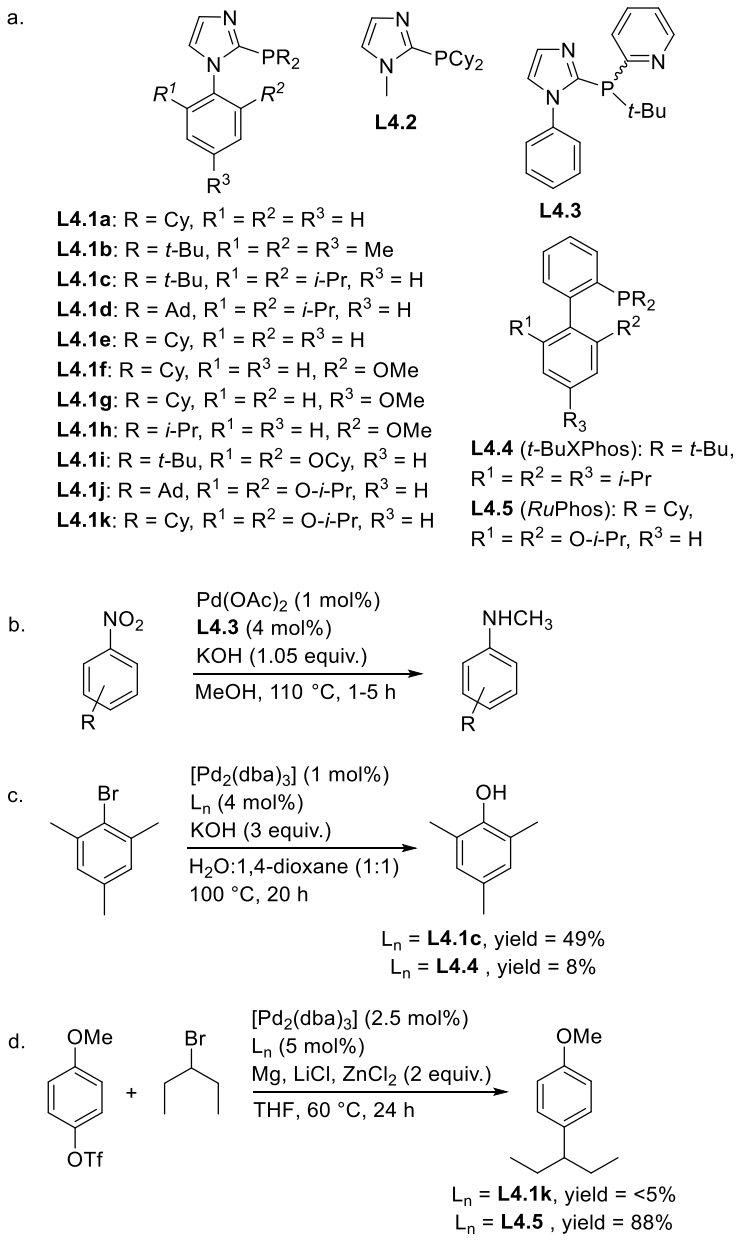

Figure 4.1. Representative Examples of 2-Phosphinyl Imidazole and Buchwald-type Ligands in Catalysis.

Despite the significant achievements highlighted above, the synthesis and applications of *P*-chiral phosphinyl imidazolyl ligands have not been reported. Traditionally, 2-phosphinyl imidazoles are synthesized by quenching C2-metalated imidazoles with the requisite chlorophosphines (Scheme 4.1a),[1,8] which requires the handling of highly sensitive reagents. The configurational instability of chlorophosphines[9] precludes the synthesis of *P*-chiral analogues via this route. In

contrast, stereoretentive reduction of chiral phosphine oxides[10] could circumvent these challenges and afford *P*-chiral phosphinyl imidazoles.

Over the past two decades, through-space 1,4-palladium migration - has emerged as a powerful strategy for the construction of C-C and C-N,[11] C-O,[12] C-B,[13] C-Si[14] and very recently, C-P[15] bonds. We envisioned that the remote C(sp^2)–H activation of imidazoles via 1,4-palladium migration could furnish palladated intermediates of various substitution patterns (Scheme 4.1b; intermediates **I** and/or **II**). The subsequent coupling of these intermediates with *P*-chiral secondary phosphine oxides (SPOs), could furnish tertiary phosphine oxides (TPOs) that could serve as precursors to *P*-chiral phosphinyl imidazoles. Herein, we report the first solvent-switchable and site-selective *P*-chiral phosphorylation of imidazoles, via 1,4-palladium migration. Additionally, we provide an example of the utility of this novel methodology towards the synthesis of a novel *P*-chiral phosphinyl imidazole ligand for asymmetric catalysis.

.

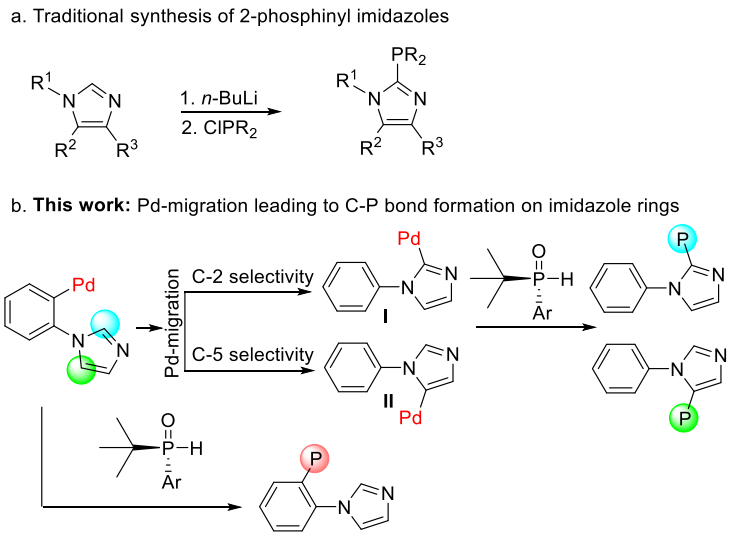

Scheme 4.1. Strategies towards the Installation of Phosphorus on Imidazoles.

4.4 Results and Discussion

We reasoned that a thorough exploration of reaction conditions may reveal parameters that would favour palladium migration to either the C2 or the C5 position of the imidazole moiety, as opposed to direct cross-coupling to the phenyl moiety. We began by investigating the effects of various catalysts, solvents, bases and temperatures on the coupling of the racemic SPO **4.1a** with imidazole **4.2a** (Table 4.1; refer to supplementary information for more details).

Table 4.1. Optimization of Reaction Conditions.

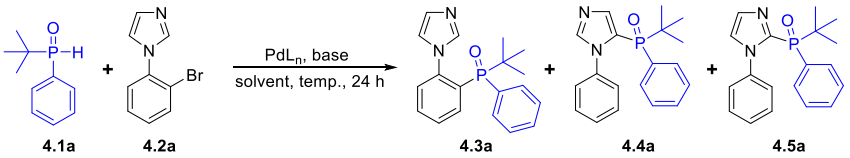

4.1a **4.2a** **4.3a** **4.4a** **4.5a**

Entry[a]	[Pd]	L_n	Base	Solvent	Temp. °C	4.3a:4.4a:4.5a[b]
1	**$Pd(PPh_3)_4$**	**-**	**DIPEA**	**DMF**	**110**	**90:9:1**
2	$Pd(PPh_3)_4$	-	DIPEA	DMSO	110	59:37:4
3	$Pd(OAc)_2$	PPh_3	DIPEA	DMSO	110	56:40:4
4	$Pd(OAc)_2$	PPh_3	DIPEA	DMSO:H_2O (1:1)	110	24:47:29
5	$Pd(OAc)_2$	PPh_3	DIPEA	DMSO:H_2O (10:1)	110	31:55:14
6	$Pd(OAc)_2$	PPh_3	DIPEA	DMSO:H_2O (10:1)	80	45:54:1
7	**$Pd(PPh_3)_4$**	**-**	**DIPEA**	**DMSO:H_2O (10:1)**	**100**	**13:74:13**
8	$Pd(PPh_3)_4$	-	DIPA	DMSO:H_2O (10:1)	100	8:64:28
9	$Pd(OAc)_2$	PPh_3	DIPEA	MeOH	110	41:28:31
10	$Pd(OAc)_2$	PPh_3	DIPEA	*n*-BuOH	110	59:26:15
11	$Pd(OAc)_2$	PPh_3	DIPEA	*i*-PrOH	110	81:14:5
12	$Pd(OAc)_2$	PPh_3	DIPEA	*t*-BuOH	110	92:7:1
13	$Pd(OAc)_2$	PPh_3	DIPEA	ethylene glycol:H_2O (10:1)	110	26:8:66
14	$Pd(OAc)_2$	PPh_3	DIPEA	ethylene glycol	110	24:8:68
15	$Pd(OAc)_2$	PPh_3	DIPEA	glycerol	110	30:26:44
16	$Pd(OAc)_2$	PPh_3	DIPEA	ethylene glycol	130	17:8:75
17	$Pd(PPh_3)_4$	-	DIPEA	ethylene glycol	130	24:3:73
18	**$Pd(PPh_3)_4$**	**-**	**DIPA**	**ethylene glycol**	**130**	**18:2:80**
19	$Pd(PPh_3)_4$	-	DIPA	DMF	130	52:26:22
20	$Pd(PPh_3)_4$	-	DIPA	DMSO:H_2O (10:1)	130	14:36:50

[a]All reactions were run in parallel without individual optimization, using racemic **4.1a** (0.10 mmol) and **4.2a** (0.15 mmol) for 24 h with either $Pd(OAc)_2$ (10 mol%)/PPh_3 (25 mol%) or $Pd(PPh_3)_4$ (10 mol%), base (4 equiv.), solvent (1.0 mL). [b]Estimated ratio based on ^{31}P NMR.

Cross-coupling catalyzed by $Pd(PPh_3)_4$ in the presence of DIPEA at 110 °C in DMF, led predominantly to the direct cross coupling at the phenyl moiety in a ratio of

the products **4.3a**:**4.4a**:**4.5a** of 90:9:1, as estimated by ^{31}P NMR (entry 1). However, replacement of DMF with DMSO as the solvent, led to an increase in the formation of the C5 coupled product **4.4a**, presumably via 1,4-palladium migration, and a decrease in **4.3a** (Table 4.1; entry 2). Changing the catalyst to $Pd(OAc)_2/PPh_3$ marginally improved the selectivity for **4.4a** (entry 3), whereas reactions catalyzed by $Pd(PPh_3)_4$ in a mixture of DMSO:H_2O (in variable ratios) and slightly lower temperatures led to more appreciable selectivity for the formation of compound **4.4a** (entries 4-8). Interestingly, replacement of DMSO:H_2O with simple alcohols, reversed the selectivity to the direct cross-coupling at the phenyl moiety (entries 9-12). However, replacement of DMSO:H_2O with ethylene glycol:H_2O (10:1) led to preferential coupling of the SPO at the C2 of the imidazole, leading to the formation of product **4.3a**:**4.4a**:**4.5a** in a ratio of 26:8:66 (entry 13).

Inspired by this phenomenon, we sought to investigate the effects of other polar and polyprotic solvents. Cross coupling of **4.1a** with **4.2a** under the same overall conditions as in entry 13 (Table 4.1), with only ethylene glycol as the solvent marginally increased the formation of **4.5a** (entry 14), whereas, the triol, glycerol, resulted in almost no site selectivity (entry 15). Reverting to ethylene glycol and increasing the temperature to 130 °C improved the selectivity for **4.5a** (entry 16). Finally, while replacing $PdOAc_2/PPh_3$ with $Pd(PPh_3)_4$ had a negligible effect on the yield of **4.5a** (entry 16 vs. 17), switching the base to DIPA, led to the formation of **4.5a** as the major product in a ratio of **4.3a**:**4.4a**:**4.5a** of 18:2:80 (entry 18). Finally, in order to gain greater insight as to the solvent and temperature effects on the site selectivity, we compared the reaction outcomes in DMF, DMSO:H_2O (10:1) and ethylene glycol at 130 °C, using $Pd(PPh_3)_4$ as the catalyst and DIPA as the base. The outcomes of these test reactions seem to indicate that **4.4a** and **4.5a** are the thermodynamic products. For example, at 130 °C in DMF, the ratio of the direct coupling product **4.3a** to the combined 1,4-palladium migration products (**4.4a** + **4.5a**) was 56:48 (entry 19), as compared to 90:10 at 110 °C (entry 1). Although the overall ratio of direct coupling to total migration products was almost the same in DMSO:H_2O (10:1) as that observed in

ethylene glycol, in the latter case, there was an increase in cross coupling to the more electron deficient C2 carbon of the imidazole ring (entry 20 vs 18). At this time, the solvent effect on the site selectivity between the C2 and C5 position of the imidazole remains unclear. However, it is plausible that although DMSO, H_2O, simple alcohols and ethylene glycol can all act as coordinating ligands to the palladium metal, only ethylene glycol can potentially form a monodentate coordination with Pd(II) and simultaneously form a hydrogen bond to the N3 of the imidazole, thus orienting palladation at the C2 position.

Subsequently, we pursued the coupling of the highly enantioenriched SPO (*S*)-**4.1a** (>99% ee)[16] with imidazoles **4.2**[17] under our optimized conditions for each of the potential products (S)-**4.3a**, (S)-**4.4a** and (S)-**4.5a** (Figure 4.2). Under the condition of entry 1 (Table 4.1) cross-coupling of (*S*)-**4.1a** with **4.2** gave (*S*)-**4.3a** in 83% ee (~83% es) and 46% isolated yield. It is noteworthy that although all of the SPO (*S*)-**4.1a** was consumed within the 18 h reaction period, we observed that a portion had oxidized to the corresponding phosphinic acid and some debromination of the imidazole **4.2** had also occurred, thus compromising the final isolated yield of (*S*)-**4.3a**. Nonetheless, we continued with our investigation into the enantioretentive properties of this methodology without further optimization of the reaction conditions.

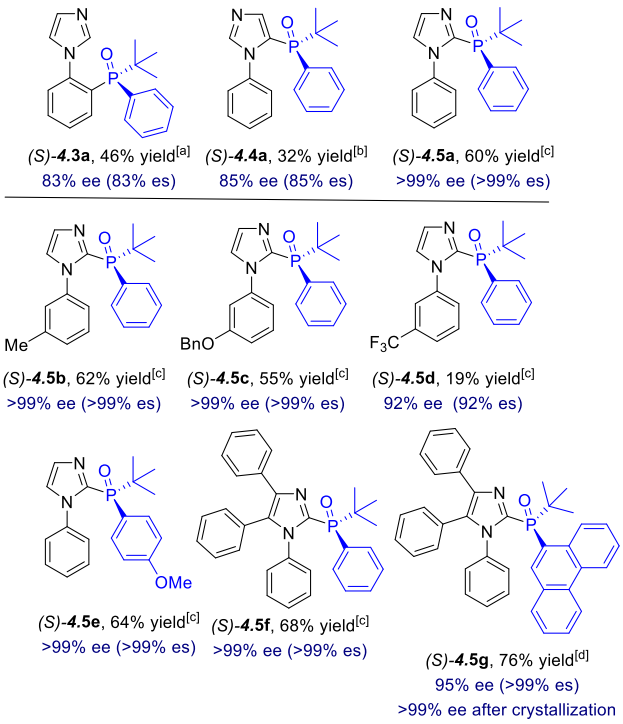

Figure 4.2. Scope of Site-Selective Coupling. [a]SPO (>99% ee) 0.20 mmol, imidazole (0.30 mmol), DIPEA (4.0 equiv.), DMF (2 mL), 110 °C, 18 h. [b]Solvent, temperature and time changed to DMSO:H_2O (10:1, 2 mL), 100 °C and 48 h. [c]Base, solvent, temperature and time changed to DIPA (4 equiv.), ethylene glycol (2 mL), 130 °C, 18 h. [d]SPO (95% ee) 1.08 mmol, imidazole (1.62 mmol), DIPA (4 equiv.), ethylene glycol (10.8 mL), 18 h.

We subsequently investigated the enantiospecificity of the conditions favoring substitution at the C5 of the imidazole using the reaction conditions of entry 7 (Table 4.1), and obtained product (*S*)-**4.4a** with minimal erosion of chiral integrity (85% ee; 85% es), *albeit* in low isolated yield (32%). For this initial study into *P*-chiral imidazole ligands, we chose to focus on the C2-imidazole phosphonylation using the optimized conditions of entry 18 (Table 4.1). We were pleased to see that the cross-coupling of (*S*)-**4.1a** (>99% ee) with **4.2** under these conditions gave (*S*)-**4.5a** without any erosion in chirality (>99% ee; >99% es) and in 60% isolated yield. This favorable outcome was also confirmed with a few other electron rich imidazoles, leading to the formation of products (*S*)-**4.5b,c,f** in >99% ee (>99% es) in all cases, with 55-68% isolated yields

(Figure 4.2). However, based on one example of an electron-deficient imidazole, product **4.5d** was obtained with slightly lower enantioretention (92% ee; 92% es) and in only 19% isolated yield. As a proof of concept, (*S*)-*tert*-butyl(4-methoxyphenyl)phosphine oxide (>99% ee) and (*S*)-*tert*-butyl(phenanthren-9-yl)phosphine oxide (95% ee) were also explored under the same reaction condition, leading to the formation of (*S*)-**4.5e** (>99% ee; >99% es) and (*S*)-**4.5g** (95% ee; >99% es; >99% ee after crystallization), respectively (Figure 4.2). Both products were formed without any loss of chiral integrity in 64-76% isolate yields. The enantiomeric purity of all products was determined by chiral HPLC. The absolute configuration of key compounds was confirmed by their single-crystal X-ray structure (Figure 4.3) and that of other compounds, assigned by analogy.

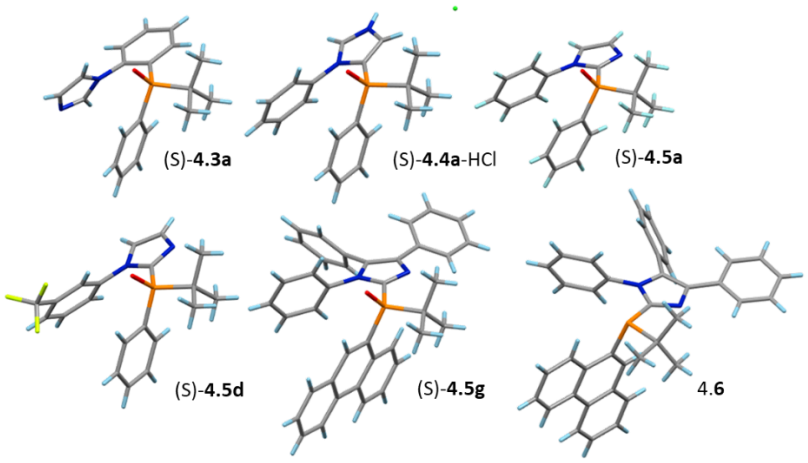

Figure 4.3. Single-Crystal X-ray Structure of *P*-chiral 2-Phosphonyl Imidazoles (S)-**4.3a**, (S)-**4.4a**-HCl**, (S)-4.5a**, (S)-**4.5d**. (S)-**4.5g** and *P*-chiral 2-phosphinyl imidazole **4.6**.

We subsequently turned our attention to the utility of these novel *P*-chiral ligands and selected to investigate the trivalent phosphine analogue of (*S*)-**4.5g**, as a model ligand, in a metal-catalyzed asymmetric reaction. Stereoretentive reduction of (*S*)-**4.5g** using catalytic[18] or stoichiometric[19] amount of $Ti(O\text{-}i\text{-}Pr)_4$ and a slight excess of TMDS were unsuccessful. However, with super-stoichiometric equivalents of both reagents,

the reduction proceeded within 72 h, to afford **4.6** in 38% isolated yield and 98% ee after column chromatography (Scheme 4.2a). The structure and absolute stereochemistry of **4.6** were also confirmed by single-crystal X-ray diffraction (Figure 4.3). As a proof of concept, we reasoned that the electron-rich nature (^{31}P NMR, CD_2Cl_2, δ = -26.5 ppm) and bulkiness of this ligand could promote the oxidative addition and reductive elimination steps of cross-coupling reactions,[4a,20] such as the asymmetric Pd-catalyzed Suzuki-Miyaura reaction. We were pleased to see that coupling of bromide **4.7** to the naphthalene boronic acid **4.8** afforded atropisomer **4.9** in 89% yield and 86% ee (Scheme 4.2b). Interestingly, although crystallization of **4.9** in Et_2O/DCM at -20 °C, led to the formation of poorly-enantioenriched crystals, the mother liquor contained this compound in >99% ee. Tang and co-workers have previously reported preparation of the same atropisomer **4.9**[21a] in slightly higher yield and enantiomeric purity using the *P*-chiral ligand (*2S,3S*)-3-(*tert*-butyl)-4-(2,6-dimethoxyphenyl)-2-methyl-2,3-dihydrobenzo[d][1,3]oxaphosphole **4.10** (Scheme 4.2c).[21b] The absolute configuration of product **4.9**, which was obtained by using our methodology, was assigned by comparison of chiral HPLC data using the same chiral HPLC conditions as those previously reported.[21a]

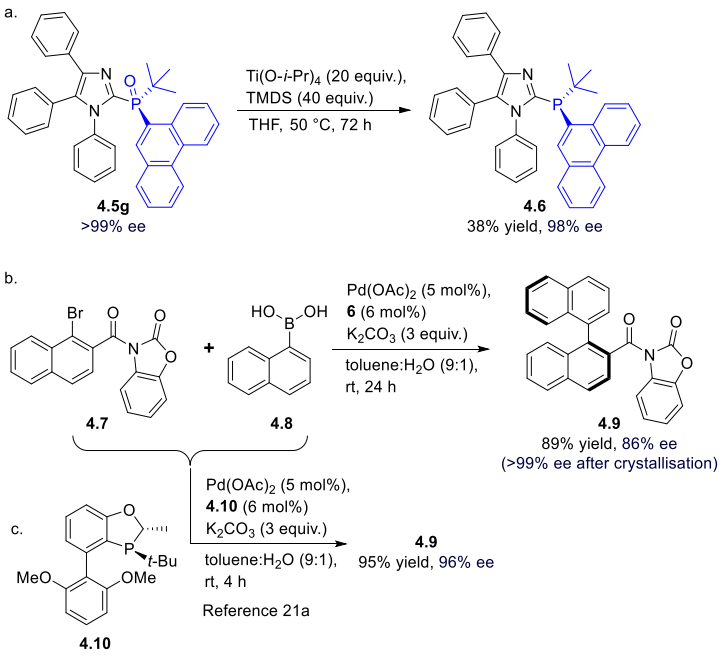

Scheme 4.2. Synthesis of *P*-Chiral 2-Phosphinyl Imidazole and its Application in an Asymmetric Suzuki-Miyaura Cross-Coupling Reaction.

In an effort to gain further insight into the mechanism of the 1,4-palladium migration, **4.1a** was subjected to conditions favoring cross-coupling to the C2 of the imidazole and leading to products **4.5a**, using the C2-deuterated imidazole ^{2}H-**4.2a** (Scheme 4.3). However, we did not observe any deuterium incorporation in product **4.5a**, suggesting that the transformation is not H-retentive in the 1,4-palladium migration step. Furthermore, we did not observe the formation of any product when the nonbrominated analog of **4.2a** (i.e. compound **4.11**) was used, eliminating the possibility of any direct C-H activation or oxidative coupling on the imidazole ring.

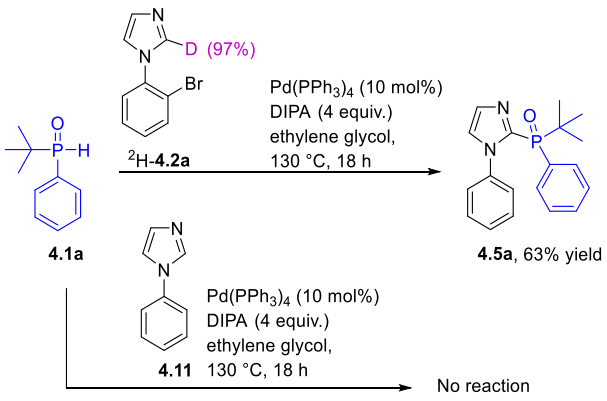

Scheme 4.3. Investigations of Deuterium Incorporation in the C2-Imidazole Site-Selective Reaction and the Possibility of Direct C-H Activation/Oxidative Coupling.

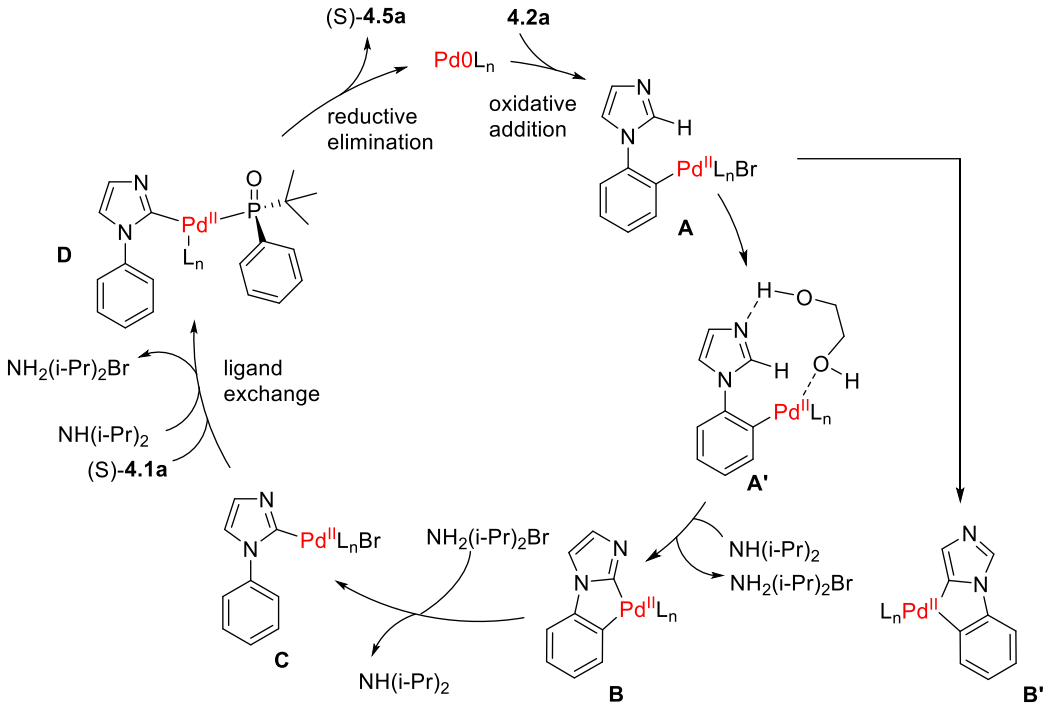

Scheme 4.4. Proposed Mechanism.

Based on all of our observations and literature precedents,[15,22] we propose the mechanism shown in Scheme 4. Oxidative addition of Pd(0) to **4.2a** is expected to generate the arylpalladium(II) species **A**. The subsequent 1,4-palladium migration can lead to the formation of palladacycles **B** and **B'**, which upon protonation would generate

C (or the corresponding **C'** intermediate; the latter is not shown). As mentioned previously, the plausible coordination effects of ethylene glycol, favoring the C2 1,4-migration of the metal is indicated in intermediate **A'**. Ligand exchange on intermediate **B**, followed by displacement of the bromide by the nucleophilic addition of the SPO is expected to give intermediate **D**, which upon reductive elimination can lead to (S)-**4.5a**. Intermediate **B'** can follow a similar catalytic cycle to give (S)-**4.4a**. An analogous mechanism has been proposed by Fu and Feng for the phosphorylation of C(sp^3)-H bonds via a 1,4-palladium migration, in the presence of non-chiral H-phosphonates.[15] In addition to this proposed Pd(0) to Pd(II) catalytic cycle the involvement of other Pd(IV) species in 1,4-palladium migration mechanisms has been proposed by Mota and Dedieu.[22b]

4.5 Conclusion

In summary, we have developed an enantiospecific solvent-switchable methodology to access various *P*-chiral 2-phosphonyl oxide imidazoles via 1,4-palladium migration. The reaction conditions that favour the C2-substituiton on the imidazole moiety are of particular interest since they provide valuable precursors for the simple preparation of *P*-chiral 2-phosphinylimidazole ligands. As a proof of concept, one such ligand was used in the successful asymmetric Suzuki-Miyaura cross-coupling reaction. Currently, the synthesis of a structurally diverse library of *P*-chiral compounds of general structures **4.4** and **4.5** is in preparation in order to fully explore the potential applications of such ligands in a variety of asymmetric transformations.

4.6 Experimental Section

General Procedure: All reactions were carried out under anhydrous conditions and under an atmosphere of dry argon, unless otherwise stated. Compounds were purified by normal phase flash column chromatography on silica gel (SDS, 60 Å C. C. 40-63 mm) as the stationary phase. Where necessary, further purification was carried out by

reversed phase column chromatography on C18 silica gel (SDS, 100 Å 20-40 μm). Thin Layer Chromatography (TLC) was performed on alumina plates pre-coated with silica gel (Merck silica gel, 60 F254), which were visualized by UV when applicable (λmax = 254 nm and/or 366 nm) and/or by staining with vanillin or anisaldehyde in acidic ethanol and/or $KMnO_4$ in basic water followed by heating. Key compounds were fully characterized by ^{1}H, $^{13}C\{^{1}H\}$ and $^{31}P\{^{1}H\}$ NMR and HRMS. Chemical shifts (δ) are reported in ppm relative to the internal deuterated solvent or external H_3PO_4 (δ 0.00 ^{31}P), unless indicated otherwise. High-resolution MS spectra were recorded using electrospray ionization (ESI+/-) and Fourier transform ion cyclotron resonance mass analyzer (FTMS).

The reactions were monitored either by TLC or analytical HPLC/MS to confirm completion and homogeneity of the products. Analytical HPLC was performed using a reversed phase C18 5 μm column on a Waters Atlantis T3 instrument and the solvent system indicated below:

Solvent A: H_2O, 0.1% formic acid

Solvent B: CH_3CN, 0.1% formic acid

Mobile phase: linear gradient from 95%A and 5%B to 5%A and 95%B in 13 min, then 2 min at 100% B

Flow rate: 1 mL/min

The enantiomeric purity of chiral compounds was determined by chiral HPLC using an Agilent 1100 series instrument and the column and solvent system indicated for each compound. The absolute configuration of key compounds was confirmed by their single-crystal X-ray structures and that of all other compounds assigned by analogy. The absolute configuration of the atropisomeric product **4.9** was assigned by comparison of its chiral HPLC chromatogram, using the same chiral HPLC conditions, as that previously reported.[21a]

Solvents used for reactions:

THF was dried and deoxygenated by distillation over sodium wire and benzophenone under a nitrogen atmosphere.

DMF was purchased from Fisher Scientific and stored over activated 3Å MS. Prior to use, it was filtered through a 0.45 μM syringe filter to remove particulates. Subsequently, it was sparged with argon for 2 hours.

Ethylene glycol was purchased from Sigma Aldrich in a Sure-Seal bottle and maintained under argon.

DMSO (HPLC grade) was used after sparging with argon for 2 hours.

Deionized water was used after sparging with argon for 2 hours.

$CDCl_3$ was purchased from Sigma Aldrich and stored over activated 3Å MS.

D_2O was purchased from Sigma Aldrich and used without further purification.

Crystallization conditions:

The desired compounds (solids) were dissolved in a minimal volume of DCM in a screw-cap vial and an equal volume of pentane or hexanes was added. The cap was loosely screwed on the vial, with gradual evaporation occurring over a 1-2 day period, to give crystals. For compound **4.6**, a minimal volume of Et_2O was used to dissolved it, followed by slow evaporation over a few hours to afford crystals. When the compound was an oil (i.e. (S)-**4.4a**), it was first converted to the HCl salt using 1M HCl in dioxane and concentrated to dryness. The resulting oil was suspended in pentane (1 mL) and vigorously stirred until a sticky white solid formed. A minimal volume of EtOAc was added dropwise, with warming, until complete dissolution occurred. The solution was allowed to evaporate to 1/3 of its volume at room temperature and then stored at -20 °C, with the formation of crystals.

Synthesis and Characterization of SPOs:

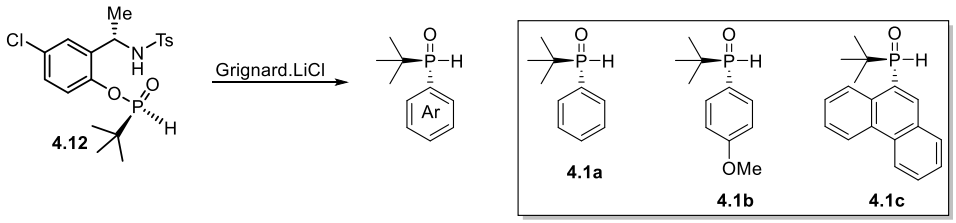

We previously reported the asymmetric synthesis of 4-chloro-2-((S)-1-((4-methylphenyl)sulfonamido)ethyl)phenyl (R)-*tert*-butylphosphinate oxide (**4.12**), as well as the asymmetric synthesis of SPOs **4.1a**, **4.1b** and **4.1c**.[16] However, the synthesis of **4.1c** was achieved in higher enatiomeric purity to that previously reported via minor modifications of the previously published protocol.

Synthesis of SPO **4.1c**:

A 100 mL oven-dried round bottom flask was equipped with an oven-dried stir bar and cooled to ambient temperature in a desiccator. LiCl (204 mg, 4.80 mmol) and Mg metal (117 mg, 4.80 mmol) were added and flame-dried under vacuum. The flask was cooled to ambient temperature under Ar, 9-bromophenanthrene (1.03 g, 4.00 mmol) was added and the flask was put through 3 cycles of evacuation and Ar back-filling. Anhydrous THF (5 ml) was added under Ar, and while stirring vigorously, 1,2-dibromoethane (6 drops) was added. The resulting yellow mixture was stirred vigorously at RT for 3 h, during which time it became warm and acquired a greenish-yellow colour. After 3 h, only residual Mg was left and the Grignard solution was used as such. While the Grignard reagent was being generated, a 100 mL oven-dried 3-neck flask was charged with an oven-dried stir bar and phosphinate oxide **4.12** (430 mg. 1.00 mmol). The flask was fitted with a thermometer, an adapter and a rubber septum, and put through 3 standard cycles of evacuation and argon-backfilling. The compound was then dissolved in THF (5.0 mL) and cooled to an internal temperature of 0 °C, and the previously generated Grignard solution was added dropwise over 20 min using a syringe pump, while maintaining the internal temperature between 0 - 5 °C. The resulting yellow solution was allowed to warm to 10 °C over a 30 min period. Subsequently, it was

removed from the cooling bath and stirred at RT for an additional 30 min. The solution was cooled back to an internal temperature of 0 °C, quenched with aqueous NH_4Cl (5 mL) and diluted with EtOAc (15 mL). The resulting mixture was directly decanted into a separatory funnel, and the salt residue was washed with EtOAc (3 x 20 mL) and filtered to remove the metal salts. The EtOAc layers were combined and extracted with brine (10 mL). The aqueous layer was further back extracted with EtOAc (2 x 15 mL) and the combined organic layers were dried over anhydrous Na_2SO_4 and concentrated under reduced pressure at RT. The crude product was purified by column chromatography on silica get using a Combi flash instrument, and a solvent gradient of 0-100% hexanes/EtOAc, to give the desired product as a white foam in 73% yield (206 mg, 0.729 mmol) and 95% ee.

Synthesis of Imidazoles:

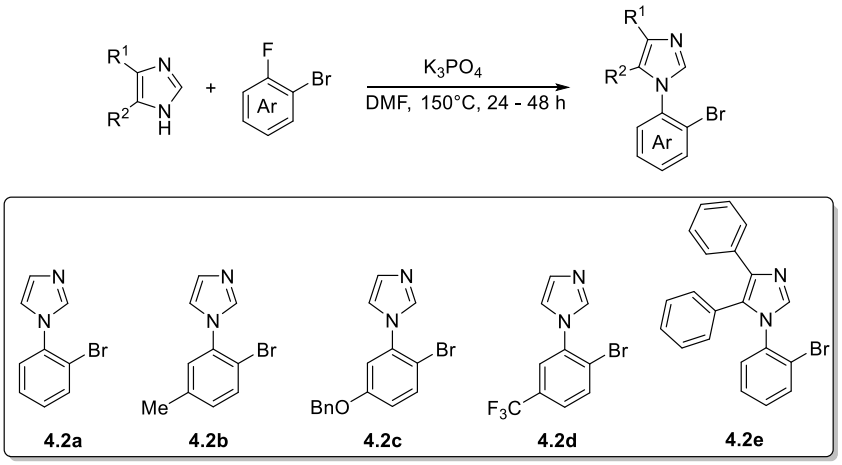

Imidazoles **4.2a-e** were synthesized according to a previously reported protocol, with minor modifications.[17]

A general protocol is provided below:

A 150 mL pressure vessel equipped with a stir bar, was charged with the imidazole precursor (8.00 mmol), K_3PO_4 (40.0 mmol), dry DMF (28 mL) and the requisite fluorobenzene (16.0 mmol). The flask was capped and stirred at 150 °C for 24 h for **4.2a-d** and 48 h for **4.2e**. The resulting reaction mixture was diluted with DCM (25 mL)

and the solution was filtered. The solid residue was washed with DCM (2 x 25 mL) and combined organic layers were concentrated under reduced pressure. The resulting oil was diluted with EtOAc (50 mL), transferred to a separatory funnel and washed with distilled water (5 x 20 mL) followed by brine (20 mL). The organic layers were dried over anhydrous Na_2SO_4 and concentrated under reduced pressure. The crude product was purified by column chromatography on silica gel using a Combi flash instrument and a solvent gradient from 0-40% EtOAc/Hexanes, to give the desired compounds in 32 – 71% yield. If necessary, the obtained solid could be triturated with a hot solution of EtOAc in hexanes (20% v/v) and then cooled to 0 °C to increase the product's purity.

1-(2-bromophenyl)-1H-imidazole (4.2a)

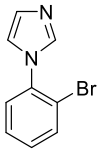

The product was obtained as a white solid. ^{1}H NMR (500 MHz, $CDCl_3$): δ 7.73 (dd, *J* = 7.9, 1.4 Hz, 1H), 7.67 (t, *J* = 1.1 Hz, 1H), 7.46 – 7.40 (m, 1H), 7.37 – 7.29 (m, 2H), 7.21 (t, *J* = 1.1 Hz, 1H), 7.14 (t, *J* = 1.4 Hz, 1H). ^{13}C NMR (126 MHz, $CDCl_3$): δ 137.7, 136.9, 134.1, 130.2, 129.5, 128.6, 128.2, 120.7, 120.1. HRMS (ESI+, m/z): calcd for $C_9H_8BrN_2O$ [M+H]+: 222.9865, found: 222.9867.

1-(2-bromo-5-methylphenyl)-1H-imidazole (4.2b)

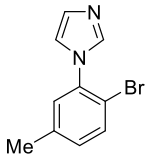

The product was obtained as a yellow oil. ^{1}H NMR (400 MHz, $CDCl_3$): δ 7.65 (s, 1H), 7.57 (d, *J* = 8.1 Hz, 1H), 7.18 (s, 1H), 7.15 – 7.09 (m, 3H), 2.36 (s, 3H). ^{13}C NMR (101 MHz, $CDCl_3$): δ 139.0, 137.7, 136.5, 133.6, 131.0, 129.4, 128.8, 120.6, 116.4, 20.9. HRMS (ESI+, m/z): calcd for $C_{10}H_{10}BrN_2$ [M+H]+: 237.0022, found: 237.0017.

1-(5-(benzyloxy)-2-bromophenyl)-1H-imidazole (4.2c)

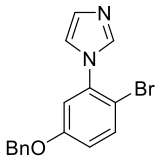

The product was obtained as a white solid. ^{1}H NMR (400 MHz, $CDCl_3$): δ 7.66 (s, 1H), 7.62 – 7.51 (m, 1H), 7.45 – 7.30 (m, 5H), 7.20 (s, 1H), 7.12 (s, 1H), 7.01 – 6.86 (m, 2H), 5.08 (s, 2H). ^{13}C NMR (101 MHz, $CDCl_3$): δ 158.7, 137.6, 137.4, 135.9, 134.4, 129.5, 128.9, 128.6, 127.6, 120.6, 116.9, 114.9, 110.3, 70.7. HRMS (ESI+, m/z): calcd for $C_{16}H_{14}BrN_2O$ [M+H]+: 329.0284, found: 329.0290.

1-(2-bromo-5-(trifluoromethyl)phenyl)-1H-imidazole (4.2d)

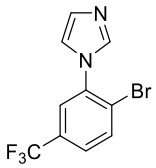

The product was obtained as a light-yellow solid. ^{1}H NMR (500 MHz, DMSO): δ 8.11 (d, J = 8.4 Hz, 1H), 7.95 (s, 1H), 7.81 (dd, *J* = 8.5, 2.2 Hz, 1H), 7.50 (s, 1H), 7.12 (s, 1H). ^{13}C NMR (126 MHz, DMSO): δ 137.8, 137.4, 134.9, 129.4 (q, *J* = 33.1 Hz), 128.9, 126.9 (q, *J* = 3.7 Hz), 125.5 (q, *J* = 3.8 Hz), 123.3 (q, *J* = 272.2 Hz),, 124.4, 121.0. ^{19}F NMR (471 MHz, DMSO): δ 61.2. HRMS (ESI+, m/z): calcd for $C_{10}H_6BrF_3N_2Na$ [M+Na]+: 312.9559, found: 312.9555.

1-(2-bromophenyl)-4,5-diphenyl-1H-imidazole (4.2e)

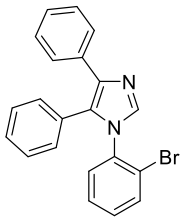

After chromatography, this compound was isolated with some minor impurities and was further purified by trituration from a hot solution of EtOAc in hexanes (20% v/v)

and then cooled to 0 °C to obtain highly pure material as an amorphous white solid. ^{1}H NMR (400 MHz, $CDCl_3$): δ 7.70 (s, 1H), 7.63 (dd, *J* = 7.7, 1.7 Hz, 1H), 7.61 – 7.57 (m, 2H), 7.32 – 7.26 (m, 2H), 7.25 – 7.16 (m, 9H). ^{13}C NMR (101 MHz, $CDCl_3$): δ 138.3, 137.7, 135.9, 134.3, 133.6, 130.8, 130.6, 130.2, 130.0, 129.4, 128.6, 128.4, 128.1, 127.2, 126.9, 122.7. HRMS (ESI+, m/z): calcd for $C_{21}H_{16}BrN_2$ [M+H]+: 375.0491, found: 375.0494.

Solvent-Switchable, Site-Selective C-H Activation via 1,4-Palladium Migration:

Table 4.2. Optimization of Reaction Conditions.

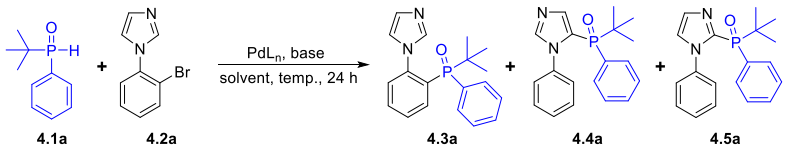

4.1a 4.2a 4.3a 4.4a 4.5a

Entry	[Pd]	L_n	Base	Solvent	Temp. °C	4.3a : 4.4a : 4.5a
1	$Pd(PPh_3)_4$	-	DIPEA	DMF	110	90 : 9 : 1
2	$Pd(PPh_3)_4$	-	DIPEA	DMSO	110	59 : 37 : 4
3	$Pd(OAc)_2$	dppb	DIPEA	DMSO	110	37 : 57 : 6
4	$Pd(OAc)_2$	PPh_3	DIPEA	DMSO	110	56 : 40 : 4
5	$Pd(OAc)_2$	PPh_3	DIPEA	DMSO:H_2O (1:1)	110	24 : 47 : 29
6	$Pd(OAc)_2$	PPh_3	DIPEA	DMSO:H_2O (10:1)	110	31 : 55 : 14
7	$Pd(OAc)_2$	PPh_3	K_3PO_4	DMSO:H_2O (10:1)	110	83 : 17 : 0
8	$Pd(OAc)_2$	PPh_3	K_2CO_3	DMSO:H_2O (10:1)	110	68 : 31 : 1
9	$Pd(OAc)_2$	PPh_3	Cs_2CO_3	DMSO:H_2O (10:1)	110	63 : 35 : 2
10	$Pd(OAc)_2$	PPh_3	$NaHCO_3$	DMSO:H_2O (10:1)	110	65 : 30 : 5
11	$Pd(OAc)_2$	PPh_3	KOAc	DMSO:H_2O (10:1)	110	51 : 40 : 9
12	$Pd(OAc)_2$	PPh_3	CsOAc	DMSO:H_2O (10:1)	110	52 : 41 : 7
13	$Pd(OAc)_2$	P(2-furyl)$_3$	DIPEA	DMSO:H_2O (10:1)	100	66 : 28 : 6
14	$Pd(OAc)_2$	CataCXium A	DIPEA	DMSO:H_2O (10:1)	100	47 : 23 : 30
15	$Pd(OAc)_2$	PPh_3	DIPEA	DMSO:H_2O (10:1)	80	45 : 54 : 1
16	**$Pd(PPh_3)_4$**	-	**DIPEA**	**DMSO:H_2O (10:1)**	**100**	**13 : 74 : 13**
17	$Pd(PPh_3)_4$	-	DIPA	DMSO:H_2O (10:1)	100	8 : 64 : 28
18	$Pd(OAc)_2$	PPh_3	DIPEA	MeOH	110	41 : 28 : 31
19	$Pd(OAc)_2$	PPh_3	DIPEA	*n*-BuOH	110	59 : 26 : 15
20	$Pd(OAc)_2$	PPh_3	DIPEA	*i*-PrOH	110	81 : 14 : 5
21	$Pd(OAc)_2$	PPh_3	DIPEA	*t*-BuOH	110	92 : 7 : 1
22	$Pd(OAc)_2$	PPh_3	DIPEA	ethylene glycol:H_2O (10:1)	110	26 : 8 : 66
23	$Pd(OAc)_2$	PPh_3	DIPEA	ethylene glycol	110	24 : 8 : 68
24	$Pd(OAc)_2$	PPh_3	DIPEA	glycerol	110	30 : 26 : 44
25	$Pd(OAc)_2$	PPh_3	DIPEA	ethylene glycol	130	17 : 8 : 75
26	$Pd(PPh_3)_4$	-	DIPEA	ethylene glycol	130	24 : 3 : 73
27	**$Pd(PPh_3)_4$**	-	**DIPA**	**ethylene glycol**	**130**	**18 : 2 : 80**
28	$Pd(PPh_3)_4$	-	DIPA	DMF	130	52 : 26 : 22
29	$Pd(PPh_3)_4$	-	DIPA	DMSO:H_2O (10:1)	130	14 : 36 : 50

Reaction conditions: **4.1a** (0.10 mmol), **4.2a** (0.15 mmol), $Pd(OAc)_2$ (10 mol%)/PPh_3 (25 mol%) or $Pd(PPh_3)_4$ (10 mol%), base (4 equiv.), solvent (1.0 mL). Product ratios were estimated by ^{31}P NMR.

General procedures for direct and site-selective enantiospecific coupling of SPOs and imidazoles:

Procedure for the synthesis of analogues **4.3**; direct coupling to the phenyl moiety:

An oven-dried pressure vessel equipped with an oven-dried stir bar was charged with imidazole **4.2** (0.300 mmol), SPO **4.1** (0.200 mmol) and $Pd(PPh_3)_4$ (10 mol%) The vial was crimp-capped and put through 3 cycles of evacuation and Ar back-filling via a needle. DMF (2 mL) was added under Ar, followed by diisopropylethylamine (0.14 mL, 0.800 mmol). and the reaction mixture was vigorously stirred in a pre-heated oil bath at 110 °C for 18 h. After cooling to ambient temperature, the solution was transferred to a flask and the pressure vessel were washed with EtOAc (2 x 1 mL). The solution was concentrated to dryness and the crude mixture was first purified on a short column of silica gel using a Combi flash instrument and 100% EtOAc as the eluent to remove some side products, followed by a gradient of a 0-10% MeOH/EtOAc to elute the desired product. This product was further purified on C18 reversed phase silica gel using a solvent gradient from 10% MeCN/H_2O to 100% MeCN; the desired product typically eluted at 40% MeCN/H_2O). The combined fractions were concentrated under a reduced pressure at 45 °C and any residual water was removed as an azeotrope by adding toluene (1 mL) and MeCN (1 mL) and evaporating at the same temperature. Toluene (1 mL) and MeCN (1 mL) were added again, followed by concentration under a reduced pressure at 45 °C to give the desired final product.

Procedure for the synthesis of analogues **4.4**; cross coupling to the C-5 of the imidazole ring via 1,4-Pd migration

An oven-dried pressure vessel equipped with an oven-dried stir bar was charged with imidazole **4.2** (0.300 mmol), SPO **4.1** (0.200 mmol) and $Pd(PPh_3)_4$ (10 mol%) The vial was crimp-capped and put through 3 cycles of evacuation and Ar back-filling via a needle. DMS0 (1.82 mL) and deionised water (0.18 mL) were added under Ar, followed by diisopropylethylamine (0.14 mL, 0.800 mmol) and the reaction mixture was vigorously stirred in a pre-heated oil bath at 100 °C for 48 h. After cooling to ambient

temperature, the solution was transferred to a flask and the pressure vessel were washed with EtOAc (2 x 1 mL) and MeOH (2 x 1 mL). The solution was concentrated to dryness and the crude mixture was first purified on a short column of silica gel using a Combi flash instrument and a gradient of 0-100% EtOAc/hexanes, followed by 0-10% MeOH/EtOAc, to elute the desired product. This product was further purified on C18 reversed phase silica gel using a solvent gradient from 10% MeCN/H_2O to 100% MeCN; the desired product typically eluted at 30% MeCN/H_2O). The combined fractions were concentrated under a reduced pressure at 45 °C and any residual water was removed as an azeotrope by adding toluene (1 mL) and MeCN (1 mL) and evaporating at the same temperature. Toluene (1 mL) and MeCN (1 mL) were added again, followed by concentration under a reduced pressure at 45 °C to give the desired final product.

General procedure for the synthesis of analogues **4.5**; cross coupling to the C-2 of the imidazole ring via 1,4-Pd migration

An oven-dried pressure vessel equipped with an oven-dried stir bar was charged with imidazole **4.2** (0.300 mmol), SPO **4.1** (0.200 mmol) and $Pd(PPh_3)_4$ (10 mol%) The vial was crimp-capped and put through 3 cycles of evacuation and Ar back-filling via a needle. Ethylene glycol (2 mL) was added under Ar, followed by diisopropylamine (0.11 mL, 0.800 mmol) and the reaction mixture was vigorously stirred in a pre-heated oil bath at 130 °C for 18 h. After cooling to ambient temperature, the mixture was transferred to a separatory funnel and diluted with DCM (20 mL). The organic layer was washed with deionised water (10 mL) and collected. The aqueous layer was further extracted with DCM (2 x 5 mL) and the combined organic fractions were washed with brine (10 mL). The resulting aqueous layer was extracted with DCM (5 mL) and combined with the previous organic fractions. The collective organic fractions were dried over anhydrous Na_2SO_4, filtered, and concentrated to dryness. The crude mixture was first purified on a short column of silica gel using a Combi flash instrument. When necessary, products were further purified on C18 reversed phase silica gel using a

solvent gradient from 10% MeCN/H_2O to 100% MeCN; the desired products typically eluted at 50 - 55% MeCN/H_2O). The combined fractions were concentrated under a reduced pressure at 45 °C and any residual water was removed as an azeotrope by adding toluene (1 mL) and MeCN (1 mL) and evaporating at the same temperature. Toluene (1 mL) and MeCN (1 mL) were added again, followed by concentration under a reduced pressure at 45 °C to give the desired final product.

(S)-(2-(1H-imidazol-1-yl)phenyl)(tert-butyl)(phenyl)phosphine oxide (4.3a)

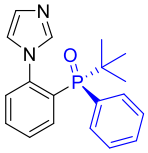

Product **4.3a** was obtained as a white solid in 46% yield (38.8 mg, 0.120 mmol) and 82% ee. ^{1}H NMR (400 MHz, $CDCl_3$): δ 8.18 (ddd, *J* = 10.5, 7.6, 1.7 Hz, 1H), 7.62 (tt, *J* = 7.7, 1.5 Hz, 1H), 7.56 (tt, *J* = 7.5, 1.8 Hz, 1H), 7.50 – 7.32 (m, 3H), 7.33 – 7.27 (m, 2H), 7.23 (ddd, *J* = 7.7, 3.7, 1.5 Hz, 1H), 6.82 (s, 1H), 6.73 (s, 1H), 1.34 (d, *J* = 14.9 Hz, 9H). ^{13}C NMR (101 MHz, $CDCl_3$): δ 141.8, 139.0, 132.8 (d, *J* = 2.2 Hz), 132.6 (d, *J* = 8.1 Hz), 131.5 (d, *J* = 2.8 Hz), 131.3 (d, *J* = 8.9 Hz), 130.8 (d, *J* = 60.5 Hz), 130.4 (d, *J* = 6.2 Hz), 129.9 (d, *J* = 50.6 Hz), 128.3, 128.0, 128.0 (d, *J* = 11.5 Hz), 122.3, 34.4 (d, *J* = 71.6 Hz), 26.0. ^{31}P NMR (162 MHz, $CDCl_3$): δ 39.3. Chiral HPLC method: Chiralpak AD, hexane/IPA = 90/10, 1 mL/min, λ = 220 nm; (R)-t_R = 26.57 min (minor), (S)-t_R = 33.17 min (major). HRMS (ESI+, m/z): calcd for $C_{19}H_{22}N_2OP$ [M+H]+: 325.1464, found: 325.1456.

(S)-tert-butyl(phenyl)(1-phenyl-1H-imidazol-5-yl)phosphine oxide (4.4a)

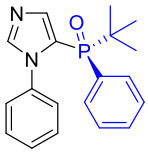

Product **4.4a** was obtained as a colourless oil in 32% yield (20.9 mg, 0.0644 mmol) and 85% ee. ^{1}H NMR (400 MHz, $CDCl_3$): δ 7.85 (s, 1H), 7.74 (s, 1H), 7.45 – 7.31 (m, 3H), 7.30 – 7.25 (m, 1H), 7.24 – 7.11 (m, 6H), 1.27 (d, *J* = 15.6 Hz, 9H). ^{13}C NMR (101

MHz, $CDCl_3$): δ 142.9, 138.5, 136.2, 132.3 (d, *J* = 8.9 Hz), 131.5 (d, *J* = 2.9 Hz), 130.3 (d, *J* = 98.7 Hz), 128.9, 128.8 (d, *J* = 81.6 Hz), 128.6, 127.9 (d, *J* = 11.6 Hz), 127.3, 34.1 (d, *J* = 76.6 Hz), 25.2. ^{31}P NMR (162 MHz, $CDCl_3$): δ 32.1. Chiral HPLC method: Chiralpak AD, hexane/IPA = 90/10, 1.0 mL/min, λ = 220 nm; (R)-t_R = 13.94 min (minor), (S)-t_R = 17.73 min (major). HRMS (ESI+, m/z): calcd for $C_{19}H_{21}N_2NaOP$ [M+Na]+: 347.1284, found: 347.1277.

(S)-tert-butyl(phenyl)(1-phenyl-1H-imidazol-2-yl)phosphine oxide (4.5a)

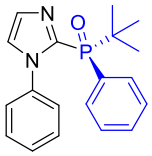

The crude product **4.5a** was first purified on silica gel, using a gradient of 0-60% hexanes/EtOAc) and then on reversed-phase C 18 silica gel to afford the desired product as a white solid in 60% yield (38.8 mg, 0.120 mmol) and >99% ee. ^{1}H NMR (400 MHz, $CDCl_3$): δ 7.66 – 7.56 (m, 2H), 7.44 – 7.34 (m, 2H), 7.35 – 7.26 (m, 2H), 7.25 – 7.14 (m, 6H), 1.33 (d, *J* = 15.8 Hz, 9H). ^{13}C NMR (101 MHz, $CDCl_3$): δ 141.0 (d, *J* = 126.6 Hz), 137.6, 132.3 (d, *J* = 8.8 Hz), 131.5 (d, *J* = 2.8 Hz), 130.5 (d, *J* = 95.8 Hz), 129.7 (d, *J* = 14.0 Hz), 128.7, 128.5, 127.9 (d, *J* = 11.5 Hz), 126.9, 125.5 (d, *J* = 2.7 Hz), 34.9 (d, *J* = 75.6 Hz), 24.6. ^{31}P NMR (162 MHz, $CDCl_3$): δ 32.9. Chiral HPLC method: Chiralpak AD, hexane/IPA = 95/5, 0.7 mL/min, λ = 254 nm; (S)-t_R = 11.87 min (single enantiomer). HRMS (ESI+, m/z): calcd for $C_{19}H_{21}N_2NaOP$ [M+Na]+: 347.1284, found: 347.1289.

(S)-tert-butyl(phenyl)(1-(m-tolyl)-1H-imidazol-2-yl)phosphine oxide (4.5b)

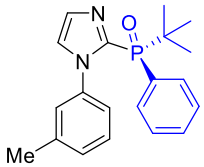

The crude product **4.5b** was first purified on silica gel, using a gradient of 0-50% hexanes/EtOAc and then on reversed-phase C 18 silica gel to afford the desired product

as a white solid in 62% yield (42.2 mg, 0.125 mmol) and >99% ee. ^{1}H NMR (400 MHz, $CDCl_3$): δ 7.64 – 7.49 (m, 2H), 7.47 – 7.34 (m, 1H), 7.34 (t, *J* = 1.4 Hz, 1H), 7.31 (ddd, *J* = 8.5, 6.8, 3.0 Hz, 2H), 7.15 (t, *J* = 1.3 Hz, 1H), 7.12 – 6.97 (m, 2H), 6.99 – 6.84 (m, 2H), 2.20 (s, 3H), 1.35 (d, *J* = 15.8 Hz, 9H). ^{13}C NMR (101 MHz, $CDCl_3$): δ 141.1 (d, *J* = 127.5 Hz), 138.4, 137.4, 132.2 (d, *J* = 8.8 Hz), 131.4 (d, *J* = 2.8 Hz), 130.7 (d, *J* = 95.8 Hz), 129.6 (d, *J* = 14.3 Hz), 129.3, 128.3, 127.8 (d, *J* = 11.5 Hz), 127.5, 125.4 (d, *J* = 2.8 Hz), 123.8, 34.8 (d, *J* = 75.6 Hz), 24.7, 21.2. ^{31}P NMR (162 MHz, $CDCl_3$): δ 32.6. Chiral HPLC method: Chiralpak AD, hexane/IPA = 96/4, 1.0 mL/min, λ = 254 nm; (S)-t_R = 9.63 min (single enantiomer). HRMS (ESI+, m/z): calcd for $C_{20}H_{24}N_2OP$ [M+H]+: 339.1621, found: 339.1629.

(S)-(1-(3-(benzyloxy)phenyl)-1H-imidazol-2-yl)(tert-butyl)(phenyl)phosphine oxide (4.5c)

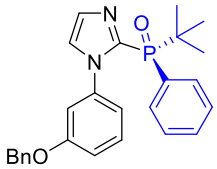

The crude product **4.5c** was purified on silica gel using a gradient of 0-50% hexanes/EtOAc to afford the desired compound as a light-yellow oil in 55% yield (47.7 mg, 0.111 mmol) and >99% ee. ^{1}H NMR (400 MHz, $CDCl_3$): δ 7.64 – 7.53 (m, 2H), 7.44 – 7.27 (m, 9H), 7.18 (t, *J* = 1.3 Hz, 1H), 7.08 (t, *J* = 8.1 Hz, 1H), 6.88 (t, *J* = 2.2 Hz, 1H), 6.83 (ddd, *J* = 8.3, 2.5, 1.0 Hz, 1H), 6.76 (ddd, *J* = 7.8, 1.9, 0.9 Hz, 1H), 4.92 (d, *J* = 11.5 Hz, 1H), 4.85 (d, *J* = 11.4 Hz, 1H), 1.36 (d, *J* = 15.8 Hz, 9H). ^{13}C NMR (101 MHz, $CDCl_3$): δ 158.6, 140.9 (d, *J* = 127.1 Hz), 138.6, 136.7, 132.2 (d, *J* = 8.8 Hz), 131.5 (d, *J* = 2.8 Hz), 130.5 (d, *J* = 95.8 Hz), 129.8 (d, *J* = 14.4 Hz), 129.3, 128.7, 128.2, 127.9 (d, *J* = 11.6 Hz), 127.7, 125.3 (d, *J* = 2.6 Hz), 119.0, 115.9, 112.9, 70.1, 34.9 (d, *J* = 75.9 Hz), 24.7. ^{31}P NMR (162 MHz, $CDCl_3$): δ 33.0. Chiralpak AD, hexane/IPA = 96/4, 1.0 mL/min, λ = 254 nm; (S)-t_R = 12.33 min (single enantiomer). HRMS (ESI+, m/z): calcd for $C_{26}H_{27}N_2NaO_2P$ [M+Na]+: 453.1702, found: 453.1701.

(S)-tert-butyl(phenyl)(1-(3-(trifluoromethyl)phenyl)-1H-imidazol-2-yl)phosphine oxide (4.5d)

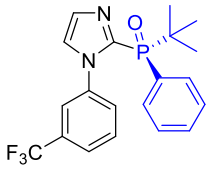

The crude product **4.5d** was first purified on silica gel using a gradient of 0-50% hexanes/EtOAc and then on reversed-phase C 18 silica gel to afford the desired product as a white solid in 19% yield (15.0 mg, 0.0382 mmol) and 92% ee. ^{1}H NMR (400 MHz, $CDCl_3$): δ 7.61 – 7.46 (m, 4H), 7.44 – 7.35 (m, 3H), 7.35 – 7.27 (m, 3H), 7.18 (s, 1H), 1.35 (d, *J* = 16.0 Hz, 9H). ^{31}P NMR (162 MHz, $CDCl_3$): δ 32.9. ^{13}C NMR (101 MHz, $CDCl_3$:) δ 141.3 (d, *J* = 125.2 Hz), 137.8, 132.0 (d, *J* = 8.8 Hz), 131.6 (d, *J* = 2.8 Hz), 130.9 (q, *J* = 33.3 Hz), 130.5, 130.0 (d, *J* = 96.0 Hz), 130.0 (d, *J* = 14.2 Hz), 129.1, 127.9 (d, *J* = 11.6 Hz), 125.3 (q, *J* = 3.7 Hz), 125.0 (d, *J* = 2.5 Hz), 123.6 (q, *J* = 3.7 Hz), 123.2 (d, J = 272.7 Hz), 34.7 (d, *J* = 75.5 Hz), 24.4. ^{31}P NMR (162 MHz, $CDCl_3$): δ 32.9. ^{19}F NMR (377 MHz, $CDCl_3$): δ -62.8. Chiralpak AD, hexane/IPA = 90/10, 1.0 mL/min, λ = 254 nm; (R)-t_R = 4.33 min (minor), (S)-t_R = 5.05 min (major). HRMS (ESI+, m/z): calcd for $C_{20}H_{20}F_3N_2NaOP$ [M+Na]+: 415.1158, found: 415.1164.

(S)-tert-butyl(4-methoxyphenyl)(1-phenyl-1H-imidazol-2-yl)phosphine oxide (4.5e)

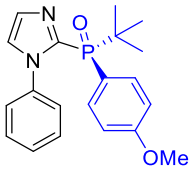

The crude product **4.5e** was first purified on silica gel using a gradient of 0-90% hexanes/EtOAc and then on reversed-phase C 18 silica gel to afford the desired product as a white solid in 64% yield (45.2 mg, 0.128 mmol) and >99% ee. ^{1}H NMR (400 MHz, $CDCl_3$): δ 7.62 – 7.51 (m, 2H), 7.34 (t, *J* = 1.3 Hz, 1H), 7.26 – 7.20 (m, 3H), 7.20 – 7.17 (m, 2H), 7.16 (t, *J* = 1.3 Hz, 1H), 6.85 – 6.80 (m, 2H), 3.80 (s, 3H), 1.30 (d, *J* = 15.8 Hz, 9H). ^{13}C NMR (101 MHz, $CDCl_3$): δ 162.2 (d, *J* = 2.9 Hz), 141.2 (d, *J* = 126.4

Hz), 137.7, 134.1 (d, *J* = 10.0 Hz), 129.6 (d, *J* = 14.2 Hz), 128.6, 128.5, 126.9, 125.4 (d, *J* = 2.6 Hz), 121.5 (d, *J* = 102.3 Hz), 113.5 (d, *J* = 12.5 Hz), 55.4, 34.9 (d, *J* = 76.6 Hz), 24.6. ^{31}P NMR (162 MHz, $CDCl_3$): δ 32.9. HRMS (ESI+, m/z): calcd for $C_{20}H_{24}N_2O_2P$ [M+H]+: 355.1570, found: 355.1578. Chiralpak IC, hexane/IPA = 90/10, 1.0 mL/min, λ = 254 nm; (S)-t_R = 42.00 min (single enantiomer).

(S)-tert-butyl(phenyl)(1,4,5-triphenyl-1H-imidazol-2-yl)phosphine oxide (4.5f)

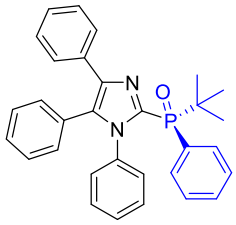

The crude product **4.5f** was purified on silica gel using a gradient of 0-60% hexanes/EtOAc to afford the desired compound as a light-yellow solid in 68% yield (64.7 mg, 0.136 mmol) and >99% ee. ^{1}H NMR (800 MHz, CD_2Cl_2,, 0 °C): δ 7.68 – 7.64 (m, 2H), 7.59 – 7.55 (m, 2H), 7.48 – 7.41 (m, 1H), 7.35 (td, *J* = 7.8, 2.9 Hz, 3H), 7.30 – 7.16 (m, 7H), 7.13 (tt, *J* = 7.5, 1.2 Hz, 1H), 7.11 – 7.09 (m, 2H), 6.84 (s, 1H), 6.44 (s, 1H), 1.38 (d, *J* = 15.7 Hz, 9H). ^{13}C NMR (201 MHz, CD_2Cl_2, 0 °C): δ 140.8 (d, *J* = 126.5 Hz), 138.9 (d, *J* = 13.2 Hz), 136.1, 134.5, 133.8, 132.6 (d, *J* = 8.8 Hz), 131.8 (d, *J* = 2.7 Hz), 131.3, 130.6 (d, *J* = 95.9 Hz), 130.1, 129.6, 128.8, 128.7 (d, *J* = 15.1 Hz), 128.6, 128.3, 128.2 (d, *J* = 11.6 Hz), 128.0, 127.4, 127.3, 35.0 (d, *J* = 75.0 Hz), 24.7. ^{31}P NMR (162 MHz, CD_2Cl_2): δ 32.2. HRMS (ESI+, m/z): calcd for $C_{31}H_{29}N_2NaOP$ [M+Na]+: 499.1910, found: 499.1917. Chiralcel OD, hexane/IPA = 96/4, 1.0 mL/min, λ = 254 nm; (S)-t_R = 6.91 min (single enantiomer).

(S)-tert-butyl(phenanthren-9-yl)(1,4,5-triphenyl-1H-imidazol-2-yl)phosphine oxide (4.5g)

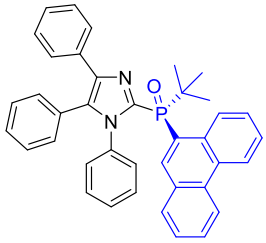

Synthesis of analogue **4.5g** was carried out using SPO **4.1c** (0.68 mmol, 95% ee), imidazole **4.2e** (1.02 mmol), diisopropylamine (0.38 mL, 2.70 mmol) and ethylene glycol (6.80 mL). The crude product was purified on silica gel using a gradient of 0-30% hexanes/EtOAc, to obtain the desired product as a light-yellow foam in 69% yield (273 mg, 0.473 mmol) and 95% ee. The foam was dissolved in a minimal volume of diethyl ether, and after a few seconds, white crystals began to form. The mixture was allowed to stand at RT for 1 h and then stored at -10 °C for 20 h. The yellow supernatant was removed to reveal white crystals. The white crystals were dissolved in a minimal volume DCM and the solvent was evaporated to reveal a foam. The foam was subsequently dissolved in a minimal quantity of hot methanol and the solution was cooled to RT, then stored at -10 °C for 18 h, with the formation of crystals. The supernatant was removed while cold and the crystals were washed with cold MeOH (1.0 mL) to give the desired product as an off-white solid in 51% overall yield, 73% recovery after crystallisation (200 mg, 0.347 mmol) and >99% ee.

The reaction was repeated on a larger scale using SPO **4.1c** (1.08 mmol, 95% ee), imidazole **4.2e** (1.62 mmol), diisopropylamine (0.61 mL, 4.31 mmol) and ethylene glycol (10.8 mL) to give **4.5g** in 76% yield (475 mg, 0.823 mmol) and 95% ee. After trituration from diethyl ether and crystallisation from MeOH as described above, **4.5g** was obtained in 59% overall yield, 76% recovery (364 mg, 0.631 mmol) and >99%ee.

^{1}H NMR (800 MHz, CD_2Cl_2, 0 °C): δ 8.64 (dd, *J* = 25.3, 8.4 Hz, 2H), 8.48 (s, 1H), 8.09 (d, *J* = 15.8 Hz, 1H), 7.86 (d, *J* = 7.7 Hz, 1H), 7.72 (ddd, *J* = 8.3, 6.9, 1.4 Hz, 1H), 7.69 – 7.64 (m, 2H), 7.62 (ddd, *J* = 8.2, 6.9, 1.3 Hz, 1H), 7.60 (ddd, *J* = 7.9, 6.9, 1.1 Hz, 1H), 7.54 (s, 1H), 7.50 (ddd, *J* = 8.2, 6.8, 1.3 Hz, 1H), 7.35 – 7.29 (m, 2H), 7.28 –

7.24 (m, 1H), 7.22 – 7.20 (m, 1H), 7.19 – 7.15 (m, 2H), 7.12 – 7.05 (m, 2H), 7.01 (s, 1H), 6.64 (t, *J* = 7.5 Hz, 1H), 6.14 (s, 1H), 5.82 (s, 1H), 1.53 (d, *J* = 15.9 Hz, 9H). ^{13}C NMR (201 MHz, CD_2Cl_2): δ 142.4 (d, *J* = 128.4 Hz), 138.9 (d, *J* = 13.3 Hz), 137.6, 135.7, 134.6, 133.6, 132.1, 131.9 (d, *J* = 2.2 Hz), 131.3, 130.6 (d, *J* = 8.7 Hz), 130.1, 130.1, 130.0 (d, *J* = 13.7 Hz), 129.6, 129.1, 128.8, 128.8, 128.6, 128.2, 128.0, 127.5, 127.4, 127.3, 127.0 (d, *J* = 5.8 Hz), 125.1 (d, *J* = 90.1 Hz), 123.1, 122.7, 36.8 (d, *J* = 75.5 Hz), 25.6. ^{31}P NMR (162 MHz, CD_2Cl_2): δ 34.85. HRMS (ESI+, m/z): calcd for $C_{39}H_{34}N_2OP$ [M+H]+: 577.2403, found: 577.2402 Chiralpak AD, hexane/IPA = 96/4, 0.6 mL/min, λ = 254 nm; (S)-t_R = 20.86 min (single enantiomer).

Stereoretentive Reduction of **4.5g** to **4.6**:

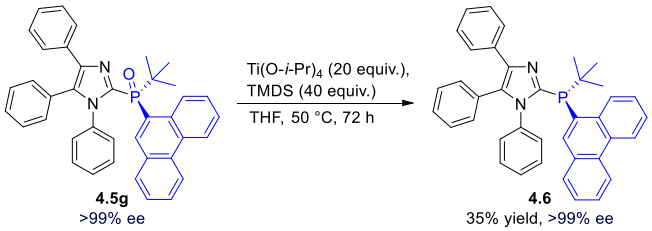

An oven-dried pressure vessel equipped with a dry stir bar was cooled to ambient temperature in a desiccator. The vessel was charged with **4.5g** (28.5 mg, 0.049 mmol. The vessel was crimp-capped and put through 3 cycles of evacuation and Ar-backfilling. Dry THF (2.0 mL) was added under Ar and the mixture was stirred at RT until complete dissolution. TMDS (0.35 mL, 1.98 mmol) and Ti(O-iPr)$_4$ (0.29 mL, 0.988 mmol) were added. The Ar inlet was removed, the vessel was wrapped in aluminum foil, immersed in a pre-heated oil bath at 50 °C and stirred for 72 h. The vessel was removed from the oil bath and allowed to cool to RT. Using a needle, the Teflon seal was carefully punctured to vent the vessel. The resulting dark-drown solution was transferred to a flask. The vessel was washed with THF (1.0 mL x2) and transferred to the flask. The solution was concentrated at 30 °C *in vacuo*, dissolved in 5% EtOAc/hexanes (ca. 1.5 mL), and wet-loaded unto activated, neutral alumina for column chromatography. Purification (0-2% EtOAc/hexanes) and subsequent concentration at RT afforded the desired compound as a white solid in 38% yield (10.6

mg, 0.0189 mmol) and 98% ee. Following crystallization from hexanes, the compound could be obtained in >99% ee. ^{1}H NMR (800 MHz, CD_2Cl_2, 0 °C): δ 8.72 (d, *J* = 8.3 Hz, 1H), 8.69 (d, *J* = 8.3 Hz, 1H), 8.65 (t, *J* = 7.6 Hz, 1H), 8.43 (d, *J* = 4.1 Hz, 1H), 7.92 (d, *J* = 7.9 Hz, 1H), 7.72 – 7.69 (m, 2H), 7.68 (ddd, *J* = 8.3, 6.8, 1.4 Hz, 1H), 7.64 (ddd, *J* = 8.2, 6.9, 1.3 Hz, 1H), 7.60 (ddd, *J* = 7.9, 6.8, 1.1 Hz, 1H), 7.53 (ddd, *J* = 8.2, 6.8, 1.3 Hz, 1H), 7.31 (t, *J* = 7.7 Hz, 2H), 7.26 – 7.17 (m, 6H), 7.15 – 7.08 (m, 2H), 7.04 (t, *J* = 7.4 Hz, 1H), 6.68 (s, 1H), 6.44 (s, 1H), 1.35 (d, *J* = 13.8 Hz, 9H). ^{13}C NMR (201 MHz, CD_2Cl_2, 0 °C): δ 147.1 (d, *J* = 11.3 Hz), 139.7, 138.0 (d, *J* = 3.8 Hz), 137.2, 135.5, 135.2 (d, *J* = 25.9 Hz), 132.3, 131.4 (d, *J* = 1.1 Hz), 131.2, 131.0, 130.9 (d, *J* = 17.5 Hz), 130.3 (d, *J* = 5.1 Hz), 129.6, 128.7, 128.6, 128.3, 128.2, 127.9, 127.8, 127.7, 127.4, 127.0, 126.9, 126.6 (d, *J* = 1.7 Hz), 126.6 (d, *J* = 2.7 Hz), 123.1, 122.7, 33.2 (d, *J* = 7.6 Hz), 28.5 (d, *J* = 14.4 Hz). ^{31}P NMR (162 MHz, CD_2Cl_2): δ -26.5. HRMS (ESI+, m/z): calcd for $C_{39}H_{34}N_2P$ [M+H]+: 561.2454, found: 561.2443.

In order to determine the %ee, an aliquot dissolved in $CDCl_3$ was oxidised using cold H_2O_2 (30% w/w). After extraction, drying over anhydrous Na_2SO_4 and concentration, the oxidised product was subjected to HPLC analysis: Chiralpak AD, hexane/IPA = 96/4, 0.6 mL/min, λ = 254 nm; t_R = 21.04 min (single enantiomer).

<u>Asymmetric Suzuki-Miyaura cross-coupling using Phosphinyl Imidazole Ligand **6**</u>:

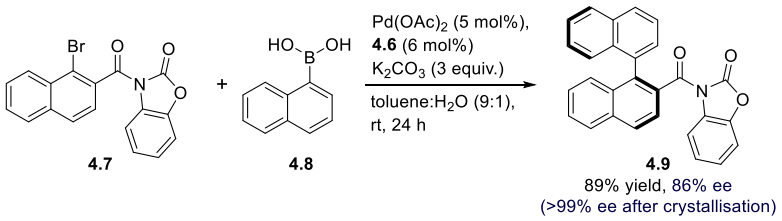

Aryl bromide **4.7** (36.9 mg, 0.100 mmol), boronic acid **4.8** (34.5 mg, 0.200 mmol), ligand **4.6** (3.4 mg, 0.006 mmol, 6.0 mol%), $Pd(OAc)_2$ (0.005 mmol, 5.0 mol%) and K_2CO_3 (41.6 mg, 0.300 mmol), were weighed into an oven-dried pressure vial. The vial was crimp-capped and put through 3 cycles of evacuation and Ar back-filling via a needle. Subsequently, dry Ar-sparged toluene (0.9 mL) and Ar-sparged deionised water (0.1 mL) were added. The mixture was vigorously stirred under Ar at RT for 24 h. The

mixture was filtered into a flask and the residue was washed with DCM (5 x 1 mL). The combined filtrate was concentrated at RT and dried under vacuum for 2 h. The crude was purified on SiO_2 (0-5% EtOAc/hexanes) to give the desired compound as a white solid in 89% yield (37.2 mg, 0.085 mmol) and 86% ee. The compound was suspended in warm Et_2O (1.0 mL) and DCM was added dropwise until dissolution. The solution was stored at -20 °C and crystals formed. The enantioenriched mother liquor was removed with a pipet and dried to give a fluffy white solid in 54% over all yield (22.3 mg, 0.0537 mmol) and >99% ee. ^{1}H NMR (400 MHz, $CDCl_3$): δ 8.09 (d, *J* = 8.5 Hz, 1H), 8.00 (d, *J* = 8.2 Hz, 1H), 7.84 – 7.64 (m, 3H), 7.58 (ddd, *J* = 8.2, 6.7, 1.4 Hz, 1H), 7.51 (dd, *J* = 7.0, 1.3 Hz, 1H), 7.45 – 7.38 (m, 4H), 7.38 – 7.29 (m, 3H), 7.12 – 7.06 (m, 1H), 7.03 – 6.96 (m, 2H). ^{13}C NMR (101 MHz, $CDCl_3$): δ 168.3, 150.6, 142.4, 137.3, 134.8, 134.4, 133.5, 132.8, 132.7, 132.2, 128.7, 128.6, 128.4, 128.4, 128.2, 127.8, 127.6, 127.4, 127.2, 126.7, 126.5, 126.2, 125.1, 124.9, 124.4, 123.7, 114.3, 109.7. Chiralpak OD, hexane/IPA = 98/2, 0.8 mL/min, λ = 254 nm; (R)-t_R = 19.03 min (minor), (S)-t_R = 21.12 min (major).

Mechanistic Studies

Synthesis of 1-(2-bromophenyl)-1*H*-imidazole-2-d (^{2}H-**4.2a**):

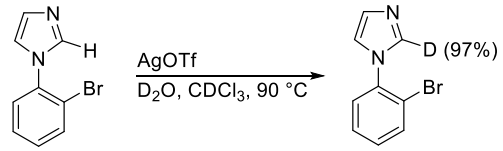

4.2a ^{2}H-**4.2a**

Compound **4.2a** with a deuterium at C-2 was synthesised according to previously reported protocol with modifications.[23] An oven-dried pressure vessel equipped with a dry stir bar was charged with 1-(2-bromophenyl)-1H-imidazole (446 mg, 2.00 mmol) and AgOTf (12.8 mg, 0.0500 mmol). The vessel was wrapped with aluminum foil to exclude light. Subsequently, D_2O (0.72 mL, 40.0 mmol) and $CDCl_3$ (1.3 mL) were sequentially added. The vessel was crimp-capped and stirred in a pre-heated oil bath at 90 °C for 18 h. The mixture was cooled to RT and transferred to a separatory funnel. The bi-phasic mixture was diluted with EtOAc (10 mL) and brine (50 mL). The organic

layer was collected and the aqueous layer was further extracted with EtOAc (10 mL). The combined organic layers were dried over anhydrous Na_2SO_4, filtered and concentrated, to give the deuterated imidazole as a light-yellow oil in 67% deuteration at C2. The solid was re-dissolved in $CDCl_3$ (2.0 mL) and transferred to a dry pressure vessel, followed by the addition of D_2O (0.72 mL, 40.0 mmol) and AgOTf (12.8 mg, 0.0500 mmol). The vessel was wrapped in aluminum foil and after stirring in a pre-heated oil bath at 90 °C for 64 h, the mixture was cooled to RT and transferred to a separatory funnel. The bi-phasic mixture was diluted with EtOAc (20 mL) and brine (20 mL). The organic layer was collected and the aqueous layer was further extracted with EtOAc (2 x 20 mL). The combined organic layers were dried over anhydrous Na_2SO_4, filtered and concentrated. The crude was purified on silica gel using a gradient of 0-60% EtOAc/hexanes, to afford the desired deuterated imidazole as a light brown oil in 70% yield (312 mg, 1.39 mmol) and 97% deuterium incorporation at C2. After storage in a freezer (ca. -10 °C), the oil solidified and remained a solid even at room temperature.

^{1}H NMR (500 MHz, $CDCl_3$): δ 7.73 (dd, *J* = 7.9, 1.4 Hz, 1H), 7.67 (s, 0.03 H), 7.47 – 7.39 (m, 1H), 7.36 – 7.29 (m, 2H), 7.21 (d, *J* = 1.4 Hz, 1H), 7.13 (d, *J* = 1.3 Hz, 1H).

^{13}C NMR (126 MHz, $CDCl_3$): δ 136.9, 134.1, 130.2, 129.6, 128.6, 128.3, 120.6, 120.1.

HRMS (ESI+, m/z): calcd for $C_9H_6BrDN_2Na$ [M+Na]+: 245.9748, found: 245.9751.

<u>Investigation of H/D scrambling under C2-favouring site-selective conditions</u>:

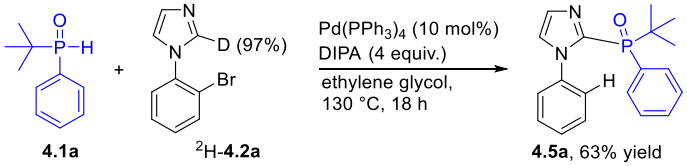

4.1a ^{2}H-**4.2a** **4.5a**, 63% yield

The crude product **4.5a** was first purified on silica gel, using a gradient of 0-60% hexanes/EtOAc) and then on reversed-phase C 18 silica gel to afford the desired product as a white solid in 63% yield (41.1 mg, 0.127 mmol) without deuterium incorporation at the *ortho*-position of the phenyl ring of the imidazole moiety.

Investigation of direct C-H activation/oxidative coupling:

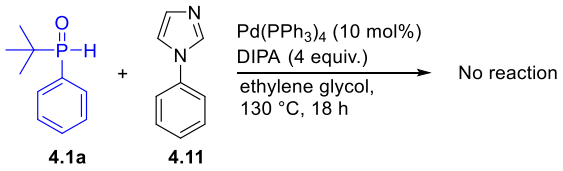

4.1a 4.11

4.7 Associated Content

NMR spectra and chiral HPLC data are provided in Appendix III.

4.8 Author Information

Corresponding Author

*Phone 514-398-3638. Fax 514-398-3797. Email: youla.tsantrizos@mcgill.ca

4.9 Acknowledgements

A doctoral scholarship awarded to I. I. M from Fonds de recherche du Québec is gratefully acknowledged. We are also grateful to the Natural Sciences and Engineering Research Council of Canada (NSERC) for financial support. We wish to thank Boehringer-Ingelheim Pharmaceuticals Inc., USA, for their generous gift of the chiral auxiliary (R)-N-(1-(5-chloro-2-hydroxyphenyl)ethyl)-4-methylbenzenesulfonamide.

4.10 References

1. Grotjahn, D. B.; Incarvito, C. D.; Rheingold, A. L. Combined Effects of Metal and Ligand Capable of Accepting a Proton or Hydrogen Bond Catalyze Anti-Markovnikov Hydration of Terminal Alkynes. *Angew. Chem. Int. Ed*. **2001**, *40*, 3884-3887.

2. For a review on monodentate phosphine ligands, see: Hayashi, T. Chiral Monodentate Phosphine Ligand MOP for Transition-Metal-Catalyzed Asymmetric Reactions. *Acc. Chem. Res*. **2000**, *33*, 354-362.

3. (a) Grotjahn, D. B.; Gong, Y.; Zakharov, L.; Golen, J. A. Rheingold, A. L. Changes in Coordination of Sterically Demanding Hybrid Imidazolylphosphine Ligands on Pd(0) and Pd(II). *J. Am. Chem. Soc*. **2006**, *128*, 438-453. (b) Díez, V.; Espino, G.; Jalón, F. A. Manzano, B. R.; Pérez-Manrique, M. Synthesis and Structure of New Palladium Complexes with the Ligand 2-(Diphenylphosphino)-1-methylimidazole: Evidence of Hemilability. *J. Organomet. Chem*. **2007**, *692*, 1482-1495. (c) Grotjahn, D. B. Bifunctional Catalysts and Related Complexes: Structures and Properties. *Dalton Trans*. **2008**, 6497-6508.

4. (a) Harkal, S.; Rataboul, F.; Zapf, A.; Fuhrmann, C.; Riermeier, T.; Monsees, A.; Beller, M. Dialkylphosphinoimidazoles as New Ligands for Palladium-Catalyzed Coupling Reactions of Aryl Chlorides. *Adv. Synth. Catal.* **2004**, *346*, 1742-1748. (b) Torborg, C.; Huang, J.; Schulz, T.; Schäffner, B.; Zapf, A.; Spannenberg, A.; Börner, A.; Beller, M. Improved Palladium-Catalyzed Sonogashira Coupling Reactions of Aryl Chlorides. *Chem. Eur. J*. **2009**, *15*, 1329-1336. (c) Schulz, T.; Torborg, C.; Schäffner, B.; Huang, J.; Zapf, A.; Kadyrov, R.; Börner, A.; Beller, M. Practical Imidazole-Based Phosphine Ligands for Selective Palladium-Catalyzed Hydroxylation of Aryl Halides. *Angew. Chem. Int. Ed*. **2009**, *48*, 918-921. (d) Wu, X-F.; Neumann, H.; Spannenberg, A.; Schulz, T.; Jiao, H. Beller, M. Development of a General Palladium-Catalyzed Carbonylative Heck Reaction of Aryl Halides. *J. Am. Chem. Soc*. **2010**, *132*, 14596–14602. (e) Fleischer, I.; Dyballa, K. M.; Jennerjahn, R.; Jackstell, R.; Franke, R.; Spannenberg, A.; Beller, M. From Olefins to Alcohols: Efficient and Regioselective Ruthenium-Catalyzed Domino Hydroformylation/Reduction Sequence. *Angew. Chem. Int. Ed.* **2013**, *52*, 2949 –2953. (f) Fleischer, I.; Wu, L.; Profir, I.; Jackstell, R.; Franke, R.; Beller, M. Towards the Development of a Selective Ruthenium-Catalyzed Hydroformylation of Olefins. *Chem. Eur. J*. **2013**, *19*, 10589-10594. (g) Wu, L.; Liu,

Q.; Spannenberg, A.; Jackstell, R.; Beller, M. Highly Regioselective Osmium-Catalyzed Hydroformylation. *Chem. Commun*. **2015**, *51*, 3080-3082.

5. Zhang, K-F.; Christoffel, F.; Baudoin, O. Barbier–Negishi Coupling of Secondary Alkyl Bromides with Aryl and Alkenyl Triflates and Nonaflates. *Angew. Chem. Int. Ed*. **2018**, *57*, 1982-1986.

6. (a) Grotjahn, D. B.; Larsen, C. R.; Gustafson, J. L.; Nair, R.; Sharma, A. Extensive Isomerization of Alkenes Using a Bifunctional Catalyst: An Alkene Zipper. *J. Am. Chem. Soc*. **2007**, *129*, 9592-9593. b) Larsen, C. R.; Grotjahn, D. B. Stereoselective Alkene Isomerization over One Position. *J. Am. Chem. Soc*. **2012**, *134*, 10357-10360.

7. Wang, L.; Neumann, H.; Beller, M. Palladium-Catalyzed Methylation of Nitroarenes with Methanol. *Angew. Chem. Int. Ed*. **2019**, *58*, 5417-5421.

8. Curtis, N. J.; Brown, R. S. An Easily Introduced and Removed Protecting Group for Imidazole Nitrogen: A Convenient Route to 2-Substituted Imidazoles. *J. Org. Chem*. **1980**, *45*, 4038-4040.

9. (a) Omelańczuk, J. The First Stereoselective Synthesis of Chiral Halogenophosphines: Optically Active Tert-butyl(phenyl)chlorophosphine. *J. Chem. Soc. Chem. Commun*. **1992**, 1718-1719. (b) Pabel, M.; Willis, A. C.; Wild, S. B. Attempted Resolution of Free (±)-Chlorophenylisopropylphosphine. *Tetrahedron: Asymmetry* **1995**, *6*, 2369-2374. (c) Humbel, S.; Bertrand, C.; Darcel, C.; Bauduin, C.; Jugé, S. Configurational Stability of Chlorophosphines. *Inorg. Chem*. **2003**, *42*, 420-427.

10. For a review, see: Hérault, D.; Nguyen, D. H.; Nuel, D.; Buono, G. Reduction of Secondary and Tertiary Phosphine Oxides to Phosphines. *Chem. Soc. Rev*. **2015**, *44*, 2508-2528.

11. For reviews, see: (a) Shi, F.; Larock, R. C. in C-H Activation. Topics in Current Chemistry, Vol. 292 (Eds.: J-Q. Yu, Z. Shi), Springer, **2009**, pp 123-164. https://doi.org/10.1007/128_2008_46 (b) Dong, X.; Wang, H. Liu, H.; Wang, F. Recent Advances in Transition Metal Migration Involving Reactions. *Org. Chem. Front*. **2020**,

7, 3530-3556. c) Li, M-Y.; Wei, D.; Feng, C-G.; Lin, G-Q. Tandem Reactions involving 1,4-Palladium Migrations. *Chem. Asian J.* **2022**, *17*, e202200456.

12. Kesharwani, T.; Larock, R. C. Benzylic C–H Activation and C–O bond Formation via Aryl to Benzylic 1,4-Palladium Migrations. *Tetrahedron* **2008**, *64*, 6090-6102.

13. (a) Hu, T-J.; Zhang, G.; Chen, Y-H.; Feng, C-G.; Lin, G-Q. Borylation of Olefin C–H Bond via Aryl to Vinyl Palladium 1,4-Migration. *J. Am. Chem. Soc.* **2016**, *138*, 2897-2900. (b) Zhang, G.; Li, M-Y.; Ye, M-B.; He, Z-T.; Feng, C-G.; Lin, G-Q. Borylation of Unactivated C(sp3)–H Bonds with Bromide as a Traceless Directing Group. *Org. Lett.* **2021**, *23*, 2948-2953.

14. Cheng, C.; Zhu, Q.; Zhang, Y. Intermolecular C–H Silylation through Cascade Carbopalladation and Vinylic to Aryl 1,4-Palladium Migration. *Chem. Commun.* **2021**, *57*, 9700-9703.

15. Ji, X-M.; Chen, Y-Z.; Fu, J-G.; Zhang, S-S.; Feng, C-G. Phosphorylation of C(sp3)–H Bonds via 1,4-Palladium Migration. *Org. Lett.* **2022**, *24*, 3781-3785.

16. (a) Li, S-G.; Yuan, M.; Topic, F.; Han, Z. S.; Senanayake, C. H. Tsantrizos, Y. S. Asymmetric Library Synthesis of P-Chiral t-Butyl-Substituted Secondary and Tertiary Phosphine Oxides. *J. Org. Chem.* **2019**, *84*, 7291-7302. (b) Kortmann, F. A.; Chang, M. C. Otten, E.; Couzijn, E. P. A.; Lutz, M.; Minnaard, A. J. Consecutive Dynamic Resolutions of Phosphine Oxides. *Chem. Sci.* **2014**, *5*, 1322-1327.

17. Matsumura, M.; Kitamura, Y.; Yamauchi, A.; Kanazawa, Y.; Murata, Y.; Hyodo, T.; Yamaguchi, K.; Yasuike, S. Synthesis of Benzo[d]imidazo[2,1-]benzoselenoazoles: Cs_2CO_3-Mediated Cyclization of 1-(2-Bromoaryl)benzimidazoles with Selenium. *Beilstein J. Org. Chem.* **2019**, *15*, 2029–2035.

18. Petit, C.; Poli, E.; Favre-Réguillon, A.; Khrouz, L.; Denis-Quanquin, S.; Bonneviot, L.; Mignani, G.; Lemaire, M. Unraveling the Catalytic Cycle of Tertiary Phosphine Oxides Reduction with Hydrosiloxane and $Ti(OiPr)_4$ through EPR and 29Si NMR Spectroscopy. *ACS Catal.* **2013**, *3*, 1431-1438.

19. Sieber, J. D.; Rodriguez, S.; Frutos, R.; Buono, F.; Zhang, Y.; Li, N.; Qu, B.; Premasiri, A.; Li, Z.; Han, Z. S.; Xu, Y.; Byrne, D.; Haddad, N.; Lorenz, J.; Grinberg, N.; Kurouski. D.; Lee, H.; Narayanan, B.; Nummy, L.; Mulder, J.; Brown, J. D.; Granger, A.; Gao, J.; Krawiec, M.; Williams, Z.; Pennino, S.; Song, J. J.; Hossain, A.; Yee, N. K.; Busacca, C.; Roschangar, F.; Xin, Y.; Mao, Z.; Zhang, X.; Hong, Y.; Senanayake, C. H. Development of a Scalable, Chromatography-Free Synthesis of t-Bu-SMS-Phos and Application to the Synthesis of an Important Chiral CF3-Alcohol Derivative with High Enantioselectivity Using Rh-Catalyzed Asymmetric Hydrogenation. *J. Org. Chem.* **2018**, *83*, 1448-1461.

20. Martin, R.; Buchwald, S. L. Palladium-Catalyzed Suzuki−Miyaura Cross-Coupling Reactions Employing Dialkylbiaryl Phosphine Ligands. *Acc. Chem. Res*. **2008**, *41*, 1461-1473.

21. (a) Tang, W.; Patel, N. D.; Xu, G.; Xu, X.; Savoie, J.; Ma, S.; Hao, M-H.; Keshipeddy, S.; Capacci, A-G.; Wei, X.; Zhang, Y.; Gao, J. J.; Li, W.; Rodriguez, S.; Lu, B. Z.; Yee, N. K.; Senanayake, C. H. Efficient Chiral Monophosphorus Ligands for Asymmetric Suzuki–Miyaura Coupling Reactions. *Org. Lett*. **2012**, *14*, 2258-2261. (b) Tang, W.; Qu, B.; Capacci, A. G.; Rodriguez, S.; Wei, X.; Haddad, N.; Narayanan, B.; Ma, S.; Grinberg, N.; Yee, N. K.; Krishnamurthy, D.; Senanayake, C. H. Novel, Tunable, and Efficient Chiral Bisdihydrobenzooxaphosphole Ligands for Asymmetric Hydrogenation. *Org, Lett.* **2010**, *12*, 176-179.

22. (a) Campo, M. A.; Zhang, H.; Yao, T.; Ibdah, A.; McCulla, R. D.; Huang, Q.; Zhao, J.; Jenks, W. S.; Larock, R. C. Aryl to Aryl Palladium Migration in the Heck and Suzuki Coupling of o-Halobiaryls. *J. Am. Chem. Soc*. **2007**, *129*, 6298-6307. (b) Mota, A. J.; Dedieu, A. Intramolecular 1,n Palladium Migrations in Polycyclic Aromatic Hydrocarbons. Palladium(II) versus Palladium(IV) Mechanisms: A Theoretical Study. *Organometallics* **2006**, *25*, 3130-3142.

23. Dong, B.; Cong, X.; Hao, N. Silver-Catalyzed Regioselective Deuteration of (Hetero)arenes and α-Deuteration of 2-Alkyl Azaarenes. *RSC Adv*. **2020**, *10*, 25475–25479.

Chapter 5: Conclusion and Contributions to Knowledge

5.1 Conclusion and Future Directions of Research Projects Presented in this Ph.D. Thesis

The three projects presented in this Ph.D. thesis focused on the rational design, synthesis and applications of novel *P*-chiral Brønsted acids and novel *P*-chiral ligands in asymmetric catalysis. In the first project (Chapter 2) a class of *P*-chiral *N*-phosphoryl sulfonamide Brønsted acid-type organocatalysts was synthesized from *P*-chiral SPOs. A systematic evaluation of their properties in the asymmetric transfer hydrogenation of quinolines revealed that these Brønsted acids, characterized by an *ortho*-substituted phenol or naphthol moiety, performed better in reactivity and enantioselectivity than comparable, commonly used BINOL-based phosphoric acid organocatalysts. In addition, extending the aromaticity of these acids, for instance, replacing the *P*-substituted phenol moiety with naphthol (Scheme 2.1, Table 2.1) enhanced reaction enantioselectivity. Within this reaction scope, the asymmetric Brønsted acid-catalyzed transfer hydrogenation of deactivated quinolines was successfully investigated for the first time.

In the effort to improve on the enantioselectivity of this reaction, the library of Brønsted acids was further expanded to include variations to the sulfonyl handle (Chapter 3). These compounds were shown to catalyze the transfer hydrogenation of C2-substituted carboxymethyl quinolines in modest yields and enantioselectivity, where BINOL-based phosphoric acid organocatalysts failed. Furthermore, the thermal stability of some *P*-chiral Brønsted acids was investigated and it was shown that at elevated temperatures, a phospha-Brook rearrangement occurs. Future studies to address this limitation may involve modulating the electronic nature of the substituents on the phosphorus atom of these compounds, and thoroughly re-evaluating their stability and catalytic properties. For instance, utilizing electron-deficient *P*-substituted naphthols may decelerate the rate of catalyst rearrangement at elevated temperatures.

Furthermore, to improve on the enantioselectivity of the transfer hydrogenation reaction, it is suggested that the *P*-substituted aromatic group is further elaborated with systems such as phenanthrol and anthracenol. In order to further explore the catalytic properties of this novel class of P-chiral Brønsted acid organocatalysts, it is imperative that reactions involving other challenging electrophiles, such as olefins, are explored.

In the third project reported in this thesis (Chapter 4), a novel, enantiospecific, site-selective, solvent-switchable 1,4-palladium migration/C-H activation cascaded was applied to the phosphonylation of imidazoles with *P*-chiral SPOs. Preliminary investigations suggest that this methodology is amenable to imidazole and SPO coupling partners of various electronic and steric demands. To demonstrate the utility of this methodology, the synthesis of a novel C2-substituted *P*-chiral phosphinyl imidazole ligand was achieved for the first time, via the stereoretentive reduction of its phosphonyl imidazole precursor. The application of this ligand was showcased in an asymmetric Suzuki-Miyaura cross-coupling reaction, to give the desired atropisomer in high yield and enantioselectivity. As a future direction for this methodology, an improvement to the yields of the products may be investigated via an extensive reaction optimization. In addition, a structurally diverse library of *P*-chiral phosphonyl imidazoles (Figure 4.2) will be synthesized and evaluated in numerous asymmetric transformations. In collaboration with experts in the field, computational studies may be carried out to probe the role of solvents in site-selectivity.

5.2 Claims to Original Knowledge

a. Contributed to the synthesis of a novel class of *P*-chiral *N*-phosphoryl sulfonamide Brønsted acids organocatalysts, and their evaluation in the biomimetic asymmetric transfer hydrogenation of quinolines. We showed that the catalytic properties of these acids are modulated by an intramolecular hydrogen bond interaction that rigidifies their cavity size, and potentially guides the hydride transfer from the

Hantzsch ester reagent to the substrate, increasing the reaction rate and enantioselectivity.

b. These Brønsted acids were also applied to the organocatalytic, asymmetric transfer hydrogenation of deactivated quinolines for the first time, yielding amino acid bioisosteres. In comparison, BINOL-based Brønsted acids failed to catalyze this transformation. Furthermore, the thermal stability of some of these *P*-chiral Brønsted acids was investigated and an unprecedented phospha-Brook rearrangement was shown to occur at elevated temperatures. While this phenomenon presents a limitation to this methodology, it may be explored as a synthetic route towards compounds such as phosphoramidates.

c. Contributed to the development of an unprecedented enantiospecific, solvent-switchable, site-selective 1,4-palladium migration/C-H activation cascade and applied it to the synthesis of *P*-chiral phosphonyl imidazoles. This methodology allowed for direct coupling, as well as imidazole-C2 and imidazole-C5 site-selectivity. To the best of our knowledge, the stereoretentive reduction of one of these compounds afforded the first *P*-chiral 2-phosphiny imidazole ligand, which was used, as an example, to achieve an asymmetric Suzuki-Miyaura cross-coupling reaction.

d. Contributed to the development of a B_2Pin_2-assisted copper-catalyzed transfer hydrogenation of aromatic sulfonylimines, delivering a variety of aryl/heteroaryl sulfonamides in good to excellent yields under mild reaction conditions and with methanol as the hydrogen source. Mechanistic studies suggest that the reaction may proceed via a transient α-borylated intermediate, followed by protodeboration to afford the sulfonamide products. This manuscript is published, however, it is not reported in this thesis.

e. Contributed to the applications of novel *P*-chiral *N*-heterocyclic carbenes as ligands for asymmetric catalysis. This manuscript is under preparation and not reported in this thesis.

5.3 Peer-Reviewed Publications and Conference Proceedings

5.3.1 Peer-Reviewed Publications

Publications Co-Authored in the Duration of this Ph.D. Research:

Mbaezue, I. I.; Topic, F.; Tsantrizos, Y. S. Re-evaluation of P-Chiral, N-Phosphoryl Sulfonamide Brønsted Acids in the Asymmetric Synthesis of 1,2,3,4-Tetrahydroquinoline-2-carboxylate Esters via Biomimetic Transfer Hydrogenation. *Synlett* **2023**, DOI: 10.1055/a-2047-8301.

He, Y.; Li, S-L.; Mbaezue, I. I.; Reddy, A. C. S.; Tsantrizos, Y. S. Copper-Boryl Mediated Transfer Hydrogenation of N-Sulfonyl Imines using Methanol as the Hydrogen Donor. *Tetrahedron* **2021**, *85*, 132063.

Yuan, M.; Mbaezue, I. I.; Zhou, Z.; Topic, F.; Tsantrizos, Y. S. P-Chiral, N-phosphoryl Sulfonamide Brønsted Acids with an Intramolecular Hydrogen Bond Interaction that Modulates Organocatalysis. *Org. Biomol. Chem*. **2019**, *17*, 8690 – 8694.

Publications Co-Authored during B.Sc. (Hons.) Research:

Mbaezue, I. I.; Ylijoki, K. E. O. [5 + 1 + 2 + 1] vs [5 + 1 + 1 + 2] Rhodium-Catalyzed Cycloaddition Reactions of Vinylcyclopropanes with Terminal Alkynes and Carbon Monoxide: Density Functional Theory Investigations of Convergent Mechanistic Pathways and Reaction Regioselectivity. *Organometallics* **2017**, *36*, 2832-2842.

Areephong, J.; Huo, B.; Mbaezue, I. I.; Ylijoki, K. E. O. Synthesis of Dihydroquinoxaline-2(1H)-ones via Palladium-Catalyzed Intramolecular C–N Bond Formation. *Tetrahedron Lett*. **2016**, *57*, 3124-3126.

5.3.2 Manuscript in Preparation

Mbaezue, I. I.; Li, S-G.; Reddy, A. C. S.; Titi, H.; Tsantrizos, Y. S. Solvent-Switchable Remote C-H Activation via 1,4-Palladium Migration Enables Site-Selective C-P Bond Formation: A New Tool for the synthesis of P-Chiral Phosphinyl Imidazole Ligands.

5.3.3 Conference Proceedings

Oral Presentation in the Duration of this Ph.D. Research:

1. Mbaezue, I. I.; Yuan, Y.; Zhou, Z.; Senanayake, C.; Topic, F.; Tsantrizos, Y. S. In Novel *P*-Chiral, *N*-Phosphoryl Sulfonamide Brønsted Acids: Design, Synthesis and Applications in the Asymmetric Transfer Hydrogenation of Quinolines, Proceedings of the 102nd Canadian Chemistry Conference and Exhibition, Quebec City, QC, June 3-7, 2019

Oral Presentations during B.Sc. (Hons.) Research:

1. Mbaezue, I. I.; Ylijoki, K. E. O. In A Spectroscopic and Computational Investigation of the Rh-catalyzed [5 + 1 + 2 + 1] Cycloaddition Reaction, Proceedings of the 42nd Annual Science Atlantic/CSC Student Chemistry Conference, St. John's, NL, May 4-6, 2017

2. Mbaezue, I. I.; Ylijoki, K. E. O. In Does the [5 + 1 + 2 + 1] Rhodium-Catalysed Cycloaddition Reaction Actually Proceed via an Alternate Pathway? The Elucidation of a [5 + 1 + 1 + 2] Mechanistic Pathway via DFT Investigation, Proceedings of the 41st Annual Science Atlantic/CIC Student Chemistry Conference, Halifax, NS, June 2-4, 2016

Poster Presentation in the Duration of this Ph.D. Research:

1. Mbaezue, I. I.; Li, S-G.; Yuan, M.; Tsantrizos, Y. S. In The Design and Synthesis of P-Chiral Molecules and their Applications in Asymmetric Transformations. Proceedings of the 23rd Gordon Research Conference in Stereochemistry, Newport, RI, July 24-29, 2022

Oral Presentations during B.Sc. (Hons.) Research:

1. Mbaezue, I. I.; Ylijoki, K. E. O. In Does the [5 + 1 + 2 + 1] Rhodium-catalysed Cycloaddition Reaction Actually Proceed via an Alternate Pathway? The Elucidation of a [5 + 1 + 1 + 2] Mechanistic Pathway via DFT Investigation, Proceedings of the 99th Canadian Chemistry Conference and Exhibition, Halifax, NS, June 5-9, 2016

2. Mbaezue, I. I.; Ylijoki, K. E. O. In A Density Functional Theory Investigation of the Rhodium-Catalysed [5 + 1 + 2 + 1] Cycloaddition Reaction, Proceedings of the 40th Annual Science Atlantic-CIC Chemistry Conference, Fredericton, NB, May 21-23, 2015

Appendix 1: NMR Spectra, HPLC Chromatograms and X-Ray Data for Chapter 2

^{1}H NMR of **2.3b**

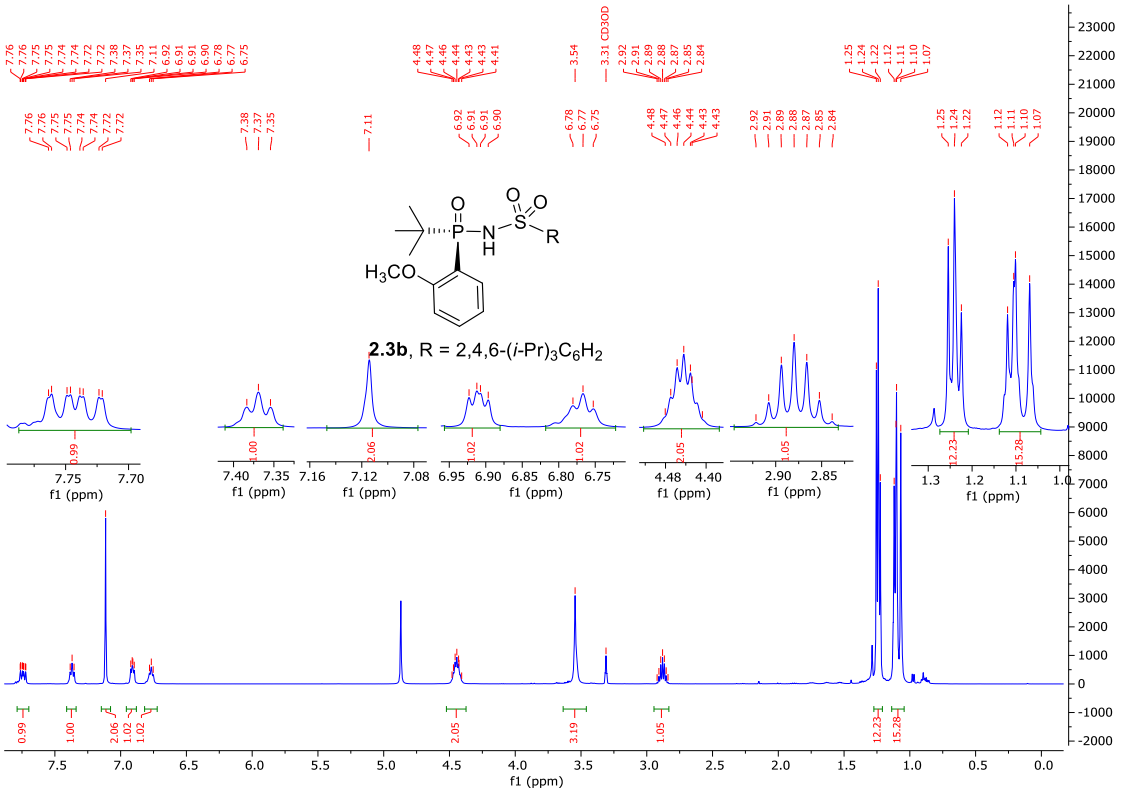

^{31}P NMR of **2.3b**

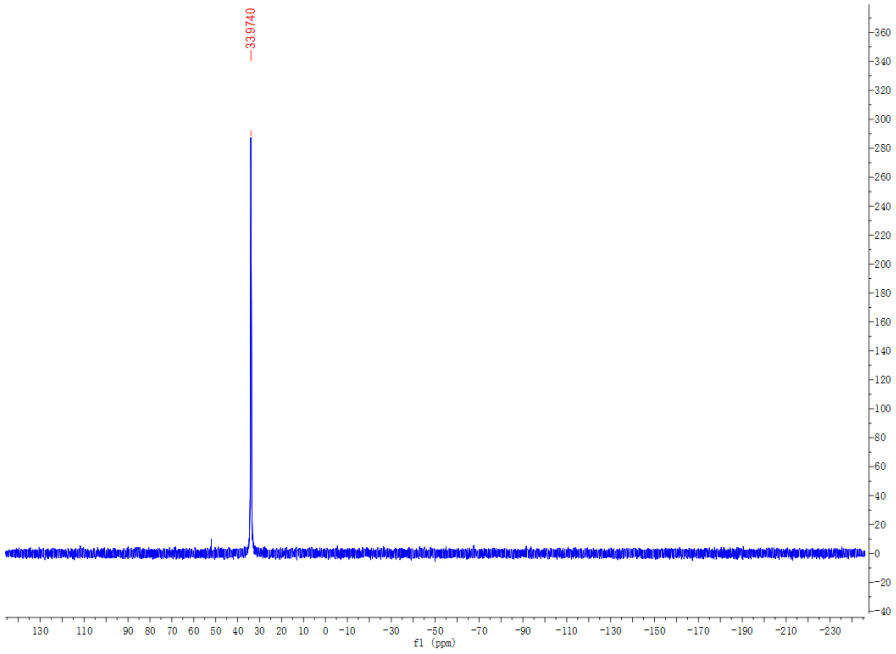

^{13}C NMR of **2.3b**

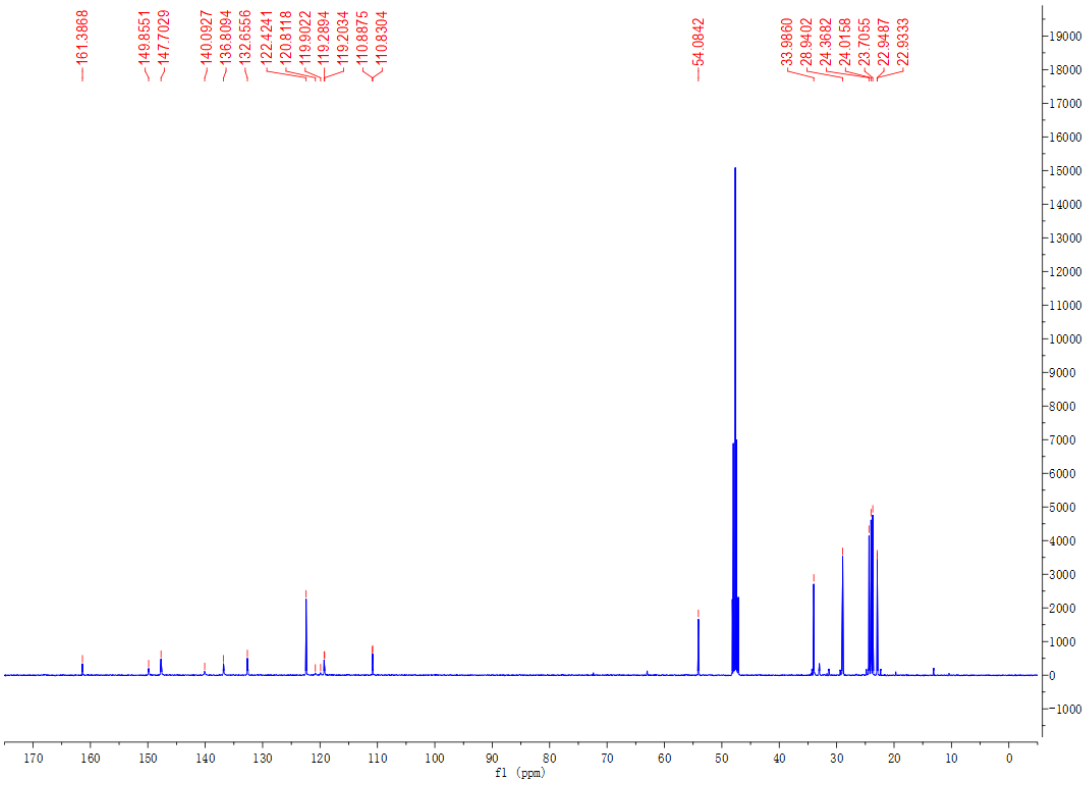

^{1}H NMR of **2.4a**

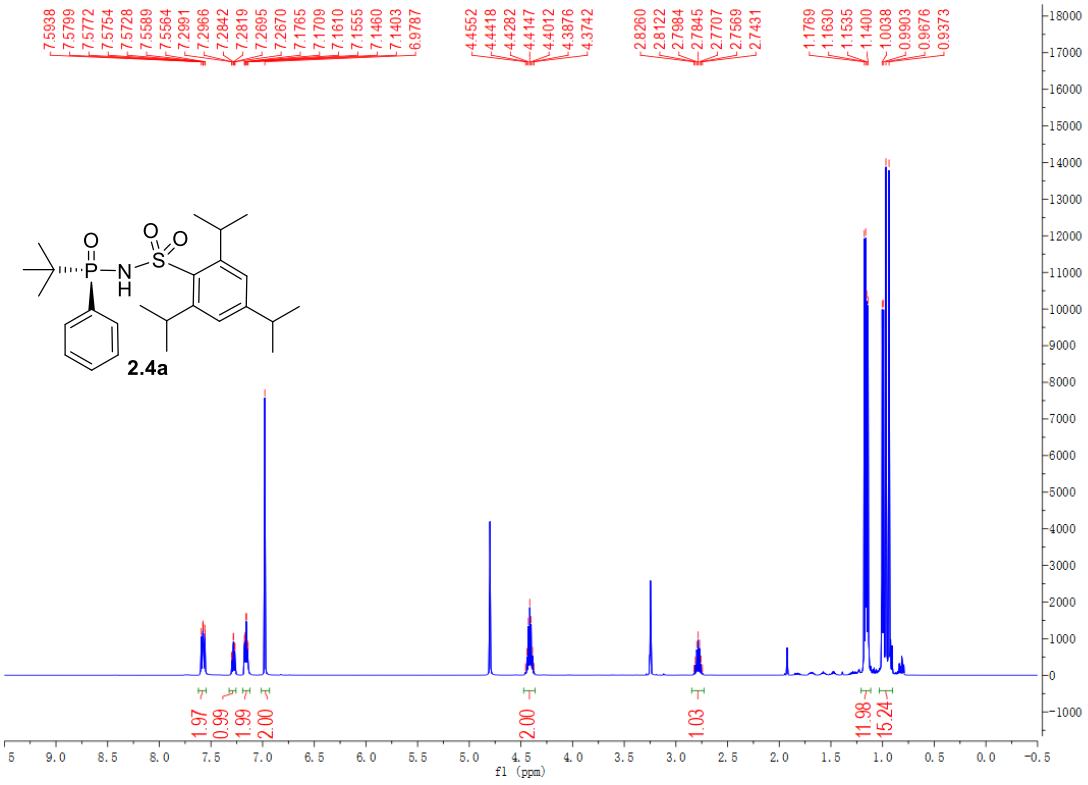

^{31}P NMR of **2.4a**

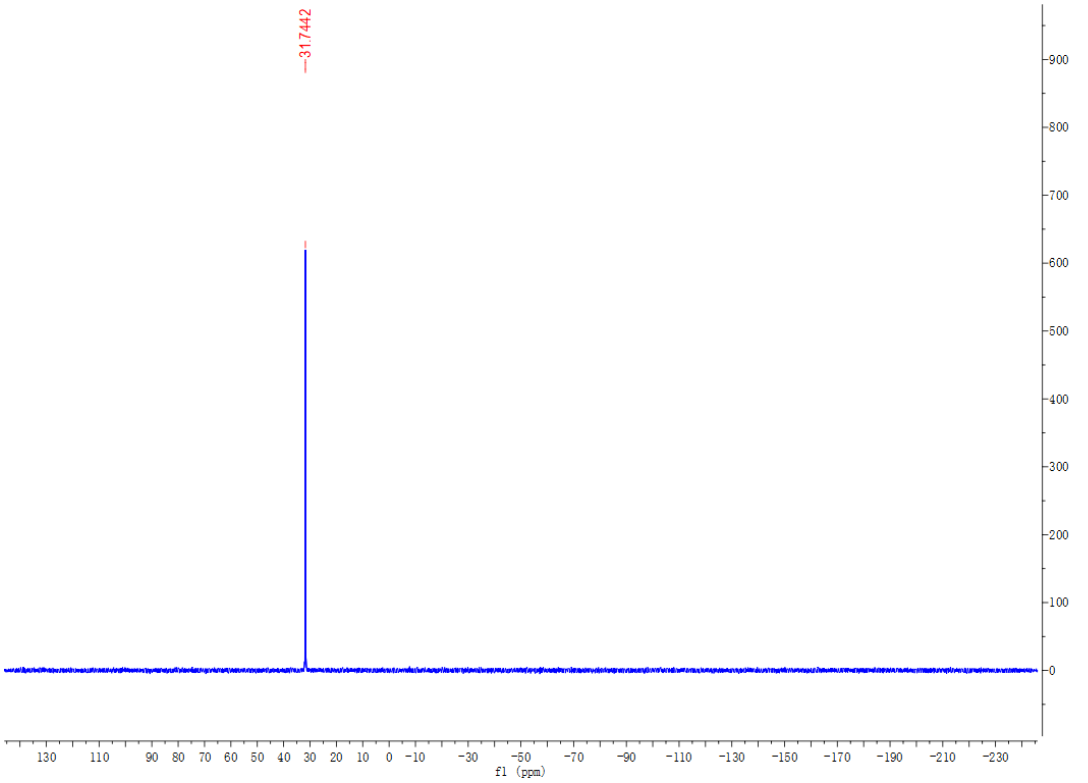

^{13}C NMR of **2.4a**

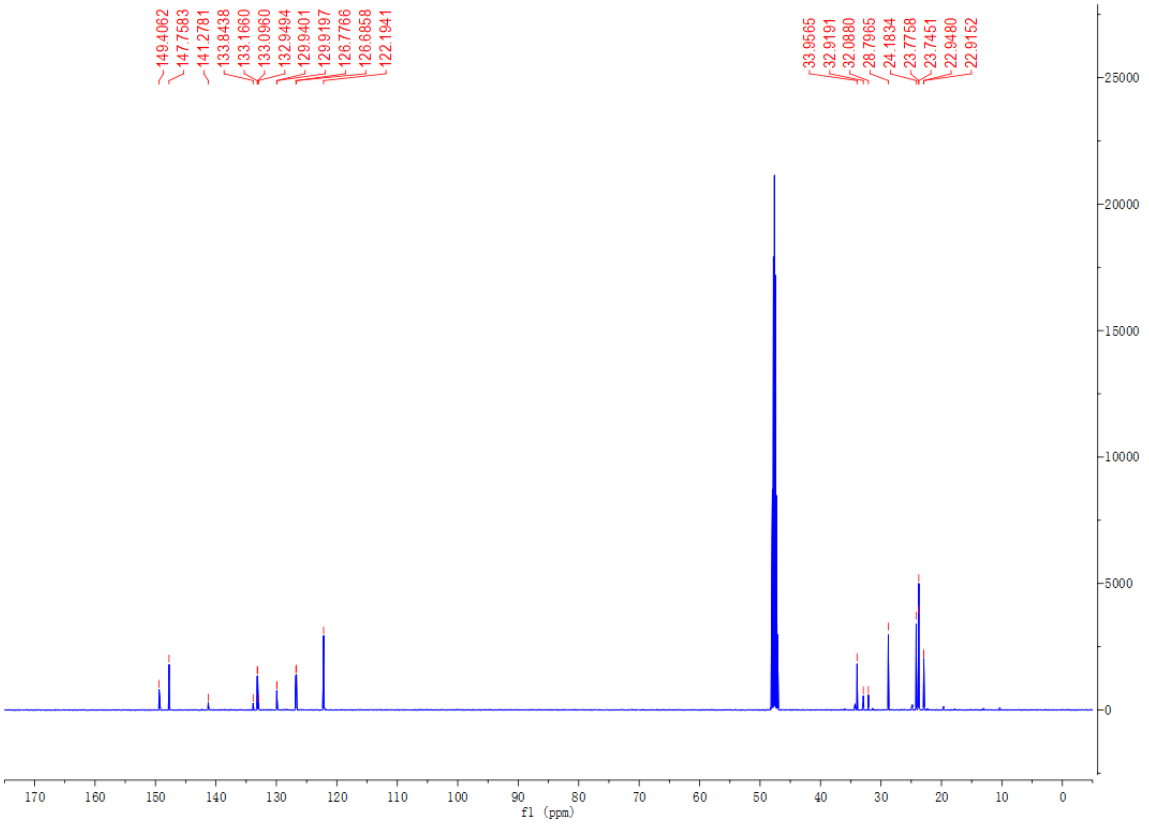

Chiral HPLC Chromatograms of **2.4a**

Method: HPLC instrument: Agilent 1260 HPLC; λ = 220 nm

Colum: Phenomenex Lux Cellulose-2, 4.6x100 mm

Solvent A: 0.1% (v/v) $HClO_4$ in water, Solvent B: CH_3CN; 50-90% solvent B in 15 min at a flow rate of 1.2 mL/min

Top panel, racemic (in red) superimposed with (*R*)-enantiomer (in blue); bottom panel (*R*)-**2.4a**; (*R*)-enantiomer t_R = 11.44 min (major), (*S*)- enantiomer t_R = 12.36 min (minor).

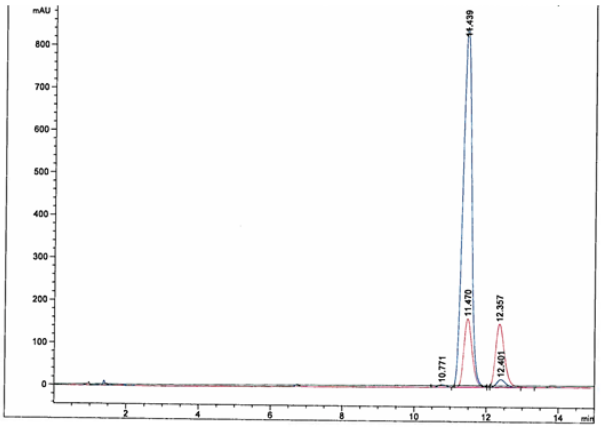

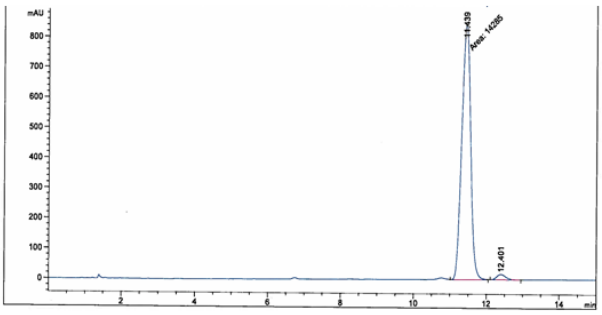

Peak #	RetTime [min]	Type	Width [min]	Area [mAU*s]	Height [mAU]	Area %
1	11.439	MM	0.2819	1.42850e4	844.44775	98.0089
2	12.401	BB	0.2276	290.20435	17.39890	1.9911
Totals :				1.45752e4	861.84665	

*** End of Report ***

[1]HNMR of **2.4c**

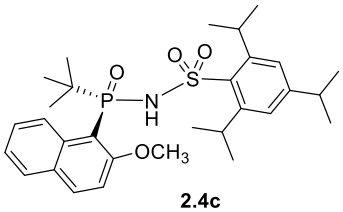

2.4c

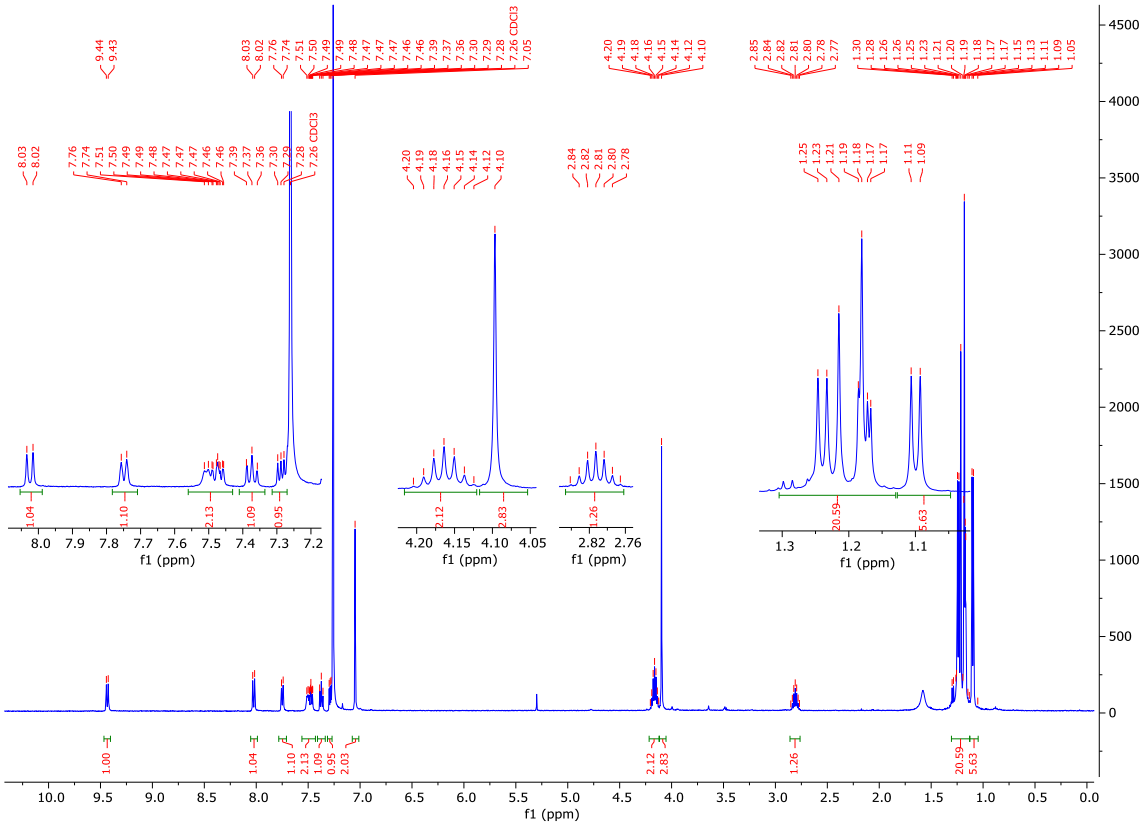

^{31}P NMR of **2.4c**

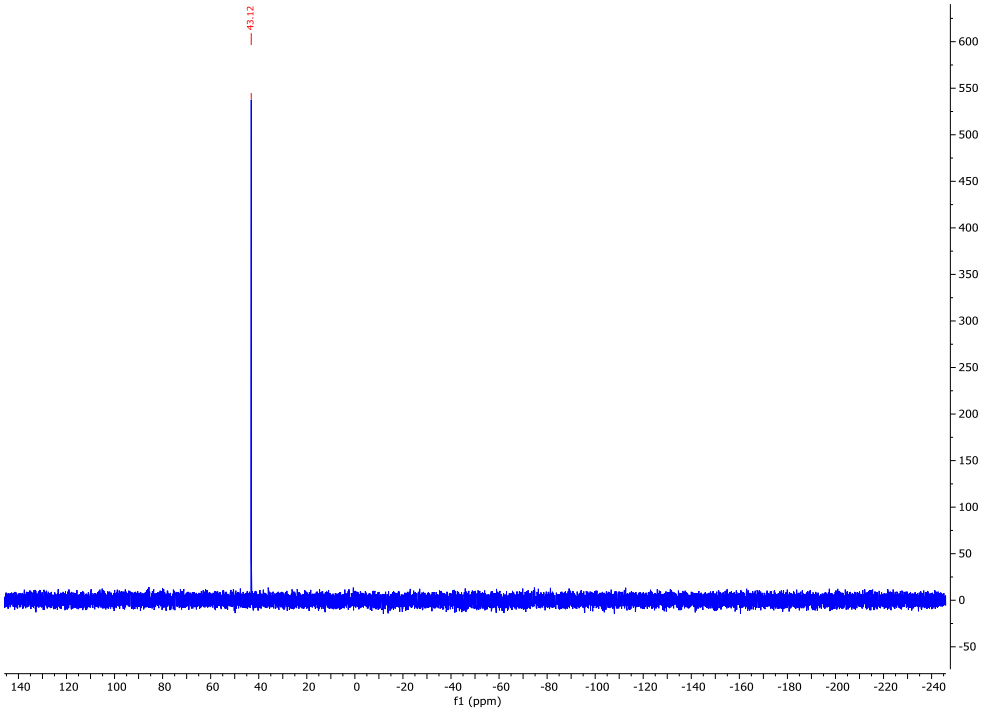

^{13}C NMR of **2.4c**

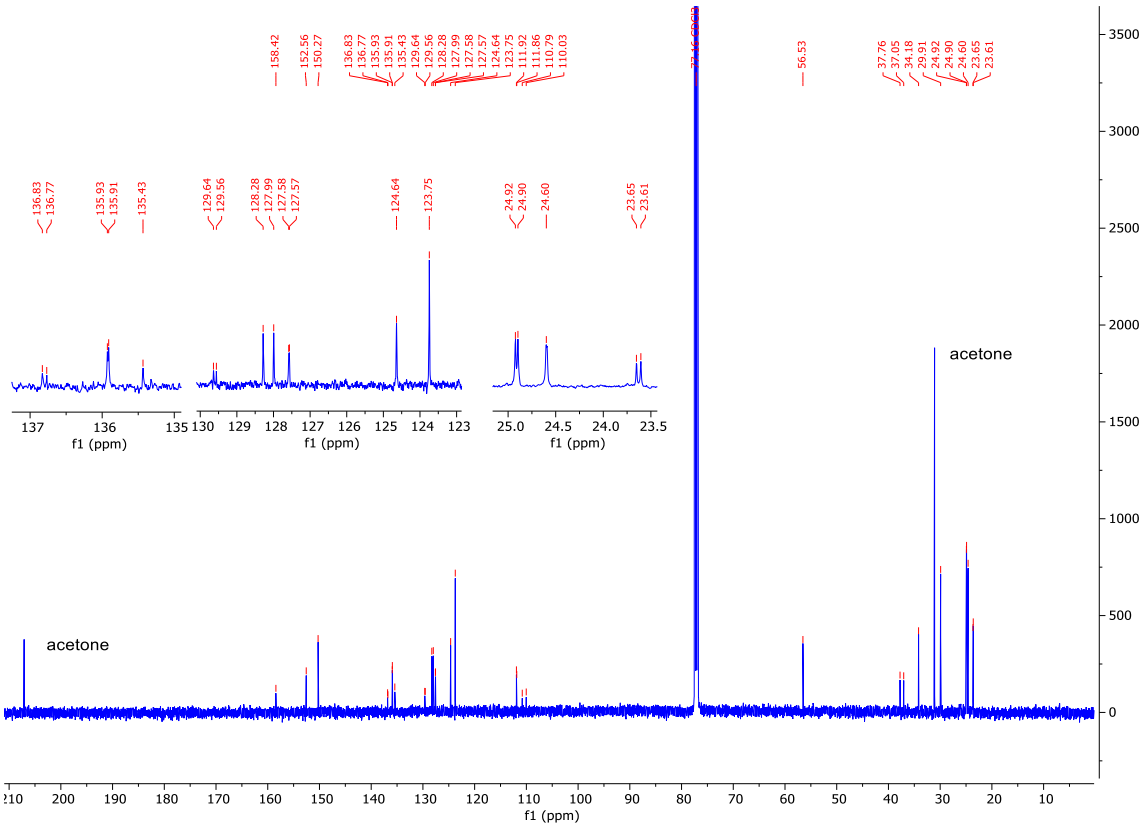

^{1}HNMR of **2.4d**

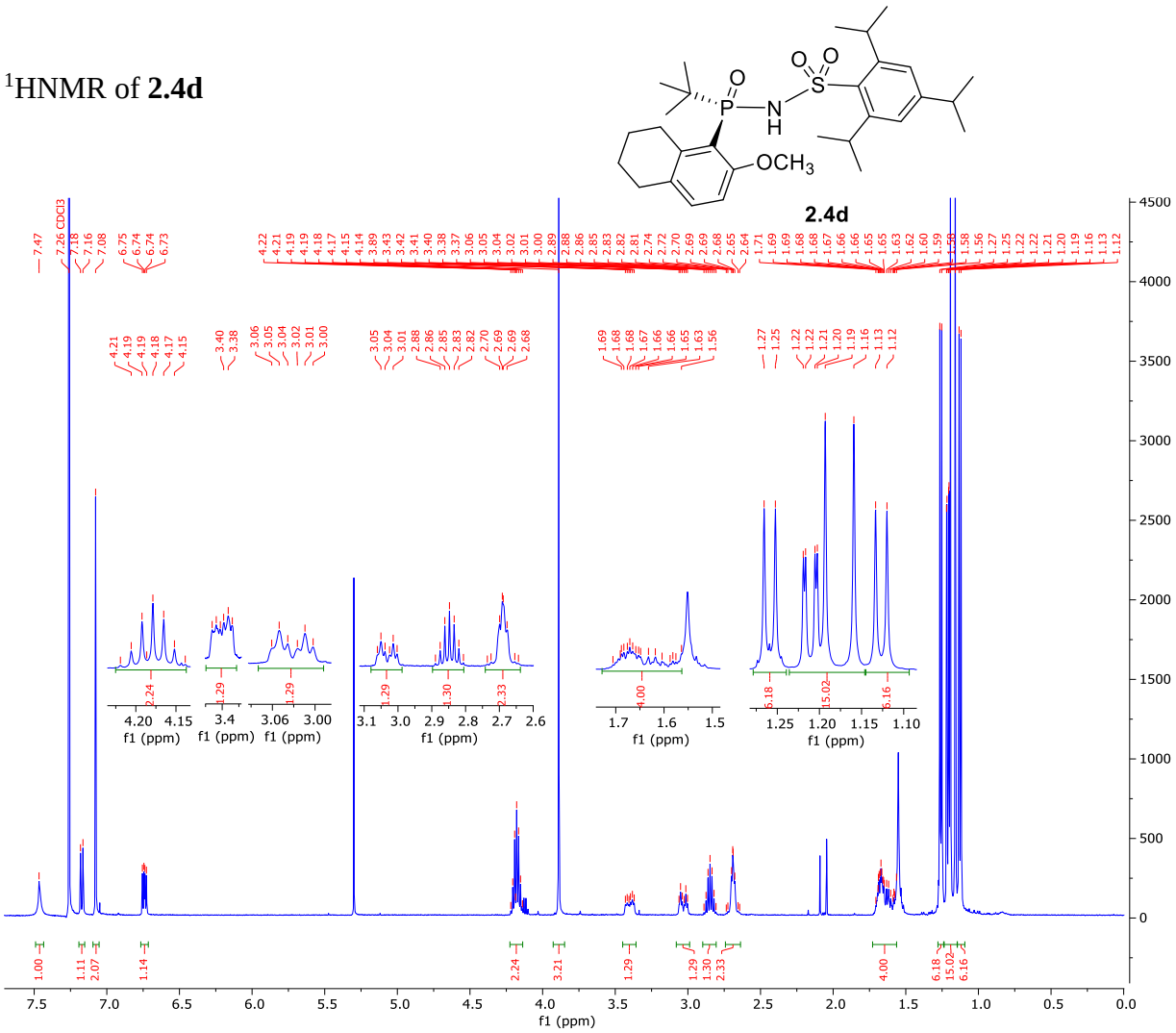

^{31}P NMR of **2.4d**

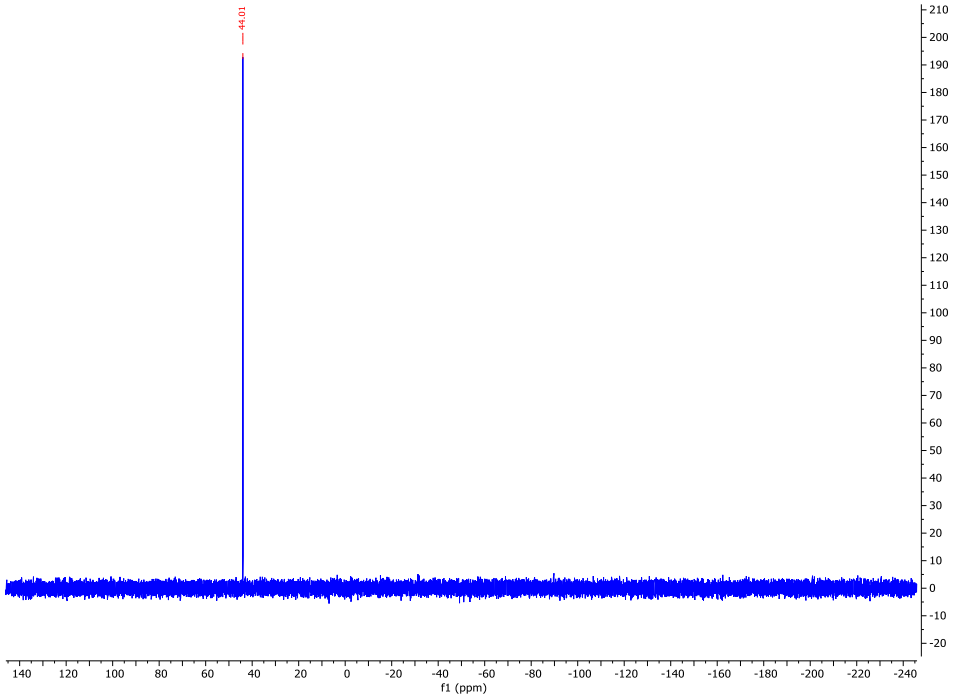

^{1}H NMR of **2.4e**

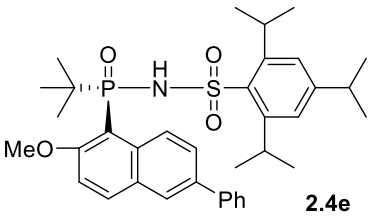

2.4e

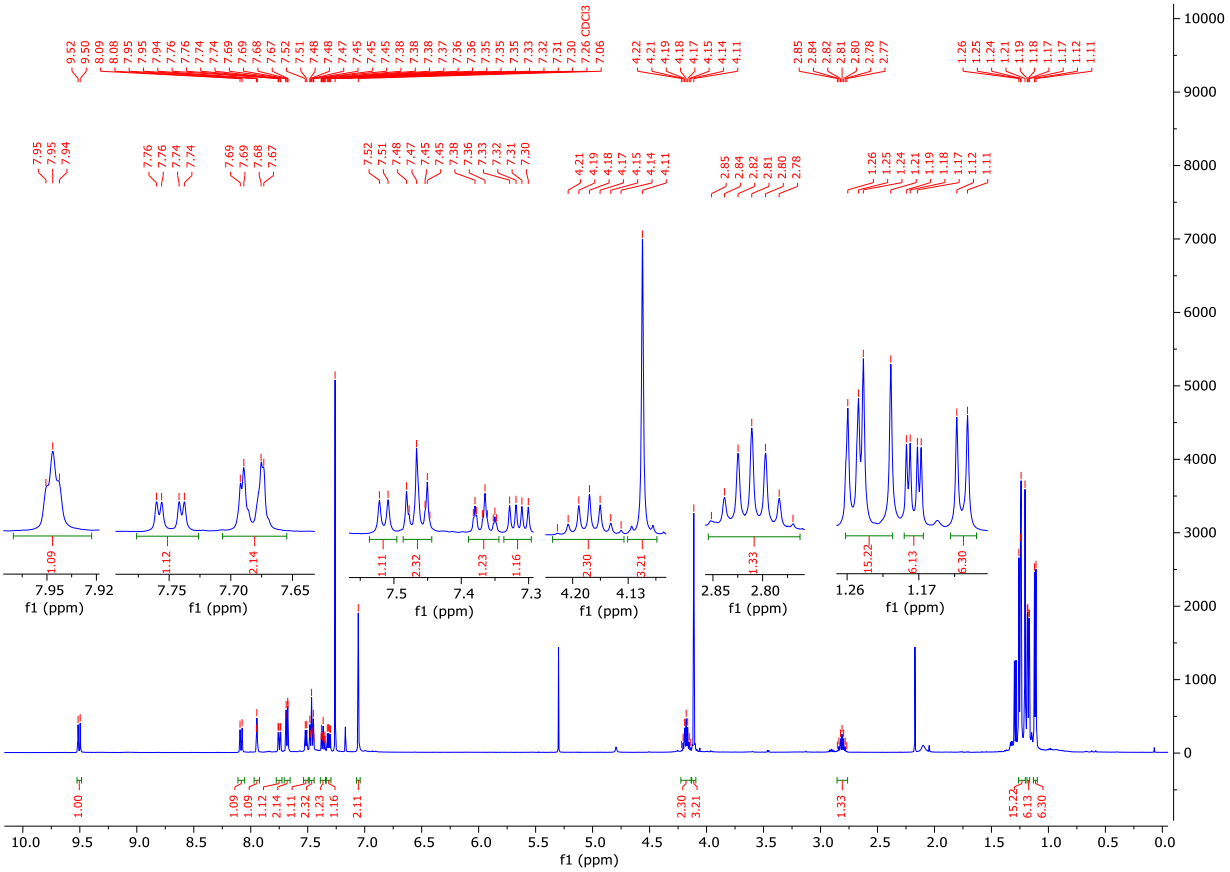

^{31}P NMR of **2.4e**

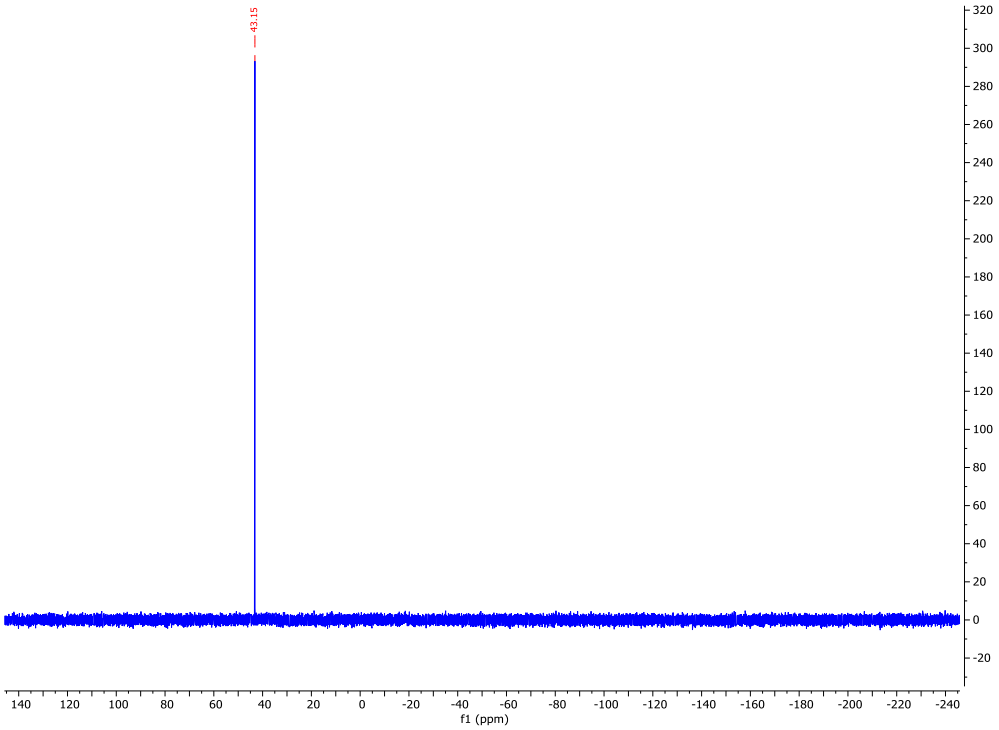

^{1}H NMR of **2.5a**

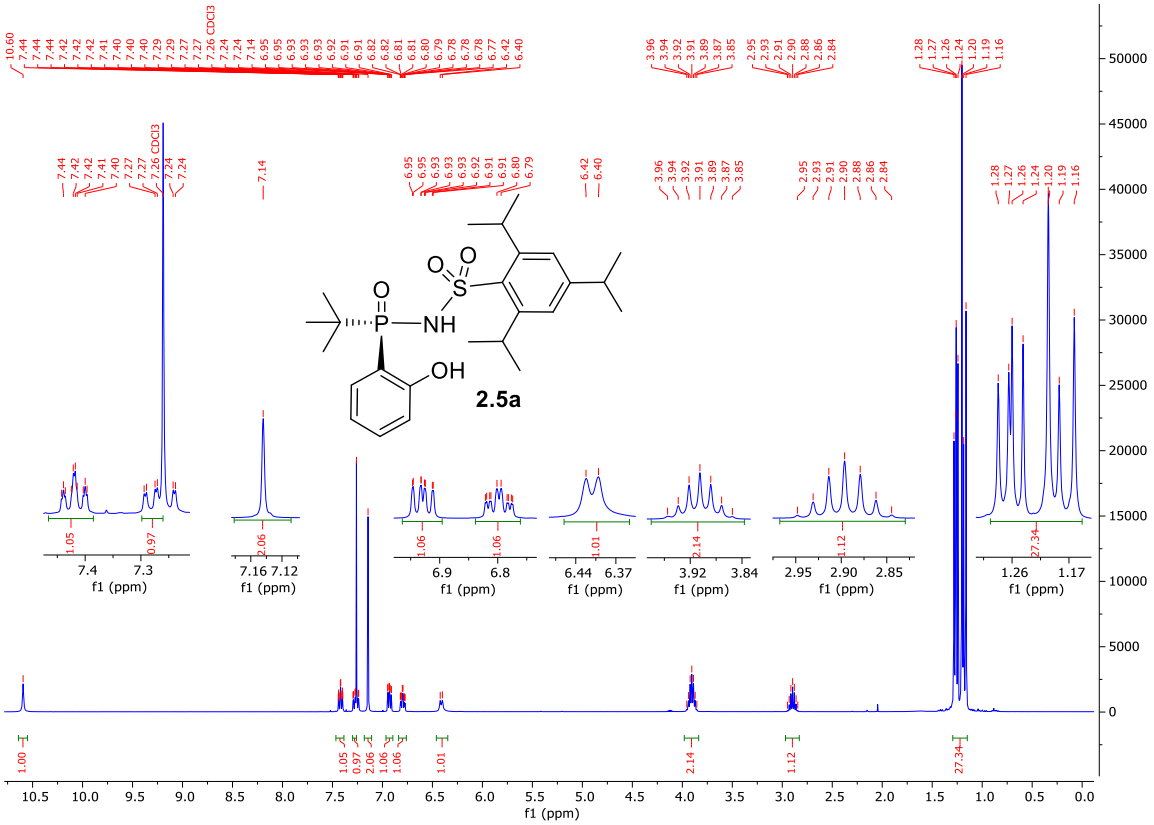

^{31}P NMR of **2.5a**

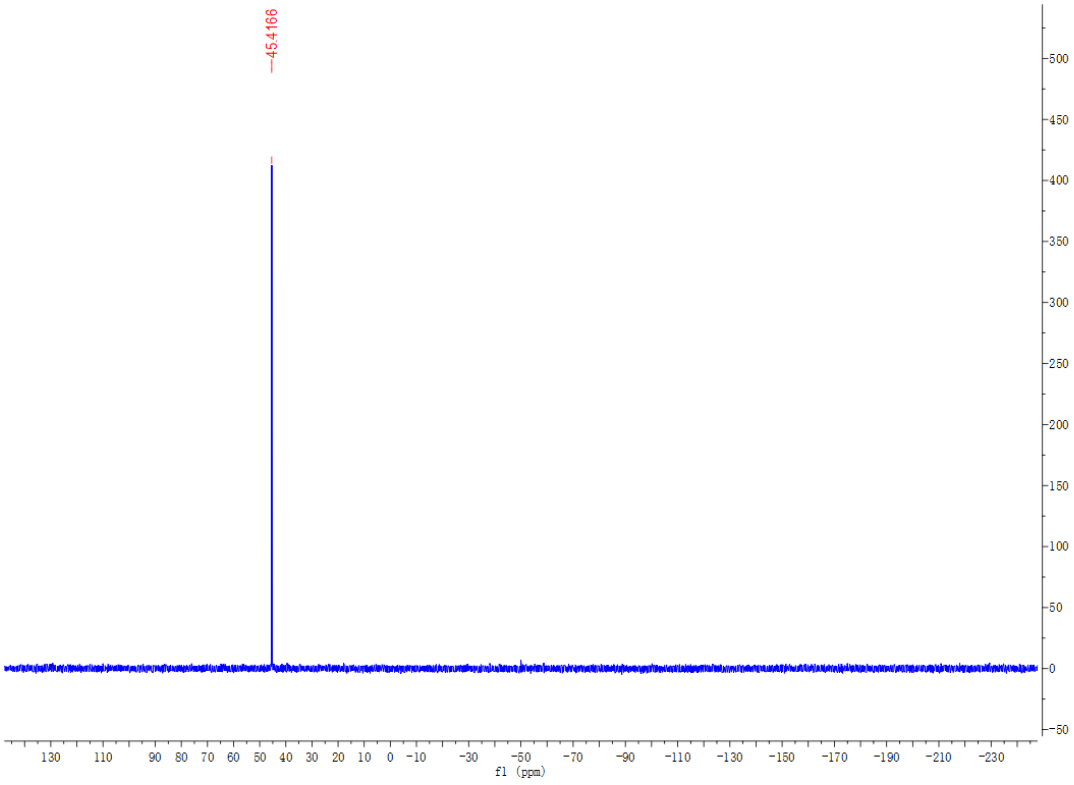

^{13}C NMR of **2.5a**

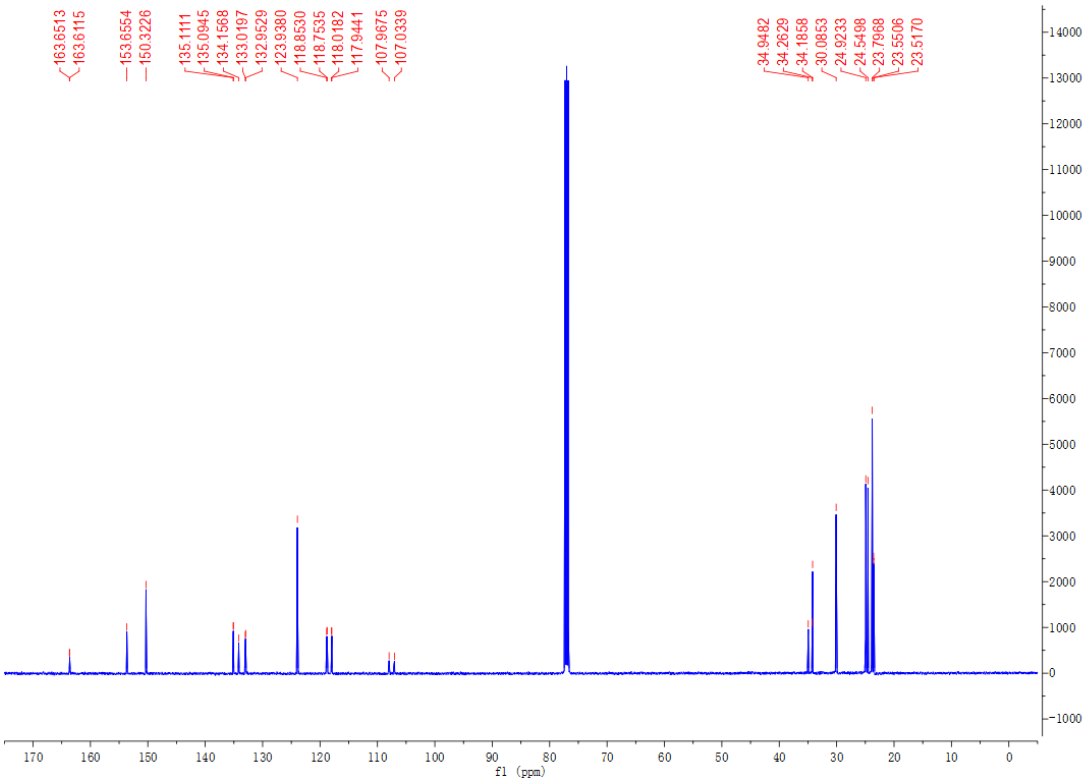

^{1}H NMR of **2.5b**

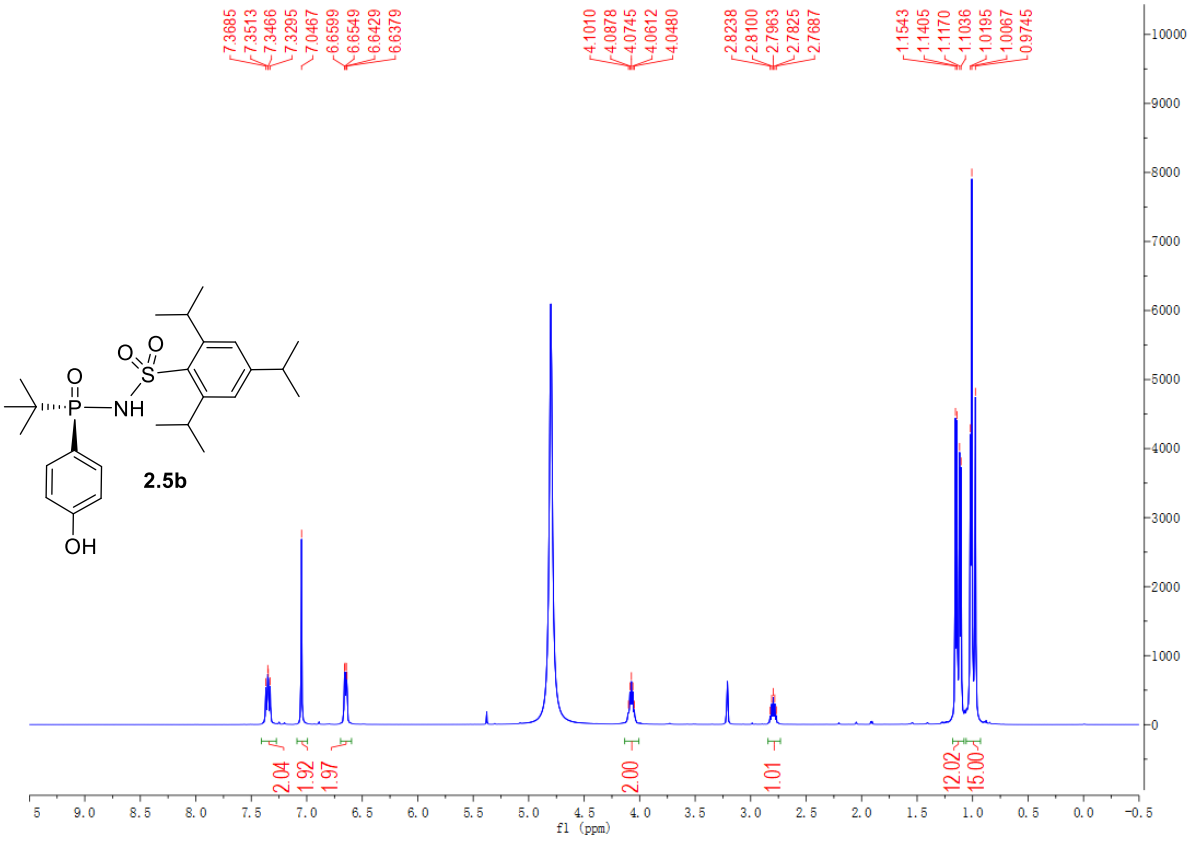
7.3685
7.3513
7.3466
7.3295
7.0467
6.6599
6.6549
6.6429
6.6379
4.1010
4.0878
4.0745
4.0612
4.0480
2.8238
2.8100
2.7963
2.7825
2.7687
1.1543
1.1405
1.1170
1.1036
1.0195
1.0067
0.9745
2.04
1.92
1.97
2.00
1.01
12.02
15.00
f1 (ppm)
2.5b

^{31}P NMR of **2.5b**

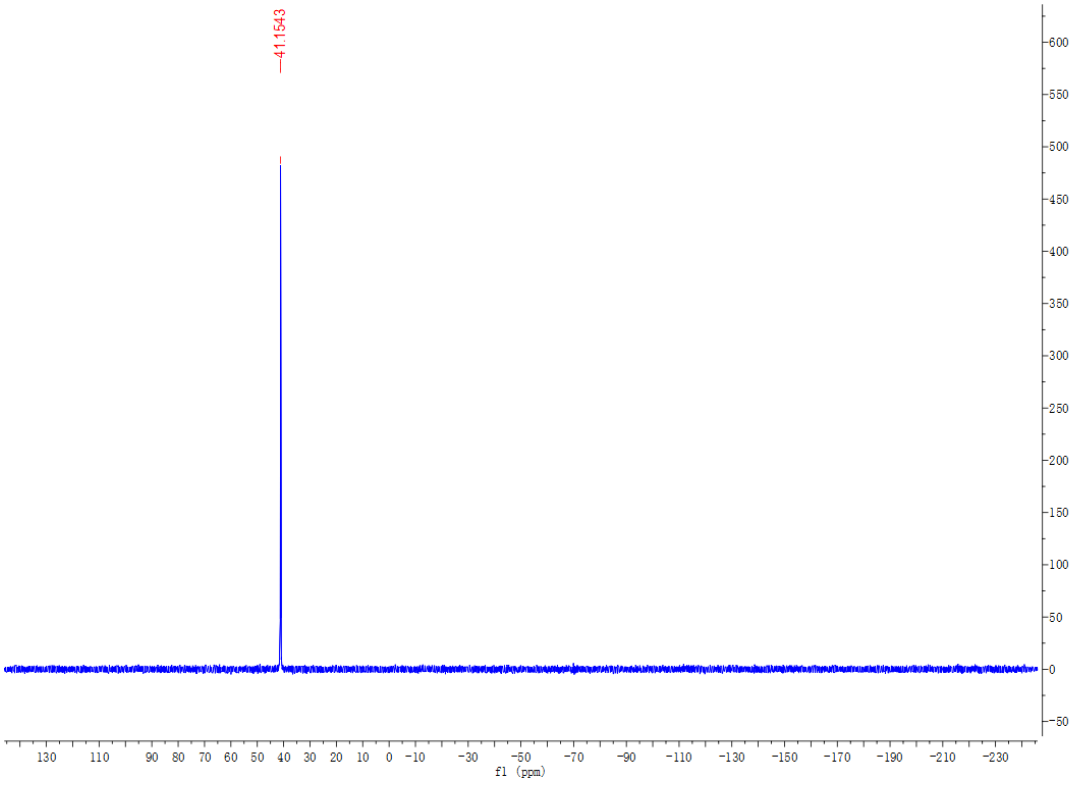

^{13}C NMR of **2.5b**

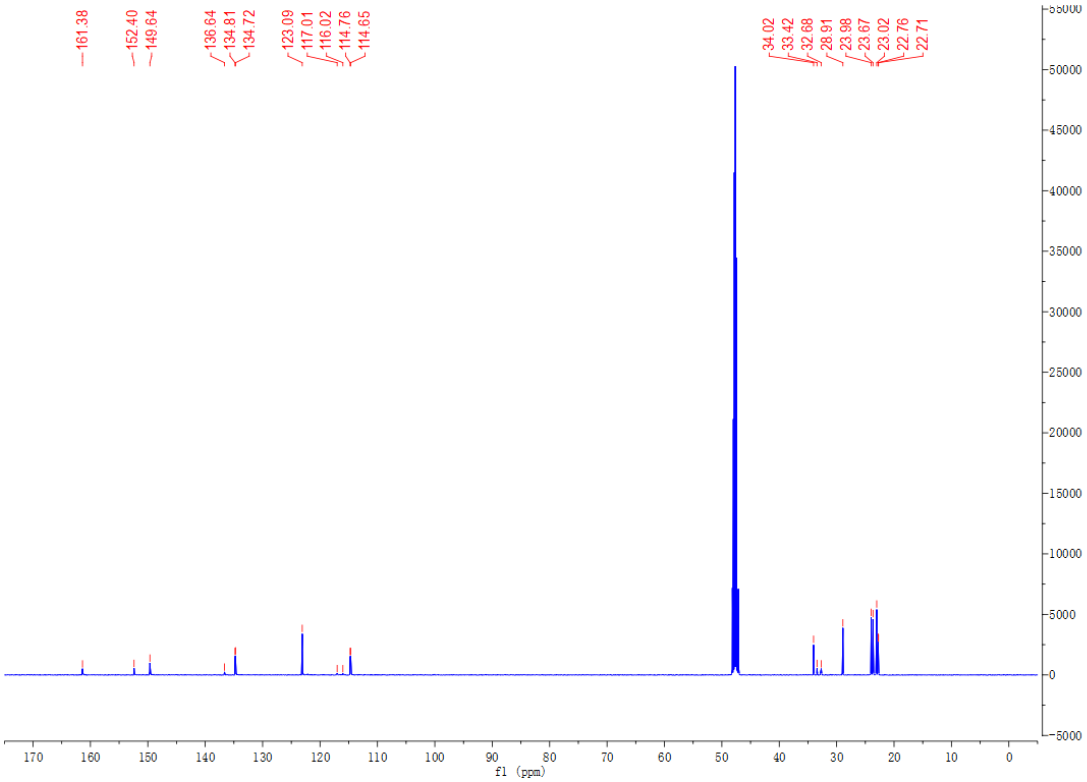

^{1}H NMR of **2.5c**

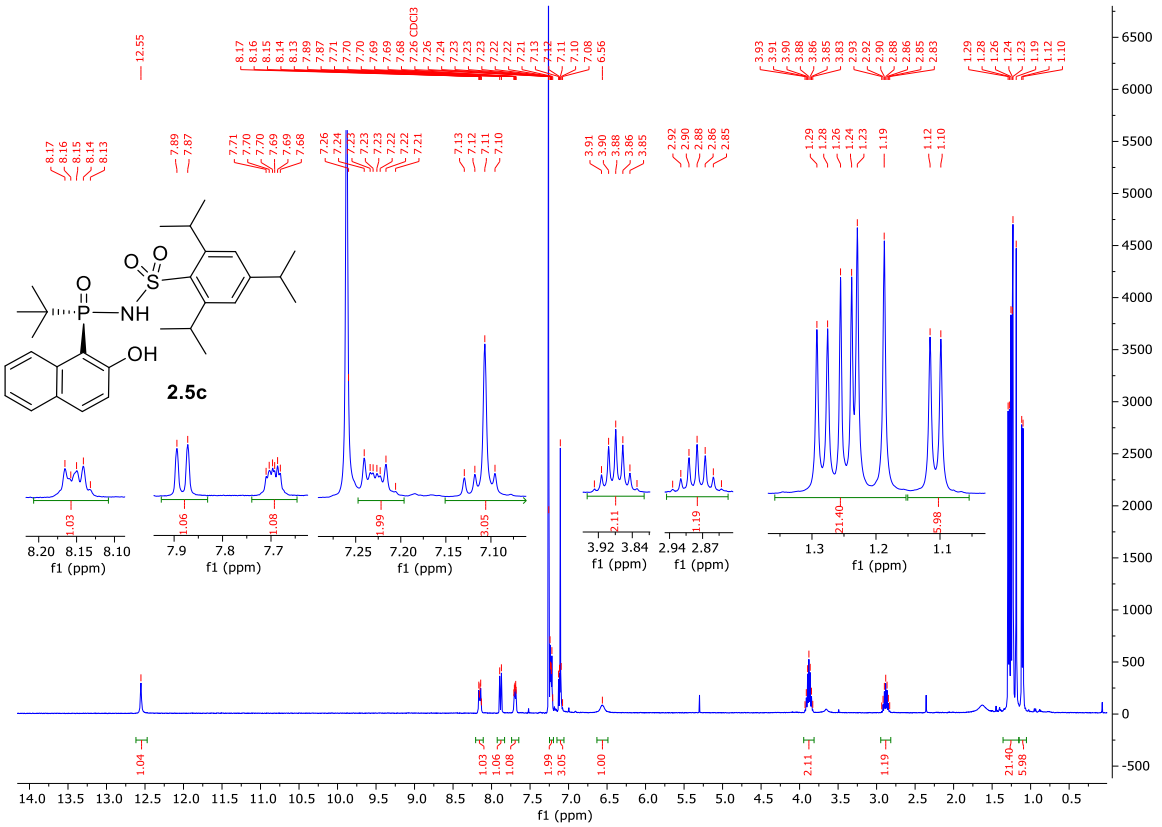

^{31}P NMR of **2.5c**

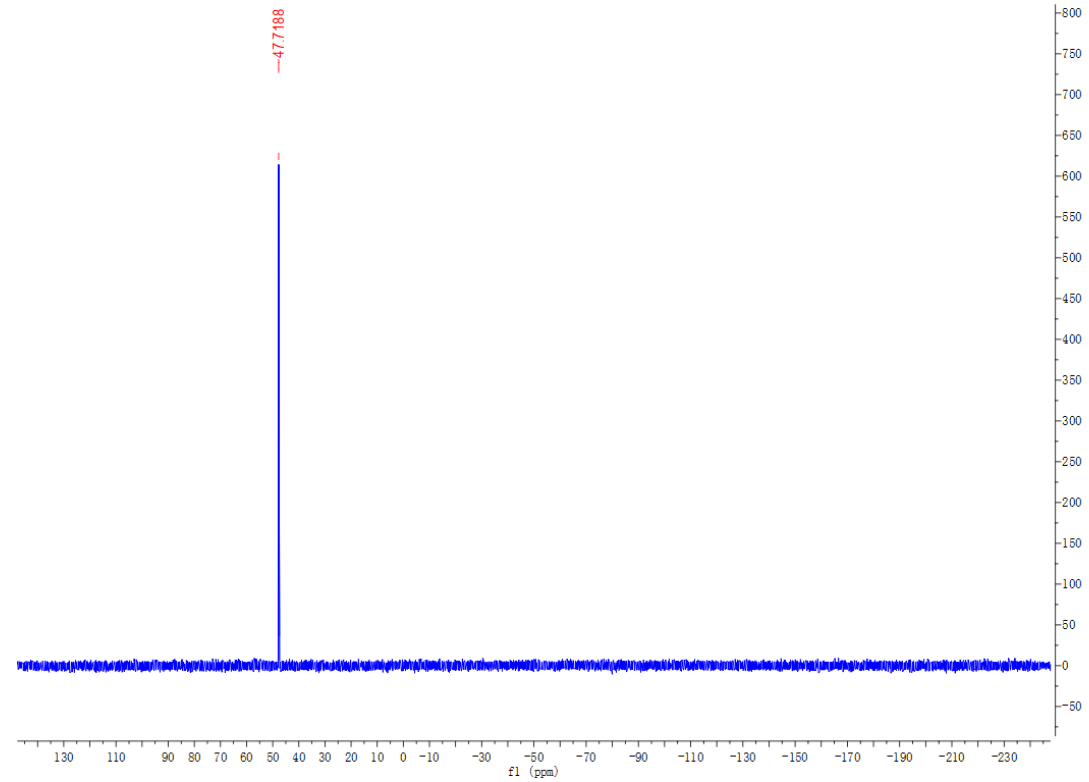

^{13}C NMR of **2.5c**

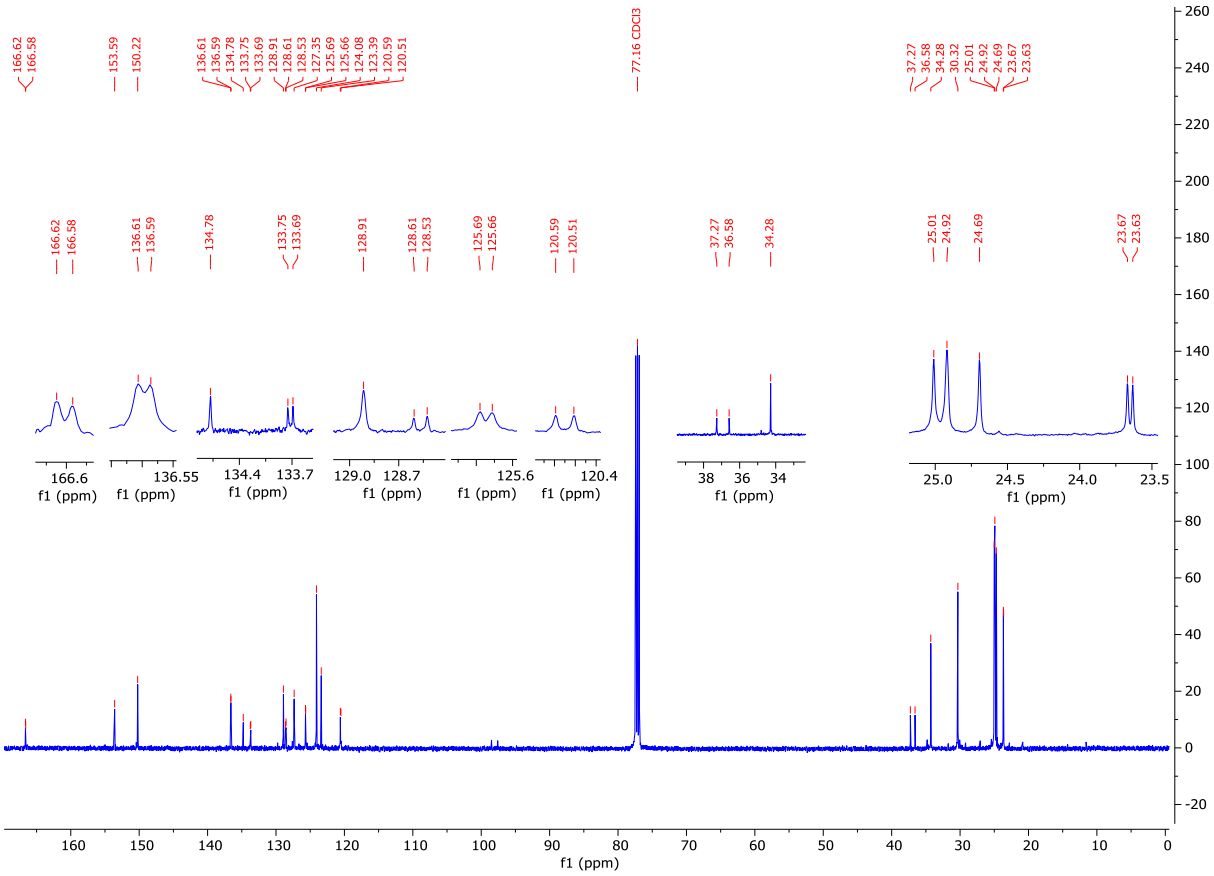

^{1}H NMR of **2.5d**

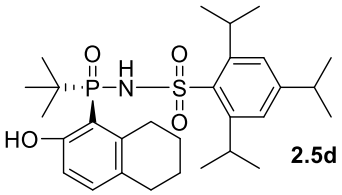

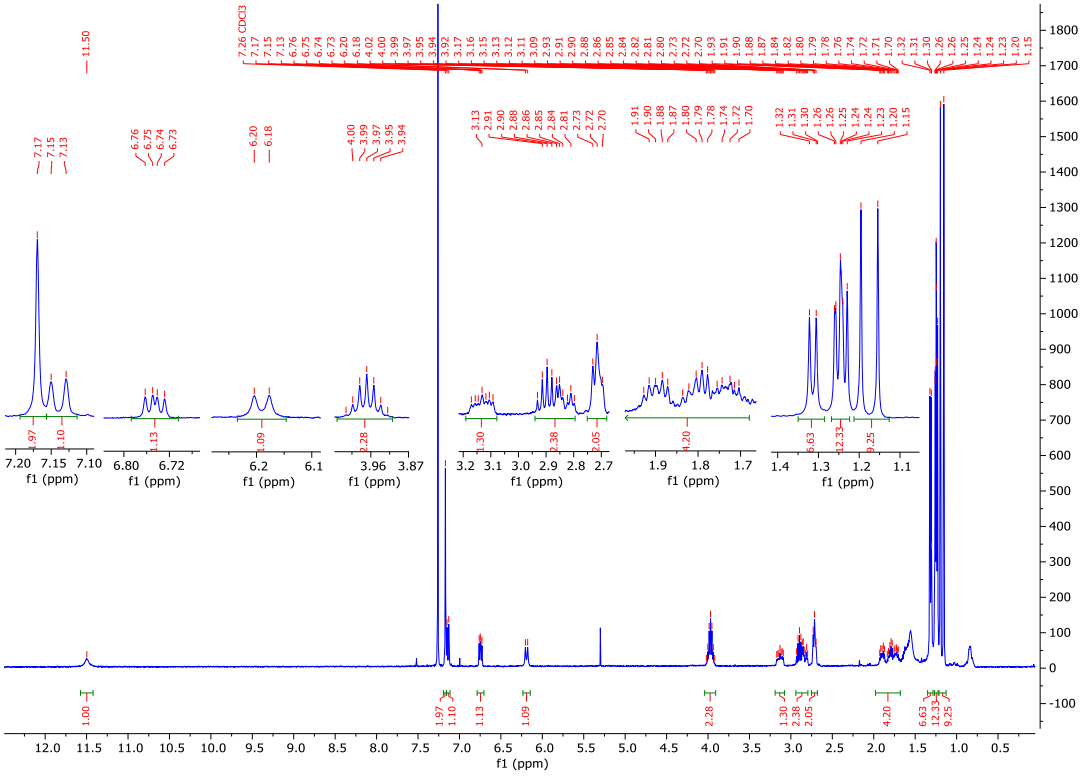

^{31}P NMR of **2.5d**

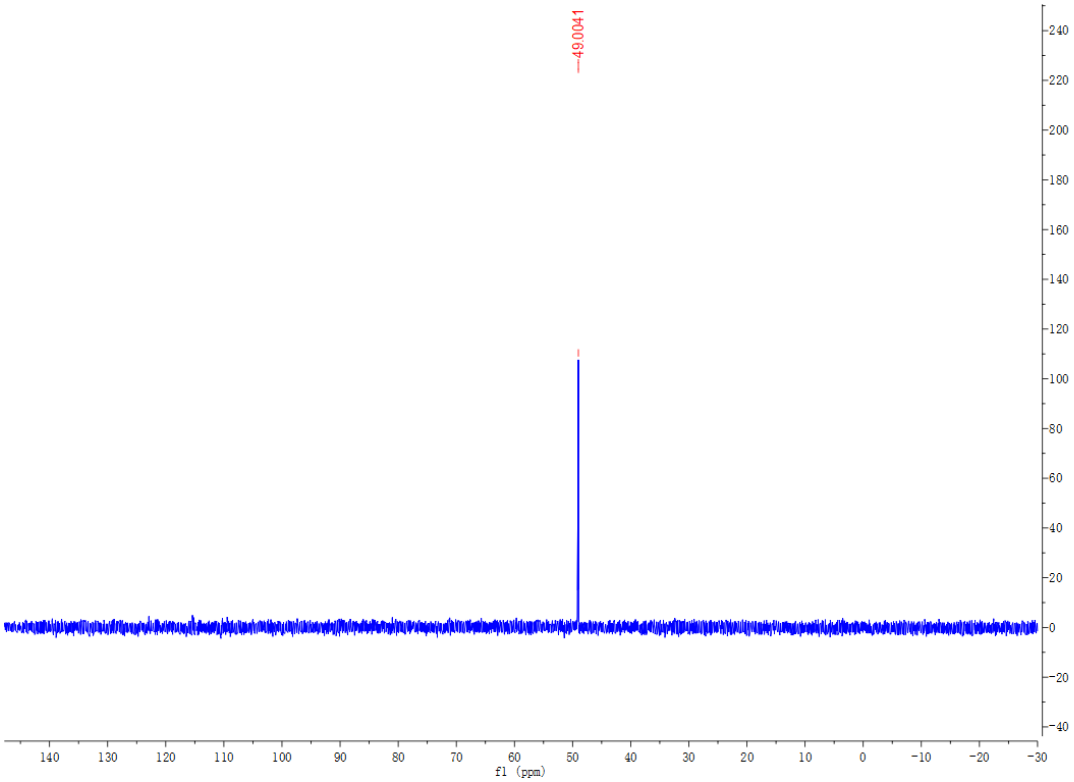

^{13}C NMR of **2.5d**

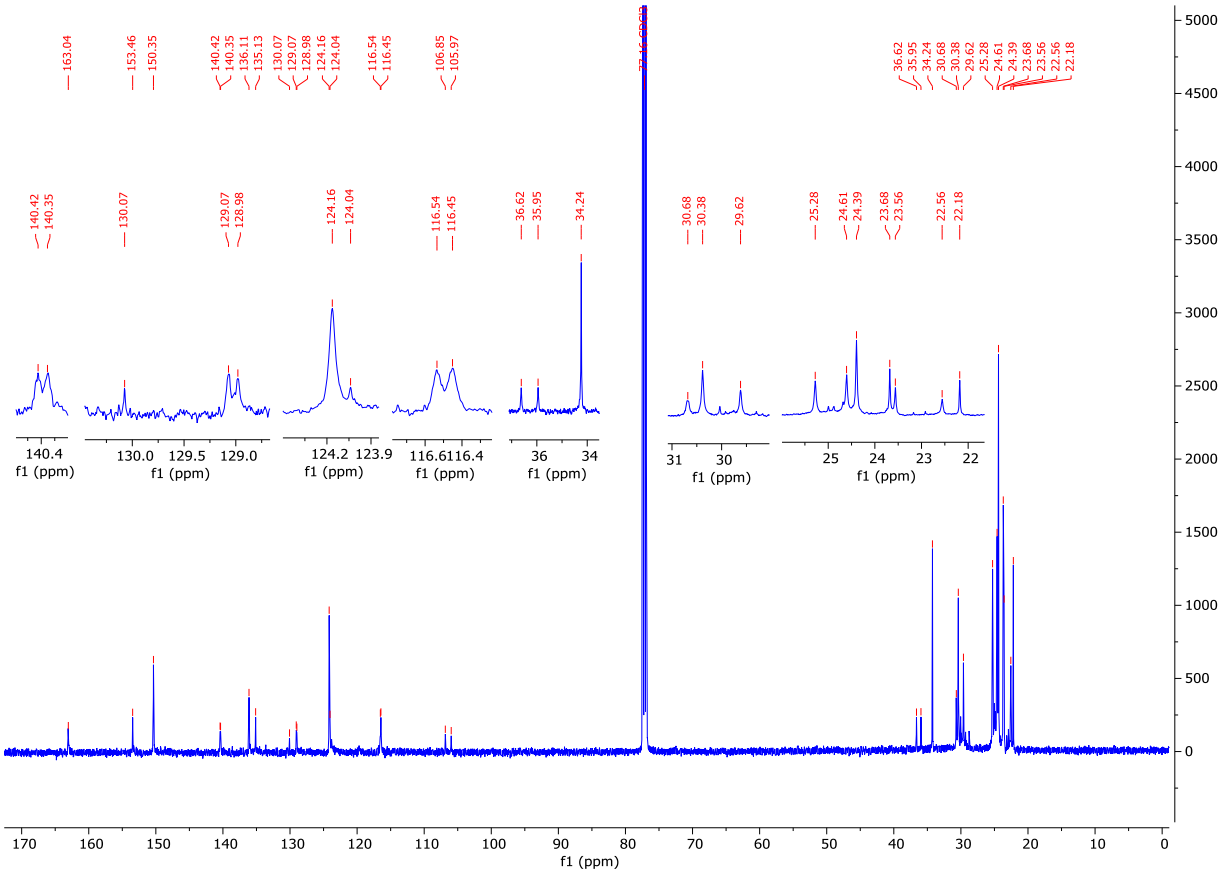

^{1}H NMR of **2.5e**

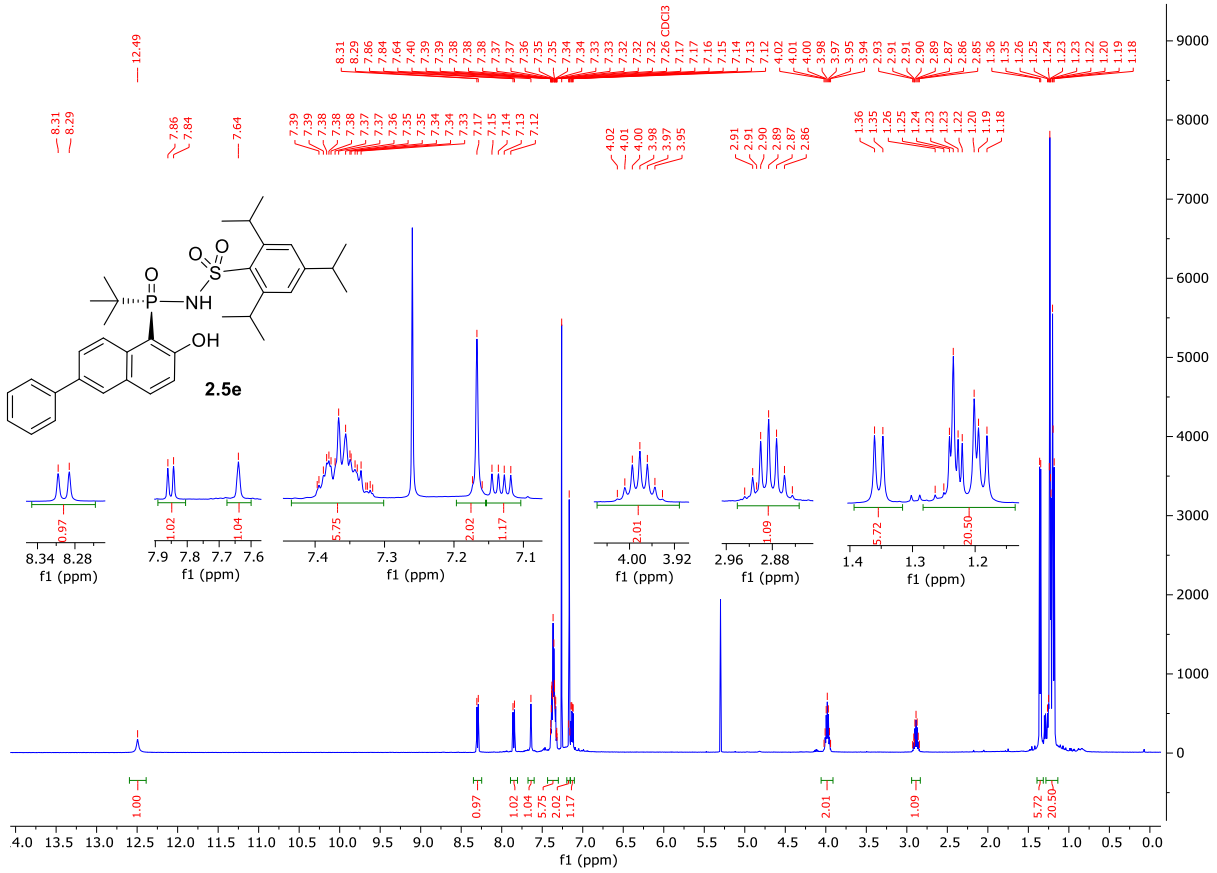

^{31}P NMR of **2.5e**

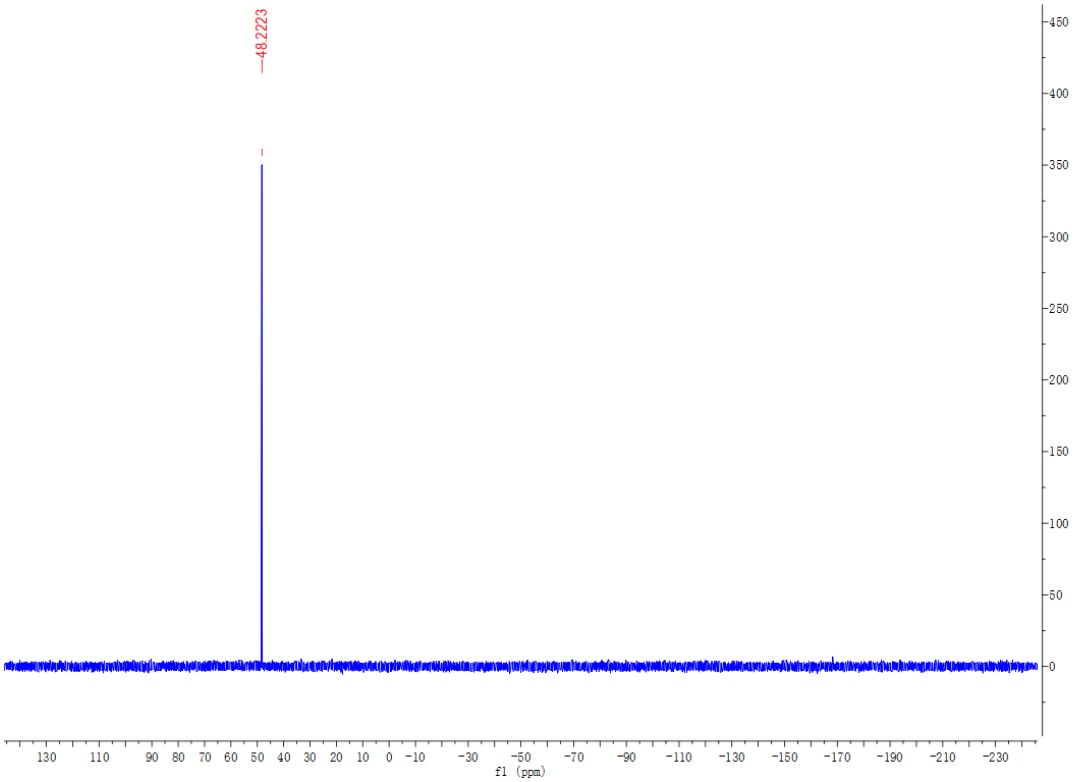

^{13}C NMR of **2.5e**

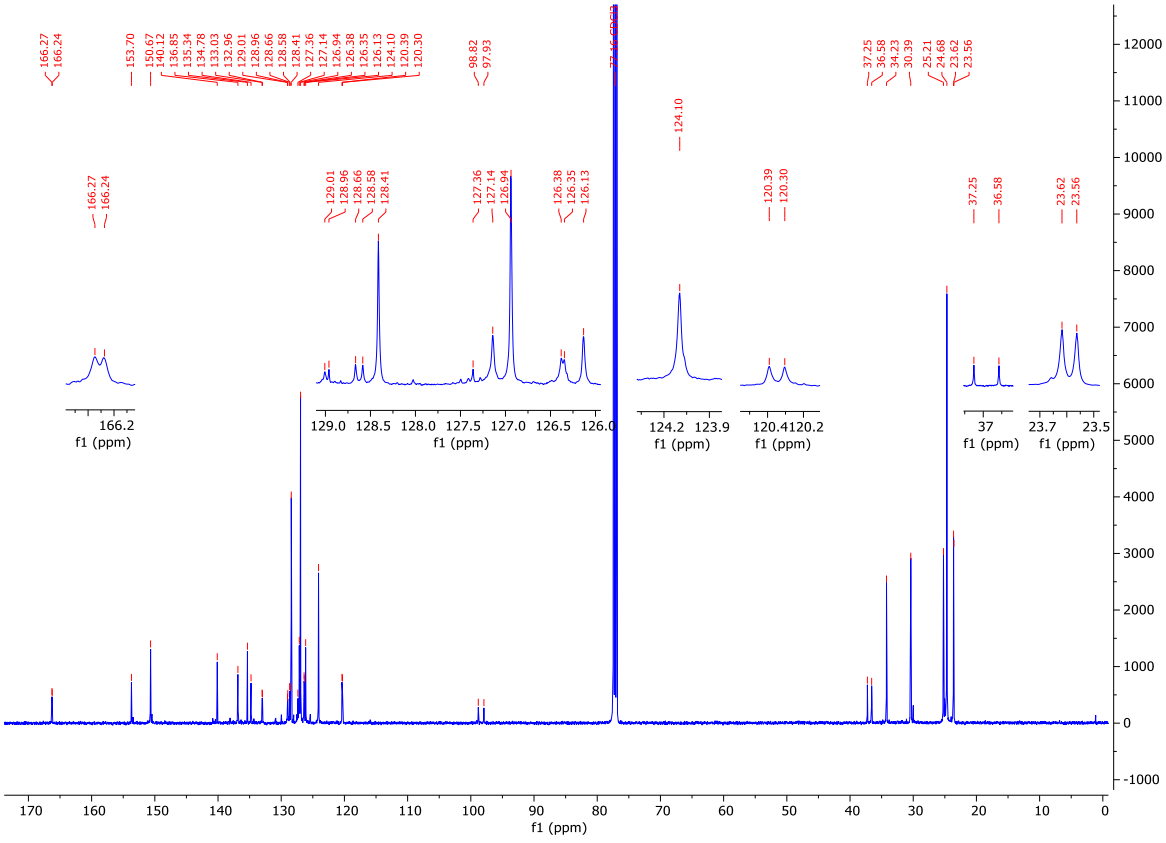

^{1}H-NMR of **2.7e**

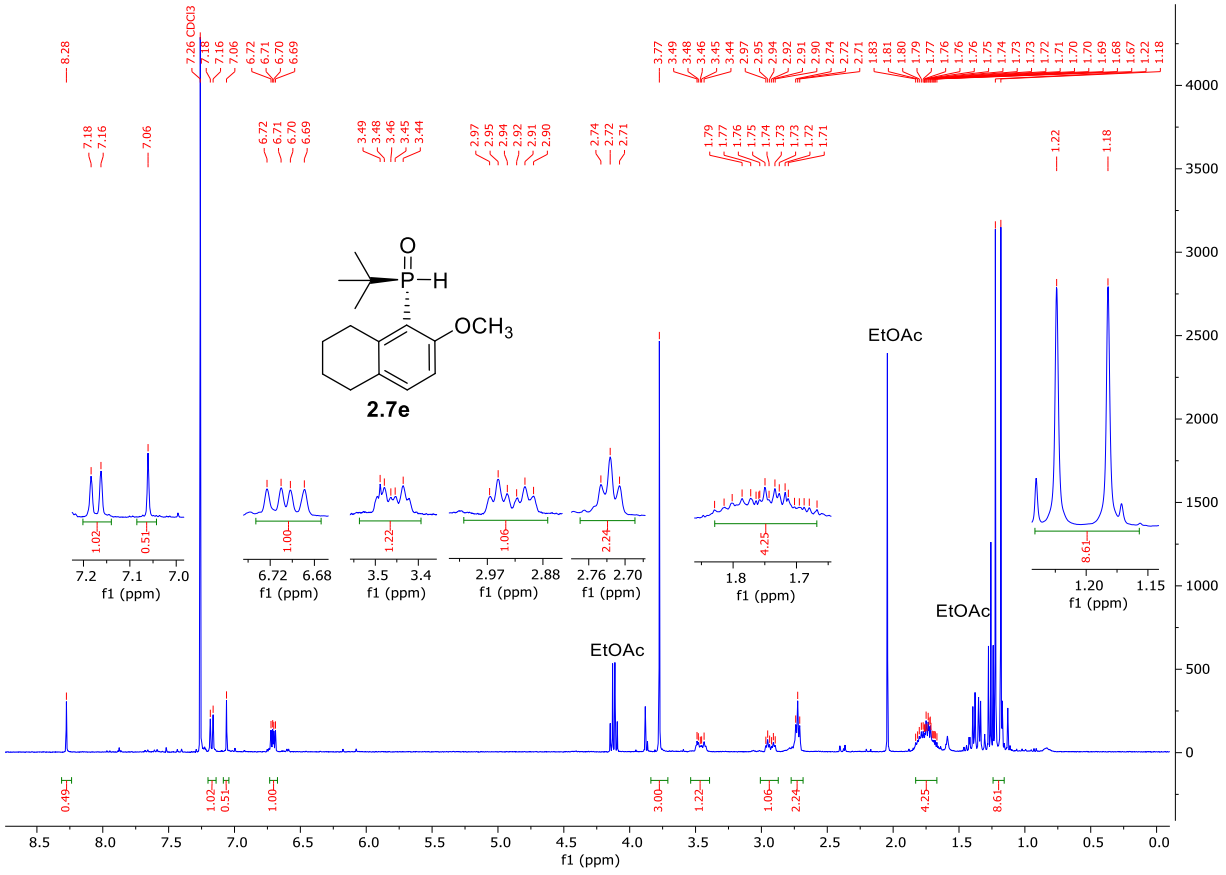

^{31}P-NMR of **2.7e**

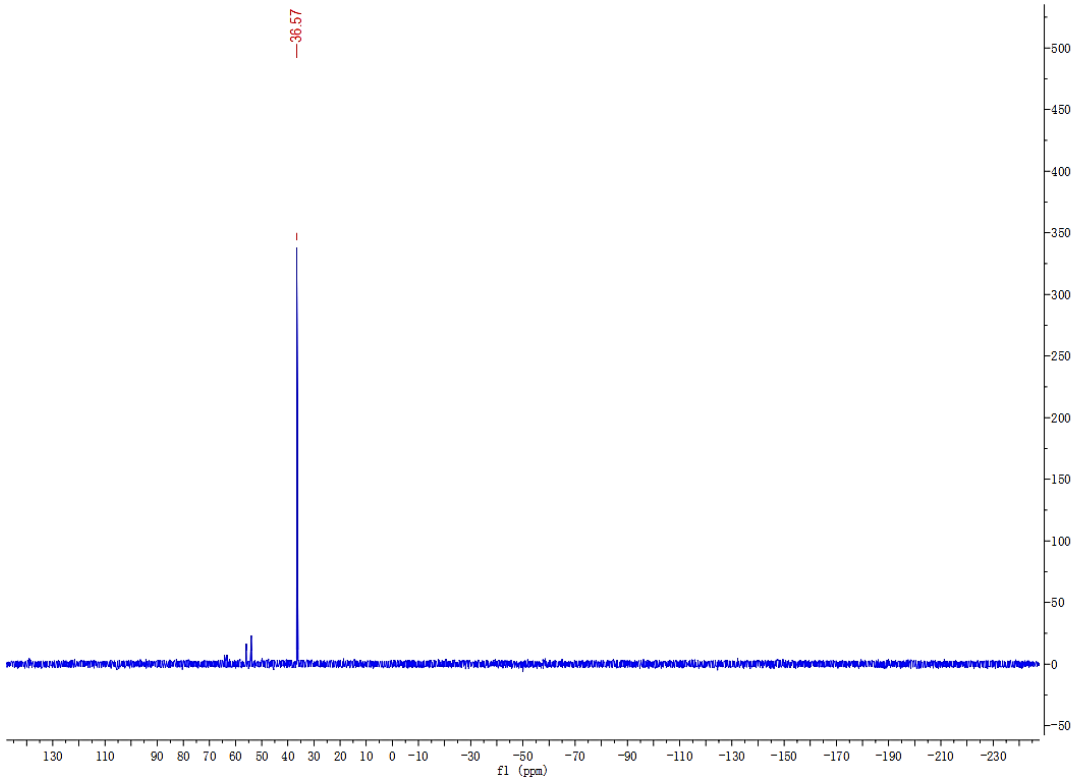

^{1}H-NMR of **2.7f**

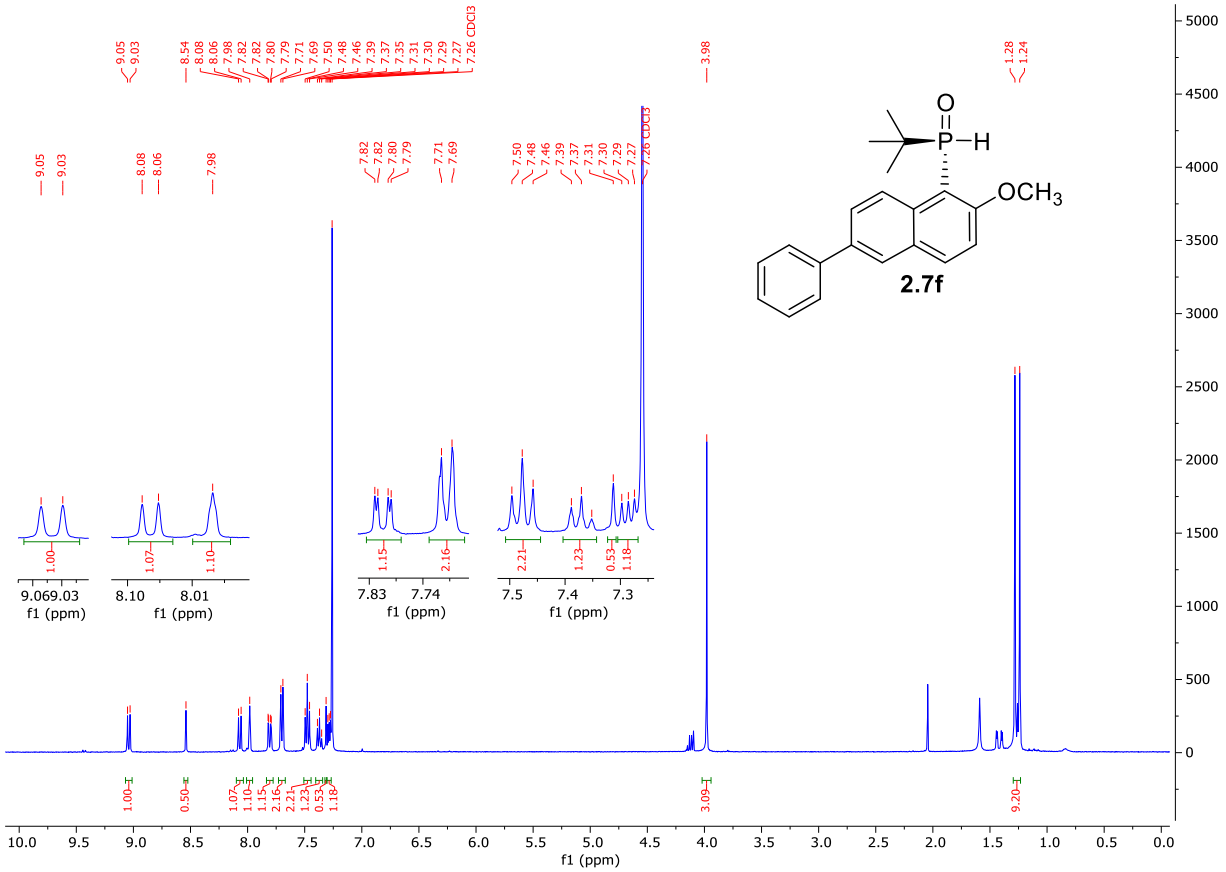
9.05
9.03
8.54
8.08
8.06
7.98
7.82
7.82
7.80
7.79
7.71
7.69
7.50
7.48
7.46
7.39
7.37
7.35
7.31
7.30
7.29
7.27
7.26 CDCl3
3.98
1.28
1.24
O
P–H
OCH3
2.7f
f1 (ppm)

^{31}P-NMR of **2.7f**

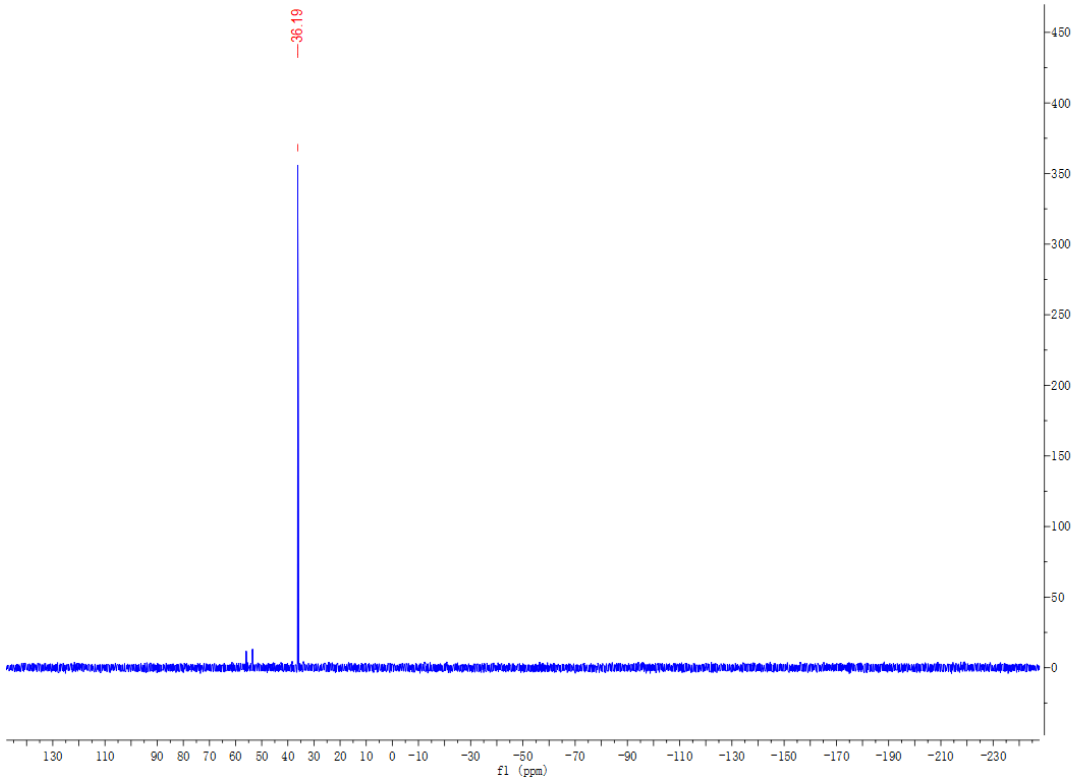

^{1}H-NMR, ^{13}C and ^{31}P NMR spectra of compound **2.8a** were consistent with those previously reported.[7]

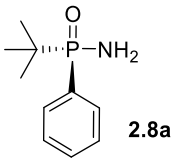

2.8a

Chiral HPLC chromatograms of **2.8a**

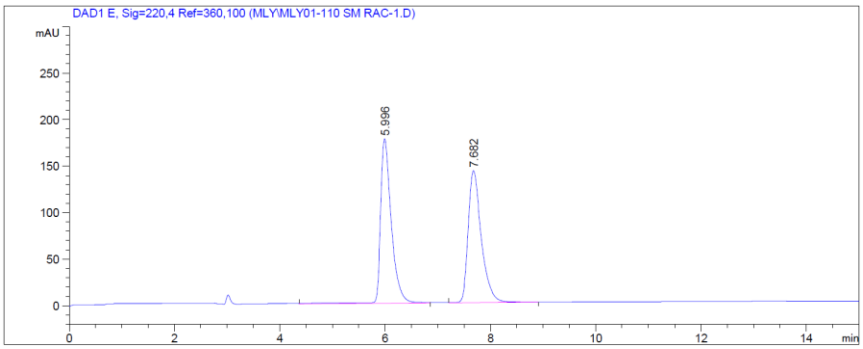

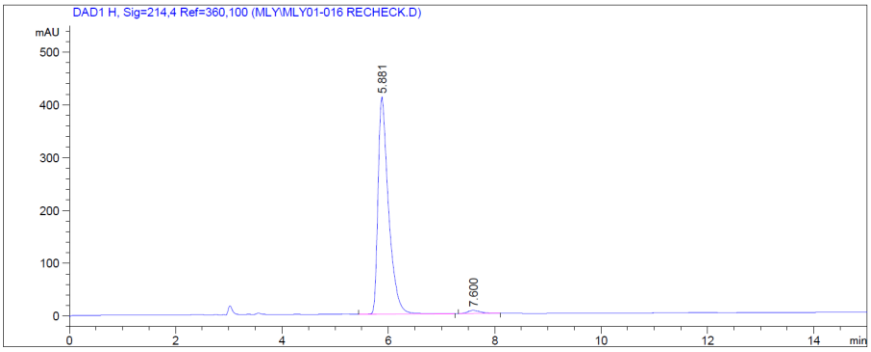

Peak #	RetTime [min]	Type	Width [min]	Area [mAU*s]	Height [mAU]	Area %
1	5.881	BB	0.2069	5673.06494	411.40399	98.3002
2	7.600	BB	0.2540	98.09958	5.90015	1.6998

^{1}H NMR of **2.8b**

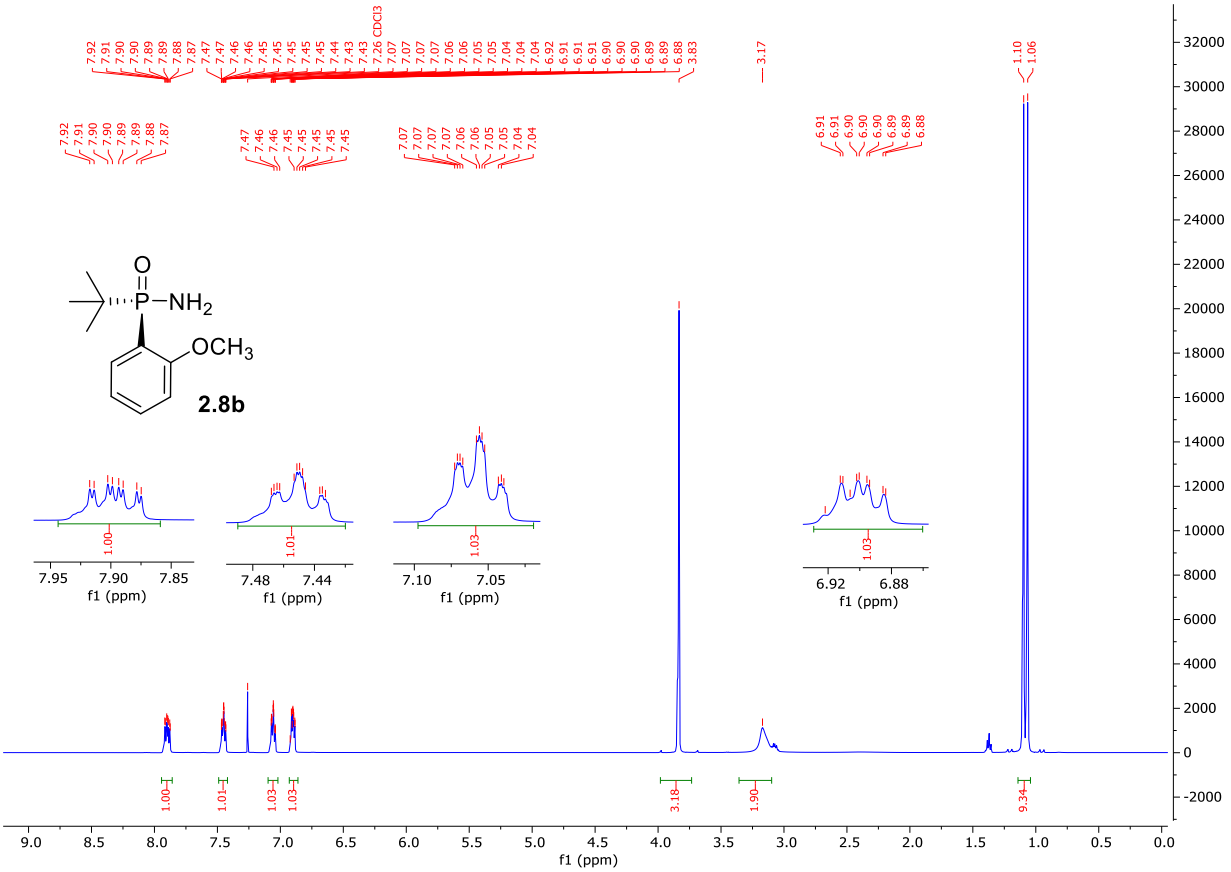

^{31}P NMR of **2.8b**

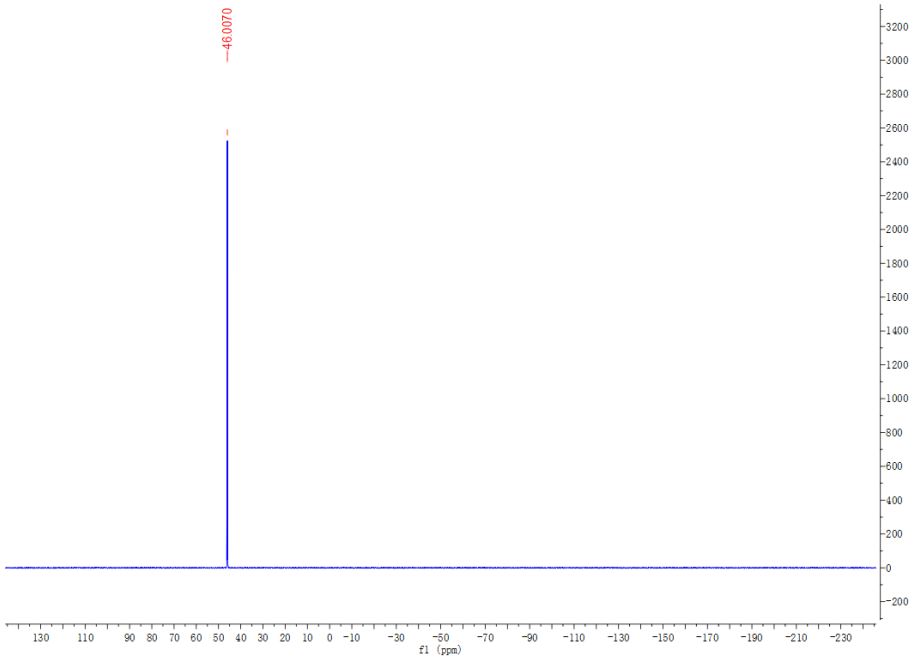

^{13}C NMR of **2.8b**

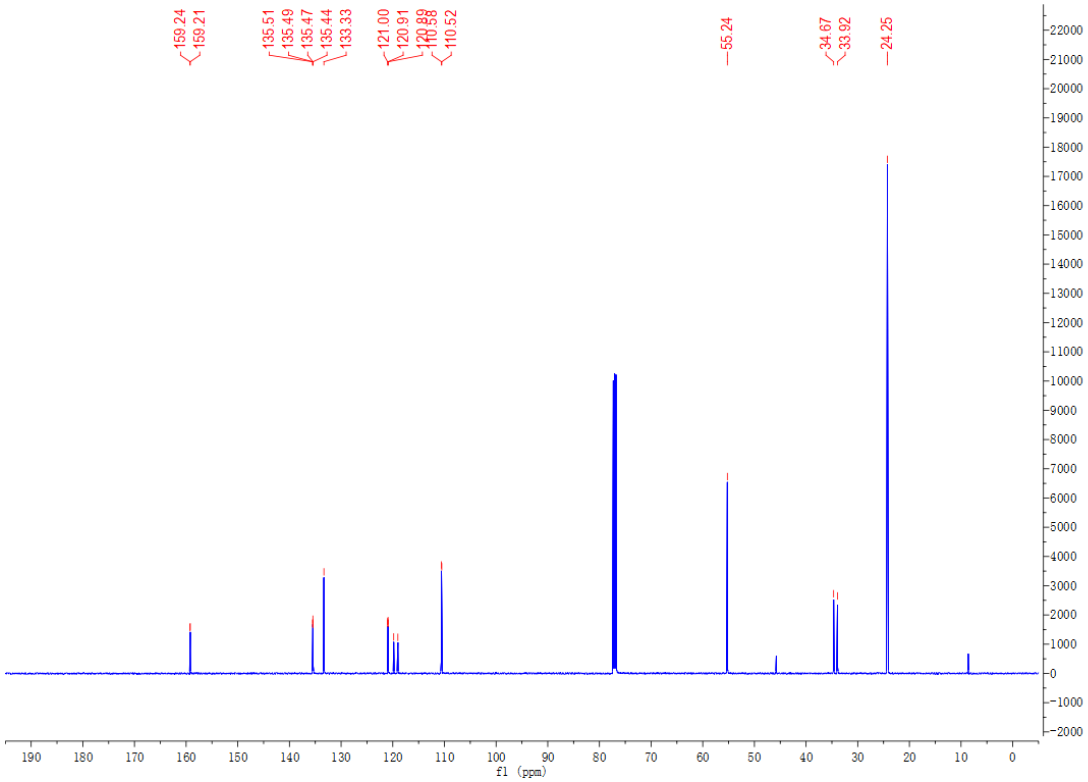

Chiral HPLC chromatograms of **2.8b**

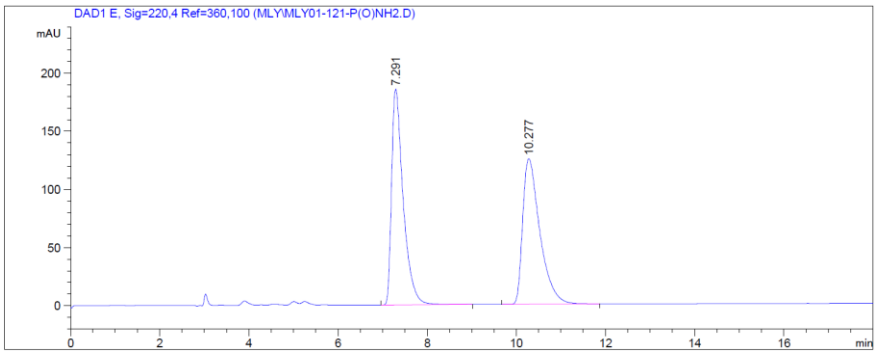

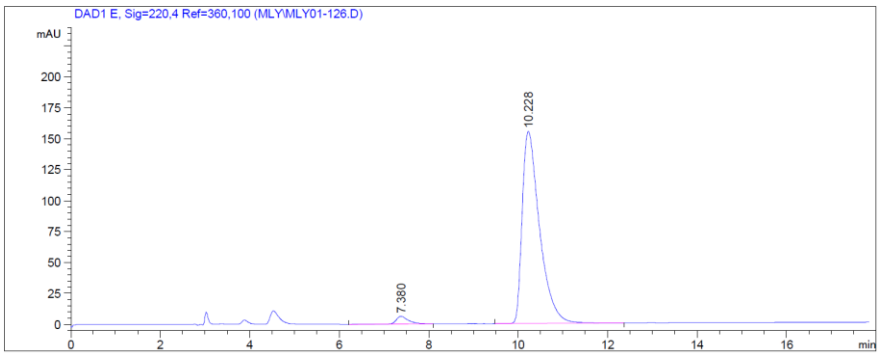

Peak #	RetTime [min]	Type	Width [min]	Area [mAU*s]	Height [mAU]	Area %
1	7.380	BB	0.2838	118.71608	6.18996	2.7608
2	10.228	BB	0.4025	4181.28223	155.10017	97.2392

^{1}H NMR of **2.8c**

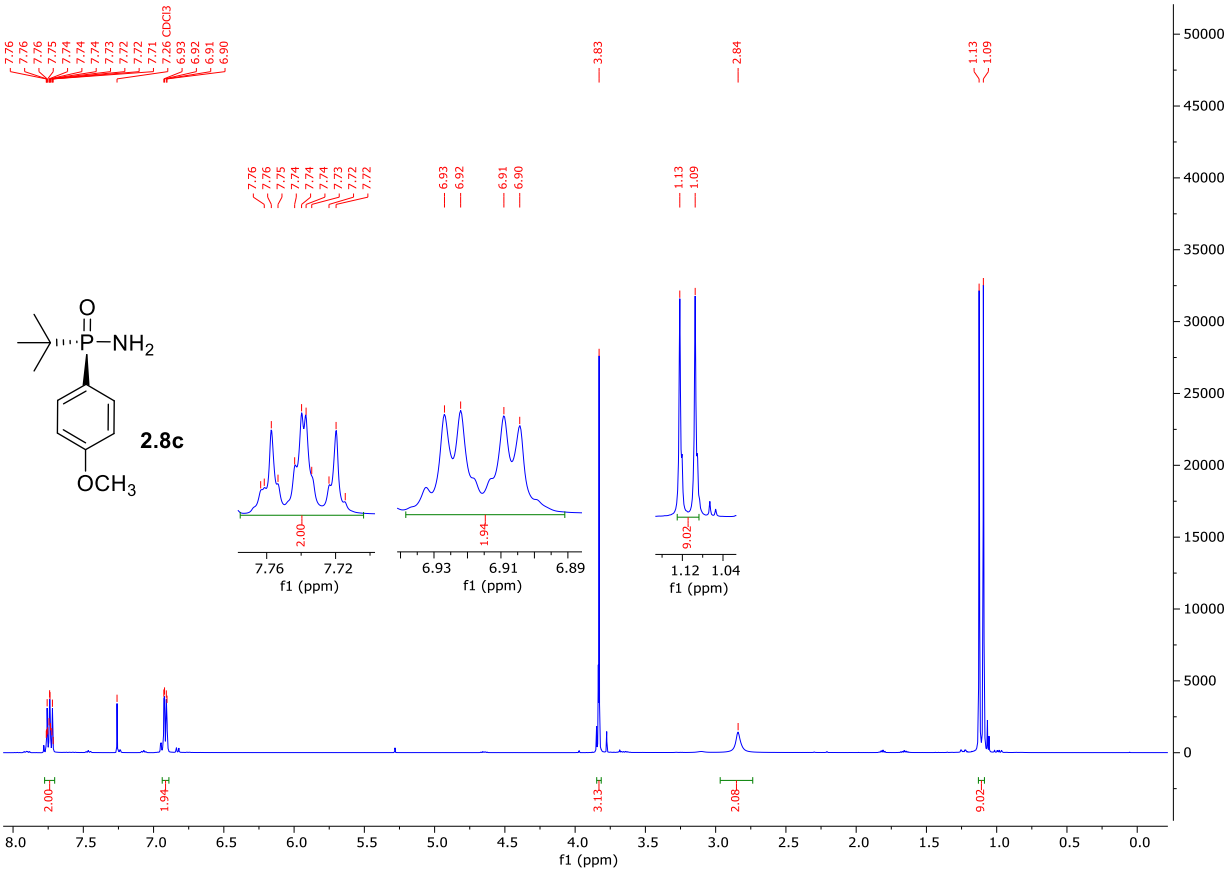
7.76
7.76
7.76
7.75
7.74
7.74
7.73
7.72
7.72
7.71
7.26 CDCl3
6.93
6.92
6.91
6.90
3.83
2.84
1.13
1.09
O
P–NH2
OCH3
2.8c
2.00
1.94
9.02
f1 (ppm)
2.00
1.94
3.13
2.08
9.02

^{31}P NMR of **2.8c**

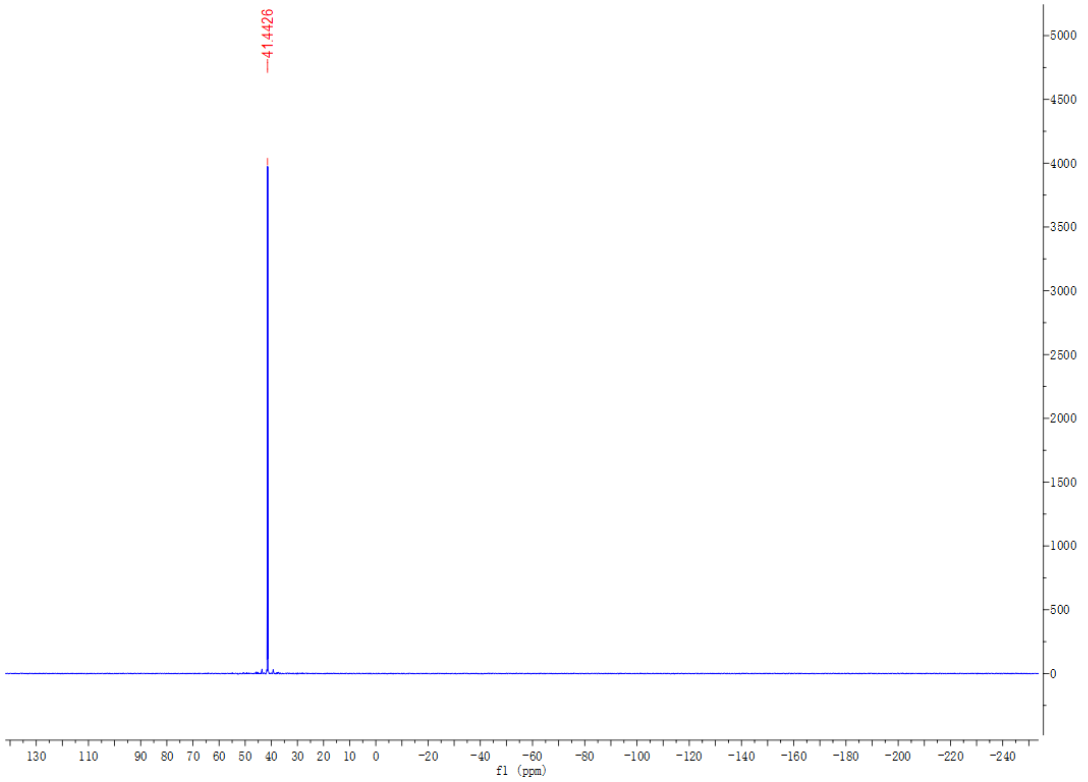

^{13}C NMR of**2. 8c**

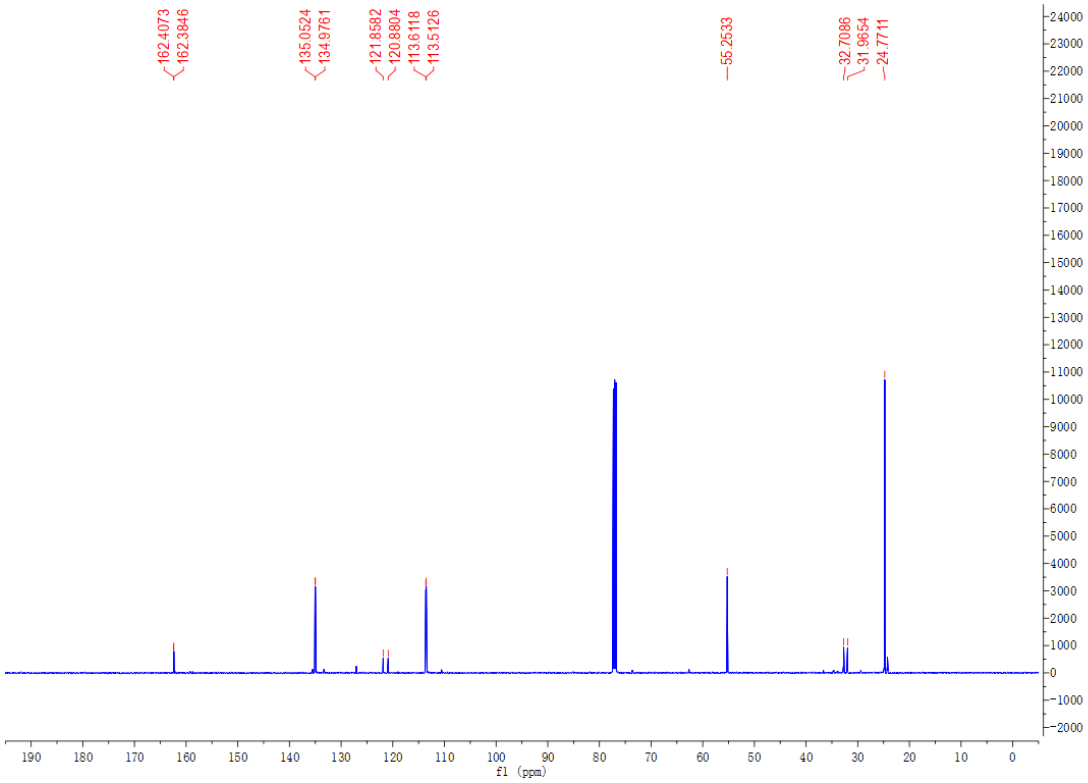

Chiral HPLC chromatograms of **2.8c**

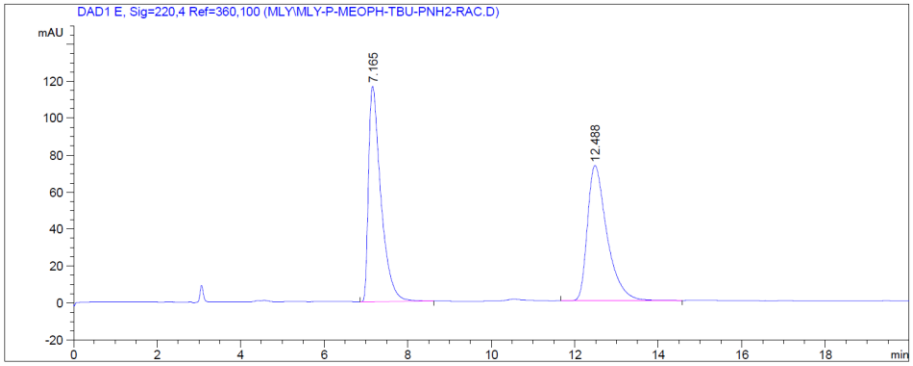

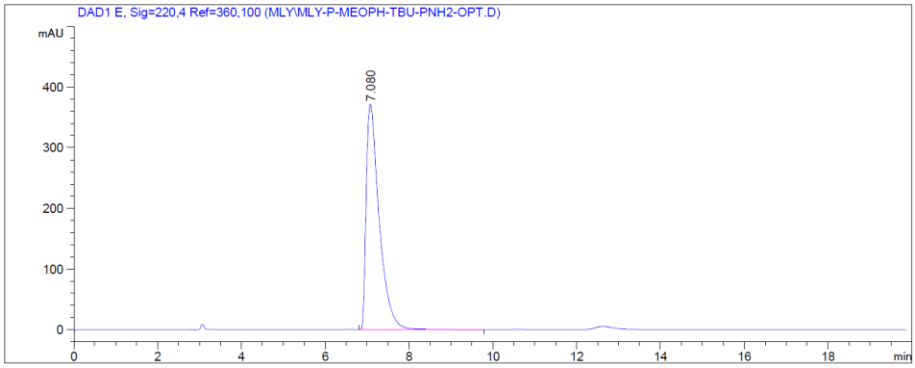

Peak #	RetTime [min]	Type	Width [min]	Area [mAU*s]	Height [mAU]	Area %
1	7.080	VV	0.3243	8036.97559	371.68729	100.0000

^{1}H NMR of **2.8d**

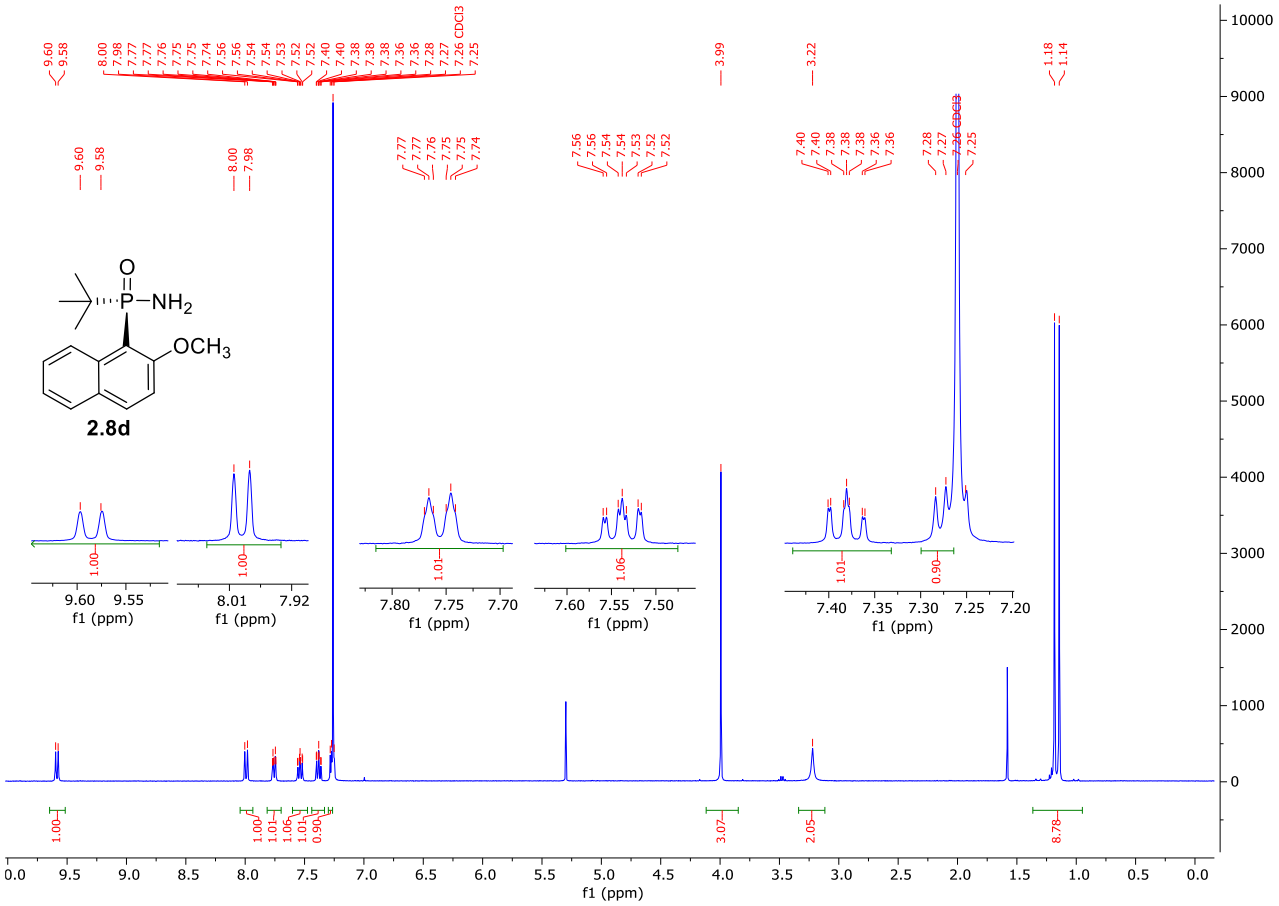

^{31}P NMR of **2.8d**

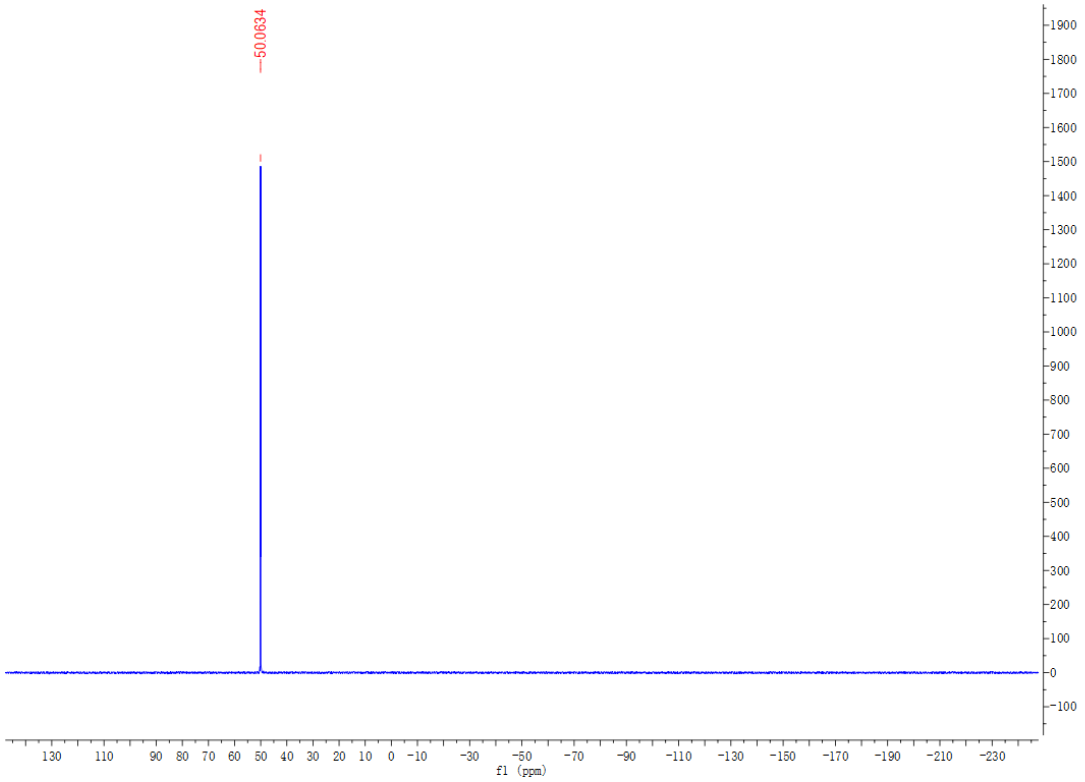

^{13}C NMR of **2.8d**

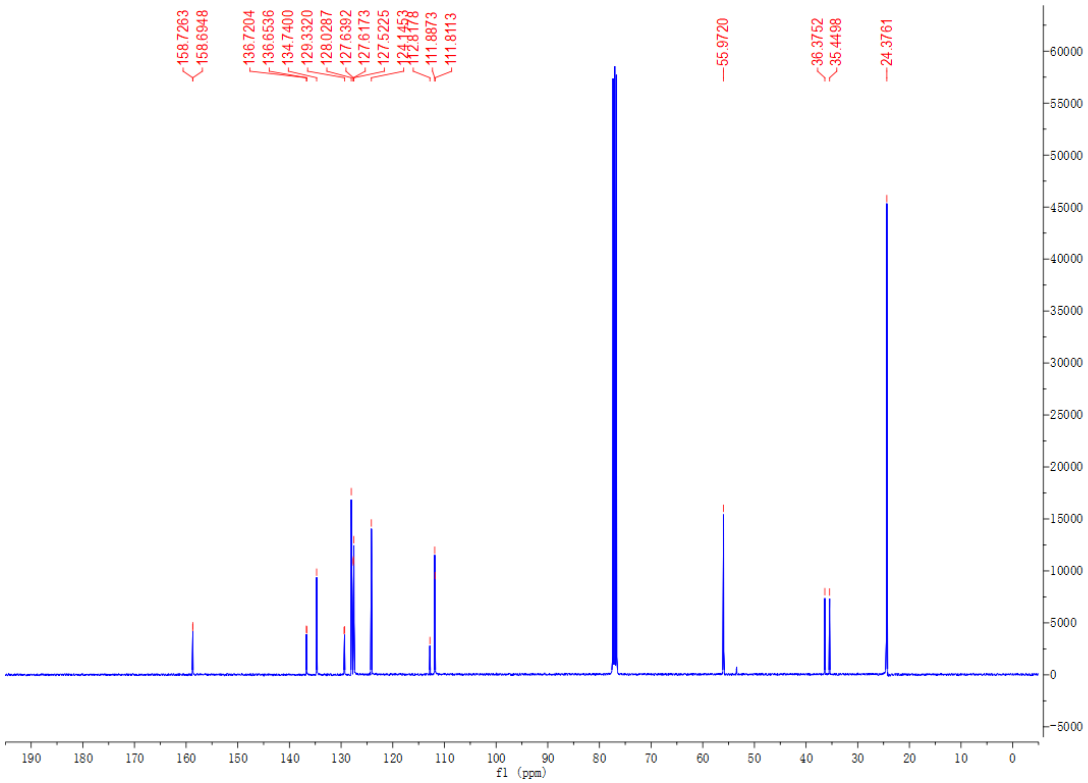

Chiral HPLC chromatograms of **2.8d**

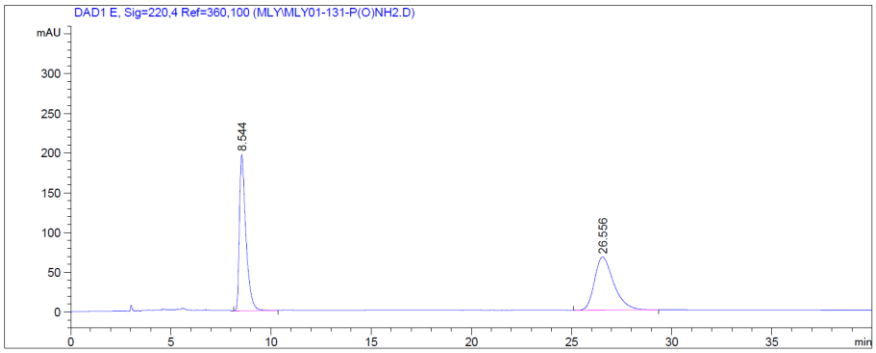

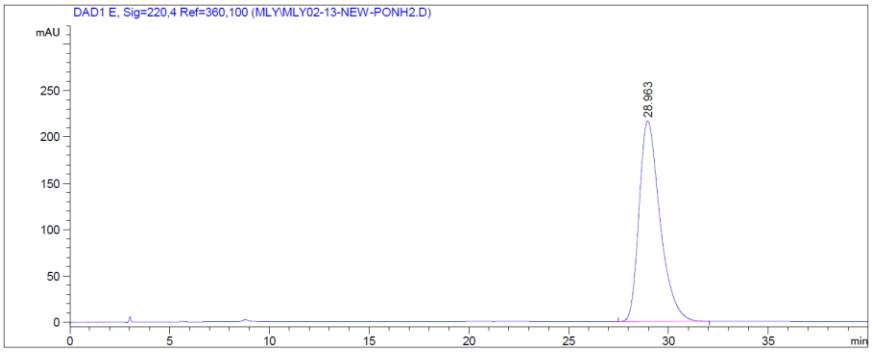

Peak #	RetTime [min]	Type	Width [min]	Area [mAU*s]	Height [mAU]	Area %
1	28.963	BB	1.0990	1.57264e4	216.10506	100.0000

^{1}H NMR of **2.8e**

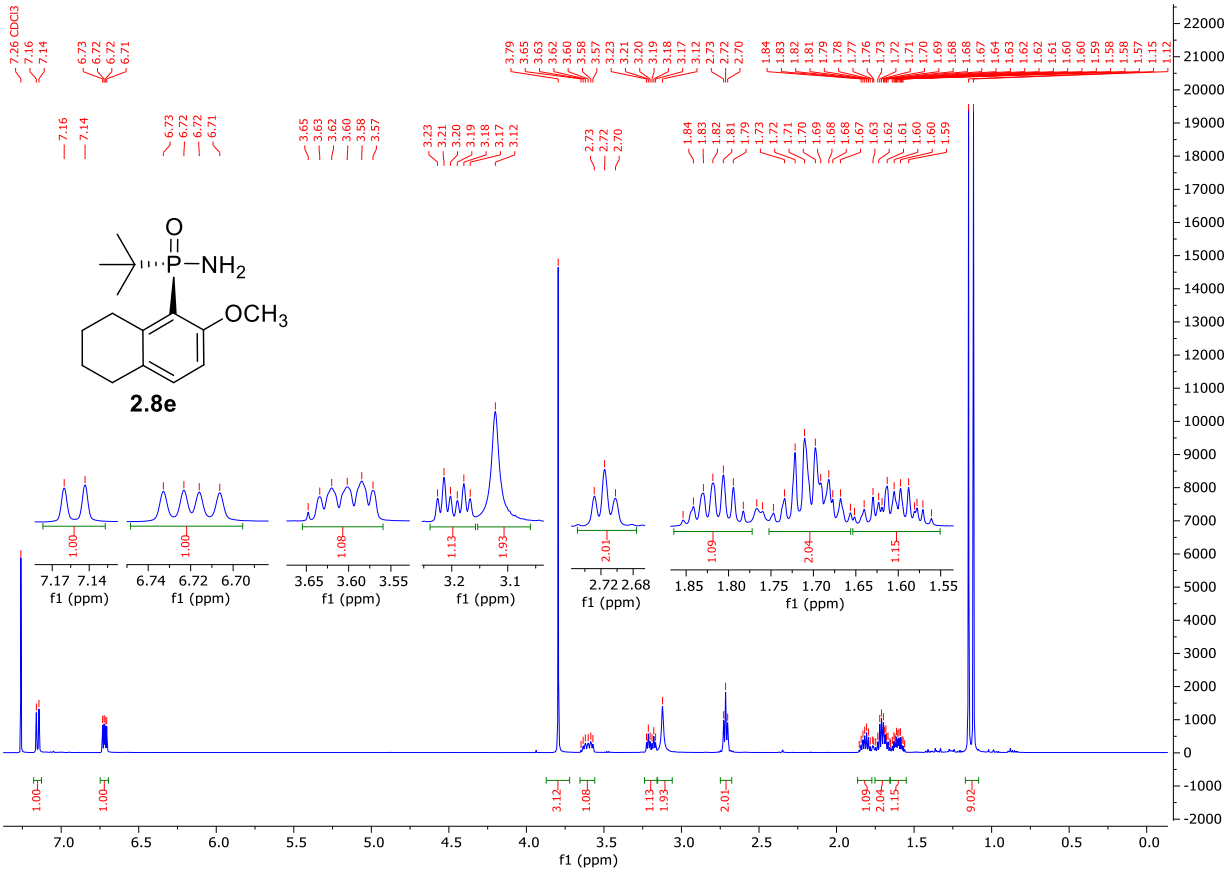

^{31}P NMR of **2.8e**

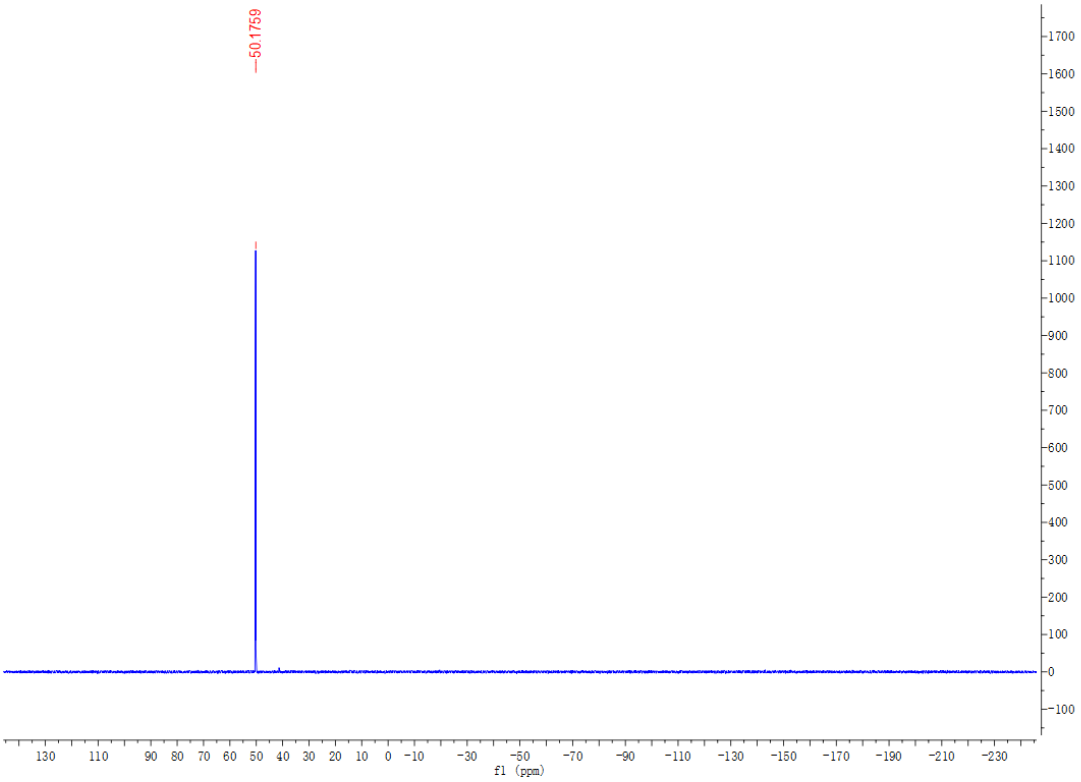

^{13}C NMR of **2.8e**

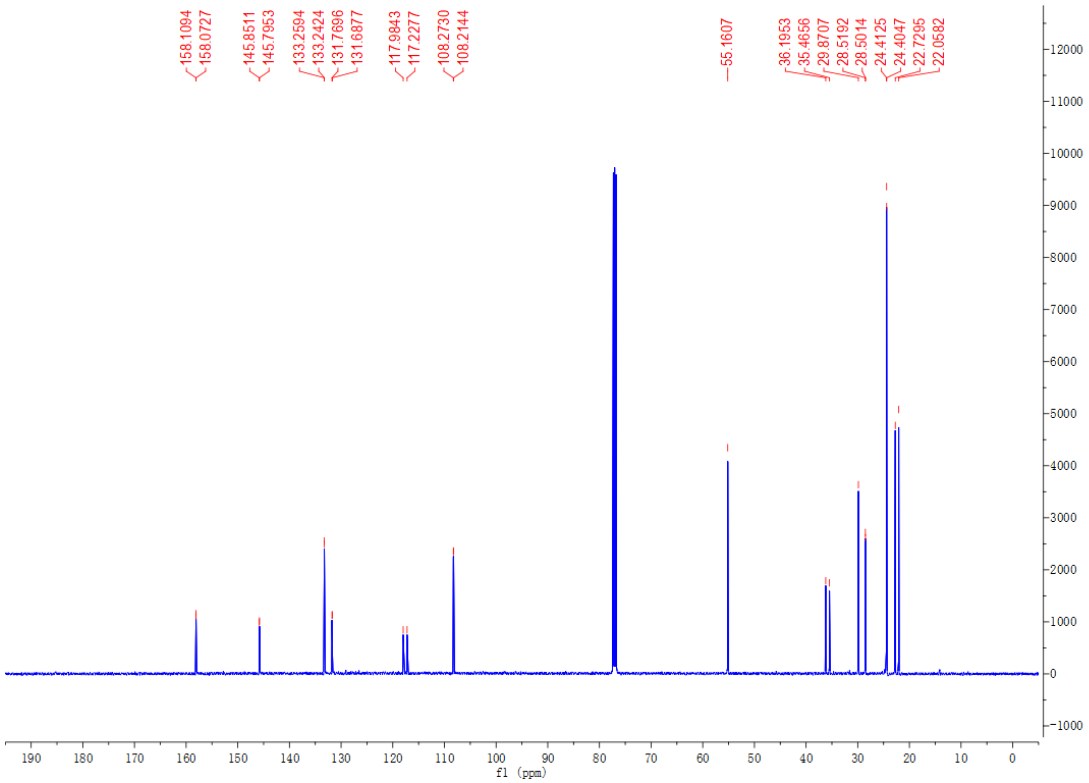

Chiral HPLC chromatograms of **2.8e**

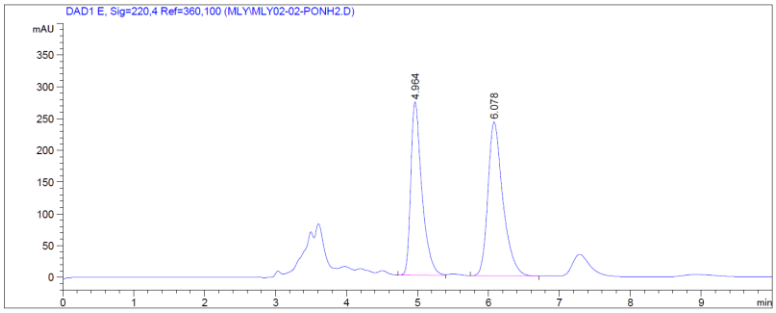

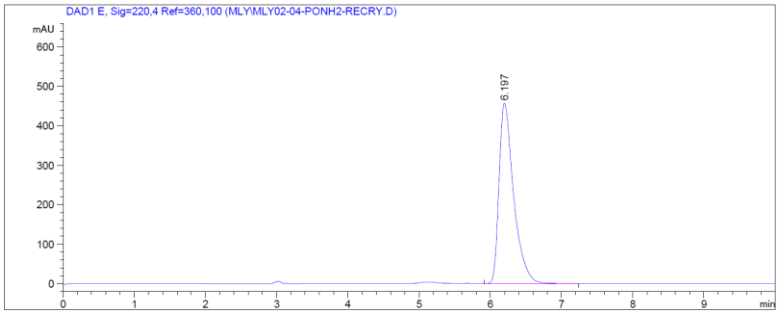

Peak #	RetTime [min]	Type	Width [min]	Area [mAU*s]	Height [mAU]	Area %
1	6.197	BV	0.2148	6538.37207	457.20520	100.0000

^{1}H NMR of **2.8f**

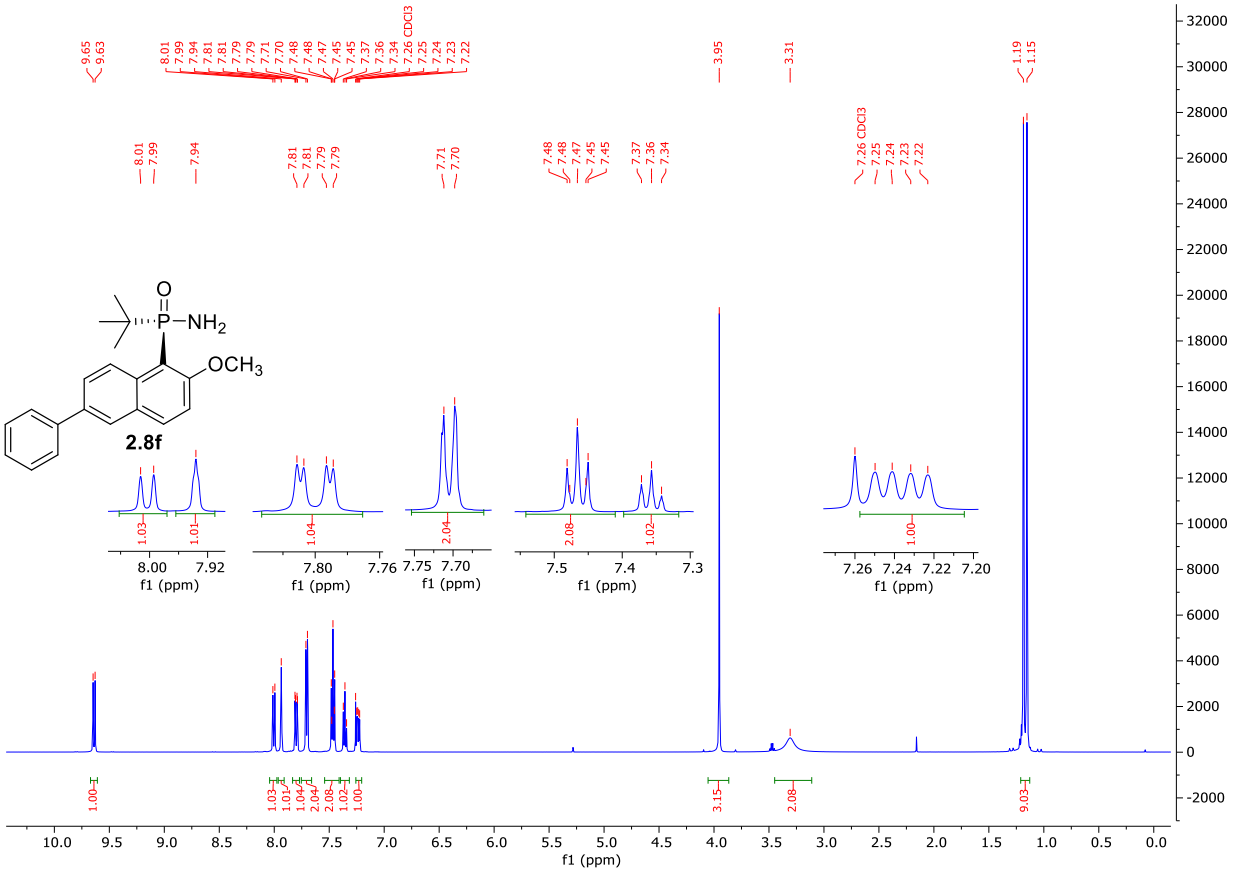

^{31}P NMR of **2.8f**

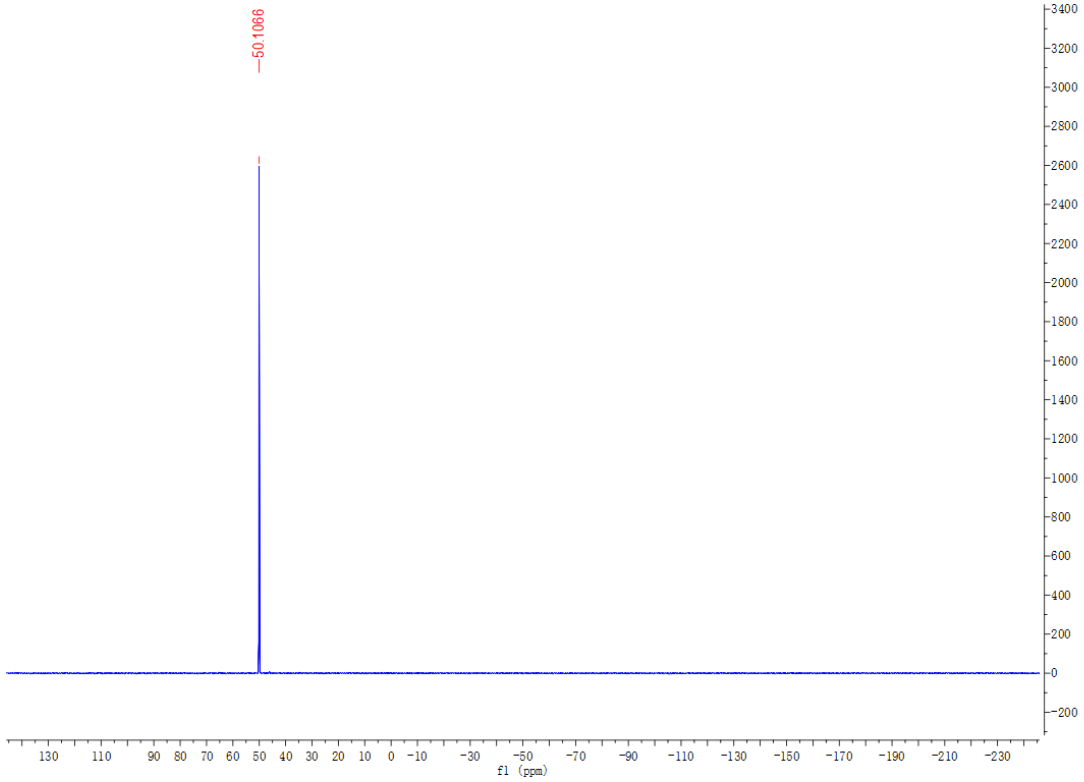

^{13}C NMR of **2.8f**

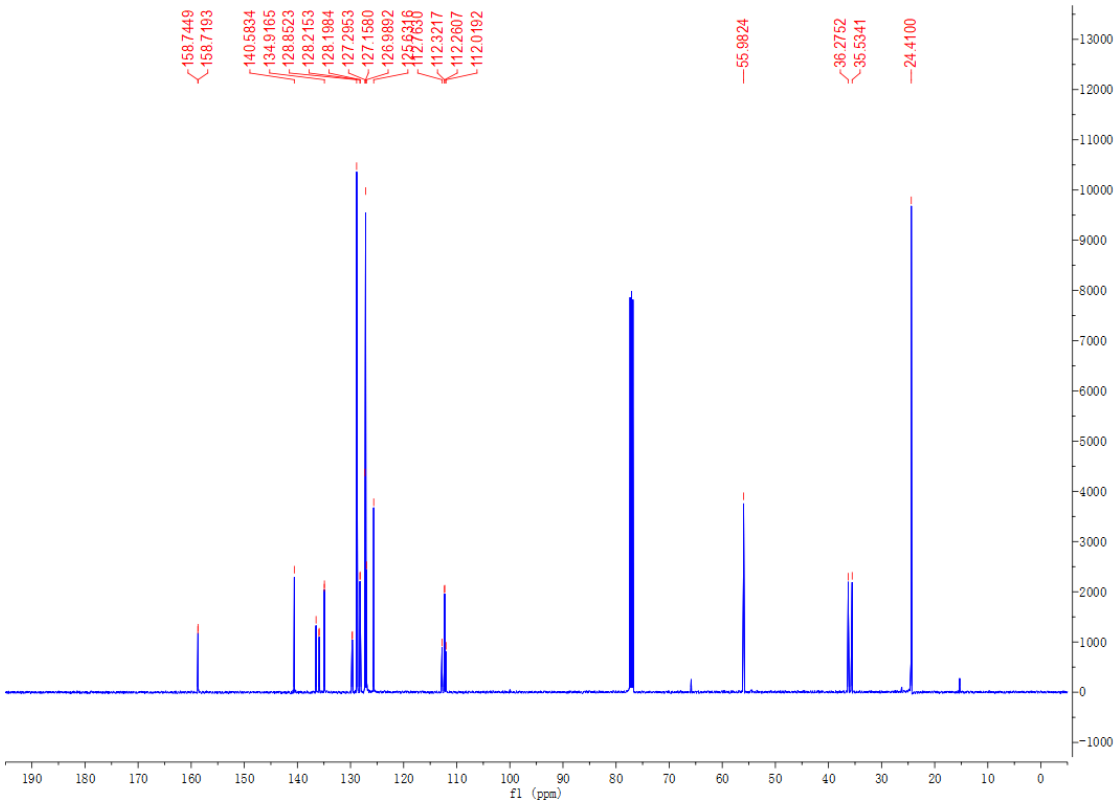

Chiral HPLC chromatograms of **2.8f**

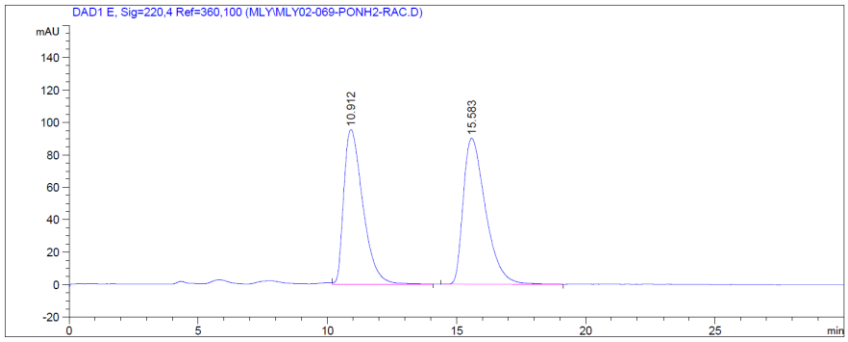

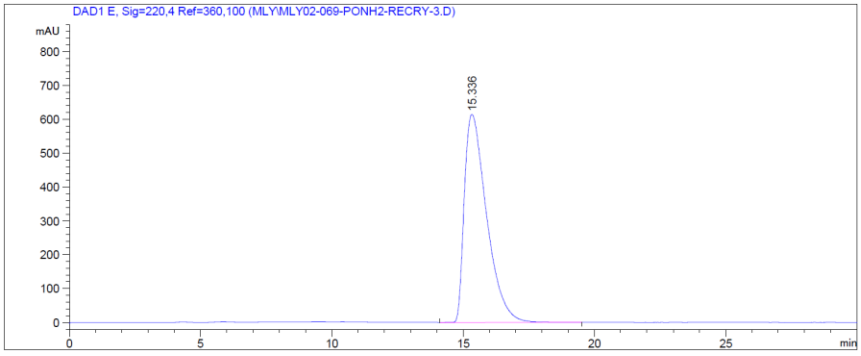

Peak #	RetTime [min]	Type	Width [min]	Area [mAU*s]	Height [mAU]	Area %
1	15.336	BV	0.9039	3.62257e4	614.41528	100.0000

(*S*)-6-bromo-2-methyl-1,2,3,4-tetrahydroquinoline (**2.11a**)

^{1}H NMR of **2.11a**

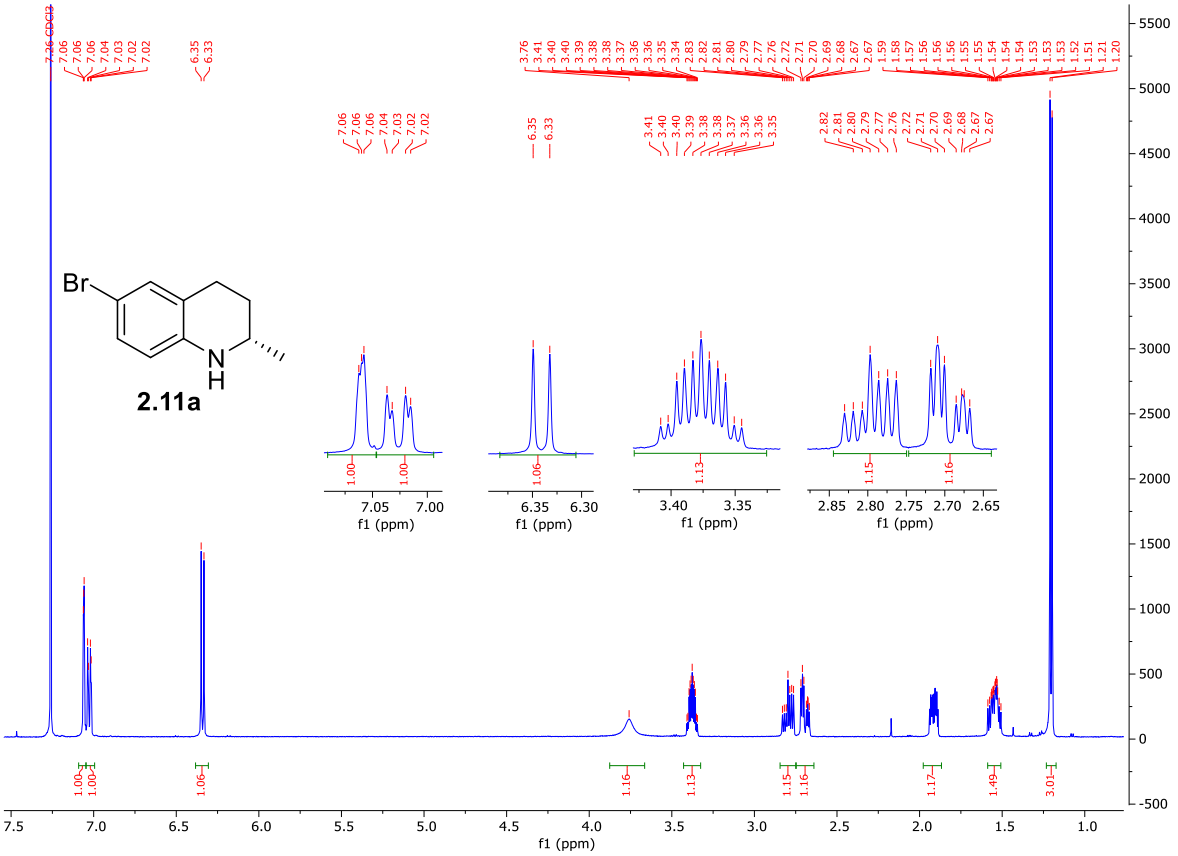

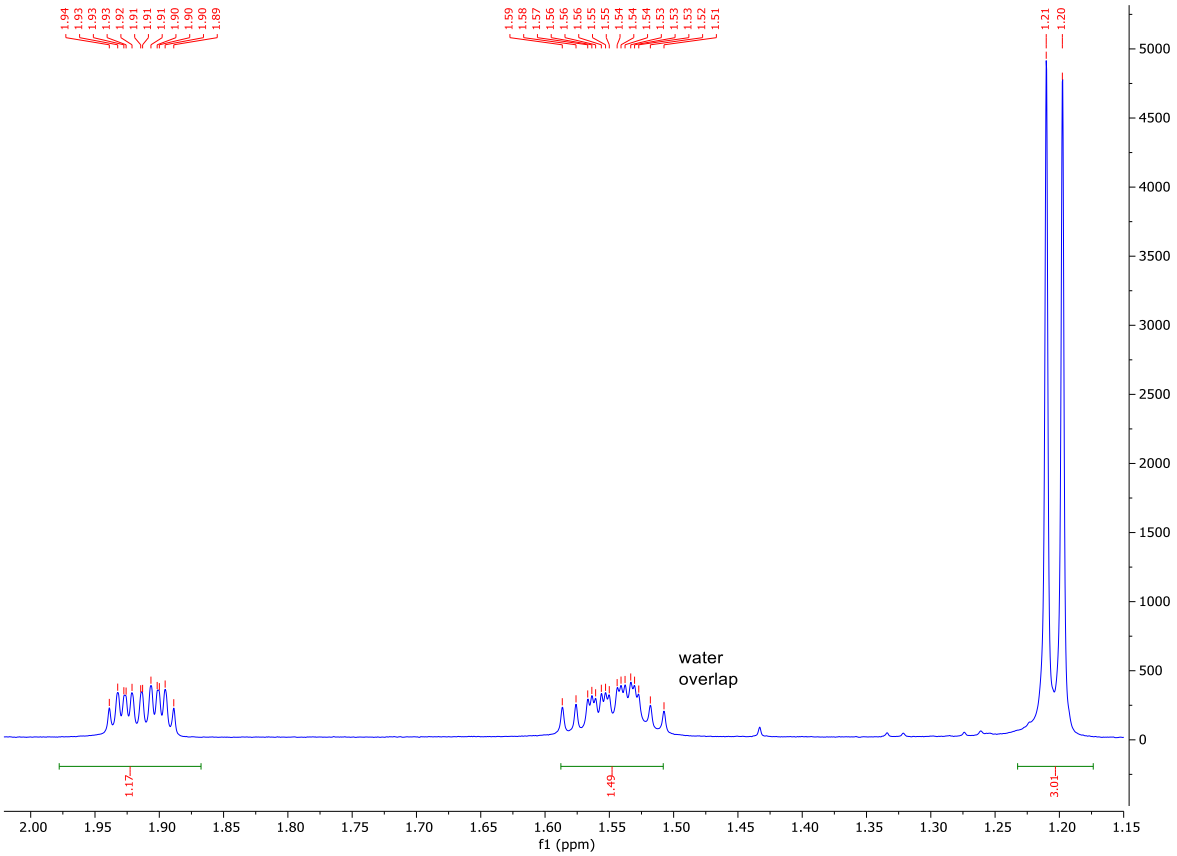
1.94
1.93
1.93
1.93
1.92
1.91
1.91
1.91
1.90
1.90
1.90
1.89
1.59
1.58
1.57
1.56
1.56
1.56
1.55
1.55
1.54
1.54
1.54
1.53
1.53
1.53
1.52
1.51
1.21
1.20
water
overlap
1.17
1.49
3.01
5000
4500
4000
3500
3000
2500
2000
1500
1000
500
0
2.00
1.95
1.90
1.85
1.80
1.75
1.70
1.65
1.60
1.55
1.50
1.45
1.40
1.35
1.30
1.25
1.20
1.15
f1 (ppm)

^{13}C NMR of **2.11a**

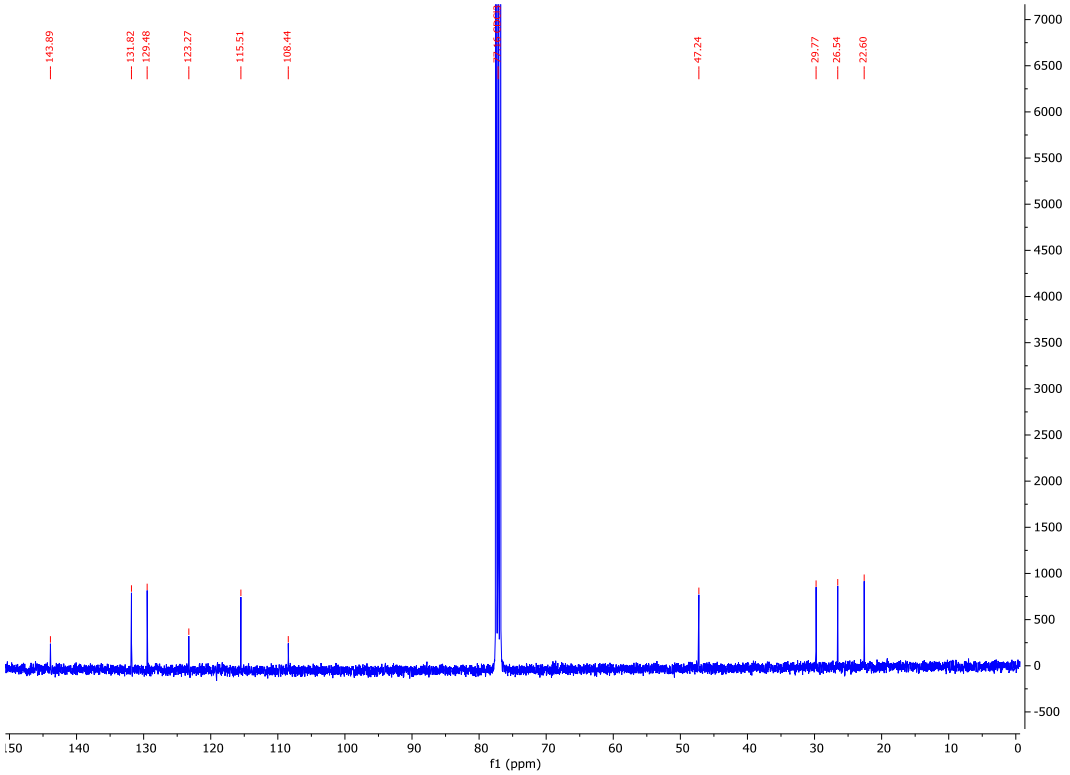

Chiral HPLC Chromatograms of **2.11a**

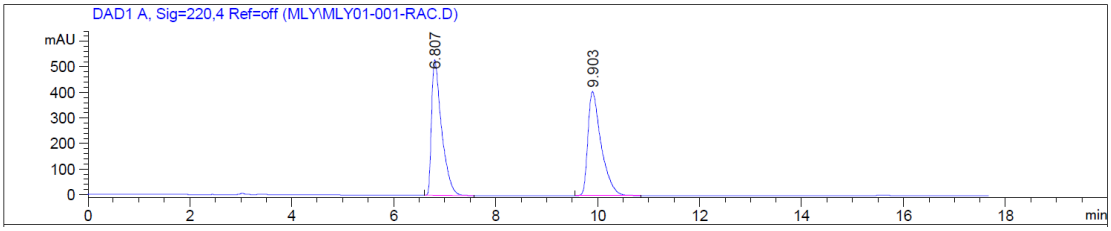

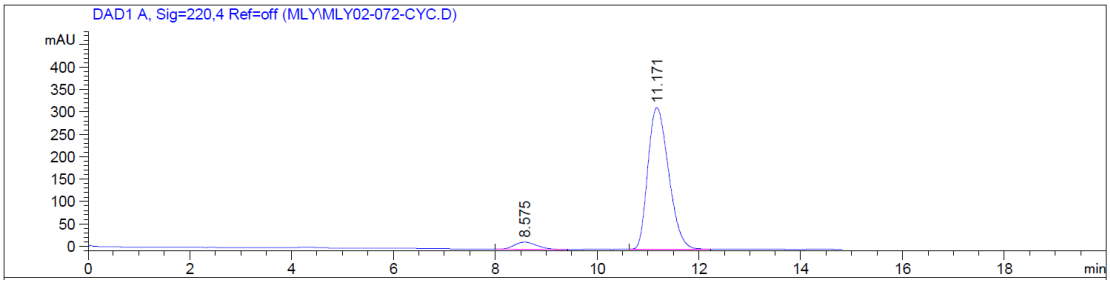

Peak #	RetTime [min]	Type	Width [min]	Area [mAU*s]	Height [mAU]	Area %
1	8.575	BB	0.4773	492.90408	16.00656	5.2228
2	11.171	BB	0.4480	8944.63574	316.22061	94.7772

For comparison compound **2.11a** was also analyzed using a chiralcel OJ-H colunn in comparison with the literature.[9]

Chiral HPLC Chromatograms of **2.11a**

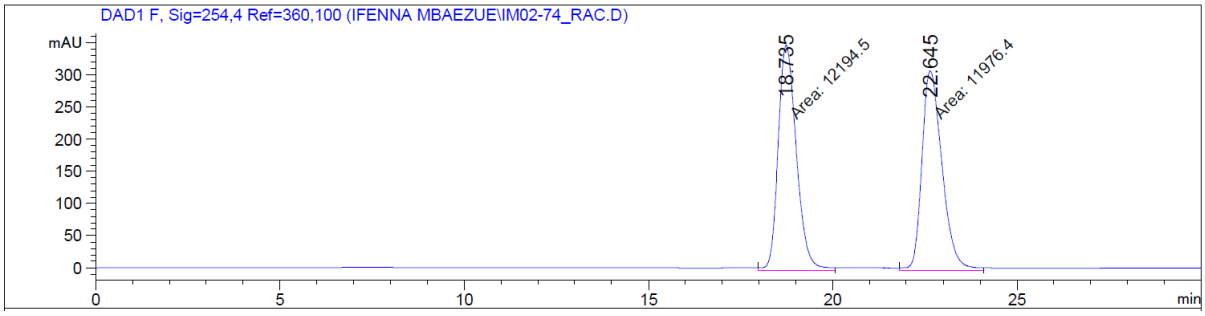

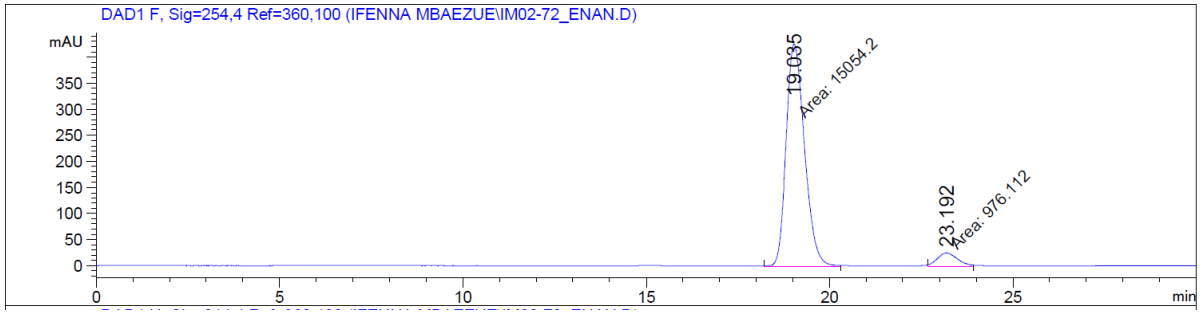

Peak #	RetTime [min]	Type	Width [min]	Area [mAU*s]	Height [mAU]	Area %
1	19.035	MM	0.5867	1.50542e4	427.68332	93.9108
2	23.192	MM	0.6424	976.11206	25.32313	6.0892

Chiral HPLC Chromatogram of crystallized product **2.11a**

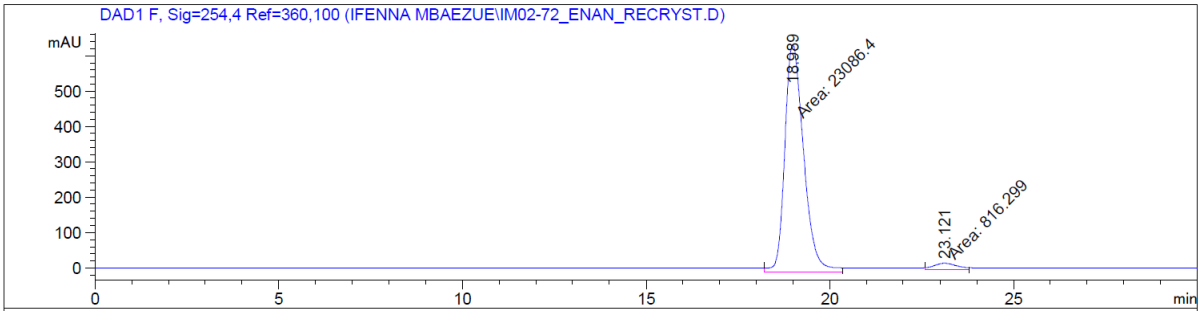

Peak #	RetTime [min]	Type	Width [min]	Area [mAU*s]	Height [mAU]	Area %
1	18.989	MM	0.5980	2.30864e4	643.44177	96.5849
2	23.121	MM	0.7581	816.29865	17.94708	3.4151

(*S*)-2-methyl-1,2,3,4-tetrahydroquinoline (**2.11b**)

^{1}H NMR of **2.11b**

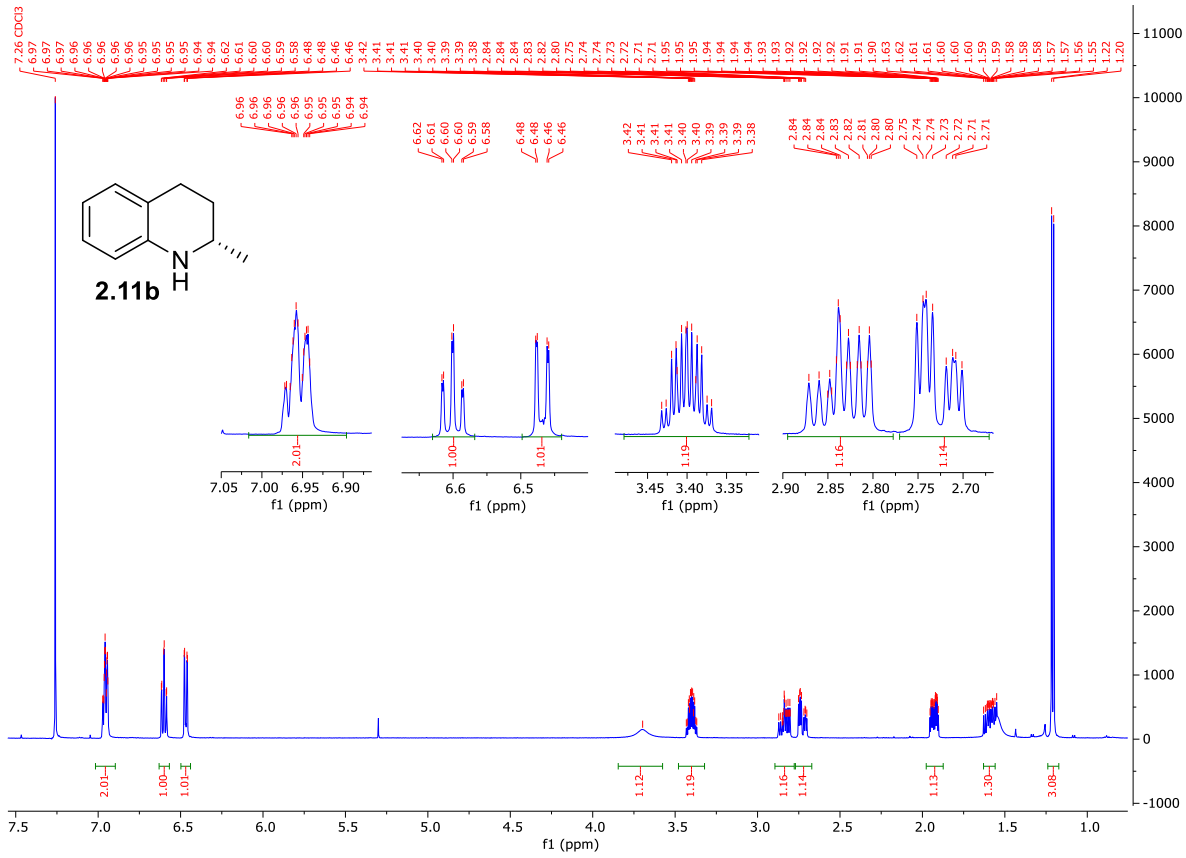

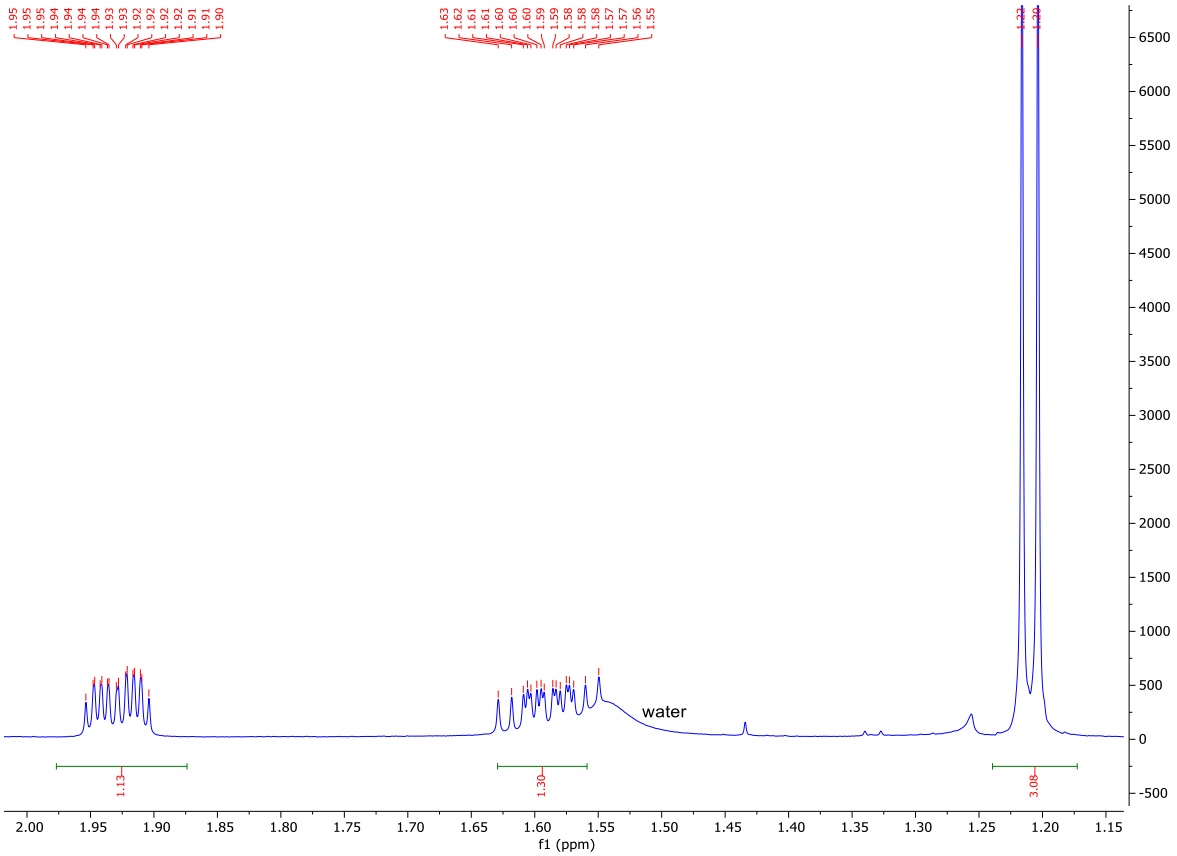

^{13}C NMR of **2.11b**

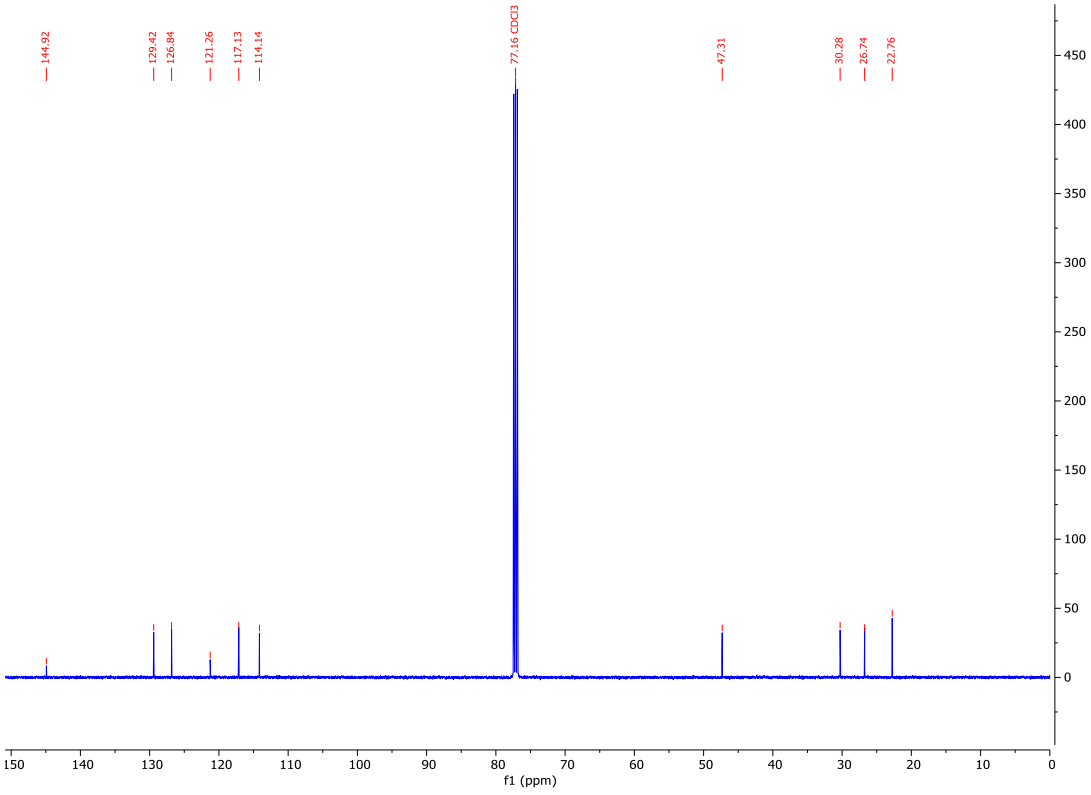

Chiral HPLC Chromatograms of **2.11b**

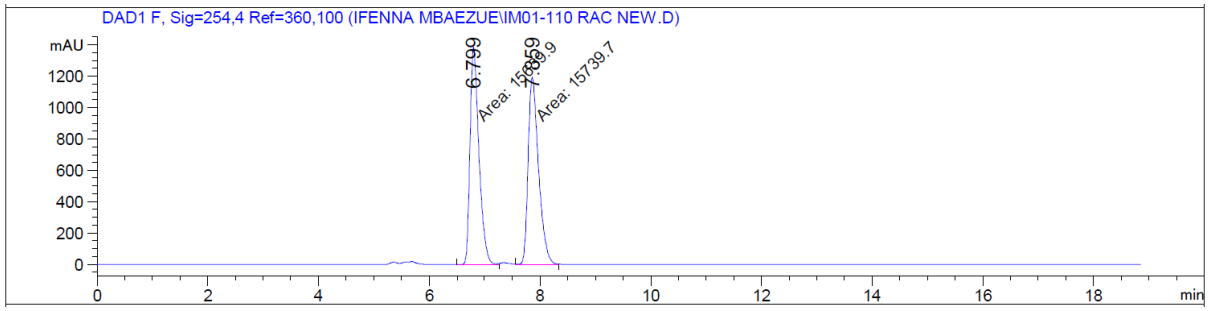

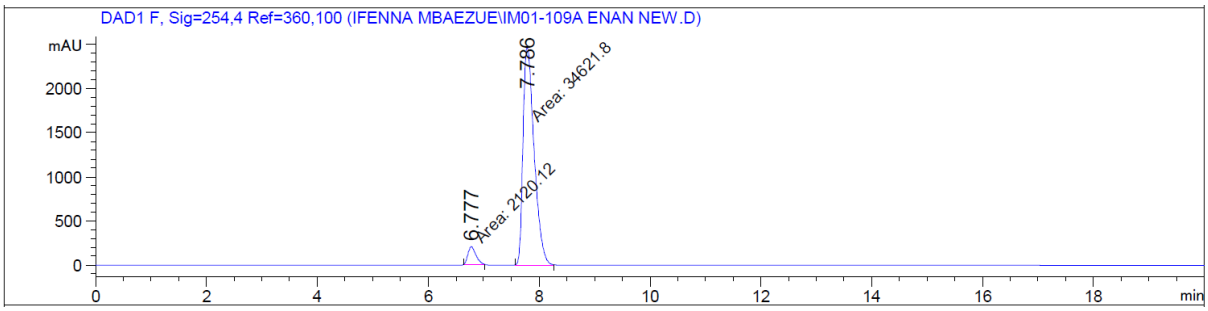

Peak #	RetTime [min]	Type	Width [min]	Area [mAU*s]	Height [mAU]	Area %
1	6.777	MM	0.1708	2120.12207	206.83456	5.7703
2	7.786	MM	0.2332	3.46218e4	2474.55640	94.2297

(*R*)-2-phenyl-1,2,3,4-tetrahydroquinoline (**2.11c**)

^{1}H NMR of **2.11c**

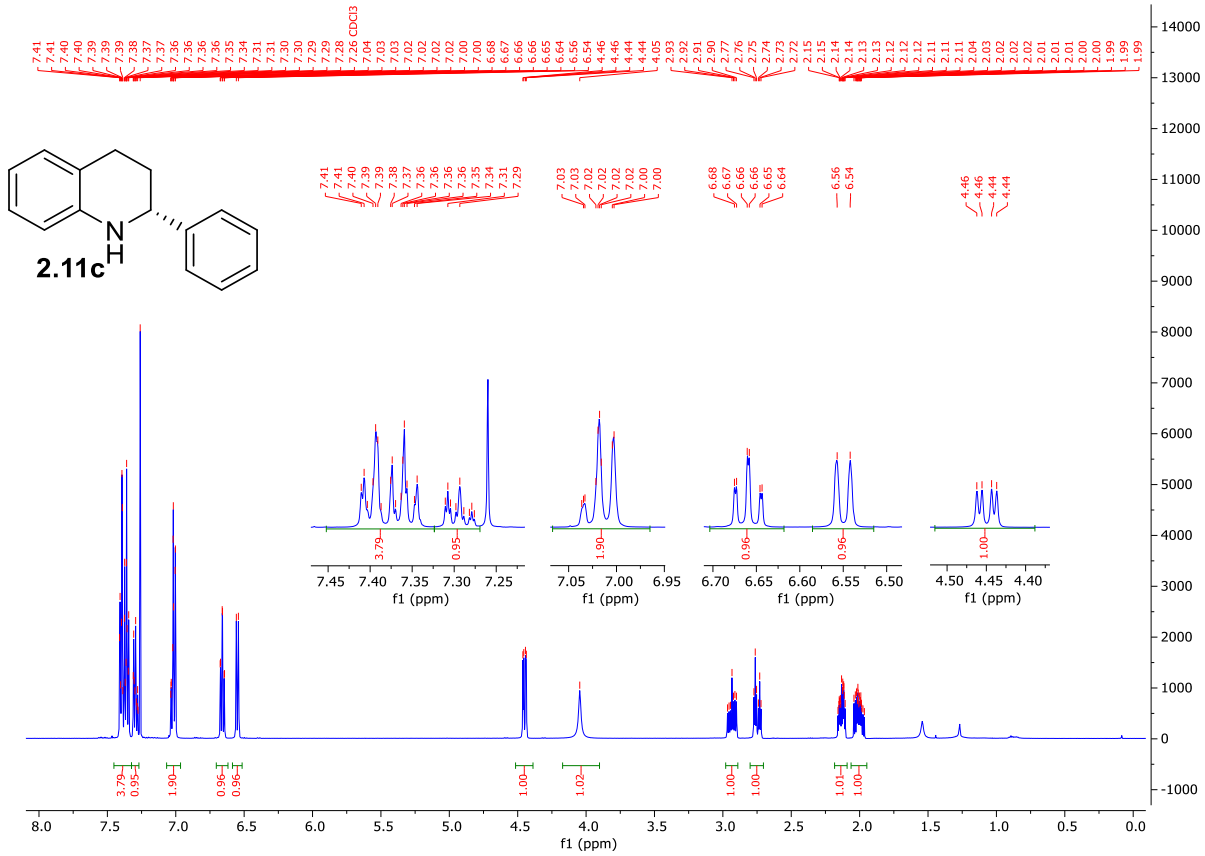

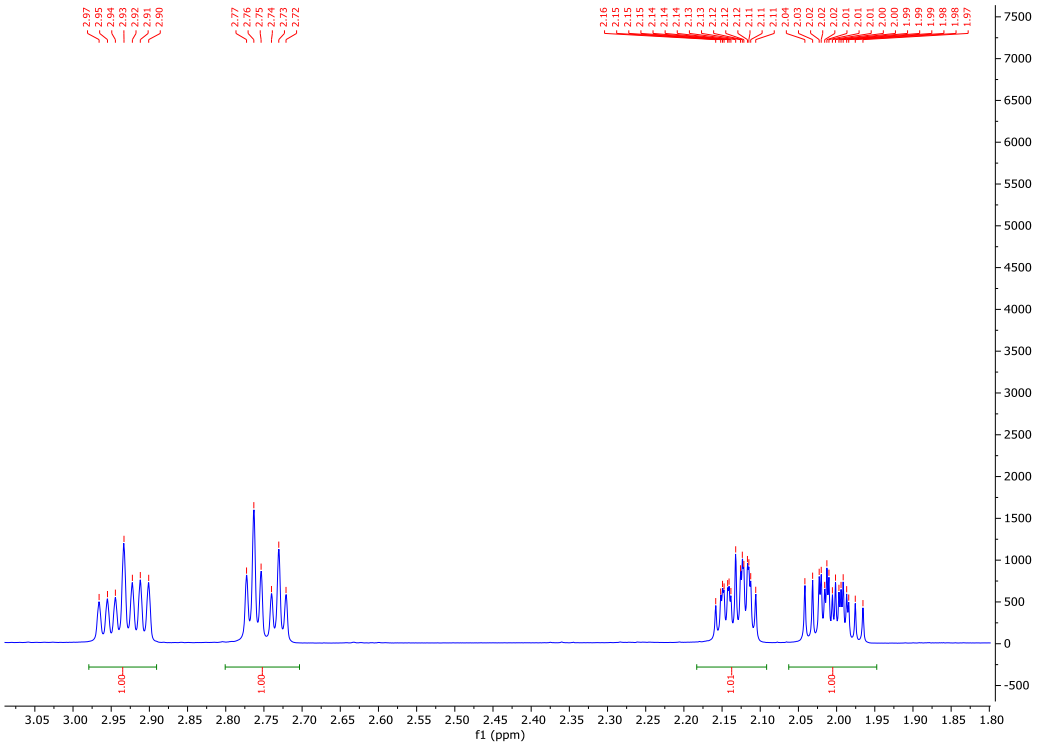

^{13}C NMR of **2.11c**

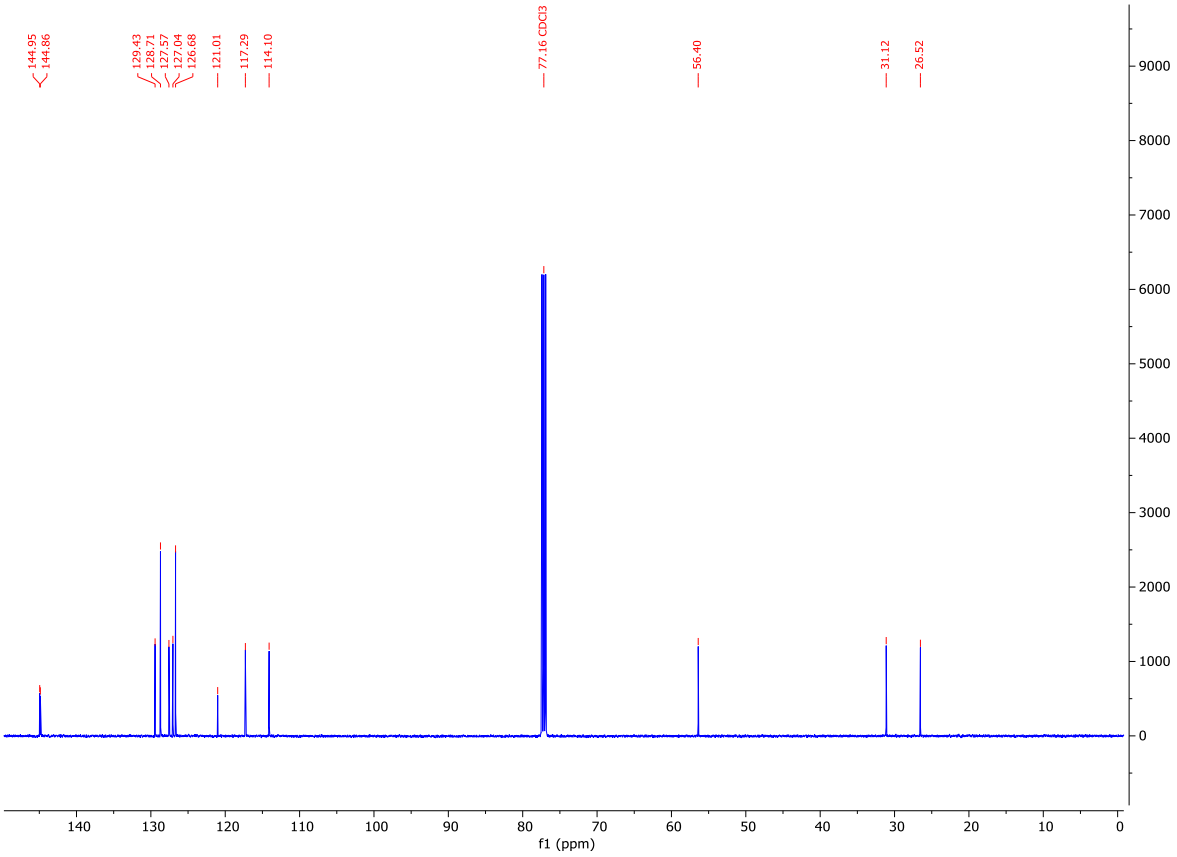

Chiral HPLC Chromatograms of **2.11c**

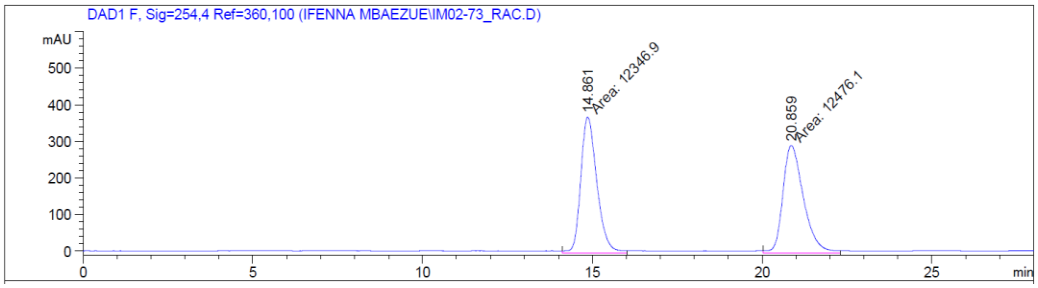

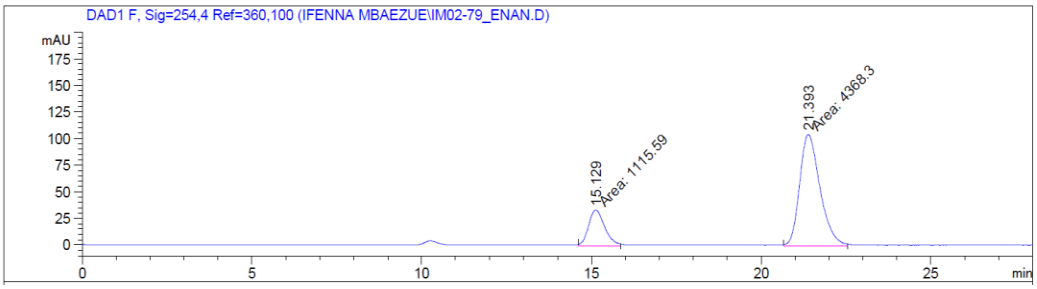

Peak #	RetTime [min]	Type	Width [min]	Area [mAU*s]	Height [mAU]	Area %
1	15.129	MM	0.5518	1115.59338	33.69407	20.3431
2	21.393	MM	0.6967	4368.30176	104.49825	79.6569

(*R*)-4-methyl-1,2,3,4-tetrahydroquinoline (**2.11d**)

^{1}H NMR of **2.11d**

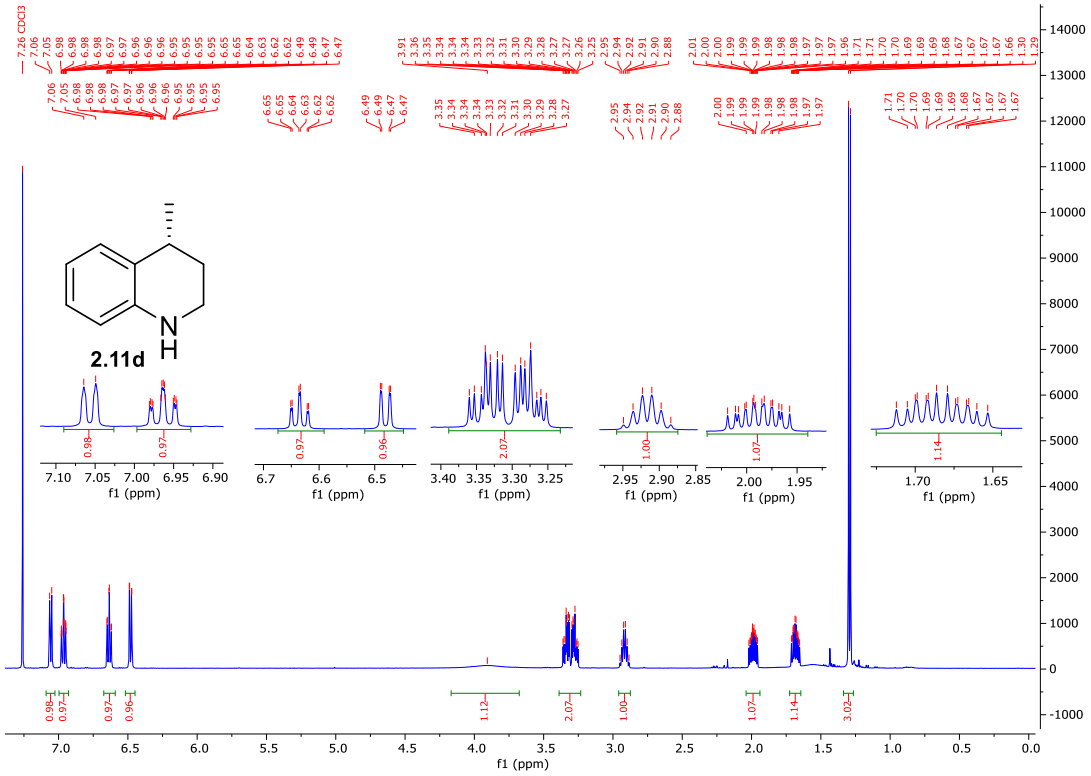

^{13}C NMR of **2.11d**

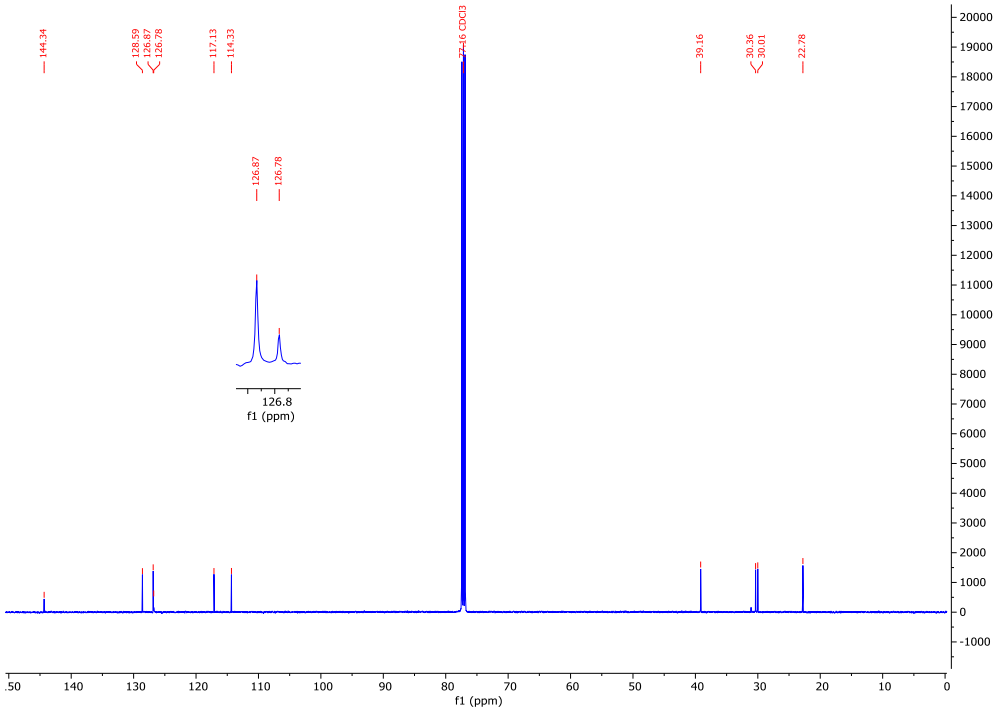

Chiral HPLC Chromatograms of **2.11d**

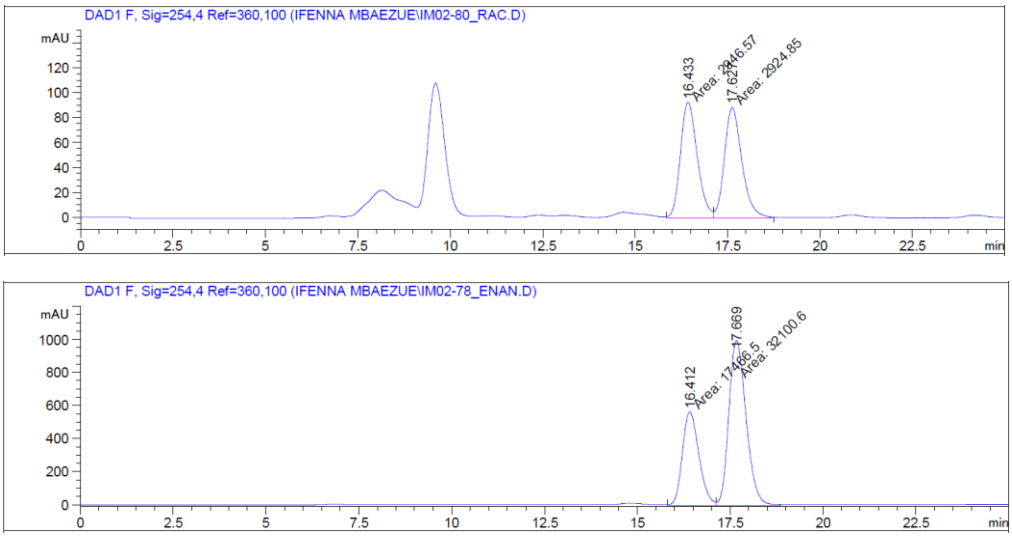

Peak #	RetTime [min]	Type	Width [min]	Area [mAU*s]	Height [mAU]	Area %
1	16.412	MM	0.5150	1.74665e4	565.20856	35.2382
2	17.669	MM	0.5373	3.21006e4	995.67267	64.7618

(*S*)-2-ethyl-1,2,3,4-tetrahydroquinoline (**2.11e**)

^{1}H NMR of **2.11e**

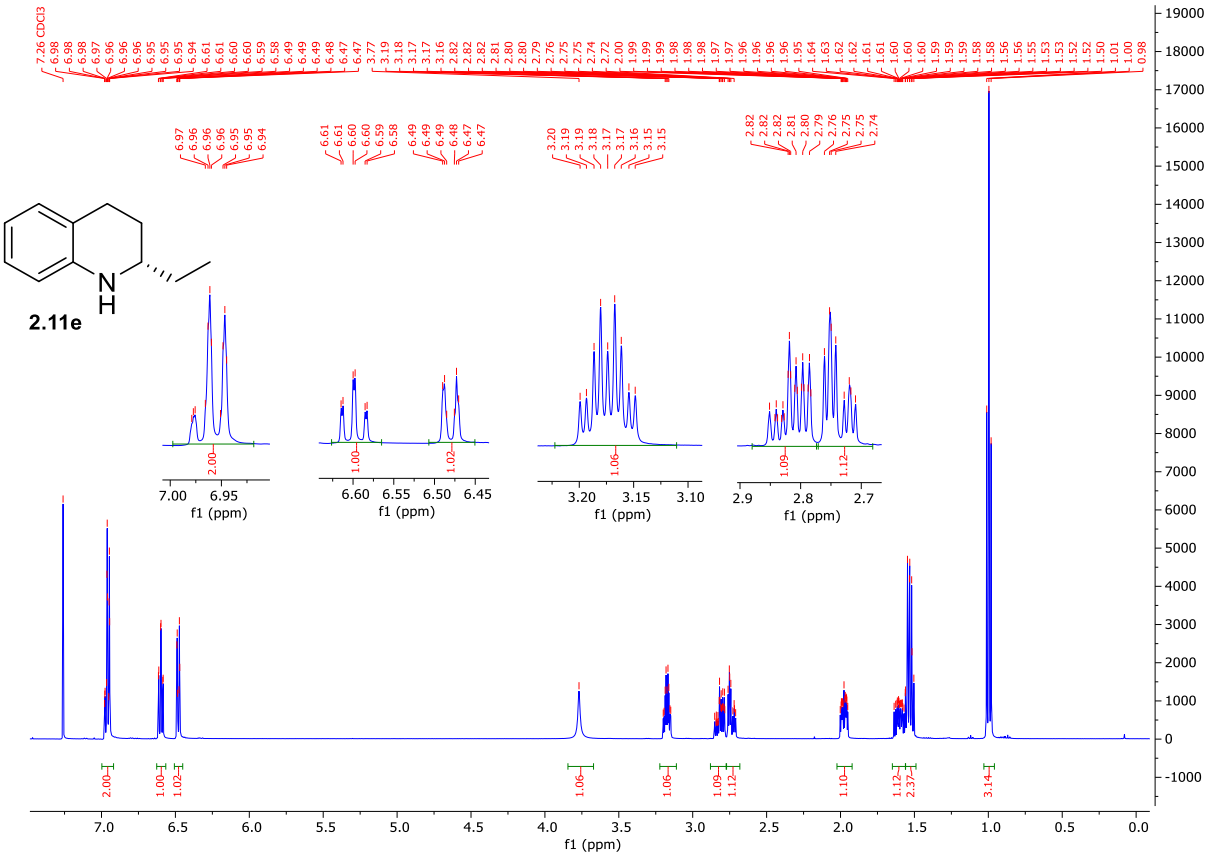

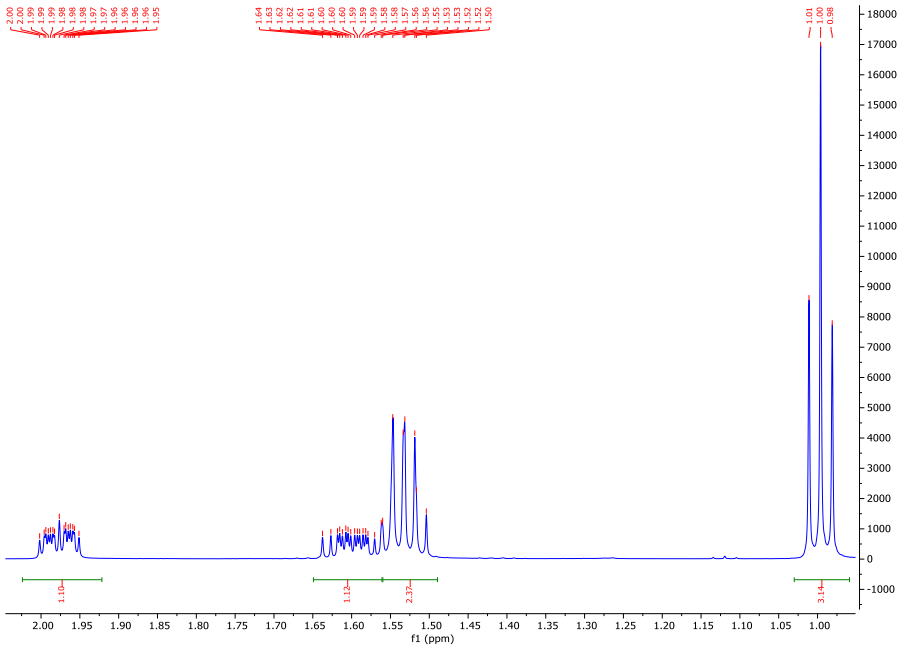

^{13}C NMR of **2.11e**

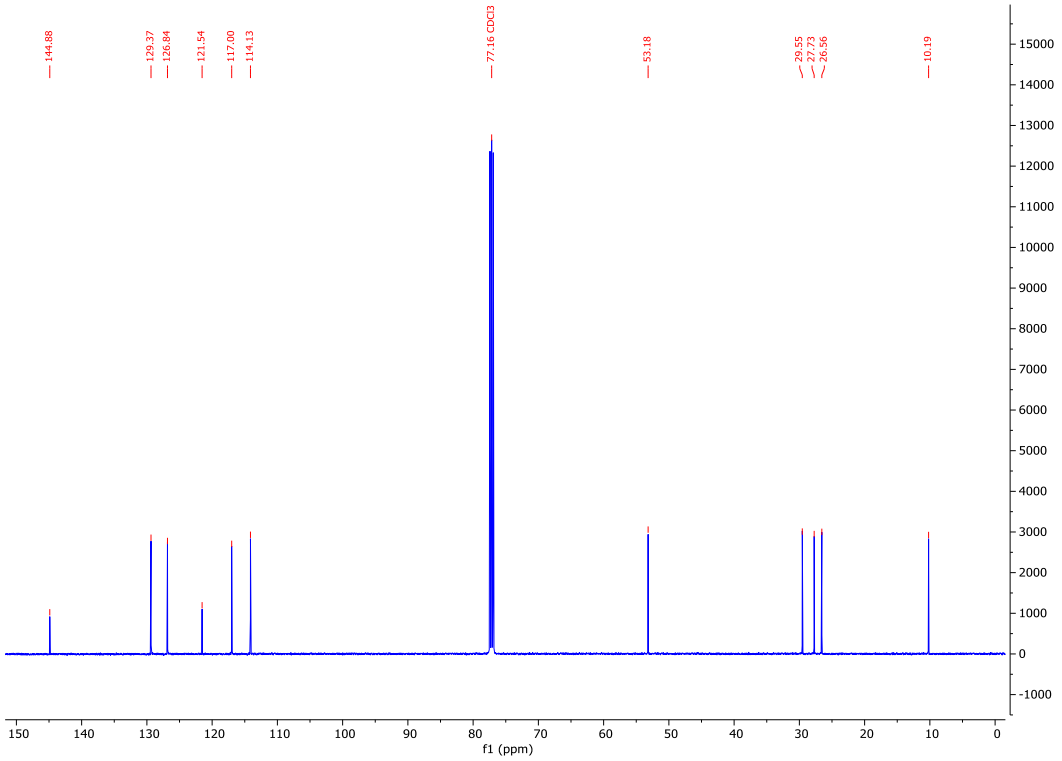

Chiral HPLC Chromatograms of **2.11e**

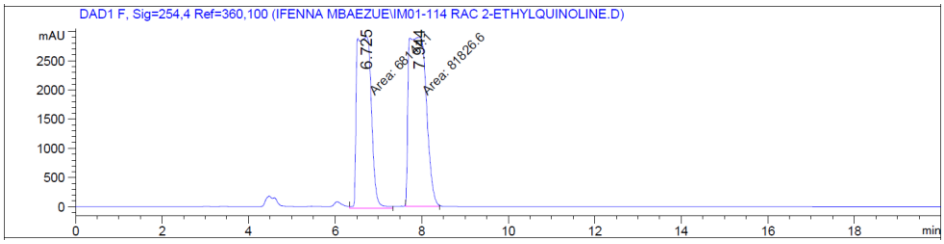

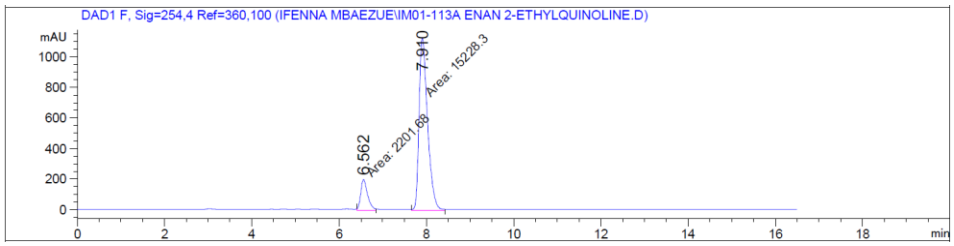

Peak #	RetTime [min]	Type	Width [min]	Area [mAU*s]	Height [mAU]	Area %
1	6.562	MM	0.1823	2201.67993	201.33543	12.6316
2	7.910	MM	0.2248	1.52283e4	1129.25708	87.3684

(*R*)-2-isopropyl-1,2,3,4-tetrahydroquinoline (**2.11f**)

^{1}H NMR of **2.11f**

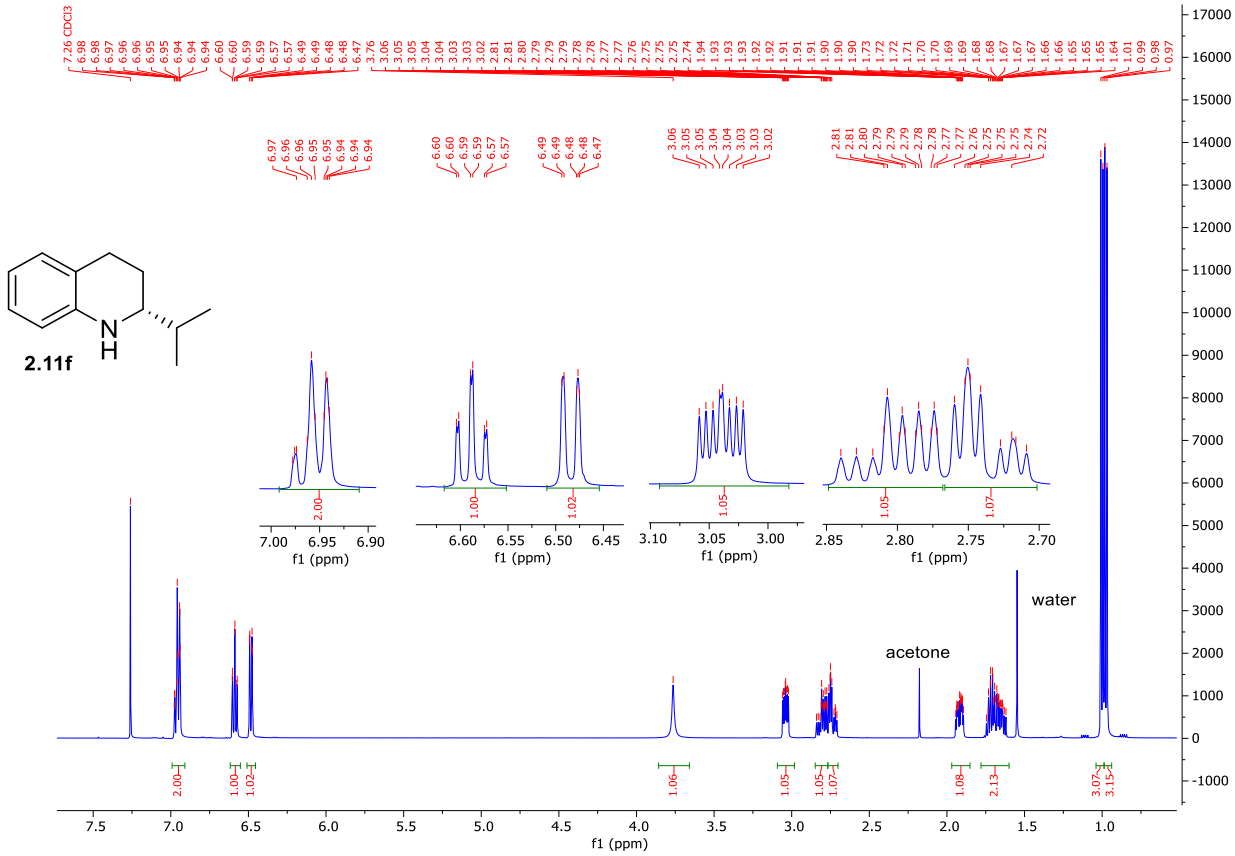

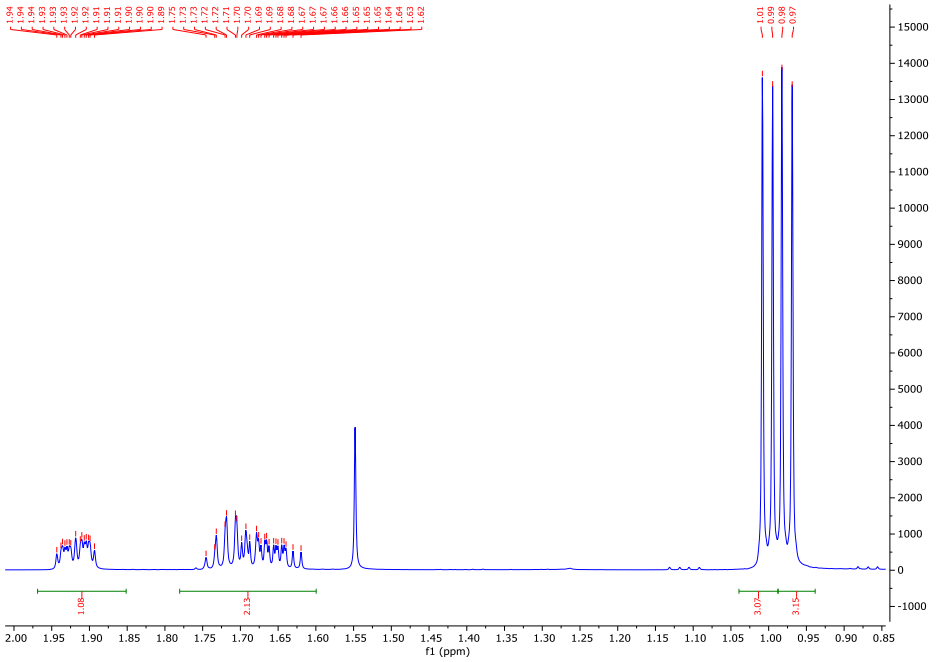

^{13}C NMR of **2.11f**

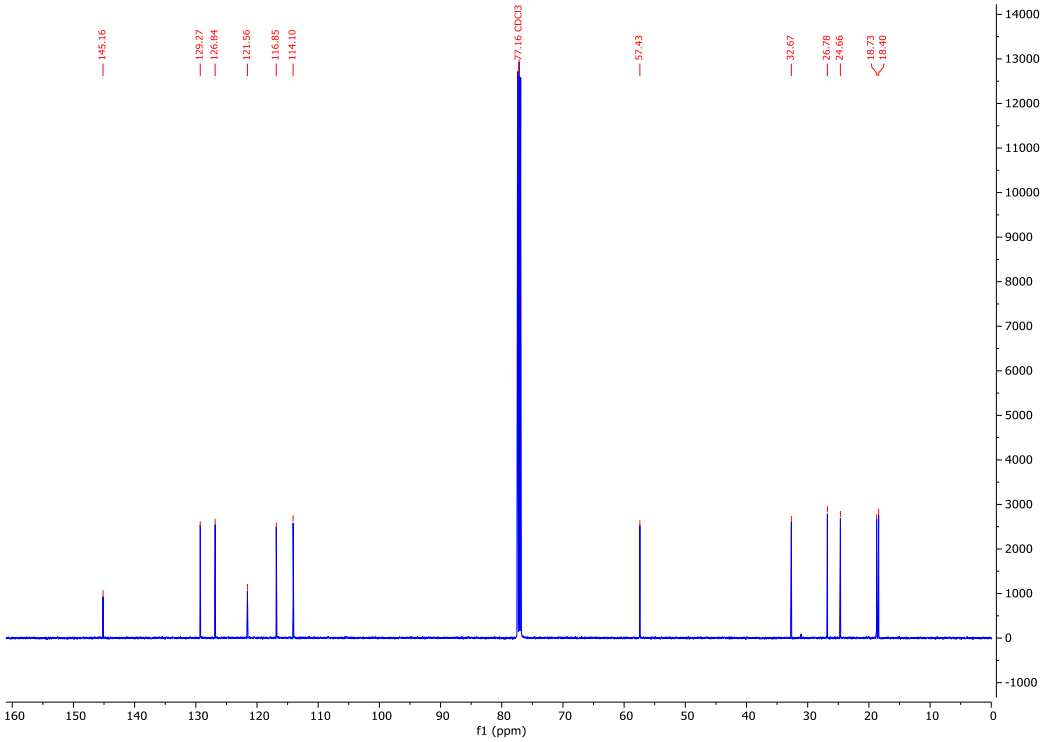

Chiral HPLC Chromatograms of **2.11f**

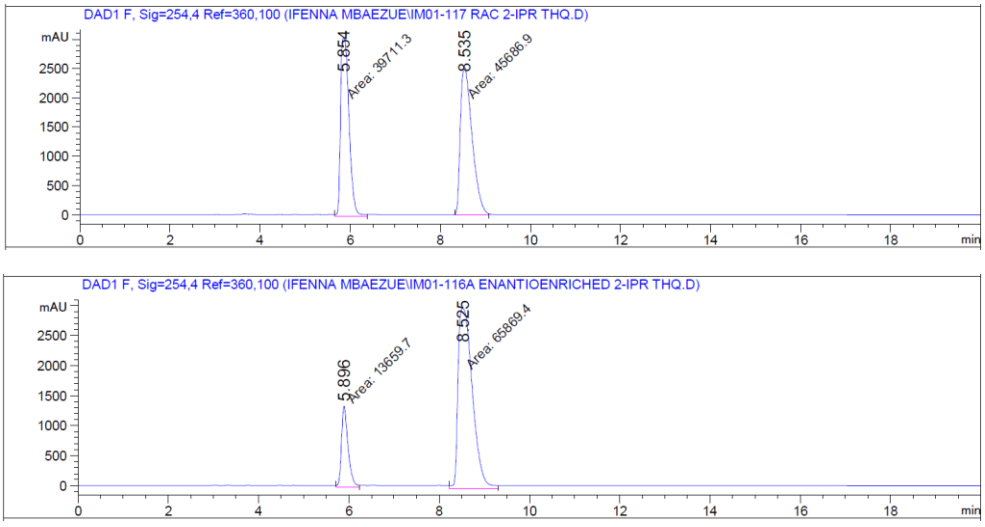

Peak #	RetTime [min]	Type	Width [min]	Area [mAU*s]	Height [mAU]	Area %
1	5.896	MM	0.1692	1.36597e4	1345.61450	17.1757
2	8.525	MM	0.3666	6.58694e4	2994.45923	82.8243

(*S*)-2-methyl-6-nitro-1,2,3,4-tetrahydroquinoline (**2.11g**)

^{1}H NMR of **2.11g**

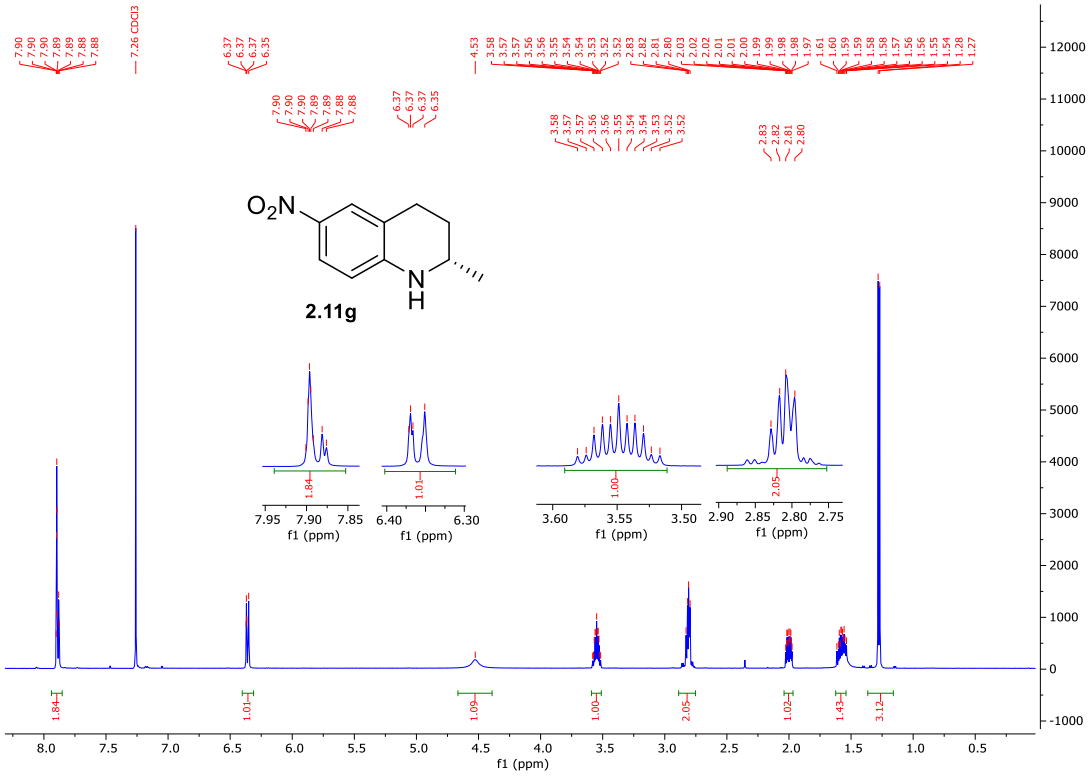

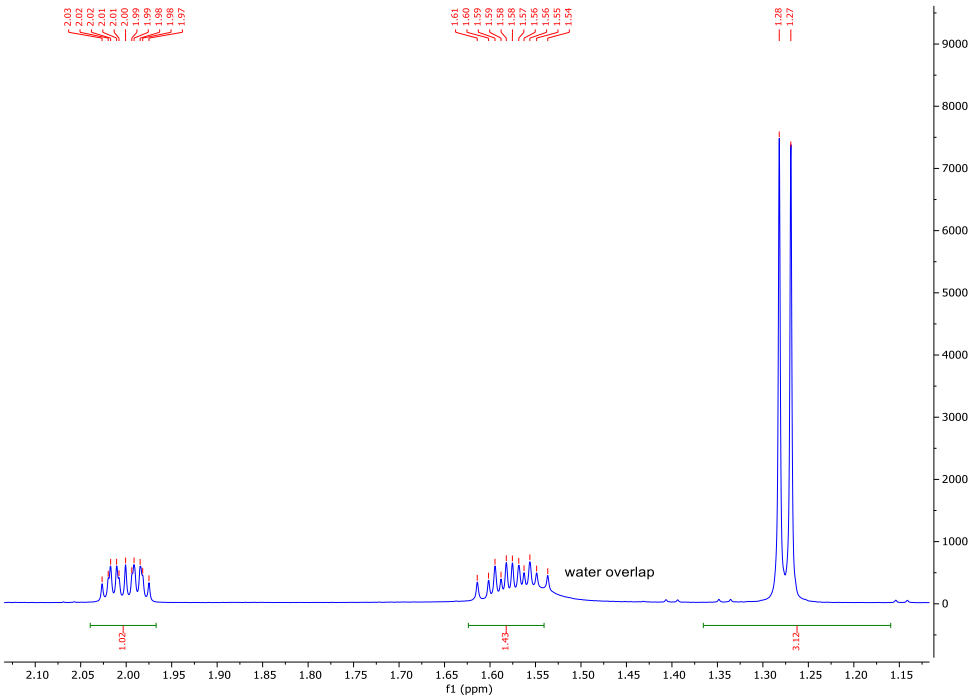

^{13}C NMR of **2.11g**

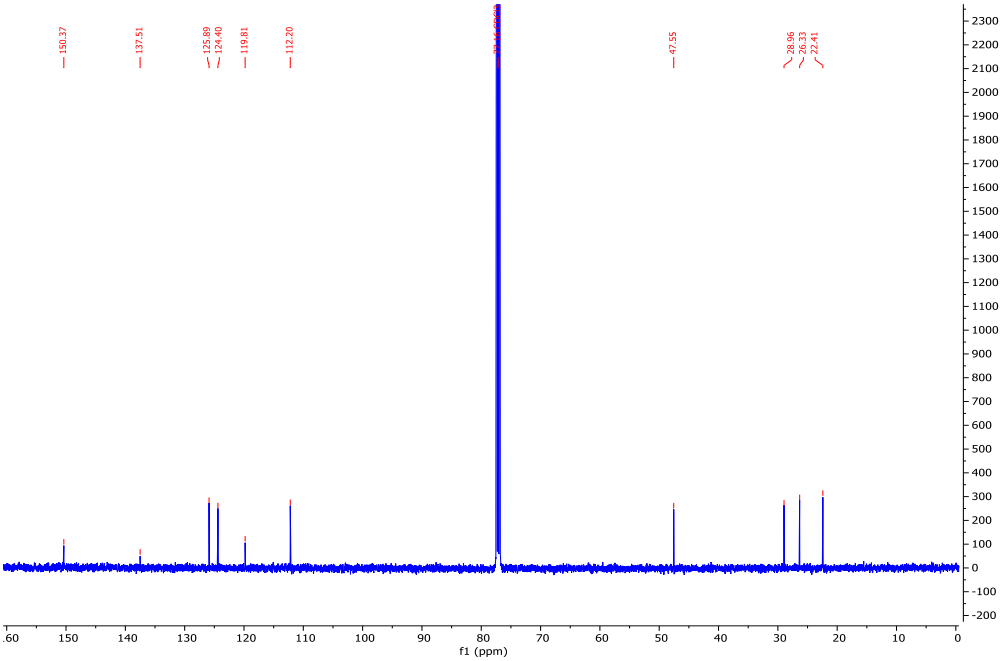

Chiral HPLC Chromatogram of **2.11g**

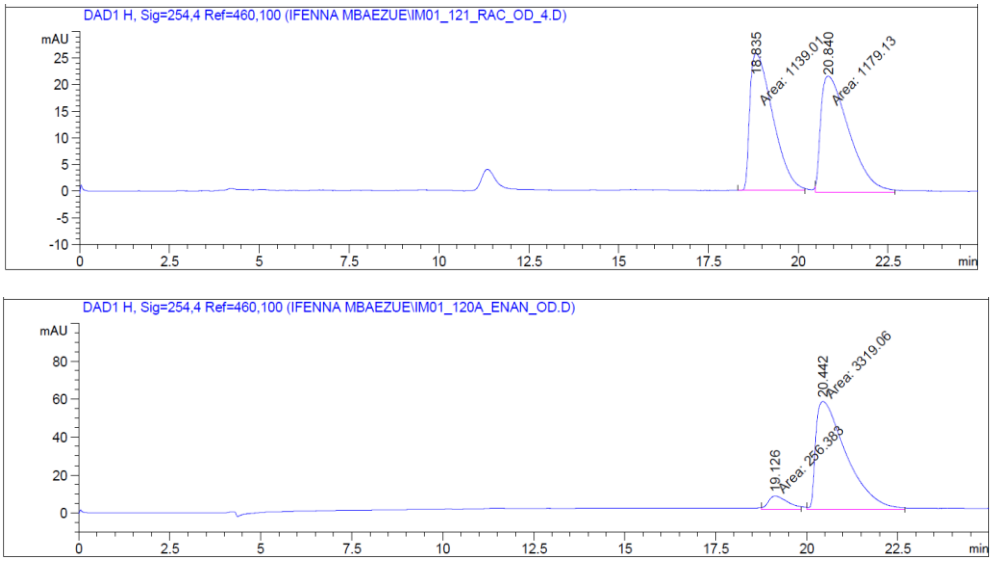

Peak #	RetTime [min]	Type	Width [min]	Area [mAU*s]	Height [mAU]	Area %
1	19.126	MM	0.6119	256.38251	6.98332	7.1706
2	20.442	MM	0.9745	3319.06494	56.76318	92.8294

Chiral HPLC Chromatogram of crystallized product **2.11g**

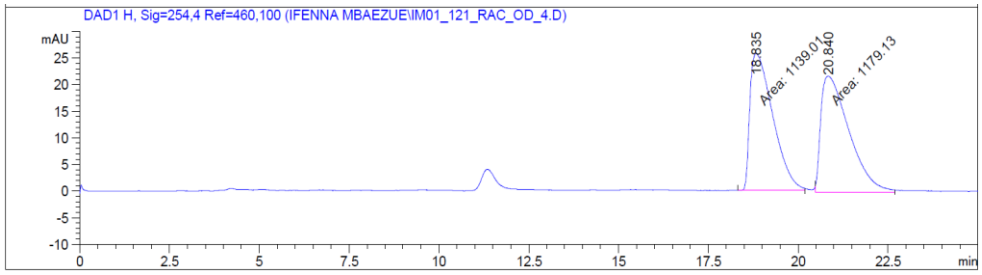

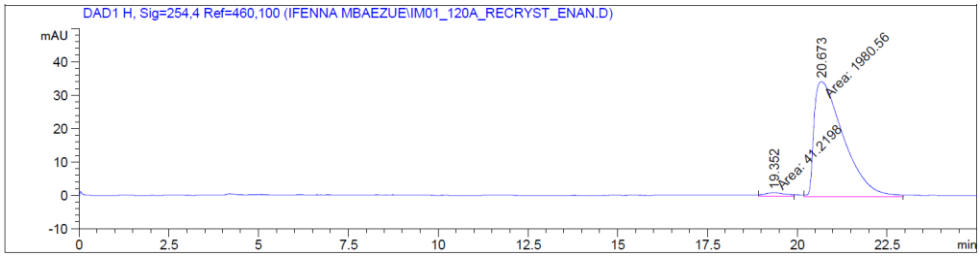

Peak #	RetTime [min]	Type	Width [min]	Area [mAU*s]	Height [mAU]	Area %
1	19.352	MM	0.6727	41.21978	1.02125	2.0388
2	20.673	MM	0.9551	1980.56396	34.56263	97.9612

^{1}H NMR of **2.11h**

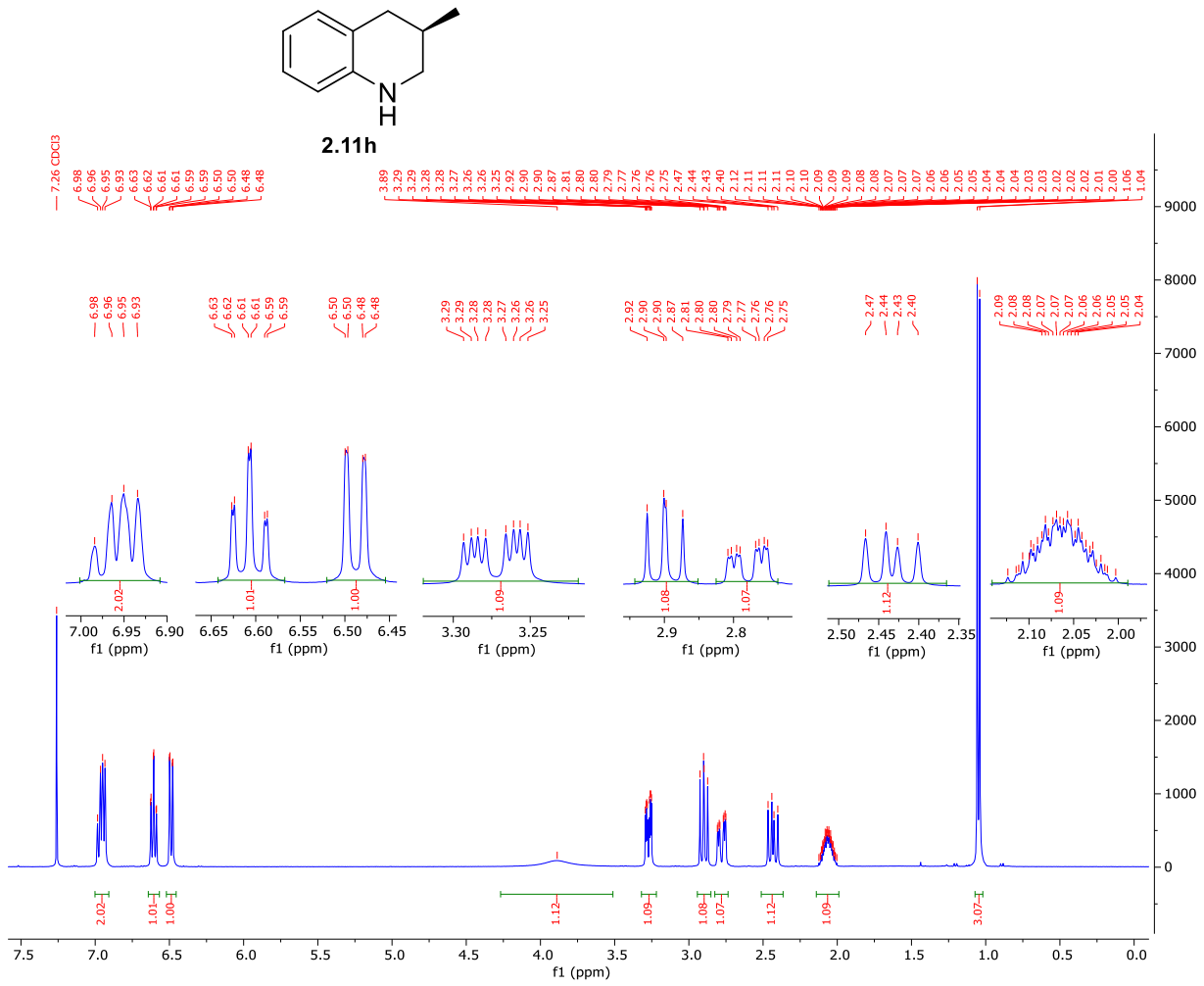

^{13}C NMR of **2.11h**

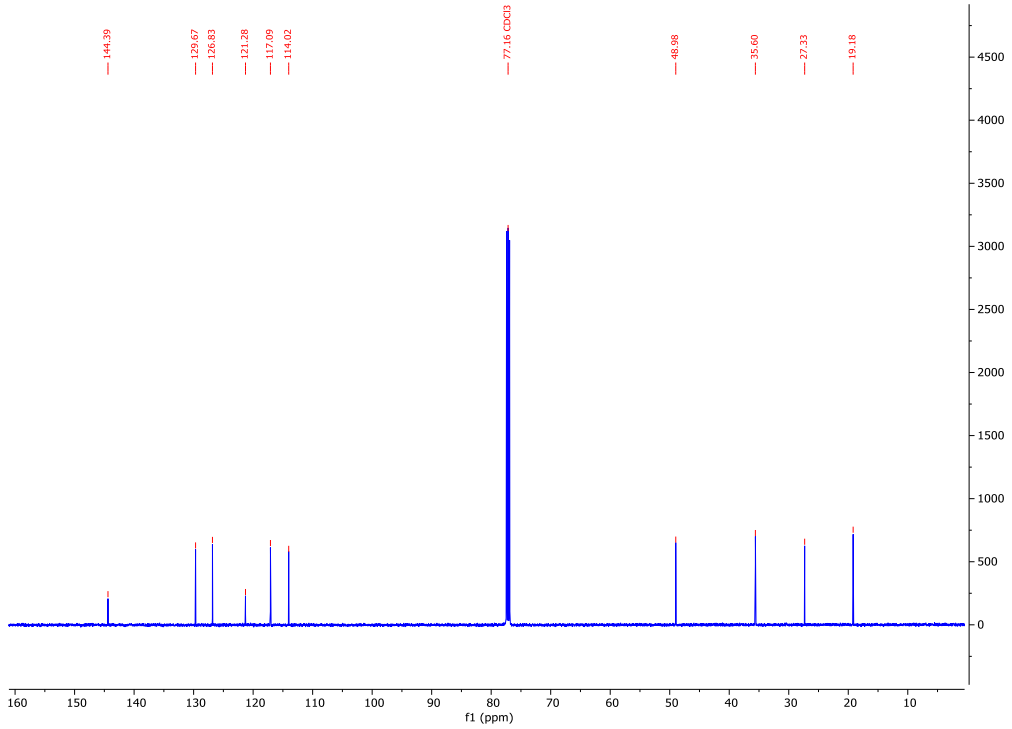

Chiral HPLC Chromatograms of **2.11h**

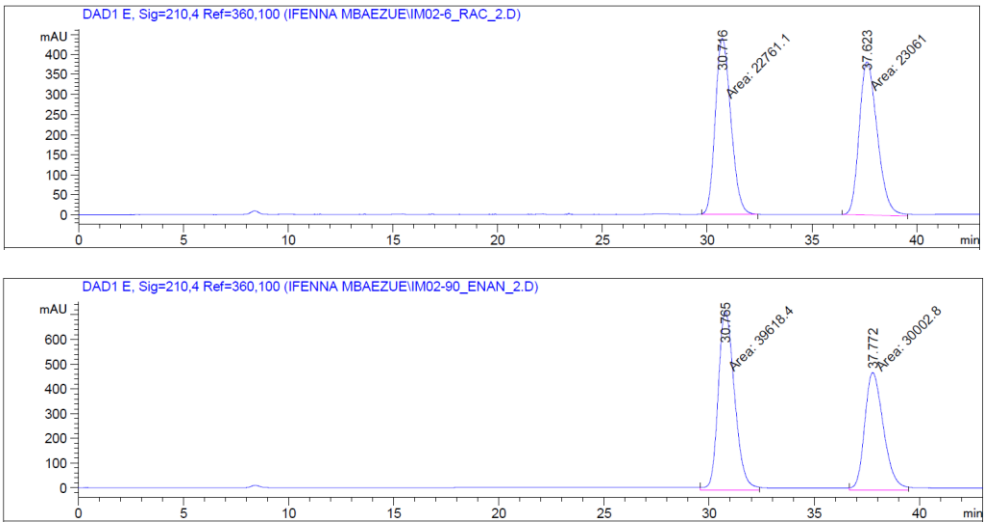

Peak #	RetTime [min]	Type	Width [min]	Area [mAU*s]	Height [mAU]	Area %
1	30.765	MM	0.9067	3.96184e4	728.26892	56.9056
2	37.772	MM	1.0490	3.00028e4	476.68146	43.0944

^{1}H NMR of **2.11i**

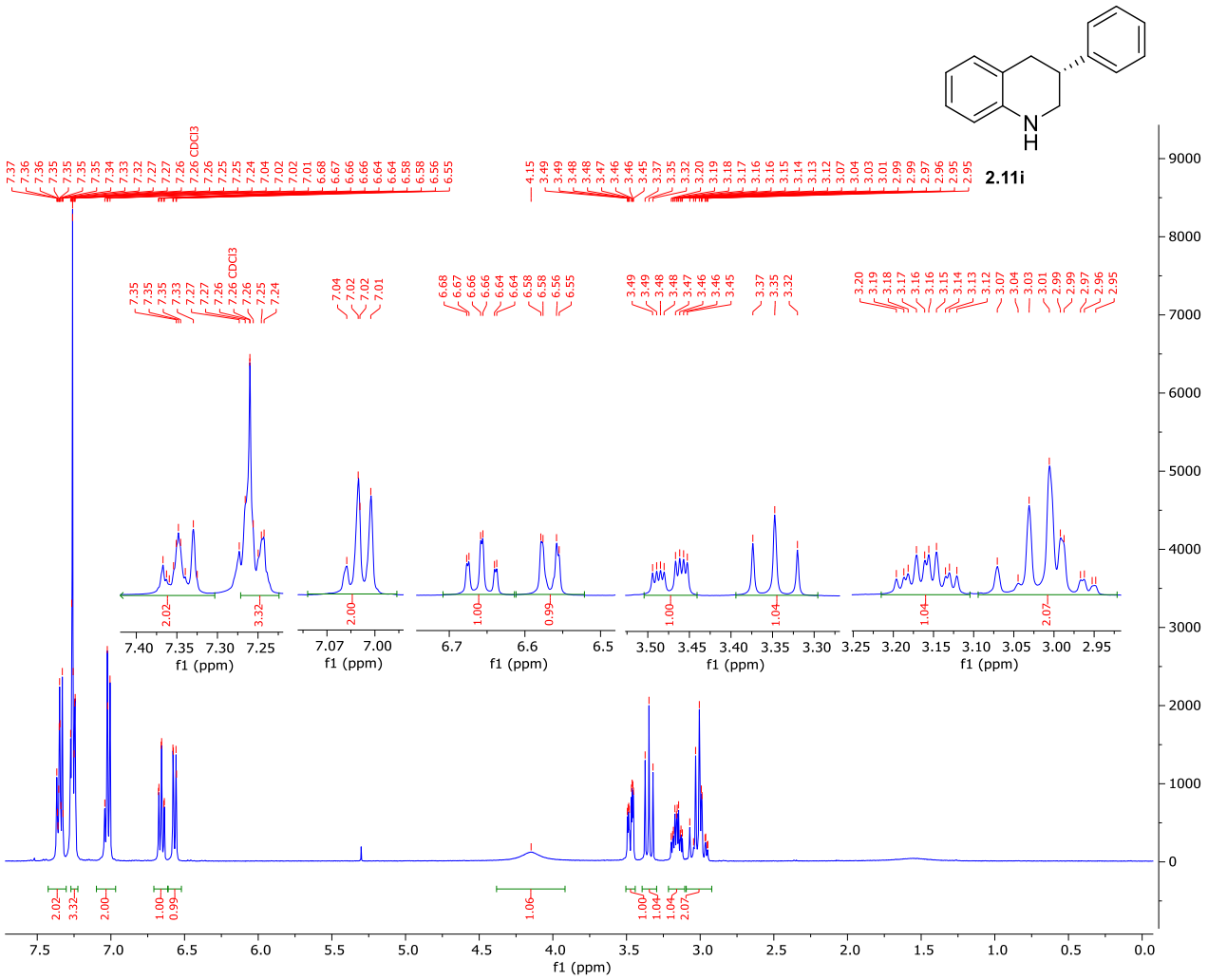

^{13}C NMR of **2.11i**

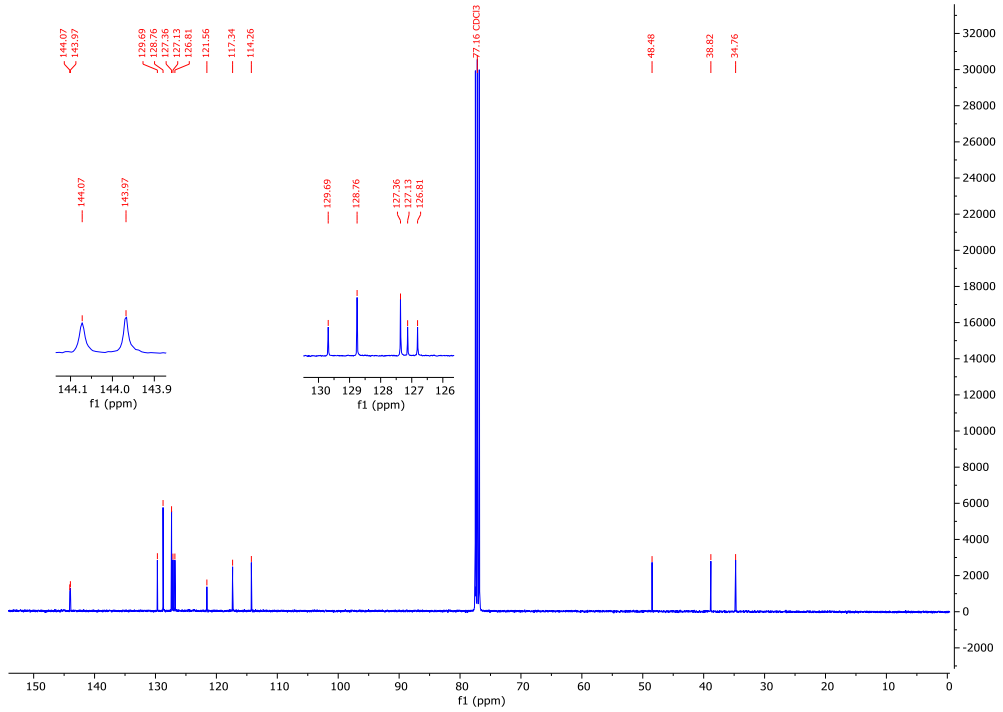

Chiral HPLC Chromatograms of **2.11i**

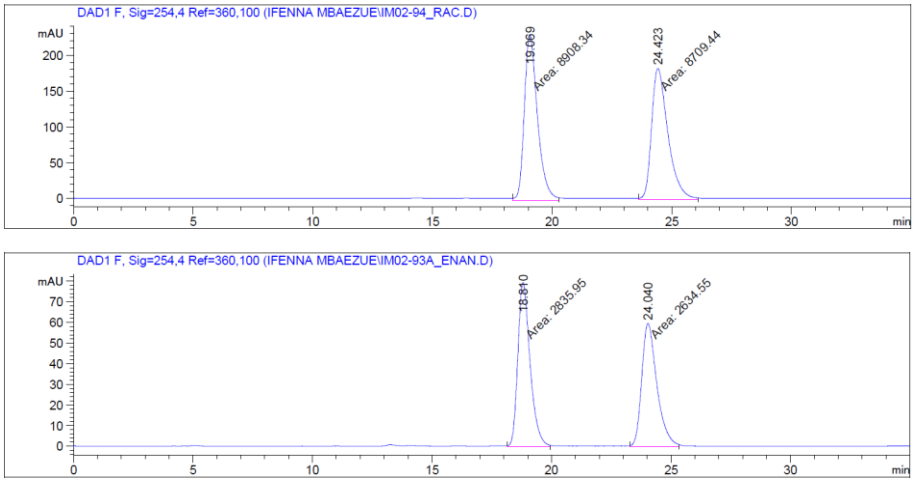

Signal 6: DAD1 F, Sig=254,4 Ref=360,100

Peak #	RetTime [min]	Type	Width [min]	Area [mAU*s]	Height [mAU]	Area %
1	18.810	MM	0.5948	2835.94873	79.46480	51.8408
2	24.040	MM	0.7355	2634.54956	59.70087	48.1592
Totals :				5470.49829	139.16567	

^{1}H NMR of **2.11j**

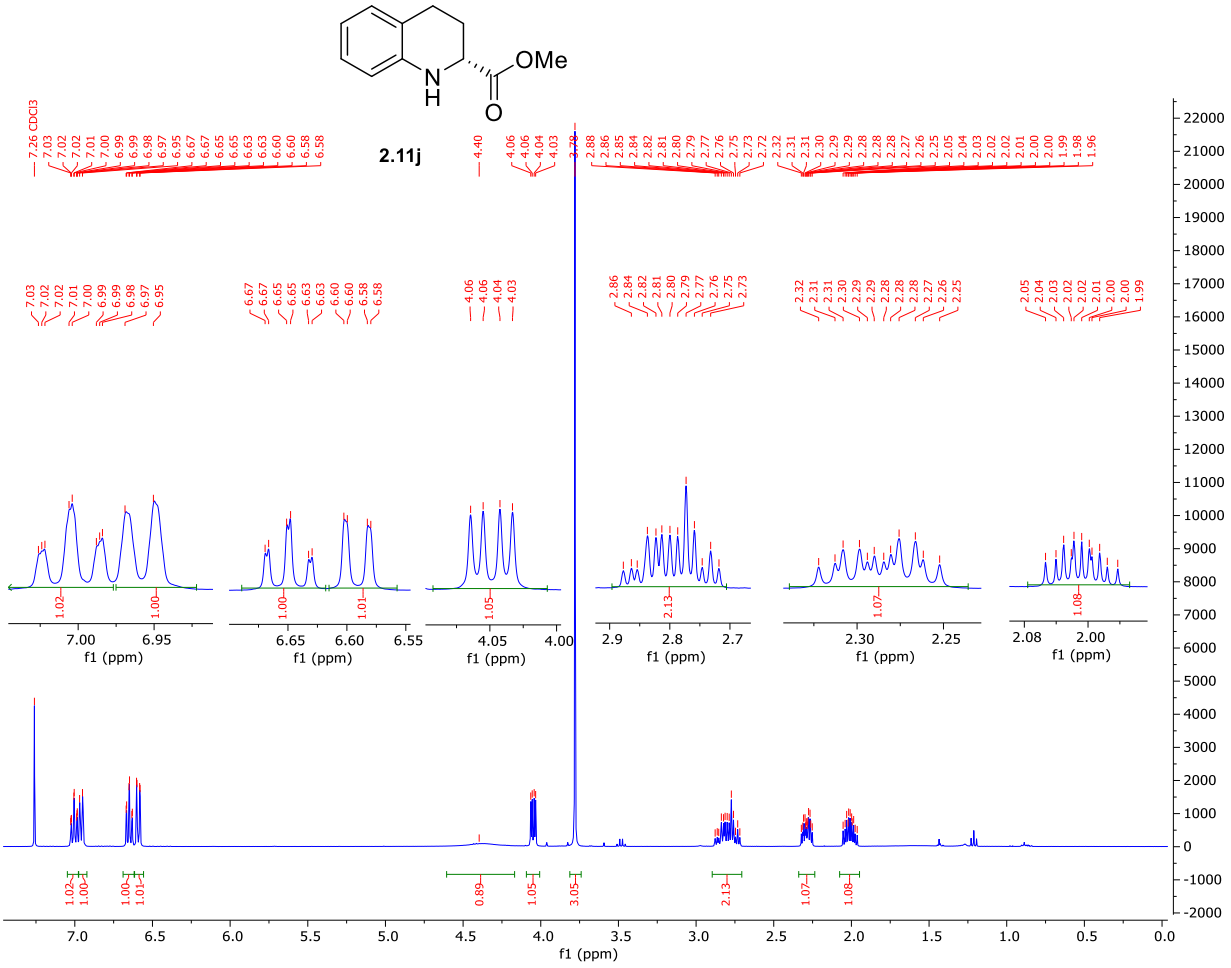

^{13}C NMR of **2.11j**

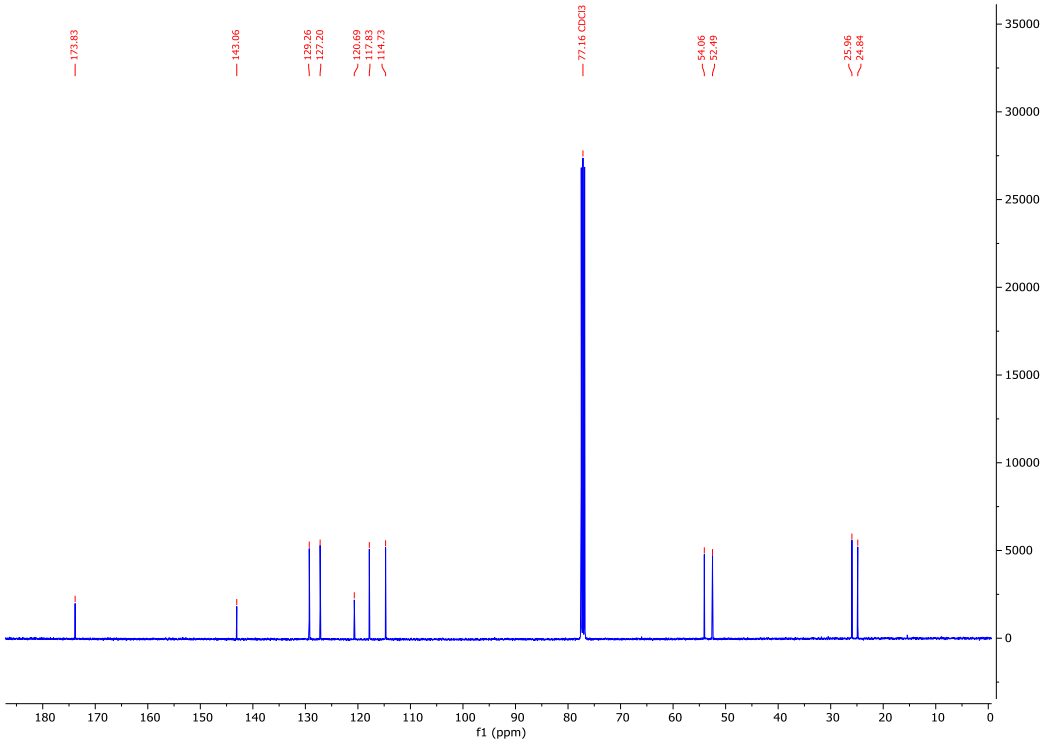

Chiral HPLC Chromatograms of **2.11j**

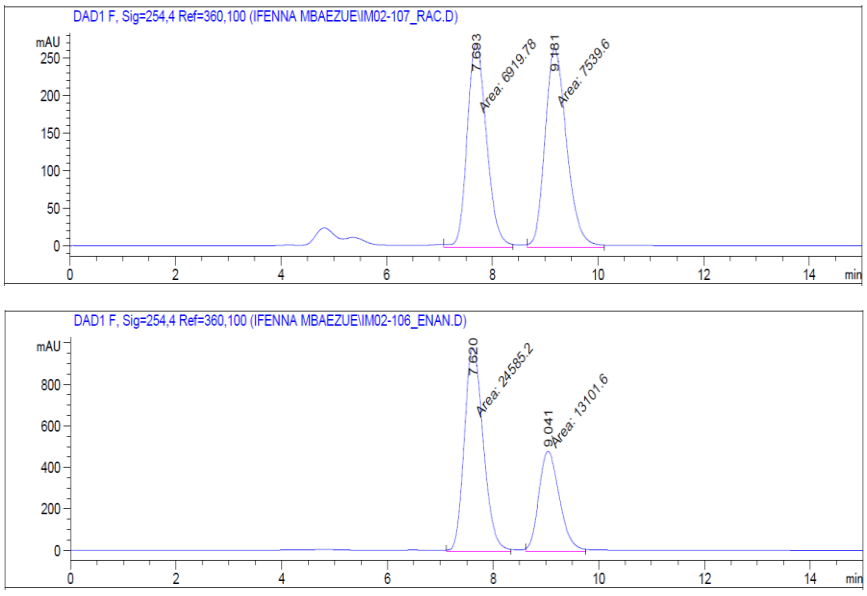

Peak #	RetTime [min]	Type	Width [min]	Area [mAU*s]	Height [mAU]	Area %
1	7.620	MM	0.4169	2.45852e4	982.85883	65.2355
2	9.041	MM	0.4524	1.31016e4	482.72311	34.7645

X-Ray Data Collection and Structural Refinement Statistics

The X-ray data were collected on a Bruker D8 Venture dual-source diffractometer equipped with a PHOTON II detector and an Oxford Cryostream 800 cooling system, using mirror-monochromatized Cu*K*α radiation (λ = 1.54184 Å) from a microfocus source, in a series of φ- and ω-scans. APEX3 software was used for data collection, integration and reduction.[43] Semi-empirical absorption correction was applied using SADABS-2016/2.[44]

The structures were solved using SHELXT-2014/5 (**5a_123K**, **11a_253K**) or SHELXT-2018/2 (**5c_253K**, **8d_253K**)[45]and refined by full-matrix least-squares using SHELXL-2018/3[46] within Olex2[47]and WinGX[48] packages. All non-hydrogen atoms were refined anisotropically. All carbon-bound hydrogen atoms were calculated to their optimal positions and treated as riding atoms using isotropic displacement parameters 1.2 (or 1.5 in case of methyl groups) times larger than the respective parent atoms. Nitrogen- and oxygen-bound hydrogen atoms were found in the difference electron density map and were modelled as constrained, with isotropic displacement parameters 1.2 (for nitrogen-bound) or 1.5 (for oxygen-bound) times larger than those of the respective parent atoms. In case of **11a_253K**, the amino group was instead allowed to refine as a rigid body to allow for the partial sp^3 character of the nitrogen, i.e. the out-of-plane position of the attached hydrogen atom. For disordered moieties, 1,2- and 1,3-interatomic distances were restrained to be equal and the anisotropic displacement parameters of the atoms were restrained to be equal for bonded and spatially close atoms. In case of **5c_253K**, the minor disorder component of the 2,4,6-triisopropylbenzenesulfonyl group was partially refined as a rigid body including the benzene ring with the attached secondary carbon atoms of isopropyl groups and the sulfonyl (–SO_2–) group. The occupancies of the disordered moieties were either allowed to refine freely (**5c_253K**) or were fixed to 0.5 as required by the proximity of a two-fold rotation axis (**8d_253K**).

CCDC 1935843–1935846 contain the supplementary crystallographic data for this paper. The data can be obtained free of charge from The Cambridge Crystallographic Data Centre via www.ccdc.cam.ac.uk/structures.

Table I-1. Crystallographic data.

Complex	**2.5a_123K**	**2.5c_253K**	**2.8d_253K**	**2.11a_253K**
CCDC Number	1935843	1935844	1935845	1935846
Empirical formula	$C_{25}H_{38}NO_4PS$	$C_{30}H_{44}NO_5PS$	$C_{31}H_{42}Cl_2N_2O_4P_2$	$C_{10}H_{12}BrN$
Formula weight	479.59	561.69	639.50	226.12
T/K	123.0(1)	253.0(1)	253.0(1)	253.0(1)
Crystal system	Monoclinic	Orthorhombic	Tetragonal	Orthorhombic
Space group	$P2_1$	$P2_12_12_1$	$P4_12_12$	$P2_12_12_1$
a/Å	10.6790(7)	10.5840(6)	10.7127(2)	16.0321(5)
b/Å	12.0178(8)	15.7917(8)	10.7127(2)	6.1532(2)
c/Å	11.2241(7)	18.4493(10)	27.9476(6)	9.7828(3)
α/°	90	90	90	90
β/°	112.3257(14)	90	90	90
γ/°	90	90	90	90
V/Å^3	1332.50(15)	3083.6(3)	3207.32(14)	965.06(5)
Z	2	4	4	4
ρ_{calc}/g cm^{-3}	1.195	1.210	1.324	1.556
μ/mm^{-1}	1.878	1.721	3.070	5.338
Max. and min. transmission	0.7543 and 0.5780	0.7536 and 0.6107	0.7536 and 0.6332	0.7543 and 0.5764
F(000)	516.0	1208.0	1352.0	456.0
Crystal color and shape	colorless, prism	yellow, lath	colorless, prism	colorless, block
Crystal size/mm^3	0.655×0.634×0.502	0.644×0.628×0.384	0.314×0.283×0.221	0.337×0.312×0.294
2θ range for data collection /°	8.952 to 161.056	7.368 to 145.612	8.84 to 144.914	10.594 to 161.068
Index ranges	$-13 \le h \le 13$, $-15 \le k \le 14$, $-14 \le l \le 14$	$-13 \le h \le 13$, $-19 \le k \le 19$, $-22 \le l \le 22$	$-13 \le h \le 13$, $-13 \le k \le 13$, $-34 \le l \le 32$	$-20 \le h \le 20$, $-7 \le k \le 7$, $-12 \le l \le 12$
Reflections collected	31499	60068	45989	25154
Reflections [R_{int}]	5643 [0.0313]	6006 [0.0411]	3167 [0.0835]	2073 [0.0457]
Data completeness (%)	99.5 to 2θ = 135.500°	97.6 to 2θ = 135.358°	99.2 to 2θ = 135.500°	97.6 to 2θ = 135.358°
Data/restraints/parameters	5643/1/300	6006/981/483	3167/20/208	2073/0/114
Goodness-of-fit on F^2	1.034	1.137	1.054	1.145
Final R indices [$I > 2\sigma(I)$]	R_1 = 0.0271, wR_2 = 0.0709	R_1 = 0.0437, wR_2 = 0.1133	R_1 = 0.0278, wR_2 = 0.0741	R_1 = 0.0656, wR_2 = 0.1579
Final R indices [all data]	R_1 = 0.0273, wR_2 = 0.0711	R_1 = 0.0440, wR_2 = 0.1137	R_1 = 0.0280, wR_2 = 0.0744	R_1 = 0.0662, wR_2 = 0.1581
Largest diff. peak/hole (e Å^{-3})	0.346/−0.258	0.477/−0.282	0.253/−0.190	0.475/−0.632
Flack parameter x	0.014(9)	0.029(4)	−0.007(5)	0.050(18)
Extinction coefficient	0.0090(10)	0.0130(15)	-	0.014(2)

Appendix II: NMR Spectra, HPLC Chromatograms of Chapter 3

^{1}H NMR ($CDCl_3$, 400 MHz) of compound **3.8a**

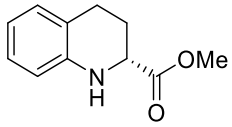

3.8a

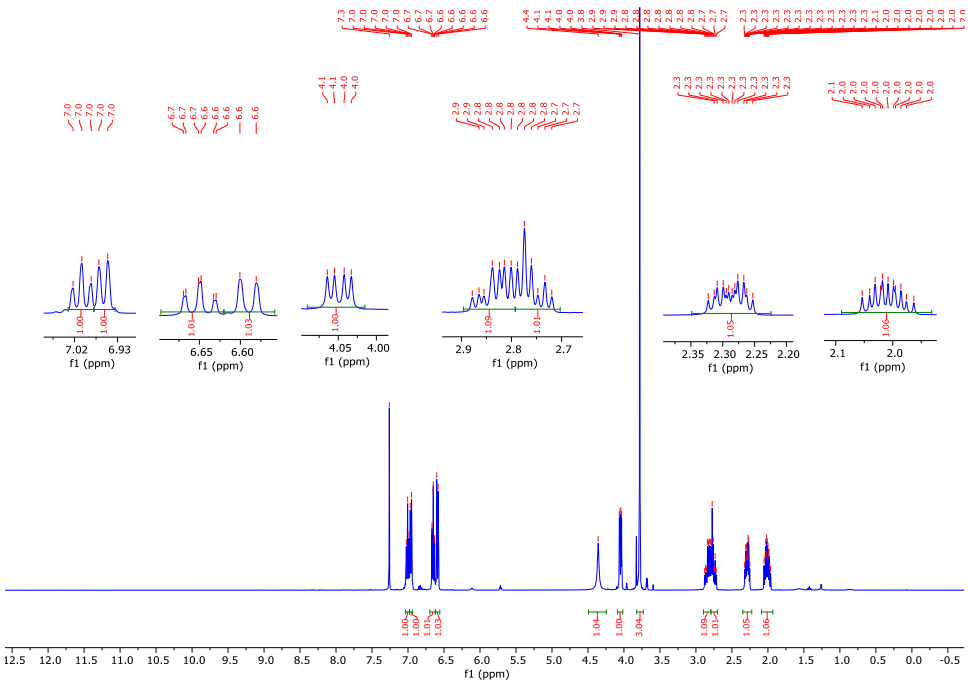

^{13}C NMR ($CDCl_3$, 101 MHz) of compound **3.8a**

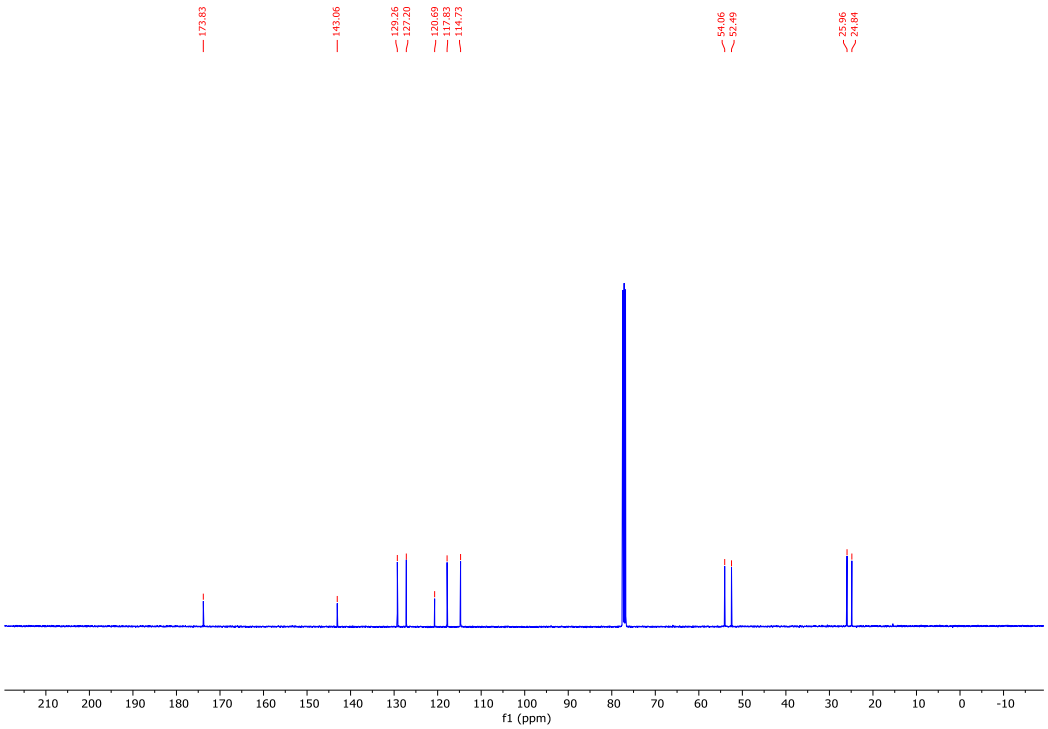

Chiral HPLC Chromatograms of **3.8a**

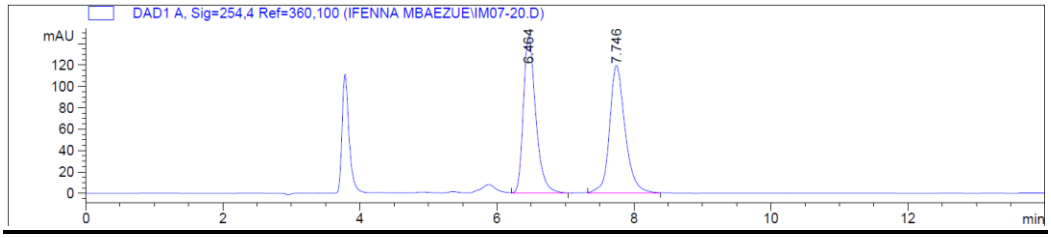

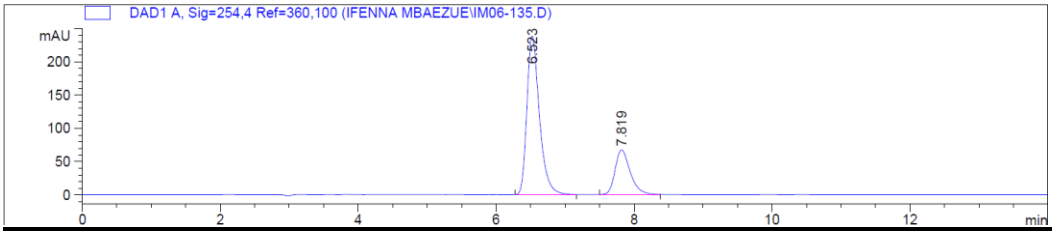

Peak #	RetTime [min]	Type	Width [min]	Area [mAU*s]	Height [mAU]	Area %
1	6.464	VB	0.1902	1836.71472	146.56891	49.4534
2	7.746	BB	0.2377	1877.31531	119.22342	50.5466

Peak #	RetTime [min]	Type	Width [min]	Area [mAU*s]	Height [mAU]	Area %
1	6.523	BB	0.1914	3015.92383	238.72182	74.4572
2	7.819	BB	0.2329	1034.62195	67.48457	25.5428

^{1}H NMR ($CDCl_3$, 500 MHz) of compound **3.8b**

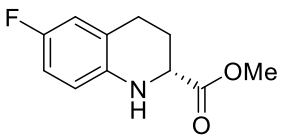

3.8b

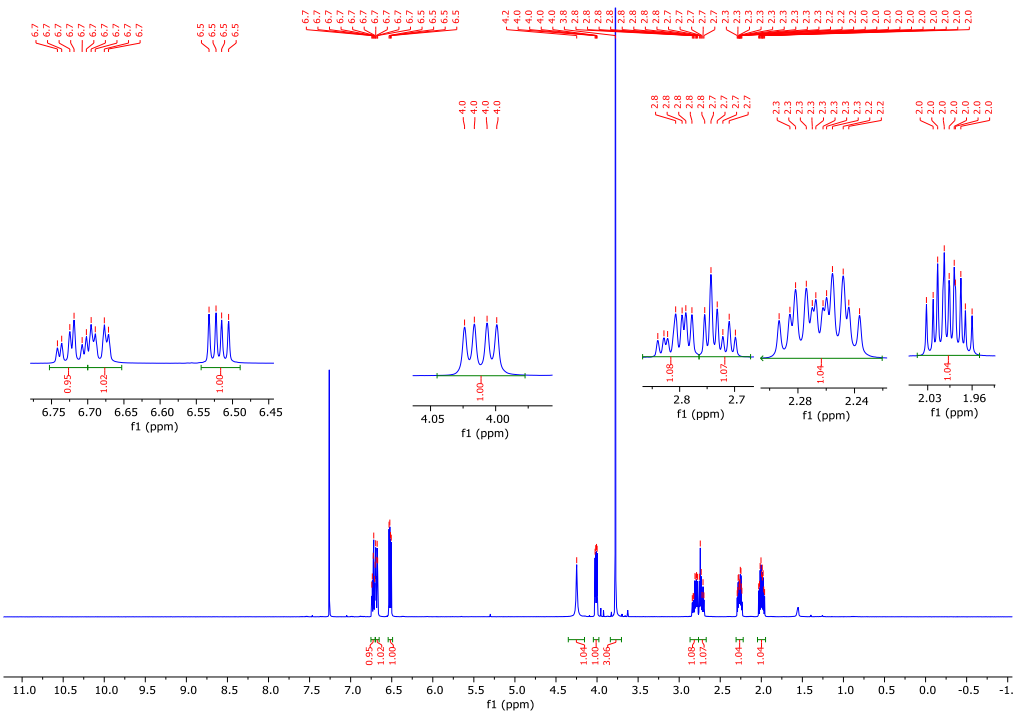

^{13}C NMR ($CDCl_3$, 126 MHz)of compound **3.8b**

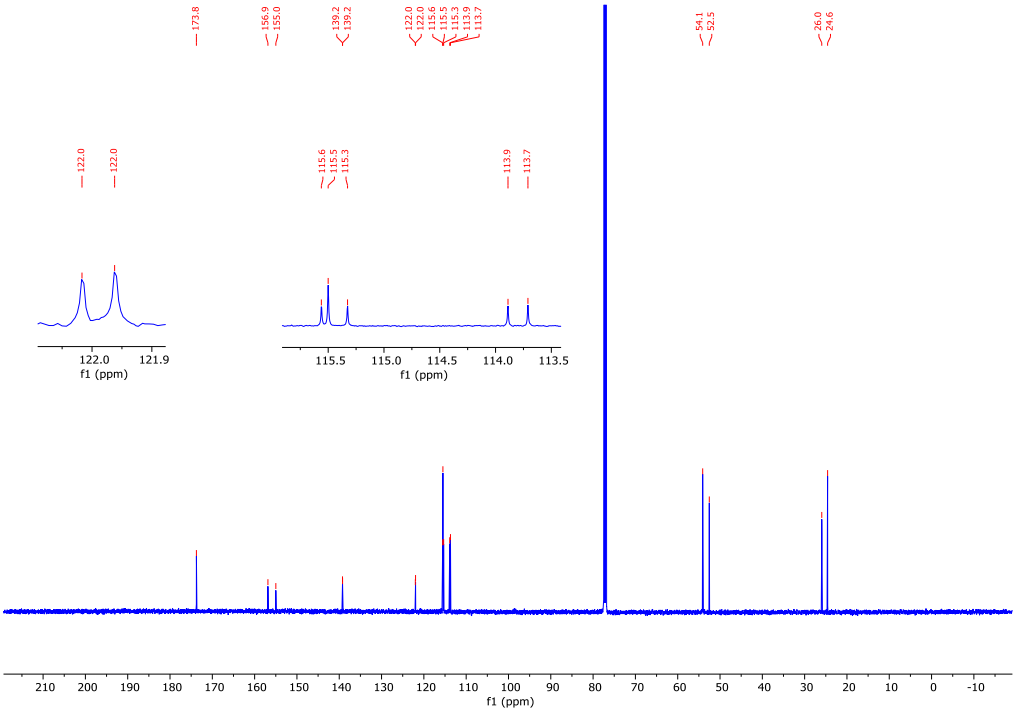

^{19}F NMR ($CDCl_3$, 471 MHz) of compound **3.8b**

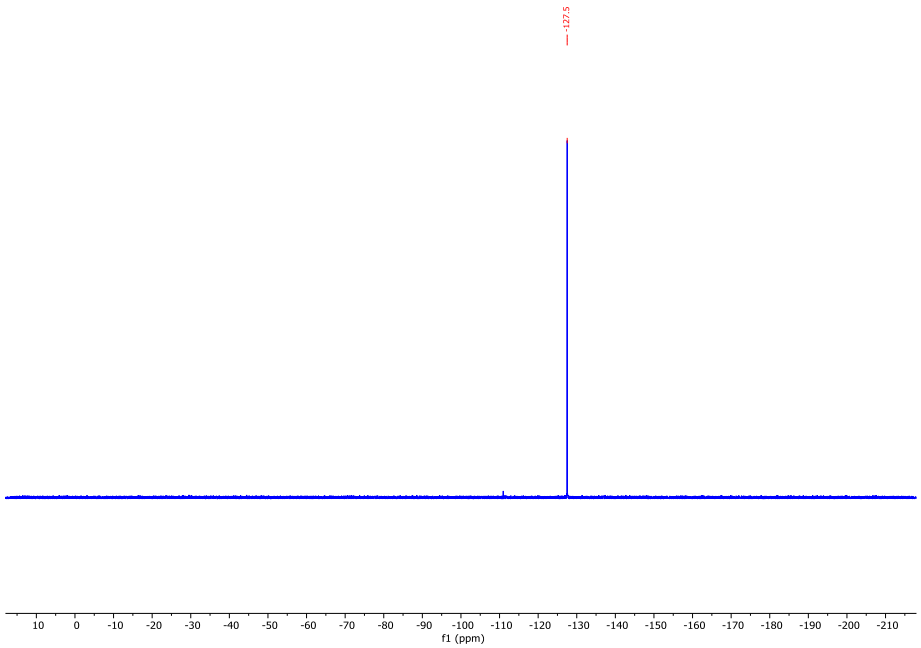

Chiral HPLC Chromatograms of **3.8b**

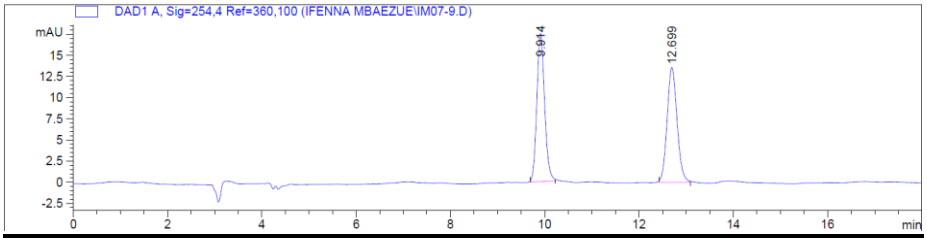

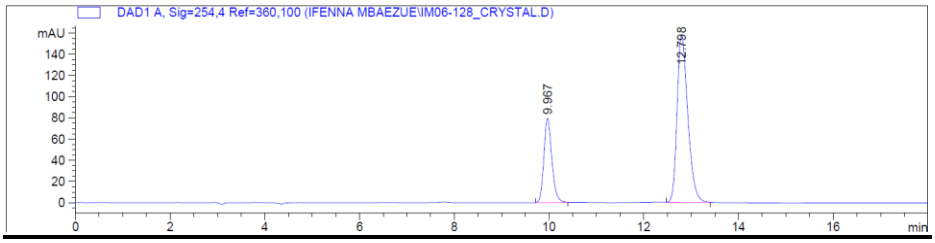

Peak #	RetTime [min]	Type	Width [min]	Area [mAU*s]	Height [mAU]	Area %
1	9.914	BB	0.1774	200.36966	17.51891	50.1694
2	12.699	BB	0.2268	199.01665	13.59466	49.8306

Peak #	RetTime [min]	Type	Width [min]	Area [mAU*s]	Height [mAU]	Area %
1	9.967	BB	0.1790	935.77582	79.66815	27.3511
2	12.798	BB	0.2394	2485.57617	158.13461	72.6489

^{1}H NMR ($CDCl_3$, 500 MHz) of compound **3.8c**

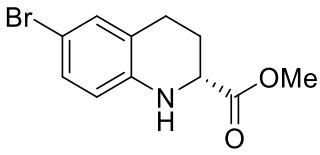

3.8c

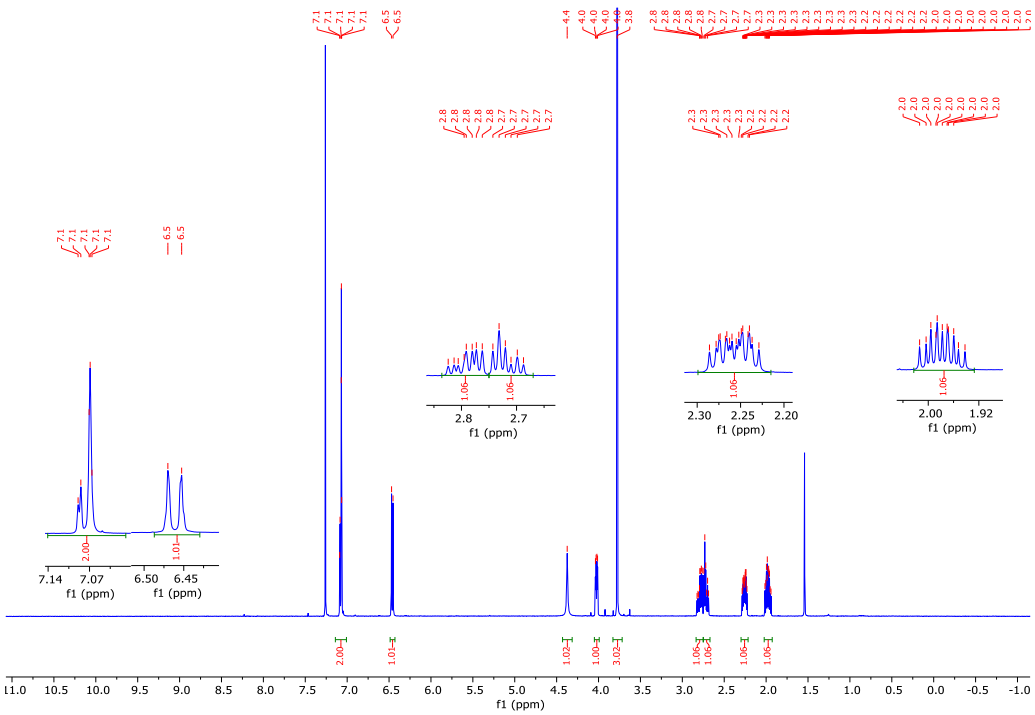

^{13}C NMR ($CDCl_3$, 126 MHz) of compound **3.8c**

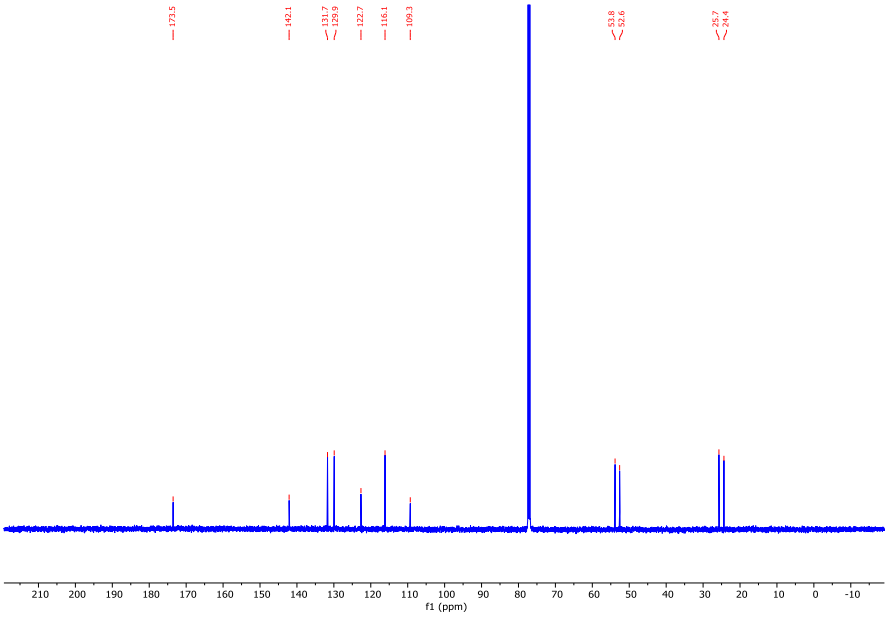

Chiral HPLC Chromatograms of 3.8c

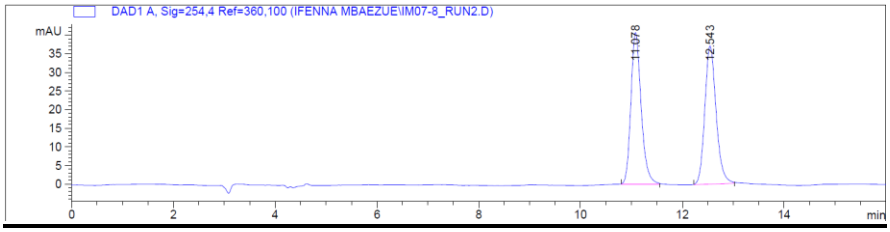

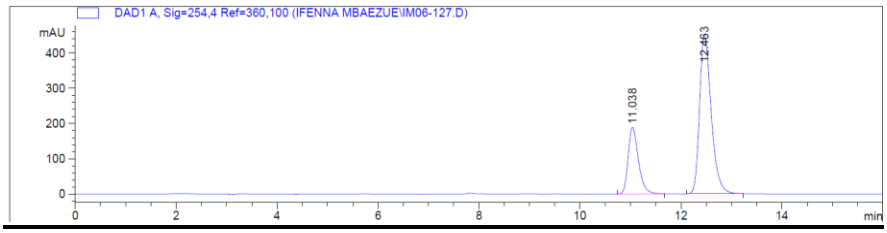

Peak #	RetTime [min]	Type	Width [min]	Area [mAU*s]	Height [mAU]	Area %
1	11.078	BB	0.2138	571.73297	40.72522	50.0334
2	12.543	BB	0.2355	570.97064	37.10265	49.9666

Peak #	RetTime [min]	Type	Width [min]	Area [mAU*s]	Height [mAU]	Area %
1	11.038	BB	0.2150	2678.41431	189.39082	26.9677
2	12.463	BB	0.2445	7253.51611	453.70108	73.0323

After Recrystallization:

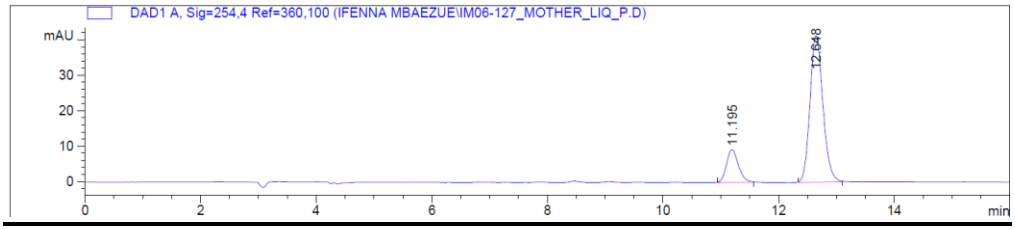

Peak #	RetTime [min]	Type	Width [min]	Area [mAU*s]	Height [mAU]	Area %
1	11.195	BB	0.2183	132.32381	9.28285	17.1056
2	12.648	BB	0.2389	641.24689	41.36087	82.8944

^{1}H NMR ($CDCl_3$, 400 MHz) of **(*R*)-*N*-(tert-butyl(2-methoxynaphthalen-1-yl)phosphoryl)-4-methylbenzenesulfonamide**

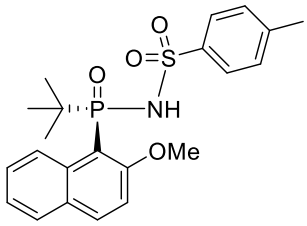

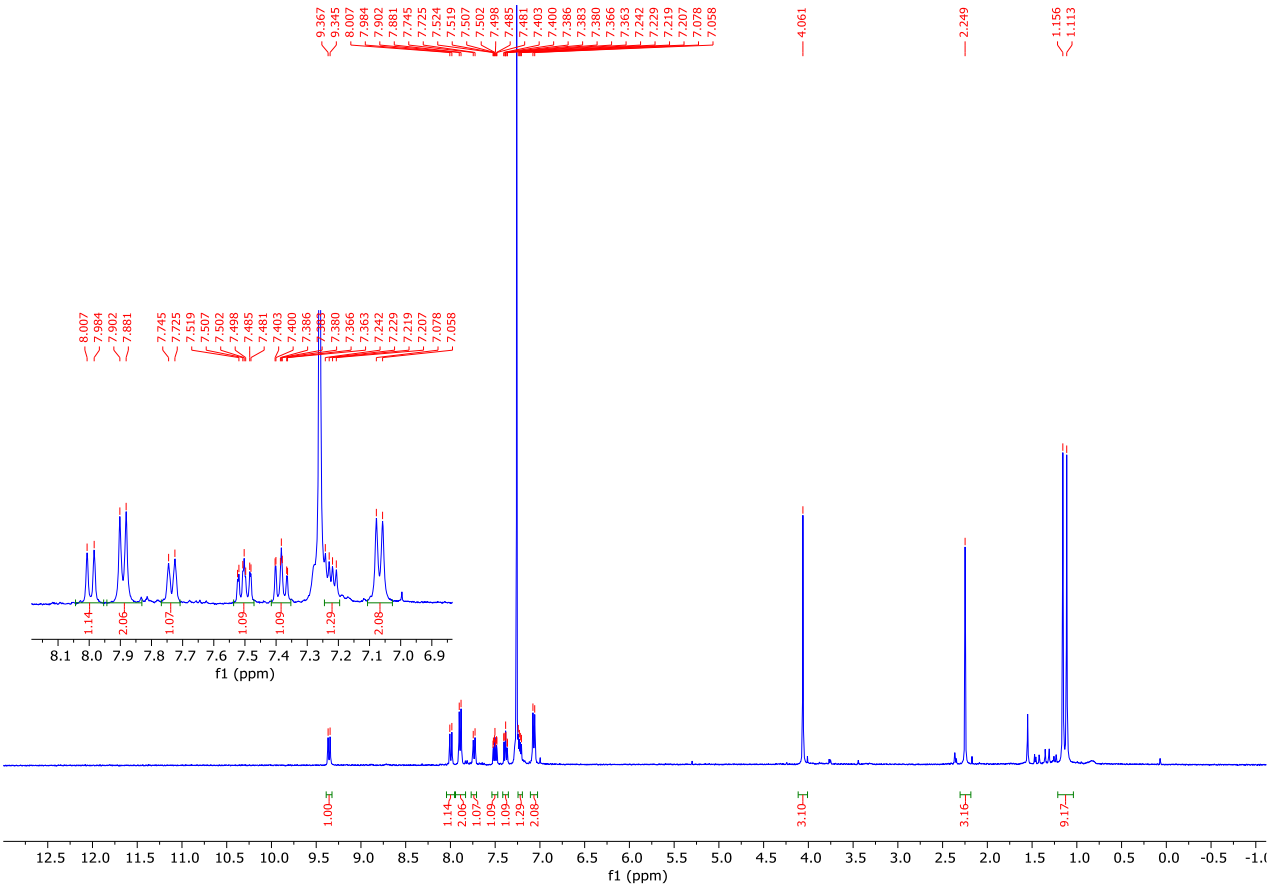

^{13}C NMR ($CDCl_3$, 126 MHz) of **(*R*)-*N*-(tert-butyl(2-methoxynaphthalen-1-yl)phosphoryl)-4-methylbenzenesulfonamide**

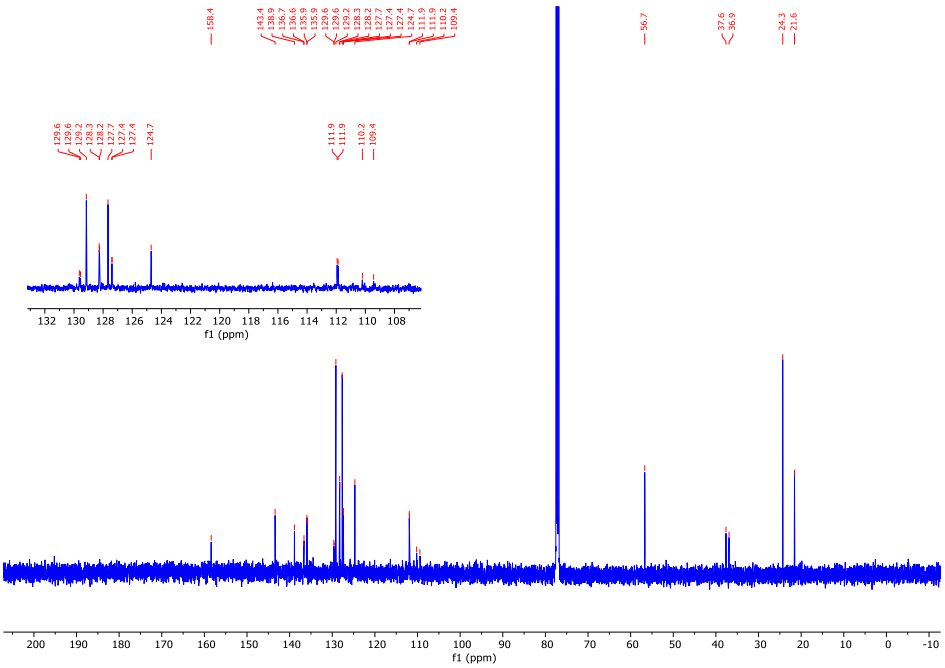

^{31}P NMR ($CDCl_3$, 162 MHz) of **(*R*)-*N*-(tert-butyl(2-methoxynaphthalen-1-yl)phosphoryl)-4-methylbenzenesulfonamide**

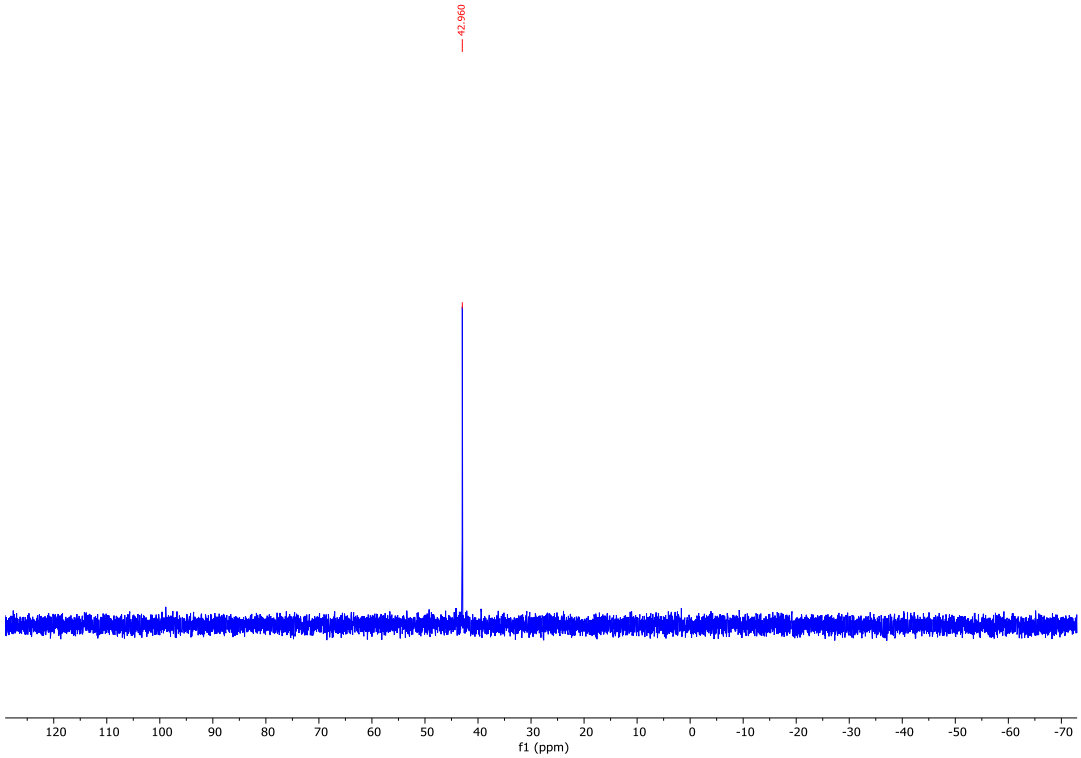

(*R*)-*N*-(tert-butyl(2-hydroxynaphthalen-1-yl)phosphoryl)-4-methylbenzenesulfonamide (3.14a)

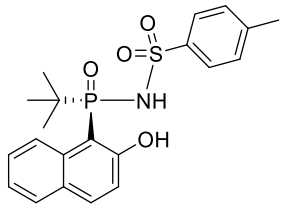

^{1}H NMR of ($CDCl_3$, 400 MHz) **3.14a**

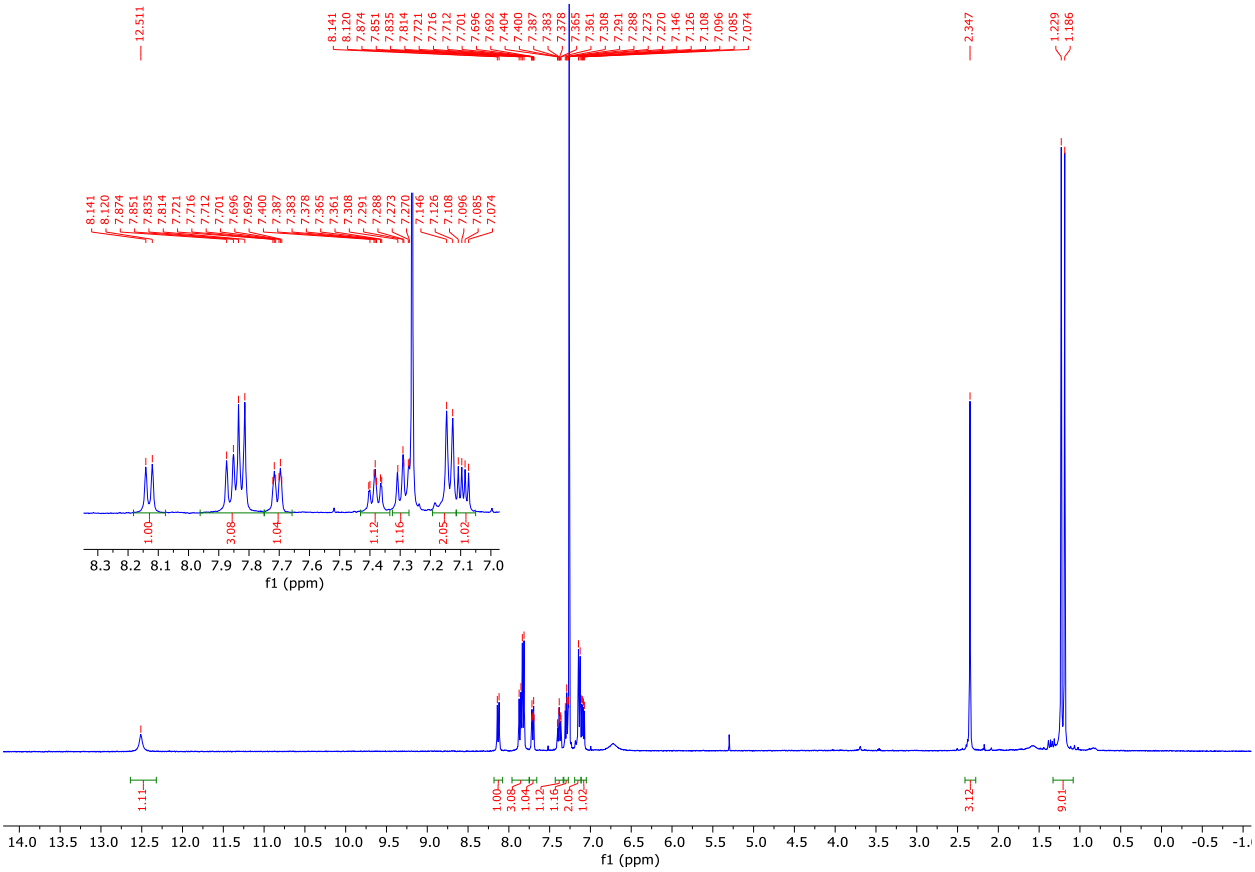

^{13}C NMR of ($CDCl_3$, 126 MHz) **3.14a**

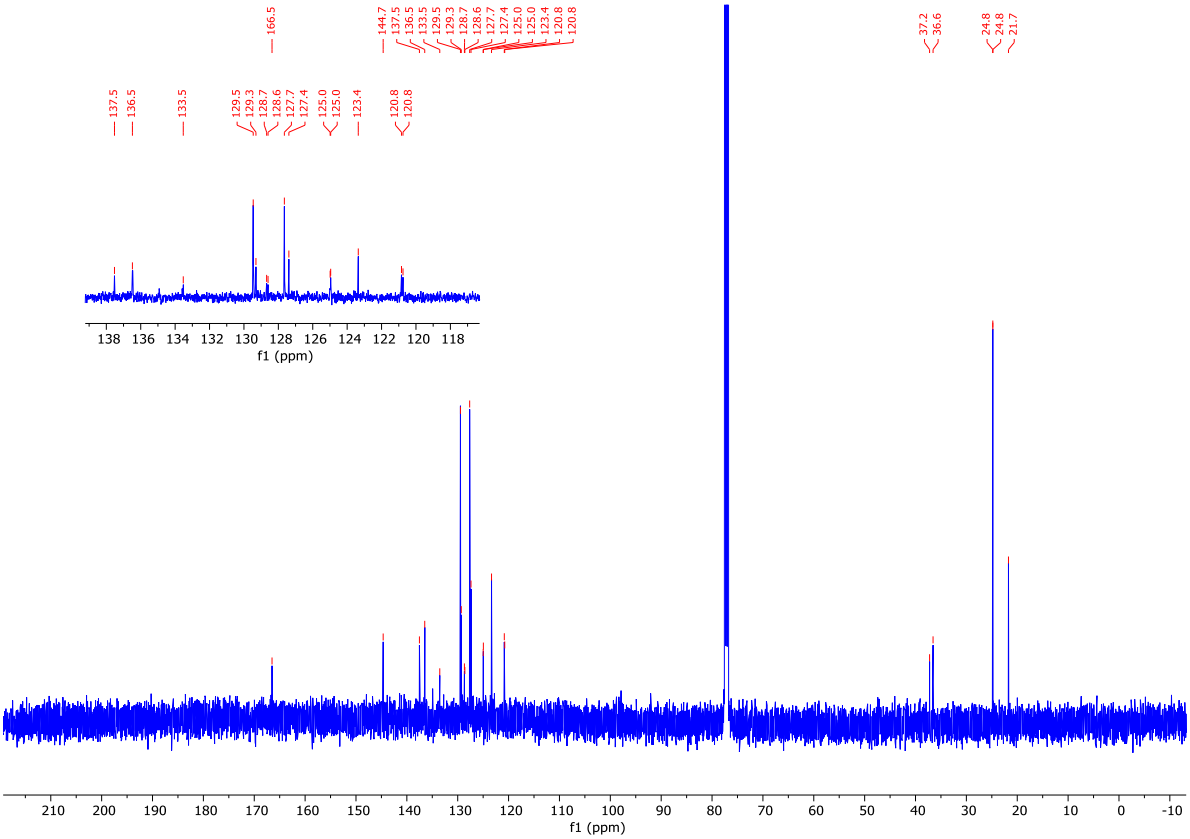

^{31}P NMR ($CDCl_3$, 162 MHz) of **3.14a**

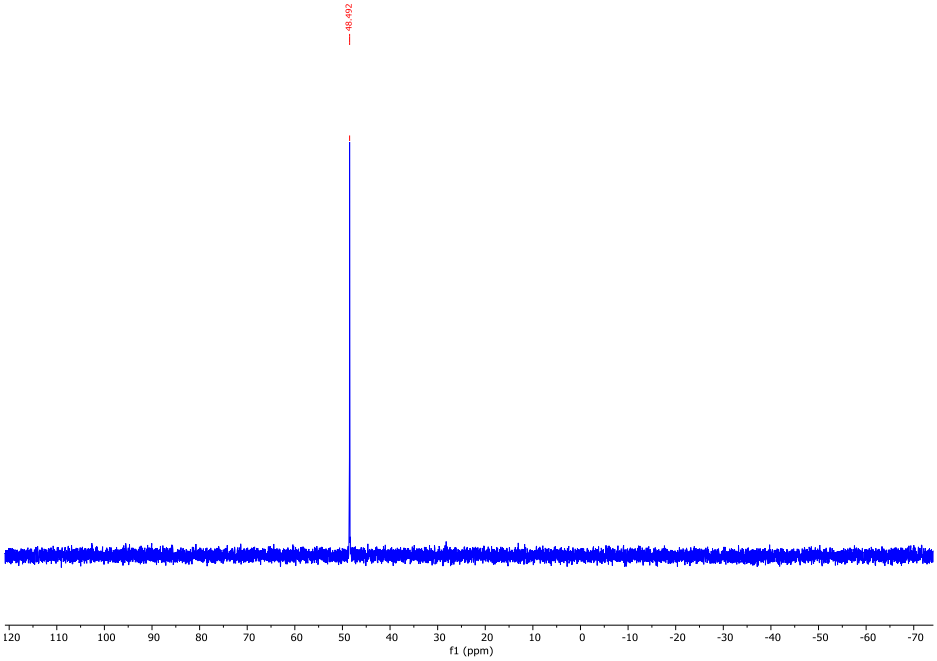

^{1}H NMR ($CDCl_3$, 400 MHz) of **(*R*)-*N*-(tert-butyl(2-methoxynaphthalen-1-yl)phosphoryl)-2,4,6-tricyclohexylbenzenesulfonamide**

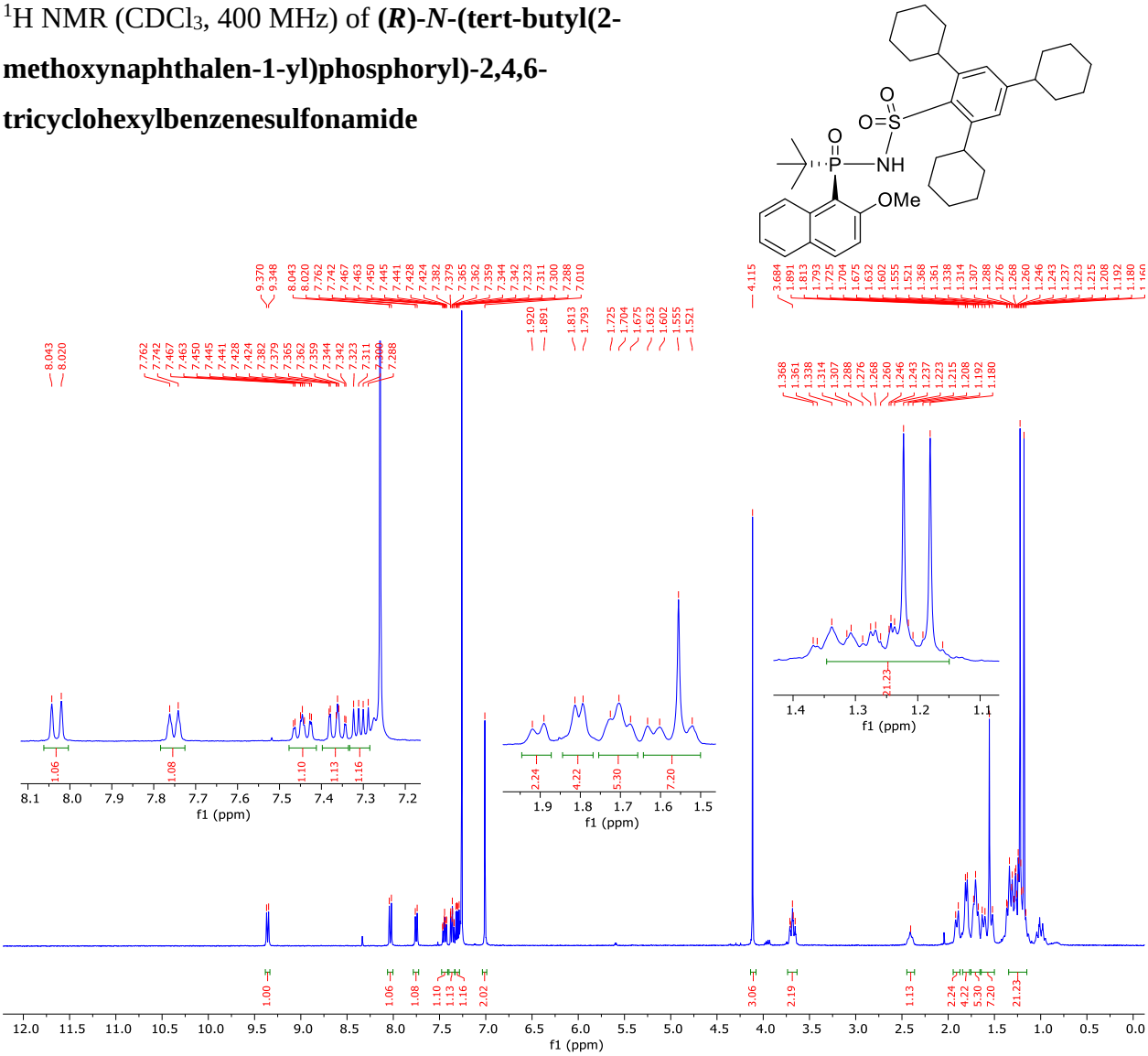

^{13}C NMR ($CDCl_3$, 126 MHz) of **(*R*)-*N*-(tert-butyl(2-methoxynaphthalen-1-yl)phosphoryl)-2,4,6-tricyclohexylbenzenesulfonamide**

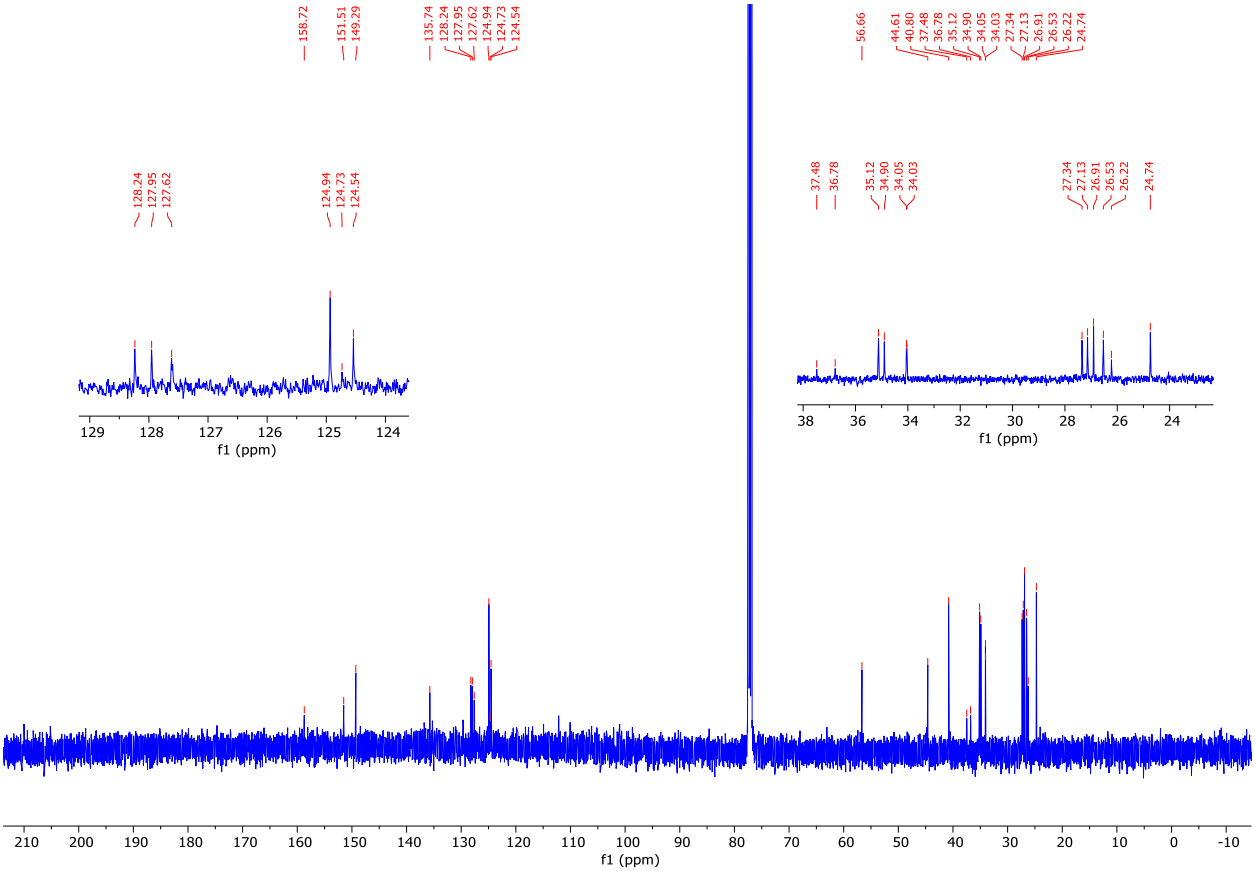

^{31}P NMR ($CDCl_3$, 162 MHz) of **(*R*)-*N*-(tert-butyl(2-methoxynaphthalen-1-yl)phosphoryl)-2,4,6-tricyclohexylbenzenesulfonamide**

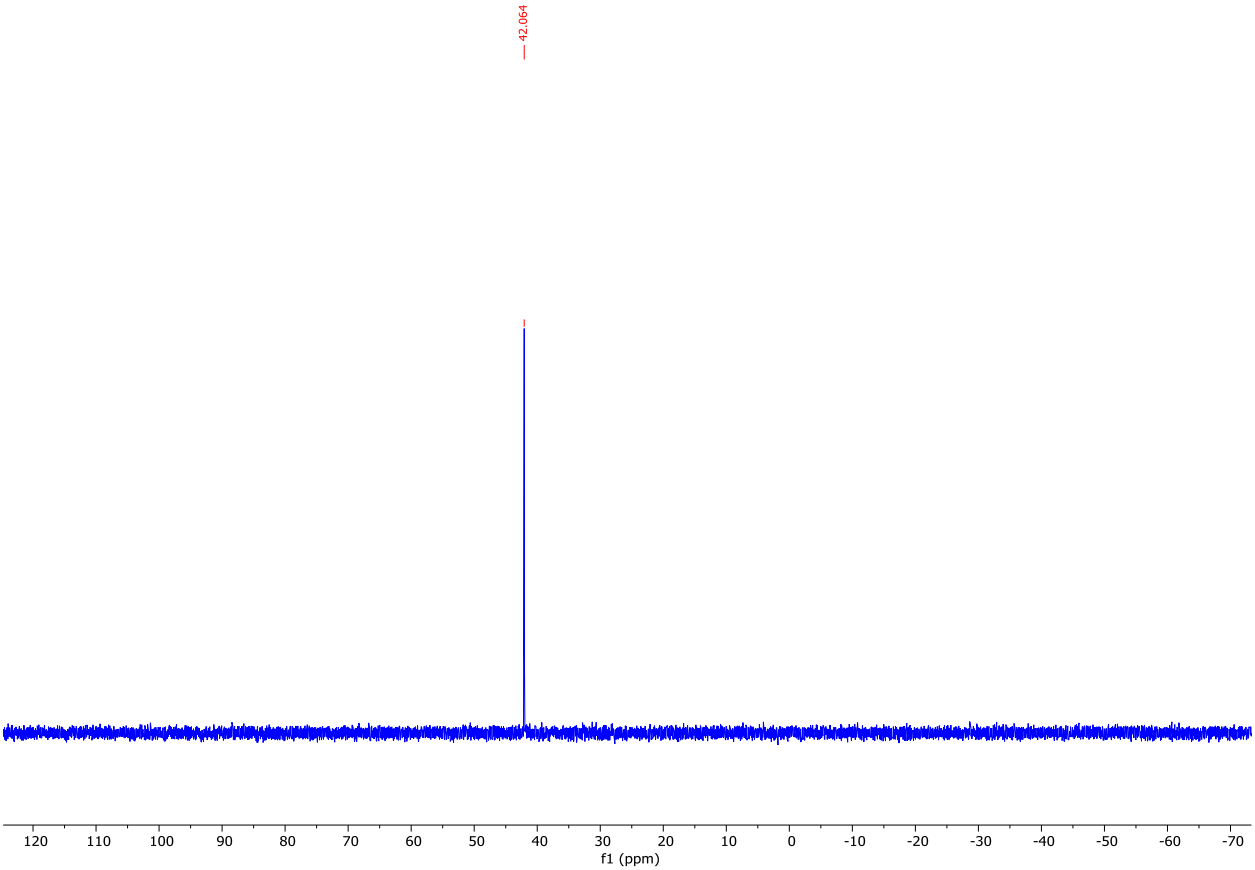

(*R*)-*N*-(tert-butyl(2-hydroxynaphthalen-1-yl)phosphoryl)-2,4,6-tricyclohexylbenzenesulfonamide (3.14c)

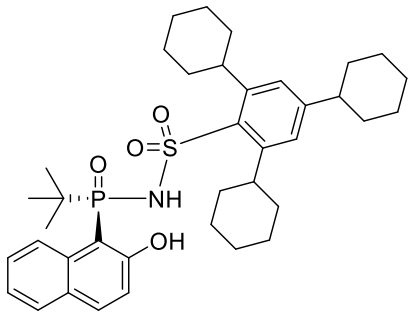

^{1}H NMR ($CDCl_3$, 400 MHz) of 3.14c

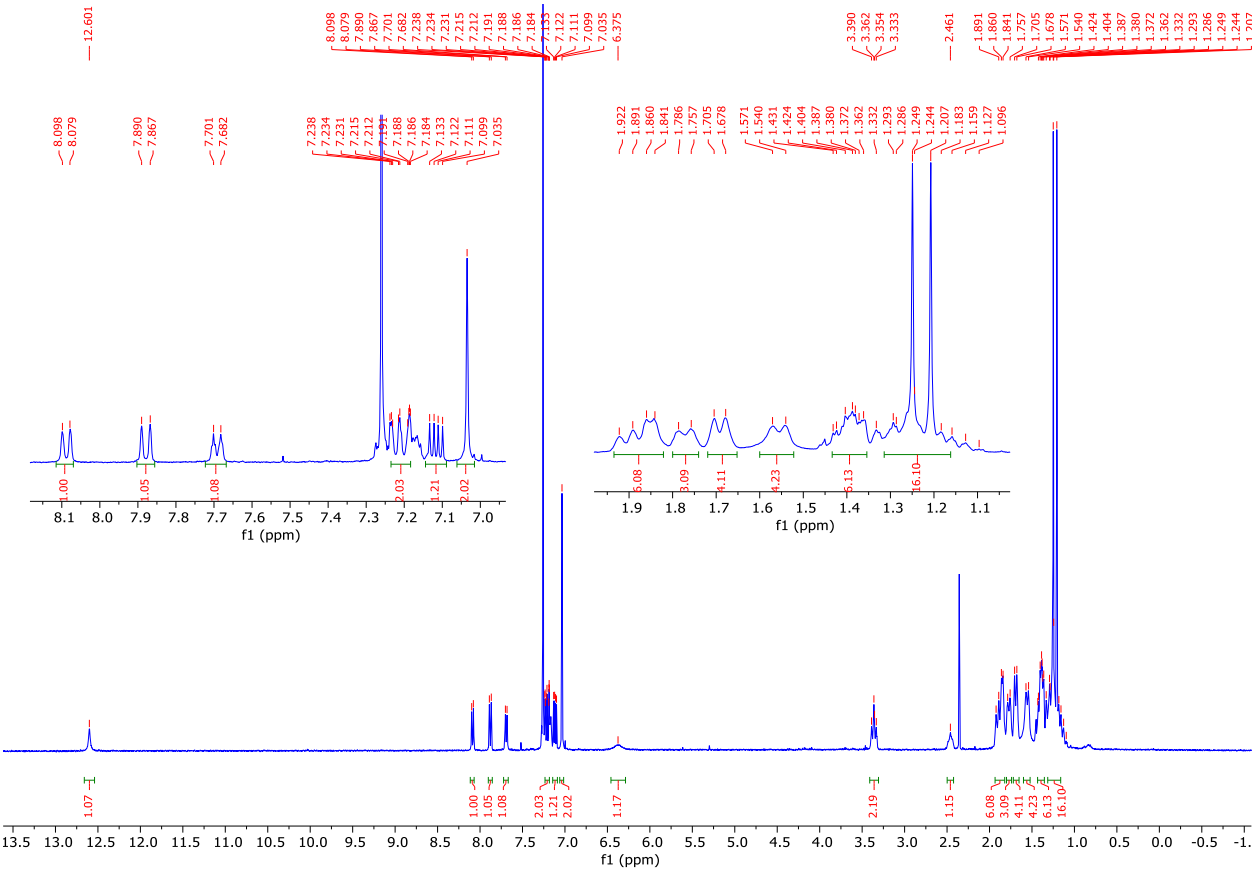

^{13}C NMR ($CDCl_3$, 126 MHz) of **3.14c**

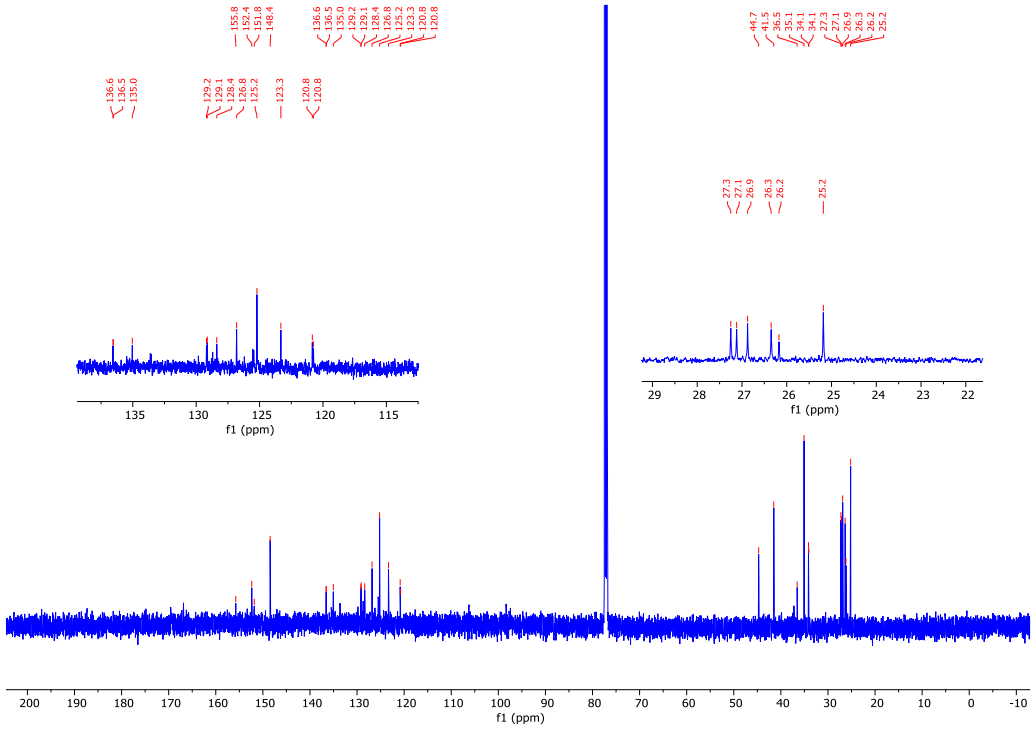

^{31}P NMR ($CDCl_3$, 162 MHz) of **3.14c**

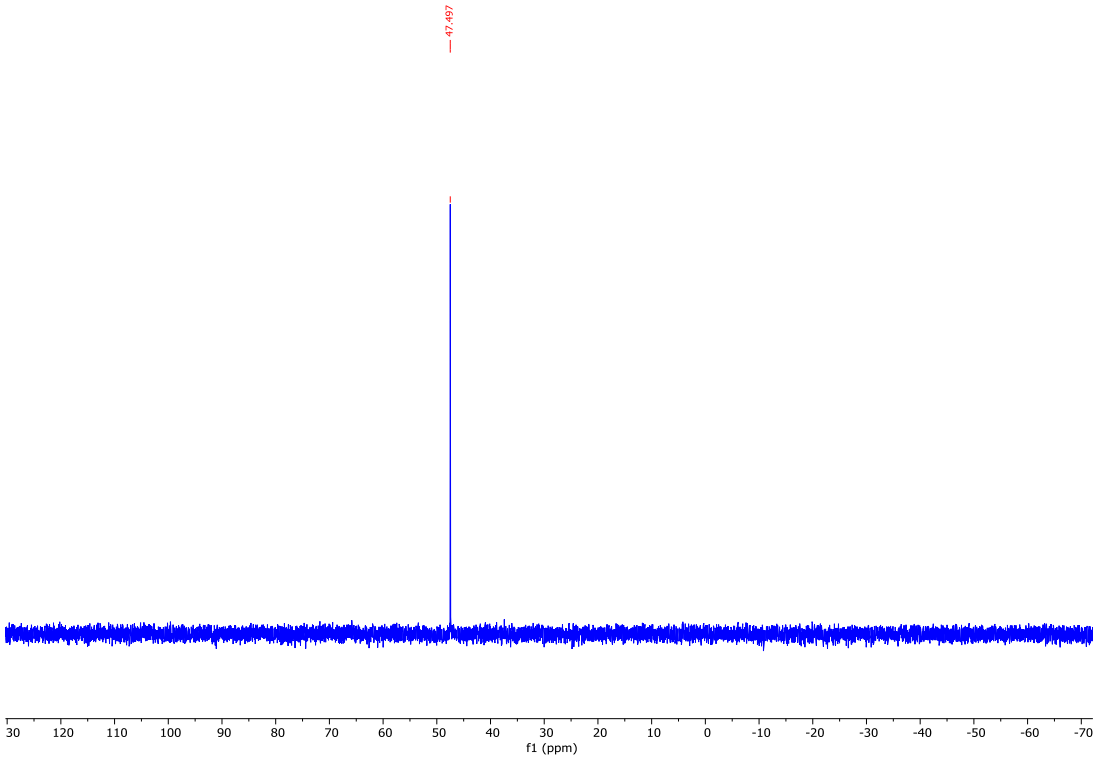

^{1}H NMR ($CDCl_3$, 400 MHz) of

(*R*)-*N*-(tert-butyl(2-methoxynaphthalen-1-yl)phosphoryl)-5'-phenyl-[1,1':3',1''-terphenyl]-2'-sulfonamide

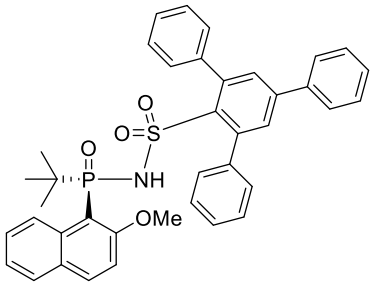

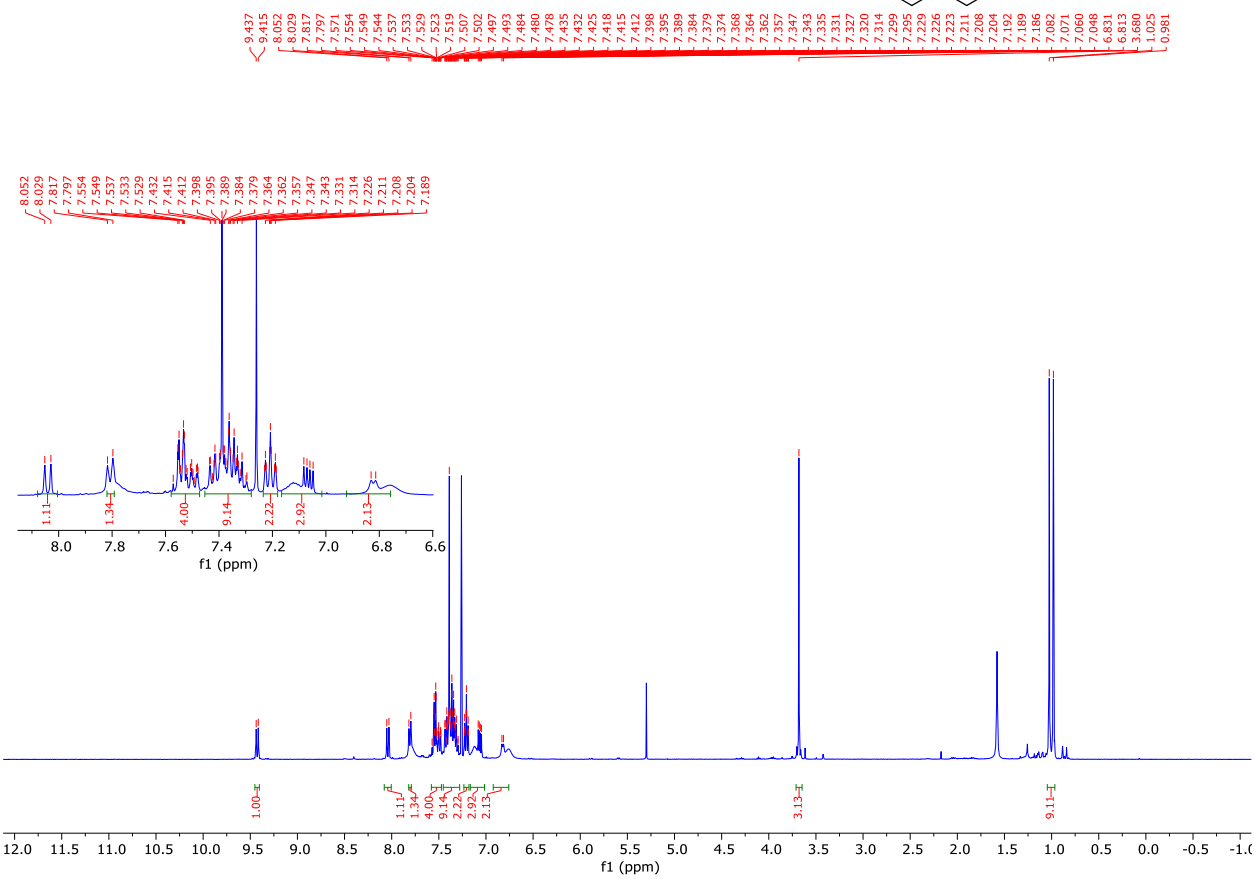

^{13}C NMR ($CDCl_3$, 126 MHz) of **(*R*)-*N*-(tert-butyl(2-methoxynaphthalen-1-yl)phosphoryl)-5'-phenyl-[1,1':3',1''-terphenyl]-2'-sulfonamide**

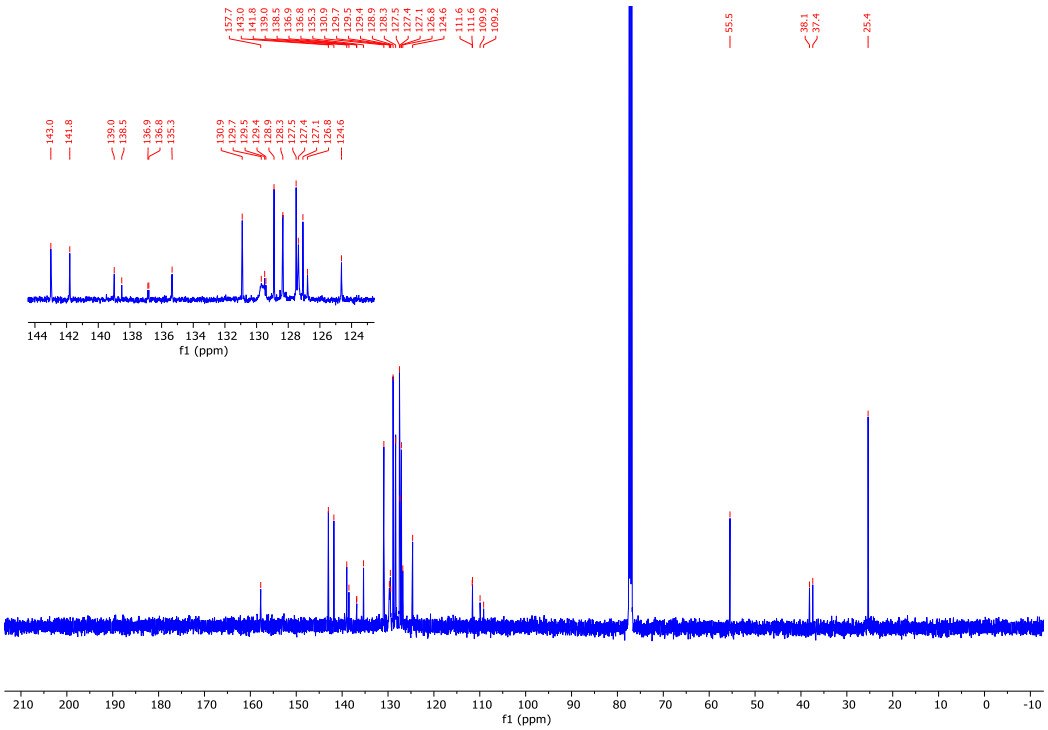

^{31}P NMR ($CDCl_3$, 162 MHz) of **(*R*)-*N*-(tert-butyl(2-methoxynaphthalen-1-yl)phosphoryl)-5'-phenyl-[1,1':3',1''-terphenyl]-2'-sulfonamide**

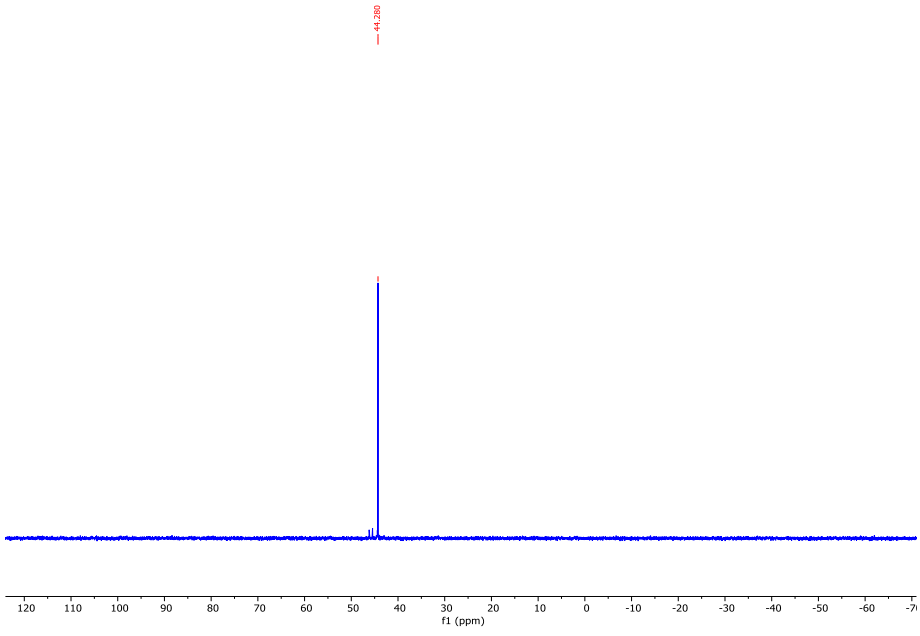

(R)-N-(tert-butyl(2-hydroxynaphthalen-1-yl)phosphoryl)-5'-phenyl-[1,1':3',1''-terphenyl]-2'-sulfonamide (3.14d)

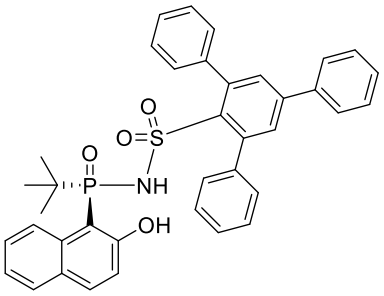

^{1}H NMR ($CDCl_3$, 400 MHz) of **3.14d**

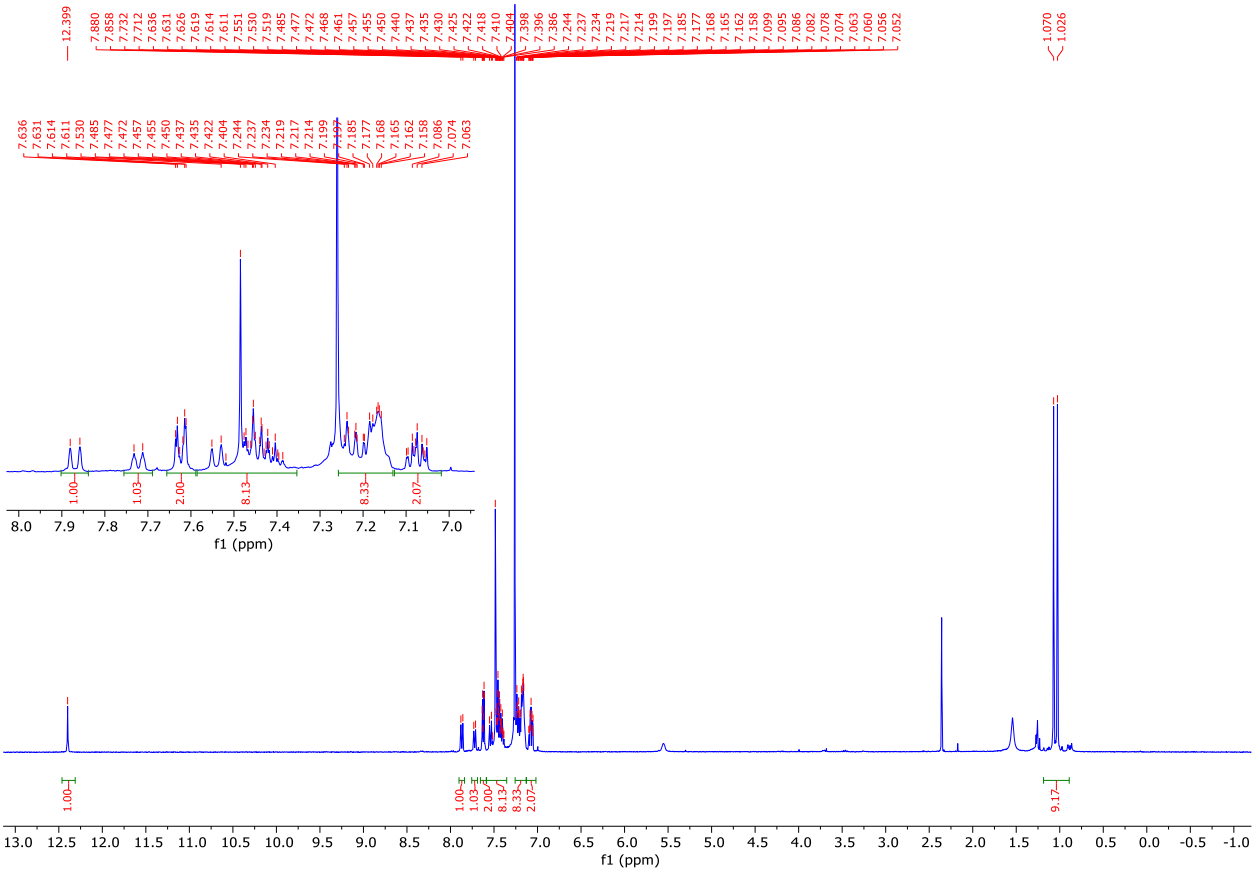

^{13}C NMR ($CDCl_3$, 126 MHz) of **3.14d**

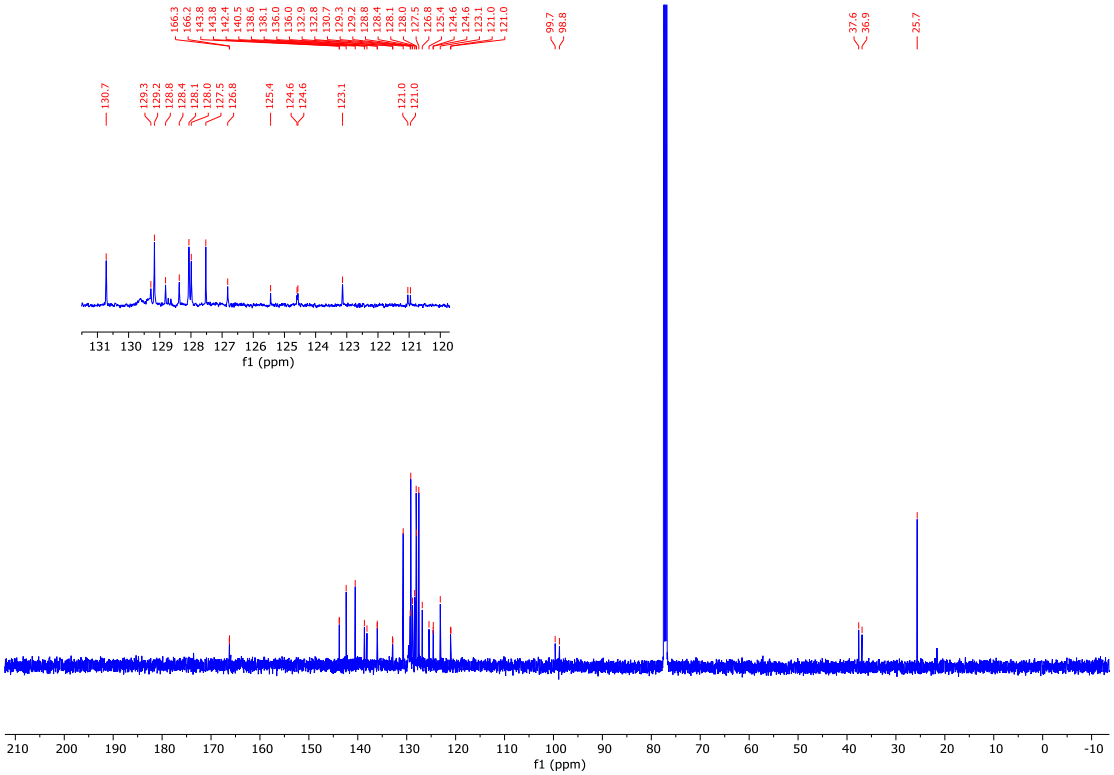

^{31}P NMR ($CDCl_3$, 162 MHz) of **3.14d**

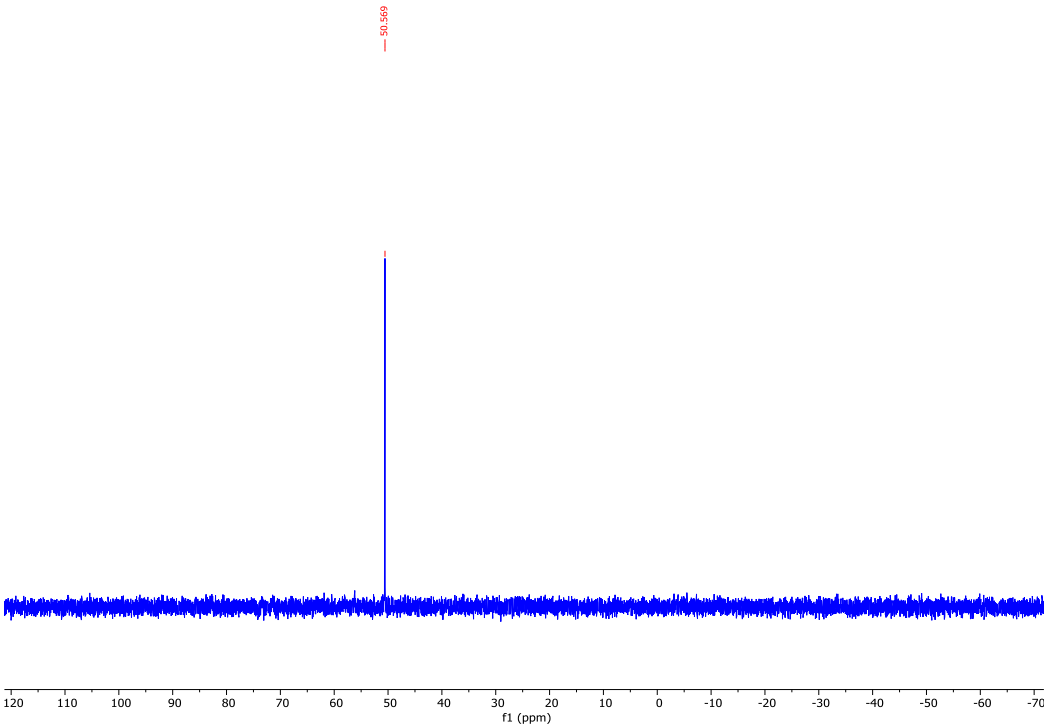

^{1}H NMR ($CDCl_3$, 500 MHz) of **(*R*)-*N*-(tert-butyl(2-methoxynaphthalen-1-yl)phosphoryl)phenanthrene-9-sulfonamide**

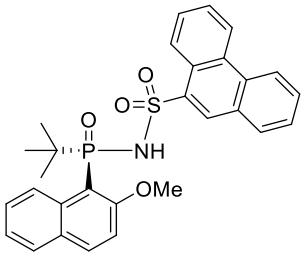

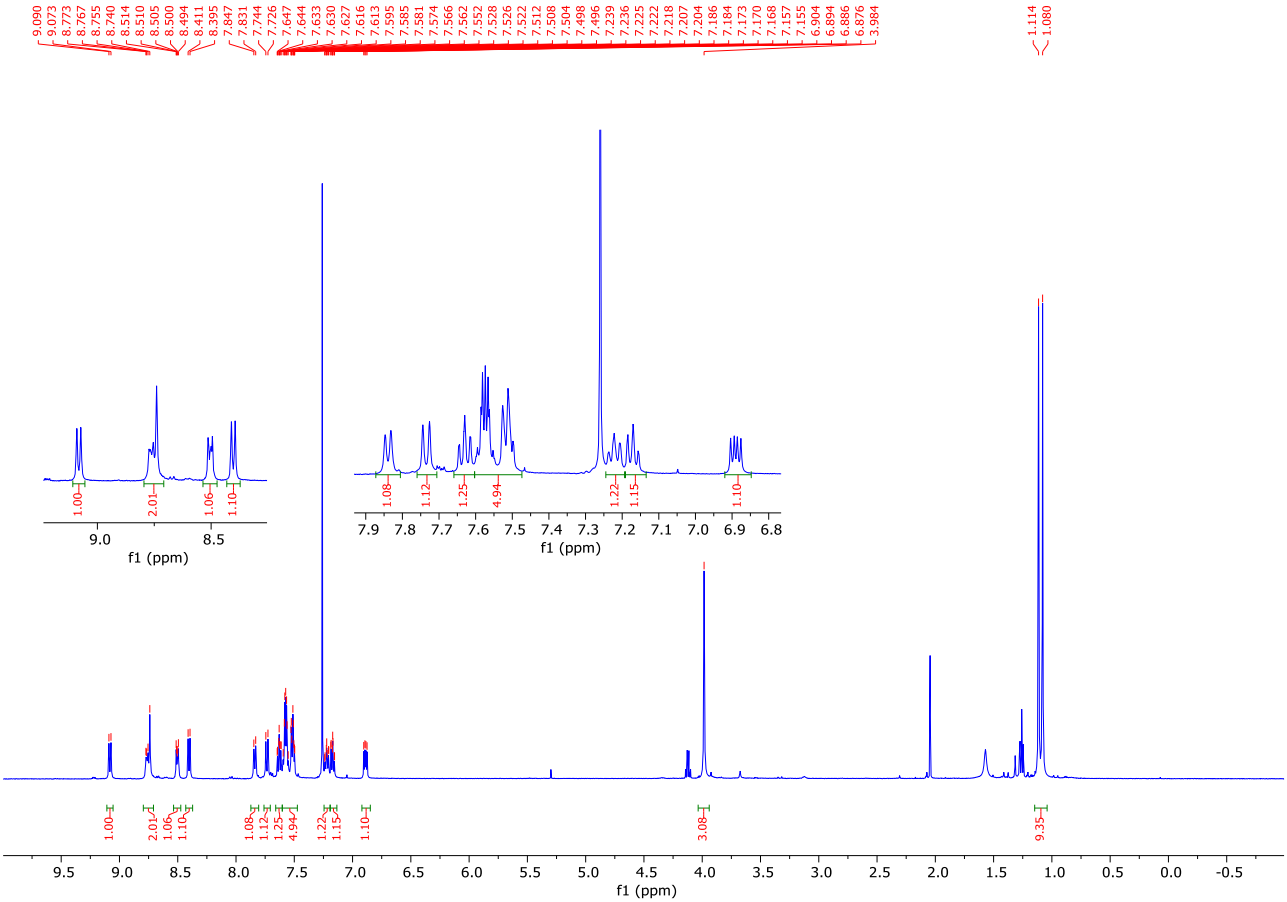

^{13}C NMR ($CDCl_3$, 126 MHz) of **(*R*)-*N*-(tert-butyl(2-methoxynaphthalen-1-yl)phosphoryl)phenanthrene-9-sulfonamide**

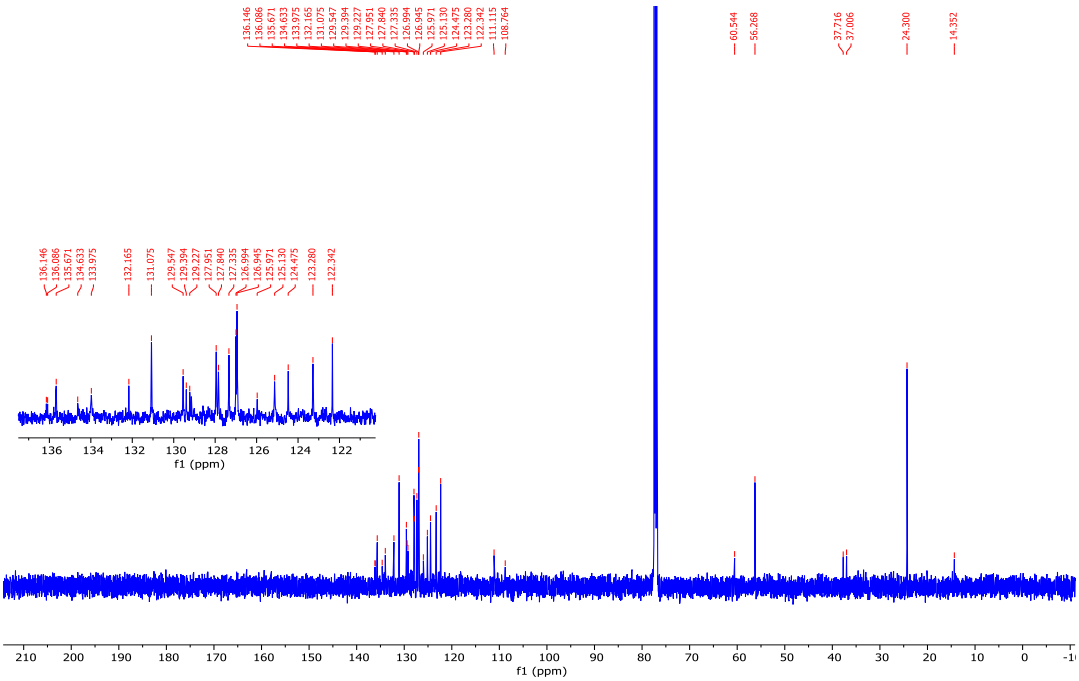

^{31}P NMR ($CDCl_3$, 203 MHz) of **(*R*)-*N*-(tert-butyl(2-methoxynaphthalen-1-yl)phosphoryl)phenanthrene-9-sulfonamide**

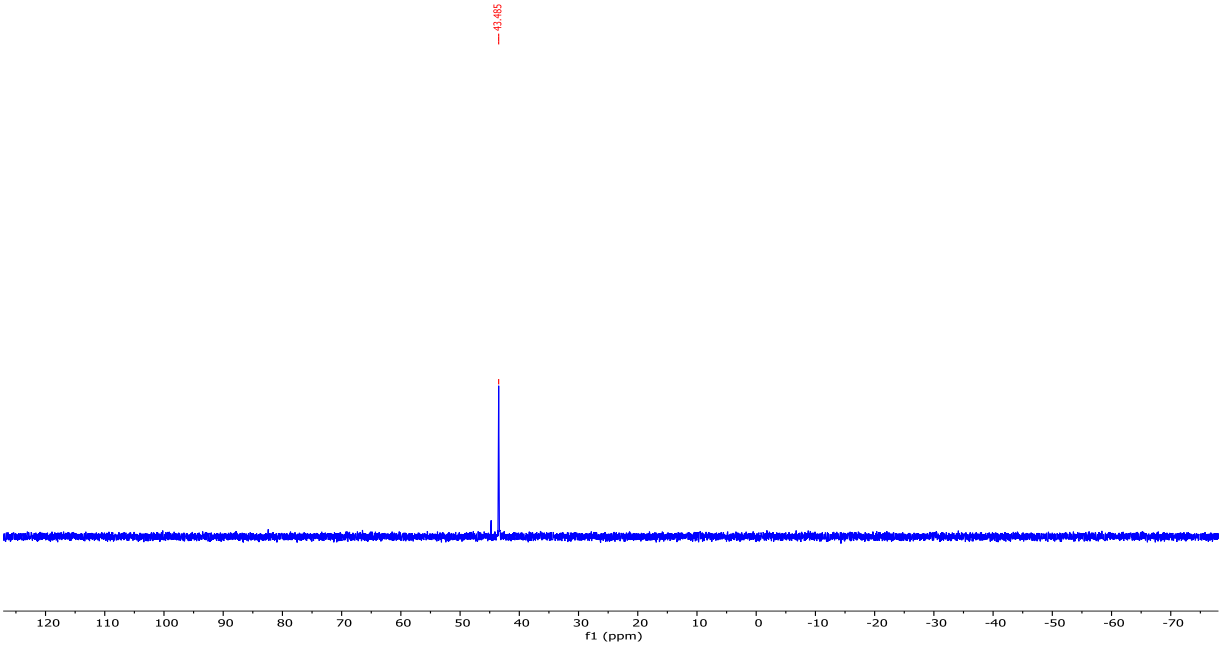

(R)-N-(tert-butyl(2-hydroxynaphthalen-1-yl)phosphoryl)phenanthrene-9-sulfonamide (3.14e)

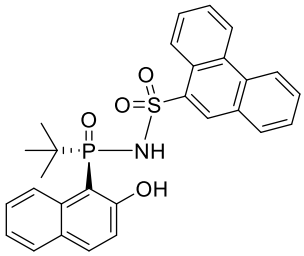

^{1}H NMR ($CDCl_3$, 500 MHz) of **compound 3.14e**

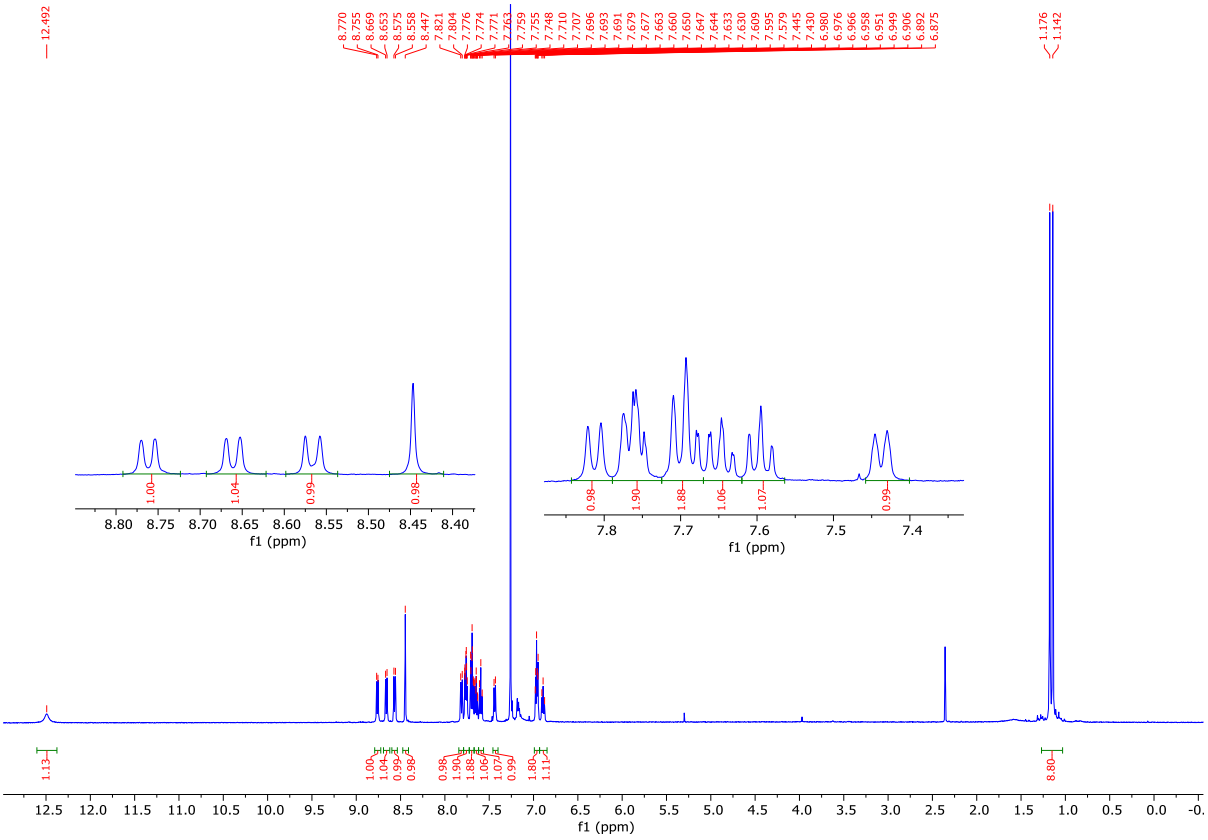

^{13}C NMR ($CDCl_3$, 201 MHz) of **compound 3.14e**

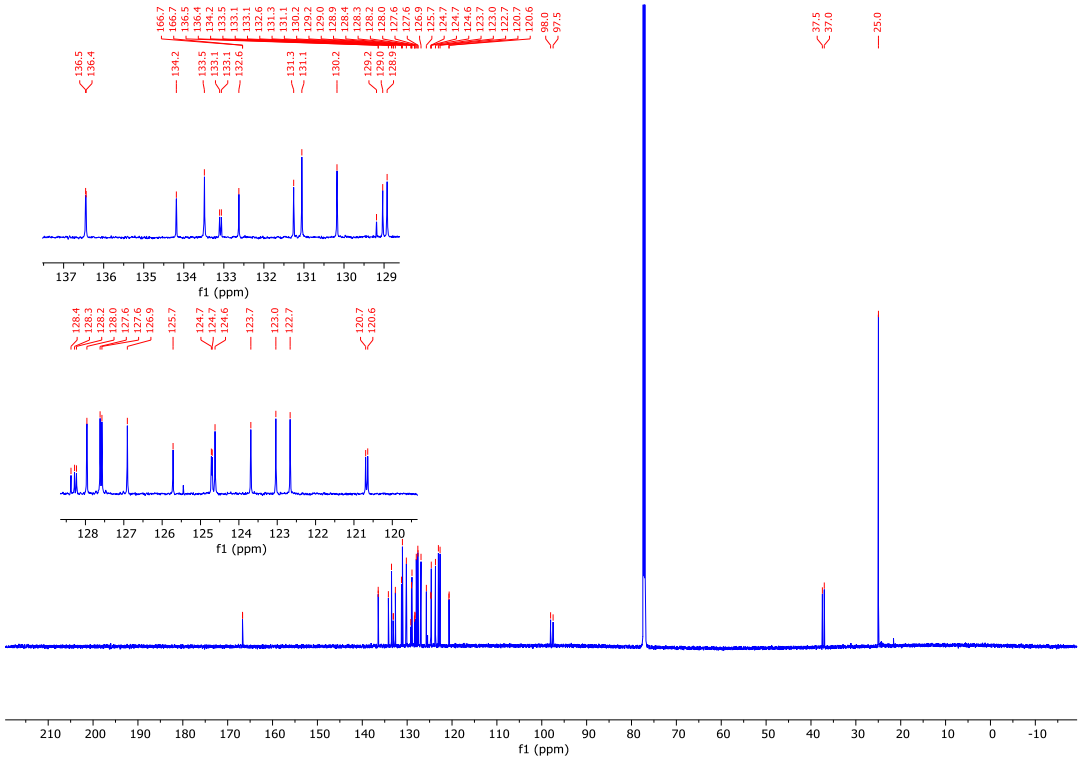

^{31}P NMR ($CDCl_3$, 203 MHz) of **compound 3.14e**

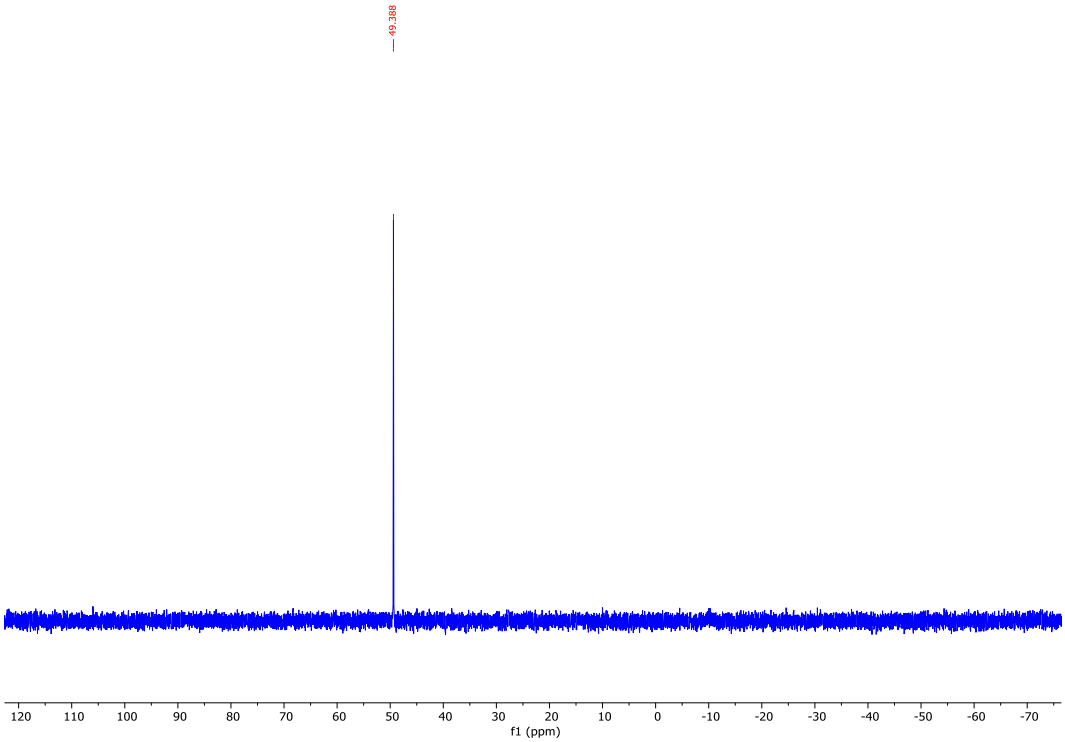

Naphthalen-2-yl P-(tert-butyl)-N-((2,4,6-triisopropylphenyl)sulfonyl)phosphonamidate (3.15)

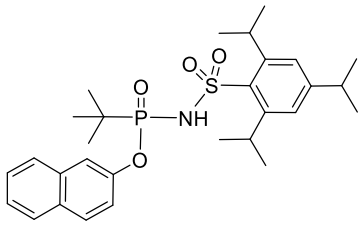

^{1}H NMR ($CDCl_3$, 500 MHz) of compound **3.15** at RT

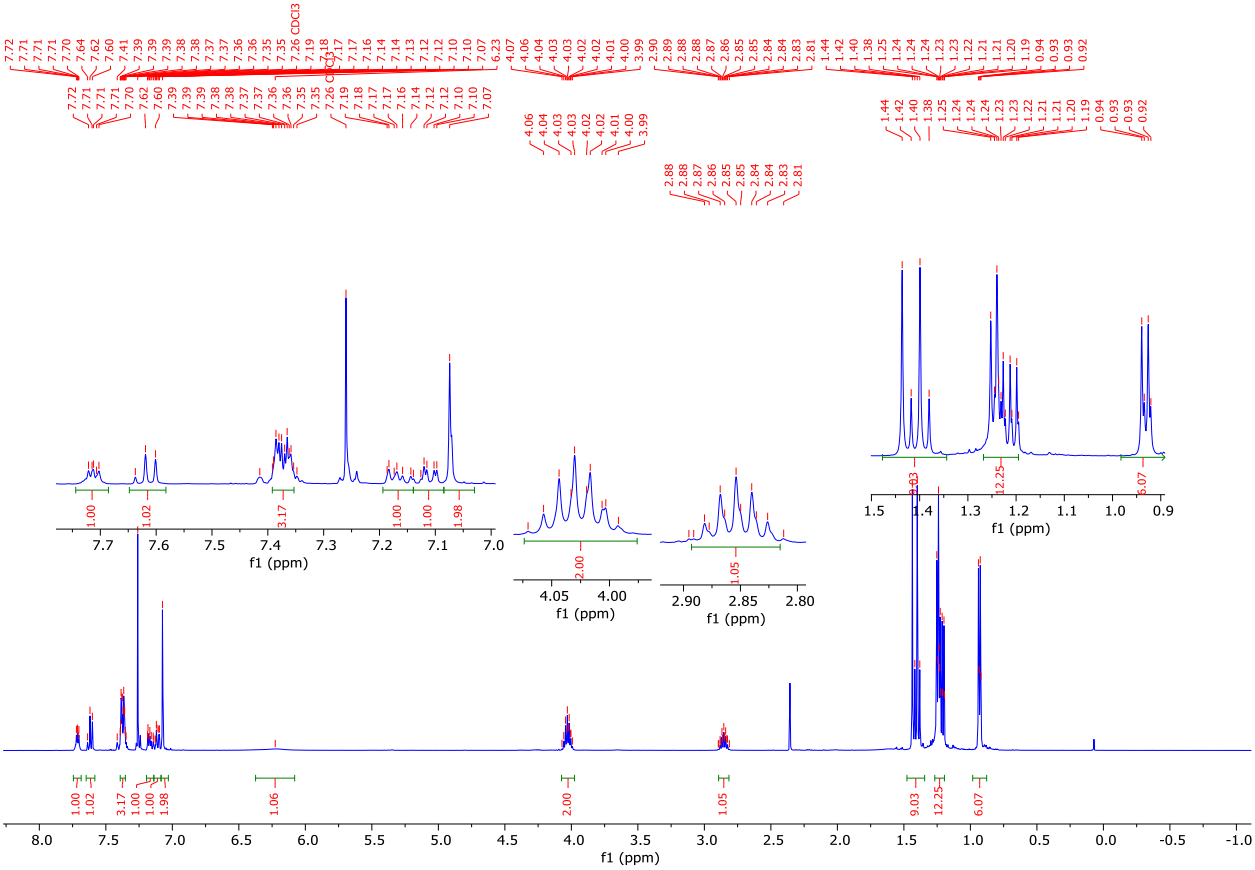

^{1}H NMR ($CDCl_3$, 400 MHz) of compound **3.15** at 50 °C showing peak coalescence

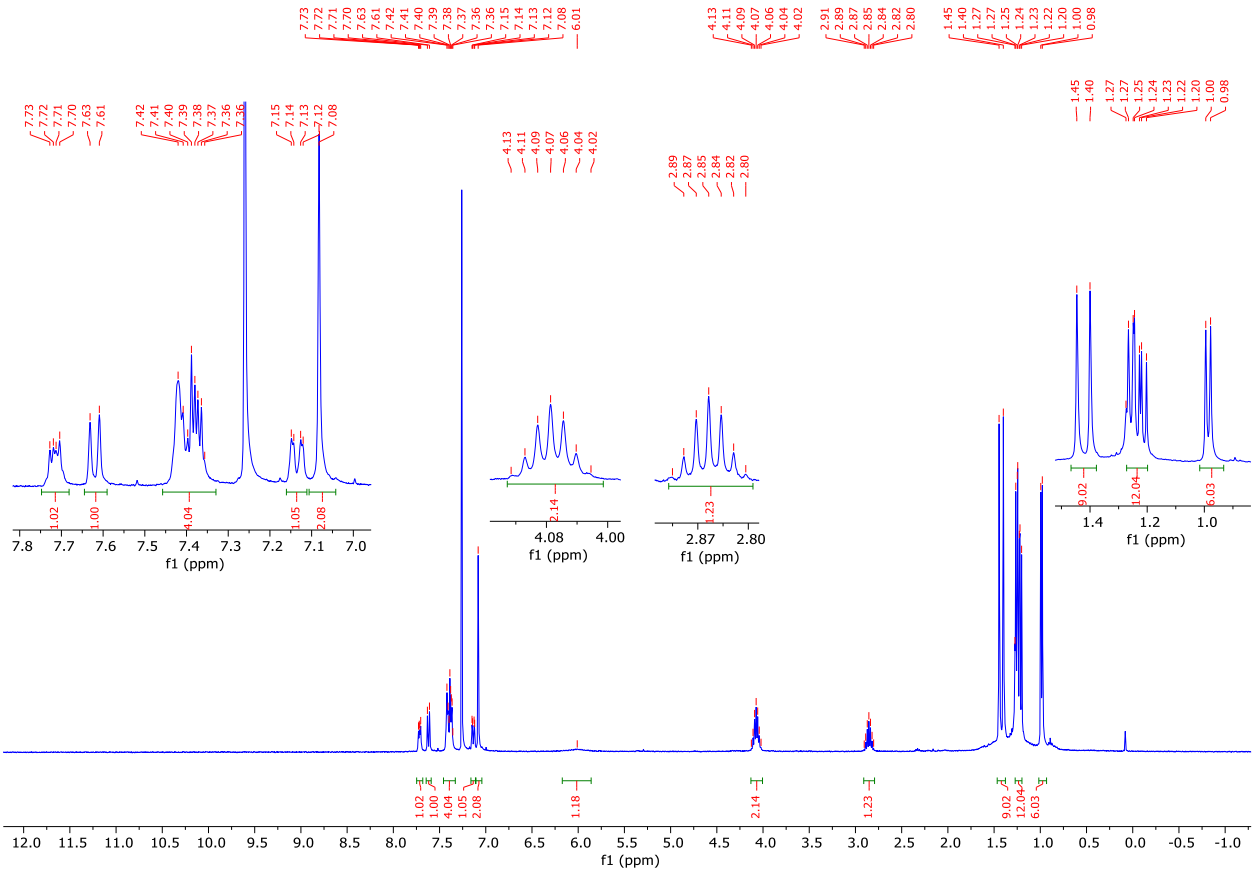

^{1}H NMR ($CDCl_3$) of compound **3.15** at RT and 50 °C showing peak coalescence

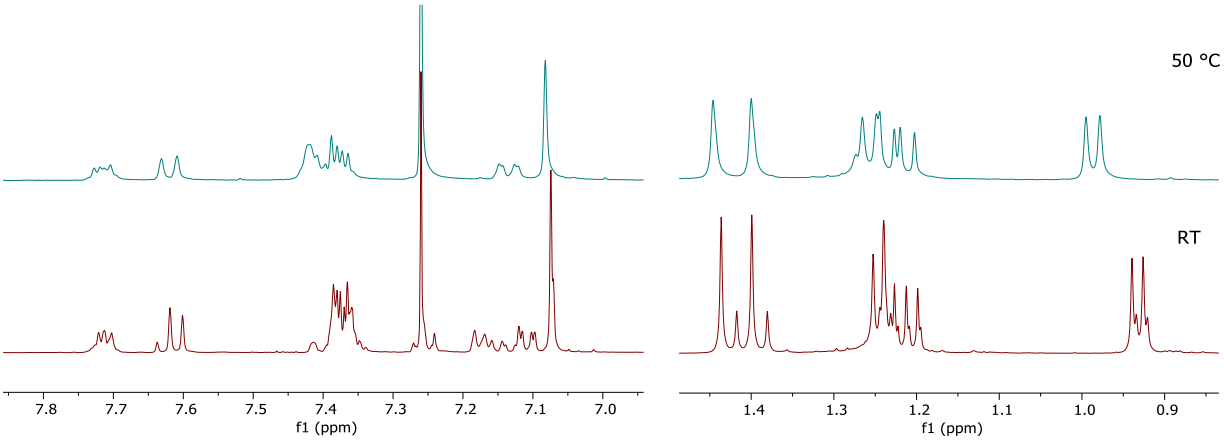

^{13}C NMR ($CDCl_3$, 126 MHz) of compound **3.15** at RT

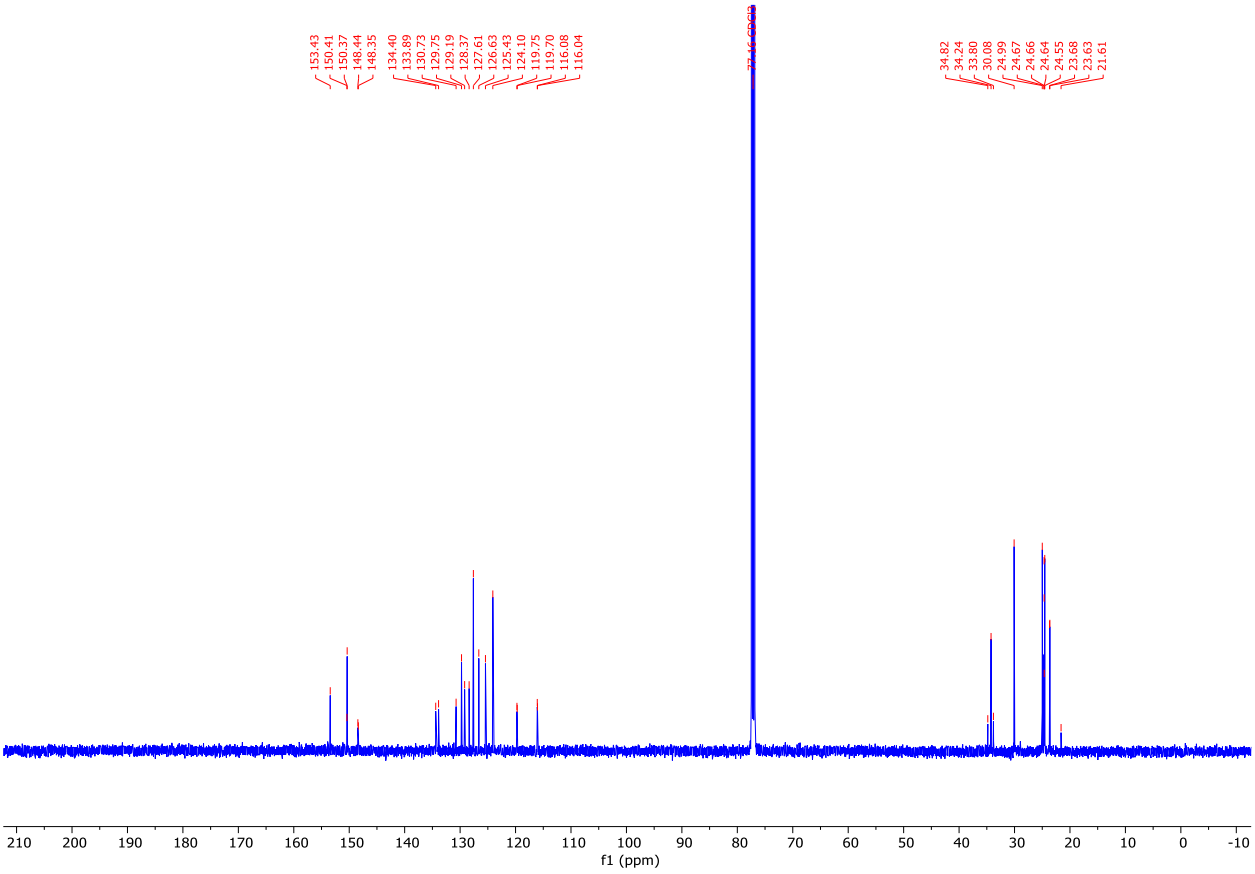

^{31}P NMR ($CDCl_3$, 203 MHz) of compound **3.15** at RT

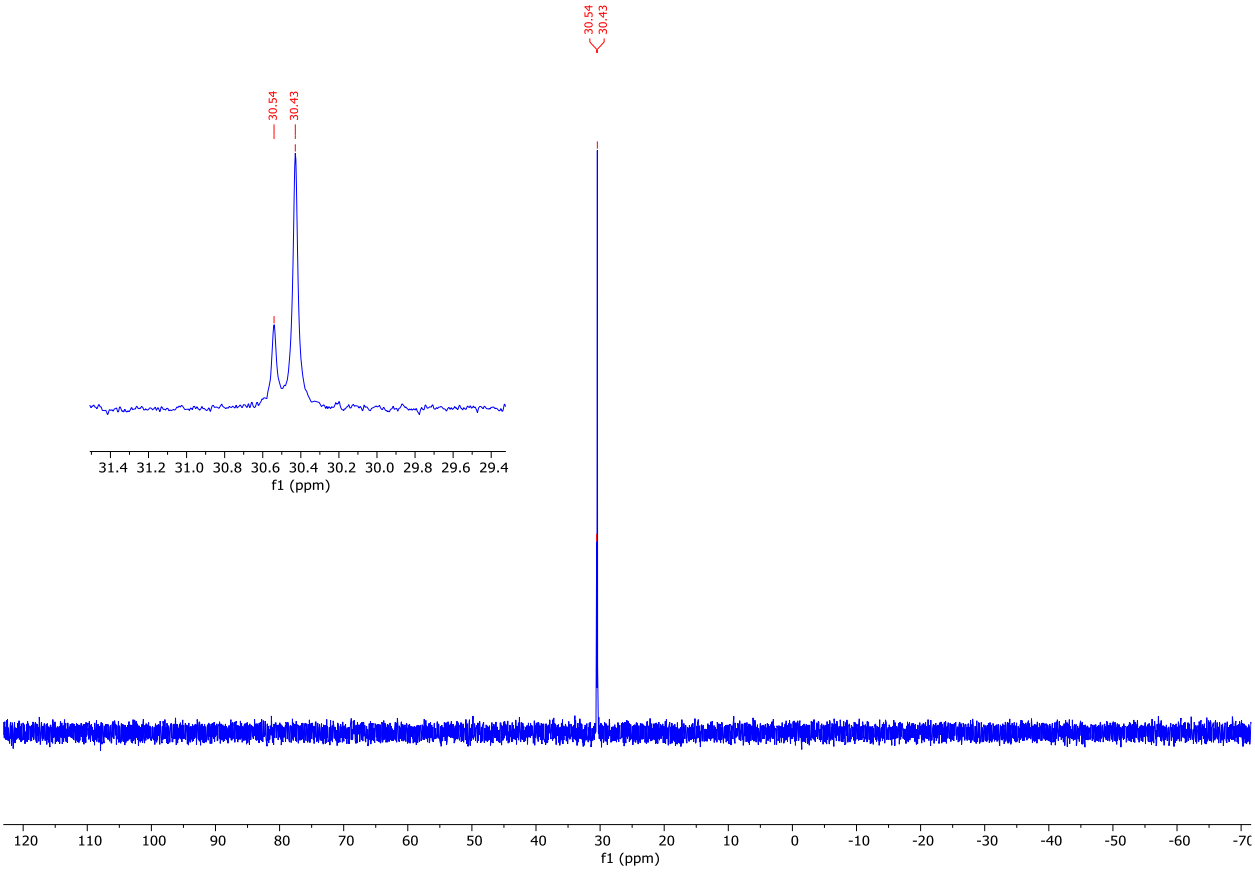

^{31}P NMR ($CDCl_3$, 162 MHz) of compound **3.15** at 50 °C showing peak coalescence

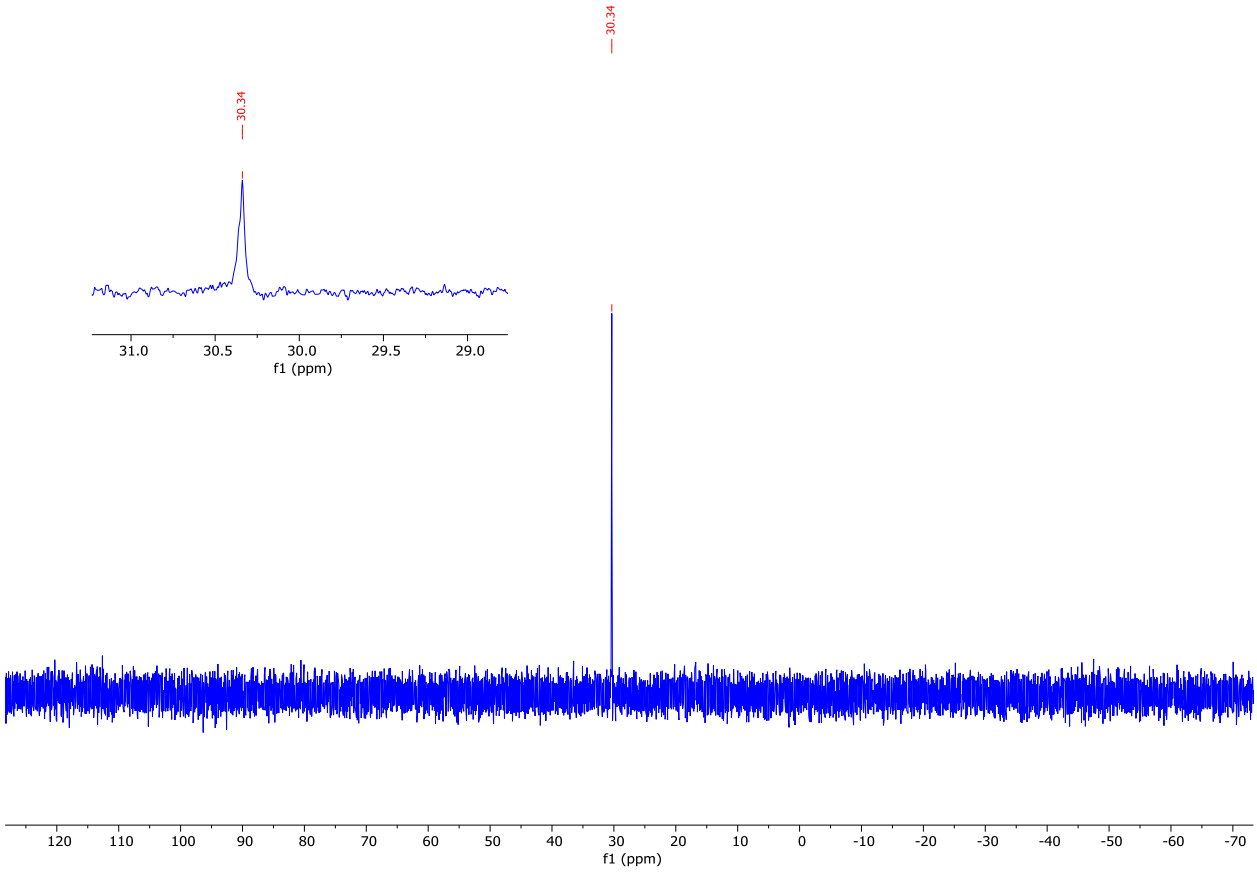

\$^{31}$P NMR ($CDCl_3$) of compound **3.15** at RT and 50 °C showing peak coalescence

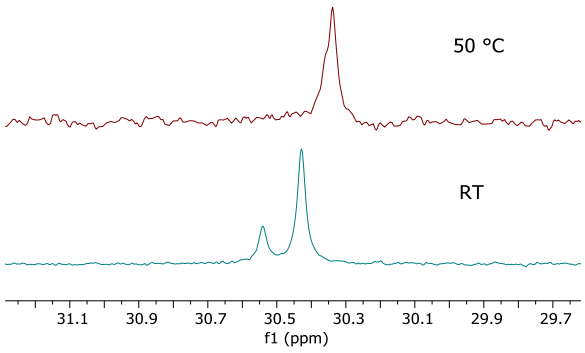

Appendix III: NMR Spectra and HPLC Chromatograms of Chapter 4

^{1}H NMR (500 MHz, $CDCl_3$) spectrum of **4.2a**

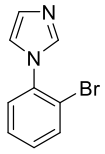

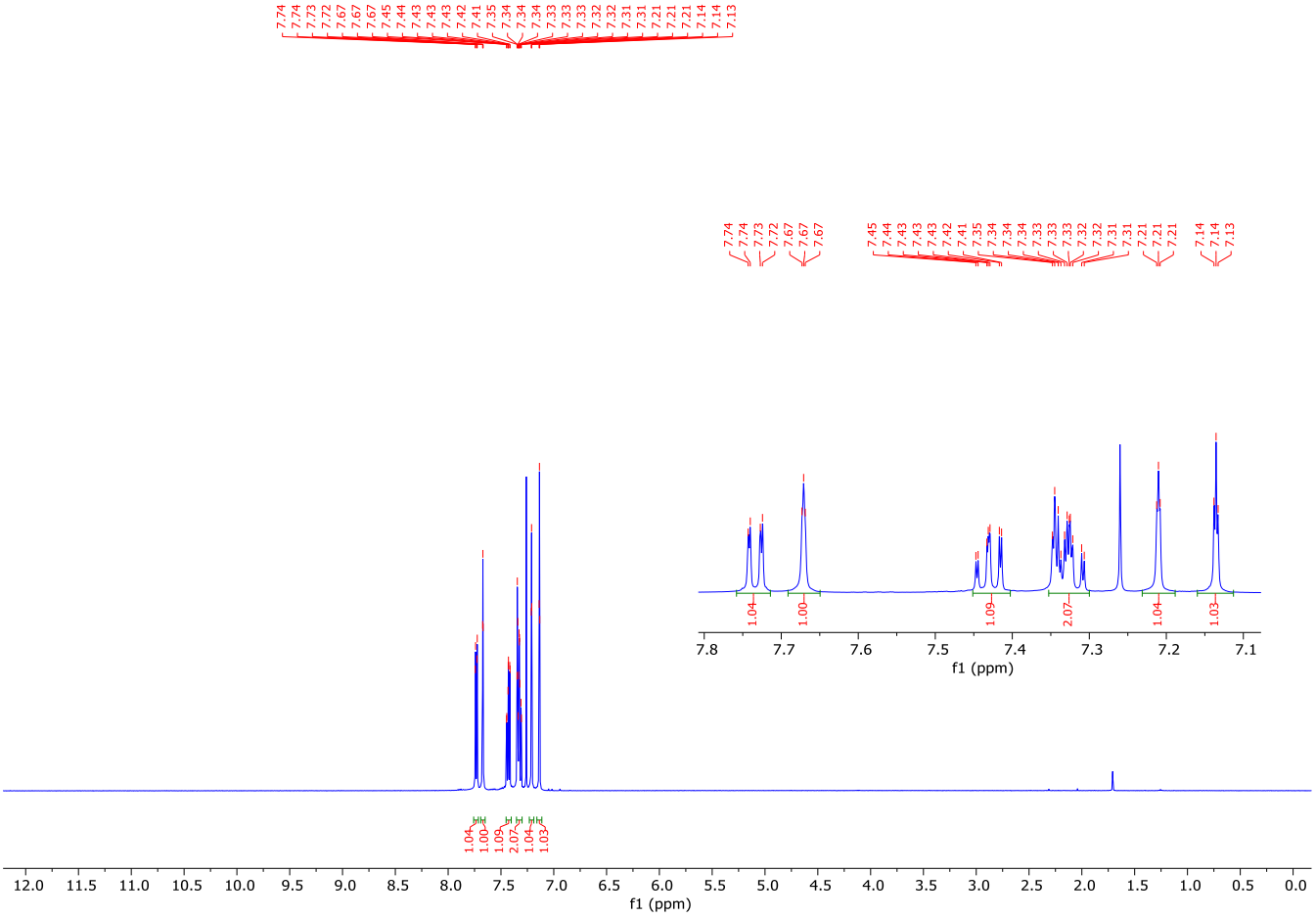

^{13}C (^{1}H) NMR (126 MHz, $CDCl_3$) spectrum of **4.2a**

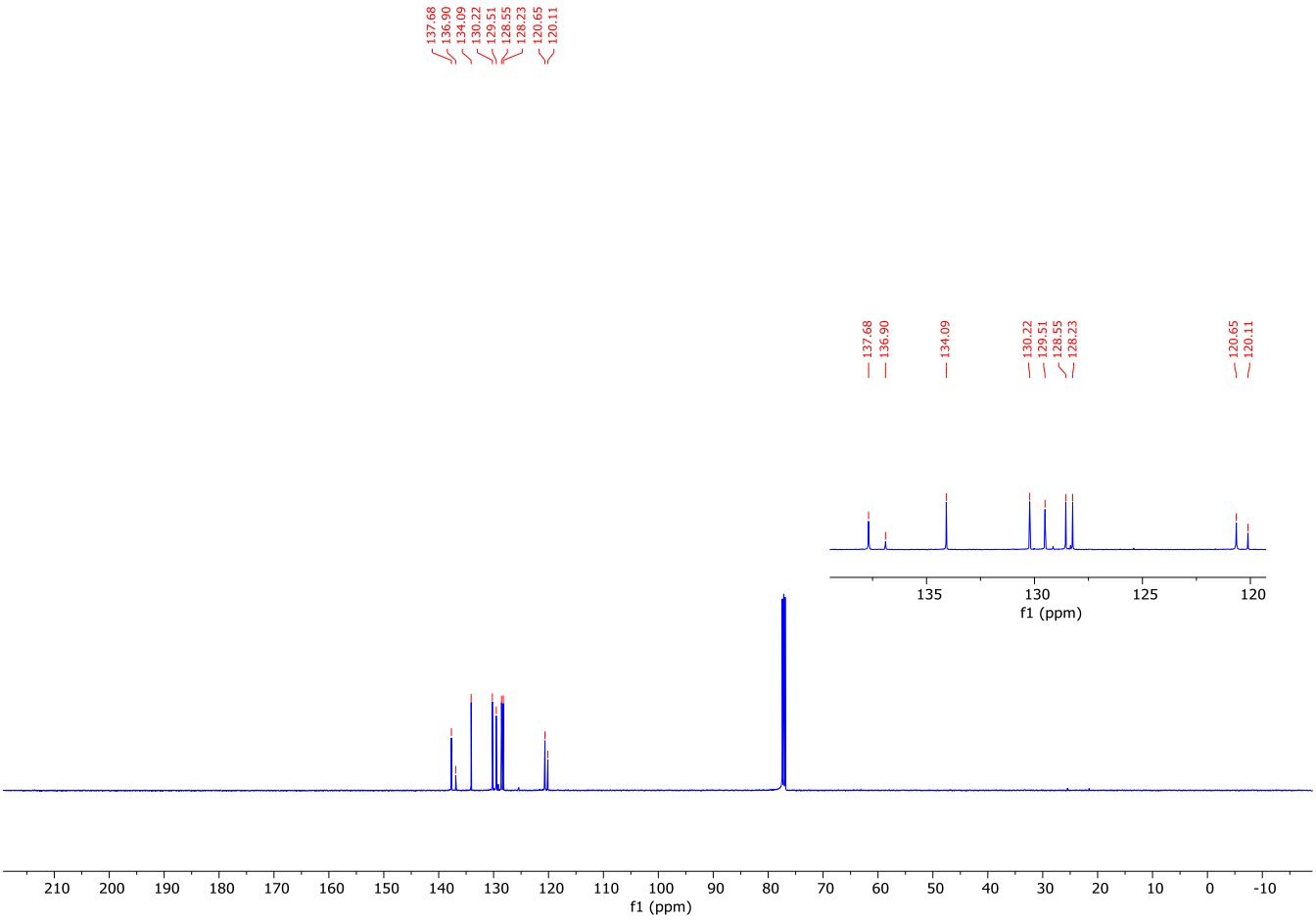

^{1}H NMR (400 MHz, $CDCl_3$) spectrum of **4.2b**

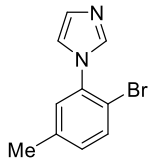

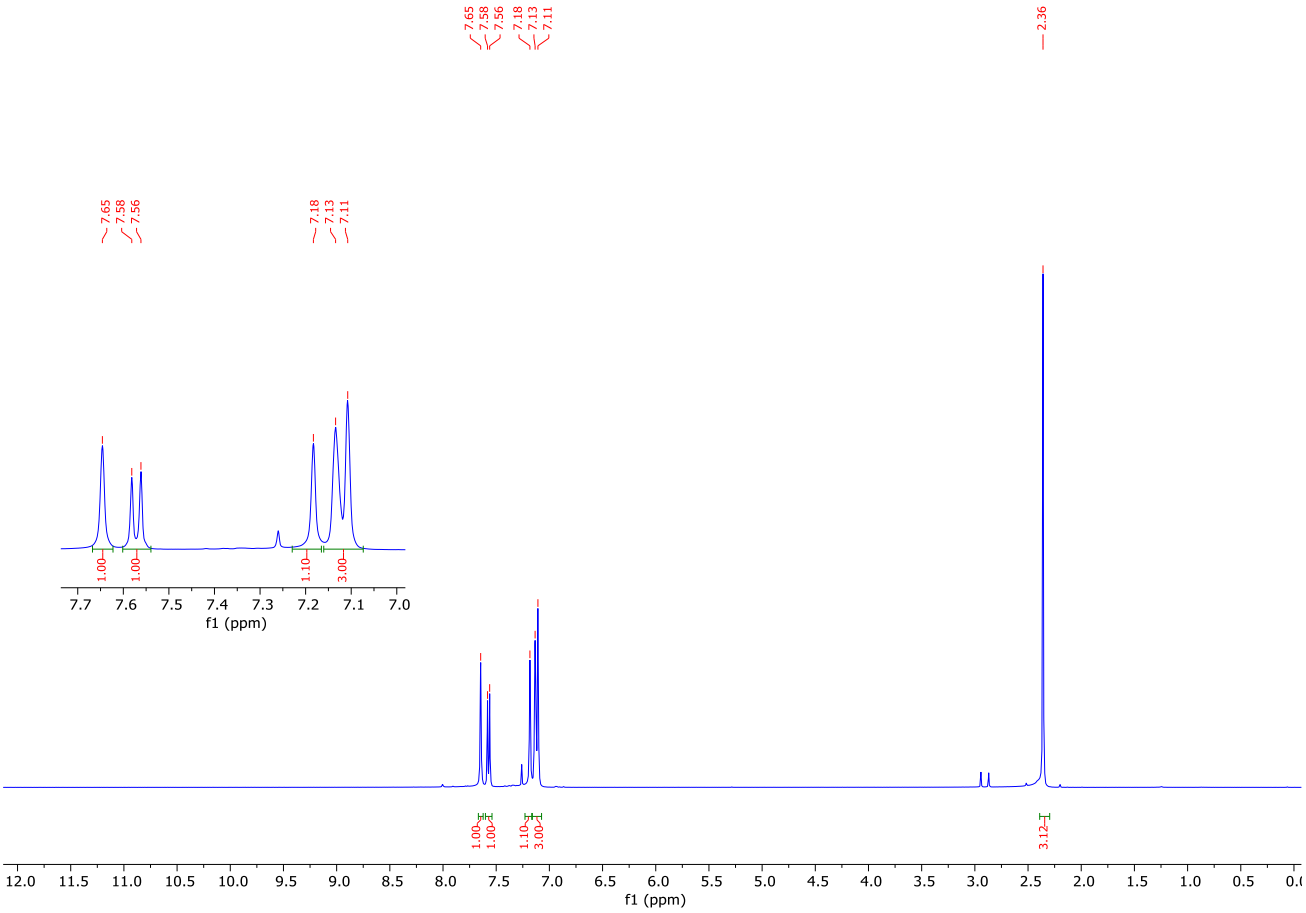

^{13}C (^{1}H) NMR (101 MHz, $CDCl_3$) spectrum of **4.2b**

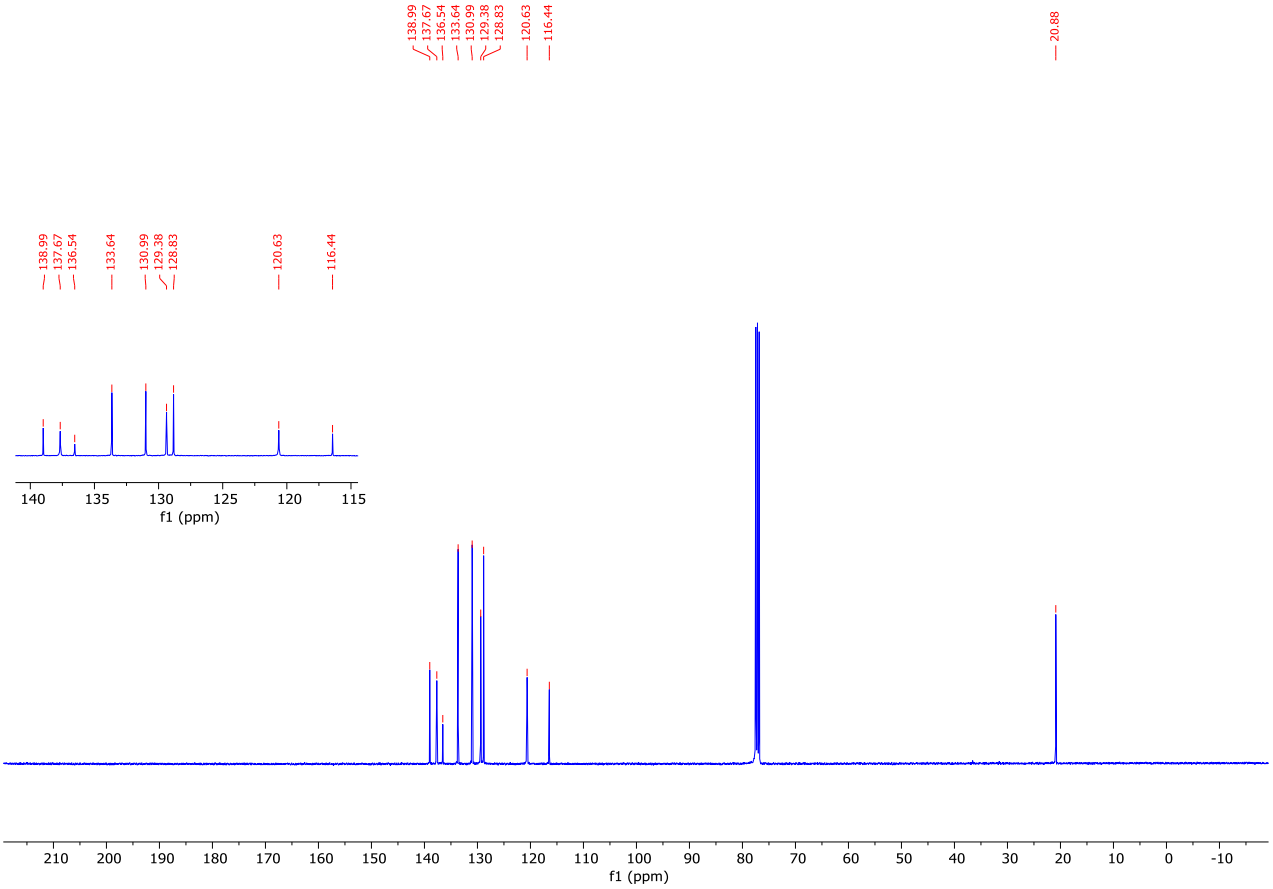

^{1}H NMR (400 MHz, $CDCl_3$) spectrum of **4.2c**

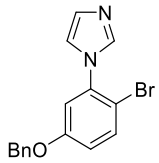

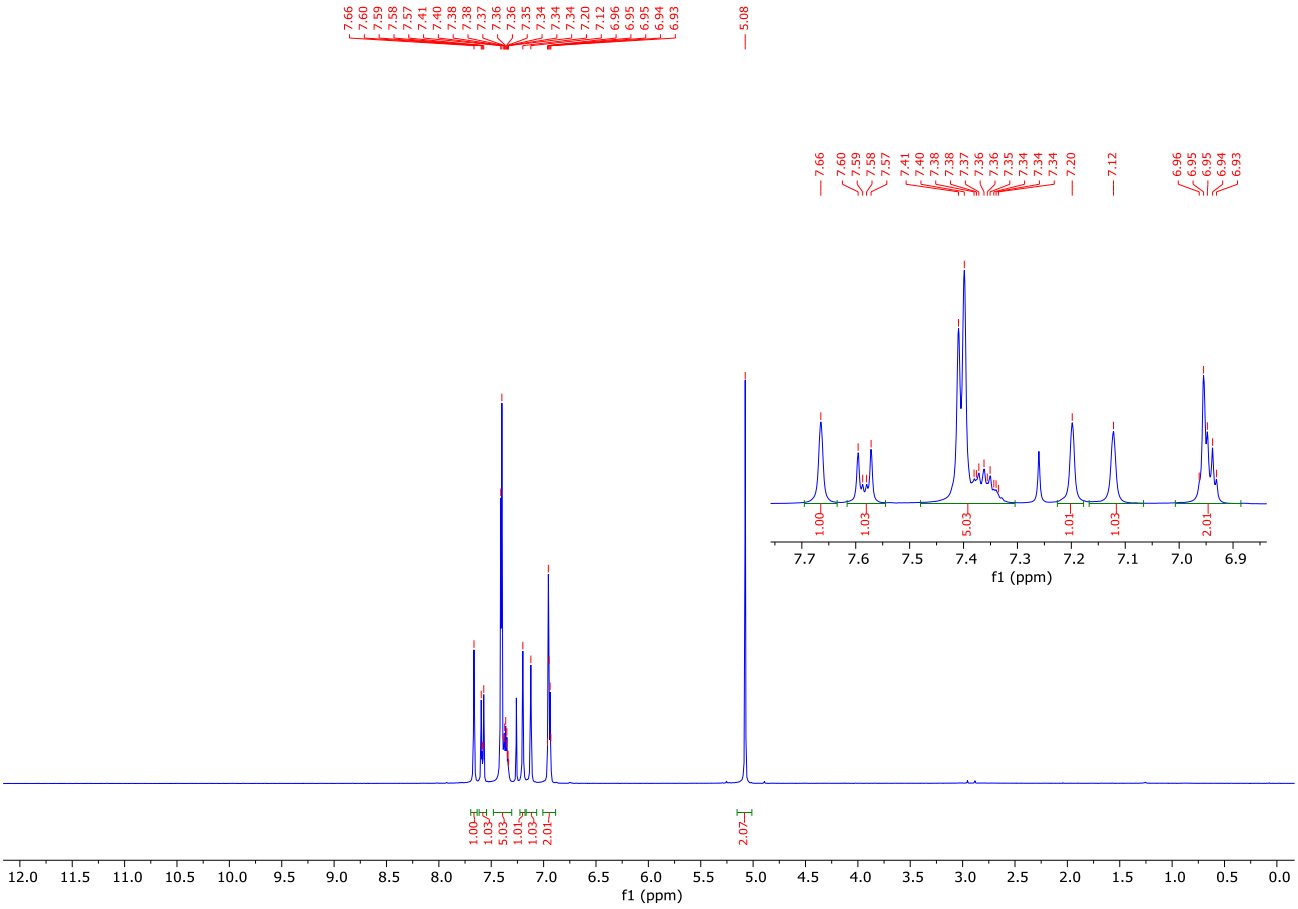

^{13}C (^{1}H) NMR (101 MHz, $CDCl_3$) spectrum of **4.2c**

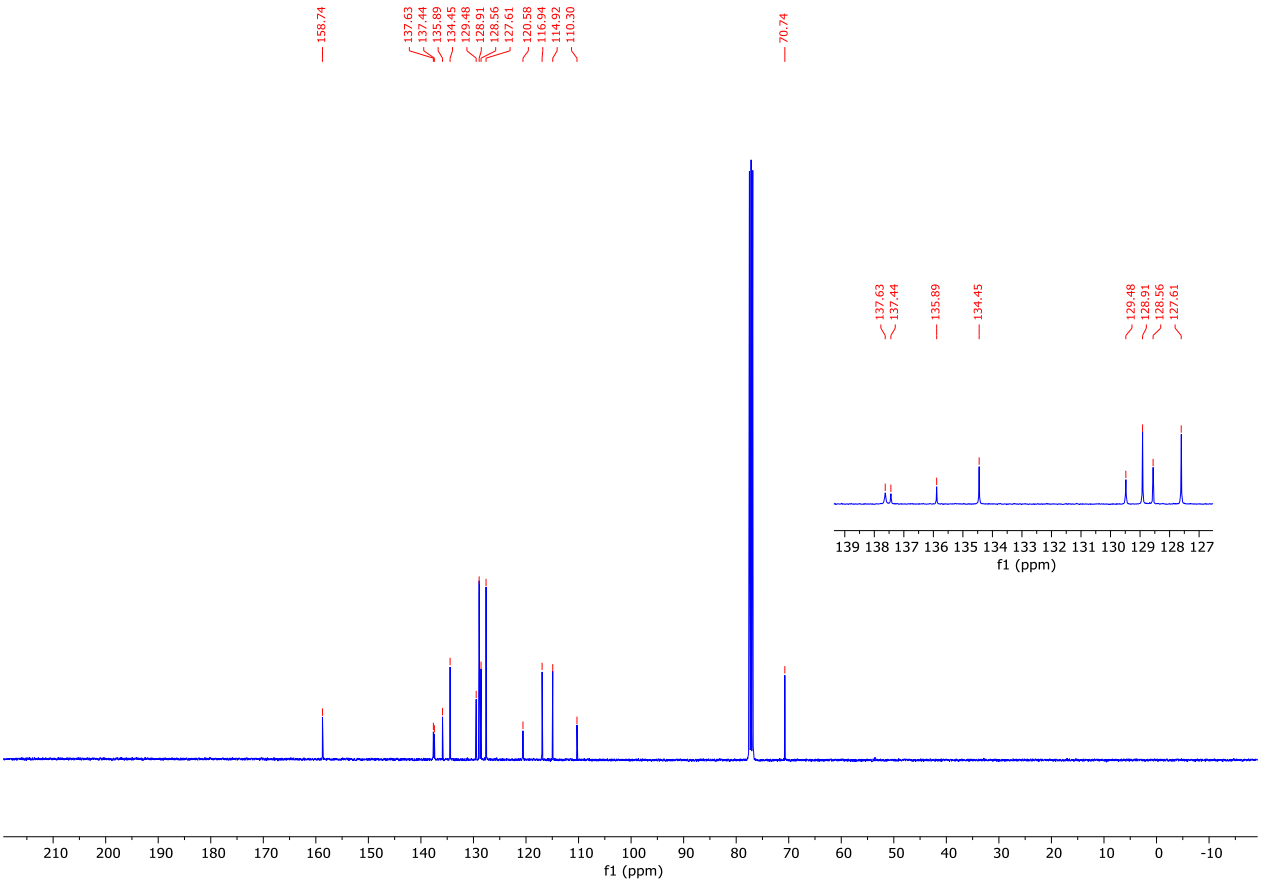

^{1}H NMR (500 MHz, DMSO) spectrum of **4.2d**

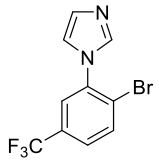

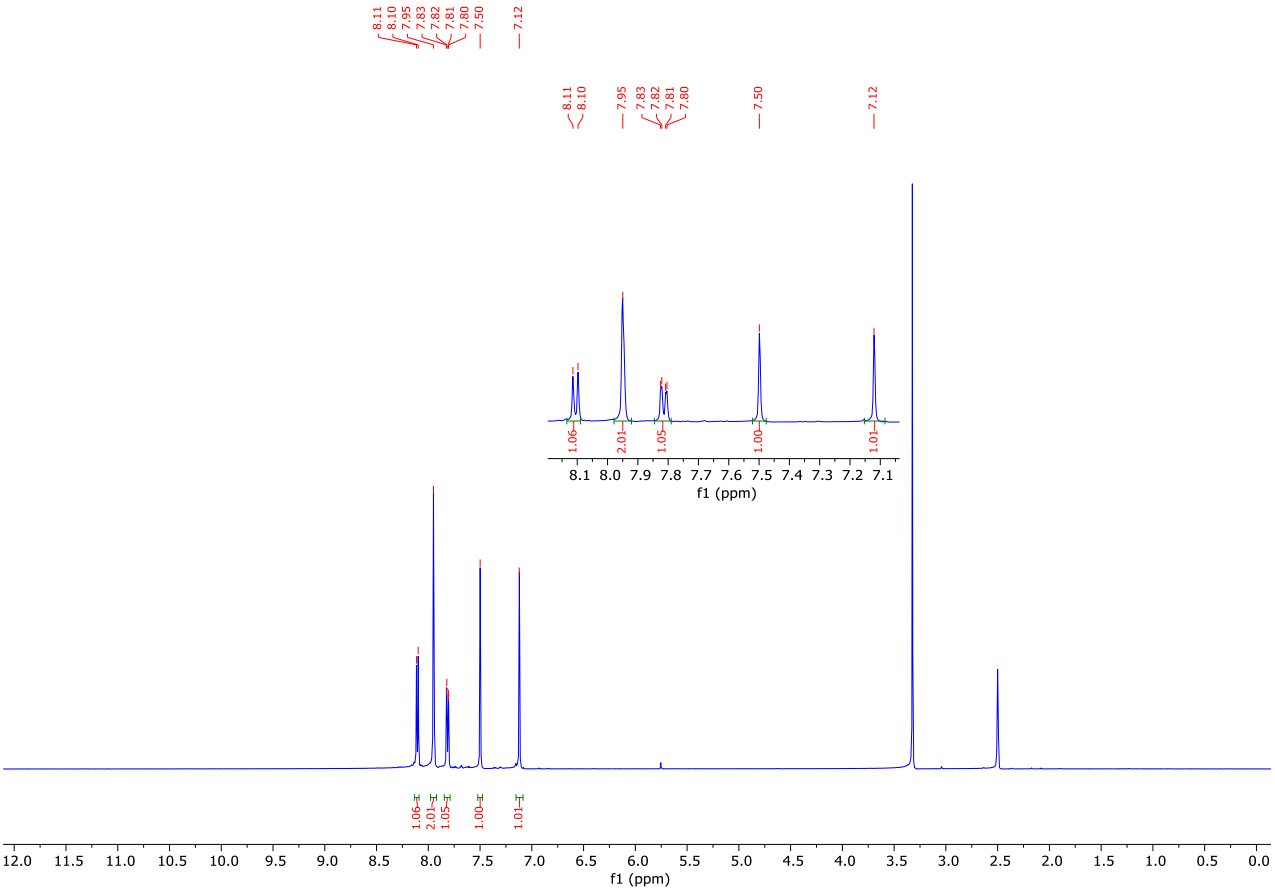

^{13}C (^{1}H) NMR (126 MHz, DMSO) spectrum of **4.2d**

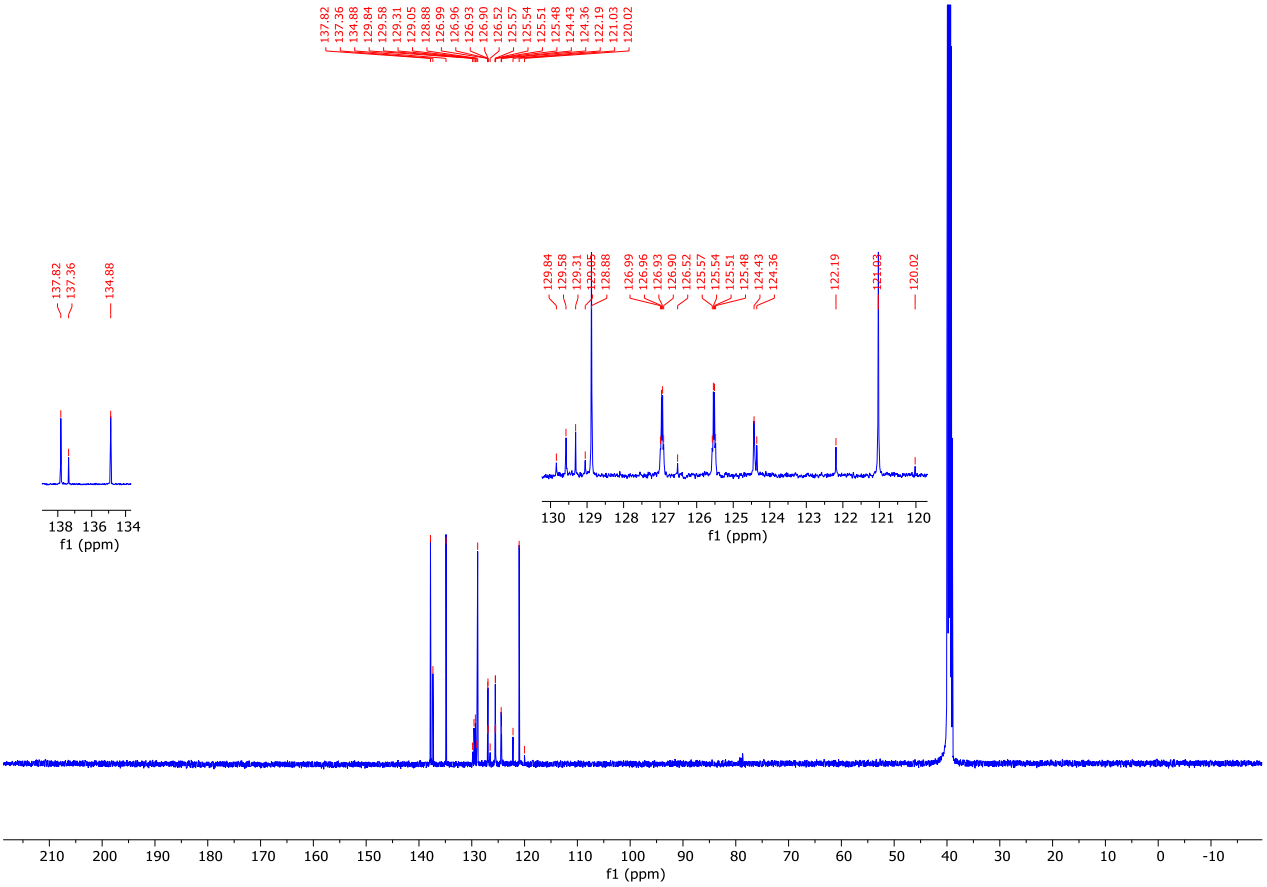

^{19}F (^{1}H) NMR (471 MHz, DMSO) spectrum of **4.2d**

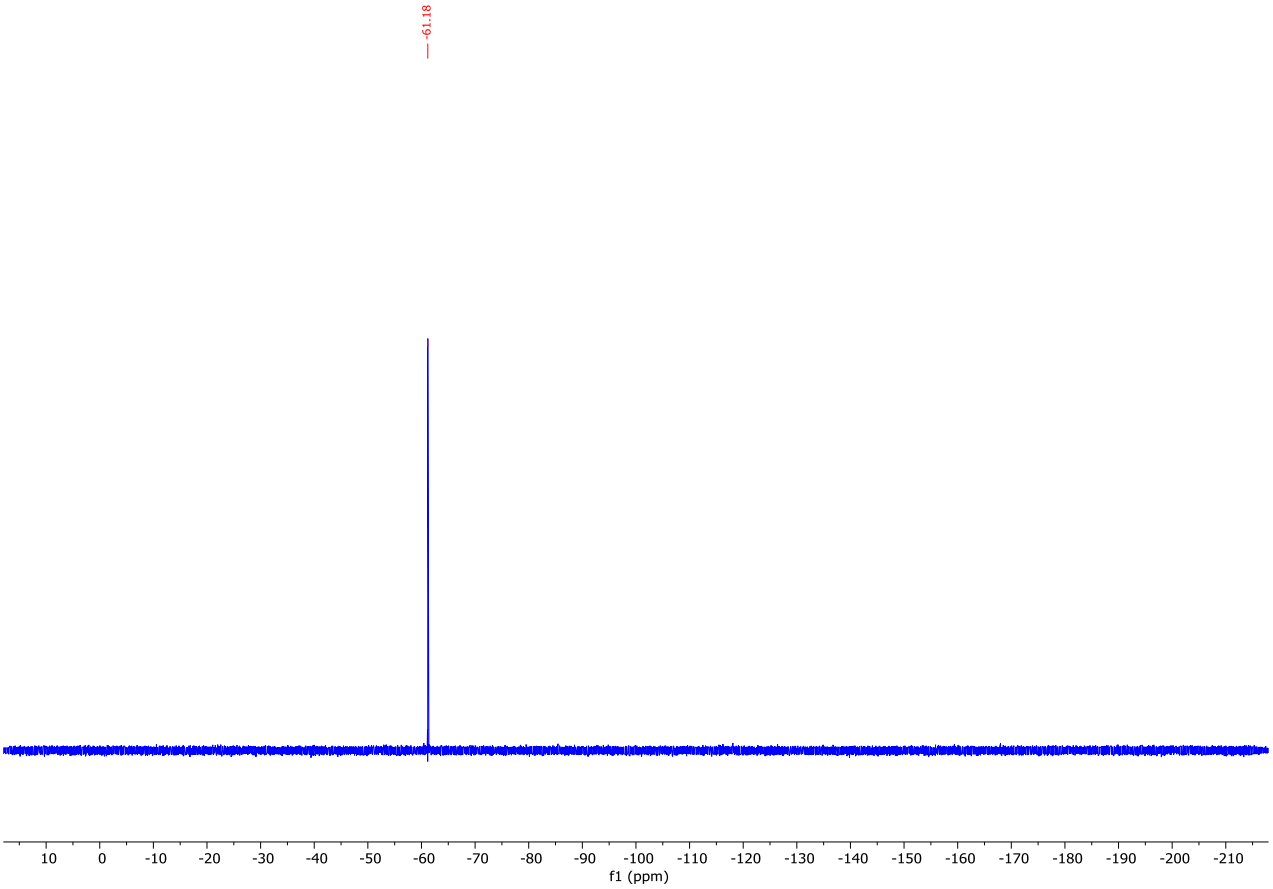

^{1}H NMR (400 MHz, $CDCl_3$) spectrum of **4.2e**

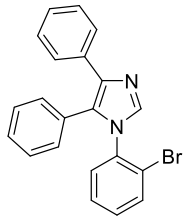

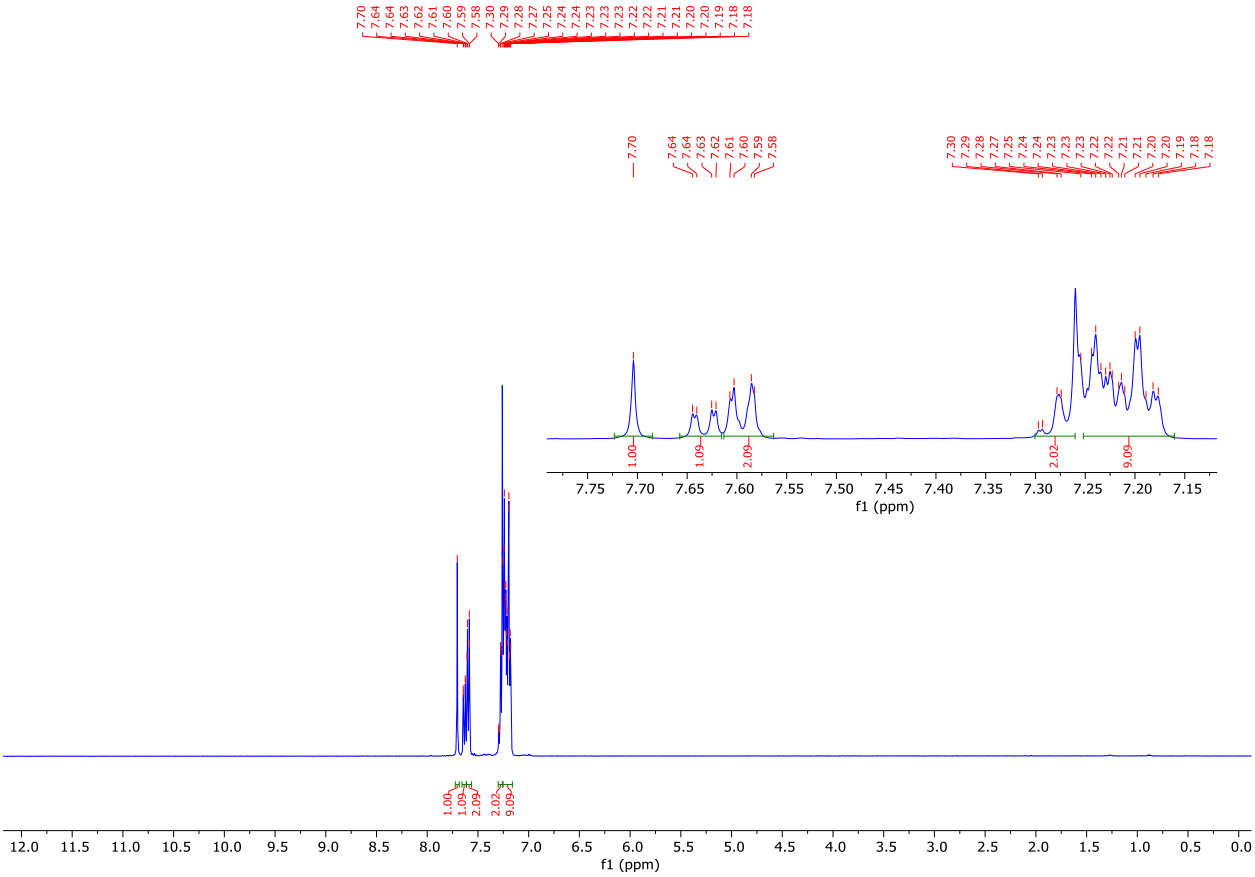

^{13}C (^{1}H) NMR (101 MHz, $CDCl_3$) spectrum of **4.2e**

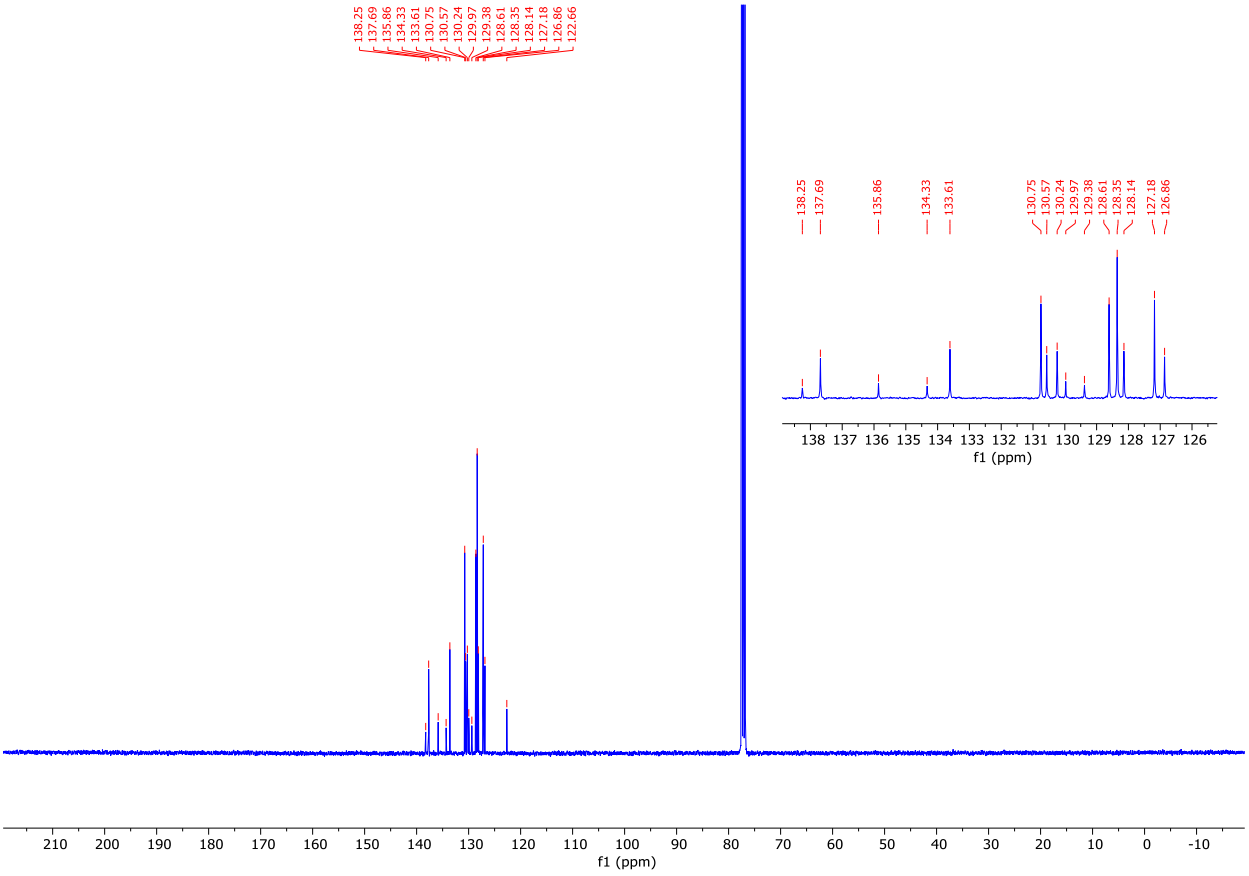

^{1}H NMR (400 MHz, $CDCl_3$) spectrum of **4.3a**

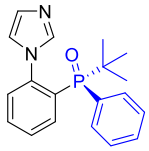

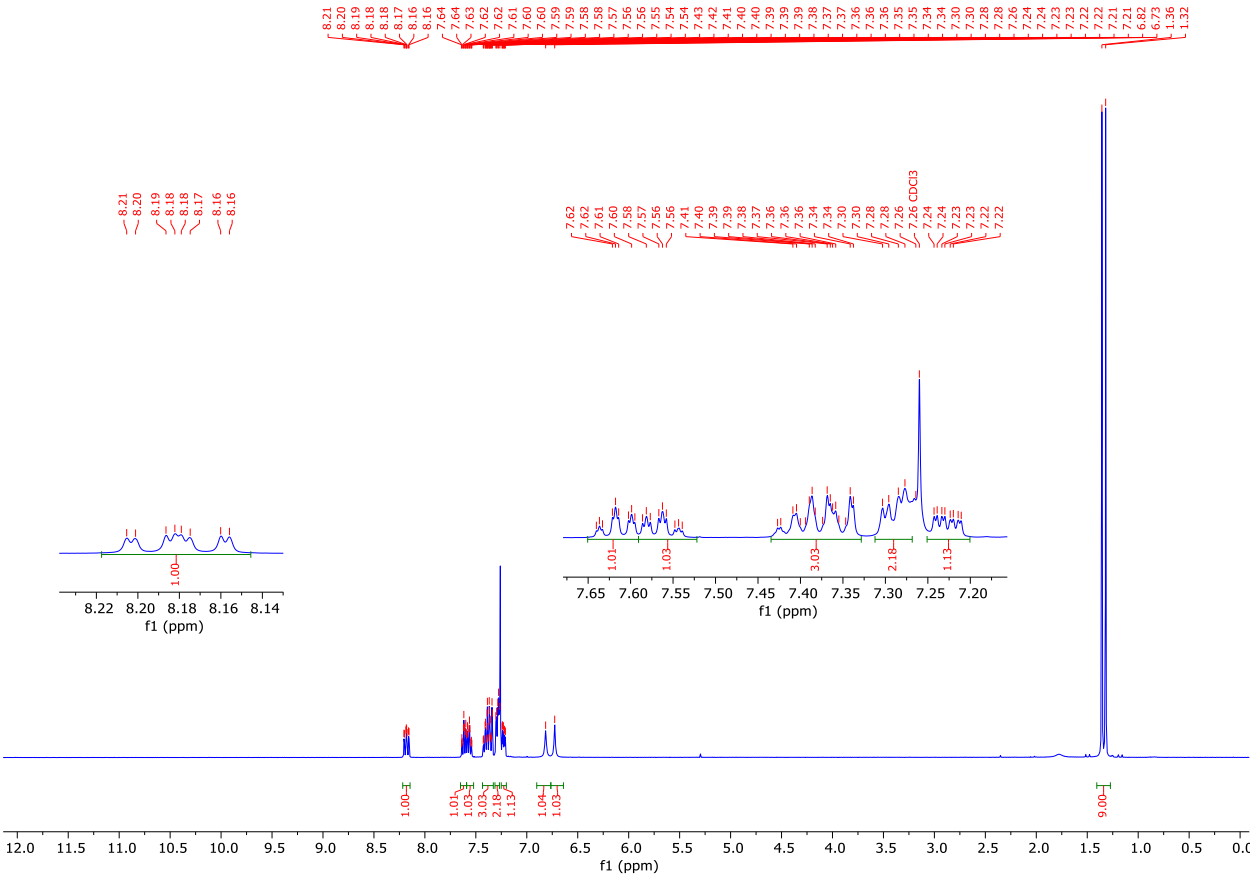

^{13}C (^{1}H) NMR (101 MHz, $CDCl_3$) spectrum of **4.3a**

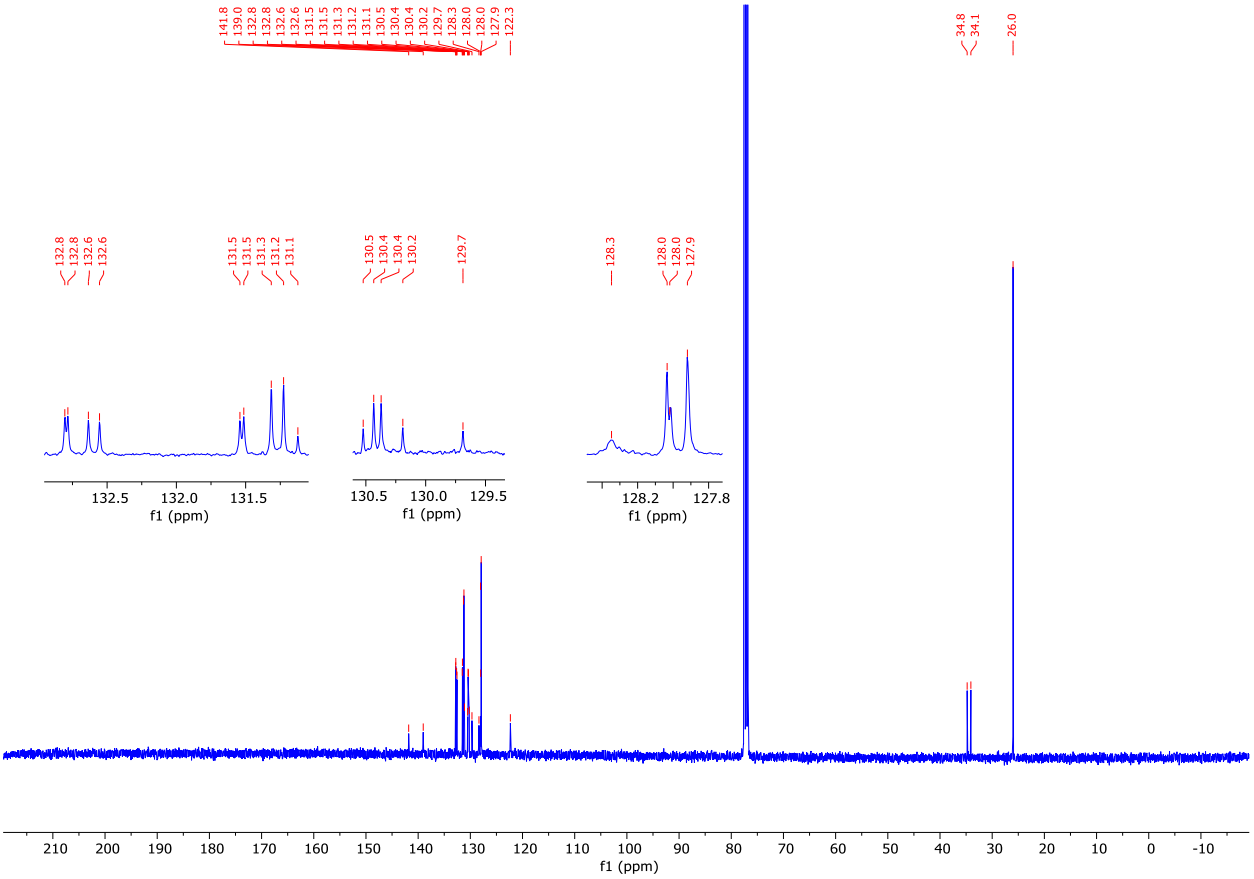

$^{31}P(^{1}H)$ NMR (162 MHz, $CDCl_3$ of **4.3a**

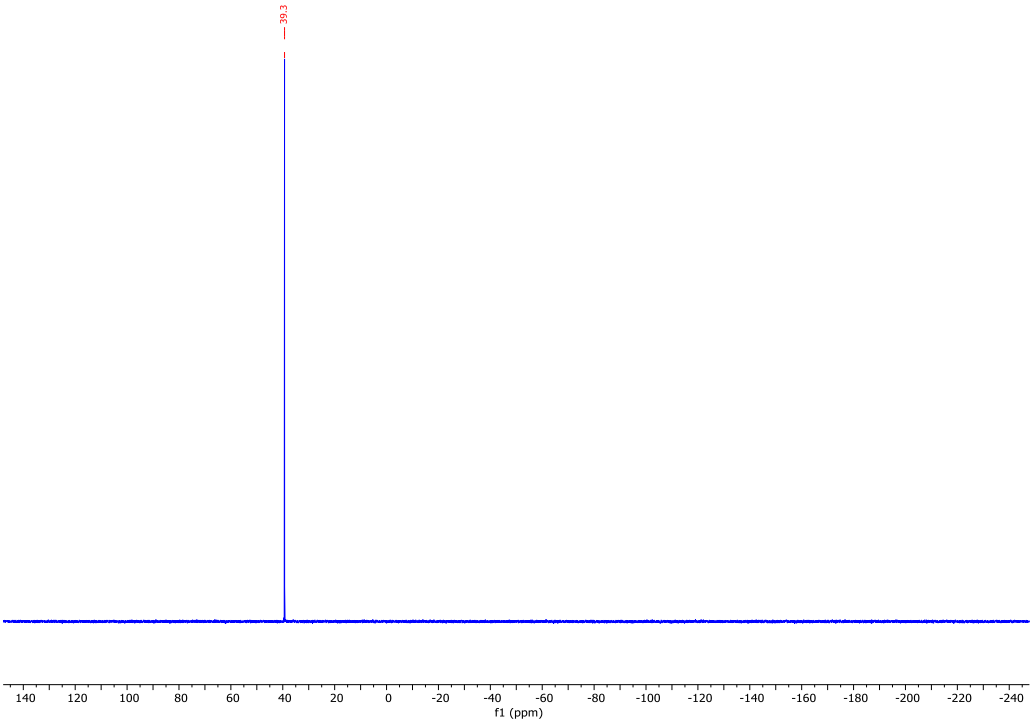

Chiral HPLC chromatogram of **4.3a**

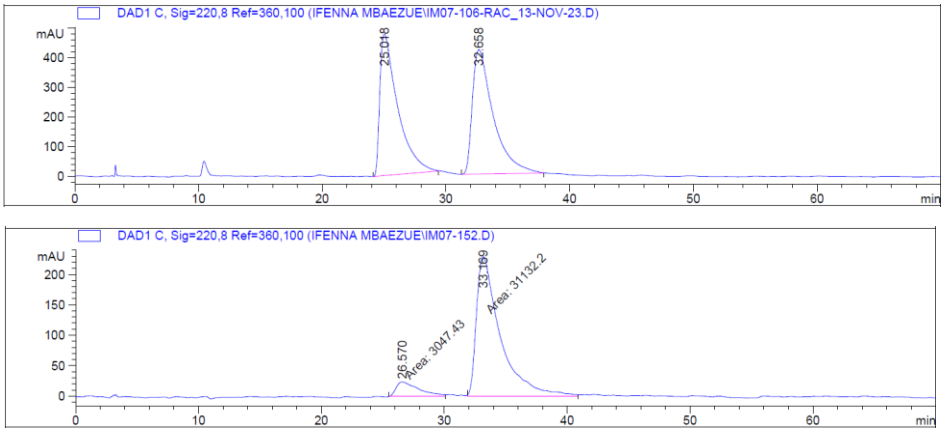

Peak #	RetTime [min]	Type	Width [min]	Area [mAU*s]	Height [mAU]	Area %
1	25.018	BB	1.3985	4.79008e4	477.43799	49.2899
2	32.658	BB	1.7217	4.92811e4	419.76245	50.7101

Peak #	RetTime [min]	Type	Width [min]	Area [mAU*s]	Height [mAU]	Area %
1	26.570	MM	2.1490	3047.43140	23.63472	8.9159
2	33.169	MM	2.2569	3.11322e4	229.90378	91.0841

^{1}H NMR (400 MHz, $CDCl_3$) spectrum of **4.4a**

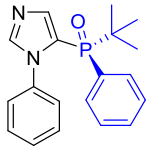

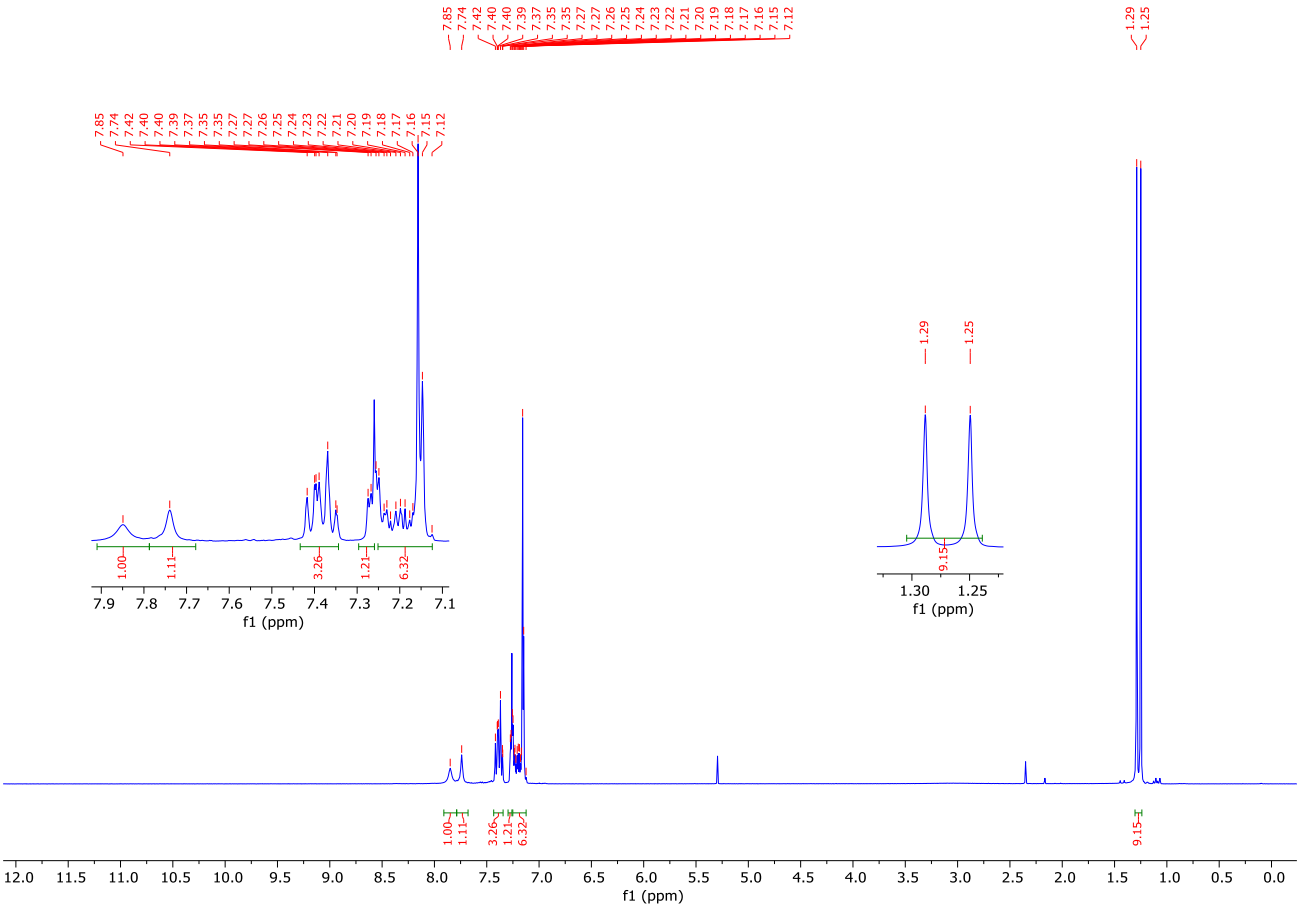

^{13}C (^{1}H) NMR (101 MHz, $CDCl_3$) spectrum of **4.4a**

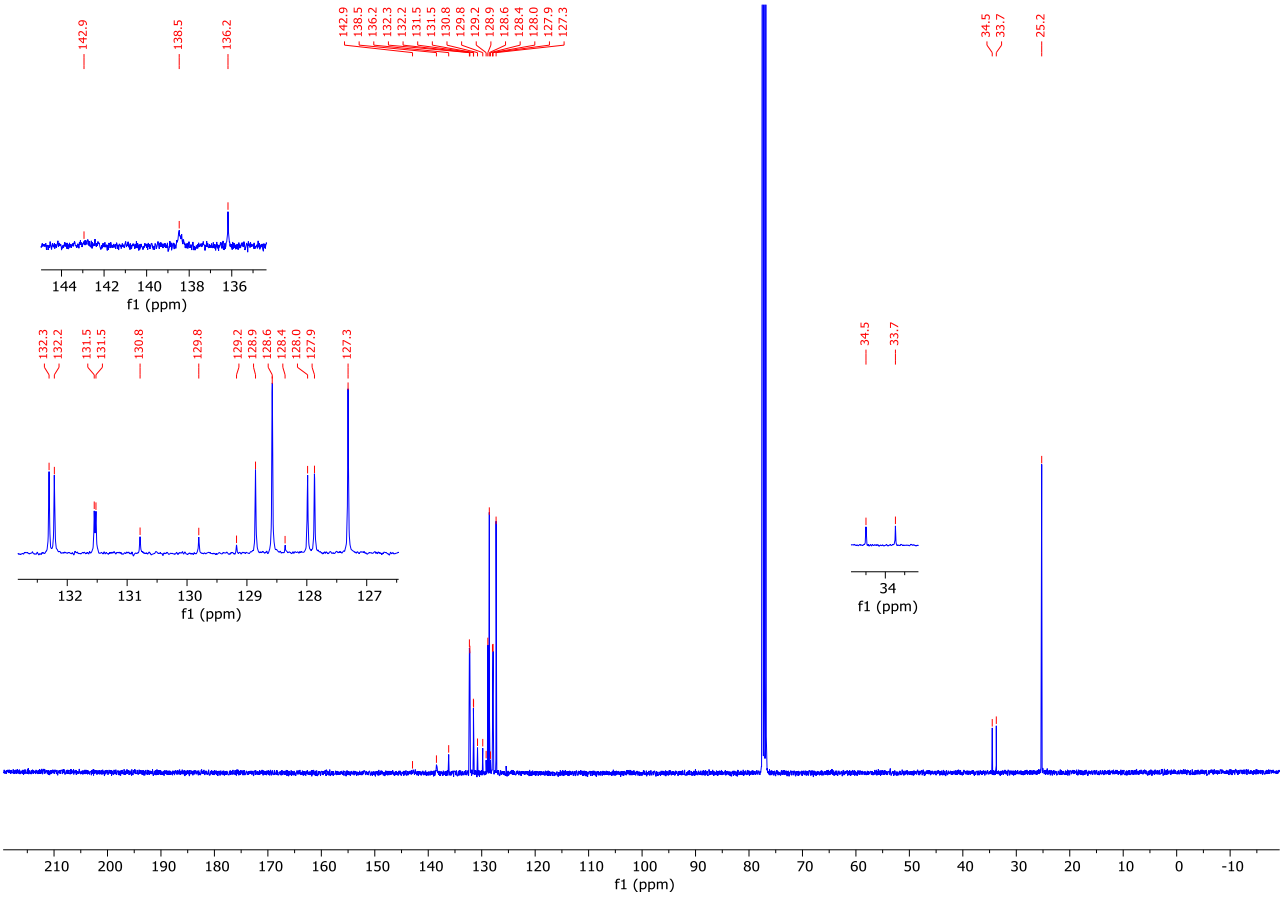

$^{31}P(^{1}H)$ NMR (162 MHz, $CDCl_3$ of **4.4a**

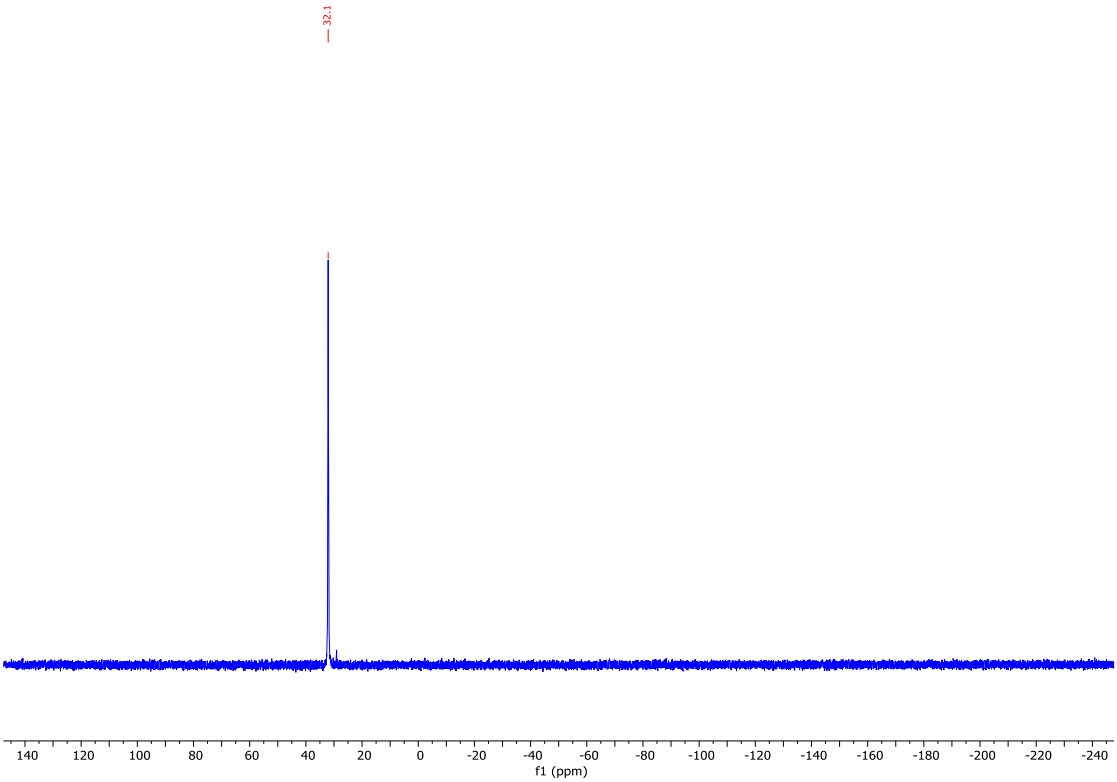

Chiral HPLC chromatogram of **4.4a**

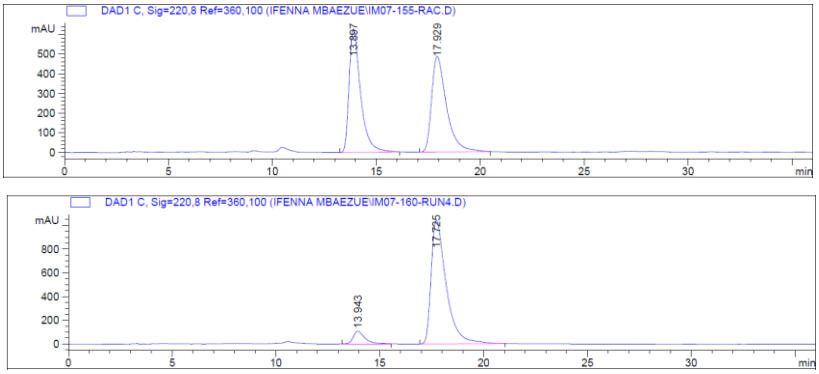

Peak #	RetTime [min]	Type	Width [min]	Area [mAU*s]	Height [mAU]	Area %
1	13.897	BB	0.5729	2.40475e4	627.78516	49.8024
2	17.929	BB	0.7458	2.42383e4	486.01501	50.1976

Peak #	RetTime [min]	Type	Width [min]	Area [mAU*s]	Height [mAU]	Area %
1	13.943	BB	0.5756	4128.88232	106.66958	7.2840
2	17.725	BB	0.7512	5.25553e4	1040.61011	92.7160

^{1}H NMR (400 MHz, $CDCl_3$) spectrum of **4.5a**

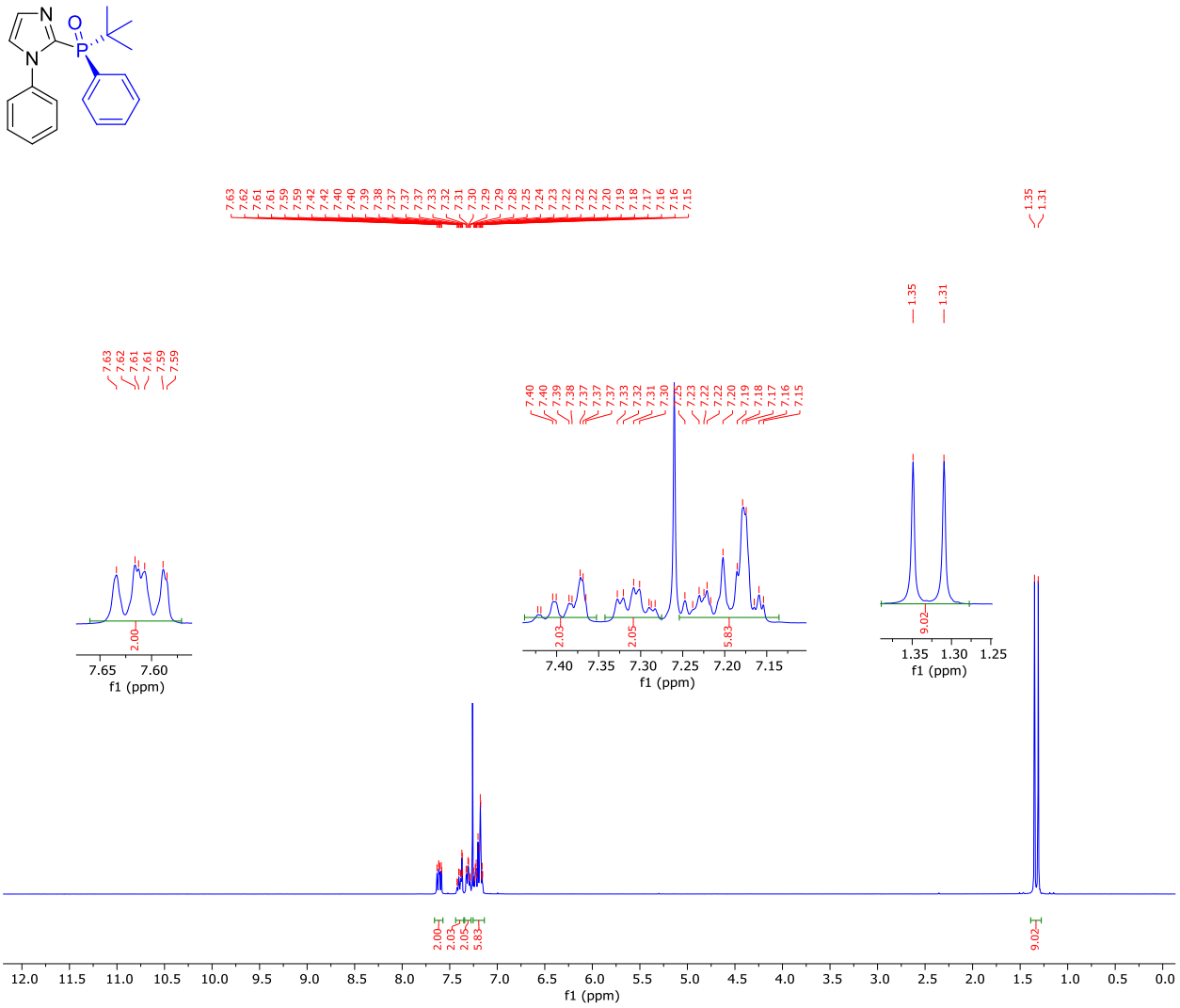

^{13}C (^{1}H) NMR (101 MHz, $CDCl_3$) spectrum of **4.5a**

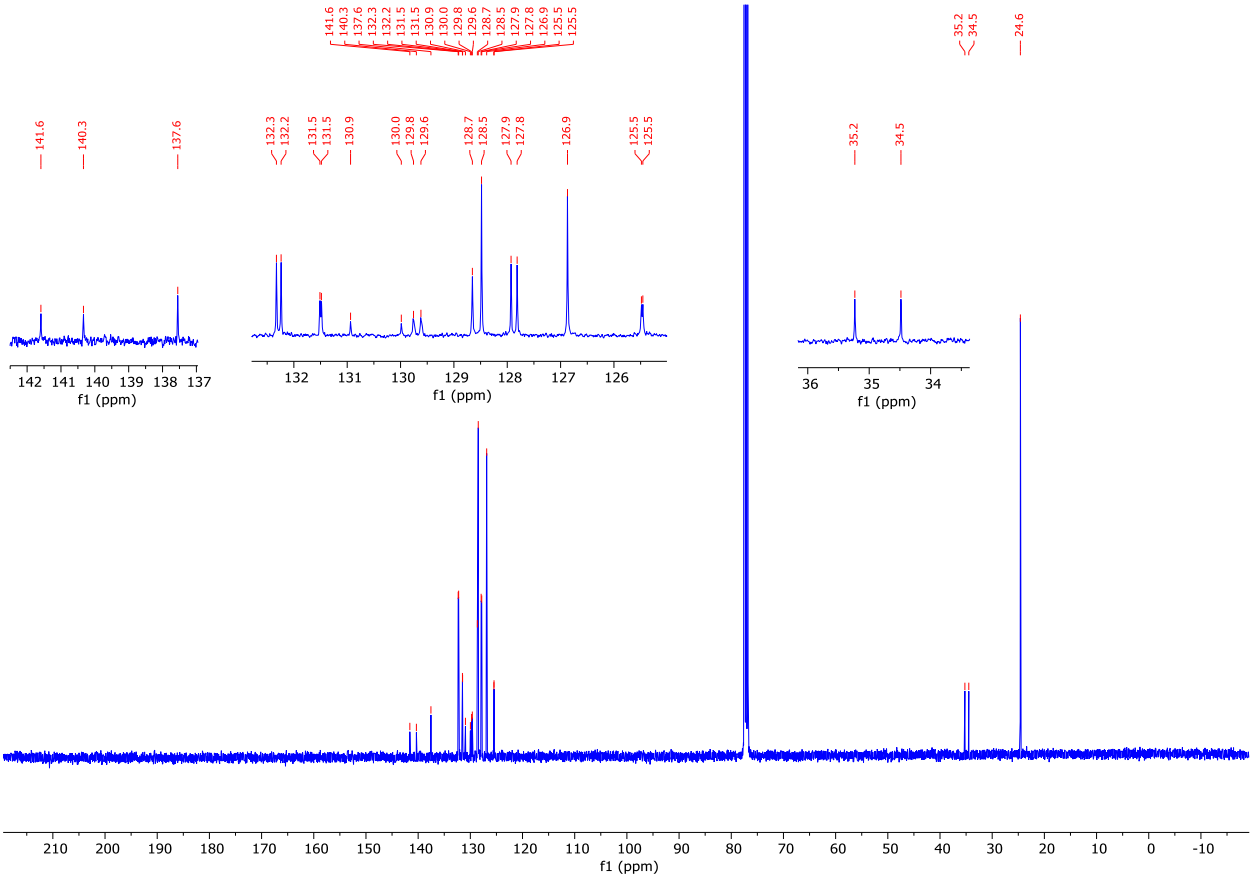

$^{31}P(^{1}H)$ NMR (162 MHz, $CDCl_3$ of **4.5a**

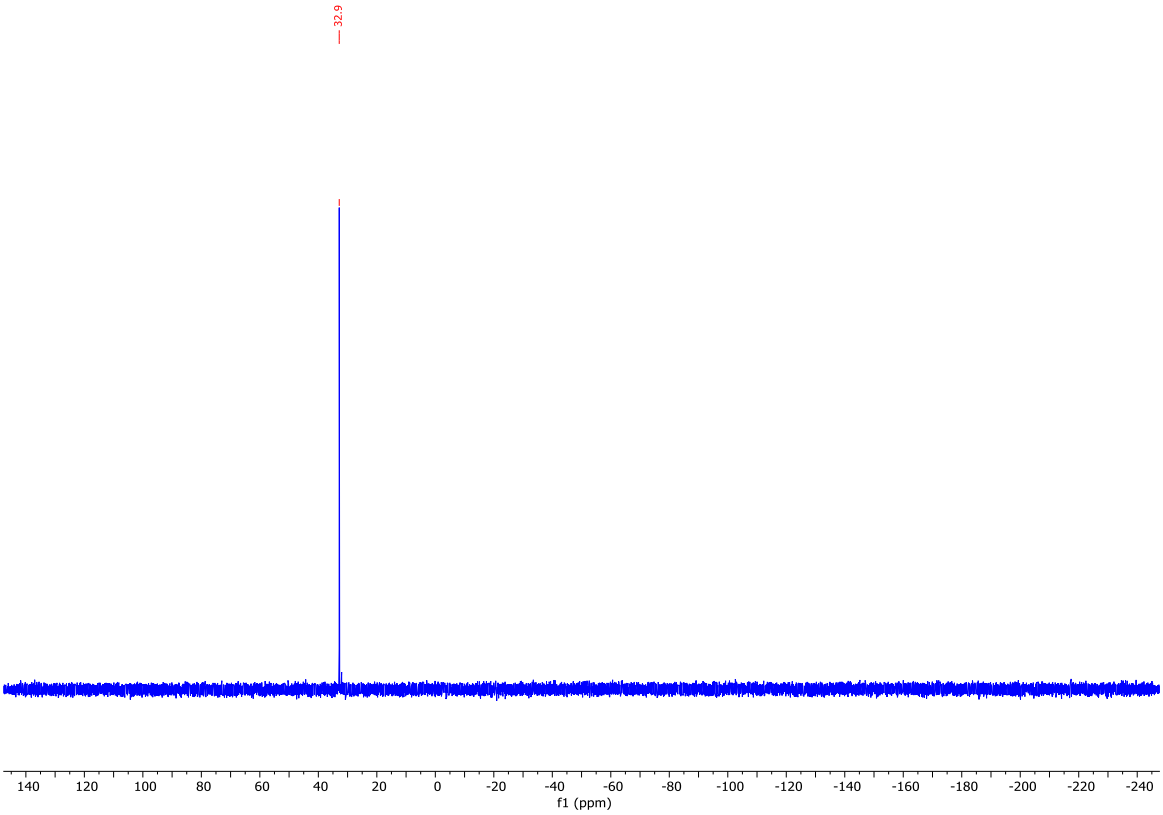

Chiral HPLC chromatogram of **4.5a**

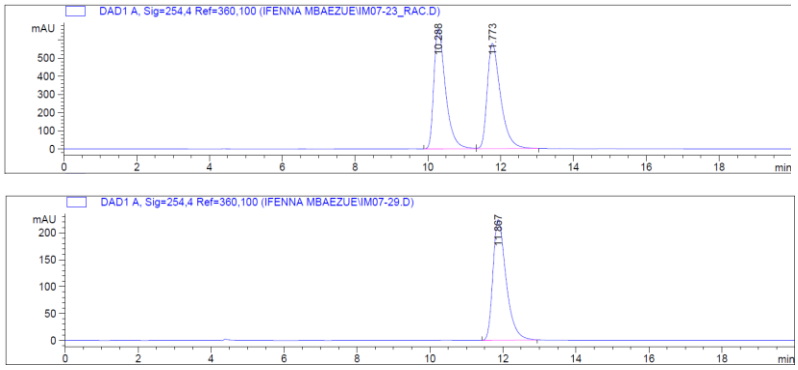

Peak #	RetTime [min]	Type	Width [min]	Area [mAU*s]	Height [mAU]	Area %
1	10.288	BV	0.3350	1.46661e4	660.74292	49.8947
2	11.773	VB	0.3849	1.47280e4	578.75311	50.1053

Peak #	RetTime [min]	Type	Width [min]	Area [mAU*s]	Height [mAU]	Area %
1	11.867	BB	0.3817	5646.22412	224.26785	100.0000

^{1}H NMR (400 MHz, $CDCl_{3,}$) spectrum of **4.5b**

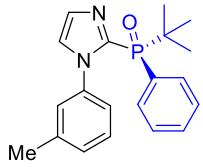

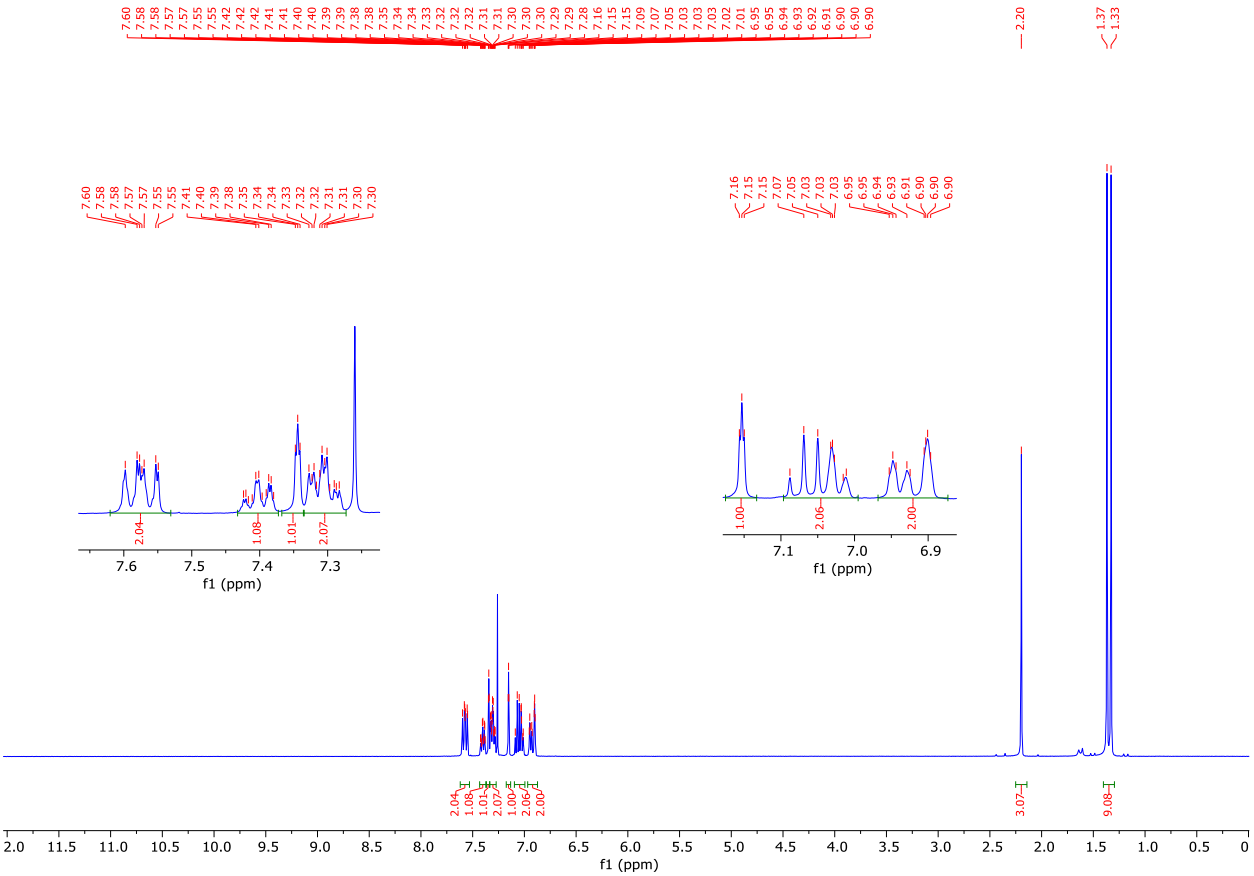

^{13}C (^{1}H) NMR (101 MHz, $CDCl_3$) spectrum of **4.5b**

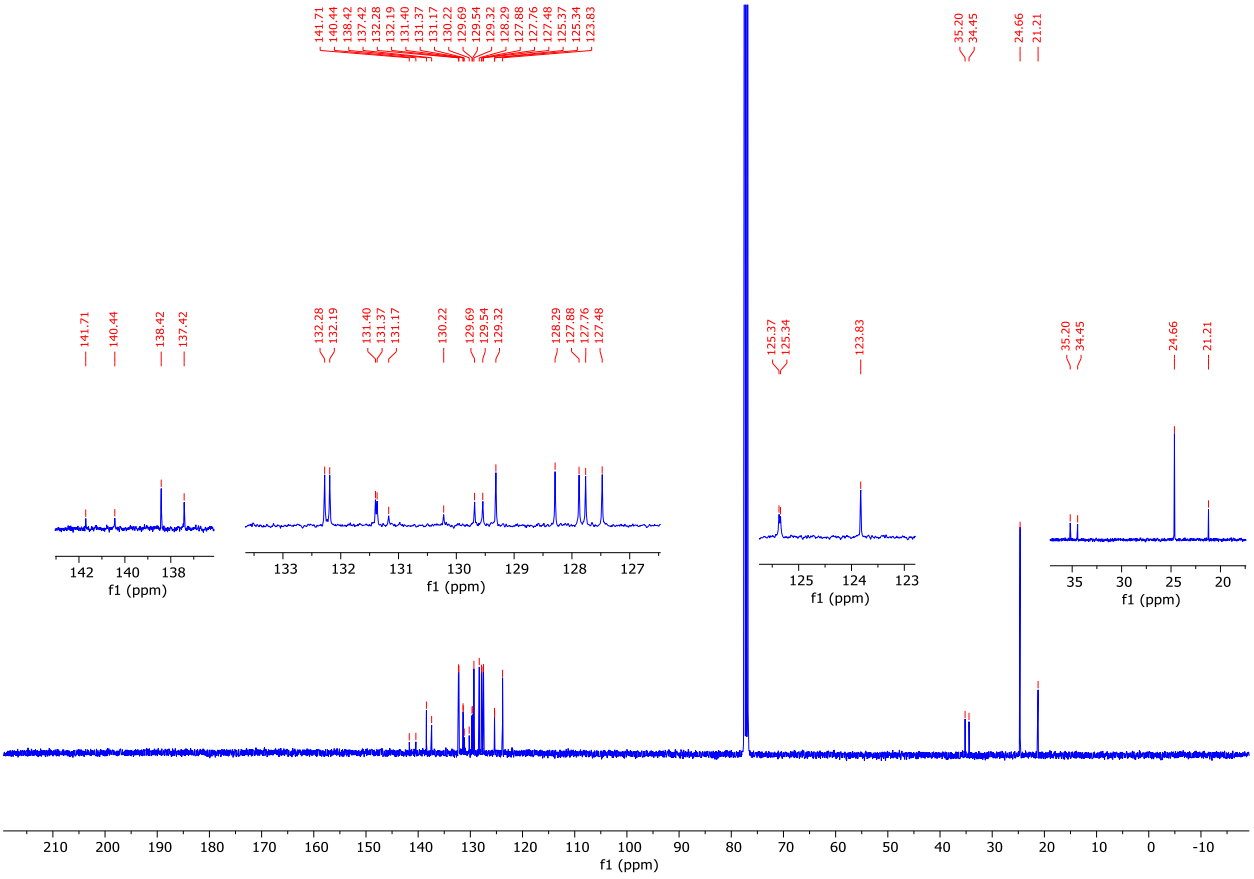

$^{31}P(^{1}H)$ NMR (162 MHz, $CDCl_3$ of **4.5b**

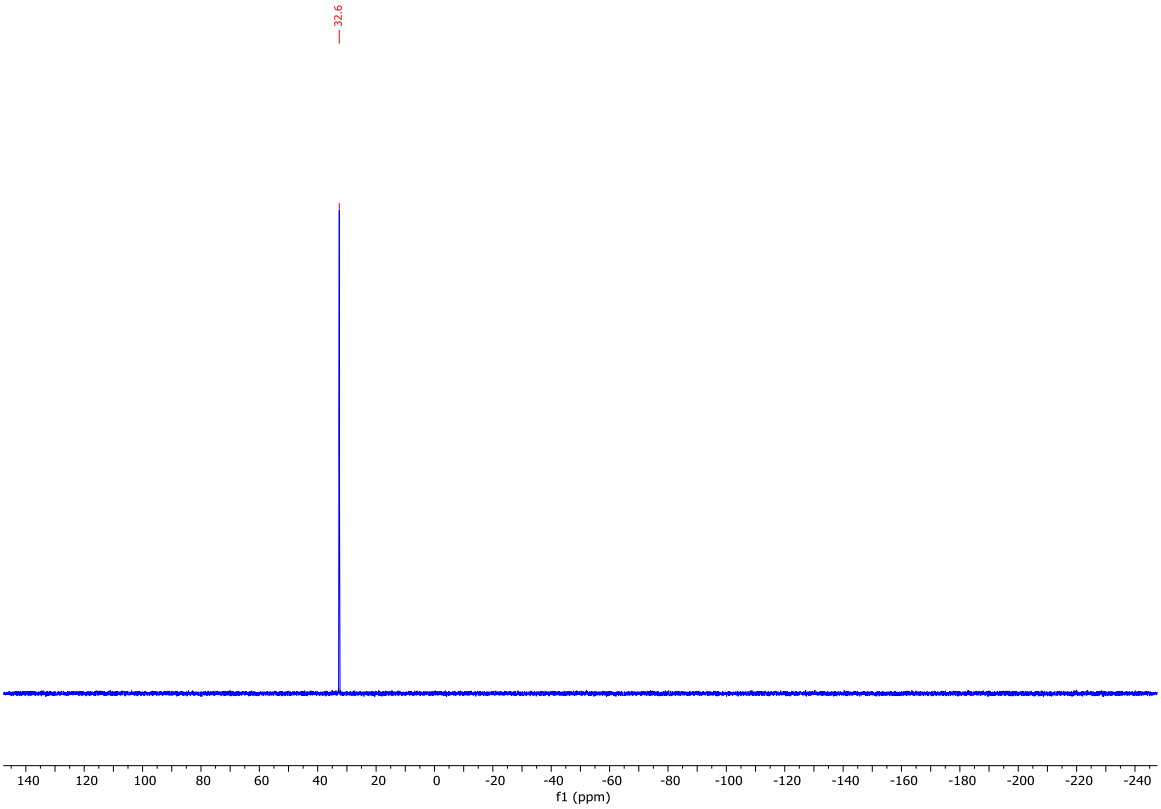

Chiral HPLC chromatogram of **4.5b**

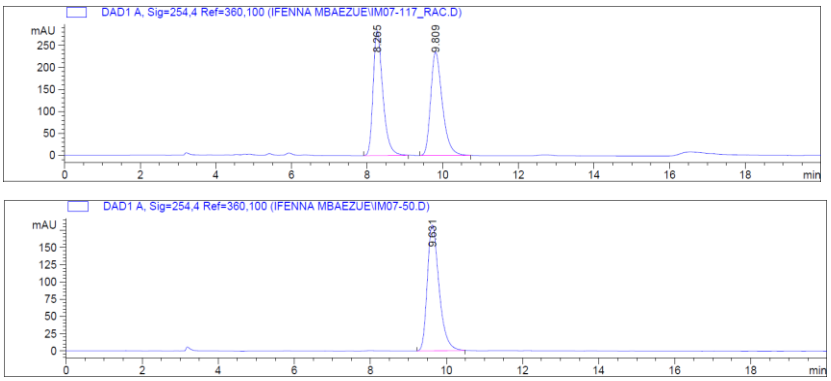

Peak #	RetTime [min]	Type	Width [min]	Area [mAU*s]	Height [mAU]	Area %
1	8.265	BB	0.2700	5050.08691	283.22394	50.1158
2	9.809	BB	0.3258	5026.75732	234.81137	49.8842

Peak #	RetTime [min]	Type	Width [min]	Area [mAU*s]	Height [mAU]	Area %
1	9.631	BB	0.3286	3921.87842	182.59357	100.0000

^{1}H NMR (400 MHz, $CDCl_{3,}$) spectrum of **4.5c**

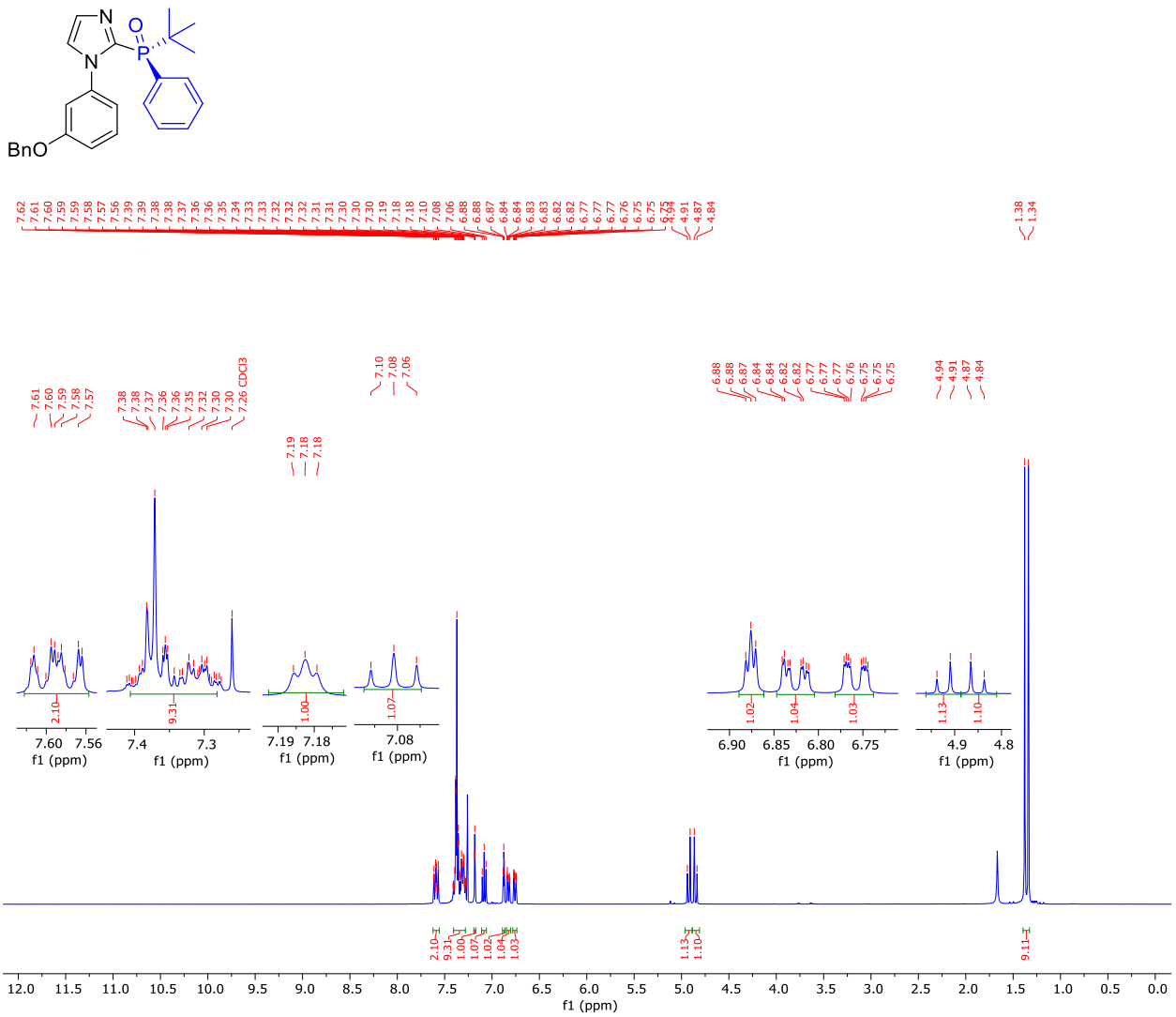

^{13}C (^{1}H) NMR (101 MHz, $CDCl_3$) spectrum of **4.5c**

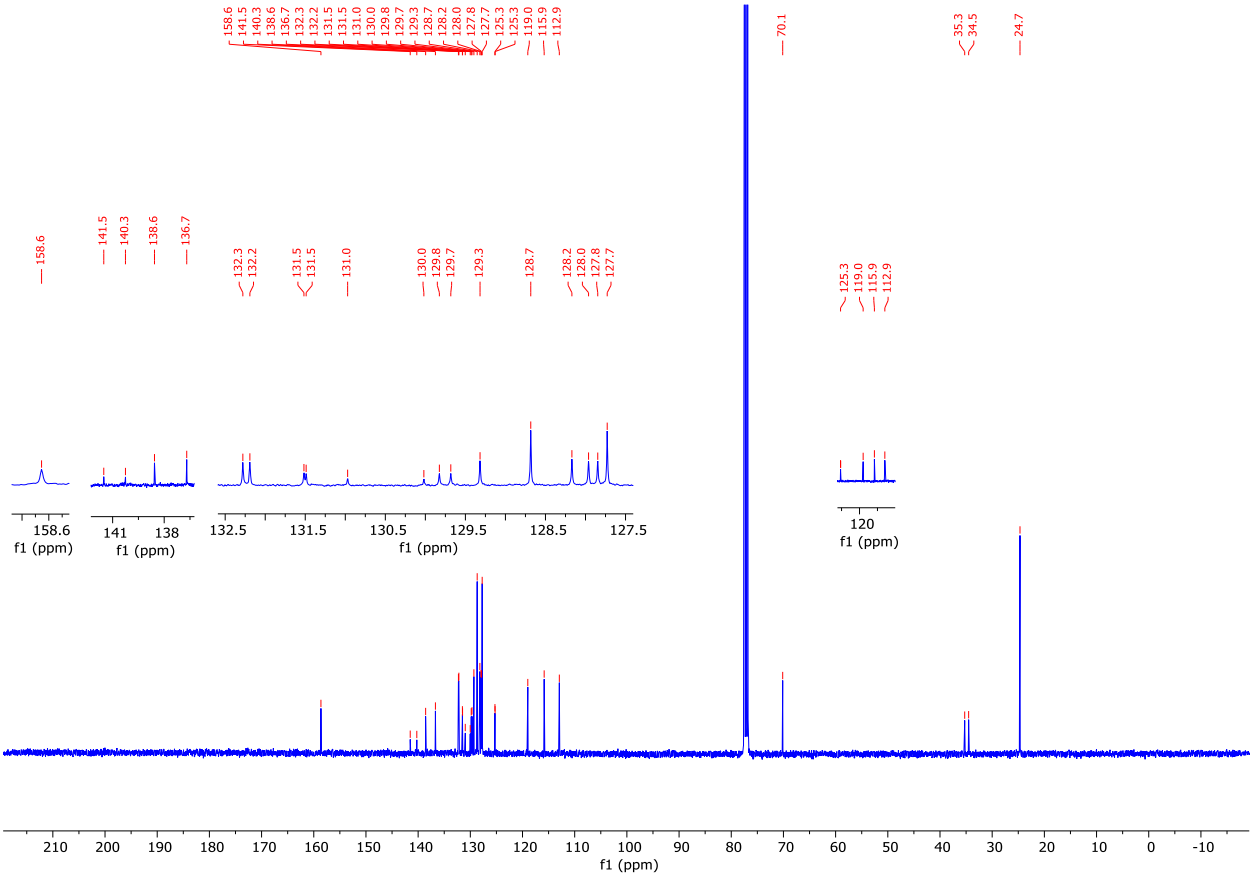

$^{31}P(^{1}H)$ NMR (162 MHz, $CDCl_3$ of **4.5c**

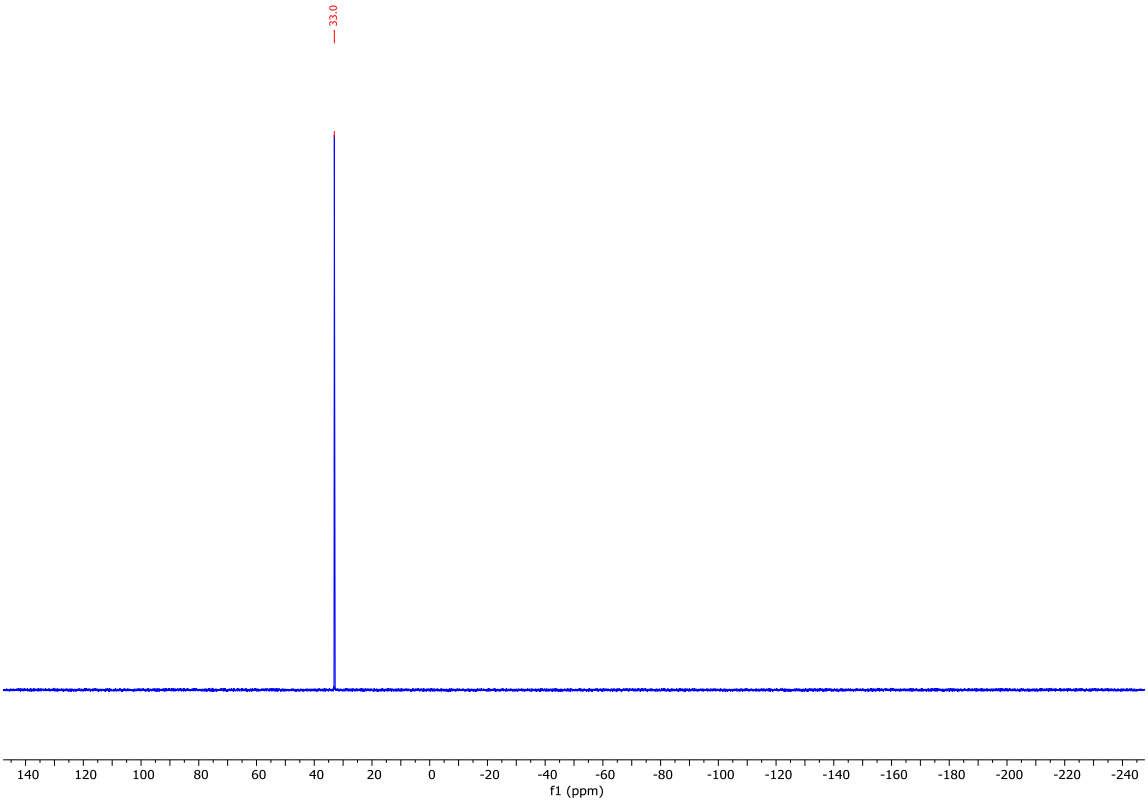

Chiral HPLC Chromatogram of **4.5c**

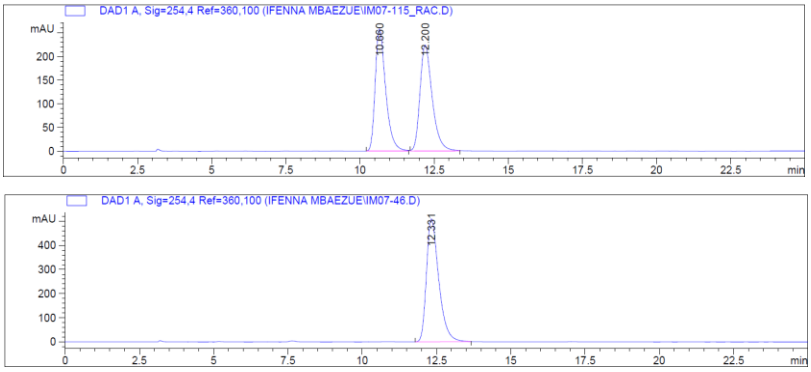

Peak #	RetTime [min]	Type	Width [min]	Area [mAU*s]	Height [mAU]	Area %
1	10.660	BB	0.3717	6300.75342	257.25934	49.7209
2	12.200	BB	0.4378	6371.49219	222.65724	50.2791

Peak #	RetTime [min]	Type	Width [min]	Area [mAU*s]	Height [mAU]	Area %
1	12.331	BB	0.4381	1.46712e4	509.32068	100.0000

^{1}H NMR (400 MHz, $CDCl_3$) spectrum of **4.5d**

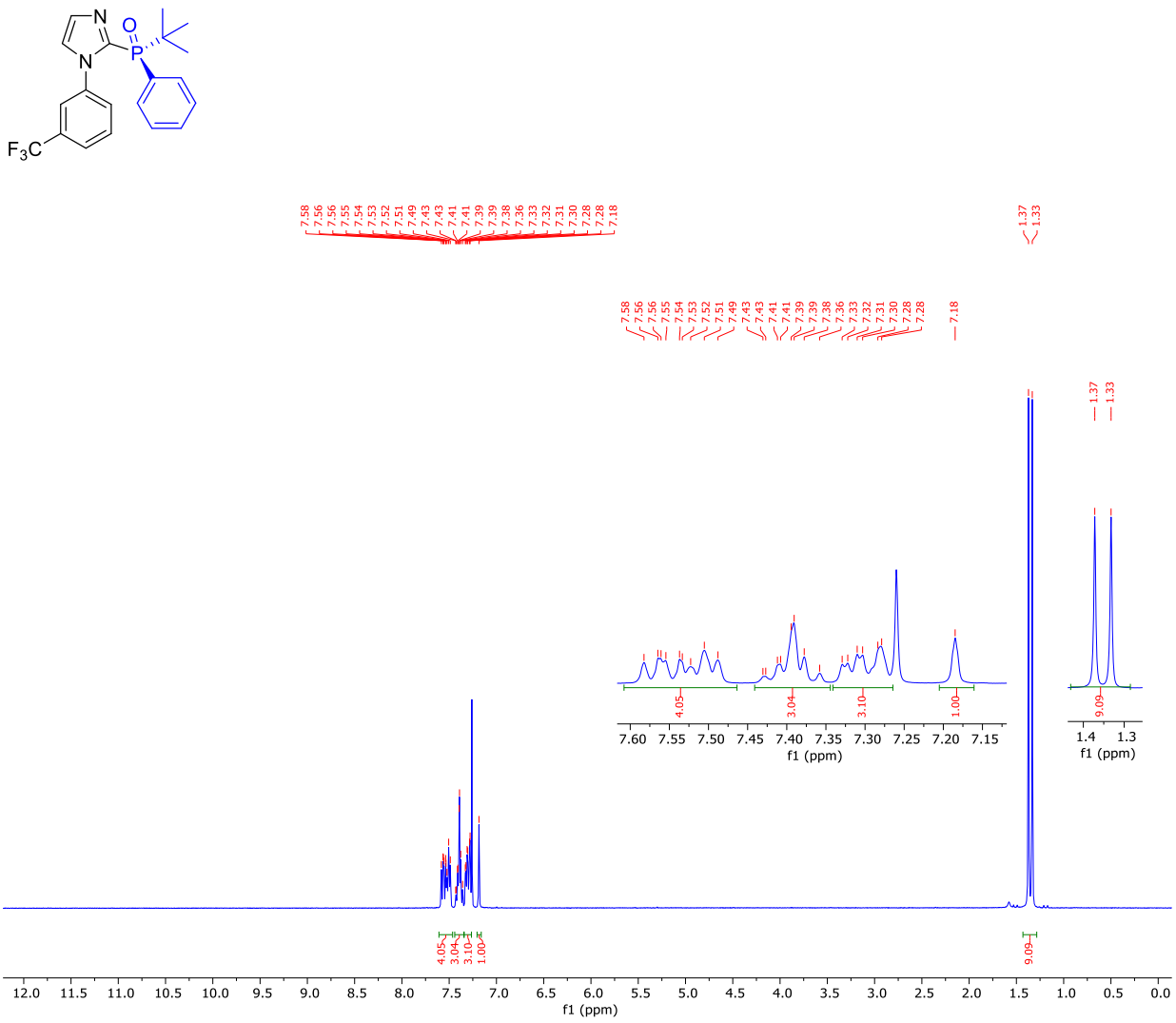

^{13}C (^{1}H) NMR (101 MHz, $CDCl_3$) spectrum of **4.5d**

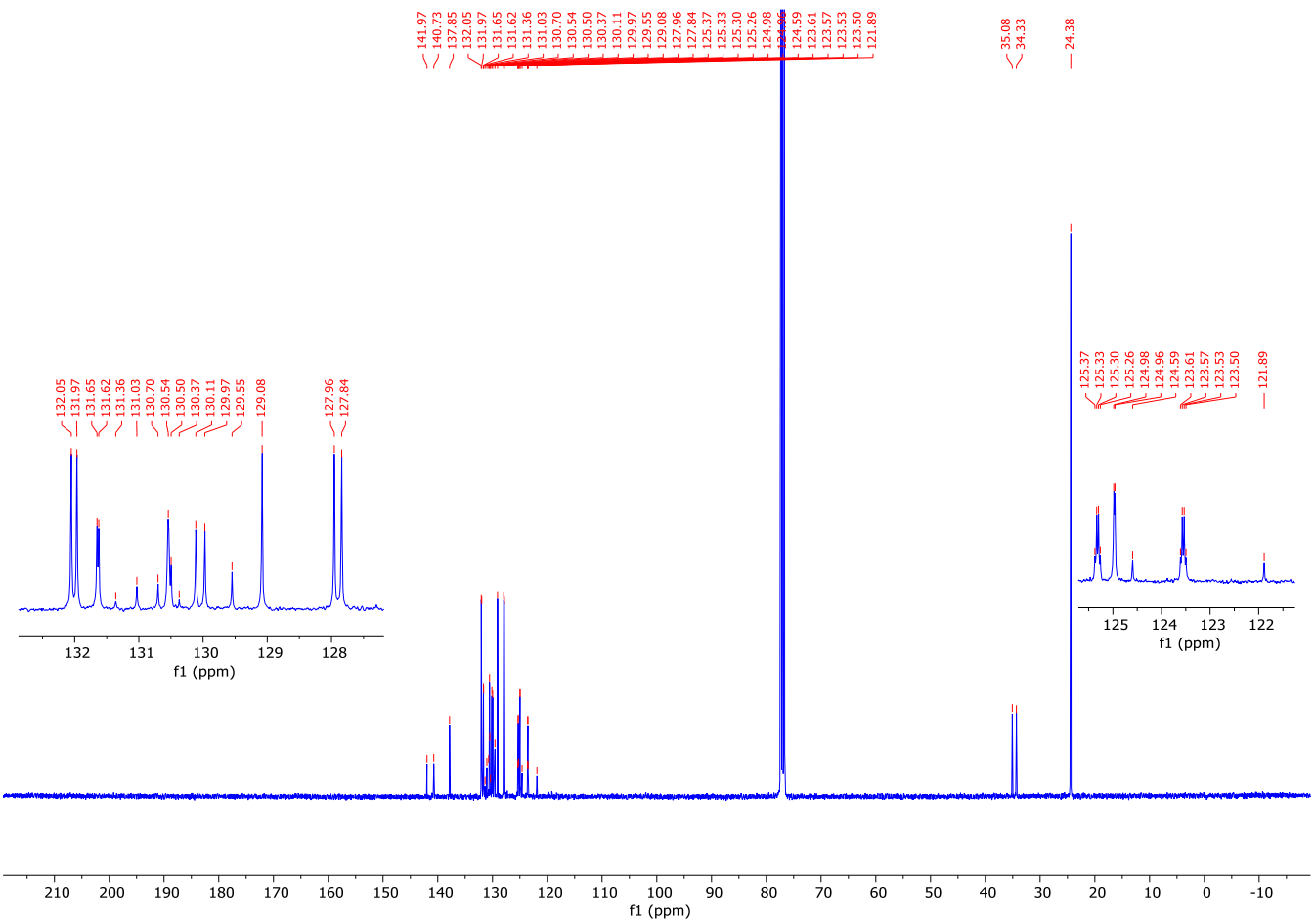

^{19}F (^{1}H) NMR (377 MHz, $CDCl_3$) spectrum of **4.5d**

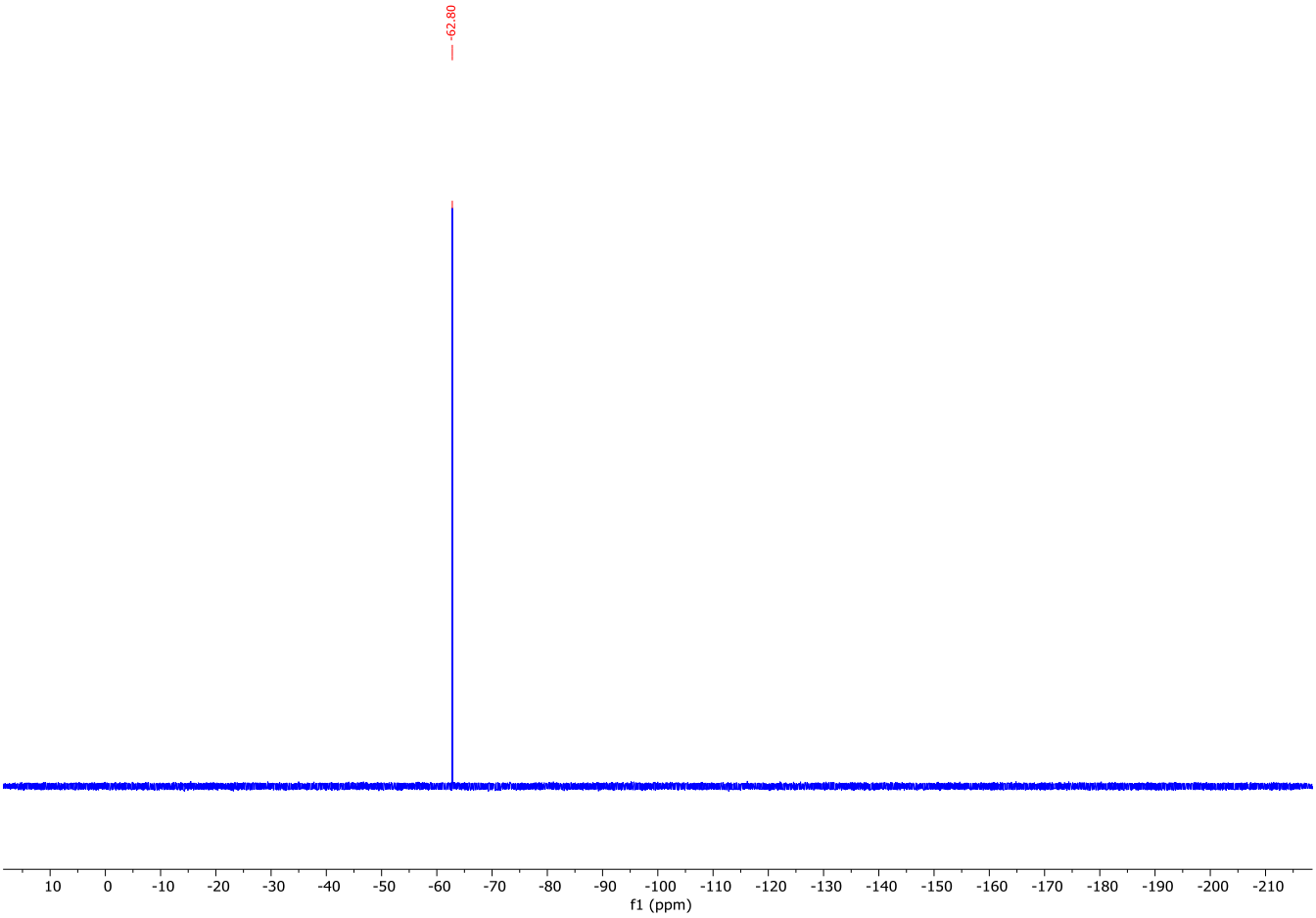

^{31}P (^{1}H) NMR (162 MHz, $CDCl_3$) spectrum of **4.5d**

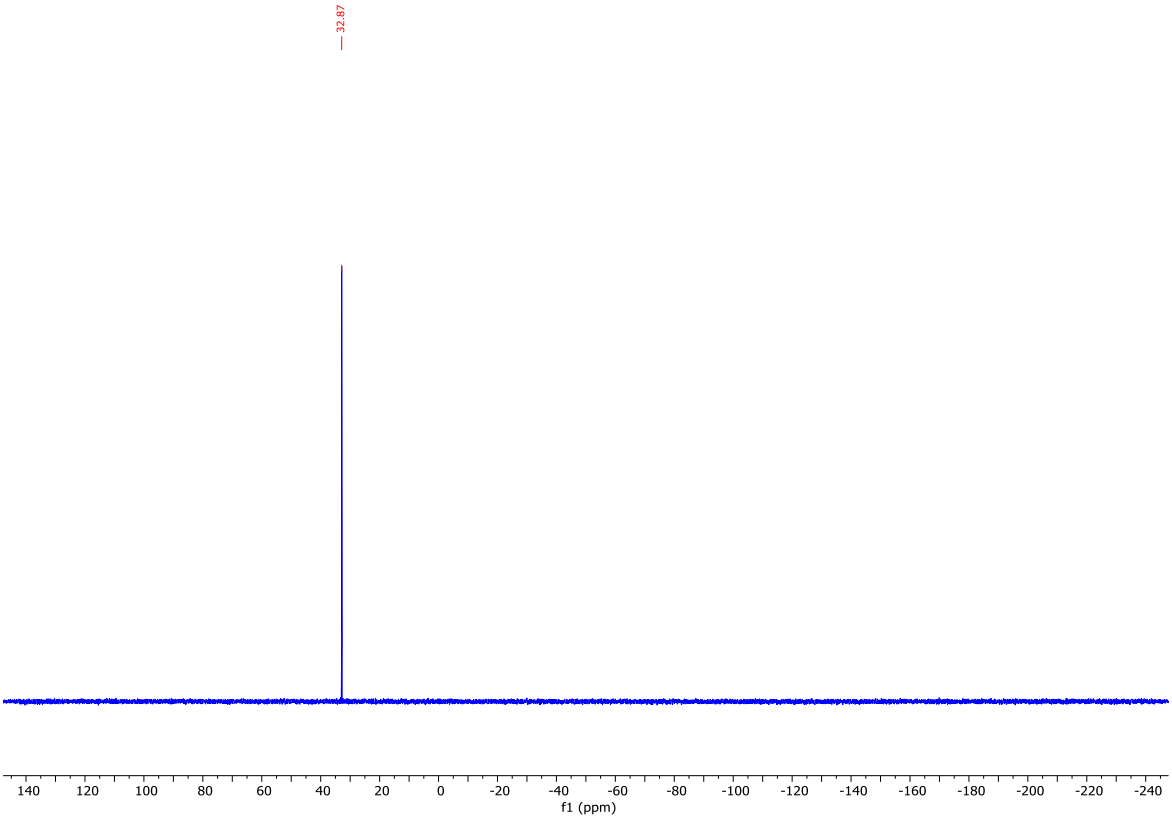

Chiral HPLC Chromatogram of **4.5d**

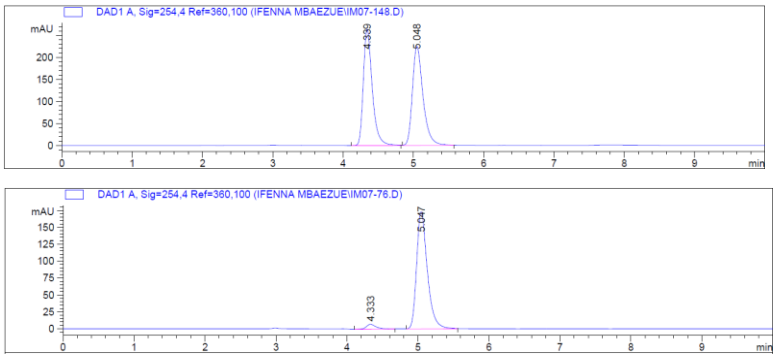

Peak #	RetTime [min]	Type	Width [min]	Area [mAU*s]	Height [mAU]	Area %
1	4.339	BB	0.1338	2355.38135	264.70190	49.9562
2	5.048	BB	0.1585	2359.50903	224.77470	50.0438

Peak #	RetTime [min]	Type	Width [min]	Area [mAU*s]	Height [mAU]	Area %
1	4.333	BB	0.1538	76.02120	7.28187	4.0083
2	5.047	BB	0.1607	1820.59058	173.06908	95.9917

^{1}H NMR (400 MHz, $CDCl_{3,}$) spectrum of **4.5e**

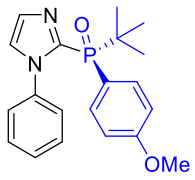

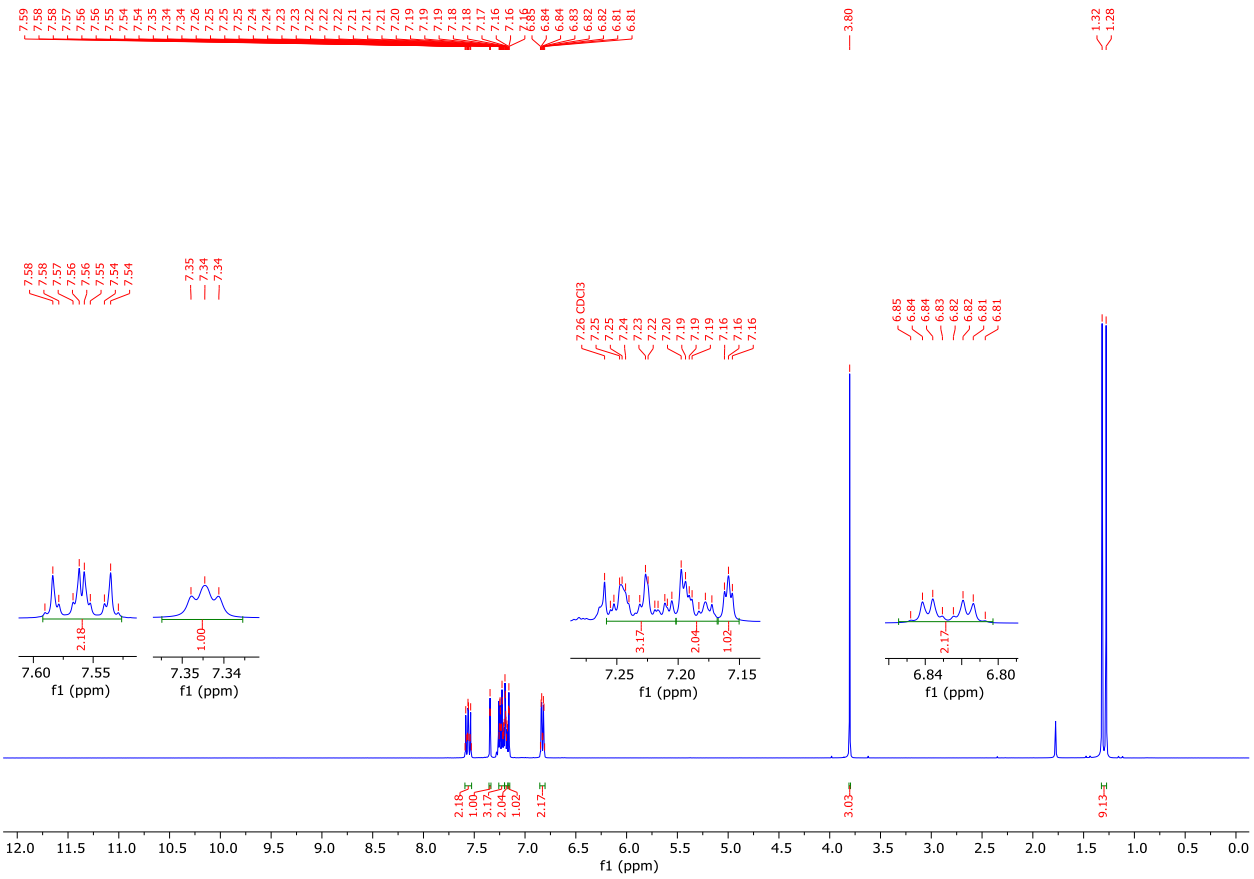

^{13}C (^{1}H) NMR (101 MHz, $CDCl_3$) spectrum of **4.5e**

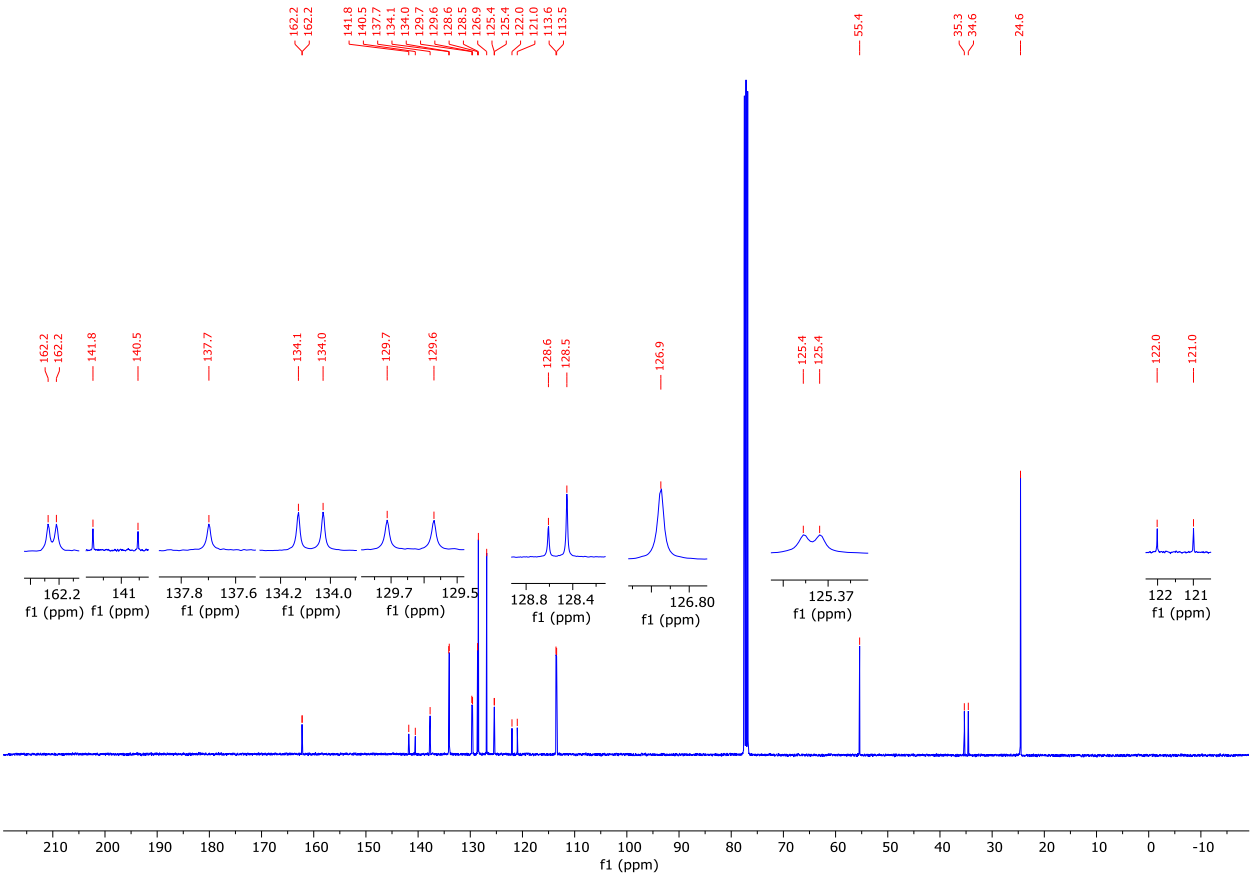

$^{31}P(^{1}H)$ NMR (162 MHz, $CDCl_3$) of **4.5e**

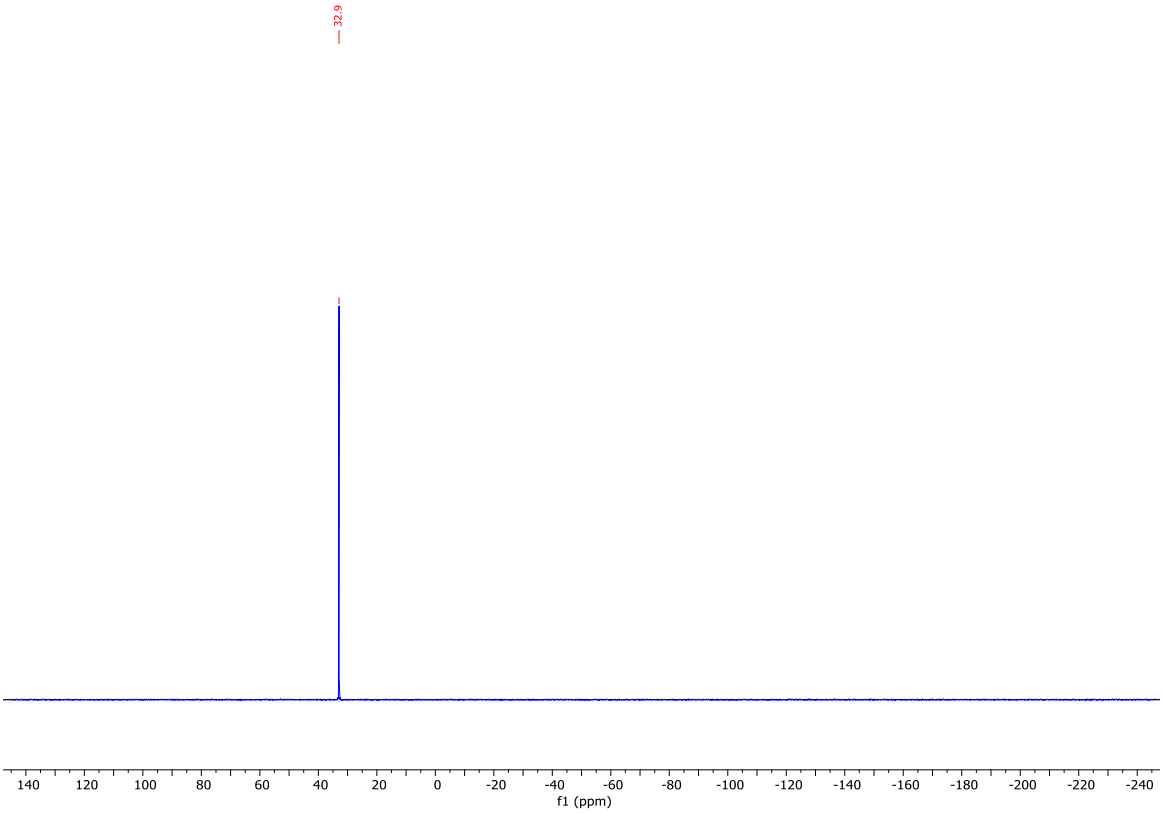

Chiral HPLC Chromatogram of **4.5e**

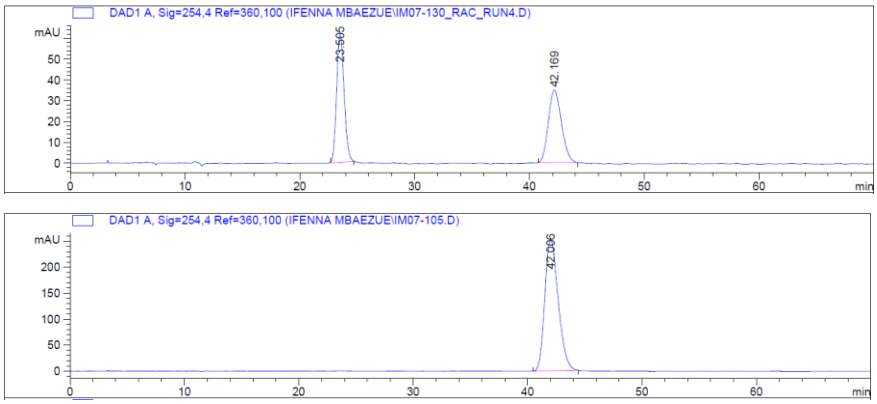

Peak #	RetTime [min]	Type	Width [min]	Area [mAU*s]	Height [mAU]	Area %
1	23.505	BB	0.6812	2798.60913	62.41037	50.2942
2	42.169	BB	1.1808	2765.86987	34.81707	49.7058

Peak #	RetTime [min]	Type	Width [min]	Area [mAU*s]	Height [mAU]	Area %
1	42.006	BB	1.2597	2.05294e4	252.19910	100.0000

^{1}H NMR (800 MHz, CD_2Cl_2, 0 °C) spectrum of **4.5f**

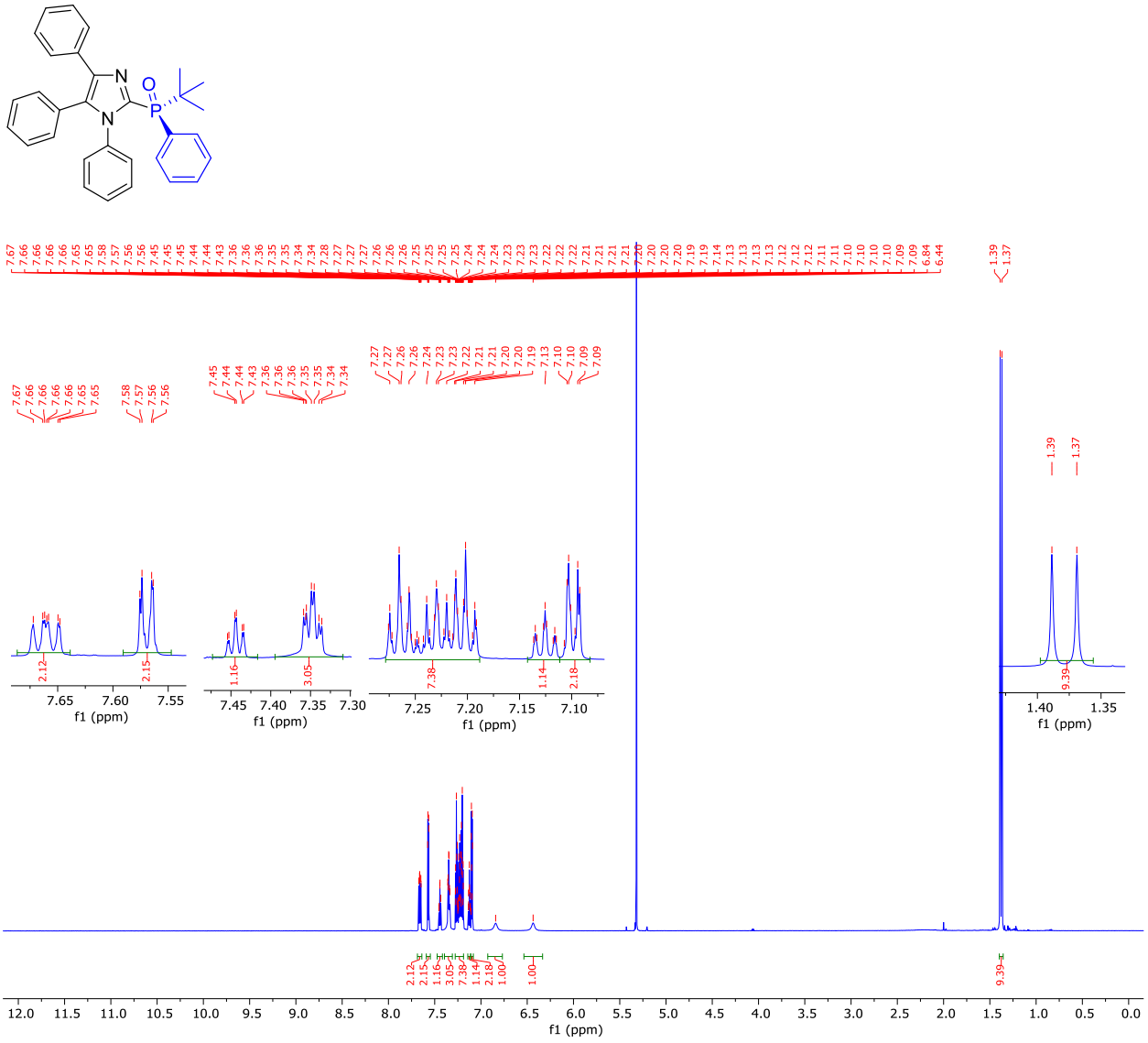

^{13}C (^{1}H) NMR (201 MHz, CD_2Cl_2, 0 °C) spectrum of **4.5f**

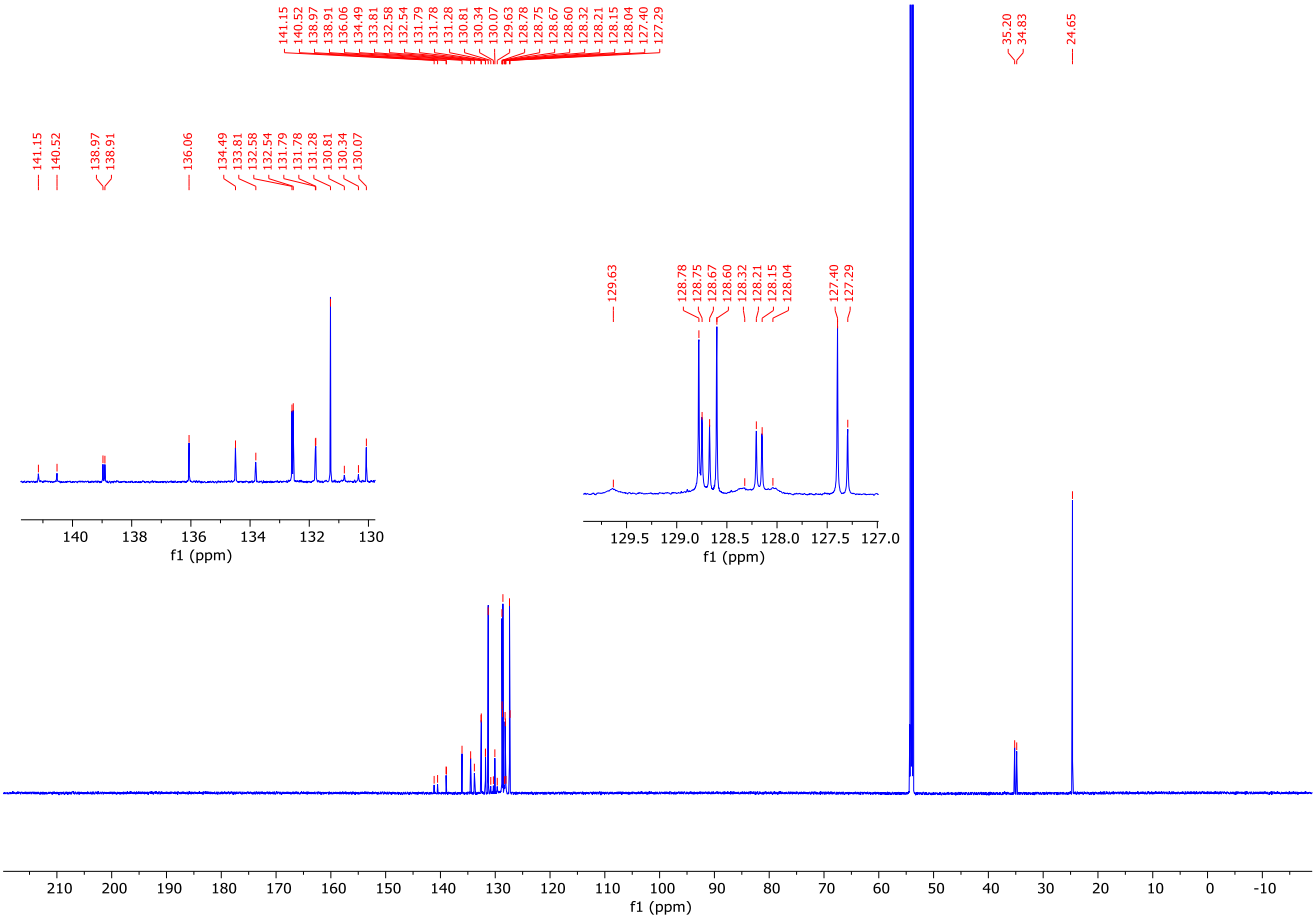

$^{31}P(^{1}H)$ NMR (162 MHz, CD_2Cl_2) of **4.5f**

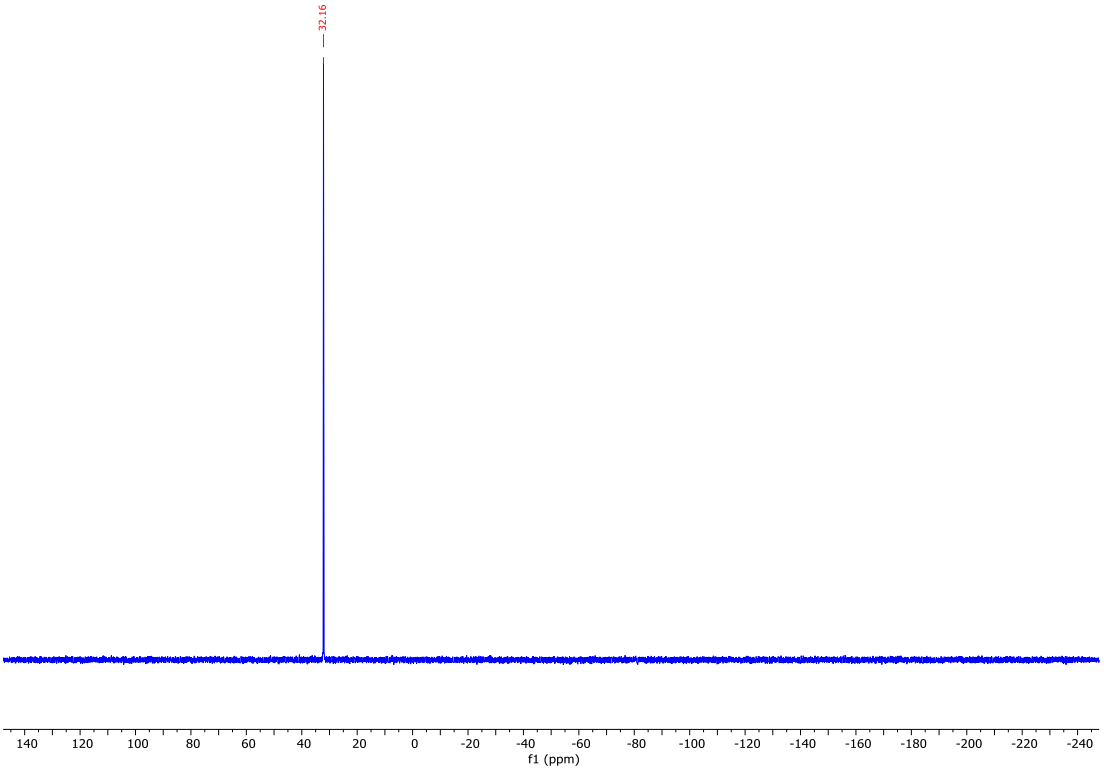

Chiral HPLC Chromatogram of **4.5f**

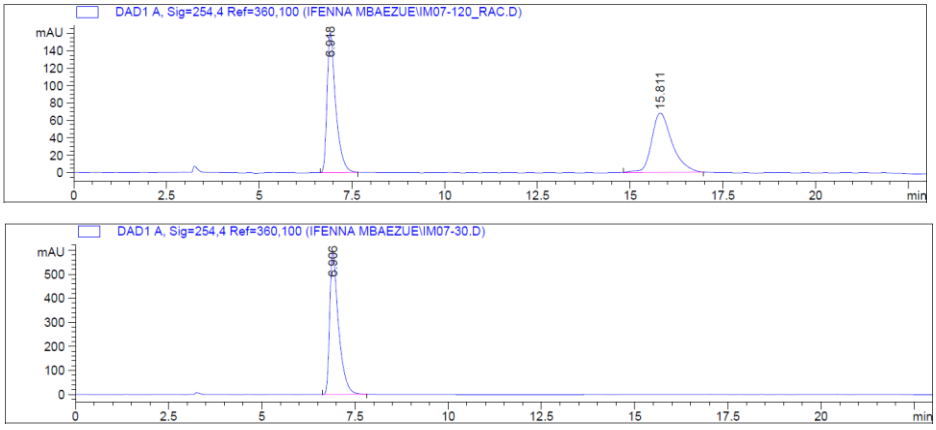

Peak #	RetTime [min]	Type	Width [min]	Area [mAU*s]	Height [mAU]	Area %
1	6.918	BB	0.2392	2607.63281	160.76247	49.7802
2	15.811	BB	0.5770	2630.66235	68.34666	50.2198

Peak #	RetTime [min]	Type	Width [min]	Area [mAU*s]	Height [mAU]	Area %
1	6.906	BB	0.2450	9773.82910	590.76819	100.0000

^{1}H NMR (800 MHz, CD_2Cl_2, 0 °C) spectrum of **4.5g**

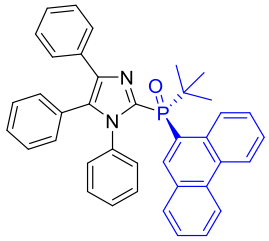

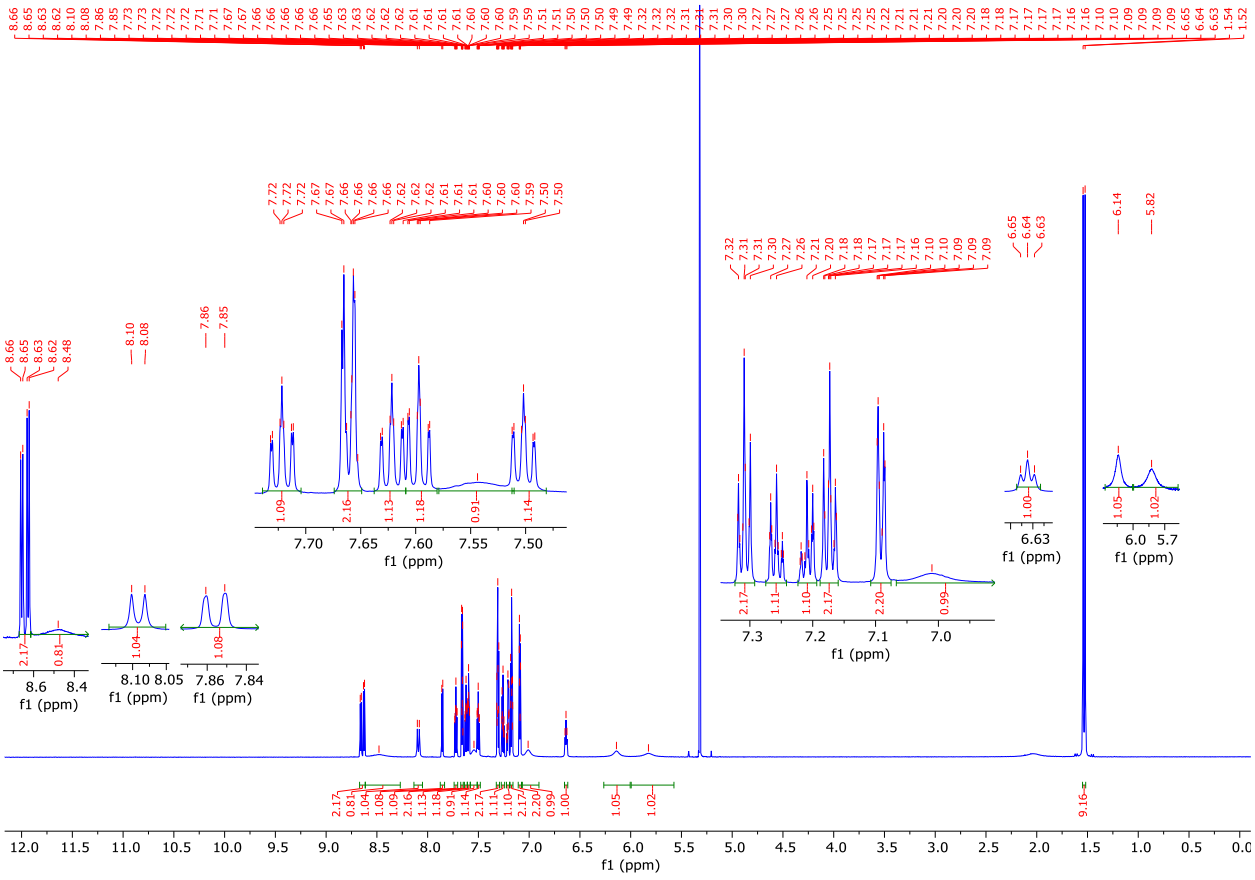

$^{13}C(^{1}H)$ NMR (200 MHz, CD_2Cl_2, 0 °C) of **4.5g**

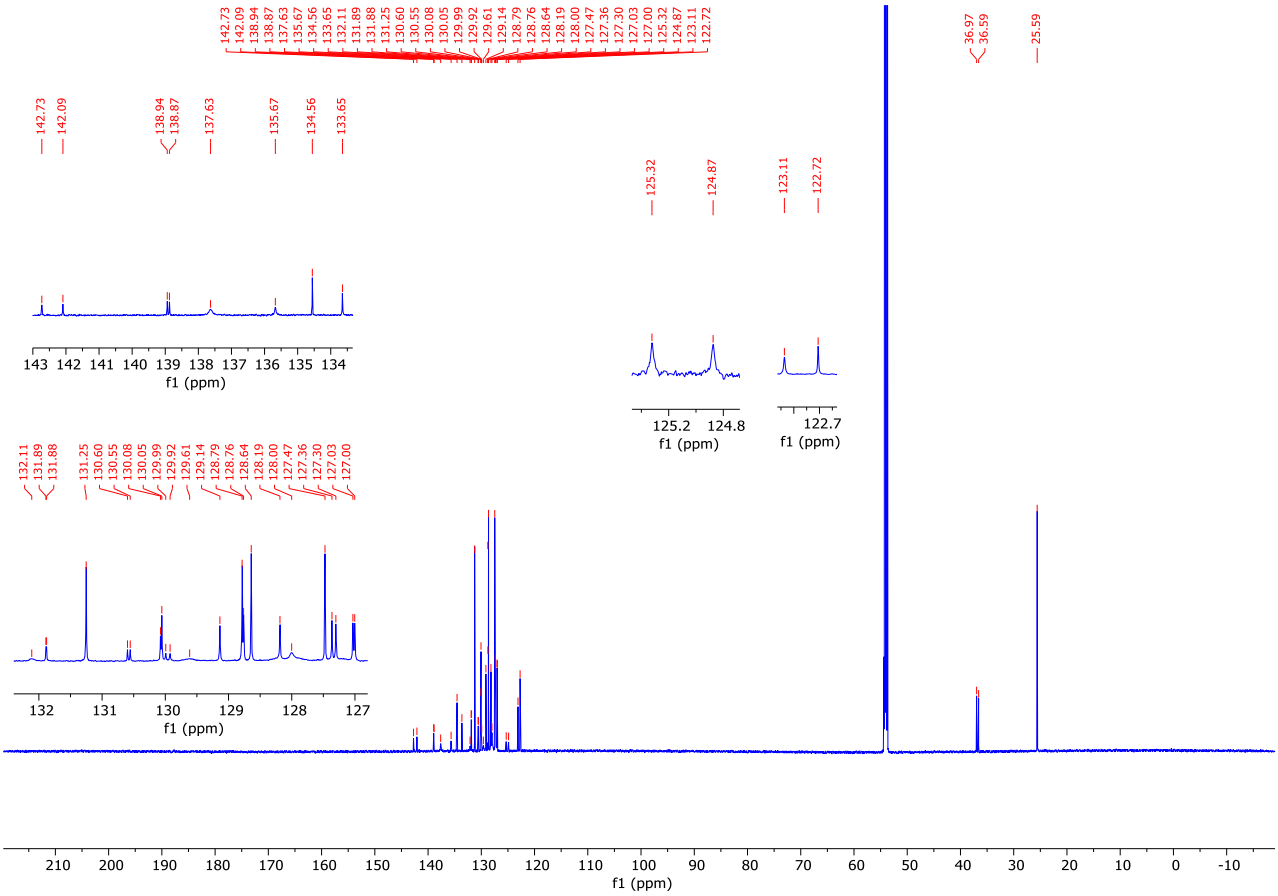

$^{31}P(^{1}H)$ NMR (162 MHz, CD_2Cl_2) of **4.5g**

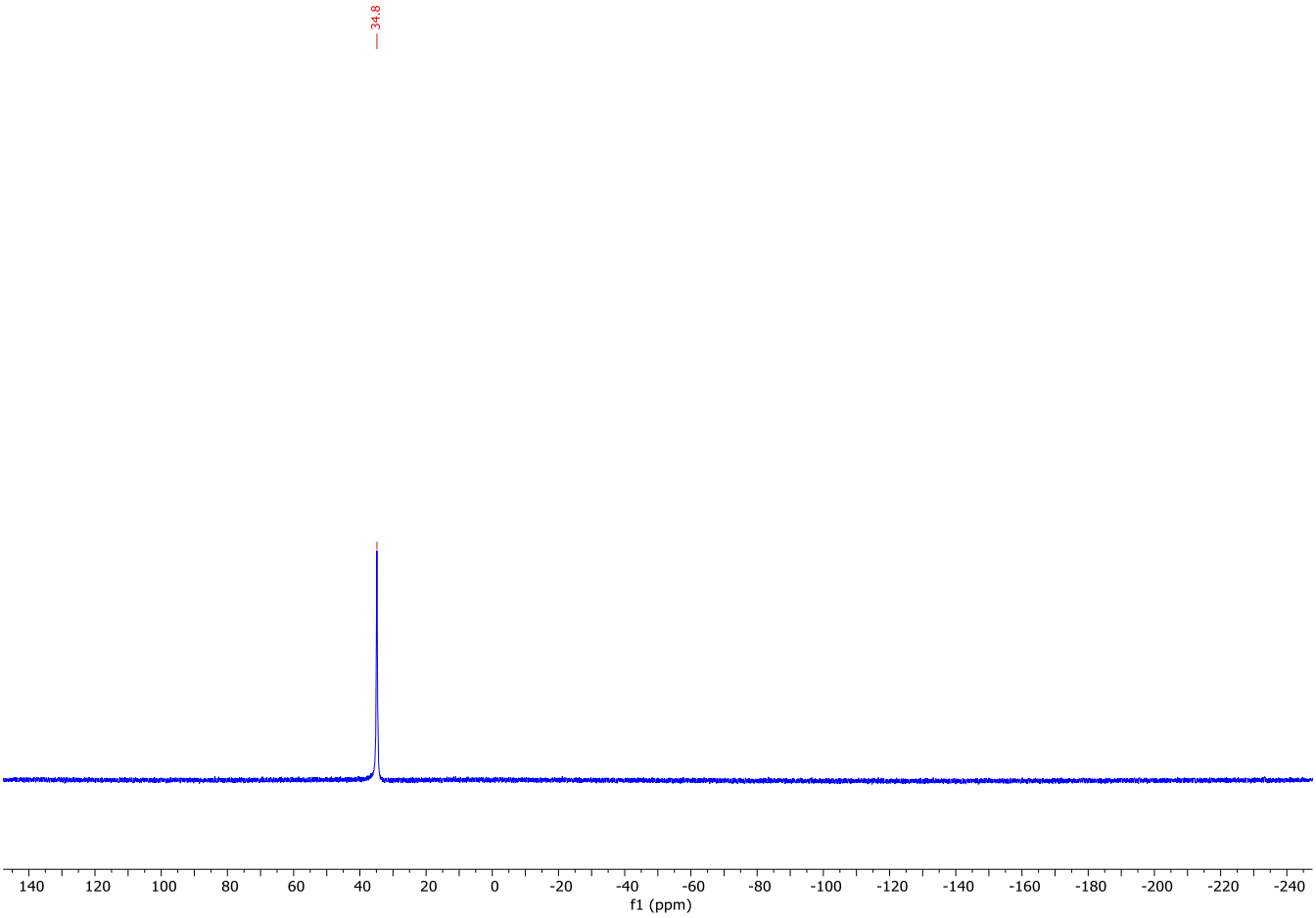

Chiral HPLC Chromatogram of **4.5g**

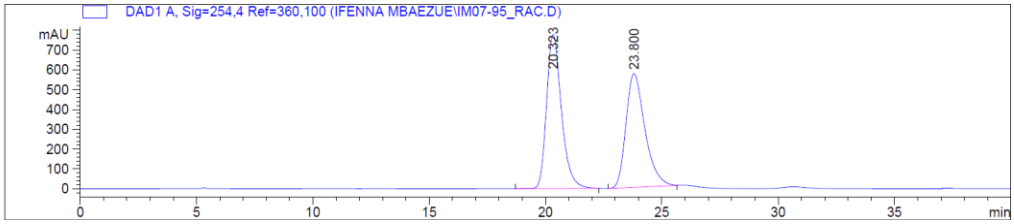

Before trituration/crystallisation

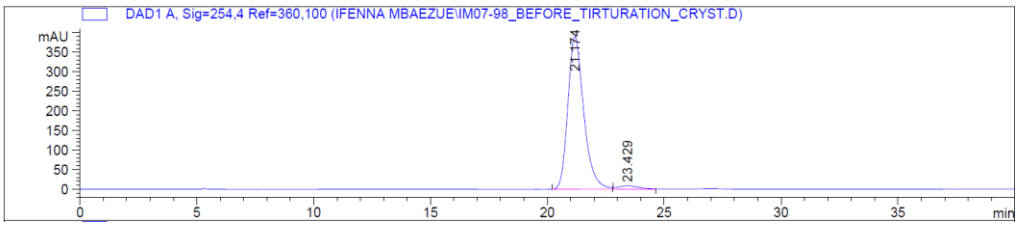

After trituration/crystallisation

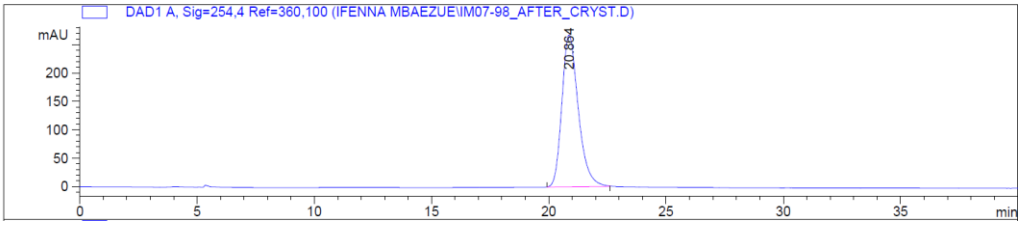

Peak #	RetTime [min]	Type	Width [min]	Area [mAU*s]	Height [mAU]	Area %
1	20.323	BB	0.6848	3.45564e4	777.08307	51.5465
2	23.800	BB	0.8670	3.24829e4	573.35223	48.4535

Peak #	RetTime [min]	Type	Width [min]	Area [mAU*s]	Height [mAU]	Area %
1	21.174	BB	0.7196	1.80496e4	381.73096	97.4310
2	23.426	BB	0.8061	475.92056	8.13980	2.5690

Peak #	RetTime [min]	Type	Width [min]	Area [mAU*s]	Height [mAU]	Area %
1	20.864	BB	0.7446	1.29933e4	267.54233	100.0000

^{1}H NMR (800 MHz, CD_2Cl_2, 0 °C) spectrum of **4.6**

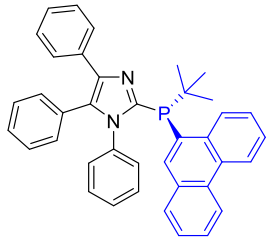

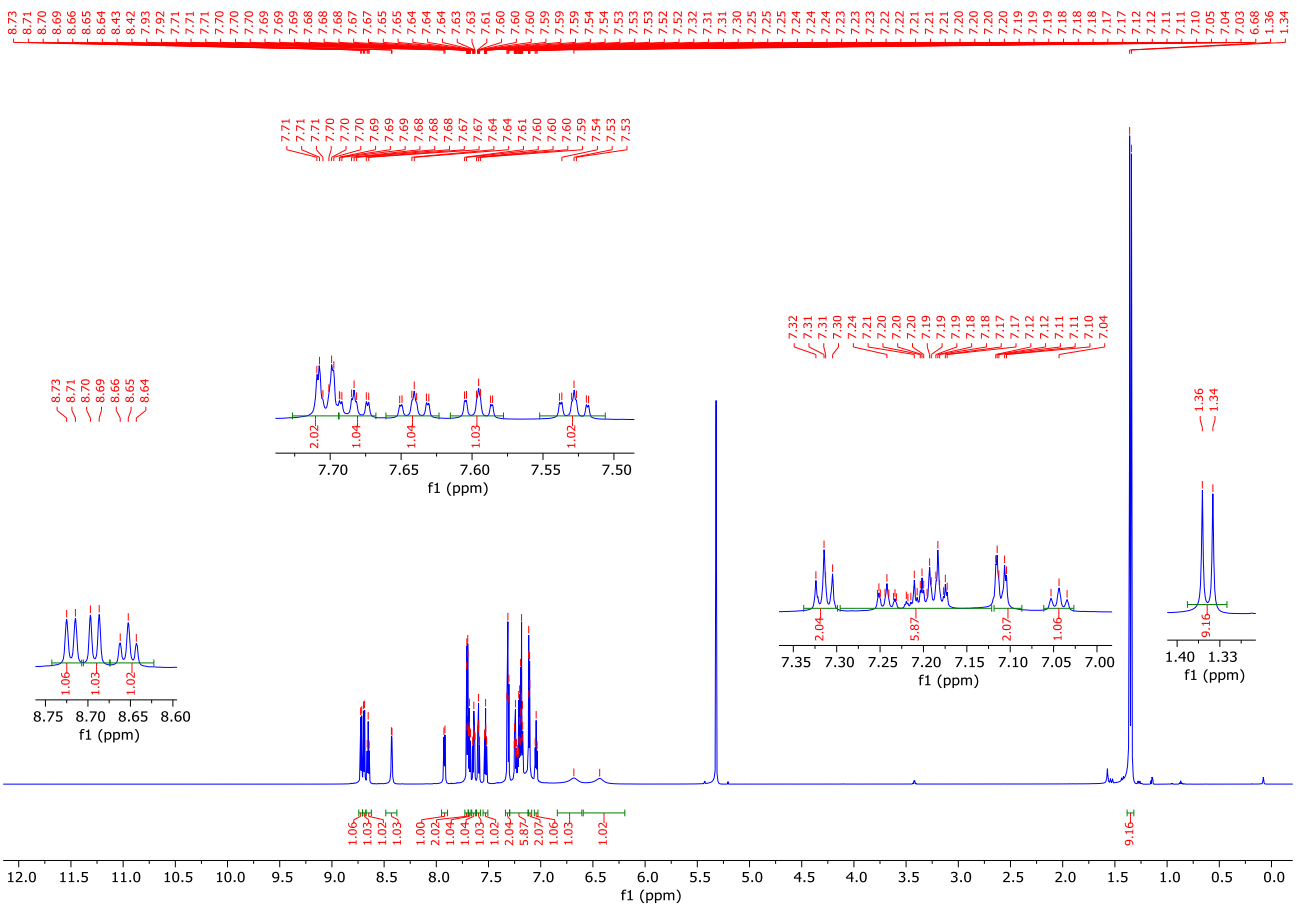

^{13}C (^{1}H) NMR (200 MHz, CD_2Cl_2, 0 °C) spectrum of **4.6**

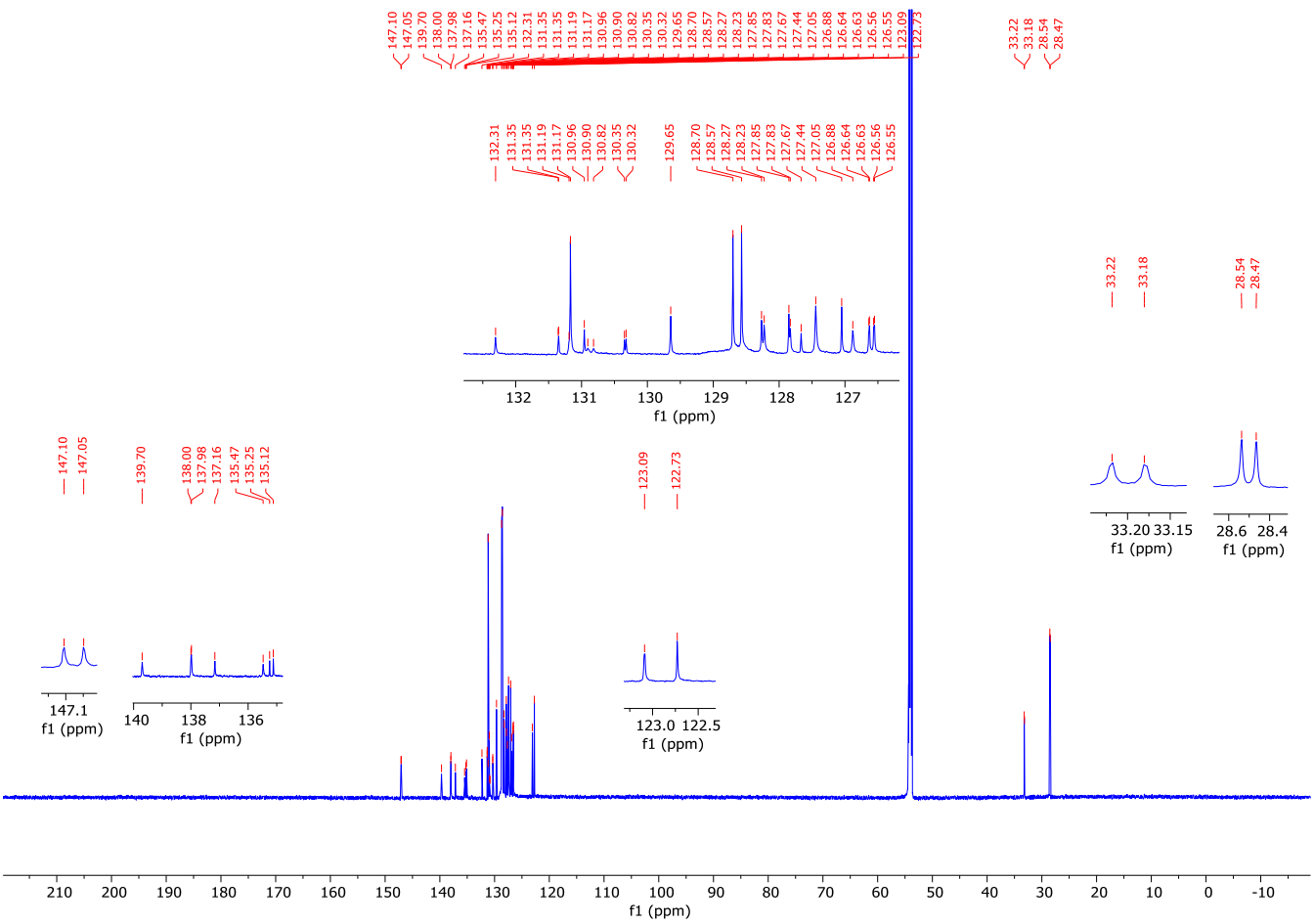

$^{31}P(^{1}H)$ NMR (162 MHz, CD_2Cl_2) of **4.6**

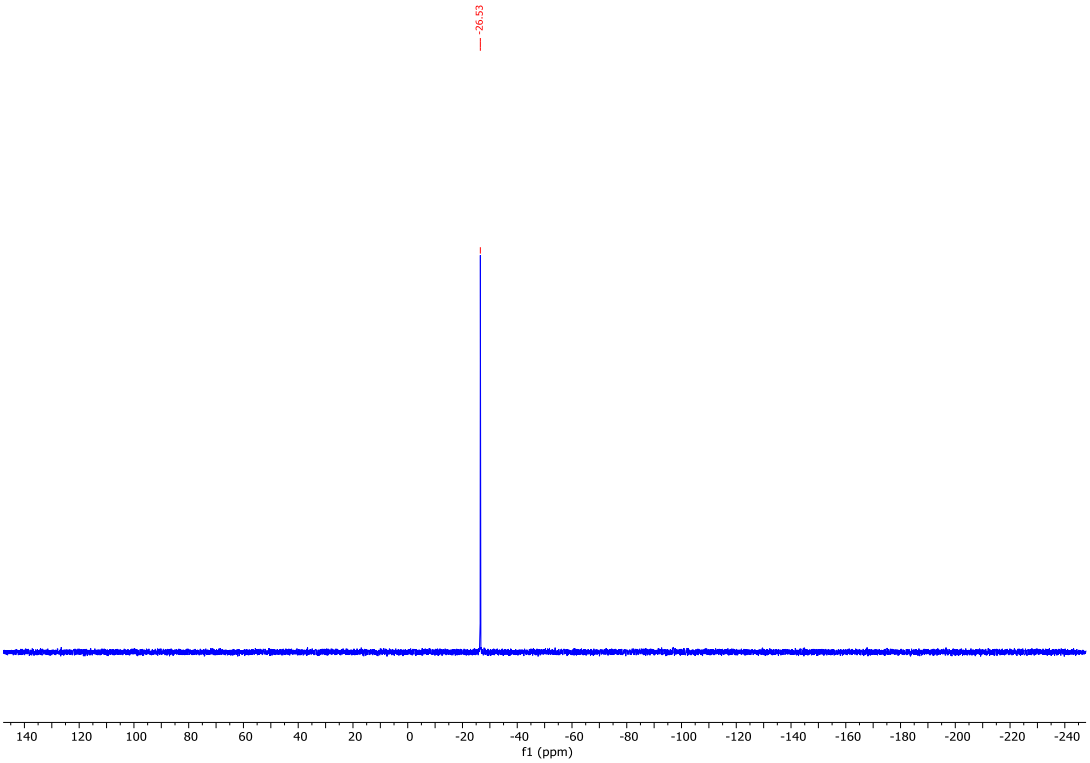

Chiral HPLC Chromatogram of oxidised **4.6**

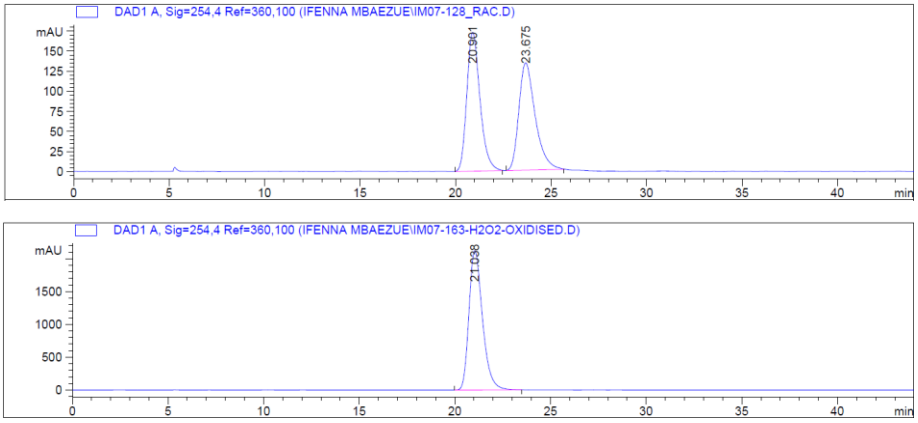

Peak #	RetTime [min]	Type	Width [min]	Area [mAU*s]	Height [mAU]	Area %
1	20.901	BB	0.7247	8270.82910	172.72525	51.0129
2	23.675	BB	0.8943	7942.39014	133.45621	48.9871

Peak #	RetTime [min]	Type	Width [min]	Area [mAU*s]	Height [mAU]	Area %
1	21.038	BB	0.7414	1.04312e5	2122.21436	100.0000

^{1}H NMR (400 MHz, $CDCl_3$) spectrum of **4.9**

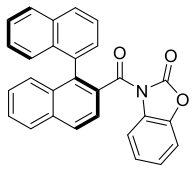

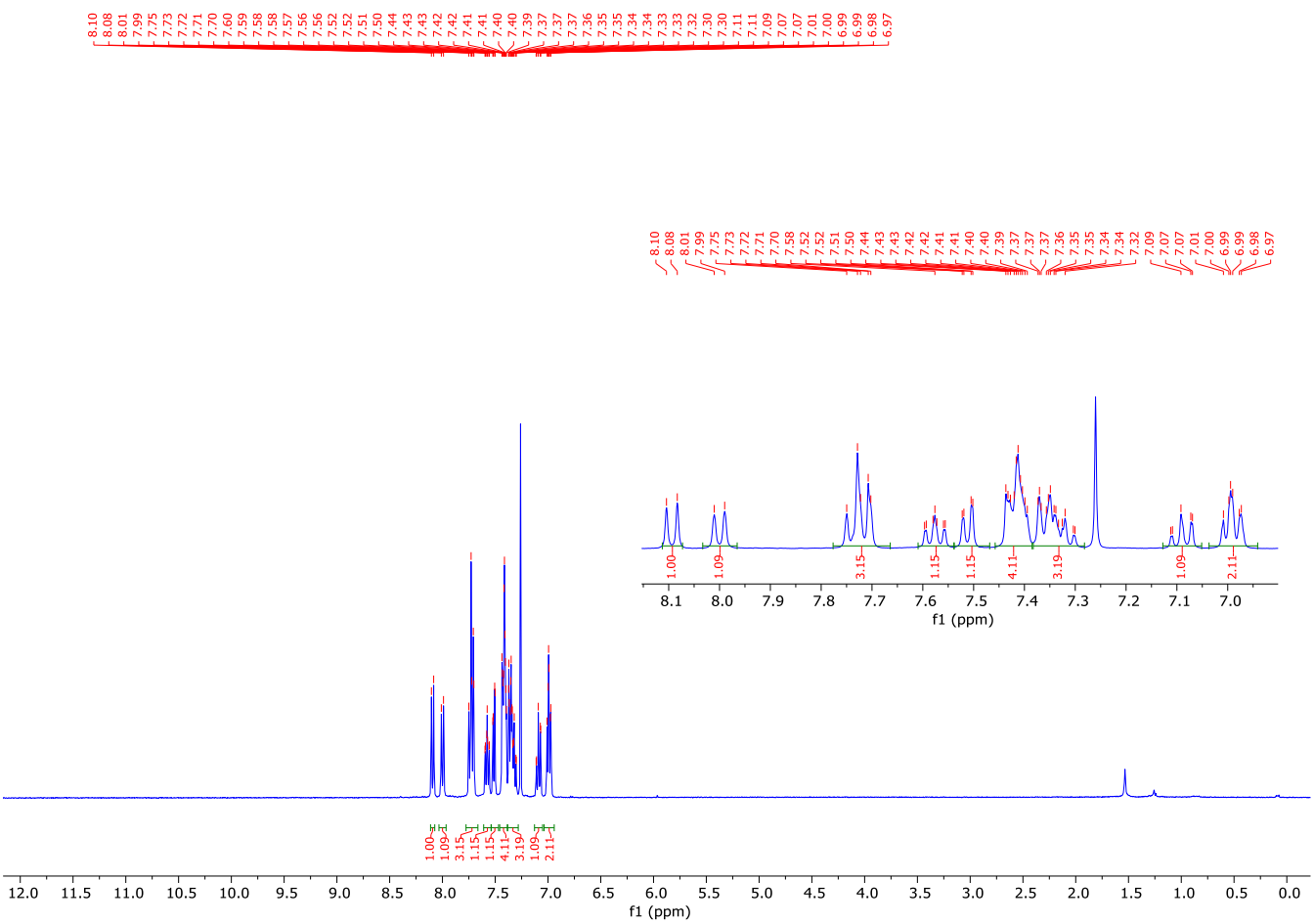

^{13}C (^{1}H) NMR (101 MHz, $CDCl_3$) spectrum of **4.9**

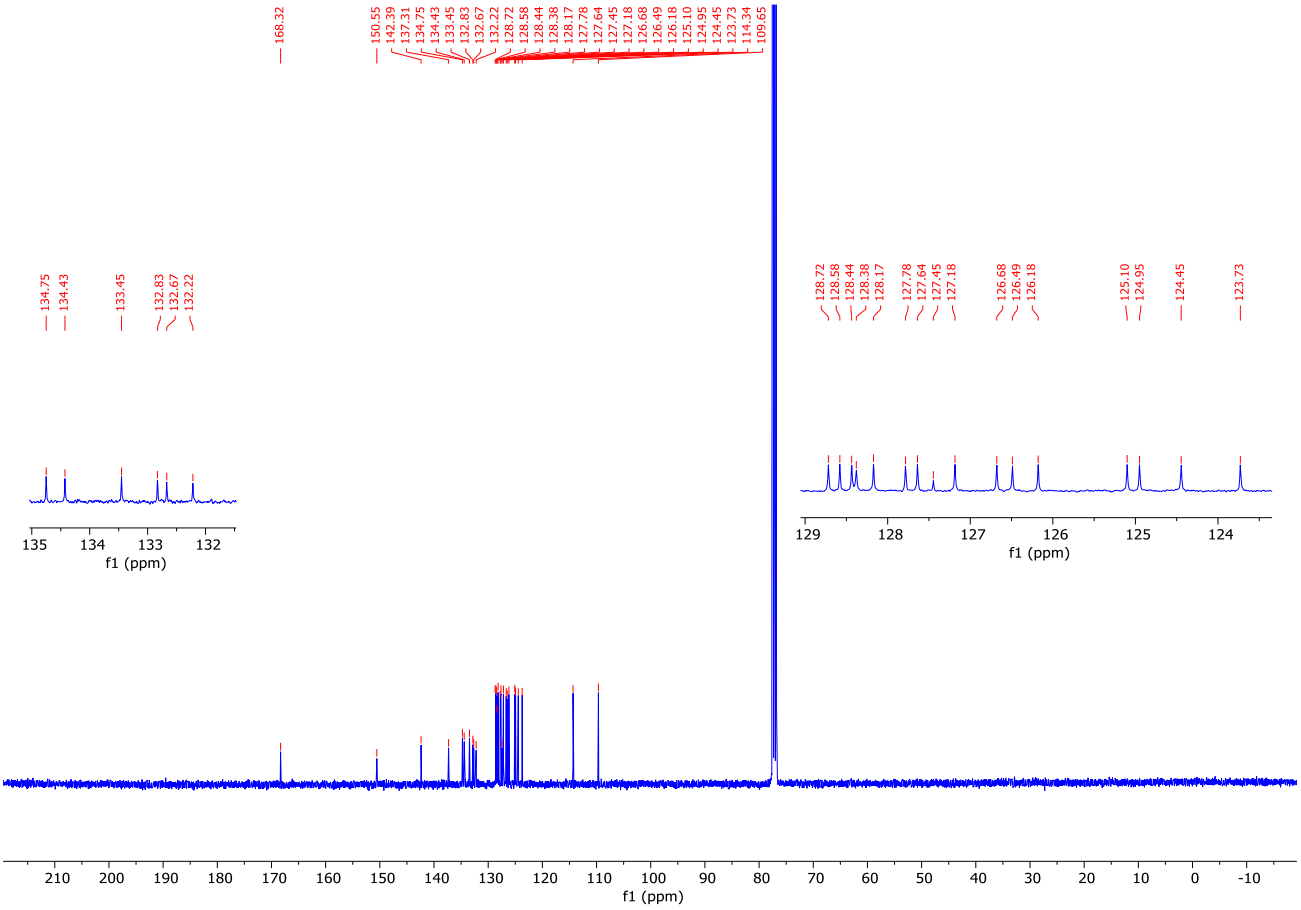

Chiral HPLC Chromatogram of **4.9**

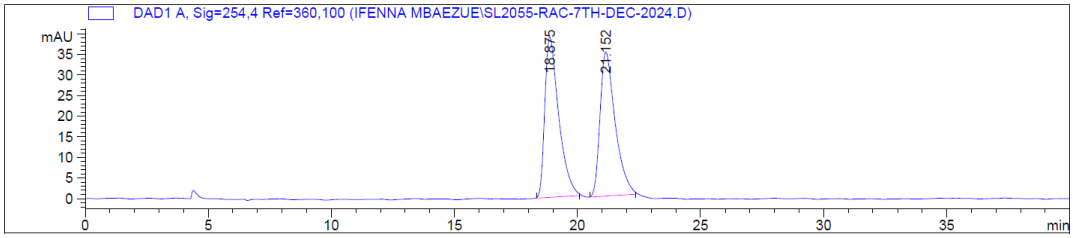

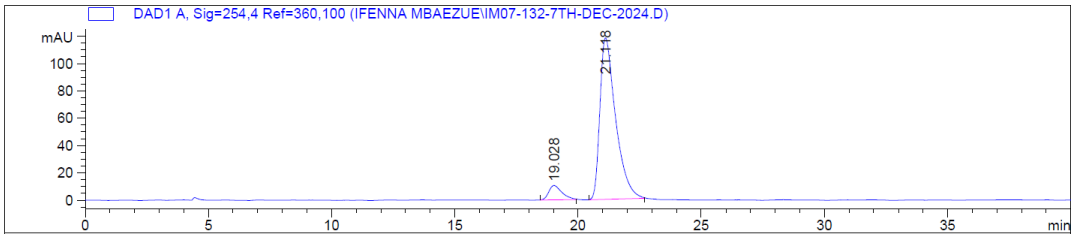

Chromatogram of product from mother liquor after crystallisation

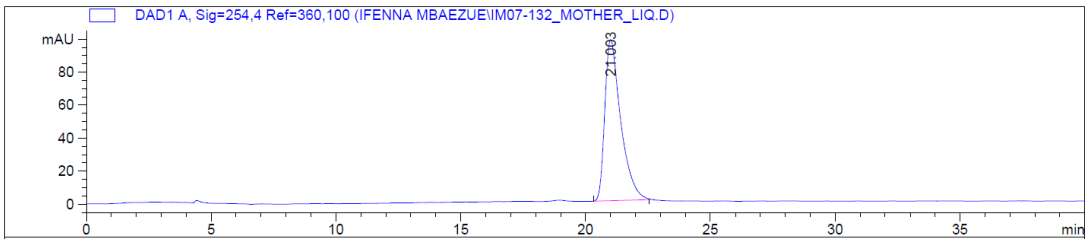

Peak #	RetTime [min]	Type	Width [min]	Area [mAU*s]	Height [mAU]	Area %
1	18.875	BB	0.5784	1527.46094	38.87504	50.5723
2	21.152	BB	0.6222	1492.89111	34.96113	49.4277

Peak #	RetTime [min]	Type	Width [min]	Area [mAU*s]	Height [mAU]	Area %
1	19.028	BB	0.5427	384.30673	10.45941	6.8359
2	21.118	BB	0.6586	5237.59570	118.27800	93.1641

Peak #	RetTime [min]	Type	Width [min]	Area [mAU*s]	Height [mAU]	Area %
1	21.003	BB	0.6597	4319.62012	97.72627	100.0000

^{1}H NMR (500 MHz, $CDCl_3$) spectrum of ^{2}H-**4.2a**

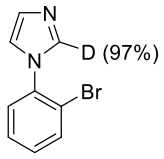

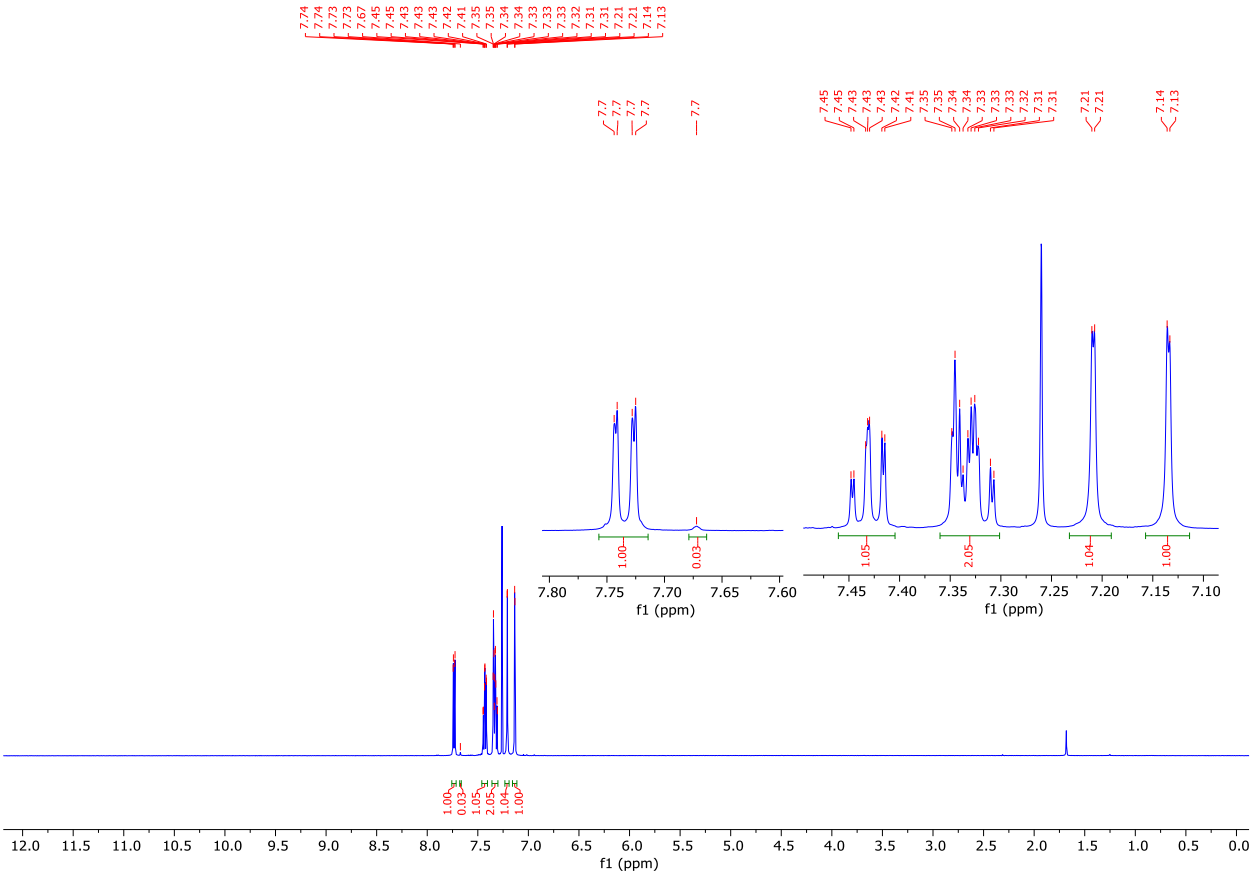

^{13}C (^{1}H) NMR (126 MHz, $CDCl_3$) spectrum of ^{2}H-**4.2a**